This is to certify that the

dissertation entitled

MAGNETIC PROPERTIES OF LAYERED VANADYL PHOSPHATES AND PHOSPHONATES: FROM MOLECULAR BUILDING BLOCKS TO EXTENDED STRUCTURES

presented by

DIMITRIS PAPOUTSAKIS

has been accepted towards fulfillment
of the requirements for

Ph. D. degree in CHEMISTRY

Daniel G. Nocera / James E. Penner-Hahn
Major professor

Date 18 November 1998

MAGNETIC PROPERTIES OF LAYERED VANADYL PHOSPHATES AND PHOSPHONATES: FROM MOLECULAR BUILDING BLOCKS TO EXTENDED STRUCTURES

By

Dimitris Papoutsakis

A DISSERTATION

Submitted to

Michigan State University

in partial fulfillment of the requirements

for the degree of

DOCTOR OF PHILOSOPHY

Department of Chemistry

1998

ABSTRACT

MAGNETIC PROPERTIES OF LAYERED VANADYL PHOSPHATES AND PHOSPHONATES: FROM MOLECULAR BUILDING BLOCKS TO EXTENDED STRUCTURES

By

Dimitris Papoutsakis

Without well–defined structure, any sensible interpretation of magnetic behavior at the molecular level is necessarily speculative. Nowhere is this difficulty more striking than in the field of the host–guest chemistry of layered metal phosphates and their organic/inorganic hybrid analogs (LVPs). In the last few years, however, hydrothermal synthesis techniques afforded such materials in crystalline form, allowing for their structural characterization. The LVPs structural environment can act as a host by encapsulating guest species like small molecules and ions. Such systems are likely to have rich magnetochemistry, since spin communication in principle could be achieved within the host layers (*intralayer coupling*), between adjacent host layers (*interlayer coupling*), among neighboring guest species (*guest–guest coupling*) and between guest and layered host species (*guest–host coupling*). A systematic investigation of low dimensional magnetic interactions involving vanadyl ions was undertaken, indicating correlation of the magnetic properties to structural changes induced to the LVPs' structural building blocks.

We have probed the *intralayer* spin–spin interactions by employing the layered framework of $VOPO_4 \cdot 2H_2O$, which upon redox intercalation of monovalent or divalent cations this simple diamagnetic host becomes magnetic by injection of half or one electron per vanadium center respectively. The magnetic properties of a series of $A_xVOPO_4 \cdot nH_2O$, with A an alkali or alkaline–

earth, were determined and correlated to the structural features of the host layers. Additional insights into the spin exchange pathway were gained by considering the magnetic behavior of a family of layered vanadyl phosphonates (LVPh's) $VO(O_3PC_6H_4–X)•H_2O$ with X = *p*–NO_2, *m*–F, *p*–F, H. In this series of compounds the magnitude of the magnetic coupling was correlated to the electronic properties of the bridging phosphonate ligands. Finally the magnitude of *interlayer coupling* is assessed by utilizing a second series of layered vanadyl phosphonates, $VO(O_3PNp)(H_2O)•nROH$, where the phosphonate pendant is a naphthalene group and various alcohols are intercalated within the interlayer space (LVNpPh's). These compounds displayed remarkable control over the *d*–spacing, since by using various alkyl alcohols adjacent layers are mechanically jacked by 1.06 Å per methylene unit. Hence, the magnetic properties of layers identical to each other, but separated at distances from 12.10 Å to 20.83 Å, were studied enabling the evaluation of the magnitude of the *interlayer coupling*.

We have also identified the potential exchange pathways of the layers responsible for the magnetic coupling. In most cases these were of dimeric nature with two vanadyl centers being bridged by two phosphate/phosphonate ligands. Molecular analogues of these exchange pathways were synthesized and their metric parameters were tuned by varying the substituents in the bridging phosphonates. The small structural changes were correlated to differences in magnetic behavior.

Finally, assembly of organic molecules by the use of an amidinium–carboxylate salt bridge offered an alternative way for the construction of layered materials. Incorporation of a nitroxyl radical within the molecular constituents afforded magnetic solids where magnetic interactions are turn on and off depending on the nature of the potential exchange pathways.

To my wife and son.

ACKNOLEDGMENTS

My days at Michigan State were interesting from many perspectives and certainly not only from a scientific point of view. I was fortunate enough to work for Dan Nocera and Ned Jackson, two individuals that I highly respect and I am grateful for their guidance during the course of my graduate studies. Through them I was exposed to the academic environment and developed a better understanding of the scientific community.

I have interacted with a number of coworkers in both groups, who I would like to thank for providing a friendly and collaborative environment.

Many thanks to the MSU Department of Public Safety and officer Collins for their hospitality and kindness during the hours that me and my wife spent with them. We especially enjoyed the picture session and certainly we are going to keep them in our memories for many years to come. In addition, the sincere interest of the Department of Chemistry and the College of Nature Science was touching.

I wish to thank Prof. Gerasimos Karabatsos and Prof. Daniel Nocera for their help and guidance during our darkest moments.

The most vivid memories were certainly coming from the exhaustive sessions of meditation with Nikos Lydakis, Spiros Kambourakis, Charalambos Soulis, Markos Katsoulakis, Zoe Soulis, Lykourgos Iordanidis, Jen Aitken, Filippos Ververidis, Fabiana Furtato, my companion Lena and occasionally with others, always accompanied by good food and wine. Their friendship was valuable and made my days and my memories enjoyable.

TABLE OF CONTENTS

LIST OF FIGURES

CHAPTER 1

CHAPTER 3

CHAPTER 4

CHAPTER 5

LIST OF TABLES

CHAPTER 1

Introduction

A. Molecular Magnetism

Magnetic effects, for many years have been mainly of concern in the world of physics and materials science. "Real" magnets utilized for industrial purposes are metallic materials, "objects that are opaque, shiny, and go clang when they hit the floor", as Peter Day defined them recently[1]. Their generic attributes include (a) atomic–based character (b) unpaired electrons residing on d or f orbitals of transition or lanthanide metal–based sites (c) extended bonding networks at least in two dimensions and (d) synthesis by high temperature metallurgical methodologies[2]. The systematic study of magnetic phenomena in these materials reveals the variety of electronic and structural factors that

influence spin communication among the "active" sites of a magnet, which often implicate the molecular and atomic constituents of the extended structure, providing the link between chemical science and magnetic phenomena.

The construction or demolition of covalent bonds, which affords interconversion among functional groups, is traditionally utilized in chemistry for the manipulation of various physical properties. These synthetic tools, along with recent advancements concerning the role of noncovalent bonding in the organization of molecular materials to extended solids and in the electronic communication of the constituent molecular building blocks[3], provide the scaffolding that chemical science administers for the study of magnetic phenomena. Through this interaction the field of molecular magnetism has emerged. This multidisciplinary field progresses upon advancements in chemical synthesis of organic and inorganic compounds, theoretical and computational chemistry, solid state chemistry and finally biochemistry since magnetic centers are buttressed within natural systems.

Molecular–based magnetic materials are expected to (a) permit the specific variation of magnetic properties by established synthetic methodologies (b) combine magnetic properties with other mechanical, electrical, and/or optical properties and (c) offer simple synthetic methodologies amenable to laboratory conditions[2]. Although the quest for compounds that mimic or exceed the properties of industrial magnets remains unfulfilled, substantial progress towards this goal has been achieved during the last thirty–five years. The early history of the field is dominated by theoretical approaches to the problem, which established its foundations[4]. However it was not till the late 1980s that the first molecular–based compound exhibiting hysteresis was reported by Miller et al[5]. Today, new exciting materials are synthesized by creative design of ligands and molecular building blocks able to self–assemble in extended structural

frameworks. A plethora of interesting magnetic phenomena have been recorded and analyzed on the basis of known theoretical models. Recognition of the factors that affect spin communication, and their correlation to the type and the strength of the magnetic interaction, are critical requirements for development of a better understanding of the field. An overview of the different ways that unpaired electrons can interact is presented below, along with the qualitative theoretical background utilized in this thesis.

1. Types of Magnetic Behavior

Magnetic effects are classified by the repulsion or attraction of a body when placed in a magnetic field. The repulsion is called diamagnetism, which is an underlying property of matter and is caused by the interaction of the magnetic field with the motions of the electrons. When unpaired electrons are present within the body, the diamagnetic behavior is masked by the much stronger interaction of the magnetic field with the eletrons' magnetic moments, also known as their spins. The theoretical formalism describing the unpaired spin behavior in the presence of magnetic field, was developed by Van Vleck in 1932[6], who derived an equation describing the molar magnetic susceptibility of a substance as:

$$\chi = \frac{N\sum_n (E_n^{(1)^2}/kT - 2E_n^{(2)}) exp(-E_n^{(0)}/kT)}{\sum_n exp(-E_n^{(0)}/kT)} \qquad (1.1)$$

where N is the Avogadro number, k is the Boltzmann constant, T is the temperature in Kelvin, $E_n^{(0)}$ is the energy of the level in the absence of the field and $E_n^{(1)}$, $E_n^{(2)}$ are the first– and the second–order Zeeman coefficients respectively. Using perturbation theory, these coefficients can be calculated as

$$E_n^{(1)} = \langle n|\hat{\mathbf{H}}|n\rangle \tag{1.2}$$

$$E_n^{(2)} = \sum_m \frac{\langle n|\hat{\mathbf{H}}|m\rangle^2}{(E_n^{(0)} - E_m^{(0)})} \tag{1.3}$$

with the summation running over the levels m with $m \neq n$. Different terms can be incorporated into the hamiltonian $\hat{\mathbf{H}}$ to account for the factors contributing to the magnetic behavior of a given compound. If the active spin sites are far enough apart and their spin–spin coupling energy J is small compared to the thermal energy, the spins behave independently, adopting random orientations with respect to each other. Such behavior is referred to as paramagnetic and is illustrated in *Figure 1(A)*. Solution of equation (1.1) for a paramagnetic substance leads to the well–known Curie expression:

$$\chi = \frac{N\mu_\beta^2}{3kT}[L(L+1) + 4S(S+1)] \tag{1.4}$$

with L and S the orbital and spin quantum numbers respectively and μ_β the Bohr magneton.

In many cases the spin–spin coupling interaction is strong enough to induce neighboring sites to take on either a parallel or antiparallel arrangement with respect to each other. The former type of behavior is known as ferromagnetic (*Figure 1(B)*) and the latter as antiferromagnetic (*Figure 1(C)*). When strong antiferromagnetic coupling occurs among dissimilar spin sites, the incomplete cancellation of the magnetic moment ensues to a net ferromagnetic interaction in polynuclear or extended spin arrays. This effect, known as ferrimagnetism (*Figure 1(D)*), constitutes one of the main strategies for the synthesis of molecular–based magnets.

Early theoretical work on exchange coupled systems, concerned chemical entities where two spin centers are juxtaposed on the same structural

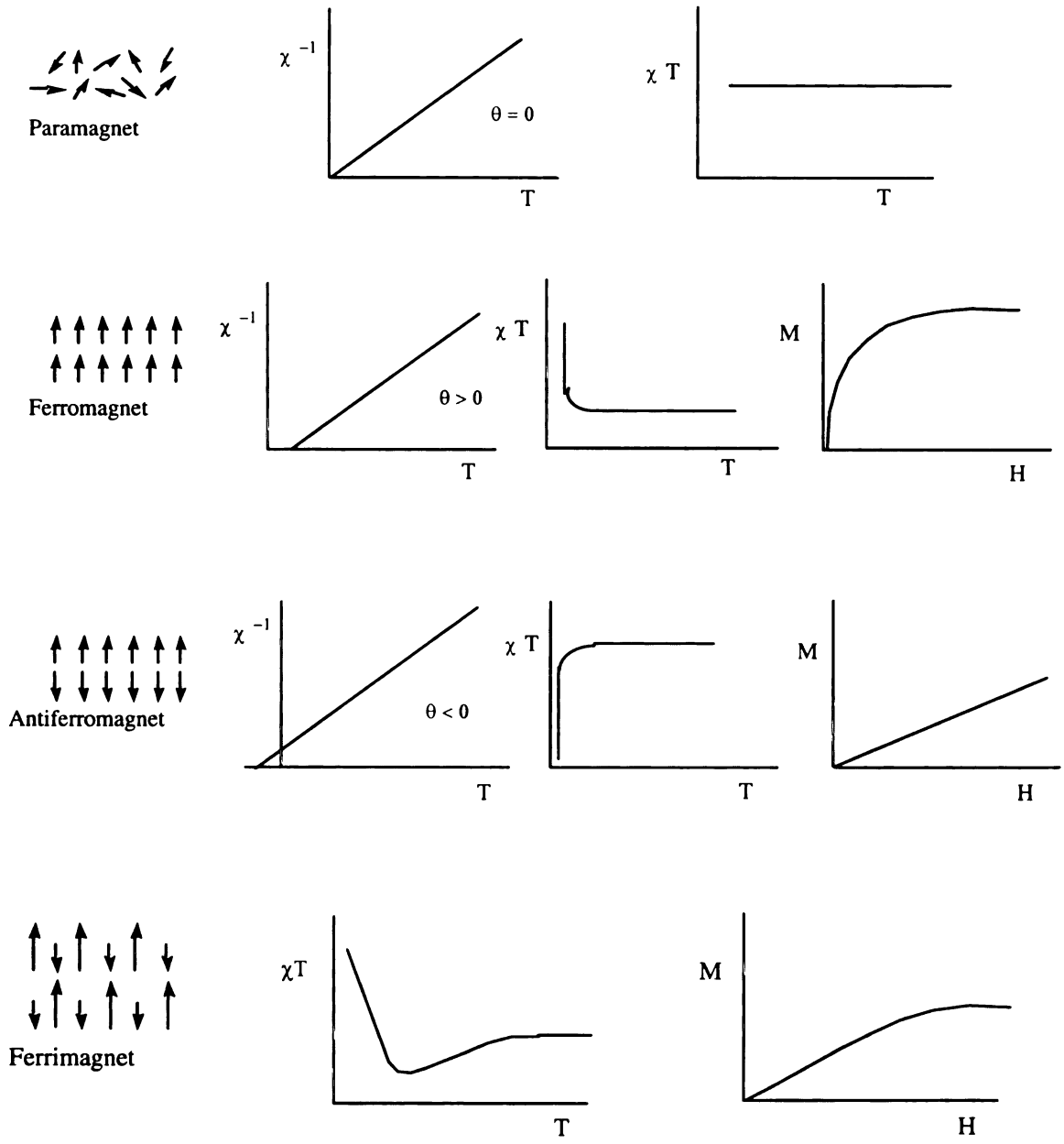

Figure 1. Relative spin orientation in different types of magnetic behavior. The plots display the typical behavior of magnetic quantities, such as inverse susceptibility (χ^{-1}), temperature product of susceptibility (χT), and magnetic moment (M), when plotted versus the temperature or the magnetic field.

framework. Few parameters needed to be considered for a successful approximation of the system, and the discovery of strong antiferromagnetic coupling on $Cu_2(CH_3COO)_4 \cdot 2H_2O$[7] provided a well–defined case. The study of magnetic effects on this dimeric entity opened widely the field of magnetism to chemists, with the realization that small variations of the structural and electronic properties of a molecule, controlled via by chemical methodology, can be manifested as changes in the magnetic behavior. Dimeric complexes containing transition metal atoms with unpaired electrons can be generally categorized according to their magnetic behavior into three main groups, depending on the strength of the metal–metal interaction. In the first type, namely the *noninteracting* group, the magnetic properties are essentially unchanged from those of the paramagnetic monomer. In the *strongly interacting* group, direct overlap between the metal orbitals that bear the unpaired spin density lead to formation of relatively strong metal–metal bonds, and the molecule displays simple diamagnetic behavior. One family of such compounds consists of the d^4 — d^4 complexes that exhibit a quadruple bonded metal core. These systems have a ground state electronic configuration of $\sigma^2\pi^4\delta^2$, with the δ bond being formed by the weak overlap of the metal's d_{xy} orbitals. The lowest lying electronic excited state of the complexes is the spin triplet configuration $\sigma^2\pi^4\delta^1\delta^{*1}$, with theoretical considerations and indirect experimental evidence[8] placing it approximately 3200 cm^{-1} above the ground state[9]. This weak bonding interaction attains its maximum strength by positioning the two monomeric ML_4 units of the dimer core in an eclipsed arrangement. By proper selection of the bridging ligand[10] a twist towards a staggered configuration can be triggered, reducing the δ–bond overlap and the energy difference between the ground singlet and the excited triplet states. When a large twist is induced in the dimer core, thermal energy is sufficient to promote population of the excited triplet–state, resulting in

a magnetic response[11] similar to those of strongly coupled antiferromagnetic systems.

The intermediate coupling regime consists of complexes where the metal centers are *weakly interacting*, mainly indirectly by way of the ligands interconnecting them. Such interactions lead to the formation of two low–lying states of different spin which can be populated at thermal energies ($\leq 1000\ cm^{-1}$). The resulting magnetic behavior may be ferromagnetic or antiferromagnetic depending on whether the high spin (spins parallel) or the low spin (spins antiparallel), is the ground state respectively. These interactions are mediated by the ligands since the metal — metal distance is large (3 – 6 Å), and are termed *superexchange* interactions. A valuable qualitative treatment of the effect is achieved through the active–electron approximation[12]. Theoretical models[13,14] have established the geometrical and electronic factors that govern the nature of the ground state. The magnetic interaction between two spin centers $\mathbf{S_A}$ and $\mathbf{S_B}$ is written according to the Heisenberg, Dirac and Van Vleck[6,15] hamiltonian

$$\mathbf{H} = -J\mathbf{S_A} \bullet \mathbf{S_B} \qquad (1.5)$$

where the exchange coupling constant J (which measures the singlet–triplet energy splitting) is positive if the spin sites align parallel with respect to each other indicating ferromagnetic interaction, and negative for paired alignment imposed by antiferromagnetic coupling. Two approaches have been developed under the active–electron approximation according to the types of magnetic orbitals utilized as the basis set. The first approach considers orthogonalized magnetic orbitals, drawn in *Figure 2(A)* for a d^9 — d^9 dibridged copper compound, where each orbital is mainly localized in one metal center but has a nonvanishing contribution from the other metal site. This tail becomes more important as the energy separation of the orthogonalized molecular orbitals

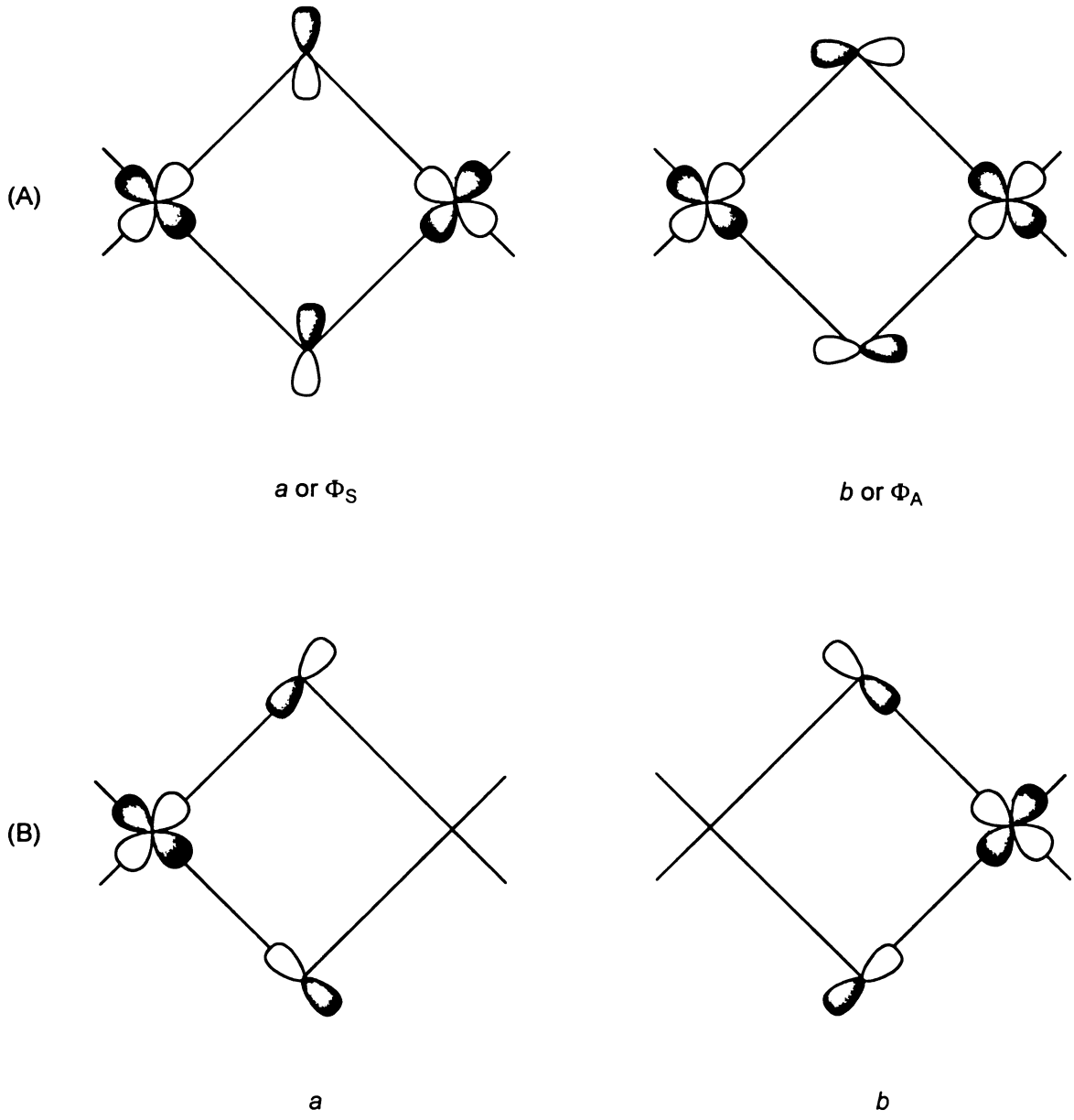

Figure 2. The symmetric ϕ_S and antisymmetric ϕ_A orthogonalized magnetic orbitals (A), and the respective natural magnetic orbitals (B), for a hydroxo–bridged Cu(II) binuclear complex.

becomes larger. The combine effect is a symmetric a (or ϕ_A) and an antisymmetric b (or ϕ_S) linear combination of metal orbitals that interact with molecular orbitals of proper symmetry from the bridging ligand. The natural magnetic orbital basis set on the other hand, considers the dimeric entity as a combination of two fragments, each one composed of one metal center and the bridging ligand. The orbitals are localized around each metal and have contributions only from the bridging ligand(s) (*Figure 2(B)*).

In order to calculate the singlet–triplet energy splitting for two orthogonalized orbitals *a* and *b* bearing one unpaired electron each, an effective electrostatic hamiltonian is considered

$$\mathbf{H} = \mathbf{h}(1) + \mathbf{h}(2) + 1/r_{12} \qquad (1.6)$$

with $\mathbf{h}(i)$ being the one electron hamiltonian for electron *i* which takes into account its kinetic energy, and its interactions with the nuclei and the core electrons. The following two one–electron and four two–electron integrals given below contribute to the energy of the states

$$\alpha = \langle a(1)|\mathbf{h}(1)|a(1)\rangle \qquad \beta = \langle a(1)|\mathbf{h}(1)|b(1)\rangle$$
$$j^0 = \langle a(1)a(2)|r_{12}^{-1}|a(1)a(2)\rangle \qquad j = \langle a(1)b(2)|r_{12}^{-1}|a(1)b(2)\rangle$$
$$k = \langle a(1)b(2)|r_{12}^{-1}|a(2)b(1)\rangle \qquad l = \langle a(1)b(2)|r_{12}^{-1}|b(1)b(2)\rangle$$

The interaction of the two electrons generates two ground states arising from the *ab* electronic configuration ($^1\Gamma_g$ and $^3\Gamma_u$) and two excited states from the charge transfer zwitterionic states a^2 or b^2 ($^1\Gamma_g$ and $^1\Gamma_u$). The singlet–triplet splitting is expressed as the sum of a ferromagnetic and an antiferromagnetic contribution

$$E_T - E_S = J_F + J_{AF} = 2k - \frac{4(\beta + l)^2}{U} \qquad (1.7)$$

with the energy diagram drawn in *Figure 3*. The first ferromagnetic term reflects the stabilization of the triplet ground state with respect to the singlet ground state as a result of the exchange interaction of the electrons. Considering second–order effects, the $^1\Gamma_g$ charge transfer state stabilizes the $^1\Gamma_g$ ground state with respect to the triplet. It is this interaction, termed kinetic exchange, that to a first approximation[14] provides the main antiferromagnetic contribution. The significance of kinetic exchange becomes clearer when it is formulated as[13]

$$J_{AF} = -\frac{(\varepsilon_1 - \varepsilon_2)^2}{j^0 - j} \qquad (1.8)$$

with ε_1 and ε_2 being the energies of the magnetic orbitals *a* and *b* depicted in *Figure 2(A)*, since magnetostructural correlations can be derived based on the effects of geometrical distortions upon these energies.

If natural magnetic orbitals are employed as the basis set, an additional one–electron integral is considered, namely the overlap integral *S* between orbitals *a* and *b* (drawn in *Figure 2(B)*). According to this approach[13] the singlet–triplet energy splitting is expressed as

$$E_T - E_S = 2k + 4\beta S - 2S^2(2\alpha + j) - \frac{4[\beta + l - (\alpha + j + k)S]^2}{U} \qquad (1.9)$$

with the terms proportional to S^2 being relatively small compared to the rest and therefore negligible within a qualitative framework. The main antiferromagnetic term was expressed by Kahn and coworkers[16] as

$$J_{AF} = -2\Delta S \qquad (1.10)$$

with Δ being the energy gap between the two molecular orbitals in the binuclear complex built from the two magnetic orbitals *a* and *b*. This formulation bases magnetostructural correlations solely upon the value of the overlap integral S,

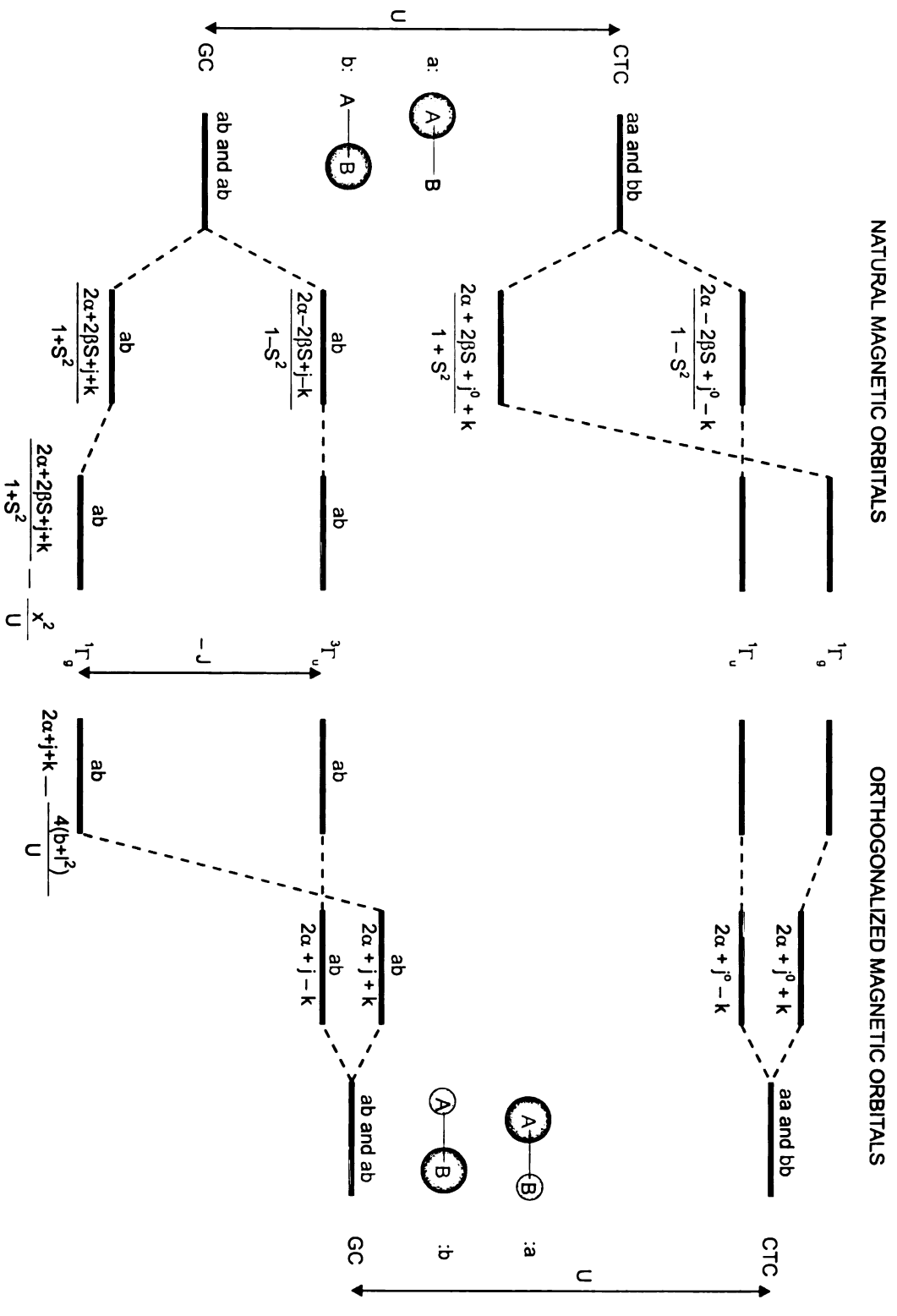

Figure 3. Comparison of the natural (left) and orthogonalized (right) orbital approaches in the active–electron approximation (GC, ground configurations; CTC, charge transfer configurations; U energy separation between GC and CTC).

which becomes larger as Δ increases favoring a singlet ground state.

2. The Effect of Geometrical Perturbations: The Case of $[L_2Cu(OH)]_2(X)_2$

Much attention is still devoted to a complete understanding of magnetic properties with respect to geometrical and electronic distortions. The title series of complexes constitutes a structurally and magnetically well–characterized group of homologous compounds[17], and has been the target of many computational studies. A recent one[18], based on Density Functional Theory (DFT), resulted in excellent agreement between calculated and experimentally determined singlet–triplet separations. The authors considered orthogonalized magnetic orbitals for their approach, with the antiferromagnetic contribution governed only by the kinetic exchange term of equation (1.8). Therefore one can focus on the difference of orbital energies, $\varepsilon_1 - \varepsilon_2$, as a probe of the singlet–triplet energy splitting. The energy gap can be tuned with the aid of synthetic methodologies, capable of modifying both the geometrical and electronic environment of the magnetic centers. This has been accomplished in the homologous series considered here, by changing the terminal ligands and the counterions of the dimeric complexes. The exchange coupling constant obeys the following empirical linear relationship[17]

$$J(cm^{-1}) = -74\alpha(deg) + 7270 \qquad (1.11)$$

with α being the Cu — O — Cu bridging angle. Equation (1.11) predicts that J equals zero for α = 97.5°, while for values above and below that angle the ground state is singlet and triplet respectively.

The highest occupied orbitals of the copper dimer are the symmetric and antisymmetric combinations of the monomer $d_{x^2-y^2}$ orbitals. These further interact

with the lower lying filled orbitals, centered on the oxygen atoms of the bridge, that derive from linear combinations of p_y and p_x atomic orbitals. The outcome of such interplay is the constitution of the two orthogonalized magnetic orbitals ϕ_S and ϕ_A respectively, shown in *Figure 2(A)*. When the bridge angle approaches 90° ϕ_S and ϕ_A become degenerate leading to a ferromagnetic interaction. By increasing the bridging angle α, the overlap (and hence the antibonding character of the predominantly metal–based orbitals) increases for ϕ_A and decreases for ϕ_S. As a consequence, the factor $(\varepsilon_1 - \varepsilon_2)$ of equation (1.8) is enlarged, affording a dominant antiferromagnetic contribution that favors the singlet state as the ground state of the dimer system. The symmetric orbital ϕ_S also interacts with the 2s atomic orbitals of the bridge, enforcing its antibonding character. A shift towards higher energies is observed, moving the crossing point for the condition $J = 0$ to $\alpha = 96°$. The latter value is in good agreement with the value predicted by the experimentally derived equation (1.11), indicating an excellent correlation of theory and experiment.

Kahn and coworkers[19] arrived at a similar conclusion by considering natural magnetic orbitals and inspecting the variation of the overlap integral S as a function of geometrical distortions. For values of the bridging angle α close to 90° the overlap integral S is approximately zero, annihilating the antiferromagnetic contribution of the exchange constant J. Such a condition is achieved by the "accidental" orthogonality of the orbitals, the term meaning that the latter condition is not an effect imposed by the symmetry properties of the orbitals, but rather by the specific geometrical arrangement of the structural framework.

3. The Effect of Electronic Perturbations: The Case of $VO(O_3PC_6H_4–X)•H_2O$

The effect of electronic perturbations on the magnitude of the exchange interaction has also been treated by theory in the framework of the active–electron approximation by Hoffmann and coworkers[13]. Using second–order perturbation theory and substituting the energies of the symmetric and the antisymmetric combinations of magnetic orbitals, the quantity of interest $\varepsilon_1 - \varepsilon_2$ ($\varepsilon_S - \varepsilon_A$) can be formulated as

$$\varepsilon_S - \varepsilon_A = \frac{|H_{id}^S|^2}{\varepsilon_d - \varepsilon_{IS}} - \frac{|H_{id}^A|^2}{\varepsilon_d - \varepsilon_{IA}} \qquad (1.12)$$

The labels I and d stand for the bridging ligand and the metal orbitals respectively, assuming that only one ligand orbital with the correct symmetry is interacting. Removal of electron density from a bridging atom that contributes to the magnetic orbitals reduces the electron–electron repulsion and lowers its atomic orbital levels, along with the energies of the molecular orbitals of the atom involved. If the energy of the atomic orbitals is lowered by an amount Δ', with $\Delta' > 0$, the new magnetic orbitals now differ in energy by

$$\varepsilon_S{}' - \varepsilon_A{}' = \frac{|H_{id}^S|^2}{\varepsilon_d - \varepsilon_{IS} + \Delta} - \frac{|H_{id}^A|^2}{\varepsilon_d - \varepsilon_{IA} + \Delta} \approx \varepsilon_S - \varepsilon_A - \Delta' \left[\frac{|H_{id}^S|^2}{(\varepsilon_d - \varepsilon_{IS})^2} - \frac{|H_{id}^A|^2}{(\varepsilon_d - \varepsilon_{IA})^2} \right] \qquad (1.13)$$

Since the quantity in the brackets is positive, the energy difference between the magnetic orbitals becomes smaller, leading to a decrease in antiferromagnetic interactions upon removal of electron density from the bridge. Conversely, electron donation would enhance antiferromagnetic coupling.

Experimentally the above observations were not very well substantiated,

since results from copper acetate[20] and formate[21] were puzzling and partially inconsistent with this qualitative theoretical framework. Firm evidence regarding the significance of substituent effects on the magnitude of the exchange interaction, was provided by the work of Le Bideau and coworkers[22] who studied the electronic tuning of the singlet–triplet energy gap on vanadyl phosphonate dimer cores incorporated within layered frameworks. The isostructural series of layered vanadyl phosphonates (LVPh's) $VO(O_3PC_6H_4–X)•H_2O$ with X = *p*–NO_2, *m*–F, *p*–F, H, was synthesized and it was found that the magnetic properties are those of isolated dimer units that exhibit a chair–like conformation. Substituent variation showed that the magnitude of the antiferromagnetic exchange interaction is weakened as electrons are withdrawn from the bridging ligands. The exchange interaction constant *J* was found to obey a linear free energy relationship with the Hammett σ parameter of the substituents, which reflects the changes upon the electronic environment of phosphorus. Detailed discussion and interpretation of these effects will follow in Chapter 3 of this thesis as the work mentioned there, is directly connected to the studies of Dr. Le Bideau.

4. Strict Orthogonality: The Case of $CuVO(fsa)_2en•CH_3OH$

The common preference of unpaired electrons for an antiparallel arrangement (Pauli Principle) is sometimes prevented by the orthogonality condition among atomic or natural molecular orbitals. In cases of homometallic species, as in some of the members of the $[L_2Cu(OH)]_2(X)_2$ series, the orthogonality of the orbitals is accidental, imposed by the structural framework. In heterometallic complexes however, it is possible by proper selection of the spin carriers to arrange for magnetic orbitals that are orthogonal by symmetry. Such a condition leads to Hund's rule–type stabilization of the triplet state by annihilating

the kinetic exchange antiferromagnetic term, which is proportional to the overlap integral S (equation (1.10)).

The above hypothesis was first tested by Kahn and coworkers[23], who synthesized the heterometallic complex $CuVO(fsa)_2en \cdot CH_3OH$ — with $H_4(fsa)_2en$ being the *N,N'*–(2–hydroxy–3–carboxybenzilidene)ethylenediamine ligand — and the respective dicopper one. Strong stabilization of the singlet state is observed for the homometallic complex as judged by the large exchange constant of – 650 cm^{-1}. The strong interaction is in accordance with the qualitative picture presented so far, since a large Cu — O — Cu (larger than 90°) bridging angle is imposed by the nature of the $H_4(fsa)_2en$ ligand. However in the heterometallic complex, the kinetic exchange term is zero since the two magnetic orbitals are orthogonal by symmetry and thus have zero overlap. This condition is termed strict orthogonality leading to a large, for a molecular compound, ferromagnetic coupling with an exchange constant of + 118 cm^{-1}. Although strict orthogonality beyond two centers is hard to achieve from a synthetic perspective, this work represented a major advancement towards the manufacture of molecular ferromagnetic materials.

5. Interaction between Pairs of Magnetic Orbitals

A frequently encountered circumstance is coupling between two metal sites juxtaposed in the same structural entity, with each of them accommodating more than one unpaired electron. Such systems are usually treated under the framework of the active–electron approximation by utilizing natural magnetic orbitals. From each pair of orbitals a_μ and b_ν localized on the A and B fragment of the dimeric complex, two molecular orbitals delocalized on the AB molecule can be constructed. If Δ_μ and D_μ denote the energy gap of the molecular and the

magnetic orbitals respectively, the exchange constant $J_{\mu\nu}$ for each pair can be again described as a sum of a ferromagnetic and an antiferromagnetic term[24]:

$$J_{\mu\nu} = 2k_{\mu\nu} - 2(\Delta_{\mu}^{2} - D_{\mu}^{2})^{1/2} S_{\mu\mu}\delta_{\mu\nu} \qquad (1.14)$$

with $k_{\mu\nu}$ the two electron integral and $S_{\mu\mu}\delta_{\mu\nu}$ the overlap integral for each pair of orbitals a_{μ} and b_{ν}. This relationship provides the formalism for qualitative rules, first proposed by Goodenough and Kanamori[25], which allow the prediction and estimation of the nature and the strength of the magnetic interaction between dissimilar metallic sites. *Figure 4* illustrates natural magnetic orbitals of metallic centers in local C_{2V} symmetry, that embody metal d– and ligand p–orbitals. Such a local environment is frequently encountered in planar double–bridged dimers with overall symmetry of C_{2V} or D_{2h}. Considering all the pairwise orbital interactions a 5×5 matrix can be constructed, by identifying the nature (ferromagnetic (F) or antiferromagnetic (AF)) and the strength (weak (w) or medium (m) or strong (s)) of the interaction. The outcomes of this approach are gathered in Table 1[12].

The strength and the nature of the $J_{\mu\nu}$ terms, depends upon the ability of the two metal orbitals to overlap through the bridging ligand orbitals (*Figure 4)*. When the magnetic orbitals are orthogonal by symmetry, a condition met by almost all the off–diagonal elements of Table 1, the nature of the interaction is ferromagnetic. Only the $d_{x^2-y^2}$ and d_{z^2} orbitals are of the same symmetry, and their exchange interaction consists of both ferromagnetic and antiferromagnetic terms. For bridging angles α larger than 90°, the kinetic exchange term prevails resulting in the stabilization of the singlet state (*Figure 2*). The interaction is weak due to the small degree of delocalization of d_{z^2} towards the bridging ligand. When the bridge angle α is close to 90°, accidental orthogonality of the orbitals is achieved and the triplet state becomes the ground state, since the net value of

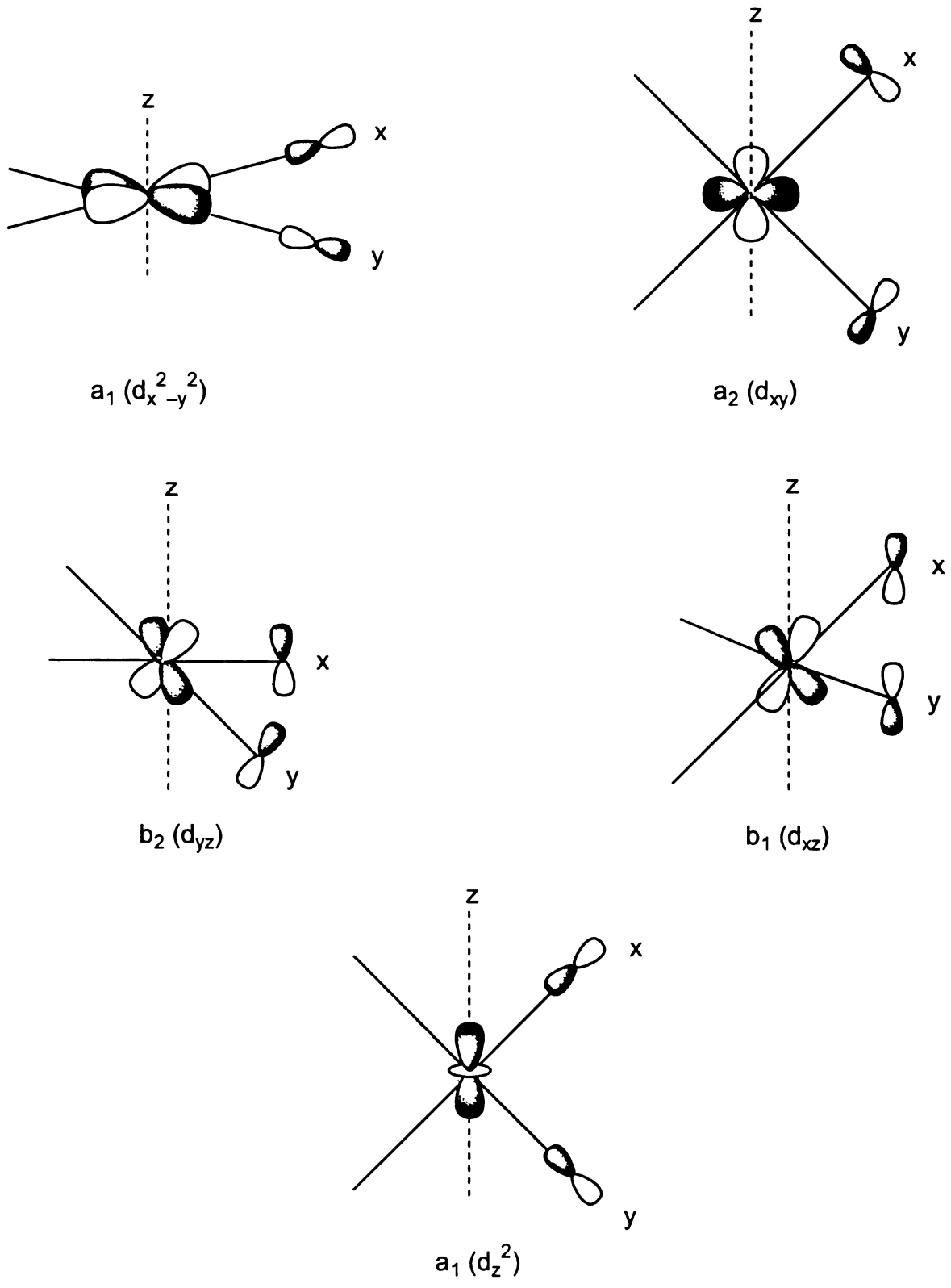

Figure 4. Magnetic orbitals of a metal fragment in the C_{2v} point group.

Table 1. Prediction of the Nature and the Order of Magnitude for Contributions $J_{\mu\nu}$ Involving Pairs of Magnetic Orbitals[a] for Binuclear Metal Complexes in the C_{2v} Point Group

$J_{\mu\nu}$	$a_2\,(d_{xy})$	$a_1(d_{z^2})$	$b_2\,(d_{yz})$	$a_1(d_{x^2-y^2})$	$b_1\,(d_{xz})$
$a_2\,(d_{xy})$	AF_m	AF_m	F_w	F_s	F_w
$a_1(d_{z^2})$		F_w to AF_w	F_w	F_w	F_w
$b_2\,(d_{yz})$			AF_w	F_w	F_w
$a_1(d_{x^2-y^2})$				F_s to AF_s	F_w
$b_1\,(d_{xz})$					AF_w

[a] F, ferromagnetic; AF, antiferromagnetic. The subscripts are w, weak; m, medium; s, strong.

the overlap integral S is zero. For the diagonal terms of Table 1, again both contributions are operative. Ferromagnetism prevails only in cases where accidental orthogonality is achieved, while in all the other cases the kinetic exchange term leads to a singlet ground state.

6. Towards Bulk Molecular Magnetism: The Case of the Prussian Blue Family of Compounds

The analysis of pair interactions among orbitals located on adjacent metal sites is a powerful qualitative method utilized for the design of molecular–based magnets. The significance of this approach has been demonstrated by the synthesis of a large family of compounds based on the three–dimensional network of Prussian Blue[26]. This structural framework presents significant advantages[27] including (a) ease of synthesis via room temperature reaction of hexacyanometallates (octahedral $[B(CN)_6]^{-k}$) –functioning as Lewis bases – with metallic cations A^{+l}, (2) the variety of oxidation states accessed by the two metal sites A and B, (3) the symmetrical nature of the structural framework, where the metal sites A juxtaposed within octahedral holes are joined via cyanide ligands with the Lewis basic sites, (4) the manipulation of the stoichiometric formula $A_k[B(CN)_6]_l \bullet nH_2O$ by incorporating cationic species within the tetrahedral holes of the structure, and (5) the nature and the strength of the coupling constant *J* can be analyzed within the binuclear fragment $(NC)_5B$ — CN — $A(NC)_5$, where B, C, N and A are collinear.

It is the latter factor that demonstrates the significance of the pair orbital analyses. Within the structural framework of the Prussian Blue family, the local coordination environment at each metal site is octahedral. Thus the electrons are distributed in two types of orbitals, namely the triply degenerate t_{2g} set and the

doubly degenerate e_g set. When the magnetic orbitals interacting are of the same type ($t_{2g} - t_{2g}$ or $e_g - e_g$), the antiferromagnetic contribution is expected to be dominant. Since no accidental orthogonality is possible as dictated by the linearity of the exchange pathway, the strength of the kinetic exchange term is determined by the strength of the overlap among the magnetic orbitals. On the other hand when the magnetic orbitals are of different types ($t_{2g} - e_g$) this overlap is zero and a parallel alignment of the spins is enforced. The simplicity of the octahedral local symmetry of the metal sites leads to two possible strategies for the design of molecular magnets based on this family of compounds. The first one depends on the specific electronic configurations of metal sites A and B, with unpaired electrons in t_{2g} orbitals in one site and in e_g orbitals in the other site. Such is the case in $Cs^{I}Ni^{II}[Cr^{III}(CN)_6]$ $\cdot 2H_2O$ where a short range ferromagnetic coupling is established among neighboring spin centers, which further leads to bulk ferromagnetism below the Curie temperature T_C = 90 K[28]. Difficulties concerning this approach arise from the small numbers of metals that meet the configuration criteria and the limited knowledge regarding the nature of the ferromagnetic contribution. On the other hand, control over the antiferromagnetic factor is better established and its magnitude can be manipulated by utilizing well–established qualitative methodologies as guides. Strong antiferromagnetic interactions among dissimilar spin sites give rise to incomplete cancellation of the spins and ferromagnetic ordering of the residual magnetic moments. The so–called ferrimagnetic approach was first demonstrated in the Prussian Blue family by the synthesis of $Cs^{I}Mn^{II}[Cr^{III}(CN)_6]$[29]. The electronic configurations of Cr^{III} and Mn^{II} are $(t_{2g})^3$ and $(t_{2g})^3(e_{2g})^2$ respectively leading to spin moments of 3/2 and 5/2. The pair orbital analysis predicts strong antiferromagnetic and weak to medium ferromagnetic contributions from the $t_{2g} - t_{2g}$ and $t_{2g} - e_g$ pairs respectively. The overall effect is

strong short–range antiferromagnetic coupling accompanied by 3D ferrimagnetic ordering at T_C = 90 K. In an effort to produce materials with enhanced curie transition temperatures Verdaguer and coworkers[27] replaced Mn^{II} by Cr^{II} synthesizing $[Cr_5(CN)_{12}]\cdot 10H_2O$ and $Cs^{I}_{0.75}[Cr_{2.125}(CN)_6]\cdot 5H_2O$, which order ferrimagnetically at 240 and 190 K respectively. Substitution of the Lewis acidic sites by Cr^{II} ions diminishes the ferromagnetic contribution on the Cr^{II} — Cr^{III} pairs, since only one electron resides in e_g orbitals. At the same time, it enhances the kinetic exchange term of the exchange constant by increasing the overlap among the magnetic orbitals, since a smaller energy mismatch corresponds to the Cr^{II} — Cr^{III} pairs than the Mn^{II} — Cr^{III} ones. Further developments along these lines, afforded a room temperature ordered ferrimagnet[30] with formula $V^{II}_{0.42}V^{III}_{0.58}[Cr^{III}(CN)_6]_{0.86}\cdot 5H_2O$, by total removal of electrons from the e_g orbitals.

The compelling results radiating from this family of compounds have shifted the target of the field towards materials that not only attain bulk magnetic behavior, but also can embody other physical properties of interest. For example the tuning of magnetic behavior by optical sources is a highly desirable combination of attributes, with numerous applications. An example is the compound $K_{0.2}Co_{1.4}[Fe(CN)_6]_2\cdot 6.9H_2O$ where changes in the magnetization are induced by red light illumination[31]. Two types of metal links are embodied within the three–dimensional network: Fe^{III} — CN — Co^{II} and Fe^{II} — CN — Co^{III}. The former contributes to the magnetic properties while the latter comprises a diamagnetic pathway. Illumination of the solid by red light results in the interconversion of the diamagnetic to the magnetic pathways, increasing the number of active spin sites and therefore the magnetization properties.

7. Double Exchange: An Alternative Mechanism for Ferromagnetic Coupling

Magnetic coupling usually propagates through well–established exchange pathways that involve filled ligand orbitals with specific geometrical and electronic attributes, which influence dramatically the strength and the nature of the magnetic interaction. Alternative strategies for the design of magnetic materials along with the necessary theoretical background[4] have been developed, based on through space[2,5] or noncovalent bonding exchange pathways[32]. However, most chemical knowledge acquired through the last century concerns synthetic control and attributes of covalent bonds. Ideally, construction of magnetic solids should therefore utilize covalent bonding as the main link between paramagnetic units. The *double–exchange* mechanism[33] is such a case, since spin communication is satisfied in a predictable manner and at the same time controlled structural design is accomplished by covalently linking the desired units. This phenomenon is observed in spin delocalized mixed–valent systems and is based on the interplay between electron exchange and electron transfer events. The archetype molecular system is $[Fe_2(\mu\text{–}OH)_3(tmtacn)_2]^{+2}$ where tmtacn represents 1,4,7–trimethyl–1,4,7–triazacyclononane. Mössbauer[34] and EXAFS[35] spectroscopy have established a delocalized dimetallic core with an S = 9/2 ground state. The spin alignment is understood within the framework of the *double–exchange* mechanism, by considering two energetically equivalent resonance structures of the mixed–valent pair, which interconvert via a one–electron transfer process (*Figure 5*). If the core spins of the two iron centers are aligned in a parallel fashion the transfer of the extra electron takes place without a spin flop (*Figure 5*, top). If an antiparallel alignment is imposed, an energetically costly spin flop is required in

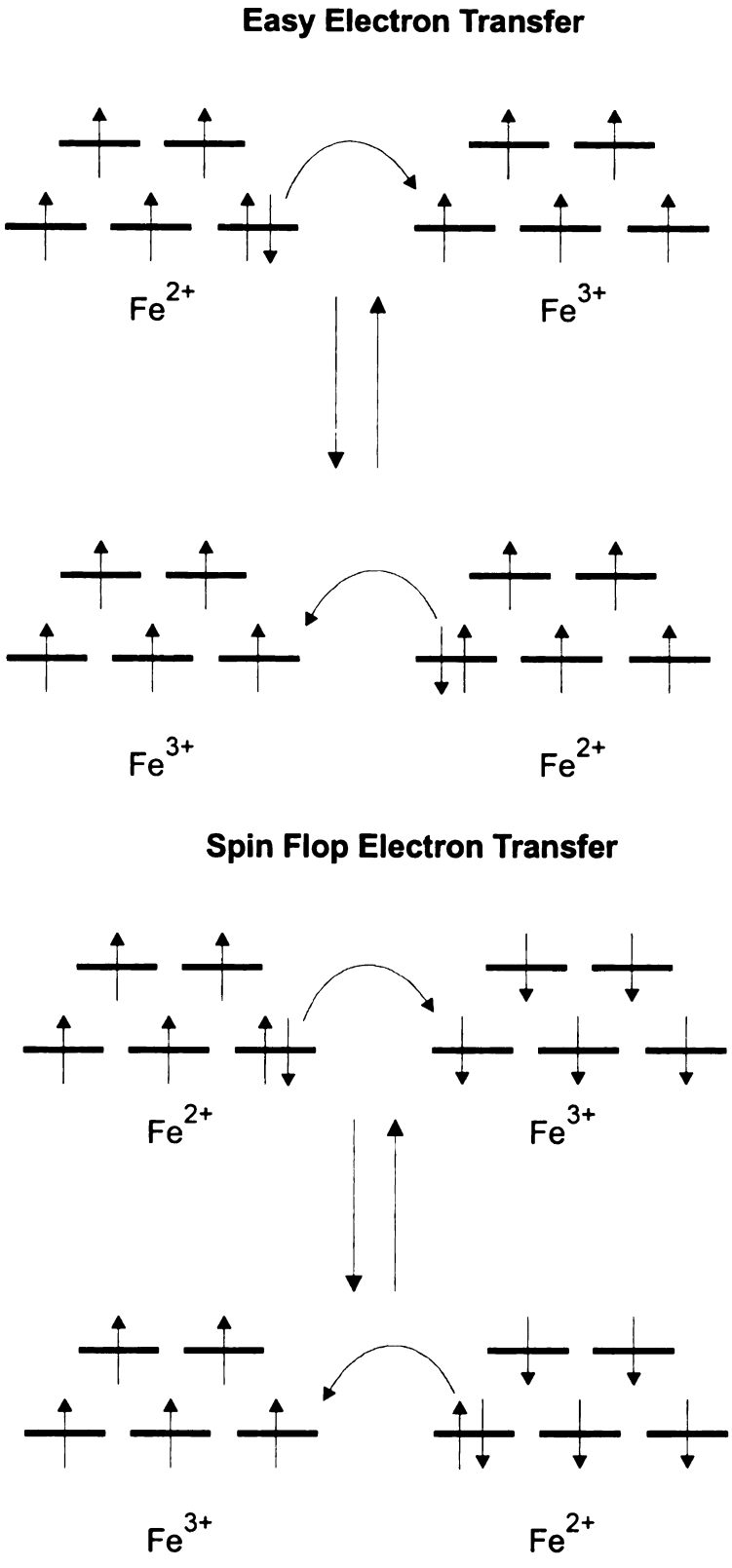

Figure 5. Easy (top) and Spin Flop (bottom) electron transfer in a Fe^{2+}/Fe^{3+} mixed valence bimetallic complex.

order for the electron transfer to be accomplished without violation of the Pauli principle (*Figure 5*, bottom). Therefore, the transfer of the excess electron effectively dictates the ferromagnetic coupling of the two metal centers.

Another family of molecular systems where ferromagnetism is the synergistic result of electron exchange and electron transfer were introduced by the work of Wieghardt and coworkers[36] who applied the above principles in trimeric clusters containing Nickel and/or Cobalt centers in various oxidation states. The *superexchange* mechanism, which considers localized oxidation states on the metal centers, does not satisfactory explain the magnetic properties of most of these compounds. The *double–exchange* concept provides a theoretical framework that explains the ground states of these compounds in which spin centers are juxtaposed within a covalent network. Although limited to these molecular examples, this theoretical picture provides new ground for creative thinking and design of molecular magnets.

B. Metal Phosphate/Phosphonate Extended Materials

The tuning of physical properties by well–established organic methodologies, has generated vast interest in the field of molecular based materials. Extended inorganic compounds, on the other hand, are difficult to manipulate via systematic, well–controlled means, which would predictably perturb their physical properties. This difficulty mainly arises from the extreme conditions needed for the synthesis of solid state inorganic materials, which requires high temperatures for interdiffusion and/or dissolution of the reactants, leading to products with bond connectivities that bear little resemblance to the starting materials[37]. Organic/inorganic hybrid materials on the other hand, are

found in the intermediate regime between molecular and extended materials. The aim of the field is to combine well–defined inorganic networks with organic pendants, generating materials with alternating inorganic and organic arrays. In addition to physical properties associated with the chemical formulation of the organic and the inorganic network, these new materials are expected to possess unique properties manifested by the synergistic interaction of the organic with the inorganic components.

Development of such materials however, has to overcome the synthetic obstacle of selecting inorganic frameworks that can be generated under conditions tolerable to the organic pendants. A major advance in this direction is the development of metal phosphate/phosphonate chemistry. These inorganic matrixes are synthesized at low temperatures and often from aqueous solutions, conditions that permit the construction of the inorganic framework without destruction of the organic part of the ligand. A large number of divalent, trivalent and tetravalent metals have been used for the synthesis of such materials[38], yielding remarkable structural diversity in the interplay of the metal ions with O — P — O linkages. These bridges may be part of the phosphate (PO_4^{-3}), hydrogenphosphate (HPO_4^{-2}), dihydrogenphosphate ($H_2PO_4^{-1}$), phosphite (PO_3^{-3}), hydrogenphosphite (HPO_3^{-2}), or phosphonate (RPO_3^{-2}) groups. Oxygen atoms belonging to these groups can be shared in different ways and numbers by metal centers juxtaposed in a variety of configurations[39].

1. Zirconium Phosphates and Phosphonates

The synthesis and characterization of these inorganic frameworks, has focused primarily on materials where the metal site is a tetravalent cation. Amorphous metal M^{IV} phosphates have been known for a long time and were

intensively investigated in the years 1955 – 1965, especially for their potential uses as inorganic ion–exchangers in processes occurring at high temperatures or under massive doses of ionizing radiation[40]. The first crystalline derivative of this family was α–$Zr(HPO_4)_2 \cdot H_2O$ synthesized by Clearfield and Stynes[41] in 1964. In the original synthesis, zirconium hydrogenphosphate gels were refluxed in 10 – 12 M phosphoric acid, yielding a white microcrystalline powder. Single crystals of this monoclinic phase were grown under hydrothermal conditions[42]. The extended structure consists of two–dimensional sheets of zirconium hydrogenphosphate, shown in *Figure 6*. The metal atoms are positioned slightly above and below the mean plane of the layers. The local coordination sphere of zirconium is supplemented by six oxygen atoms belonging to different hydrogenphosphate groups, in an octahedral arrangement. Medium sized eight–member "chair–like" rings are formed by interconnection of two zirconium centers with two hydrogenphospates, and are further fused to two types of linear chains. The first one consists of corner sharing dimers with nearest neighbors dividing up the metal site, and the second one of edge sharing dimers that form ladders by having joint use of a Zr — O — P fragment. The chains are disposed vertically with respect to each other sharing common edges, an arrangement that develops to the two–dimensional network, shown in *Figure 6(A)*. Each hydrogenphosphate group uses three oxygen atoms for metal coordination and the fourth one, a hydroxyl group, points into the interlayer space, where water molecules reside in hydrophilic pockets. The layers, simply held by van der Waals forces, are staggered such that a phosphorus atom on one layer lines up with a zirconium atom in the adjacent layer (*Figure 6(B)*).

Replacement of the hydrogenphosphate group by alkyl– and arylphosphonates generates an extended family of organic/inorganic hybrids with various structural frameworks and physical properties[38]. In addition to the

(A)

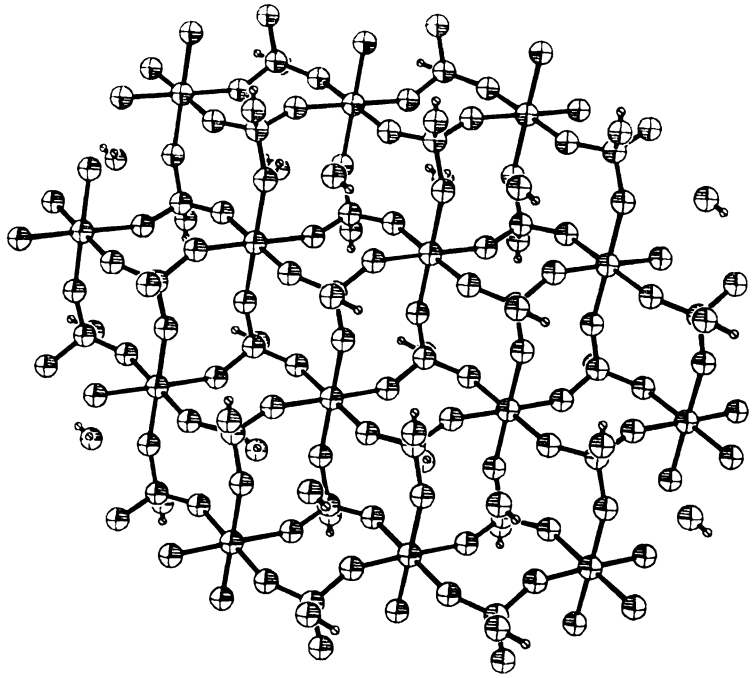

(B)

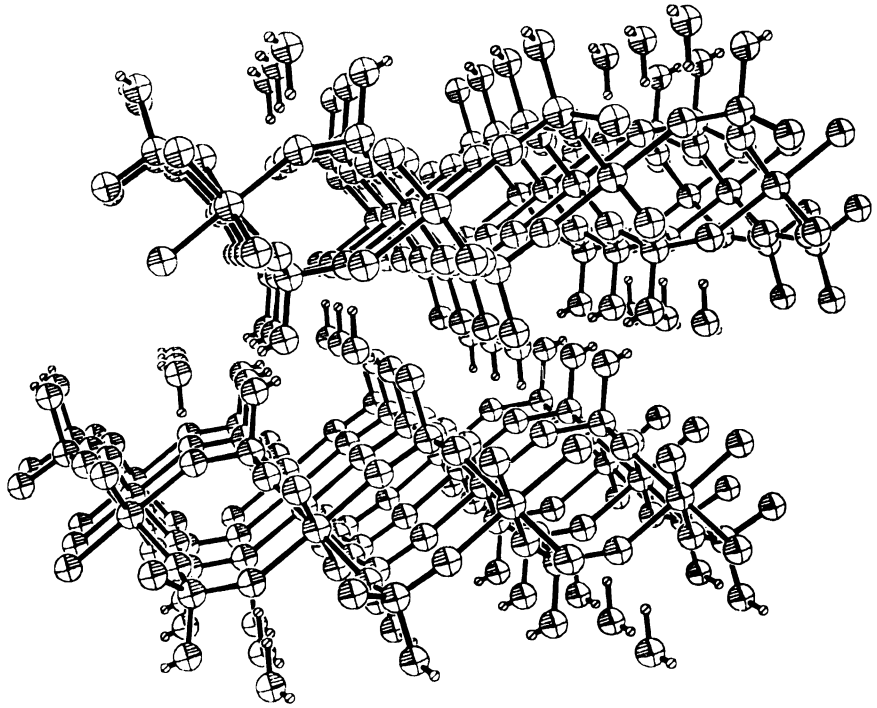

Figure 6. Layer segment of α–$Zr(HPO_4)_2 \cdot H_2O$ displaying the framework of the eight–member "chair" like rings (A). The layered sheets are staggered forming hydrophilic pockets occupied by water molecules (B).

prototype zirconium phenylphosphonate[43], the mild synthesis conditions give access to functional groups attached to the organic part of the phosphonate[44]. More recent advances[45], include mixed–component phases[46] where two or more organic pendant groups are incorporated in the layers, porous pillared biphosphonates where adjacent layers are covalently bound generating medium–sized cavities[47], and sulfophosphonates that can act as proton conductors[48] and ion exchangers[49].

2. Vanadyl Phosphates and Phosphonates

Apart from zirconium, vanadium also exhibits rich chemistry with the phosphate/phosphonate moieties. It displays three stable oxidation states, namely III, IV, and V, resulting in a large number of extended materials with homo– or hetero–valent metal centers[50]. However many of the research efforts to date have targeted species containing the oxavanadium group. This interest is stimulated by the use of vanadyl–phosphate based catalysts in industry for the synthesis of maleic anhydride from light (C4) hydrocarbons[51]. In addition, the structural diversity offered by vanadyl(IV) phosphates/phosphonates (VOP) generates a large number of materials that yield low dimensional magnetic interactions[52]. Hence, the theoretical and experimental study of magnetostructural correlations becomes a challenging task in these systems.

Oxovanadium(V) phosphate dihydrate, $VOPO_4 \cdot 2H_2O$, is considered as the chemical precursor of a wide family of oxovanadium(IV or V) derivatives. It was first synthesized by Ladwig[53] upon refluxing V_2O_5 in 85% phosphoric acid. Its structural determination was performed by X–ray[54] and neutron diffraction[55] techniques, revealing the layer material depicted in *Figure 7*. The two–dimensional framework consists of VO_6 distorted octahedra connected to four

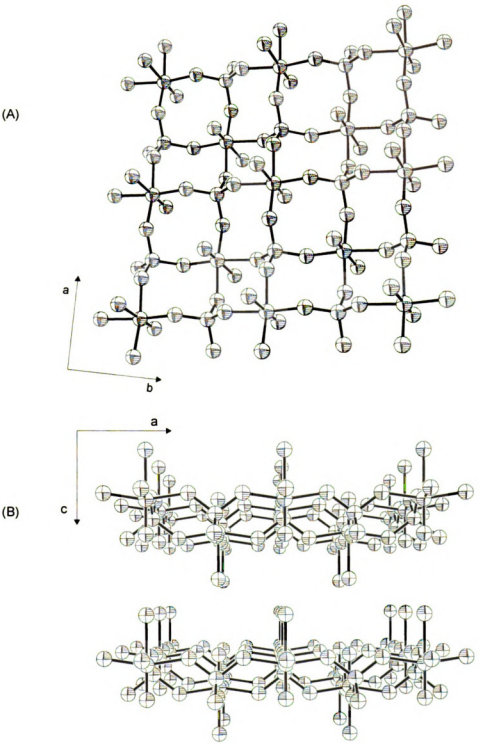

Figure 7. The two–dimensional network of $VOPO_4 \cdot 2H_2O$ constructed by edge–sharing "chair" like units (A). these sheets are further assembled to a layered material (B).

different PO_4 tetrahedra, as shown in *Figure 7(A)*. The short vanadyl bond (1.57(1) Å) is complemented in the axial direction by a weakly bound water molecule, with both groups pointing out in the interlayer space where unbound water molecules are also located. Medium–sized eight–membered chair–like rings, similar to those found in α–$Zr(HPO_4)_2 \cdot H_2O$, are formed by interconnection of two vanadyl centers with two phosphate groups. These dimers are further assembled to two–dimensional sheets by edge sharing the V — O — P faces. The interlayer space can readily accommodate a variety of neutral molecules[56] by substitution of the unbound water molecules, and small ions[57] by reversible redox intercalation reactions.

Substitution of the phosphate group by other O — P — O linkages and/or incorporation of cationic species, dramatically expands the number of compounds that belong to the VOP family[58]. When an organic pendant is incorporated into the linkage, a large series of organic/inorganic hybrides can be synthesized. They can be prepared either by hydrothermal techniques[59], or in alcoholic solutions by direct interaction of V_2O_5 and the corresponding phosphonic acid in the presence of catalytic amounts of hydrochloric acid[60]. The latter is a reductive process that results in materials with all vanadium sites bearing one unpaired electron. In addition, solvent alcohol molecules are incorporated in these materials, occupying the axial sites of the vanadyl ion. These can be exchanged by other alcohols or Lewis basic molecules in a controlled and predictable manner[60,61]. For example, Torgerson and Nocera[62] intercalated different $CH_3(CH_2)_nOH$ alcohols in $V(O)O_3PNp$ (Np stands for the naphthyl group), and by these means mechanically jack the layers apart, by 1.06 Å per methylene unit. When the neighboring naphthalene rings were in registry, excimer formation (monitored by excimer emision) was achieved.

3. Magnetostructural Correlations in Vanadyl Phosphates and Phosphonates

A large number of magnetic studies is available for vanadyl phosphates and phosphonates. However the geometrical flexibility of the O — P — O linkage creates diverse environments around the vanadyl magnetic centers. As a result magnetostructural correlations in these systems are difficult, and need to be studied in a systematic way. Towards this direction Villeneuve[58,63] and coworkers have identified the most common structural building blocks embodied in the VOP's frameworks. They are displayed in *Figure 8* along with the notation that these authors have used. In all the building blocks the coordination environment of vanadium is that of a highly distorted axial octahedron. Vanadium forms a short bond to an oxygen atom along the molecular z–axis, defining the vanadyl group. The trans– position is occupied either by a weakly bound water molecule or by the vanadyl oxygen of a different unit. The latter arrangement is denoted as O–type in *Figure 8*. The phosphate or phosphonate groups can display single (M–type) or double (D–type) bridging modes. A remarkable feature is that in no case does the ligand trans– to the vanadyl oxygen atom come from a phosphate or a phosphonate[58].

In the VOP's the unpaired electron resides in a d_{xy} orbital[64], since the local symmetry can be approximated as C_{4V}. These are slightly destabilized by the π–mixing interaction with in–plane oxygen *p*–atomic orbitals, resulting in magnetic orbitals delocalized towards the xy plane of the building block. Consequently, significant coupling through μ–oxo bridges (O–type) is orientationally precluded. Most likely the major exchange pathways would involve the phosphate/phosphonate bridges. The structural diversity and the many geometrical parameters involved in building blocks bridged by these O — P — O

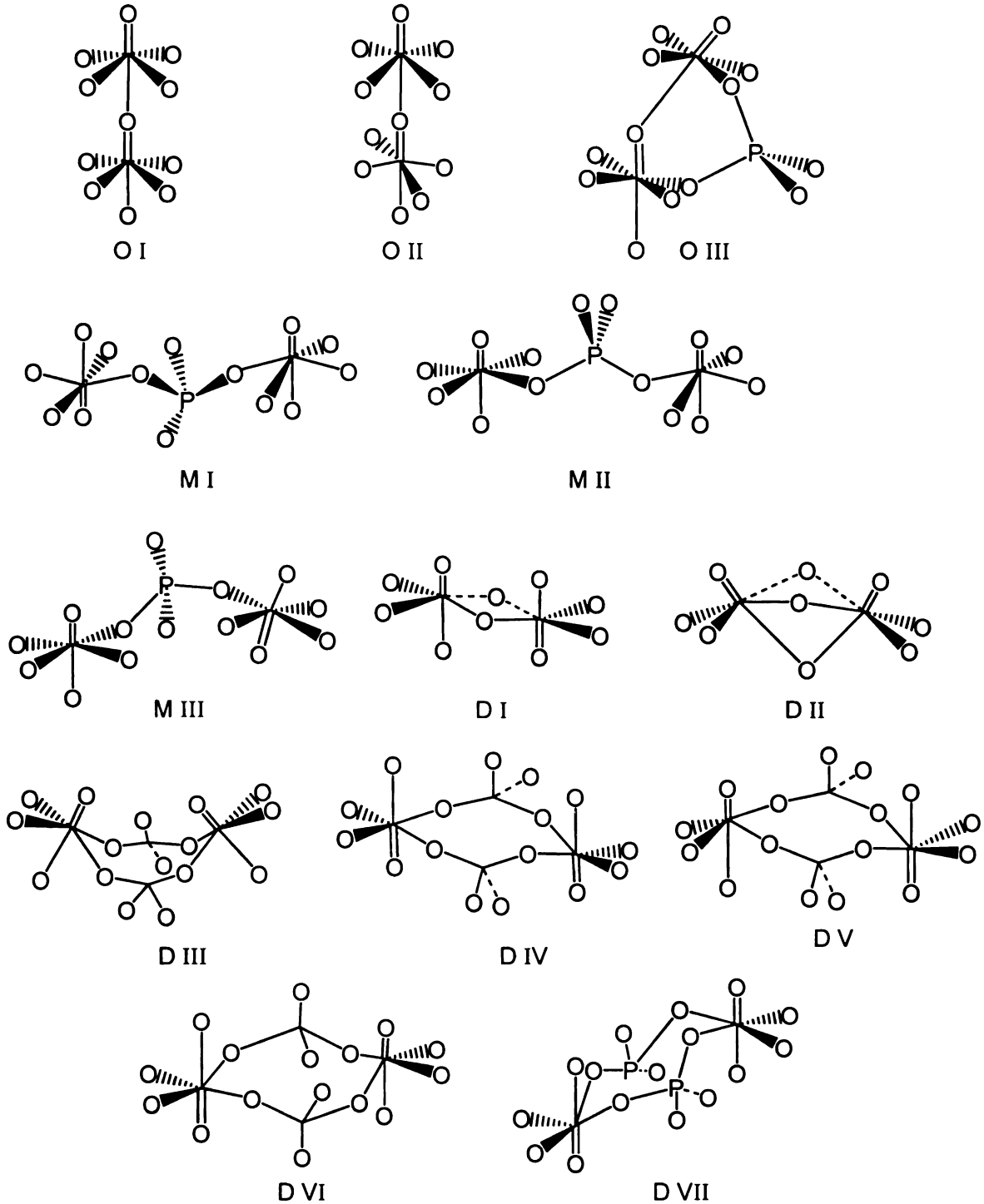

Figure 8. Common structural building blocks found in vanadyl phosphates and phosphonates. They consist of dimeric entities bridged either through the vanadyl group (O–type), or via single (M–type) or double (D–type) phosphate/phosphonate bridges.

linkages further impede the prediction of magnetic properties. Nevertheless the authors provide qualitative arguments regarding the optimum matching of magnetic orbitals. Coplanarity and the relative orientation of the local coordinate systems of adjacent VO_6 octahedra are critical variables for efficient coupling. Double bridging modes (D–type) lead to stronger interactions than do single ones (M–type). Likewise di–μ–phosphato–(O) bridges (D I and D II in *Figure 8*) minimizing vanadium — vanadium distances should enhance in spin communication compared to the di–μ–phosphato–(O, O') ones (D III to D VII in *Figure 8*).

The above considerations are summarized as series where stronger interactions are expected to occur from right to left:

These relationships have been used qualitatively to explain the magnetic properties of some members of the VOP family. The strategy is based on the identification of potential exchange pathways in a given extended material, and estimation of their relative weight on the overall magnetic properties.

C. Organization of this Thesis

The scope of this thesis is the study of the magnetic properties in layered vanadyl phosphates and phosphonates. Magnetostructural correlations in these systems are further explored via the synthesis and study of the magnetic properties of molecular complexes which resemble the common structural building blocks of the extended materials.

Chapter 2 elaborates the experimental procedures used for the synthesis and physical characterization of both the extended and molecular compounds.

Chapter 3 refers to the extended layered materials. The first part concerns

the synthesis, structural characterization and magnetic properties of metal–intercalated layered vanadyl phosphates. In the second part, the magnetic properties of the organic/inorganic hybrid series of layered vanadyl naphthhylphosphonates is presented, along with the related studies of Dr. Jean Le Bideau on layered vanadyl *p*–substituted phenylphosphonates. The structural building blocks responsible for the transmission of magnetic properties are identified, and preliminary conclusions for magnetostructural correlations are derived.

Chapter 4 presents the synthesis, structural characterization and magnetic properties of two series of dimeric vanadyl phosphinates, which model structural building blocks of layered vanadyl phosphates and phosphonates. Their magnetic properties are studied in detailed and magnetostructural correlations are drawn based on the experimental results.

Chapter 5 presents a study of the amidinium–carboxylate salt bridge as a structural element in crystal engineering. In addition molecule–based magnetic materials are assembled via this salt bridge, and the transmission of magnetic properties through hydrogen bonded radical centers is demonstrated.

LIST OF REFERENCES

(1) Day, P. *Science* **1993**, *261*, 431.

(2) Miller, J. S.; Epstein, A. J. *Angew. Chem. Int. Ed. Engl.* **1994**, *33*, 385.

(3) (a) Vögtle, F. *Supramolecular Chemistry*; Wiley: Chichesyer 1991. (b) Lehn, J.–M. *Macrocyclic Chemistry*; VCH: New York 1993. (c) Lehn, J.–M. *Supramolecular Chemistry*; VCH: Weinheim 1995. (d) Balzani, V.; Scandola, F. *Supramolecular Photochemistry*; Ellis Horwood: West Sussex 1991. (e) Cram, D. J. *Container Molecules and their Guests*; Royal Society of Chemistry: Cambridge 1994.

(4) (a) McConnell, H. M. *J. Chem. Phys.* **1963**, *39*, 1910. (b) McConnell, H. M. *Proc. R. A. Welch Found. Chem. Res.* **1967**, *11*, 44.

(5) (a) Miller, J. S.; Calabrese, J. C.; Epstein, A. J.; Bigelow, R. W.; Zhang, J. H.; Reiff, W. M. *J. Chem. Soc. Chem. Commun.* **1986**, 1026. (b) Miller, J. S.; Calabrese, J. C.; Dixon, D. A.; Epstein, A. J.; Bigelow, R. W.; Zhang, J. H.; Reiff, W. M. *J. Am. Chem. Soc.* **1987**, *109*, 769. (c) Chittipeddi, S.; Cromack, K. R.; Miller, J. S.; Epstein, A. J. *Phys. Rev. Lett.* **1987**, *22*, 2695. (d) Miller, J. S.; Epstein, A. J. *Acc. Chem. Res.* **1988**, *23*, 114. (e) Miller, J. S.; Epstein, A. J. *Science*, **1988**, *240*, 40.

(6) Van Vleck, J. H. *The Theory of Electric and Magnetic Susceptibilities*; Oxford University Press: Oxford 1932.

(7) (a) Bleaney, B.; Bowers, K. D. *Proc. R. Soc. London* **1952**, *Ser. A 214*, 451. (b) van Niekerk, J. N.; Schoening, F. K. L. *Acta Cryst.* **1953**, *6*, 227.

(8) (a) Hansen, A. E.; Ballhausen, C. J. *Trans. Faraday Soc.* **1965**, *61*, 631. (b) Miskowski, V. M.; Goldbeck, R. A.; Kliger, D. S.; Gray, H. B. *Inorg. Chem.* **1979**, *18*, 86.

(9) Hay, P. J. *J. Am. Chem. Soc.* **1982**, *104*, 7007.

(10) (a) Best, S. A.; Smith, T. J.; Walton, R. A. *Inorg. Chem.* **1978**, *17*, 99. (b) Abbott, E. H.; Bose, K. S.; Cotton, F. A.; Hall, W. T.; Sekutowski, J. C. *Inorg. Chem.* **1978**, *17*, 3240. (c) Cotton, F. A.; Fanwick, P. E.; Fitch, J. W.; Glicksman, H. D.; Walton, R. A. *J. Am. Chem. Soc.* **1979**, *101*, 1752. (d) Schrock, R. R.; Sturgoff, L. G.; Sharp, P. R. *Inorg. Chem.* **1983**, *22*, 2801. (e) Cotton, F. A.; Powell, G. L. *Inorg. Chem.* **1983**, *22*, 1507. (f) Agaskar, P. A.; Cotton, F. A.; Fraser, I. F.; Peacock, R. D. *J. Am. Chem. Soc.* **1984**, *106*, 1851.

(11) Hopkins, M. D.; Zietlow, T. C.; Miskowski, V. M.; Gray, H. B. *J. Am. Chem. Soc.* **1985**, *107*, 510.
(12) Kahn, O. *Molecular Magnetism*; VCH Publishers: New York 1993.

(13) Hay, P. J.; Thibeault, J. C.; Hoffmann, R. *J. Am. Chem. Soc.* **1975**, *97*, 4884.

(14) de Loth, P.; Cassoux, P.; Daudey, J. P.; Malrieu, J. P. *J. Am. Chem. Soc.* **1981**, *103*, 4007.

(15) (a) Dirac, P. A. M. *Proc. R. Soc. London* **1926**, *Ser. A 112*, 661. (b) Heisenberg, W. *Z. Phys.* **1926**, *38*, 411. (c) Heisenberg, W. *Z. Phys.* **1928**, *49*, 619.

(16) Kahn, O; Charlot, M. F. in *Quantum Theory of Chemical Reactions, Volume II*; D. Riedel Publishing Company: 1980.

(17) (a) Lewis, D. L.; Hatfield, W. E.; Hodgson, D. J. *Inorg. Chem.* **1972**, *11*, 2216. (b) McGregor, K. T.; Watkins, N. T.; Lewis, D. L.; Drake, R. F.; Hodgson, D. J.; Hatfield, W. E. *Inorg. Nucl. Chem. Lett.* **1973**, *9*, 423. (c) Lewis, D. L.; McGregor, K. T.; Hatfield, W. E.; Hodgson, D. J. *Inorg. Chem.* **1974**, *13*, 1013. (d) Estes, E. D.; Hatfield, W. E.; Hodgson, D. J. *Inorg. Chem.* **1974**, *13*, 1654. (e) Crawford, W. H.; Richardson, H. W.; Wasson, J. R.; Hodgson, D. J.; Hatfield, W. E. *Inorg. Chem.* **1976**, *15*, 2107.

(18) Ruiz, E.; Alemany, P.; Alvarez, S.; Cano, J. *J. Am. Chem. Soc.* **1997**, *119*, 1297.

(19) Charlot, M. F.; Kahn, O. *Nouv. J. Chim.* **1980**, *4*, 567.

(20) (a) Kato, M.; Jonassen, H. B.; Fanning, J. C. Chem. Rev. 1964, 64, 99. (b) Jotham, R. W.; Kettle, S. F. A.; Marks, J. A. *J. Chem. Soc. Dalton Trans.* **1972**, 428.

(21) Goodgame, D. M. L.; Hill, N. J.; Marsham, D. F.; Skapski, A. C.; Smart, M. L.; Troughton, P. G. H. *Chem. Commun.* **1969**, 629.

(22) Le Bideau, J.; Papoutsakis, D.; Jackson, J. E.; Nocera, D. G.; *J. Am. Chem. Soc.* **1997**, *119*, 1313.

(23) Kahn, O.; Galy, J.; Journaux, Y.; Morgenstern–Badarau, I. *J. Am. Chem. Soc.* **1982**, *104*, 2165.

(24) Kahn, O. *Struct. Bonding (Berlin)* **1987**, *68*, 89.

(25) (a) Goodenough, J. B. *Phys. Rev.* **1955**, *100*, 564. (b) Kanamori, J. *J. Phys. Chem. Solids* **1959**, *10*, 87. (c) Goodenough, J. B. *Magnetism and the Chemical Bond*; Interscience: New York 1963. (d) Ginsberg, A. P.

Inorg. Chim. Acta Rev. **1971**, *5*, 45.

(26) Dunbar, K. R.; Heintz, R. A. *Progress in Inorganic Chemistry* **1997**, *45*, 283.

(27) Mallah, T.; Thiébaut, S.; Verdaguer, M.; Veillet, P. *Science* **1993**, *262*, 1554.

(28) Gadet, V.; Mallah, T.; Castro, I.; Veillet, P.; Verdaguer, M. *J. Am. Chem. Soc.* **1992**, *114*, 9213.

(29) Griebler, W. D.; Babel, D. *Z. Naturforsch. Teil B* **1982**, *87*, 832.

(30) Ferlay, S.; Mallah, T.; Ouahès, R.; Veillet, P.; Verdaguer, M. *Nature* **1995**, *378*, 701.

(31) Sato, O.; Iyoda, T.; Fujishima, A.; Hashimoto, K. *Science* **1996**, *272*, 704.

(32) (a) Tamura, M.; Nakazawa, Y.; Shiomi, D.; Nozawa, K.; Hosokoshi, Y.; Ishikawa, M.; Takahashi, M.; Kinoshita, M. *Chem. Phys. Lett.* **1991**, *186*, 401. (b) Nakazawa, Y.; Tamura, M.; Shirakawa, N.; Shiomi, D.; Takahashi, M.; Kinoshita, M.; Ishikawa, M.; *Phys. Rev.* **1992**, *B 46*, 8906. (c) Hernàndez, E.; Mas, M.; Molins, E.; Rovira, C.; Veciana, J. *Angew. Chem. Int. Ed. Engl.* **1993**, *32*, 882. (d) Sugawara, T.; Matsushita, M. M.; Izuoka, A.; Wada, N.; Takeda, N.; Ishikawa, M. *J. Chem. Soc. Chem. Commun.* **1994**, 1723. (e) Veciana, J.; Cirujeda, J.; Rovira, C.; Vidal–Gancedo, J.; *Adv. Mater.* **1995**, *7*, 221. (f) Lang, A.; Pei, Y.; Quahab, L.; Kahn, O. *Adv. Mater.* **1996**, *8*, 60. (g) Matsushita, M. M.; Izuoka, A.; Sugawara, T.; Kobayashi, T.; Wada, N.; Takeda, N.; Ishikawa, M. *J. Am. Chem. Soc.* **1997**, *119*, 4369. (h) Deumal, M.; Cirujeda, J.; Veciana, J.; Kinoshita, M.; Hosokoshi, Y.; Novoa, J. J. *Chem. Phys. Lett.* **1997**, *265*, 190.

(33) (a) Zener, C. *Phys. Rev.* **1951**, *81*, 440. (b) Anderson, P. W.; Hasegawa, H. *Phys. Rev.* **1955**, *100*, 675. (c) Blondin, G.; Girerd, J. –J. *Chem. Rev.* **1990**, *90*, 1359. (d) Blondin, G.; Borshch, S.; Girerd, J. –J. *Comm. Inorg. Chem.* **1992**, *12*, 315.

(34) (a) Drüeke, S.; Chaudhuri, P.; Pohl, K.; Wieghardt, K.; Ding, X. –Q.; Bill, E.; Sawaryn, A.; Trautwein, A. X.; Winkler, H.; Gurman, S. J. *J. Chem. Soc. Chem. Commun.* **1989**, 59. (b) Ding, X. –Q.; Bominaar, E. L.; Bill, E.; Winkler, H.; Trautwein, A. X.; Drüeke, S.; Chaudhuri, P.; Wieghardt, K. *J. Chem. Phys.* **1990**, *92*, 178. (c) Gamelin, D. R.; Bominaar, E. L.; Kirk, M. L.; Wieghardt, K.; Solomon, E. I. *J. Am. Chem. Soc.* **1996**, *118*, 8085. (d) Gamelin, D. R.; Bominaar, E. L.; Mathoniere, C.; Kirk, M. L.; Wieghardt, K.; Girerd, J. –J.; Solomon, E. I. *Inorg. Chem.* **1996**, *35*, 4323.

(35) Peng, G.; van Elp, J.; Jang, H.; Que, L., Jr.; Armstrong, W. H.; Cramer, S. P. *J. Am. Chem. Soc.* **1995**, *117*, 2515.

(36) Beissel, T.; Birkelbach, F.; Bill, E.; Glaser, T.; Kesting, F.; Krebs, C.; Weyhermüller, T.; Wieghardt, K.; Butzlaff, C.; Trautwein, A. X. *J. Am. Chem. Soc.* **1996**, *118*, 12376.

(37) Cao, G.; Hong, H. –J.; Mallouk, T. E. *Acc. Chem. Res.* **1992**, *25*, 420.

(38) Clearfield, A. *Progress in Inorganic Chemistry* **1998**, *47*, 371.

(39) Alberti, G.; Casciola, M.; Costantino, U.; Vivani, R. *Adv. Mater.* **1996**, *8*, 291.

(40) Amphlett, C. B. *Inorganic Ion Exchangers*, Elsevier: Amsterdam 1964.

(41) Clearfield, A.; Stynes, J. A. J. *Inorg. Nucl. Chem.* **1964**, *26*, 117.

(42) (a) Clearfield, A.; Smith, G. D. *Inorg. Chem.* **1969**, *8*, 431. (b) Troup, J. M.; Clearfield, A. *Inorg. Chem.* **1977**, *16*, 3311.

(43) (a) Alberti, G.; Costantino, U.; Allulli, S.; Tomassini, N. *J. Inorg. Nucl. Chem.* **1978**, *40*, 1113. (b) Poojary, D. M.; Hu, H. –L.; Campbell, F. L., III; Clearfield, A. *Acta Cryst.* **1993**, *B 49*, 996.

(44) (a) Alberti, G.; Costantino, U.; Luciani Giovagnotti, M. L. J. Chromatog. **1979**, *180*, 45. (b) Maya, L. *Inorg. Nucl. Chem. Lett.* **1979**, *15*, 207. (c) Yamanaka, S.; Tsujimoto, M.; Tanaka, M. *J. Inorg. Nucl. Chem.* **1979**, *41*, 615. (d) Yamanaka, S.; Hattori, M. Chem. Lett. **1979**, 1073. (e) Dines, M. B.; Di Giacomo, P. M. *Inorg. Chem.* **1981**, *20*, 92. (f) Alberti, G.; Costantino, U. in *Intercalation Chemistry*, Whittingham, M. S.; Jacobson, A. J., Eds., Academic: New York 1982.

(45) Vermeulen, L. A. *Progress in Inorganic Chemistry* **1997**, *44*, 143.

(46) (a) Alberti, G.; Costantino, U.; Kornyei, J.; Luciani Giovagnotti, M. L. React. Polym. **1985**, *4*, 1. (b) Alberti, G.; Costantino, U.; Perego, J. *J. Solid State Chem.* **1986**, *63*, 455. (c) Wang, J. D.; Clearfield, A.; Peng, G. –J. *Mater. Chem. Phys.* **1993**, *35*, 208. (d) Clearfield, A.; Wang, J. D.; Tian, Y.; Stein, E.; Bhardwaj, C. *J. Solid State Chem.* **1995**, *117*, 275.

(47) (a) Dines, M. D.; Di Giacomo, P. M.; Callahan, K. P.; Griffith, P. C.; Lane, R. H.; Cooksey, R. E. in *Chemically Modified Surfaces in Catalysis and Electroanalysis*, Miller, J. S., Eds., American Chemical Society Symposium Series: Washington 1982. (b) Clearfield, A. in *Design of New Materials*, Cocke, D. L.; Clearfield, A., Eds., Plenum: New York 1987. (c) Alberti, G.; Costantino, U.; Marmottini, F.; Vivani, R.; Zappelli, P. *Angew. Chem. Int. Engl. Ed.* **1993**, *32*, 1357. (d) Derouane, E. G.; Jullien–Lardot, V. Stud. Surf. Sci. Catal. **1994**, *83*,11.

(48) (a) Alberti, G.; Casciola, M.; Costantino, U.; Peraio, A.; Montoneri, E. *Solid State Ionics* **1992**, *50*, 315. (b) Alberti, G.; Casciola, M.; Palombari, R.;

Peraio, A. *Solid State Ionics* **1992**, *58*, 339. (c) Stein, E. W.; Clearfield, A.; Subramanian, M. A. *Solid State Ionics* **1996**, *83*, 113.

(49) (a) Kullberg, L. H.; Clearfield, A. *Solv. Extr. Ion Exch.* **1989**, *7*, 527. (b) Kullberg, L. H.; Clearfield, A. *Solv. Extr. Ion Exch.* **1990**, *8*, 187.

(50) Khan, M. I.; Zubieta, J. *Progress in Inorganic Chemistry* **1995**, *43*, ?.

(51) (a) Bordes, E.; Courtine, P. *J. Catal.* **1979**, *57*, 236. (b) Hodnett, B. L. *Catal. Rev. –Sci. Eng.* **1985**, *27*, 373. (c) Centi, G.; Trifiro, F.; Ebner, J. R.; Franchetti, V. M. *Chem. Rev.* **1988**, *88*, 55. (d) Coulston, G. W.; Bare, S. R.; Kung, H.; Birkeland, K.; Bethke, G. K.; Harlow, R.; Herron, N.; Lee, P. L. *Science*, **1997**, 275, 191.

(52) Villeneuve, G.; Amoros, P.; Beltran, D.; Drillon, M. in *Organic and Inorganic Low Dimensional Crystalline Materials*; *NATO ASI Series 8*, 168; Delhaes, P.; Drillon, M., Eds., Plenum: New York 1987.

(53) Ladwig, G. *Z. Anorg. Allg. Chem.* **1965**, *338*, 266.

(54) Tietze, H. R. *Aust. J. Chem.* **1981**, *34*, 2035.

(55) Tachez, M.; Theobald, F.; Bernard, J. *Rev. Chim. Min.* **1982**, *19*, 291.

(56) (a) Johnson, J. W.; Jacobson, A. J.; Brody, J. F.; Rich, S. M. *Inorg. Chem.* **1982**, *21*, 3820. (b) Beneš, L.; Votinský, J.; Kalousová, J.; Klikorka, J. *Inorg. Chim. Acta* **1986**, *114*, 47. (c) Beneš, L.; Hyklová, R.; Kalousová, J.; Votinský, J. *Inorg. Chim. Acta* **1990**, *177*, 71.

(57) (a) Johnson, J. W.; Jacobson, A. J. *Angew. Chem. Int. Ed. Engl.* **1983**, *22*, 412. (b) Johnson, J. W.; Jacobson, A. J.; Brody, J. F.; Scanlon, J. C.; Lewandowski, J. T. *Inorg. Chem.* **1985**, *24*, 1782. (c) Šišková, R.; Beneš, L.; Zima, V.; Vlcek, M.; Votinský, J.; Kalousová, J. *Polyhedron* **1993**, *12*, 181.

(58) Beltran–Porter, D.; Beltran–Porter, A.; Amoros, P.; Ibañez, R.; Martinez, E.; Le Bail, A.; Ferey, G.; Villeneuve, G. *Eur. J. Solid State Inorg. Chem.* **1991**, *28*, 131.

(59) (a) Huan, G.; Jacobson, A. J.; Johnson, J. W.; Cocoran, E. W., Jr. *Chem. Mater.* **1990**, *2*, 91. (b) Huan, G.; Johnson, J. W.; Brody, J. F.; Goshorn, D. P.; Jacobson, A. J.; *Mater. Chem. Phys.* **1993**, *35*, 199.

(60) (a) Johnson, J. W.; Jacobson, A. J.; Brody, J. F.; Lewandowski, J. T. *Inorg. Chem.* **1984**, *23*, 3844. (b) Johnson, J. W.; Jacobson, A. J.; Butler, W. M.; Rosenthal, S. E.; Brody, J. F.; Lewandowski, J. T. *J. Am. Chem. Soc.* **1989**, *111*, 381.

(61) Johnson, J. W.; Brody, J. F.; Alexander, R. M.; Pilarski, B.; Katrizky, A. R.

Chem. Mat. **1990**, *2*, 198.

(62) Torgerson, M. R.; Nocera, D. G. *J. Am. Chem. Soc.* **1996**, *118*, 8739.

(63) Beltran–Porter, D.; Amoros, P.; Ibañez, R.; Martinez, E.; Beltran–Porter, A.; Le Bail, A.; Ferey, G.; Villeneuve, G. *Solid State Ionics* **1989**, *32/33*, 57.

(64) Ballhausen, C. J.; Gray, H. B. *Inorg. Chem.* **1962**, *1*, 111.

CHAPTER 2

Experimental Methods

A. Instrument Setups

1. Powder X–ray Diffraction

The powder X–ray diffraction data were recorded on a Rotaflex system from Rigaku with a Bragg–Brentano geometry. The Cu–K_α line was obtained from a rotating Copper anode (45 kV, 100 mA) and directed toward the sample chamber using a 1/6° divergence slit and a 1/6° receiving slit. The diffracted X–ray beam was further refined by a curved graphite single crystal monochromator (1.05° scatter slit and 1/6° monochromator receiving slit), which was set for detection of the secondary X–ray diffraction line. The compounds were mounted

in glass sample holders available from Rigaku. The glass sample holder consisted of a 1.5 cm × 3 cm plate of glass, 3 mm thick with a recess ground into the surface of the slide to pack the sample. The recess in the slides used was 1 cm × 1 cm in area and ground to a depth of 0.2 mm. The powdered specimens were placed in the recess of the sample holder and packed tightly into place by pressing and sliding them with a clean glass microscope slide. Under these conditions layered materials pack preferentially oriented along the 00l direction. As a consequence, reflections diffracted by the intralayer arrangement are not observed. The problem is partially overcome by randomly orienting the powder with the aid of a volatile solvent, like diethylether or acetone. The resulting data were recorded and processed using the manufacturer provided DMAXB software on an IBM personal computer under the MS–DOS operating system.

2. Single Crystal X–ray Structure Determination

$Rb_{0.5}VOPO_4 \cdot 1.5H_2O$, (3.1A and 3.1B). A Rigaku diffractometer with Mo Kα radiation (λ = 0.71073 Å) was used to collect data to a maximum of 2θ = 60° from crystals of 0.42 × 0.24 × 0.02 mm dimensions at 296 K (**3.1A**) and at 173 K (**3.1B**). A total of 1623 (1703 at 173 K) independent reflections were collected, of which 1498 (1349) reflections were considered observed ($I > 2\sigma(I)$) after Lorentz polarization (Lp) and absorption correction (correction was based on ψ scans of a few suitable reflections with χ values close to 90°). The structure was solved by using direct methods (SIR-88) and refined by using full-matrix least-squares procedures based on F^2 (SHELXL–93) with R1 = 0.0517 (0.0556), wR2 = 0.1474 (0.1508). The structure crystallized with 1.5 molecules of water per formula unit. The rubidium atom and the 0.5 water molecules, which were placed at special positions, were disordered and refined over two sites with a total occupancy of

0.5. Structure refinement gave a value of $Rb_{0.46}$, but forcing a total value of $Rb_{0.5}$ (two sites) only increased the wR2 factor by 0.0007.

{bpyVO[μ–$(C_6H_5)_2PO_2$]$_{1.5}$}$_2${ClO_4}, (4.1) . Data collection and structure solution were conducted at the X–ray Crystallographic Laboratory, 160 Kolthoff Hall, Chemistry Department, The University of Minnesota by Dr. Victor G. Young, Jr.

A crystal of the compound was attached to a glass fiber and mounted on the Siemens Smart system for data collection at 173(2) K. An initial set of cell constants was calculated from reflections harvested from three sets of 20 frames. These were oriented such that orthogonal wedges of reciprocal space were surveyed. This produced orientation matrices determined from 207 reflections. Final cell constants were calculated from a set of strong reflections from the actual data collection. The data collection technique used for this specimen is generally known as a hemisphere collection. Here a randomly oriented region of the reciprocal space is surveyed to the extent of 1.3 hemispheres to a resolution of 0.84 Å. Three major swaths of frames were collected with 0.30° steps in ω. Since the lattice was triclinic some additional sets of frames were collected to better model the absorption correction.

The space group $P\bar{1}$ was determined based on systematic absences and intensity statistics[1]. A successful direct–methods solution was calculated which provided most nonhydrogen atoms from the E–map. Several full–matrix least squares / difference Fourier cycles were performed which located the remainder of the nonhydrogen atoms. All nonhydrogen atoms were refined with anisotropic displacement parameters. All hydrogen atoms were placed in ideal positions and refined as riding atoms with group isotropic displacement parameters.

During the refinement several regions of difference Fourier peaks (2–3 electrons) were identified, and attempts were made to model these features as

fully and/or partially occupied methanol solvates, but these attempts were by and large unsuccessful. The PLATON[2] facility SQUEEZE was used to deal with the disordered solvent. PLATON identified a potential solvent volume of 381.4 $Å^3$, or 12.9% of the unit cell volume, and corrected the structure factors for 106.4 e / cell. These values indicate that between 6 and 10 disordered methanol molecules could be present in the cell based on the positive electron count and void volume, respectively. The refinement continued and was converged with the SQUEEZE corrected data. Therefore several crystallographic quantities (empirical formula, formula weight, absorption coefficient, F(000), d_{calc}, etc.) do not reflect the presence of the disordered solvent and are therefore known to be incorrect.

{dmbpyVO[μ–$(C_6H_5)_2PO_2$]$_{1.5}$}$_2${ClO_4}•4CH_3OH, (4.2). A crystal of the compound was attached to a glass fiber and mounted on a Siemens Smart system for data collection at 173(2) K. An initial set of cell constants was calculated from reflections harvested from three sets of 15 frames. These were oriented such that orthogonal wedges of reciprocal space were surveyed. This produced orientation matrices determined from 137 reflections. Final cell constants were calculated from a large number of strong reflections from the actual data collection. Since the lattice was triclinic four major swaths of frames were collected with 0.30° steps in ω.

The space group $P\bar{1}$ was determined based on systematic absences and intensity statistics [1]. A successful direct–methods solution was calculated which provided most nonhydrogen atoms from the E–map. Several full–matrix least squares / difference Fourier cycles were performed which located the remainder of the nonhydrogen atoms. All nonhydrogen atoms were refined with anisotropic

displacement parameters. All hydrogen atoms were placed in ideal positions and refined as riding atoms with group isotropic displacement parameters.

The dimer molecule and the perchlorate anion were found to be crystallographically unique. In addition, four methanol molecules per formula unit were located on Fourier differences maps and were successfully refined with anisotropic temperature factors.

{tmbpyVO[μ–$(C_6H_5)_2PO_2]_{1.5}$}$_2${ClO_4}•3.5CH_3OH, (4.3). A crystal of the compound was attached to a glass fiber and mounted on the Siemens Smart system for data collection at 173(2) K. An initial set of cell constants was calculated from reflections harvested from three sets of 15 frames. These were oriented such that orthogonal wedges of reciprocal space were surveyed. This produced orientation matrices determined from 41 reflections. Final cell constants were calculated from a set of strong reflections from the actual data collection. Three major swaths of frames were collected with 0.30° steps in ω.

The space group $P\bar{1}$ was determined based on systematic absences and intensity statistics [1]. A successful direct–methods solution was calculated which provided most nonhydrogen atoms from the E–map. Several full–matrix least squares / difference Fourier cycles were performed which located the remainder of the nonhydrogen atoms. All nonhydrogen atoms were refined with anisotropic displacement parameters. All hydrogen atoms were placed in ideal positions and refined as riding atoms with group isotropic displacement parameters.

Two crystallographically independent dimer molecules crystallized in the unit cell along with one perchlorate ion and 3.5 methanol molecules per dimer. Large anisotropic temperature factors were found for the solvent molecules, contributing into the observed high WR2 values.

{bpyVO[μ–(p-FC_6H_4)$_2PO_2$]$_{1.5}$}$_2${ClO4}•1.5CH_3OH, (4.4). Data collection and structure solution were conducted at the X–ray Crystallographic Laboratory, 160 Kolthoff Hall, Chemistry Department, The University of Minnesota by Dr. Victor G. Young, Jr.

A crystal of the compound was attached to a glass fiber and mounted on the Siemens Smart system for data collection at 173(2) K. An initial set of cell constants was calculated from reflections harvested from three sets of 20 frames. These were oriented such that orthogonal wedges of reciprocal space were surveyed. This produced orientation matrices determined from 81 reflections. Final cell constants were calculated from a set of strong reflections from the actual data collection. Three major swaths of frames were collected with 0.30° steps in ω.

The space group *P2,2,2,* was determined based on systematic absences and intensity statistics [1]. A successful direct–methods solution was calculated which provided most nonhydrogen atoms from the E–map. Several full–matrix least squares / difference Fourier cycles were performed which located the remainder of the nonhydrogen atoms. All nonhydrogen atoms were refined with anisotropic displacement parameters. All hydrogen atoms were placed in ideal positions and refined as riding atoms with group isotropic displacement parameters.

The dimer compound crystallized with 1.5 molecules of methanol per asymmetric unit. The specimen did not diffract well so data collection proceeded with 45 second frames. The vanadium complex appears well ordered, but the methanol solvents exhibit disorder and partial occupancy. The first one, O(13) C(57), refines to an occupancy of ~0.50 so this was fixed at half occupancy. The other methanol, O(14) C(58), refines to an occupancy of 0.9 and this was fixed at full occupancy. Both methanol molecules have large anisotropic displacement

parameters and shortened O — C bond lengths. The methanols were placed in the best positions to maximize hydrogen bonding.

{bpyVO[μ–(*p*-ClC$_6$H$_4$)$_2$PO$_2$]$_{1.5}$}$_2${ClO4}, (4.5). Data collection and structure solution were conducted at the X–ray Crystallographic Laboratory, 160 Kolthoff Hall, Chemistry Department, The University of Minnesota by Dr. Victor G. Young, Jr.

A crystal of the compound was attached to a glass fiber and mounted on the Siemens Smart system for data collection at 173(2) K. The specimen did not index initially. 50 reflections were harvested from three sets of 20 frames for input into DIRAX[3]. Two twin fragments were identified that were rotated approximately 10° about b* so both the a* and c* axes were found in the same respective directions. Reflection overlap occurs for this specimen at all low indices and along 0k0. Final cell constants were calculated from a set of strong reflections from the actual data collection. Three major swaths of frames were collected with 0.30° steps in ω.

The space group $P2_1/c$ was determined based on systematic absences and intensity statistics [1]. A successful direct–methods solution was calculated which provided most nonhydrogen atoms from the E–map. Several full–matrix least squares / difference Fourier cycles were performed which located the remainder of the nonhydrogen atoms. All nonhydrogen atoms were refined with anisotropic displacement parameters. All hydrogen atoms were placed in ideal positions and refined as riding atoms with group isotropic displacement parameters.

The specimen did not diffract well so data collection proceeded with 45 second frames. Both twins were integrated. The predominant twin was used for refinement. The presence of the minor twin did not affect the data significantly.

15 noticeably reflections twinned or blocked by the beam stop were eliminated from the refinement. The highest resolution shell of data (between 0.84 and 0.87 Å) was truncated from the refinement due to its poor quality, an action that eliminated from the refinement 1077 reflections. It was noticed during the construction of unit cell plots, that there could be an inclusive void near the center of the unit cell. The SQUEEZE utility in PLATON[2] was used to check for the void and it was determined that 10.0% of the volume of the unit cell, or 630.2 Å, was void space. No difference Fourier peaks greater than 1.5 e / $Å^3$ were found at this point. The refinement was continued with the data treated by PLATON. This pocket could potentially host 16 methanol solvent molecules, but that would require some order. PLATON determined the presence of disordered solvent to the extent of 91 electrons in the unit cell. This would reduce the amount of methanol locked in this cavity to about 5 per unit cell. The overall improvement in the refinement after the application of PLATON/SQUEEZE was about 0.5%. Several crystallographic quantities (empirical formula, formula weight, absorption coefficient, F(000), d_{calc}, etc.) do not reflect the presence of the disordered solvent and are therefore known to be incorrect.

{bpyVO[μ–(p-$CH_3OC_6H_4)_2PO_2$]$_{1.5}$}$_2${ClO4}, (4.6). Data collection and structure solution were conducted at the X–ray Crystallographic Laboratory, 160 Kolthoff Hall, Chemistry Department, The University of Minnesota by Dr. Victor G. Young, Jr.

A crystal of the compound was attached to a glass fiber and mounted on the Siemens Smart system for data collection at 173(2) K. An initial set of cell constants was calculated from reflections harvested from three sets of 20 frames. These were oriented such that orthogonal wedges of reciprocal space were surveyed. This produced orientation matrices determined from 116 reflections.

Final cell constants were calculated from a set of strong reflections from the actual data collection. Three major swaths of frames were collected with 0.30° steps in ω. Since the lattice was triclinic some additional sets of frames were collected to better model the absorption correction.

The space group $P\bar{1}$ was determined based on systematic absences and intensity statistics [1]. A successful direct–methods solution was calculated which provided most nonhydrogen atoms from the E–map. Several full–matrix least squares / difference Fourier cycles were performed which located the remainder of the nonhydrogen atoms. All nonhydrogen atoms were refined with anisotropic displacement parameters. All hydrogen atoms were placed in ideal positions and refined as riding atoms with group isotropic displacement parameters.

The perchlorate anion was disordered over two closely spaced sites in a 0.73:0.27 ratio. 40 restraints and constraints were imposed on it to 1) maintain idealized tetrahedral symmetry on both partially occupied groups and 2) model rigid–body restraints on the anisotropic displacement parameters. One methoxy group, C(41), is disordered over two sites in a 0.51:0.49 ratio. The disorder in the perchlorate is likely responsible for the higher than expected residuals.

{tmbpyVO[μ–(*p*-$CH_3OC_6H_4)_2PO_2$]$_{1.5}$}$_2${ClO4}•$2CH_3COCH_3$, (4.6A). A crystal of the compound was attached to a glass fiber and mounted on a Siemens Smart system for data collection at 173(2) K. A data set of poor quality was collected mainly due to the operation of the instrument at 34 KV, 30 mA instead of the standard 50 KV, 40 mA conditions. All reflections were of low intensity with most of them being below the 2σ(I). Nevertheless, an attempt to solve the structure in the monoclinic system, $P2_1/n$ space group, afforded reasonable results with final R1 = 0.1049 for reflections with I > 2σ(I). The structure was solved by direct methods and the nonhydrogen atoms were located from the E–map and from

several full–matrix least squares / difference Fourier cycles. All nonhydrogen atoms were refined with anisotropic displacement parameters. All hydrogen atoms were placed in ideal positions and refined as riding atoms with group isotropic displacement parameters.

The formula unit includes, in addition to the dimer complex, a perchlorate anion and two acetone molecules, which displayed large temperature factors.

$\{HB(pz)_3VO[\mu\text{–}(C_6H_5)_2PO_2]\}_2 \cdot CH_2Cl_2$, (4.7). A crystal of the compound was attached to a glass fiber and mounted on the Siemens Smart system for data collection at 143(2) K. An initial set of cell constants was calculated from reflections harvested from three sets of 15 frames. These were oriented such that orthogonal wedges of reciprocal space were surveyed. This produced orientation matrices determined from 90 reflections. Final cell constants were calculated from a set of strong reflections from the actual data collection. Since the lattice was triclinic four major swaths of frames were collected with 0.30° steps in ω.

The space group $P\bar{1}$ was determined based on systematic absences and intensity statistics [1]. A successful direct–methods solution was calculated which provided most nonhydrogen atoms from the E–map. Several full–matrix least squares / difference Fourier cycles were performed which located the remainder of the nonhydrogen atoms. All nonhydrogen atoms were refined with anisotropic displacement parameters. All hydrogen atoms were placed in ideal positions and refined as riding atoms with group isotropic displacement parameters.

Two crystallographically independent dimers crystallize within the unit cell along with one molecule of dichloromethane per asymmetric unit. Only half of each dimer is unique. The vanadium complex appears well ordered, but the

dichloromethane solvent exhibits disorder. It was modeled as two molecules each one fixed to an occupancy of 0.5

$\{HB(pz)_3VO[\mu\text{–}(p\text{-}CH_3OC_6H_4)_2PO_2]\}_2 \cdot CH_3CN$, (4.8). Data collection and structure solution were conducted at the X–ray Crystallographic Laboratory, 160 Kolthoff Hall, Chemistry Department, The University of Minnesota by Dr. Victor G. Young, Jr.

A crystal of the compound was attached to a glass fiber and mounted on the Siemens Smart system for data collection at 173(2) K. An initial set of cell constants was calculated from reflections harvested from three sets of 20 frames. These were oriented such that orthogonal wedges of reciprocal space were surveyed. This produced orientation matrices determined from 93 reflections. Final cell constants were calculated from a set of strong reflections from the actual data collection. Three major swaths of frames were collected with 0.30° steps in ω.

The space group *C2/c* was determined based on systematic absences and intensity statistics [1]. A successful direct–methods solution was calculated which provided most nonhydrogen atoms from the E–map. Several full–matrix least squares / difference Fourier cycles were performed which located the remainder of the nonhydrogen atoms. All nonhydrogen atoms were refined with anisotropic displacement parameters. All hydrogen atoms were placed in ideal positions and refined as riding atoms with group isotropic displacement parameters.

The dimer complex crystallized with one molecule of acetonitrile, which resided on the crystallographic two–fold axis. Therefore there is one molecule of solvent for every dimer complex.

{HB(pz)$_3$VO[μ–(*p*-F–C$_6$H$_4$)$_2$PO$_2$]}$_2$•2CH$_3$CN, (4.9). A crystal of the compound was attached to a glass fiber and mounted on the Siemens Smart system for data collection at 131(2) K. An initial set of cell constants was calculated from reflections harvested from three sets of 15 frames. These were oriented such that orthogonal wedges of reciprocal space were surveyed. This produced orientation matrices determined from 55 reflections. Final cell constants were calculated from a set of strong reflections from the actual data collection. Four major swaths of frames were collected with 0.30° steps in ω.

The space group $P\bar{1}$ was determined based on systematic absences and intensity statistics [1]. A successful direct–methods solution was calculated which provided most nonhydrogen atoms from the E–map. Several full–matrix least squares / difference Fourier cycles were performed which located the remainder of the nonhydrogen atoms. All nonhydrogen atoms were refined with anisotropic displacement parameters. All hydrogen atoms were placed in ideal positions and refined as riding atoms with group isotropic displacement parameters.

Two crystallographically independent dimers crystallized within the unit cell along with two molecules of acetonitrile per asymmetric unit. Only half of each dimer is unique.

{HB(pz)$_3$VO[μ–(*p*-CH$_3$C$_6$H$_4$)$_2$PO$_2$]}$_2$•2CH$_3$CN, (4.10). Data collection and structure solution were conducted at the X–ray Crystallographic Laboratory, 160 Kolthoff Hall, Chemistry Department, The University of Minnesota by Dr. Victor G. Young, Jr.

A crystal of the compound was attached to a glass fiber and mounted on the Siemens Smart system for data collection at 173(2) K. An initial set of cell constants was calculated from reflections harvested from three sets of 20 frames. These were oriented such that orthogonal wedges of reciprocal space were

surveyed. This produced orientation matrices determined from 65 reflections. Final cell constants were calculated from a set of strong reflections from the actual data collection. Three major swaths of frames were collected with 0.30° steps in ω.

The space group $P2_1/c$ was determined based on systematic absences and intensity statistics [1]. A successful direct–methods solution was calculated which provided most nonhydrogen atoms from the E–map. Several full–matrix least squares / difference Fourier cycles were performed which located the remainder of the nonhydrogen atoms. All nonhydrogen atoms were refined with anisotropic displacement parameters. All hydrogen atoms were placed in ideal positions and refined as riding atoms with group isotropic displacement parameters.

The dimer crystallized with the addition of two acetonitrile solvent molecules per whole complex. The asymmetric unit contains half of these contents.

$\{HB(pz)_3VO[\mu\text{–}(p\text{-}CH_3C_6H_4)_2PO_2]\}_2 \cdot 2CH_2Cl_2$, (4.11). A crystal of the compound was attached to a glass fiber and mounted on the Siemens Smart system for data collection at 133(2) K. An initial set of cell constants was calculated from reflections harvested from data collection frames. This produced orientation matrices determined from 183 reflections. Final cell constants were calculated from a set of strong reflections from the actual data collection. Four major swaths of frames were collected with 0.30° steps in ω.

The space group $P2_1/c$ was determined based on systematic absences and intensity statistics [1]. A successful direct–methods solution was calculated which provided most nonhydrogen atoms from the E–map. Several full–matrix least squares / difference Fourier cycles were performed which located the

remainder of the nonhydrogen atoms. All nonhydrogen atoms were refined with anisotropic displacement parameters. All hydrogen atoms were placed in ideal positions and refined as riding atoms with group isotropic displacement parameters.

The dimer crystallized with the addition of two dichloromethane solvent molecules per whole complex. The asymmetric unit contains half of these contents. The solvent molecule was disordered and modeled by placing each chlorine atom at two different sites with a total occupancy of one.

$\{HB(pz)_3VO[\mu\text{–}(p\text{-}NO_2C_6H_4O)_2PO_2]\}_2 \cdot 2CH_2Cl_2$, (4.12). A crystal of the compound was attached to a glass fiber and mounted on the Siemens Smart system for data collection at 143(2) K. Four major swaths of frames were collected with 0.30° steps in ω. After the collection of the first three sets the crystal was recentered before the collection of the final swath. The data were integrated separately and then combined to a unique data set.

The space group $P\bar{1}$ was determined based on systematic absences and intensity statistics [1]. A successful Patterson–methods solution was calculated which provided the heavy atoms from the E–map. Several full–matrix least squares / difference Fourier cycles were performed which located the remainder of the nonhydrogen atoms. All nonhydrogen atoms were refined with anisotropic displacement parameters. All hydrogen atoms were placed in ideal positions and refined as riding atoms with group isotropic displacement parameters.

The dimer crystallized with the addition of two dichloromethane solvent molecules per whole complex. The asymmetric unit contains half of these contents.

$\{HB(pz)_3VO[\mu\text{–}(p\text{-}NO_2C_6H_4O)_2PO_2]\}_2 \cdot 2CH_3COCH_3$, (4.13). A crystal of the compound was attached to a glass fiber and mounted on the Siemens Smart

system for data collection at 173(2) K. An initial set of cell constants was calculated from reflections harvested from data collection frames. This produced orientation matrices determined from 283 reflections. Final cell constants were calculated from a set of strong reflections from the actual data collection. Four major swaths of frames were collected with 0.30° steps in ω.

The space group $P\bar{1}$ was determined based on systematic absences and intensity statistics [1]. A successful Patterson–methods solution was calculated which provided the heavy atoms from the E–map. Several full–matrix least squares / difference Fourier cycles were performed which located the remainder of the nonhydrogen atoms. All nonhydrogen atoms were refined with anisotropic displacement parameters. All hydrogen atoms were placed in ideal positions and refined as riding atoms with group isotropic displacement parameters.

The dimer crystallized with the addition of two acetone solvent molecules per whole complex. The asymmetric unit contains half of these contents.

$\{HB(pz)_3VO[\mu\text{–}(p\text{-}NO_2C_6H_4O)_2PO_2]\}_2 \cdot 2C_4H_5N$, (4.14). A crystal of the compound was attached to a glass fiber and mounted on the Siemens Smart system for data collection at 173(2) K. An initial set of cell constants was calculated from reflections harvested from three sets of 15 frames. These were oriented such that orthogonal wedges of reciprocal space were surveyed. This produced orientation matrices determined from 67 reflections. Final cell constants were calculated from a set of strong reflections from the actual data collection. Four major swaths of frames were collected with 0.30° steps in ω.

The space group $P\bar{1}$ was determined based on systematic absences and intensity statistics [1]. A successful Patterson–methods solution was calculated which provided the heavy atoms from the E–map. Several full–matrix least squares / difference Fourier cycles were performed which located the remainder

of the nonhydrogen atoms. All nonhydrogen atoms were refined with anisotropic displacement parameters. All hydrogen atoms were placed in ideal positions and refined as riding atoms with group isotropic displacement parameters.

The dimer crystallized with the addition of two pyrrole solvent molecules per whole complex. The asymmetric unit contains half of these contents.

{HB(pz)$_3$VO[μ–(*p*-NO$_2$C$_6$H$_4$O)$_2$PO$_2$]}$_2$•2C$_4$H$_4$S, (4.15A). A crystal of the compound was attached to a glass fiber and mounted on the Siemens Smart system for data collection at 296(2) K. An initial set of cell constants was calculated from reflections harvested from three sets of 15 frames. These were oriented such that orthogonal wedges of reciprocal space were surveyed. This produced orientation matrices determined from 56 reflections. Final cell constants were calculated from a set of strong reflections from the actual data collection. Four major swaths of frames were collected with 0.30° steps in ω.

The space group $P\bar{1}$ was determined based on systematic absences and intensity statistics [1]. A successful Patterson–methods solution was calculated which provided the heavy atoms from the E–map. Several full–matrix least squares / difference Fourier cycles were performed which located the remainder of the nonhydrogen atoms. All nonhydrogen atoms were refined with anisotropic displacement parameters. All hydrogen atoms were placed in ideal positions and refined as riding atoms with group isotropic displacement parameters.

The dimer crystallized with the addition of two thiophene solvent molecules per whole complex. The asymmetric unit contains half of these contents. The solvent was disordered as judged by the large thermal parameters of the constituent atoms.

{HB(pz)$_3$VO[μ–(*p*-NO$_2$C$_6$H$_4$O)$_2$PO$_2$]}$_2$•2C$_4$H$_4$S, (4.15B). A crystal of the compound was attached to a glass fiber and mounted on the Siemens Smart

system for data collection at 173(2) K. An initial set of cell constants was calculated from reflections harvested from three sets of 15 frames. These were oriented such that orthogonal wedges of reciprocal space were surveyed. This produced orientation matrices determined from 50 reflections. Final cell constants were calculated from a set of strong reflections from the actual data collection. Four major swaths of frames were collected with 0.30° steps in ω.

The space group $P\bar{1}$ was determined based on systematic absences and intensity statistics [1]. A successful Patterson–methods solution was calculated which provided the heavy atoms from the E–map. Several full–matrix least squares / difference Fourier cycles were performed which located the remainder of the nonhydrogen atoms. All nonhydrogen atoms were refined with anisotropic displacement parameters. All hydrogen atoms were placed in ideal positions and refined as riding atoms with group isotropic displacement parameters.

The dimer crystallized with the addition of two thiophene solvent molecules per whole complex. The asymmetric unit contains half of these contents.

$\{HB(pz)_3VO[\mu\text{–}(p\text{-}NO_2C_6H_4O)_2PO_2]\}_2 \cdot 2C_2H_4S_2$, (4.16A). A crystal of the compound was attached to a glass fiber and mounted on the Siemens Smart system for data collection at 296(2) K. An initial set of cell constants was calculated from reflections harvested from data collection frames. This produced orientation matrices determined from 98 reflections. Final cell constants were calculated from a set of strong reflections from the actual data collection. Three major swaths of frames were collected with 0.30° steps in ω, at which point data collection was terminated due to a shutter error.

The space group $P\bar{1}$ was determined based on systematic absences and intensity statistics [1]. A successful Patterson–methods solution was calculated

which provided the heavy atoms from the E–map. Several full–matrix least squares / difference Fourier cycles were performed which located the remainder of the nonhydrogen atoms. All nonhydrogen atoms were refined with anisotropic displacement parameters. All hydrogen atoms were placed in ideal positions and refined as riding atoms with group isotropic displacement parameters.

The specimen did not diffract well so data collection proceeded with 40 second frames. The dimer crystallized with the addition of two 1,2–ethanedithiol solvent molecules per whole complex, with the asymmetric unit containing half of these contents. The solvent was disordered and was best modeled by considering two fragments refined at occupancies 0.70:0.30. In addition O(7), O(8), and O(9) were disordered and refined at partial occupancies over two sites. These atoms were refined anisotropically with the aid of DELU and SIMU restraints.

$\{HB(pz)_3VO[\mu\text{–}(p\text{-}NO_2C_6H_4O)_2PO_2]\}_2 \cdot 2C_2H_4S_2$, (4.16B). A crystal of the compound was attached to a glass fiber and mounted on the Siemens Smart system for data collection at 173(2) K. An initial set of cell constants was calculated from reflections harvested from three sets of 15 frames. These were oriented such that orthogonal wedges of reciprocal space were surveyed. This produced orientation matrices determined from 35 reflections. Final cell constants were calculated from a set of strong reflections from the actual data collection. Four major swaths of frames were collected with 0.30° steps in ω.

The space group $P\bar{1}$ was determined based on systematic absences and intensity statistics [1]. A successful Patterson–methods solution was calculated which provided the heavy atoms from the E–map. Several full–matrix least squares / difference Fourier cycles were performed which located the remainder of the nonhydrogen atoms. All nonhydrogen atoms were refined with anisotropic

displacement parameters. All hydrogen atoms were placed in ideal positions and refined as riding atoms with group isotropic displacement parameters.

Data collection proceeded with 35 second frames. The dimer crystallized with the addition of two dithioethane solvent molecules per whole complex, with the asymmetric unit containing half of these contents. Only S(2) was found disordered and refined at partial occupancies over two sites.

3–amidinium benzoate, (5.1). A Rigaku diffractometer with Mo Kα radiation (λ = 0.71073 Å) was used to collect data to a maximum of 2θ = 50° from crystals of 0.65 × 0.40 × 0.20 mm dimensions at 296 K. Cell parameters were calculated from 24 reflections. A total of 1397 independent reflections were collected, of which 1288 reflections were considered observed ($I > 2\sigma(I)$) after Lorentz, polarization (Lp), and absorption corrections (absorption correction was based on ψ scans of a few suitable reflections with χ values close to 90°). The space group $P\bar{1}$ was determined based on systematic absences and intensity statistics [1]. A successful direct–methods solution was calculated which provided the nonhydrogen atoms. All nonhydrogen atoms were refined with anisotropic displacement parameters. All hydrogen atoms were placed in ideal positions and refined as riding atoms with group isotropic displacement parameters, except the amidinium protons which were located from Fourier difference maps and allowed to refine with isotropic temperature factors.

2,2,5,5–tetramethyl–3–carboxypyrroline–1–oxyl, (5.2). A crystal of the compound was attached to a glass fiber and mounted on the Siemens Smart system for data collection at 173(2) K. An initial set of cell constants was calculated from reflections harvested from three sets of 15 frames. These were oriented such that orthogonal wedges of reciprocal space were surveyed. This produced orientation matrices determined from 76 reflections. Final cell

constants were calculated from a set of strong reflections from the actual data collection. Four major swaths of frames were collected with 0.30° steps in ω.

The space group $P2_1/n$ was determined based on systematic absences and intensity statistics [1]. A successful direct–methods solution was calculated which provided the nonhydrogen atoms from the E–map. All nonhydrogen atoms were refined with anisotropic displacement parameters unless stated otherwise. All hydrogen atoms were located by successive Fourier difference maps and allowed to refine isotropically.

benzamidinium–2,2,5,5–tetramethyl–3–carboxypyrroline–1–oxyl hydrate, (5.3). A Rigaku diffractometer with Mo Kα radiation (λ = 0.71073 Å) was used to collect data to a maximum of 2θ = 50° at 296 K. Cell parameters were calculated from 24 reflections. Data were corrected for Lorentz and polarization effects. Absorption correction was based on ψ scans of a few suitable reflections with χ values close to 90°.

The space group $P2_1/n$ was determined based on systematic absences and intensity statistics [1]. A successful Direct–methods solution was calculated which provided the nonhydrogen atoms. All nonhydrogen atoms were refined with anisotropic displacement parameters unless stated otherwise. All hydrogen atoms were placed in ideal positions and refined as riding atoms with group isotropic displacement parameters, except the amidinium protons which were located from Fourier differences maps and allowed to refine with isotropic temperature factors.

***m*–cyanobenzamidinium–2,2,5,5–tetramethyl–3–carboxypyrroline–1–oxyl, (5.4).** A Rigaku diffractometer with Mo Kα radiation (λ = 0.71073 Å) was used to collect data to a maximum of 2θ = 50° at 296 K. Cell parameters were calculated from 22 reflections. Data were corrected for Lorentz and polarization effects.

Absorption correction was based on ψ scans of a few suitable reflections with χ values close to 90°.

The space group $P2_1/c$ was determined based on systematic absences and intensity statistics [1]. A successful Direct–methods solution was calculated which provided the nonhydrogen atoms. All nonhydrogen atoms were refined with anisotropic displacement parameters unless stated otherwise. All hydrogen atoms were placed in ideal positions and refined as riding atoms with group isotropic displacement parameters, except the amidinium protons which were located from Fourier differences maps and allowed to refine with isotropic temperature factors.

3. Absorption Spectroscopy

The electronic absorption spectra of solution samples were recorded on a Cary 17 spectrometer modified with a computer controlled data acquisition system by On–Line Instruments (OLIN) Corporation. All absorption measurements were collected by using quartz sample cells with a 1 cm path. The molar extinction coefficients were obtained by recording the spectra of each compound in at least four different concentrations. Their value was subsequently derived from Beer–Lambert plots[4].

4. Thermogravimetric Analysis (TGA)

A thermogravimetric analyzer TGA–50 from Shimadzu was used to record TGA plots of layered vanadyl phosphates and phosphonates. Powder specimens were placed in quartz sample holders and were heated up to 600 °C under a nitrogen flow of approximately 88 ml/min. Typical heating rates were 2.5 °C/min,

while the sample temperature was maintained at 600 °C for 30 min before cooling to room temperature.

5. Infrared Spectroscopy

Solid state infrared spectra were recorded either on a Perkin Elmer Spectrum 2000 spectrometer or on the departmental Nicolet FT–IR instrument. Powder samples were prepared as KBr pellets and placed into the FT–IR sample chamber. Collection of the data was accomplished by acquiring 8 scans at 4 cm^{-1} or 1 cm^{-1} resolution in the Perkin Elmer Spectrum 2000 spectrometer, or by 32 scans and 4 cm^{-1} resolution in the Nicolet FT–IR instrument.

6. Magnetic Susceptibility

Magnetic susceptibilities were measured on a SHE 800 series variable–temperature SQUID magnetometer controlled by an IBM–PC computer. The magnetic samples were ground to fine powders and placed either in a plastic capsule or in a small pouch constructed by heat sealing polyethylene film. The capsule or the pouch were then placed within a plastic straw and attached to the sample holder. Data collection was performed in the temperature regime 1.8 K to 300 K, with each measurement performed three times at each temperature before recording a data point. The data were corrected from diamagnetic correction by either using Pascal's constants or by fitting a modified Curie–Weiss law that accounts for both diamagnetic and temperature independent paramagnetism (TIP) contributions.

7. Electron Spin Resonance Studies

EPR spectra were obtained at X–band on a Bruker ESP300E spectrometer by using a Bruker ST4102 EPR cavity. The microwave frequency was measured with an EIP Microwave Model 25B frequency counter. The samples were cooled to low temperatures with the aid of a cryostat (Oxford Instruments) via a stream of Helium gas utilizing an Oxford Instruments GFS–600 transfer line. The temperature was controlled by an Oxford Instruments ITC–0502 temperature controller.

Solution samples were prepared by dissolving the solid materials in the desired solvent at concentration ranges of 10^{-3} to 10^{-4} M, followed by thorough deoxygenation via several freeze-thaw cycles under vacuum. Spectra simulations were performed by using Bruker's simulation program SimFonia.

8. Solid State Nuclear Magnetic Resonance

Solid–state ^{31}P–NMR spectra were recorded in a VARIAN VXR–400S spectrometer. The powder samples were placed in a VARIAN CPMAS probe (7 mm diameter) externally cooled via an Oxford Instruments transfer line by a stream of liquid nitrogen. Variable temperature spectra were collected with the aid of an Oxford Instruments temperature controller. The shifts of the lines were referenced to 85% H_3PO_4(aq) measured in the same probe.

B. Materials and Synthesis

1. Layered Metal–Intercalated Vanadyl Phosphates Hydrates, $A_xVOPO_4 \cdot nH_2O$

Materials. Vanadium pentoxide V_2O_5 (98%), vanadium oxide V_2O_4 (99.9%), vanadium trioxide V_2O_3 (99%), rubidium hydroxide RbOH (99.9%, 50% wt solution in water), cobalt oxide CoO (99%), strontium hydroxide $Sr(OH)_2 \cdot 8H2O$ (96%), sodium hydroxide NaOH (97%), potassium hydroxide KOH (85%), and phosphoric acid H_3PO_4 (85% in water) were purchased from Aldrich.

General Considerations. All materials were synthesized by utilizing hydrothermal procedures according to the general methodology employed by Lii and coworkers[5]. The reagents were placed in 23–ml Teflon–lined autoclaves (Parr Instruments), and were subsequently heated within a Fischer Scientific Isotemp Programmable Oven (model 838F), equipped with a temperature controller. The temperature was increased to 220 °C at a rate of 4 °C/min and was maintained there for a period of two to six days, before slow cooling to room temperature at a rate of 0.1 °C/min. In each case the products were filtered off, washed several times with water and ethanol and dried overnight at room temperature.

Synthesis of $Na_{0.5}VOPO_4 \cdot 2H_2O$. The title compound was prepared from a 10 ml aqueous solution of 0.402 g (2.42 mmol) of V_2O_4, 0.205 g (1.12 mmol) of V_2O_5, 0.203 g (5 mmol) of NaOH, and 1.5 ml of H_3PO_4 contained in a 23–ml Teflon–lined autoclave. The reaction vessel was maintained at 220 °C for five days and then cooled to room temperature at 0.1 °C / min. The products were black–green rectangular platelets, which were isolated as described in the general

considerations section. Chemical Analysis, Calcd. (Found): Na, 5.48 (5.21) %; V, 24.32 (24.02) %; P, 14.79 (15.01) %.

Synthesis of $K_{0.5}VOPO_4 \cdot 1.5H_2O$. The title compound was prepared as a single–phase material under various conditions four times. One of those procedures was from a 10 ml aqueous solution of 0.402 g (2.42 mmol) of V_2O_4, 0.205 g (1.12 mmol) of V_2O_5, 0.280 g (5 mmol) of KOH, and 1.6 ml of H_3PO_4 contained in a 23–ml Teflon–lined autoclave. The reaction vessel was maintained at 220 °C for two days and then cooled to room temperature at 0.1 °C / min. The products were black–green rectangular platelets. Chemical Analysis, Calcd. (Found): K, 9.38 (9.15) %; V, 24.43 (23.93) %; P, 14.85 (14.99) %.

Synthesis of $Rb_{0.5}VOPO_4 \cdot 1.5H_2O$. The title compound was prepared from a 10 ml aqueous solution of 0.402 g (2.42 mmol) of V_2O_4, 0.205 g (1.12 mmol) of V_2O_5, 0.6 ml (5 mmol) of RbOH (99.9%, 50% wt solution in water), and 1.6 ml of H_3PO_4 contained in a 23–ml Teflon–lined autoclave. The reaction vessel was maintained at 220 °C for six days and then cooled to room temperature at 0.1 °C / min. The products were black–green rectangular platelets. Chemical Analysis, Calcd. (Found): Rb, 18.45 (16.64) %; V, 22.40 (22.77) %; P, 13.62 (13.70) %.

Synthesis of $Sr_{0.5}VOPO_4 \cdot 2H_2O$. The title compound was prepared from a 10.5 ml aqueous solution of 0.445 g (2.68 mmol) of V_2O_4, 0.709 g (2.67 mmol) of $Sr(OH)_2 \cdot 8H_2O$, and 1.2 ml of H_3PO_4 contained in a 23–ml Teflon–lined autoclave. The reaction vessel was maintained at 220 °C for five days and then cooled to room temperature at 0.1 °C / min. The product was a bluish powder. Chemical Analysis, Calcd. (Found): Sr, 18.12 (17.96) %; V, 21.07 (20.96) %; P, 12.81 (12.78) %.

Synthesis of $Co_{0.5}VOPO_4 \cdot 2H_2O$. The title compound was prepared as a single–phase material under various conditions three times. One of those procedures was from a 15 ml aqueous solution of 0.200 g (1.33 mmol) of V_2O_3, of 0.243 g (1.33 mmol) of V_2O_5, 0.200 g (2.67 mmol) of CoO, and 1.6 ml of H_3PO_4 contained in a 23–ml Teflon–lined autoclave. The reaction vessel was maintained at 220 °C for five days and then cooled to room temperature at 0.1 °C / min. The product was a green–bluish powder.

2. Layered Vanadyl Napthylphosponate Hydrate Alcoholates, $VO(O_3PNp) \cdot H_2O \cdot nROH$

This series of materials was synthesized by Dr. M. R. Torgerson[6], while thermogravimetric analysis (TGA), electron magnetic resonance (EPR) and powder susceptibility measurements were part of this thesis.

3. Synthesis of bis(*p*–Substituted Phenyl) Phosphinic Acids

Materials. *p*–Bromochlorobenzene (99%), *p*–bromofluorobenzene (99%), *p*–bromotoluene (98%), phosphorous oxychloride $POCl_3$ (99%), diethyl phosphite $(EtO)_2P(O)H$ (94%) and magnesium granules (~ 20 mesh, 98%) were purchased from Aldrich. Diphenylphosphinic acid (99%) and bis(4–nitrophenyl) phosphate hydrate (99%) were also purchased from Aldrich.

Synthesis of bis(*p*-chlorophenyl) Phosphinic Acid. This compound was synthesized according to a literature procedure[7]. In a degassed 500 ml three–neck flask containing 2.43 g (0.1 mol) of Mg turnings, a catalytic amount of iodine, and 50 ml of dry diethyl ether, 1.9 g (0.01 mol) of *p*–bromochlorobenzene dissolved in 10 ml of dry diethyl ether were slowly added under N_2 atmosphere. When the reaction turned cloudy indicating initiation of the Grignard reaction,

17.2 g (0.09 mol) of *p*–bromochlorobenzene dissolved in 100 ml of dry diethyl ether were added dropwise maintaining gentle reflux. At the end of the addition the reaction was refluxed for three more hours. The Grignard reagent was added dropwise via a cannula over a period of one and a half hour to a degassed 1000 ml three–neck flask containing 15.3 g (0.1 mol) of $POCl_3$ in 250 ml of dry diethyl ether maintained in a gentle reflux. A white–yellowish solid precipitate and refluxing continued for an additional hour. The solution was allowed to stand undisturbed overnight and the organic layer was decanted from the solid precipitate. The latter was treated with 300 gr of ice–water. It was triturated with 1 l of warm dilute sodium hydroxide solution, filtered and the filtrate acidified with dilute hydrochloric acid. The precipitated product was filtered, dried and recrystallized from dilute ethanol. m.p 131–133 °C (literature: 133 °C). ^{1}H NMR (DMSO–d_6); δ ppm: 7.71 (dd, J_{H-H} = 4.9 Hz, J_{P-H} = 8.5 Hz, 2 H), 7.54 (dd, J_{H-H} = 4.9 Hz, J_{P-H} = 1.3 Hz, 2 H). ^{31}P NMR (DMSO–d_6); δ ppm : 23.7 (s, 1 P).

Synthesis of bis(*p*-fluorophenyl) Phosphinic Acid. This compound was synthesized according to a literature procedure[8]. In a degassed 500 ml three–neck flask containing 4.86 g (0.2 mol) of Mg turnings, a catalytic amount of iodine, and 100 ml of dry diethyl ether, 1.75 g (0.01 mol) of *p*–bromofluorobenzene dissolved in 10 ml of dry diethyl ether were slowly added under N_2 atmosphere. When the reaction turned cloudy indicating initiation of the Grignard reaction, 33.25 g (0.19 mol) of *p*–bromofluorobenzene dissolved in 200 ml of dry diethyl ether were added dropwise maintaining gentle reflux. At the end of the addition the reaction was refluxed for three more hours. The Grignard reagent was filtered via a filtered–canula to a degassed 1000 ml three–neck flask. A solution of 8 ml (0.06 mol) of $(EtO)_2P(O)H$ in 20 ml of dry diethyl ether was slowly added. The two–layer mixture was refluxed overnight, and then

allowed to cool at room temperature. To cold solution placed in a 1000 ml flask containing 50 g of ice and 30 ml of HCl (36%) were added. Most of the diethyl ether evaporated during the addition while the oily residue was dissolved. The solution was subsequently condensed to one third of its initial volume. Bromine was added dropwise with stirring until a faint permanent color remained. The precipitated acid was collected, dissolved in potassium hydroxide and reprecipitated by acidification. Repeated recrystallizations from dilute alcohol afforded the pure compound. ^{1}H NMR (DMSO–d_6); δ ppm : 7.76 (ddd, J_{H-H} = 7.8 Hz, J_{P-H} = 11.5 Hz, J_{F-H} = 5.9 Hz, 2 H), 7.30 (td, J_{H-H} = 7.8 Hz, J_{P-H} = 2.2 Hz, J_{F-H} = 10.2 Hz, 2 H), 2.31 (s, 3 H); ^{31}P NMR (DMSO–d_6); δ ppm : 26.9 (s, 1 P).

Synthesis of bis(*p*-methylphenyl) Phosphinic Acid. The title compound was synthesized by the general synthetic method[8] described above. ^{1}H NMR (DMSO–d_6); δ ppm : 7.57 (dd, J_{H-H} = 8.1 Hz, J_{P-H} = 11.7 Hz, 2 H), 7.25 (dd, J_{H-H} = 8.1 Hz, J_{P-H} = 2.8 Hz, 2 H), 2.31 (s, 3 H); ^{31}P NMR (DMSO–d_6); δ ppm : 29.5 (s, 1 P).

4. Synthesis of Potassium Hydrotris(1–pyrazolyl) Borate, K[HB(pz)$_3$]

The title compound was synthesized according to a literature procedure[9]. In a flame dried three–neck flask were placed 27.2 g (0.4 mol) of pyrazole and 5.4 g (0.1 mol) of potassium borohydride. The mixture was heated in a sand bath under an argon atmosphere at 190 °C for three hours. The hydrogen observed at the initial stage of the reaction had ceased by the end of the three hour period time. The mixture was poured hot into 100 ml of toluene resulting in immediate precipitation of a white solid. The powder was filtered, washed several times with hot toluene and air dried for a few hours at room temperature. 19.9 g (yield 79%) of pure material was obtained by recrystallization from anisole. m.p 187–189 °C

(literature: 189 °C). ^{1}H NMR (DMSO–d_6); δ ppm : 7.31 (d, J_{H-H} = 1.2 Hz), 7.29 (d, J_{H-H} = 1.5 Hz), 5.99 (t, J_{H-H} = 1.5 Hz). I.R.; 3609, 3304, 3119, 2425, 1737, 1641, 1499, 1416, 1386, 1289, 1256, 1215, 1201, 1185, 1125, 1112, 1083, 1072, 1048, 1040, 965, 920, 882, 850, 792, 776, 756, 737, 723.

Heating overnight at 190 °C followed by an isolation procedure like that above afforded potassium tetra(1–pyrazolyl) borate. m.p 252 °C (literature: 252 °C). ^{1}H NMR (DMSO–d_6); δ ppm : 7.38 (s), 7.19 (s), 6.02 (s).

Heating for three hours at 100 °C and similar as above isolation afforded potassium dihydrobis(1–pyrazolyl) borate.

5. Synthesis of Vanadyl complexes

Materials. Vanadium(IV) chloride VCl_4, 2,2'–bipyridyl (99%), 4,4'–dimethyl–2,2'–bipyridyl (99%), vanadyl acetylacetonate (95%) were purchased from Aldrich.

Synthesis of $VOCl_2(CH_3OH)_3$. The title compound was synthesized according to a literature procedure[10]. 5 ml of VCl_4 were dissolved in 15 ml of anhydrous carbon tetrachloride and 12.5 ml of methanol (dissolved in 10 ml of carbon tetrachloride) were slowly added to the solution. A brown precipitate is formed at the early stages of the addition accompanied by vigorous gas evolution. The reaction is driven to completion by heating at 50 °C for 15 minutes. A mixture consisting of a light green carbon tetrachloride layer and a layer of a dark green oil were formed upon cooling to room temperature. The two layers were separated and the solvent was removed from the latter producing a dense green liquid, which was further reacted without any purification. The compound was structurally characterized by single crystal X–ray diffraction methods from crystals grown upon standing at room temperature for several days.

Synthesis of L_2VOCl_2 (L_2 = substituted 2,2'–bipyridyl ligand). Complexes of the L_2VOCl_2 type were synthesized for 2,2'–bipyridyl, 4,4'–dimethyl–2,2'–bipyridyl, and 3,3',4,4'–tetramethyl–2,2'–bipyridyl following the synthetic procedure reported for the 2,2'–bipyridyl ligand[11]. A solution of the corresponding ligand in dry diethyl ether was added to an equimolar solution of $VOCl_2(CH_3OH)_3$ in the same solvent. Immediate precipitation of a light green solid was observed and stirring continued at ambient temperature for one hour. The solids were filtrated and repeatedly washed with diethyl ether. They were allowed to air–dry overnight.

IR data: $C_8H_8N_2VOCl_2$: 1601, 1497, 1474, 1444, 1317, 1172, 1158, 1029, 974, 895, 765, 733; $C_{10}H_{12}N_2VOCl_2$: 1618, 1559, 1488, 1447, 1379, 1304, 1286, 1244, 1031, 978, 925, 902, 835; $C_{12}H_{16}N_2VOCl_2$: 1612, 1509, 1487, 1448, 1385, 1292, 1251, 1237, 1155, 1015, 994, 975, 961, 897.

Synthesis of $\{L_2VO[\mu\text{–}(p\text{-}X\text{–}C_6H_4)_2PO_2]_{1.5}\}_2\{ClO_4\}$ Dimers, (L_2 = substituted 2,2'–bipyridyl, and X = H–, CH_3–, Cl–, F–). In 10 ml of dry deoxygenated methanol was dissolved 1 mmol of the corresponding L_2VOCl_2 starting material under an argon atmosphere. To the clear green solution was slowly added, via a cannula, a methanolic solution containing 2 mmol of the corresponding phosphinic acid. The resulting mixture was stirred at ambient temperature for two hours prior the addition of 1.5 mmol of $NaClO_4$. Immediate precipitation of a green solid was observed and stirring continued for an additional hour. The solid was filtrated and washed with ether. It can be recrystallized either by acetone or methanol. Single crystals for X–ray structure determination were obtained by allowing a methanolic solution to slowly evaporate over a period of several days.

Synthesis of $[HB(pz)_3]VO(acac)$, (acac = 2,5–pentadione). The title compound was synthesized according to a literature procedure[12]. In a round bottom flask

containing 5.3 g (0.02 mol) of vanadyl acetylacetonate under an argon atmosphere, were added 50 ml of dry methanol. To the violet solution was added dropwise 5.04 g (0.02 mol) of potassium hydrotris(1–pyrazolyl) borate dissolved in 20 ml of methanol. The solution was refluxed for four hours resulting in the precipitation of a violet solid. It was filtrated, washed twice with methanol and once with ether and air dried overnight. Upon recrystallization with acetonitrile were isolated 4.25 g (yield: 56%) of pure product. I.R.; 3436, 3103, 2478, 1589, 1573, 1535, 1521, 1504, 1431, 1406, 1393, 1369, 1309, 1279, 1214,1118, 1111, 1097, 1076, 1051, 1031, 987, 976, 967, 938,888.

Synthesis of $\{HB(pz)_3VO[m–(X–Ph)_2PO_2]\}_2$ Dimers, (X = H–, CH_3–, CH_3O–, F–). A series of four dimers were synthesized by following a literature procedure[13]. $[HB(pz)_3]VO(acac)$ (0.76 g, 0.002 mol) was dissolved in 40 ml of acetonitrile and an equimolar amount of the corresponding phosphinic acid was added along with 1–2 ml of water. The solution was refluxed producing a gradual change of color from violet to blue and affording the precipitation of a blue solid. After two hours of refluxing, the solution was cooled down to room temperature and the blue solid was filtrated and washed repeatedly with fresh acetonitrile. It was recrystallized by dichloromethane. Suitable crystals for X–ray structure determination were grown by slow evaporation of an acetonitrile or dichloromethane solution.

6. Synthesis of Amidinium–Carboxylate Salts

Materials. Benzamidine hydrochloride hydrate (97%), 1,3–dicyanobenzene (98%), 2,2,5,5–tetramethyl–3–carbomidopyrroline (99%) and 1,8–diazabicyclo[5.4.0]undec–7–ene (DBU 98%) were purchased from Aldrich and used without further purification.

General Synthesis. The salts were prepared by slow evaporation of aqueous solutions containing equimolar amounts of the amidinium chloride and the 2,2,5,5–tetramethyl–3–carboxypyrroline–1–oxyl neutralized by 1,8–diazabicyclo[5.4.0]undec–7–ene (DBU). Crystals were removed from the solution prior to complete evaporation of the water.

Synthesis of *m*–Cyanobenzamidinium Chloride. 1,3–Dicyanobenzene (5.125 gr, 40 mmol) was placed in a flame dried Schlenk flask, equipped with a magnetic stirrer, under an argon atmosphere. A freshly generated solution of sodium methoxide in methanol (0.46 gr, 20mmol, of Na in 100 ml of methanol) was added dropwise at ambient temperature. The solid was dissolved within 30 min, and the clear solution was stirred at room temperature for an additional two hours. Ammonium chloride (5.35 gr, 100 mmol) was added and stirring continued overnight. The solvent was removed under vacuum and the white solid was heated at 80 °C under vacuum for an additional three hours. It was washed with ether and methanol and recrystallized from water producing fine white needles, which were air dried for 24 hours. ^{1}H NMR (DMSO–d_6), δ 9.57 (s, 4H), 8.34 (s, 1H), 8.16 (t, 2H, J = 9 Hz), 7.80 (t, 1H, J = 9 Hz); IR, 3435, 3079, 3047, 2235, 1659, 1638, 1599, 1578, 1481, 1424, 1148, 906, 807, 680.

Benzamidinium 2,2,5,5–tetramethyl–3–carboxypyrroline–1–oxyl hydrate. Yellow square crystals were isolated. IR; 3406, 3252, 2979, 2931, 2868, 1673, 1639, 1613, 1572, 1532, 1478, 1466, 1453, 1427, 1392, 1367, 1355, 1316, 1210, 1163, 1148, 1079, 1061, 1000, 952, 801, 787, 706.

***m*–Cyanobenzamidinium–2,2,5,5–tetramethyl–3–carboxypyrroline–1–oxyl.** Yellow square crystals were isolated. IR; 3170, 2976, 2929, 2866, 2239, 1656, 1642, 1609, 1574, 1544, 1512, 1478, 1465, 1450, 1427, 1388, 1375, 1366, 1316,

1272, 1228, 1208, 1173, 1161, 1150, 1113, 1063, 1001, 949, 878, 817, 801, 781, 730, 712, 678.

LIST OF REFERENCES

(1) SHELXTL–PLUS V5.0, Siemens Industrial Automation, Inc., Madison, WI.

(2) Spek, A. L. *Acta Cryst.* **1990**, *A46*, C34.

(3) Duisenberg, A. J. M. *J. Appl. Cryst.* **1992**, *25*, 92.

(4) Struve, W. S. in *Fundamentals of Molecular Spectroscopy*, John Wiley: New York 1989.

(5) (a) Wang, S. L.; Kang, H. Y.; Cheng, C. Y.; Lii, K. H. *Inorg. Chem.* **1991**, *30*, 3496. (b) Kang, H. Y.; Lee, W. C.; Wang, S. L.; Lii, K. H. *Inorg. Chem.* **1992**, *31*, 4743. (c) Lii, K. H. *J. Chin. Chem. Soc.* **1992**, *39*, 569.

(6) Torgerson, M. R. *Ph. D. Dissertation* M.S.U. 1996.

(7) Kosolapoff, G. M. *J. Am. Chem. Soc.* **1942**, *64*, 2982.

(8) (a) Kosolapoff, G. M.; Struck, R. F. *J. Chem. Soc.* **1959**, 3950. (b) Petrov, K. A.; Parshina, V. A.; Daruze, G. L. *J. Gen. Chem. USSR* **1960**, *30*, 2972.

(9) Trofimenko, S. *J. Am. Chem. Soc.* **1967**, *89*, 3170.

(10) von Funk, H.; Mohaupt, G.; Paul, A. *Z. Anorg. Allg. Chem.* **1959**, *302*, 199.

(11) Fowles, G. W. A.; Rice, D. A.; Wilkins, J. D. *Inorg. Chim. Acta* **1973**, *7*, 642.

(12) Mohan, M.; Holmes, S. M.; Butcher, R. J.; Jasinski, J. P.; Carrano, C. J. *Inorg. Chem.* **1992**, *31*, 2029.

(13) Dean, N. S.; Bond, M. R.; O' Connor, C. J.; Carrano, C. J. *Inorg. Chem.* **1996**, *35*, 7643.

CHAPTER 3

Magnetic Studies on Layered Vanadyl Phosphates and Phosphonates

A. Introduction

Without well–defined structure, any sensible interpretation of magnetic behavior at the molecular level is necessarily speculative. Nowhere is this difficulty more striking than in the field of the host–guest chemistry of layered metal phosphates and their organic/inorganic hybrid analogs (LVP's). In the last few years, however hydrothermal synthesis techniques[1] afforded such materials in crystalline form, allowing for their structural characterization. A systematic investigation of low dimensional magnetic interactions involving vanadyl ions was then undertaken, initially in the family of vanadyl monohydrogenphosphates. The magnetic properties of the $VO(HPO_4)\cdot nH_2O$ compounds with n equal to 0.5[2,3,4],

1.5^2, 2^5, or $4^{2,4,6}$ were thoroughly investigated by susceptibility methods. Villeneuve and coworkers[3,7] established the role of the O—P—O linkages as active exchange pathways, and identified the common building blocks responsible for spin communication. The geometrical and electronic factors responsible for the strength and the sign of the magnetic interaction are harder to evaluate. The complexity of the problem becomes apparent by a simple inspection of the common structural units of these low dimensional materials, depicted in *Figure 8* in Chapter 1. Many factors have to be taken into consideration in order to validate any conclusions regarding the correlation of structure to physical properties.

The approach we have followed towards this problem is schematically represented in *Figure 1*. The LVP's structural environment can act as a host by encapsulating guest species, like small molecules and ions. Such systems are likely to have rich magnetochemistry, since spin communication in principle could be achieved within the host layers (*intralayer coupling*), between adjacent host layers (*interlayer coupling*), among neighboring guest species (*guest–guest coupling*) and between guest and layered host species (*guest–host coupling*).

The *intralayer* spin–spin interactions were investigated by employing the layered framework of $VOPO_4 \cdot 2H_2O$, whose structure is depicted in *Figure 6* Chapter I. Upon redox intercalation of monovalent or divalent cations[8] this simple diamagnetic host becomes magnetic by injection of half or one electron per vanadium center respectively. In the original solution synthesis, described by Jacobson and coworkers[8] and later by Votinský and coworkers[9], metal intercalation was nonstoichiometric resulting in a large number of phases, which contained variable amounts of guest species. Lii and coworkers[10] however, by employing hydrothermal techniques, were able to synthesize and structurally characterize stoichiometric metal intercalated vanadyl phosphates,

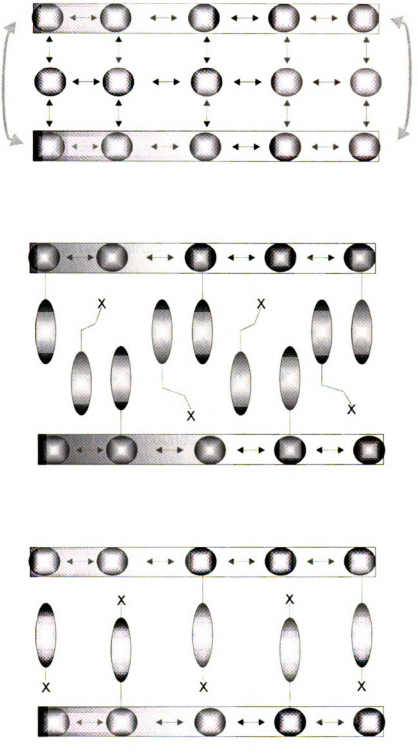

Figure 1. Schematic outline indicating the means that magnetic properties can be tuned in vanadyl phosphates and phosphonates: by small ion intercalation (top), by molecularly jacking the layer (middle), and by controlling the spin flow among adjacent centers (bottom).

$A_xVOPO_4 \cdot nH_2O$, with A an alkali, alkaline–earth or a transition metal. We have also utilized the latter synthetic strategy for the preparation of a series of these materials. In the first part of this chapter improved synthesis of compounds previously obtained as a mixture of phases are described, along with the synthesis and structural characterization of a new member of the family. The magnetic properties of metal intercalated LVP's, determined by magnetic susceptibility, solid state NMR, and solid state ESR techniques are reported and initial conclusions that relate structure and magnetic properties are drawn.

Additional insights into the spin exchange pathway in layered vanadyl phosphates are gained by considering the magnetic behavior of a family of layered vanadyl phosphonates (LVPh's) $VO(O_3PC_6H_4–X) \cdot H_2O$ with X = *p*–NO_2, *m*–F, *p*–F, H, synthesized and characterized by Dr. J. Le Bideau[11]. His results are briefly presented in the second part of this chapter and a detailed discussion concerning both families of compounds will follow.

Finally the magnitude of *interlayer coupling* is assessed by utilizing a second series of layered vanadyl phosphonates, $VO(O_3PNp)(H_2O) \cdot nROH$, where the phosphonate pendant is a naphthalene group and various alcohols are intercalated within the interlayer space (LVNpPh's). These compounds (synthesized by Dr. M. R. Torgerson[12]) display remarkable control over the *d*–spacing, since by using various alkyl alcohols adjacent layers are mechanically jacked by 1.06 Å per methylene unit. Hence, the magnetic properties of layers identical to each other, but separated at distances from 12.10 Å to 20.83 Å, were studied enabling the evaluation of the magnitude of the *interlayer coupling*.

B. Results

1. Metal Intercalated Vanadyl Phosphates (LVP's) $A_xVOPO_4 \cdot nH_2O$

a. Synthesis and Characterization

In a series of benchmark papers Lii and coworkers reported the synthesis and crystal structure determinations for several $A_xVOPO_4 \cdot nH_2O$ systems[10]. Of specific interest to this thesis were the alkali metal compounds $Na_{0.5}VOPO_4 \cdot 2H_2O$ and $K_{0.5}VOPO_4 \cdot 1.5H_2O$[13], as well as the alkaline earth and transition metal intercalates $Sr_{0.5}VOPO_4 \cdot 2H_2O$ and $Co_{0.5}VOPO_4 \cdot 2H_2O$[14] respectively. These materials were originally synthesized by hydrothermal procedures, and were obtained as minor or major phases of polycrystalline mixtures. Since the aim of this work is the study of their magnetic properties, the desired single–phases were obtained by modifying the original synthetic conditions. Pure compounds became available by changing the relative ratios of the starting materials and in some instances by varying the reaction time. Details on the syntheses are reported in Chapter 2.

In addition to the already known materials a new member of this series, namely $Rb_{0.5}VOPO_4 \cdot 1.5H_2O$, was synthesized and structurally characterized[15]. The crystallographic data are summarized in Table 1 for both temperatures where single crystal X–ray data were collected, while additional details can be found in Chapter II. The structure of $Rb_{0.5}VOPO_4 \cdot 1.5H_2O$ is discussed along with its differences and similarities to the rest of the metal vanadyl phosphate derivatives.

$Rb_{0.5}VOPO_4 \cdot 1.5H_2O$ crystallizes in the triclinic system, space group $P\bar{1}$. *Figure 2(A)* shows the view down on a segment of its layer. As with the other alkali metal systems[13] and the alkaline earth analog[14], the layer is

Table 1. Crystallographic Data for $Rb_{0.5}VOPO_4 \cdot 1.5H_2O$

	(A) Crystal Parameters	
formula	$H_3Rb_{0.5}O_{6.5}PV$	$H_3Rb_{0.5}O_{6.5}PV$
FW	227.40	227.40
crystal size (mm^3)	0.42×0.24×0.02	0.42×0.24×0.02
crystal system	triclinic	triclinic
space group	$P\bar{1}$ (#2)	$P\bar{1}$ (#2)
a (Å)	6.285(1)	6.272(6)
b (Å)	6.291(1)	6.278(4)
c (Å)	6.849(2)	6.797(5)
α (deg)	89.73(2)	89.70(6)
β (deg)	107.79(2)	107.77(8)
γ (deg)	90.15(1)	90.10(80
V ($Å^3$)	257.8(1)	254.9(3)
Z	2	2
d_{calc} (g/cm^3)	2.929	3.019
F(000)	219	223
μ(Mo Kα), cm^{-1}	64.13	69.63
	(B) Data Collection	
$2\theta_{max}$ (deg)	50	60
index ranges	$0 \le h \le 8$ $-8 \le k \le 8$ $-9 \le l \le 9$	$0 \le h \le 8$ $-8 \le k \le 8$ $-9 \le l \le 9$
scan speed (deg/min in ω)	2	2
temperature	293(2) K	173(2)K
reflections collected	1623	1703
unique reflections	1498	1349
R(merg) (%)	2.09	10.77
	(C) Refinement	
Refinement method	Full–matrix least–squares on F^2	Full–matrix least–squares on F^2
R indices ($I > 2\sigma(I)$)	R1 = 0.0517 WR2 = 0.1474	R1 = 0.0556 WR2 = 0.1508
R indices all data	R1 = 0.0921 WR2 = 0.1711	R1 = 0.0924 WR2 = 0.1703
Δ(ρ) ($e^-/Å^3$)	1.197 and – 0.906	1.590 and – 1.614
Extinction coefficient	0.023(8)	0.118(19)
GOF	1.149	1.064

Table 2. Selected Bond (Å) for $A_xVOPO_4 \cdot nH_2O$

Bond	Na^{+} [a, c]	K^{+} [a]	Rb^{+} [d]	Rb^{+} [e]	Sr^{2+} [b, c]	Co^{2+} [b]
$V—O_{ax.}$ [f]	1.581	1.587	1.598	1.601	1.589	1.60
$V—O_{w(1)}$ [g]	2.351	2.318	2.348	2.332	2.411	—
$V—O_{eq(1).}$ [h]	1.948	1.946	1.943	1.945	1.996	1.971
$V—O_{eq(2).}$ [h]	1.960	1.954	1.952	1.948	2.004	1.971
$V—O_{eq(3).}$ [h]	1.961	1.959	1.953	1.961	2.013	1.971
$V—O_{eq(4).}$ [h]	1.965	1.965	1.971	1.977	2.016	1.971
$A^{x+}—O_{w(1)}$ [g]	2.455	2.923	3.045	3.009	2.68	—
$A^{x+}—O_{w(2)}$ [i]	2.404	3.142	3.15	3.139	2.576	2.11
$A^{x+}—O_{ax.}$ [f]	—	2.793	2.842	2.830	2.80	2.14

[a] Taken from reference 13. [b] Taken from reference 14. [c] Mean bond distances. [d] X-ray structure determination was conducted at 293 K. [e] X-ray structure determination was conducted at 173 K. [f] Refers to the vanadyl oxygen atom. [g] Refers to the water molecule coordinated axially to the vanadium center. [h] Refers to the phosphate oxygen atoms. [i] Refers to the interlayer water molecule, which is not coordinated to the vanadium atom.

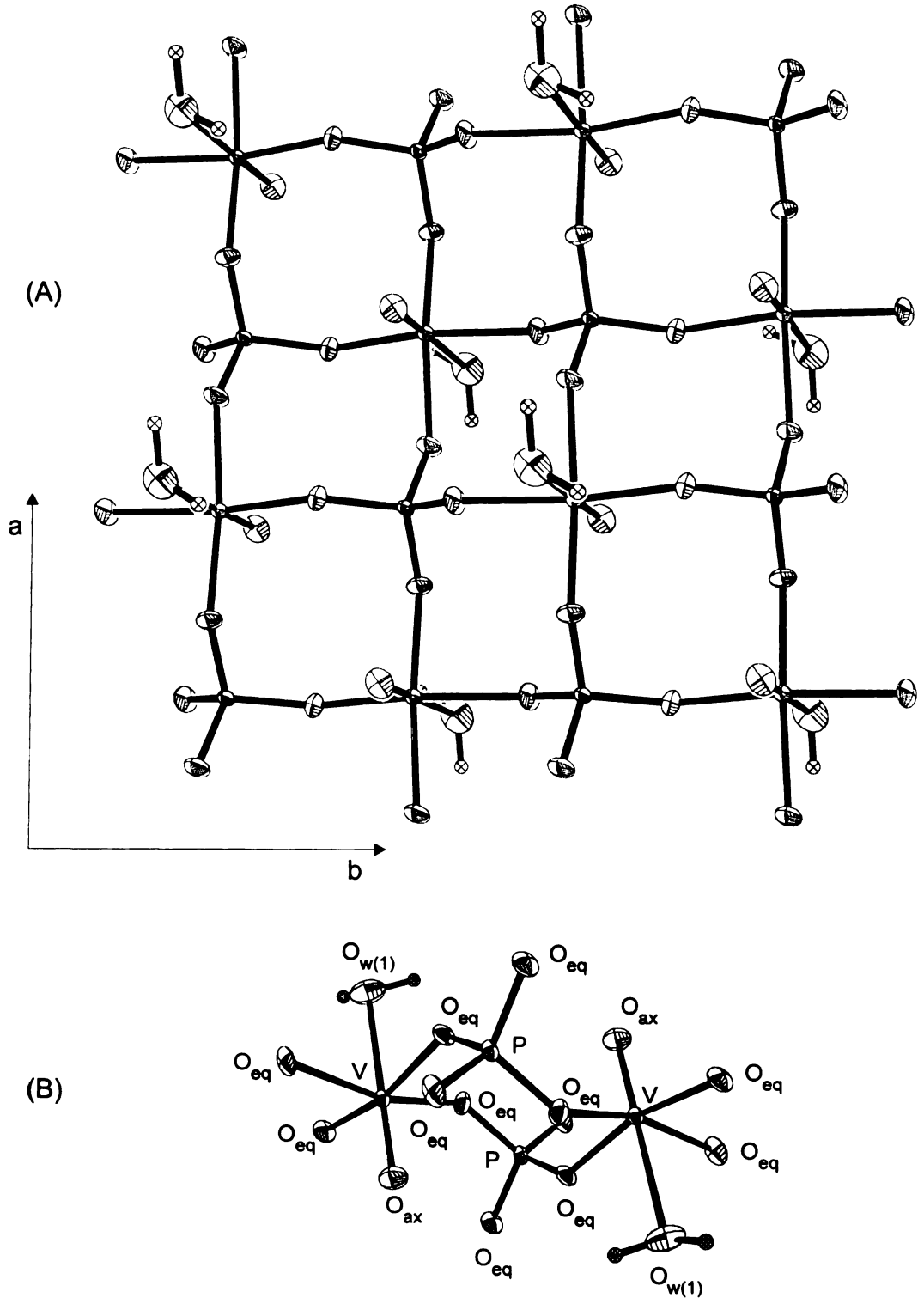

Figure 2. Intralayer framework of $Rb_{0.5}VOPO_4 \cdot 1.5H_2O$ (A). The layer is built up by fusion of chair–like eight–membered rings displayed in (B).

composed of distorted vanadium octahedra and phosphate tetrahedra. Each vanadium octahedron shares its four equatorial oxygen atoms with four different phosphates. The mean V—$O_{eq.}$ bond distance is approximately 1.96 Å for the alkali metal derivatives, and slightly higher at 2.01 Å for the alkaline earth (Table 2). The axial positions are occupied by a vanadyl oxygen (mean distance 1.59 Å) and a weakly coordinated water molecule that forms a long O — V bond ranging from 2.32 to 2.41 Å. Such an arrangement leads to the formation of eight–member rings, which adopt a chair–like conformation designated as D VII (*Figure 2(B)*) by Villeneuve and coworkers[3,7]. The intercalated ions are located within polar pockets created by the phosphate oxygen atoms. Their coordination sphere includes the water molecules bound to the vanadyl axial positions in relatively close proximity for the Na^+ and Sr^{2+} ions, but at much longer distances for the K^+ and Rb^+ ones (Table 2). An additional interlayer water molecule is located so that it can hydrogen bond to phosphates of different layers (*Figure 3*), complementing the coordination sphere of the metal ions.

The single crystal X–ray structure determination of the Rb^+ derivative at two different temperatures (293 and 173 K), revealed no major structural differences. In both instances only one unique vanadium atom is found in the unit cell indicating that the mean oxidation state of each metal center is +4.5. Efforts to solve the structure in the non–centrosymmetric space group *P1* were unsuccessful since an R1 factor of 14% was obtained.

These four derivatives are isostructural with only subtle differences in the intralayer framework arising from ion size and dissimilar numbers of water molecules coordinated to the metal cations. However, the relative positions of adjacent layers vary, resulting in crystallization of these materials in different space groups[10]. Upon metal intercalation, one electron reduction of half and all vanadium sites occurs for the alkali and alkaline earth cations respectively. The

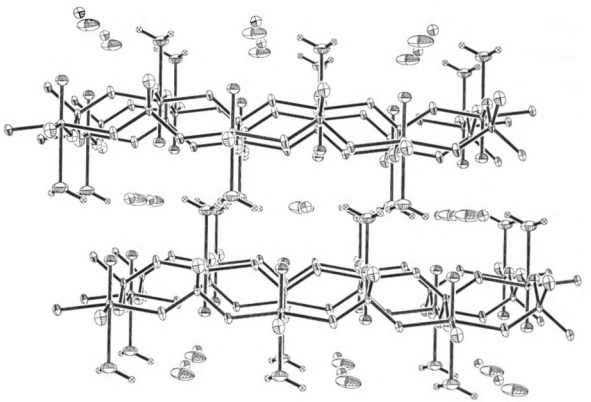

Figure 3. The three–dimensional structure of layered $Rb_{0.5}VOPO_4 \cdot 1.5H_2O$.

negatively charged layers are brought closer together by electrostatic interaction with the metal ions. Interlayer d–spacings of 6.57, 6.40, 6.51, 6.33 Å are observed for intercalates of the hydrated metal cations, $Na^+ \cdot 2H_2O$, $K^+ \cdot 1.5H_2O$, $Rb^+ \cdot 1.5H_2O$, and $Sr^{2+} \cdot 2H_2O$ respectively. The variations among these numbers are small in light of the ~1 Å electrostatic compression, relative to the d–spacing of 7.43 Å[16] for the neutral parent $VOPO_4 \cdot 2H_2O$ layered compound.

The $Co_{0.5}VOPO_4 \cdot 2H_2O$ derivative[14] displays a slightly different bonding scheme, with vanadium centers being five–coordinated adopting a square pyramidal stereochemistry. The sixth position, axial to the vanadyl, is empty due to the coordination requirements of the paramagnetic Co^{2+} ion. Four water molecules located in the interlayer space hydrate this ion in the equatorial plane (*Figure 4*) with Co — O_w distance of 2.11 Å, while the axial positions are occupied by weakly bound vanadyl oxygen atoms of adjacent layers (Co — $O_{ax.}$ 2.14 Å) forming linear V — O_{ax} — Co — $O_{ax.}$ — V chains. The local symmetry around the Co^{2+} ion is D_{4h} with the 4–fold rotation axis passing through the linear chain. Due to this interlayer arrangement an expanded d–spacing of 6.71 Å is observed.

The purity of the five compounds synthesized was mainly verified by powder X–ray methods (PXRD). From the known positional parameters and crystallographic data, theoretical PXRD patterns were calculated and compared to actual experimental data. These layered materials are susceptible to preferred orientation effects upon packing of the powders on the sample holder by a glass slide (experimental details can be found in Chapter 2). A less biased pattern is obtained when the powder samples are dispersed with the aid of a low boiling solvent, like ether. Both approaches were followed for the sample preparation.

Figure 5 displays the PXRD plots of the Na^+, Rb^+, and Sr^{2+} derivatives with the main diffraction lines indexed. In addition to the usual 00l lines expected for

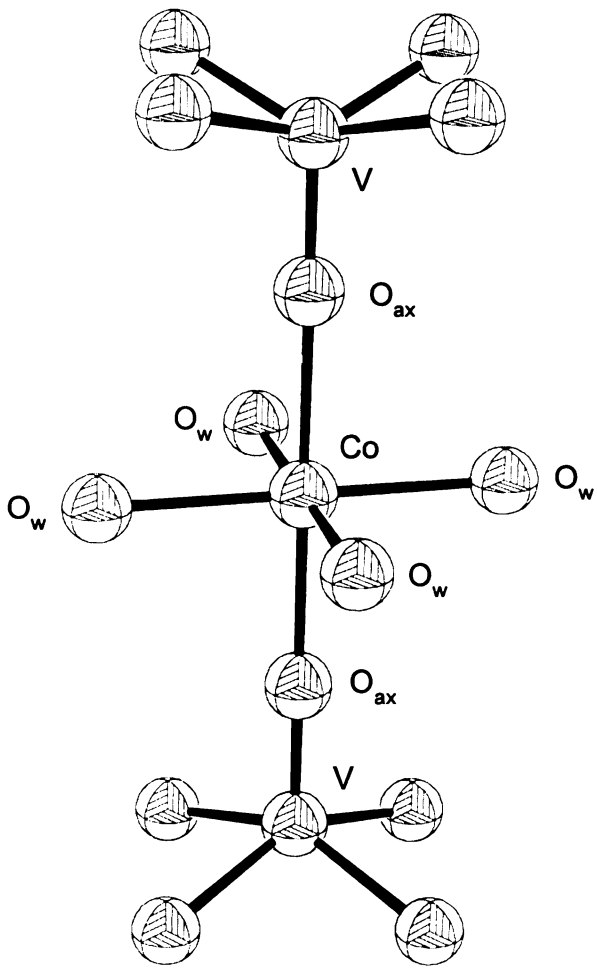

Figure 4. The D_{4h} coordination octahedron of the Co^{2+} ion in $Co_{0.5}VOPO_4 \cdot 2H_2O$.

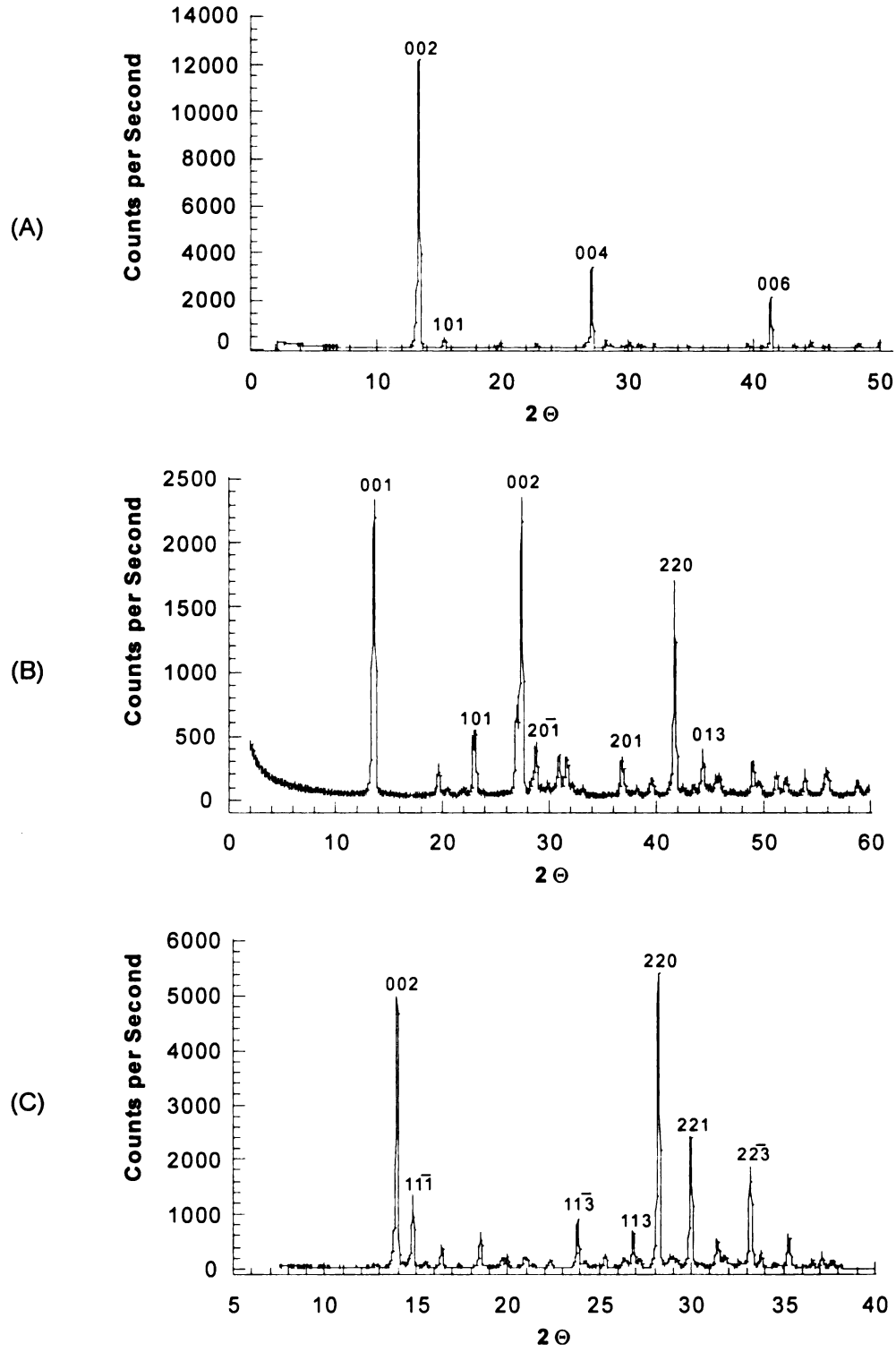

Figure 5. Powder X–ray spectra of the Na^{+} (A), Rb^{+} (B), and Sr^{2+} (C) derivatives of the vanadyl phosphate layered material. On the top of the main diffraction lines are indicated the corresponding hkl indices.

layered materials, a large number of diffraction peaks originating from intralayer order are observed. A detailed comparison of theoretical and experimental diffraction patterns indicates the materials' purity. On the other hand, the cases of the K^+ and Co^{2+} derivatives were not trivial. Repeated synthetic attempts formed multi–phase products, as judged by diffraction lines not corresponding to the theoretical PXRD pattern (shown in *Figure 6(A)* and *Figure 7(A)* respectively). Small adjustments in the ratio of starting materials and increased reaction times led to the isolation of single–phases, whose spectra are depicted in *Figure 6(B)* and *Figure 7(B)* respectively.

The thermogravimetric analysis plots (TGA) of the intercalated derivatives displayed a two–step water loss (*Figure 8(A)*). The first step, corresponding to the loss of the weakly coordinated intralayer water, occurred at ~100 C° for the Na^+, ~80 C° for the K^+, and ~75 C° for the Rb^+ ions. The second step, corresponding to the water molecule coordinated to the vanadium atom, occurred at higher temperatures (~230 C° for Na^+, ~185 C° for K^+, and ~175 C° for Rb^+). The water loss temperature correlates with the cation to water bond distance as depicted in *Figure 9*.

For the Co^{2+} intercalated derivative much higher temperature were required to remove the intralayer water, which is in close proximity (2.11 Å) with the paramagnetic ion (*Figure 8(C)*). Multi–phase materials on the other hand displayed TGA plots similar to those obtained by the alkali metal derivatives (*Figure 8(B)*). In addition, the water content calculated for a single–phase was 1.9 per formula unit, while the corresponding amount for various multi–phase samples varied from 2.2 to 2.6 per formula unit. Gentle heating at low temperatures (~ 45 to 50 C°) resulted in removal of most of the additional water, but complete transformation of the multi–phase materials to a single–phase was never achieved.

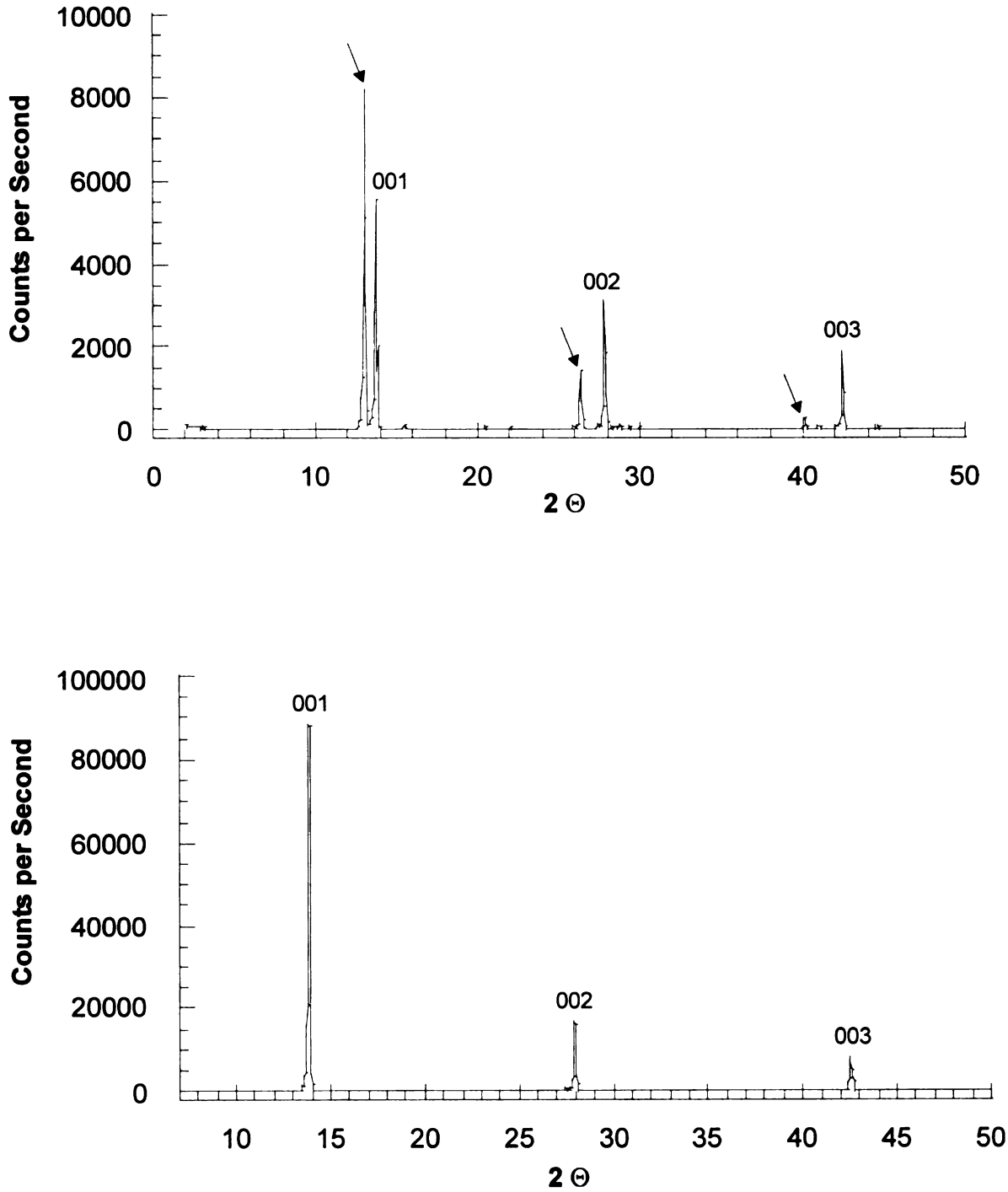

Figure 6. Powder X–ray spectra of the K^+ derivative. The top spectrum belongs to a multi–phase sample, with the arrows indicating the peaks that do not correspond to the calculated diffraction lines (A). The spectrum of a single–phase material is shown below with the main diffraction lines indexed (B).

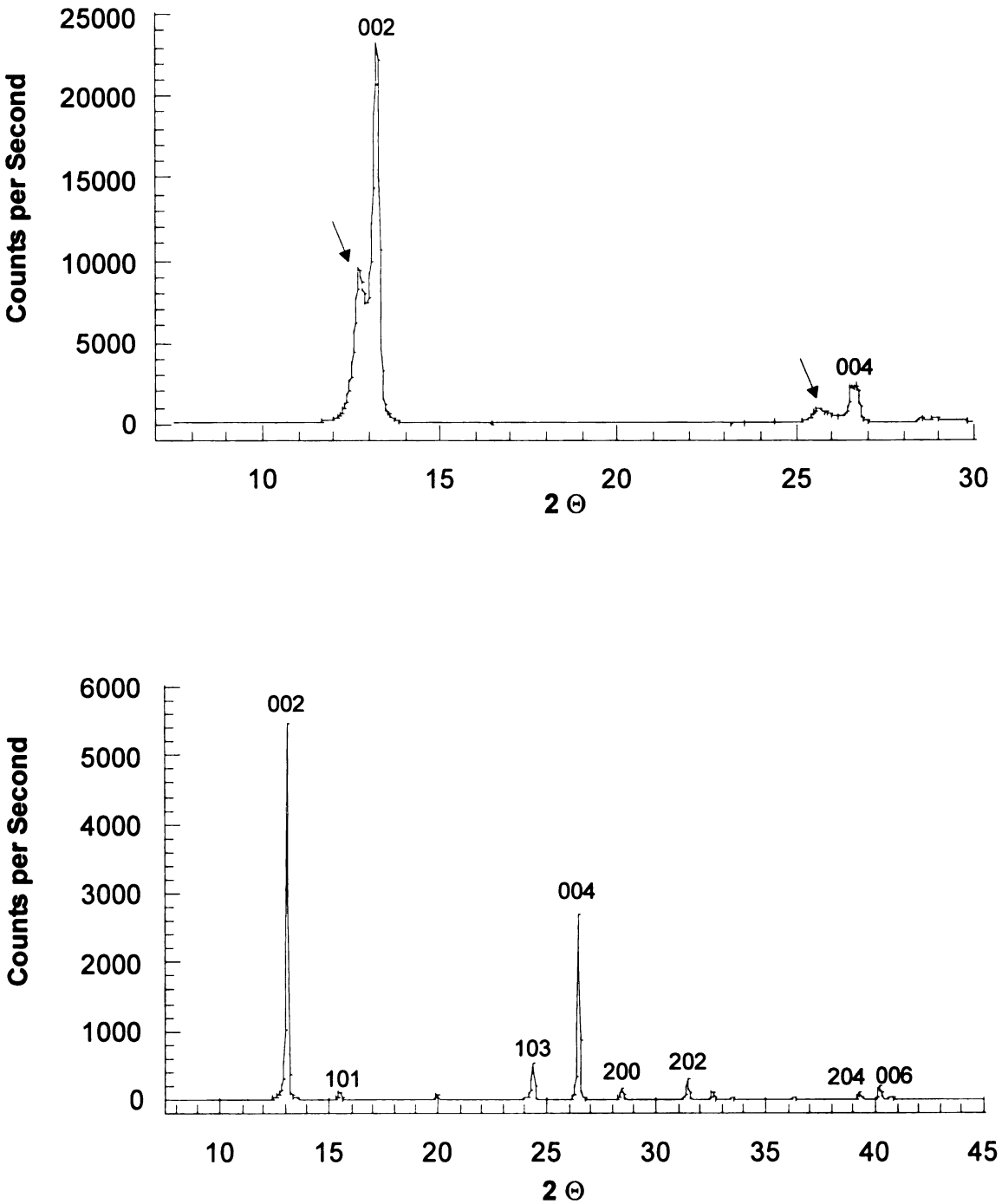

Figure 7. Powder X–ray spectra of the Co^{2+} derivative. The top spectrum belongs to a multi–phase sample, with the arrows indicating the peaks that do not correspond to the calculated diffraction lines (A). The spectrum of a single–phase material is shown below with the main diffraction lines indexed (B).

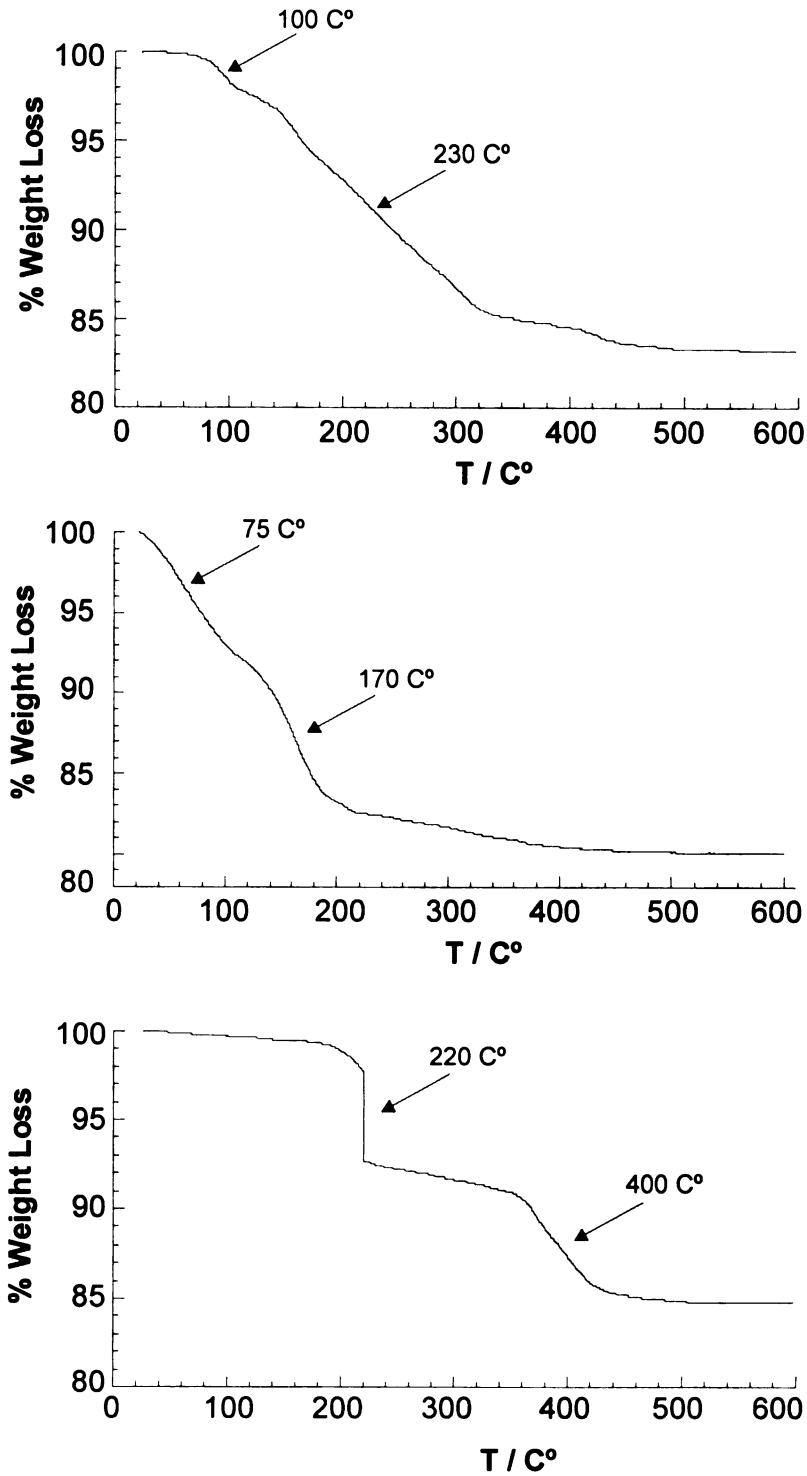

Figure 8. TGA plots of the Na^{+} (A), multi–phase Co^{2+} (B), and single–phase Co^{2+} (C) intercalated derivatives of layered vanadyl phosphate. The water loss steps are centered around the temperatures indicated by the arrows.

(A)

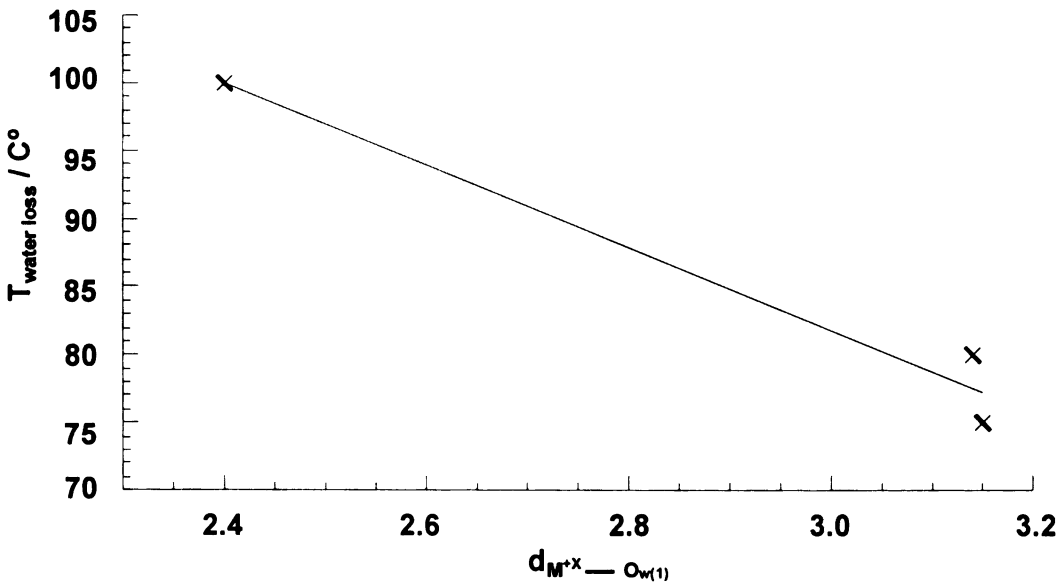

(B)

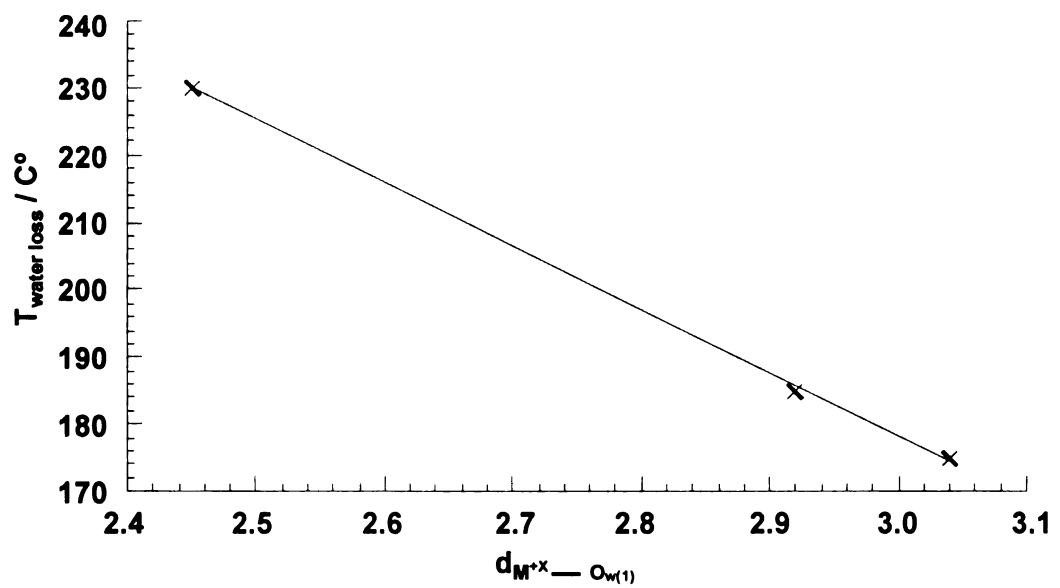

Figure 9. Correlation of the water loss temperature with the cation to water bond distance (for the Na^+, K^+, and Rb^+ derivatives), for each crystallographically unique water molecule ((A) and (B)).

Infrared spectra recorded for powder samples display characteristic peaks listed and assigned in Table 3. The alkali and the alkaline earth derivatives display a relatively similar infrared pattern indicating the isostructural nature of the intralayer framework. It is interesting to note the complexity of the spectrum in the region corresponding to P — O, V=O, and V — O stretches for these derivatives; these regions show only two lines in the more symmetric interlayer framework of the Co^{2+} one. On the other hand, a multi–phase sample of the latter compound, which contains a higher amount of interlayer water, displays a pattern similar to that of the former derivatives (*Figure 10*).

b. Magnetic Properties

Static Solid State ^{31}P NMR. Oxovanadium(IV) phosphates offer a large variety of crystal structures yielding different types of low–dimensional magnetic interactions[2]. Their magnetic behavior originates either from isolated vanadyl dimers, or from regular and double vanadyl chains, or from two–dimensional lattices[7]. Although all of the structural frameworks are based on linking of VO_6 octahedra to PO_4 tetrahedra, the magnetic properties differ not only on the type of interaction but also on their strength. The classification of exchange pathways by Villeneuve and coworkers[3,7], postulated the involvement to some extent of the phosphate tetrahedra (*Figure 8*, Chapter 1). Firm evidence for the above hypothesis was provided from ^{31}P–NMR spectroscopy[5,17], which revealed nonzero spin density on phosphorus. We have applied the same approach to the layered $A_xVOPO_4 \cdot nH_2O$ family, in order to elucidate the nature of the superexchange pathway.

In a transition metal or lanthanide complex, where unpaired electrons reside on the metal nuclei, some of the spin density might be transferred to the

Table 3. Infrared Peaks and Assignment for $A^{x+}_{0.5}VOPO_4 \cdot nH_2O$

Na	K	Rb	Sr	$Co_{s.ph.}$	$Co_{m.ph.}$	
3550 (m)	3528 (m)	3547 (m)	3561 (m)	3504 (m)		
3528 (m)	3415 (m)	3415 (m)	3421 (m)	3345 (m)	3435	$\nu_{(OH)}$
3460						
to	3169	3169 (m)	3080 (m)	3286 (s)	3284	
3335						
1653	1650			1653	1653	
to	to	1655 (m)		to	to	
1603	1640			1603	1603	
		1646				
		to	1632 (m)			
		1634				
	1615 (m)	1617 (m)				$\delta_{(HOH)}$
		1607 (m)				
1171 (m)	1171 (m)	1171 (m)				
1088 (s)	1088 (s)	1097	1122 (m)	1121 (m)	1081 (m)	
		to				$\nu_{as(PO)}$
		1082				
	1034 (s)	1034 (s)	1050 (s)		1035 (s)	
1009 (s)		1013 (s)	1010 (s)	1013 (s)	999 (s)	$\nu_{(V=O)}$
967(s)	967 (s)	964 (s)	986 (s)		959 (s)	$\nu_{(V—O)}$
904 (s)	906 (s)	904 (s)	898 (m)			$\nu_{(PO)}$

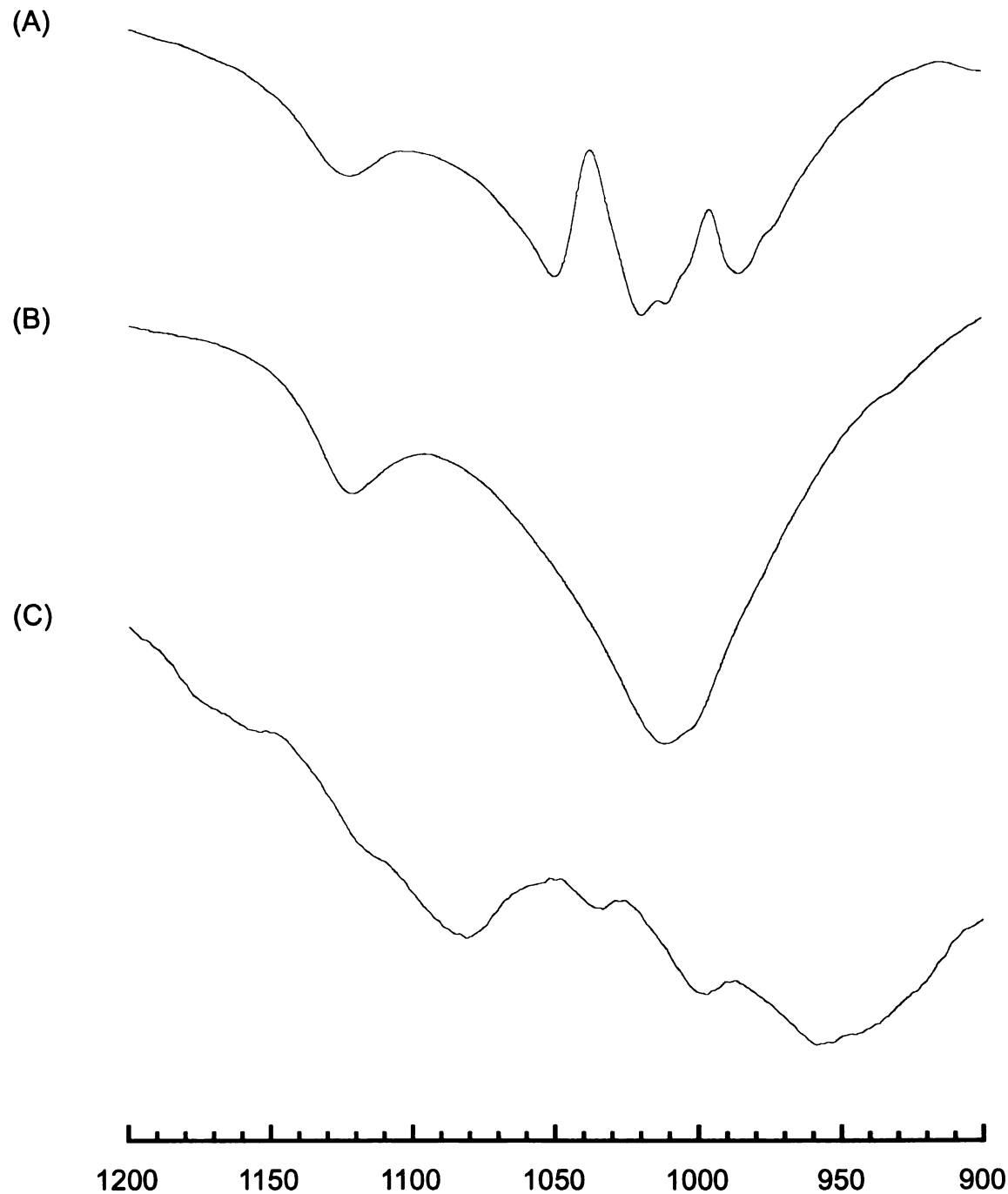

Figure 10. Detail of the infrared spectra of $Sr_{0.5}VOPO_4 \cdot 2H_2O$ (A), single–phase $Co_{0.5}VOPO_4 \cdot 2H_2O$ (B), and multi–phase $Co_{0.5}VOPO_4 \cdot 2H_2O$ (C).

diamagnetic ligands. For ligands possessing magnetic nuclei ($I \neq 0$), the spin and nuclear moments may interact via the Fermi contact[18] or dipole–dipole[19] coupling. The former term involves the interaction of the nuclear moment with the electric currents arising from electron density at the nucleus and takes the form

$$H_1 = A_s \mathbf{S} \bullet \mathrm{I} \tag{3. 1}$$

giving rise to observable contact shifts in the NMR spectrum[20] or nuclear multiplet structure in the EPR spectrum[21] with

$$A_s = (8\pi/3)\gamma_N \hbar g \beta |\Psi(0)|^2 \tag{3. 2}$$

where $|\Psi(0)|^2$ is the probability of finding the electron on the nucleus. Thus isotropic Fermi coupling constants arise only from spin in *s* orbitals, and A_s is a linear function of this spin density.

Dipolar shifts on the other hand arise from a through–space dipolar interaction between the electronic magnetic moment μ and the magnetic moment $\hbar\gamma_N \mathrm{I}$ of the resonating nucleus which does not vanish for magnetically anisotropic systems. The corresponding hamiltonian takes the form

$$H_2 = \hbar\gamma_N g\beta \left\{ \frac{3(\mathbf{r} \bullet \mathbf{S})(\mathbf{r} \bullet \mathrm{I})}{r^5} - \frac{\mathbf{S} \bullet \mathrm{I}}{r^3} \right\} \tag{3. 3}$$

with **r** being the vector locating the electron relative to nucleus. This term averages over the probability distribution $|\Psi(\mathbf{r})|^2$ for the electron, which is zero for a spherical distribution as it is for *s* type orbitals.

The above effects influence the NMR shifts of nuclei located in relatively close proximity to paramagnetic centers. A large paramagnetic shift is observed with respect to shifts of the corresponding nuclei in similar diamagnetic environments. In the $A_xVOPO_4 \cdot nH_2O$ family, intercalation of the metal ion places unpaired electrons on the vanadyl centers and therefore their ^{31}P–NMR spectra

are expected to differ significantly from that of their diamagnetic parent $VOPO_4 \cdot 2H_2O$.

Figure11(A) displays the nonspinning solid–state ^{31}P–NMR of the latter compound at 293 K. A single narrow peak is observed centered at 6.98 ppm with reference to 85% H_3PO_4, comparing well to literature data concerning diamagnetic phosphates[22]. Similar chemical shifts have also been observed in vanadium phosphate compounds (VPO) utilized in industry for the catalytic transformation of *n*–butane to maleic anhydride, for the phosphate groups located in the vicinity of diamagnetic V^{5+} centers[23]. Additional spectra recorded at temperatures ranging from 173 to 293 K indicated that this resonance is temperature independent. Doping of the $VOPO_4 \cdot 2H_2O$ lattice with Co^{2+} ions places one electron per vanadyl center on the metal's d_{xy} orbital. *Figure 11(B)* displays the ^{31}P–NMR spectrum of the intercalated phase at room temperature, where a single resonance is observed centered at 453 ppm. Such a large paramagnetic shift may be caused by strong spin–orbit coupling[24] and/or magnetic exchange[25]. For V^{4+} ions only the latter is operating[5]. The exchange mechanism should involve spin transfer through *s* and *p* phosphorus orbitals. The spin density in *s* orbitals is the origin of the isotropic shift originating from the Fermi contact term (eq. 3.1), while the contribution of the *p* orbitals manifests itself in the anisotropy of the line, including the dipole–dipole term (eq. 3). Given the low local symmetry of the vanadyl centers (C_{4V}) in the intralayer framework, the ground state term corresponds to a B_2 state with low–lying excited states not thermally accessible[26]. Hence, mixing of excited states into the ground state is possible only via spin–orbit coupling, which is relatively small for the V^{4+} ion, resulting in a small g factor anisotropy. To a first approximation, considering also the large displacement between the electron located on the V^{4+} ion and the ^{31}P magnetic nucleus, the dipole–dipole term can be ignored[27]. Thus, taking only into

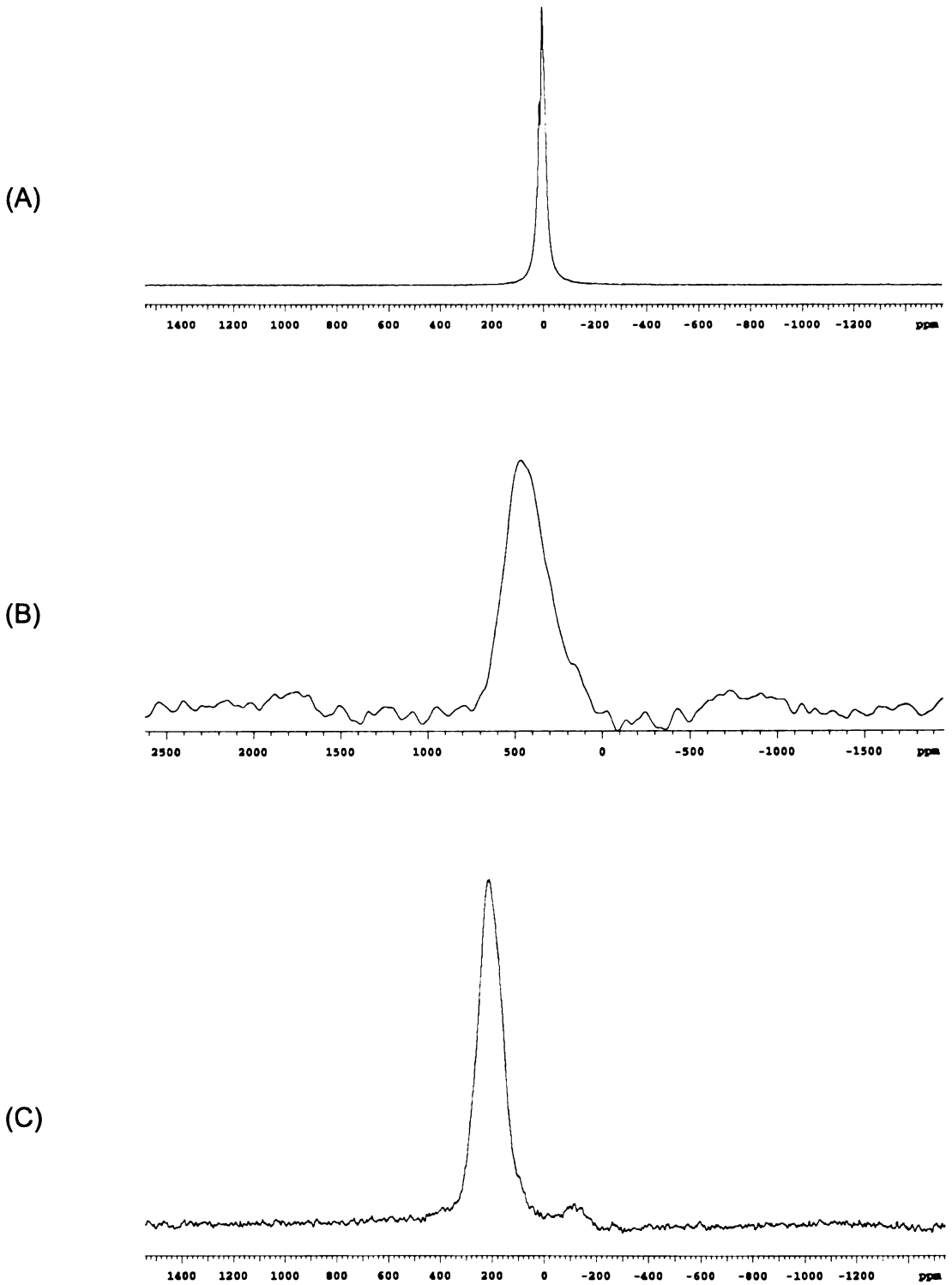

Figure 11. Room temperature ^{31}P–NMR spectra of $VOPO_4 \cdot 2H_2O$ (A) and of its Co^{2+} (B) and Na^{+} (C) metal intercalated derivatives.

account the electron and the nuclear Zeeman terms and the Fermi contact coupling, the following expression describes the isotropic shift

$$\Delta\delta = \frac{g\beta S(S+1)}{3k\gamma_N(T-\Theta)} A_s \qquad (3.4)$$

where Θ is the Weiss constant.

Equation 3.4 gives an estimation of the spin density transfer into the atom's *s* atomic orbitals. It also implies that the isotropic shift should be temperature dependent in a linear fashion. Indeed, the ^{31}P–NMR shift of the Co^{2+} intercalate displays such a linear variation with temperature (*Figure 12(D)*). Equation 3.4 was fitted to the data, where each point in the y–axis is the inverse of the difference between the observed chemical shift and the ^{31}P shift corresponding to the diamagnetic parent compound $VOPO_4 \cdot 2H_2O$. An A_s value of 6.5 MHz was obtained (Table 4) corresponding to a spin density of 6.4×10^{-4} unpaired electron per phosphorus 3*s* orbital (for a unit spin density in the phosphorus 3*s* orbital the hyperfine coupling constant is 10178 MHz[28]). However, the electronic states of phosphorus in phosphates are better described by sp^3 hybridization. Thus, the presence of one electron in an sp^3 orbital would correspond to a hyperfine coupling constant equal to one–fourth that for the free atom, resulting in an estimated transferred spin density of 2.5×10^{-3} unpaired electron, assuming the spin density resides in an sp^3 hybrid.

When the monovalent Na^+, K^+, and Rb^+ ions are intercalated within the vanadyl phosphate layered framework, half of the vanadyl centers are reduced resulting in mixed–valence compounds. Their ^{31}P–NMR spectra also display paramagnetic shifts towards low fields, but to a lesser extent than in the Co^{2+} intercalate. *Figure 11(C)* shows the room temperature spectra of the Na^+ intercalate, which consists of one resonance centered at 207 ppm. Similar peaks

(A)

(B)

(C)

(D)

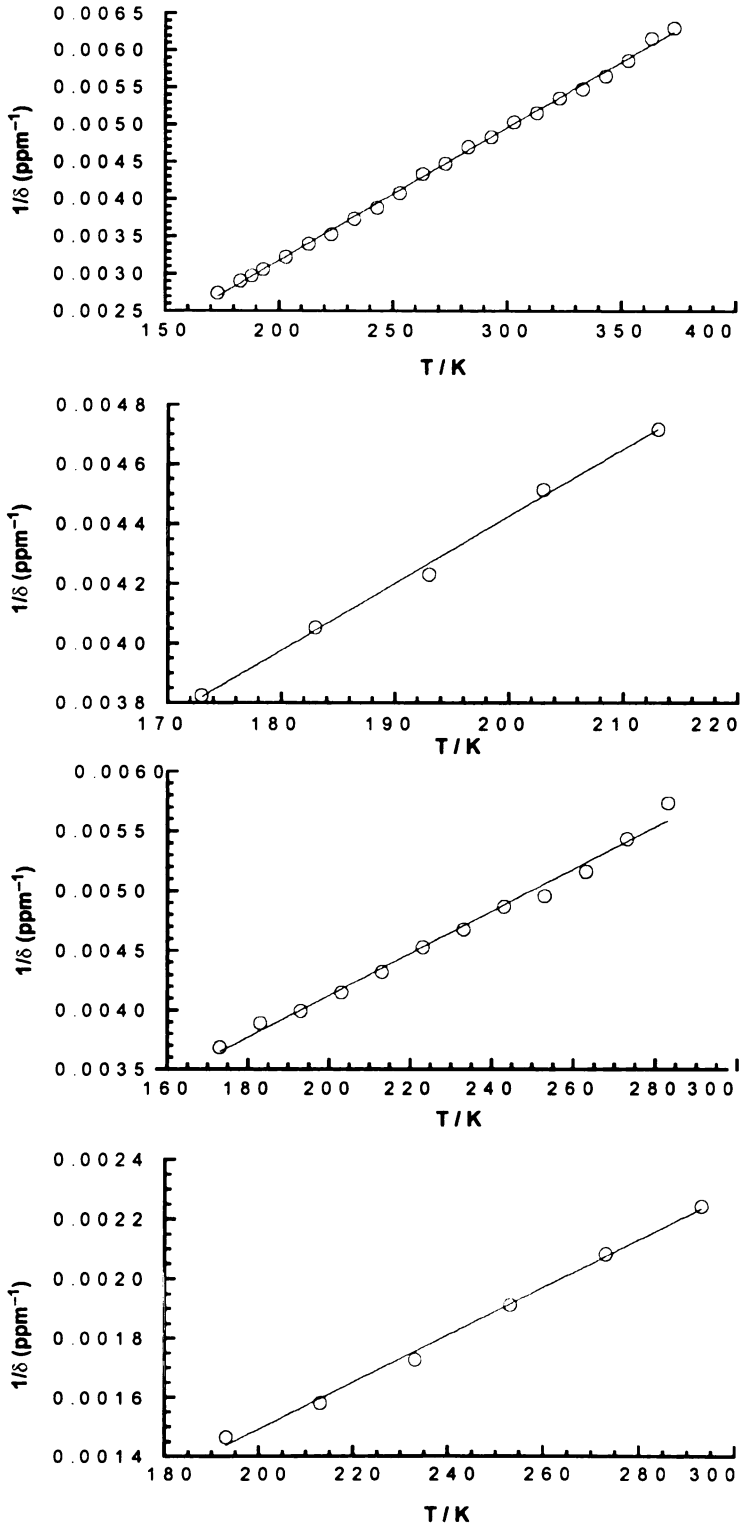

Figure 12. Temperature dependence of the inverse paramagnetic shift of Na^+ (A), K^+ (B), Rb^+ (C), and Co^{2+} (D) derivatives.

Table 4. Formula, structure and magnetic data for $A_{0.5}VOPO_4 \cdot nH_2O$

Formula & Structure			Magnetic Data			NMR Data	
A^{x+}	n	*d*–Space / Å	T_{max} / K	g_{exp}	*J/k* / K	A_{iso} / MHz	$\Delta\delta^{\alpha}$ / ppm
Na^{+}	2.0	6.57		1.96	+ 0.6	2.9	207
K^{+}	1.5	6.40		1.96	+ 0.6	2.5	
Rb^{+}	1.5	6.51		1.96	+ 0.6	2.9	165
Sr^{2+}	2.0	6.33	6.0	1.96	– 2.5		232
Co^{2}	2.0	6.71	5.5			6.5	446

[a] Values obtained at 293 K.

are displayed by the K^+, and Rb^+ derivatives (Table 4), which also show a linear temperature dependence enabling estimation of A_s (*Figure 12*). The values for the three compounds are 2.9, 2.5, and 2.9 MHz (Table 4) corresponding to spin density transferred of 2.8×10^{-4} unpaired electron per phosphorus 3*s* orbital for the Na^+ and Rb^+ intercalants. Due to the mixed valence nature of the material, every electron on a vanadyl center is exchange coupled by two phosphorus sp^3 orbitals, resulting in 5.7×10^{-4} unpaired electron per phosphorus sp^3 orbital.

A unique feature in the ^{31}P–NMR spectra of the monovalent intercalates is the splitting of the single resonance in to three peaks at low temperature. *Figure 13* displays the spectra of the Na^+ derivative in the temperature range 173 K to 233 K. Three low field peaks are observed and as the temperature is raised, they collapse to the central peak. All three lines display linear temperature dependencies indicating the paramagnetic origin of the shift. However due to the broad shape of the lines accurate determination of each resonance is a difficult task. Hence A_s values were determined only for the central peak of each compound (the problem was pronounced in the K^+ analogue and thus only five points were used to estimate the A_s value of 2.5 MHz). The small high field peak centered approximately at –150 ppm is probably due to a diamagnetic impurity[29].

Powder Susceptibility and EPR Studies. The thermal variation of the products of the molar susceptibility with temperature (χT), are given in *Figure 14(A)* for the alkali and alkaline earth derivatives. All four compounds follow the Curie–Weiss law at higher temperatures. The Curie constants of 0.358, 0.365, 0.351, and 0.355 for Na^+, K^+, Rb^+, and Sr^{2+} respectively, are all close to the spin–only value of ~0.369 (g = 1.966, determined from solid state EPR measurements), indicating good agreement between chemical analyses (given in Chapter 2) and magnetic measurements. The upturns seen in the data of the alkali intercalates

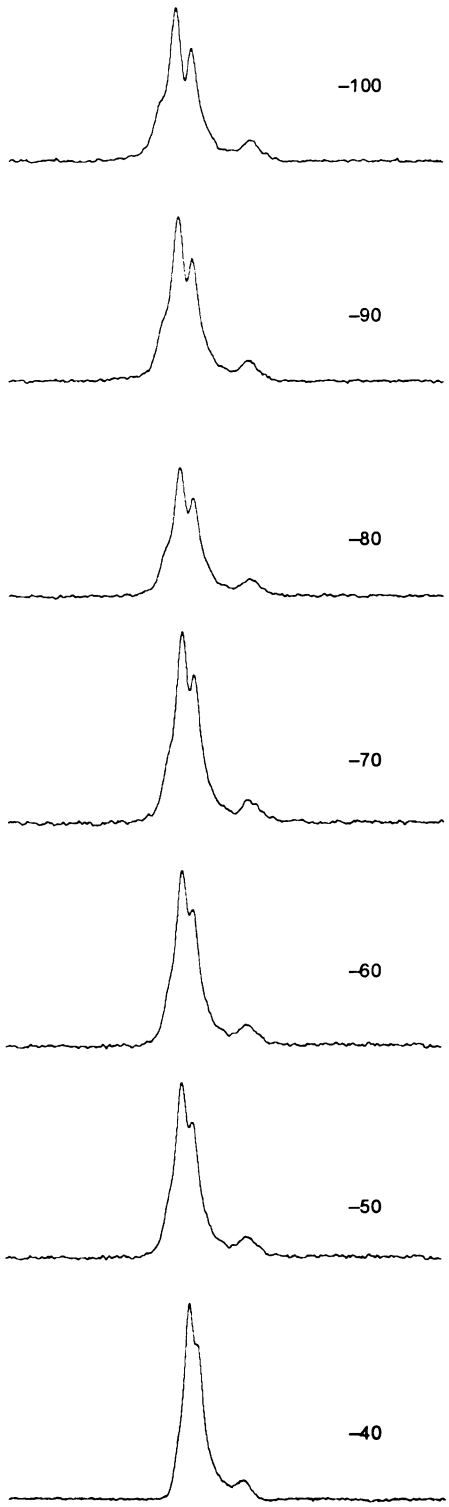

Figure 13. ^{31}P–NMR spectra of $Na_{0.5}VOPO_4 \cdot 2H_2O$ recorded at various temperatures (in C°).

(A)

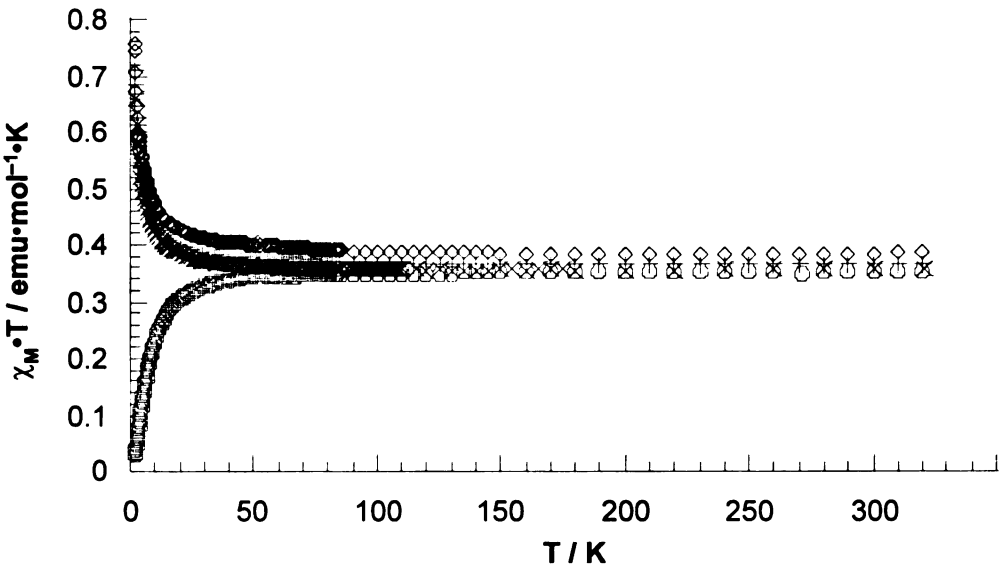

(B)

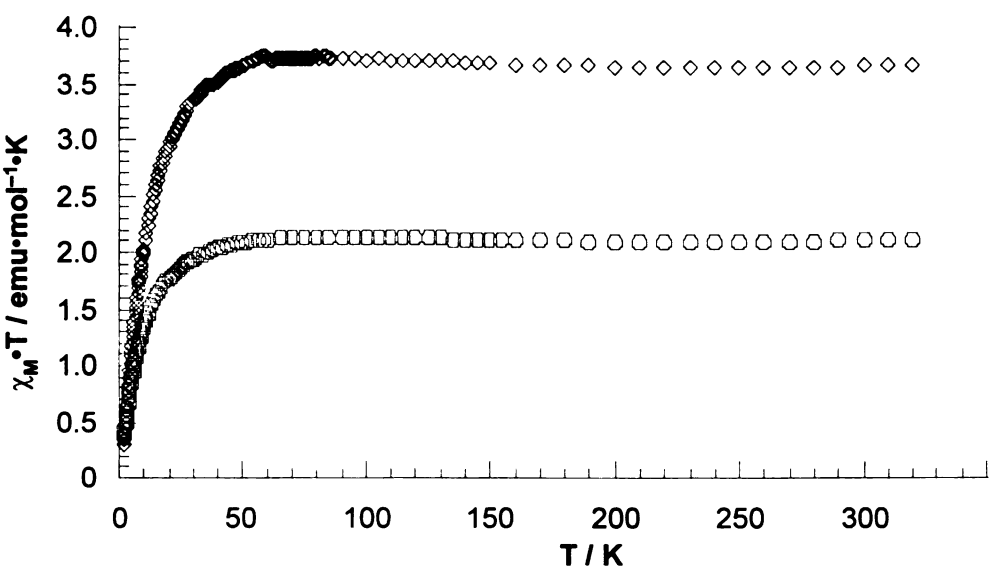

Figure 14. χT plot vs temperature of Na^+ (×), K^+ (+), Rb^+ (◊), and Sr^{2+} (o) derivatives of layered vanadyl phosphate (A). The spectrum below displays the behavior of the χT product for a two–phase (o) and a single–phase (◊) Co^{2+} derivative (B).

reveal ferromagnetic couplings in the layers, while the downturn in the alkaline earth data indicates short–range antiferromagnetic coupling. This finding is in contradistinction to earlier magnetic measurements for the Na^+ derivative, which was synthesized by the reaction of NaI with $VOPO_4 \cdot 2H_2O$ in acetone and characterized by indexing the lattice parameters from powder X–ray diffraction data[30]. Here the magnetic susceptibility was determined over a range of relatively high temperatures (T = 90 – 300 K), and weak antiferromagnetic interactions were assigned on the basis of a small negative Weiss constant. Susceptibility measurements in K^+ phases containing impurities in the form of extra intercrystalline water molecules also displayed weak antiferromagnetic behavior, but repeated measurement on different single–phase alkali intercalate samples clearly displayed the characteristic upturn in the χT data, indicative of short–range ferromagnetic interactions.

The two–dimensional structure of the $A_xVOPO_4 \cdot nH_2O$ materials is built up by interconnection of eight member rings containing two vanadium octahedra and two phosphate tetrahedra, which adopt a chair–like conformation designated as D VII (*Figure 2(B)*). Such an arrangement results in a two–dimensional magnetic lattice with each metal center participating in four D VII rings, and therefore the susceptibility data were fitted to a two–dimensional Heisenberg model for a square lattice. The expression for the molar magnetic susceptibility can be determined from a high temperature series for the quadratic layered Heisenberg ferromagnet[31] by using an isotropic exchange Hamiltonian. The following susceptibility expression was derived

$$\chi_M = \frac{Ng^2\mu_\beta^2}{4k_BT} \times \left(1 - \frac{2}{x} + \frac{2}{x^2} - \frac{1.333}{x^3} + \frac{0.25}{x^4} - \frac{0.4833}{x^5} + \frac{0.003797}{x^6}\right)^{-1} \qquad (3.5)$$

where $x = k_B T / J_{ij}$. The alkali derivatives gave values of J/k_B = + 0.6 K, while the best fit for the alkaline earth material to a high temperature series for the quadratic layer Heisenberg antiferromagnet gave J/k_B = – 2.5 K (Table 4).

Intercalation of the Co^{+2} paramagnetic ion injects one electron per vanadyl center in the layer. Different synthetic attempts produced multi– and single–phase materials, whose susceptibility properties in the form of χT plots are displayed in *Figure 14(B)*. Both compounds show the characteristic downturn in the χT product, indicative of weak antiferromagnetic interactions. Surprisingly, the electronic configuration of the Co^{2+} ion is different in the single– and the multi–phase materials. In the former the intercalated cations are high spin, since a $\mu_{eff.}$ of 5.33 was obtained from the data which compares well to the value expected for five unpaired electrons (5.73). In the latter derivative on the other hand a $\mu_{eff.}$ of 4.1 was obtained which is close to the theoretically expected value for three unpaired electrons (3.87).

No attempt was made to fit the susceptibility data in a theoretical model. Apart from the intralayer exchange interactions encountered in the other derivatives, the paramagnetic nature of the guest also raises the possibility of host–guest and guest–guest interactions. In addition, the highly symmetric coordination environment of the intercalant indicates that the orbital angular momentum is not totally quenched, further complicating the derivation of an analytical susceptibility expression since different Lánde factors should be assigned for the V^{4+} and Co^{2+} ions.

2. Layered Vanadyl *p*– or *m*–Substituted Phenyl Phosphonates (LVPh's) $VO(O_3PC_6H_4–X)•H_2O$

a. Synthesis and Characterization

Significant steps toward structural understanding are seen in the correlation of magnetic coupling with the geometrical parameters in molecular building blocks. Nowhere is this approach better illustrated than in the well–studied d^9—d^9 $Cu(\mu^2–OH)_2Cu$ dimers, in which the relationship between *J* coupling and the Cu — O — Cu angle has been mapped out in elegant detail[32]. These ideas have been extended to $VO(\mu^2\text{-}OR)_2VO$ dimers, a series with d^1—d^1 electron counts[33], and to other oxo–bridged bimetallic complexes[34,35,36]. Dimers of the $M(\mu^2\text{-}OR)_2M$ class have also served to illuminate basic electronic questions. The isostructural d^9—d^n $Cu(\mu^2\text{-}OR)_2M$ (M = VO, Fe, Ni, Cu) molecular complexes, where a dinucleating ligand template (derived from *N,N′*–(2–hydroxy–3–carboxybenzilidene)ethylenediamine) enforces the pairwise relationship,[37] have permitted examination within a unified framework of the relationship between orbital parentages and magnetic couplings. Yet a systematic understanding of the coupling between the same magnetic orbitals in an isostructural framework remains elusive. Such insight would allow the magnetic properties of materials to be analyzed in terms of fundamental chemical concepts familiar to molecular chemistry, and separate from simple geometrical issues.

Our strategy to define magnetic correlations in an isomorphic and isoelectronic family of compounds is to exploit the structural control available in self–assembled extended arrays[38,39,40,41]. In particular, the layered vanadyl phosphonates (LVPhs) $VO(O_3PC_6H_4–X)•nH_2O$, described in this section, allow structural orthogonalization of substituent variations from the magnetic network.

The LVPhs retain the key $V(OPO)_2V$ chairs of the metal intercalated vanadyl phopsphate derivatives, but permit modification of the P atom's electronic environment via variations in the pendant aryl group. Because the organic pendants project into the interlayer region, substituent variations (out–of–plane) are orthogonal, and hence structurally isolated, from the (in–plane) magnetically active V,O,P layers. Substituent effects on magnetism should then be purely due to electronic perturbations. To exploit these characteristics a series of five new substituted $VO(O_3PC_6H_4–X)\cdot nH_2O$ LVPs (X = *p*-NO_2, *m*-F, *p*-F for n = 1; *p*-Cl, *p*-CH_3 for n = 1.5) were synthesized hydrothermally by Dr. J. LeBideau[11]. These studies are complementary to the ones reported in the previous section and hence they are briefly presented in this thesis.

The X–ray structure of the prototype LVP, $VO(O_3PC_6H_5)\cdot H_2O$ (i.e. X = H above), has been reported by Jacobson and Johnson and coworkers[42]. Alternating inorganic and organic strata comprise, respectively, distorted octahedral vanadium and tetrahedral phosphorus oxide subunits, and phosphonate phenyl groups that converge in a bilayer arrangement from adjacent oxide layers. A view perpendicular to the layer plane is shown in *Figure 15*. Within the oxide layer, pairs of paramagnetic vanadyl centers are joined via chair–like $V(OPO)_2V$ links of the DV type (see *Figure 8*, Chapter 1), analogous but not similar to those discussed in the metal intercalated $VOPO_4$ systems[15]; these subunits are then stacked together, forming V=O···V=O chains. Adjacent vanadium octahedra along the chains are further connected via single O — P — O bridges, forming almost flat six–membered rings along the b–axis designated as O III (see *Figure 8*, Chapter 1).

Based on powder X–ray diffraction, IR spectra (Table 5), and TGA, the fluoro and nitro compounds (X = *p*-F, *m*-F and *p*-NO_2) are found to be isostructural with the parent (X = H). The b and c cell parameters, which describe

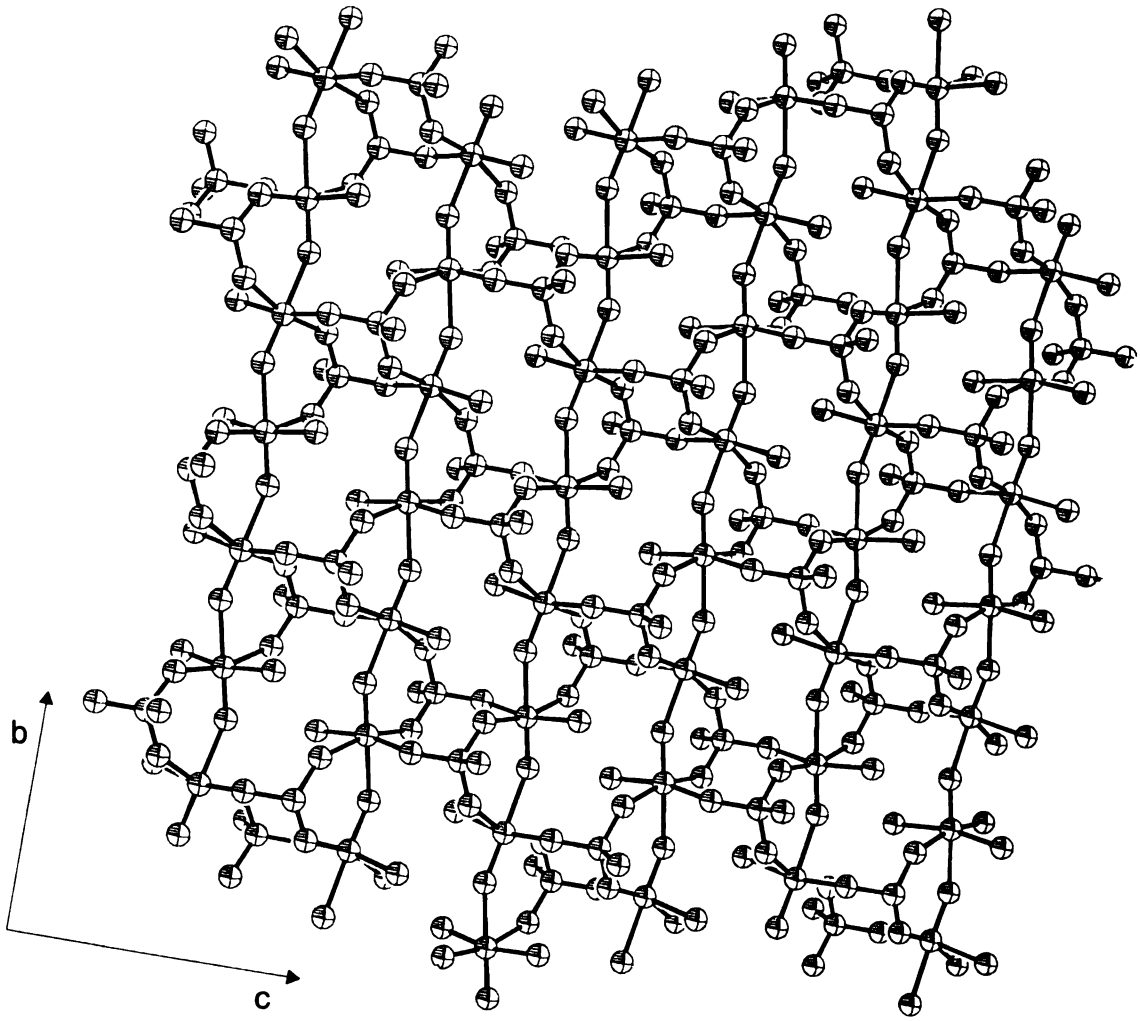

Figure 15. In–plane segment of the $VO(O_3PC_6H_4–X)\cdot H_2O$ (X = *p*-NO_2, *m*-F, *p*-F and H) structure type.

Table 5. Selected structural, vibrational and magnetic data for $VO(O_3PC_6H_4–X)\bullet H_2O$ LVPs and Hammett σ values for $C_6H_4–X$[a]

–X	C_6H_5	C_6H_4–*p*-F	C_6H_4–*m*-F	C_6H_4–*p*-NO_2
a (Å)	28.50	28.59(3)	28.60(1)	30.50(5)
b (Å)	7.18	7.16(1)	7.15(1)	6.98(1)
c (Å)	9.42	9.45(1)	9.44(1)	9.55(2)
β (°)	97.1	97.6(1)	97.5(1)	97.1(1)
d-spacing (Å)	14.14	14.17	14.18	15.13
$\nu_{(V=O)}$ (cm^{-1})	883	885	882	895
$\nu_{(P—O)}$ (cm^{-1})	1046	1044	1043	1051
C ($emu\bullet Kmol^{-1}$)[a]	0.360	0.359	0.368	0.374
Θ (K)[a]	–2.3	–1.1	–3.5[d]	–0.1
μ_{eff} (μ_B)[a]	1.70	1.69	1.72	1.73
T(χ_{max}) (K)	7	5.5	4.0	0
J/k (K)[b]	–5.5	–4.5	–3.3	0
σ[c]	0.0	0.15	0.34	0.81

[a] Determined over the range T = 50-100 K. [b] From Bleaney-Bowers fit (eq (2)) to data over the range T = 2-100 K. [c] Substituent constants from March, J. "Advanced Organic Chemistry," 4th Ed., John Wiley & Sons, New York, 1992. [d] This low value is inaccurate due to curvature in the $1/\chi$ vs. T plot in the 50-100 K temperature region of interest.

the inorganic layer, are similar as expected for an isostructural LVP series. It is the a dimension and hence the interlayer (or d) spacing that varies due to X substitution on the phenyl ring; d spacings derived from the a cell parameters of Table 5 are 14.14, 14.17, 14.18, and 15.13 Å for X = H, *p*-F, *m*-F, and *p*-NO_2, respectively. Infrared spectra for the four are qualitatively similar, with sharp V=O and P — O bands that show small variations in stretching frequencies.

There are three different structural types of the vanadyl phosphonate materials, each with a different water content (n = 1.0, 1.5, 2.0)[42,43]. Thus, besides the structurally characteristic IR spectra, and X–ray powder diffraction data, the water content provides additional definitive support for structural assignments. The TGA results of 1 H_2O per formula unit further solidify the assignment of the *p*-F, *m*-F, and *p*-NO_2 phenylphosphonates to the same structural class as the parent $VO(O_3PC_6H_5) \cdot H_2O$.

Thermogravimetric analysis on the remaining two LVP derivatives (where X is Cl and CH_3) indicates the presence of 1.5 H_2O per formula unit. Taking also into consideration IR data, it appears that these compounds are isostructural with the alkyl phosphonates $VO(O_3PR) \cdot 1.5H_2O$ (R = CH_3, C_2H_6, n–C_3H_7) series. From a partial structure solution of $VO(O_3PCH_3) \cdot 1.5H_2O$[43], it was concluded that these compounds have the same layered framework as $VO(HOPO_3) \cdot 0.5H_2O$[4(a)], whose intralayer structure is depicted in *Figure 16*. This complex structural framework consists of chains along the *a* direction where $V(\mu^2\text{-}O)_2V$ dimers of the D II type are alternating with boat–like eight–membered rings of the D III type (see *Figure 7*, Chapter I). Fusion of the chains to a two–dimensional network is accomplished by generation of tapes of eight–membered rings of the D V type. The aromatic pendants are incorporated within the interlayer space.

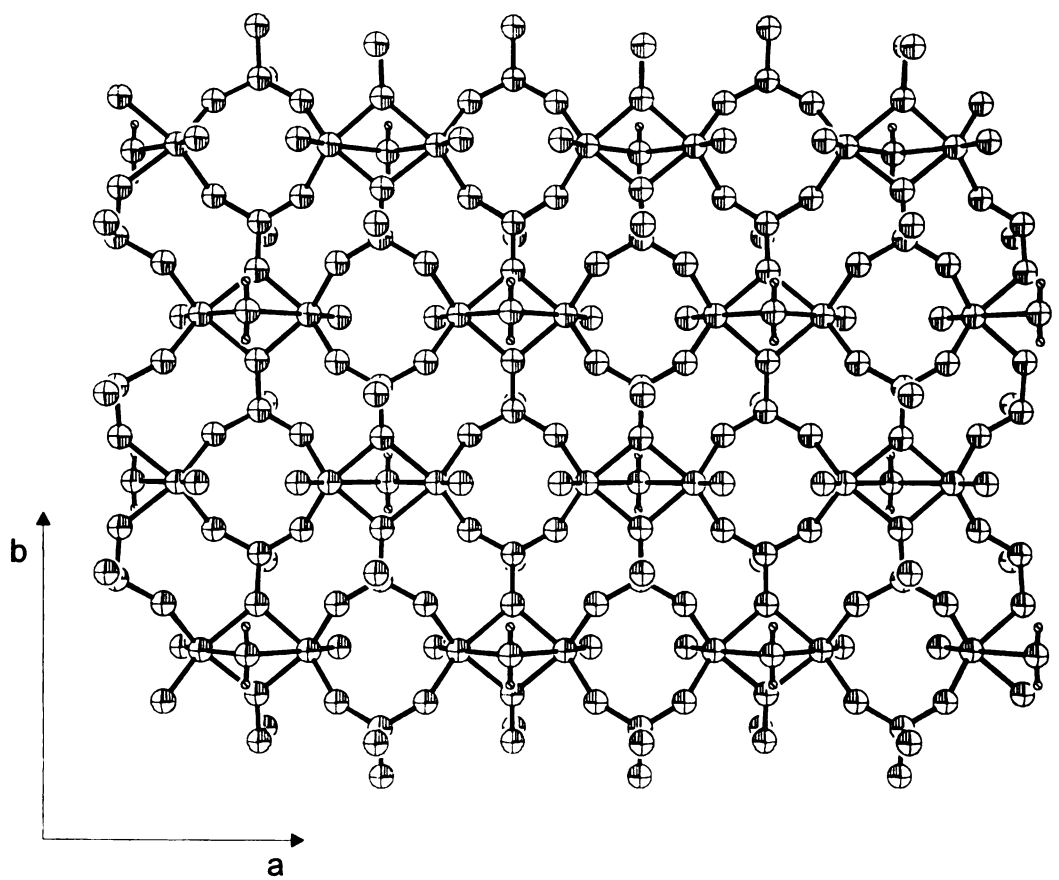

Figure 16. In-plane segment of vanadyl hydrogenphosphate hemihydrate, $VO(HPO_4)\cdot 0.5H_2O$, which is isostructural with the $VO(O_3PC_6H_4\text{–}X)\cdot 1.5H_2O$ (X = Cl, CH_3) as described in the text.

b. **Magnetic Properties**

Powder Susceptibility Studies. *Figure 17* shows the temperature dependent magnetic susceptibilities for the four LVPs with X = *p*-NO_2, *m*-F, *p*-F, and H. The LVP (X = *p*-NO_2) is a simple paramagnet, exhibiting Curie behavior with a negligible Weiss constant of – 0.1 K. Conversely, the downturns seen in the data for X = H, *m*-F, and *p*-F indicate intralayer antiferromagnetic couplings between the V^{4+} centers. Although no indication of long range magnetic ordering can be traced down to 2 K, the broad paramagnetic maximum observed in *Figure 17* for these compounds is characteristic of low dimensional antiferromagnetic interactions. The magnetic data for the four compounds are summarized in Table 5. The values of the Curie constants C at high temperatures are all close to the spin–only value of 0.367(4) indicating good agreement between chemical analyses[11] and magnetic measurements. These quantities were obtained from the Curie expression (eq 3.6), where *N* is Avogadro's number, μ_B is the Bohr magneton, and *k* is the Boltzmann constant), evaluated at the high

$$C = \frac{Ng^2\mu_B^2}{3k} S(S+1) = \chi T \qquad (3.6)$$

temperature limit, using the value of g = 1.98(1) determined from the solid state EPR measurements for the four LVPs. The four EPR spectra were essentially identical; a representative example, shown in *Figure 18*, is broadened and symmetrical like those seen in the d^1 dimer–containing $VOHPO_4$ layers[7] and related systems[44,45].

Owing to the highly coupled network within the layers (*Figure 15*), a complete model for the magnetism in these systems is difficult to derive. Nevertheless, the dominant magnetic subunits in these systems are originally thought to be the chair–like $V(OPO)_2V$ exchange pathways of the DV type

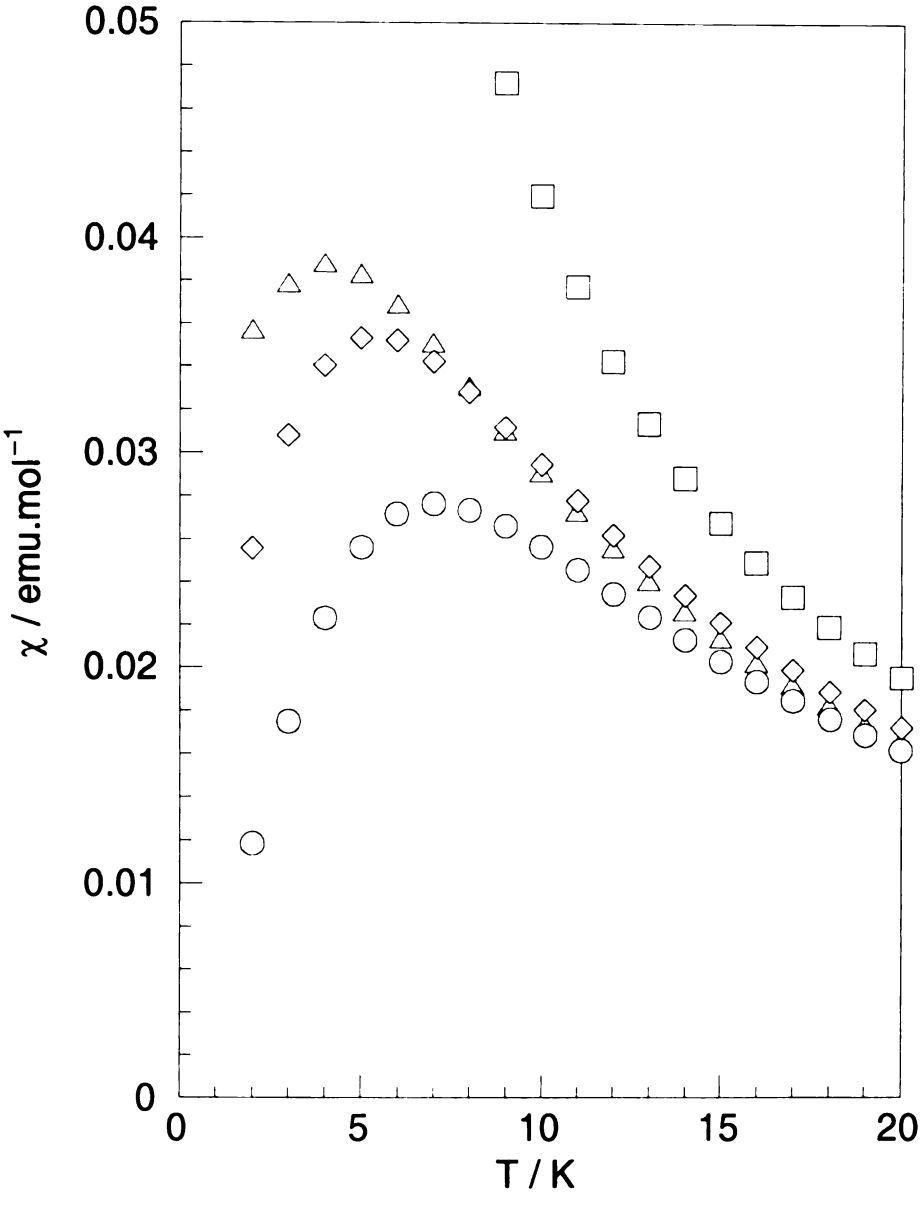

Figure 17. Plot of χ vs. T for $VO(O_3PC_6H_4–X)\cdot H_2O$ (X = *p*-NO_2 (square), *m*-F (triangle), *p*-F, (diamond), and H (circle)) showing the broad paramagnetic maxima for the latter three.

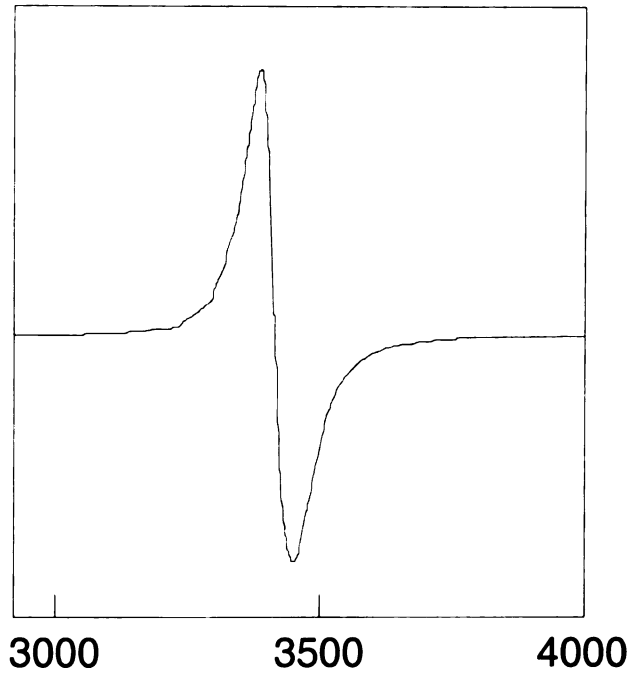

Figure 18. EPR spectrum of $VO(O_3PC_6H_4–p\text{-}NO_2)\cdot H_2O$ (the microwave frequency was 9.450 GHz and g = 1.98).

described above[11]. Thus, to a first approximation using a Heisenberg Hamiltonian $H = -2JS_iS_j$, the magnetic interaction was estimated with a Bleaney-Bowers model for dimers,[46]

$$\chi = (1-f)\left\{\frac{Ng^2\mu_B{}^2}{kT} \bullet \frac{1}{3+exp(-2J/kT)}\right\} + f\frac{C}{T} \qquad (3.7)$$

where *f* is the amount of paramagnetic impurities taken as isolated V^{4+} ions, and g = 1.98. The *J/k* values of Table 5 were obtained from fits of eq 3.7 with f = 0.05, 0.1, and 0.0 for X = H, *p*-F, and *m*-F, respectively.

The X = Cl and CH_3 derivatives have magnetic properties substantially different than those of the four LVP's mentioned above. Variable temperature susceptibility data for these compounds show antiferromagnetic downturns, with $T(\chi_{max})$ values at 54 (X = *p*-Cl) and 58 K (X = *p*-CH_3), significally higher than those seen in *Figure 17*, and consistent with the known stronger coupling ability of the $V(\mu^2\text{-}O)_2V$ dimer magnetic pathway[3]. The Bleaney–Bowers–derived J/k values (– 42 and – 48 K, respectively) for these new arylphosphonate systems are in the same range as those found in the alkylphosphonate cases (– 43 to – 52 K for simple alkyl groups)[43] and in the vanadyl hydrogenphosphate hemihydrate (– 43 K)[7].

3. Alcohol Intercalated Layered Vanadyl 2–Napthylphosphonates, $VO(O_3PNp)(H_2O)\bullet nROH$

a. Synthesis and Characterization

This homologous series of layered materials, which are members of the general family of the $VO(O_3PR)(H_2O)_2$ structural type[47], was prepared by following the methodology developed by Jacobson and Johnson[48]. Finely ground

V_2O_5 is added to the corresponding alcohol solution of 2–napthylphosphonic acid, along with a catalytic amount of 1 M HCl[49]. The two–phase mixture is heated with stirring for one to three days. During this period, the yellow–brown V_2O_5 is consumed in the reaction leaving its place to the blue vanadyl phosphonate solid, which is recovered by filtration[12].

Four different alcohols, namely ethanol, butanol, hexanol, and octanol, were intercalated within the vanadyl naphthylphosphonate host. In addition, an alcohol free derivative was synthesized by heating the ethanol or butanol intercalated analog. The purity of these materials was determined by PXRD methods, where single narrow peaks, mainly attributed to the 00l diffraction lines, were observed. Upon the alcohol intercalation, adjacent layers are mechanically jacked with a d–spacing expansion ranging from 12.10 Å in the alcohol free material to 20.83 Å in the octanol intercalated derivative. The interlayer spacing is determined by the first diffraction line, which as shown in *Figure 19* varies linearly with the number of alcohol's carbon atoms. A slope of 1.06 Å per methylene unit is obtained indicating that the naphthalene pendants adopt an interdigitated arrangement[48,50].

Interdigitation of the organic pendant is possible only with a relatively "open" intralayer topology, where adjacent phosphorus sides are relatively distant from each other. Although the actual structure of the $VO(O_3PR)(H_2O)_2$ type is not known, indirect evidence from magnetic and thermogravimetric data along with the unit cell determination from powder X–ray data[51], suggest a structure similar to that of newberyite[52], $MgHPO_4 \cdot 3H_2O$. *Figure 20* displays the intralayer structure of $VO(O_3PR)(H_2O)_2$ generated by using the lattice parameters from ref. 51 and the fractional atomic coordinates of newberyite[52]. The inorganic framework consists of octahedrally coordinated vanadium atoms where the axial positions are occupied by a vanadyl oxygen and a water molecule, while

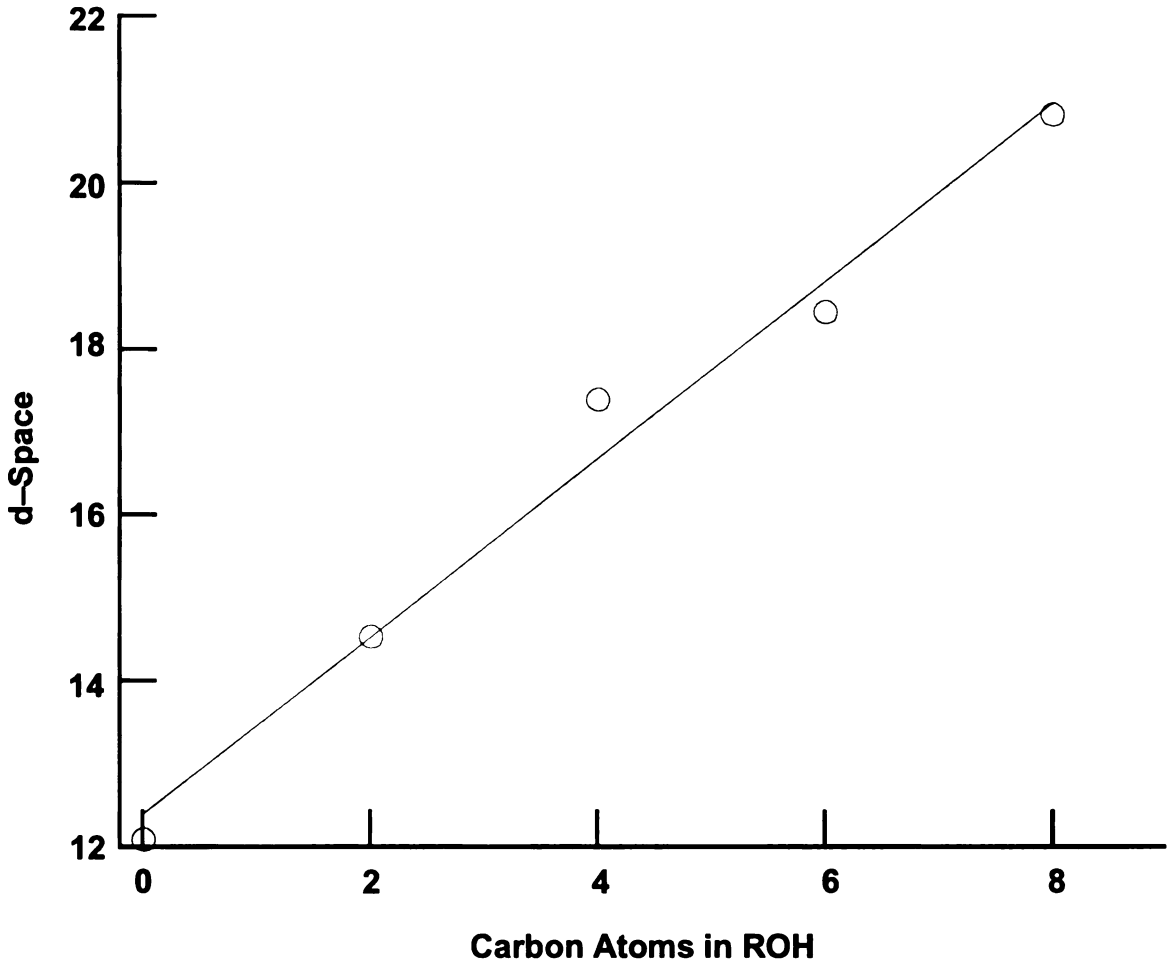

Figure 19. Interlayer spacing of $(VO)(O_3PNp)(H_2O)\bullet nROH$ plotted as a function of the carbon atoms in the alkyl group R.

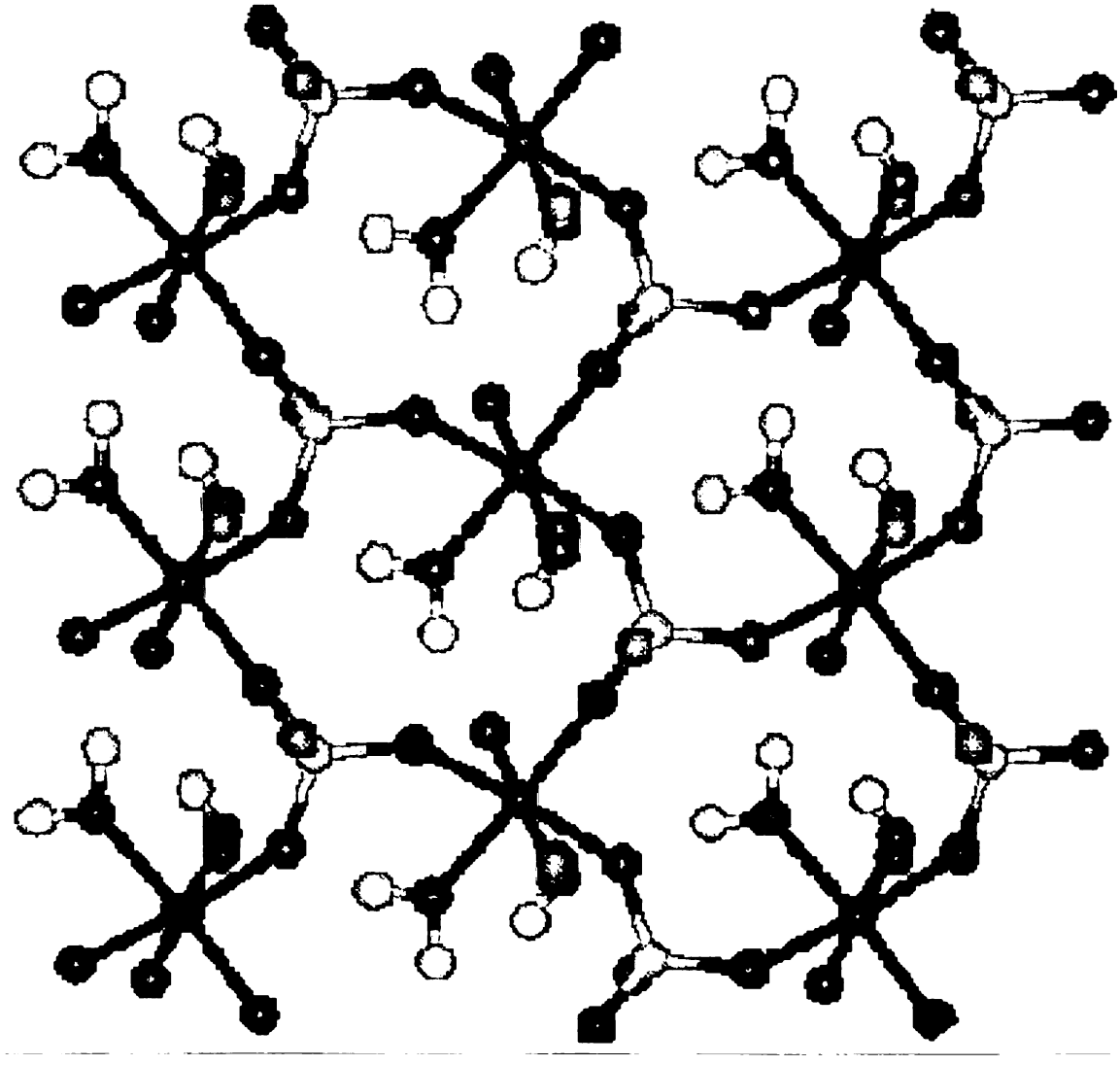

Figure 20. Intralayer structure of $VO(O_3PNp)(H_2O)\cdot nROH$.

coordination in the equatorial plane is furnished by three oxygen atoms belonging to different phosphonate groups and a water molecule. As a consequence of this arrangement, three vanadium octahedra and three phosphorus tetrahedra form medium–sized closed–loops where the equatorial water molecules are pointing in. The axial water molecules on the other hand, are placed within the interlayer space and upon alcohol intercalation are readily substituted. This process is reversible and has been thoroughly utilized for the synthesis of host–guest materials[48,49].

Thermogravimetric analysis (TGA) on the $VO(O_3PNp)(H_2O)\bullet nROH$ homologous series, supports the observation of Johnson and coworkers[53] that the vanadyl 2–napthylphosphonate belongs to this structural type. The TGA plots are depicted in *Figure 21*, for ethanol, butanol, hexanol, and octanol. The ethanol and butanol intercalated derivatives display a two–stage weight loss, with the second stage starting at approximately 155 C°. The first stage corresponds to the removal of the intercalated alcohol which weakly coordinates to the vanadium axial side. The second one is attributed to the loss of the intralayer water, which complements the vanadium equatorial plane. Although not so distinctive due to the increased boiling point of the intercalant alcohol, the other two derivatives also display a step–wise TGA plot, with the second stage starting at approximately 155 C°, as indicated by the arrows in *Figure 21*.

The presence of two well–resolved steps in the TGA of the butanol derivative, enabled the accurate determination of the water and butanol content. Solution of two quadratic equations resulted in values of 0.9 water and 0.7 butanol molecules per formula unit. For the rest of the derivatives, a water molecule content of 1.0 was assumed in order to determine the amount of intercalated alcohol, which varies from 0.7 to 0.9 (*Table 6*) for these single–phase materials in accordance with recent observations[53].

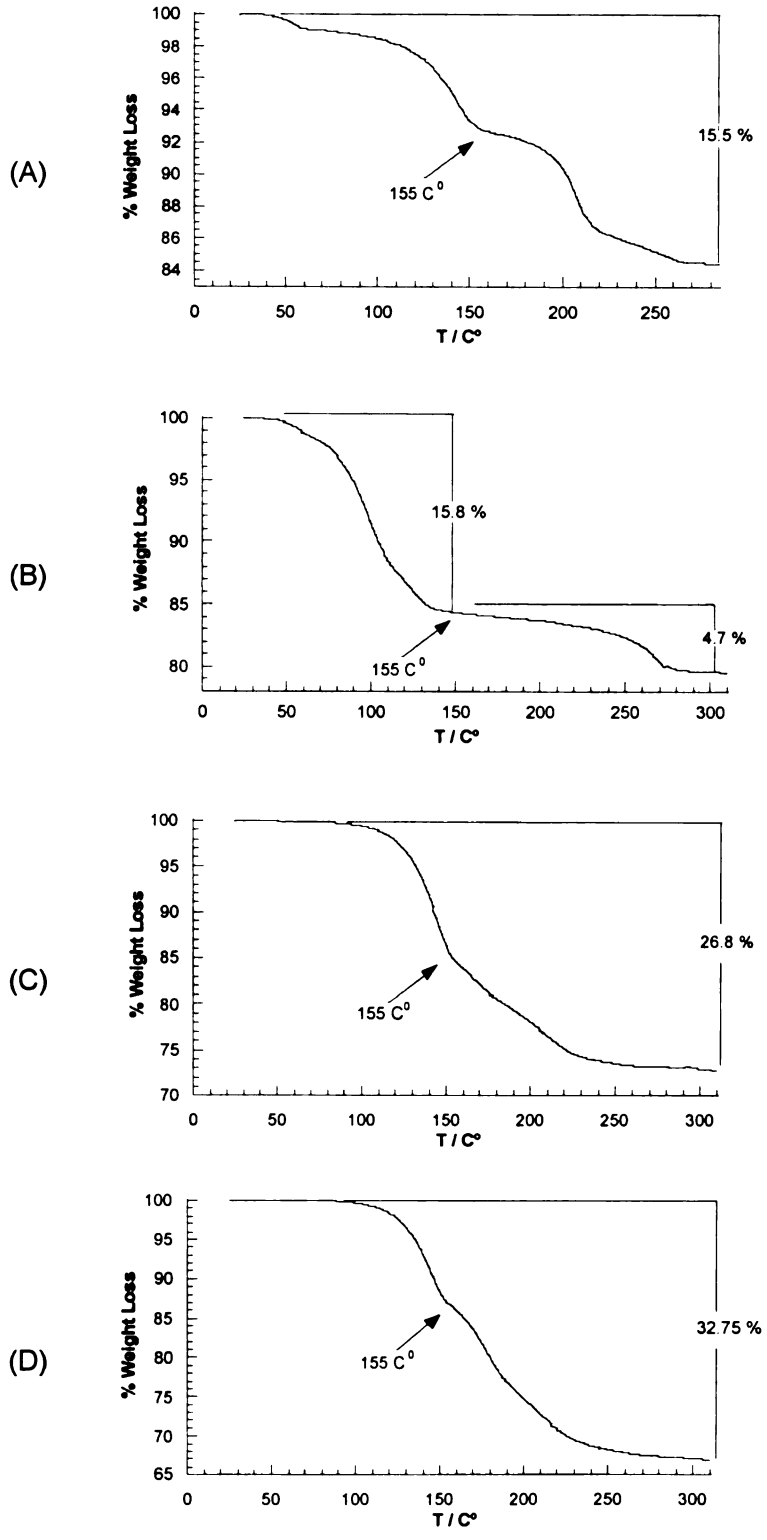

Figure 21. Thermogravimetric analysis plots of the $(VO)(O_3PNp)(H_2O)\bullet nROH$ homologous series, for ethanol (A), butanol (B), hexanol (C), and octanol (D). The arrow indicates the temperature where removal of the equatorial molecules is starting to take place.

Table 6. Formula, structure, magnetism and emission data for $VO(O_3PNp)(H_2O)\bullet nROH$

Formula & Structure			**Magnetic Data**			**Emission Data**
ROH	n	*d*–Space / Å	T_{max} / K	g_{exp}	J/k / K	λ_{max} / nm
None	0	12.10	3.8	1.961	– 1.6	405 (excimer)
Ethanol	0.7	14.54	3.8	1.961	– 1.6	377 (monomer)
Butanol	0.7	17.40	3.8	1.961	– 1.6	378 (monomer)
Hexano	0.8	18.45	3.8	1.961	– 1.6	377 (monomer)
Octanol	0.9	20.83	3.8	1.961	– 1.6	379 (monomer)

b. Magnetic Properties

Powder Susceptibility Studies. The magnetic properties of the $VO(O_3PNp)(H_2O)\cdot nROH$ homologous series were determined by powder susceptibility and EPR measurements. All five compounds exhibited identical magnetic behavior, and hence only the susceptibility of the hexanol intercalate is plotted vs temperature in *Figure 22*. The downturn seen in the susceptibility data indicates intralayer antiferromagnetic couplings between the V^{4+} centers. Although no indication of long range magnetic ordering can be found down to 2 K, the broad paramagnetic maximum centered at 3.8 K for these compounds is characteristic of low dimensional antiferromagnetic interactions.

Close examination of the layered structure (*Figure 20*) reveals that adjacent vanadyl centers are joined by single phosphonate bridges. This bridging mode corresponds to the M II type of exchange pathways displayed in *Figure 7* Chapter I. Taking into consideration the structural intralayer features the data were analyzed by using a two–dimensional Heisenberg model for a square lattice. The terms of the series are taken from Lines[54] yielding the following susceptibility expression

$$\chi_M = \frac{Ng^2\mu_\beta^2}{4k_BT} \times \left(1+\frac{2}{x}+\frac{2}{x^2}+\frac{1.333}{x^3}+\frac{0.25}{x^4}+\frac{0.4833}{x^5}+\frac{0.003797}{x^6}\right)^{-1} \qquad (3.8)$$

The experimental data produce a satisfactory fit to equation (3.8) by using a value of $J_{ij}/k_B = -1.6$ K. These results along with structural and emission data[55] are collected in Table 6.

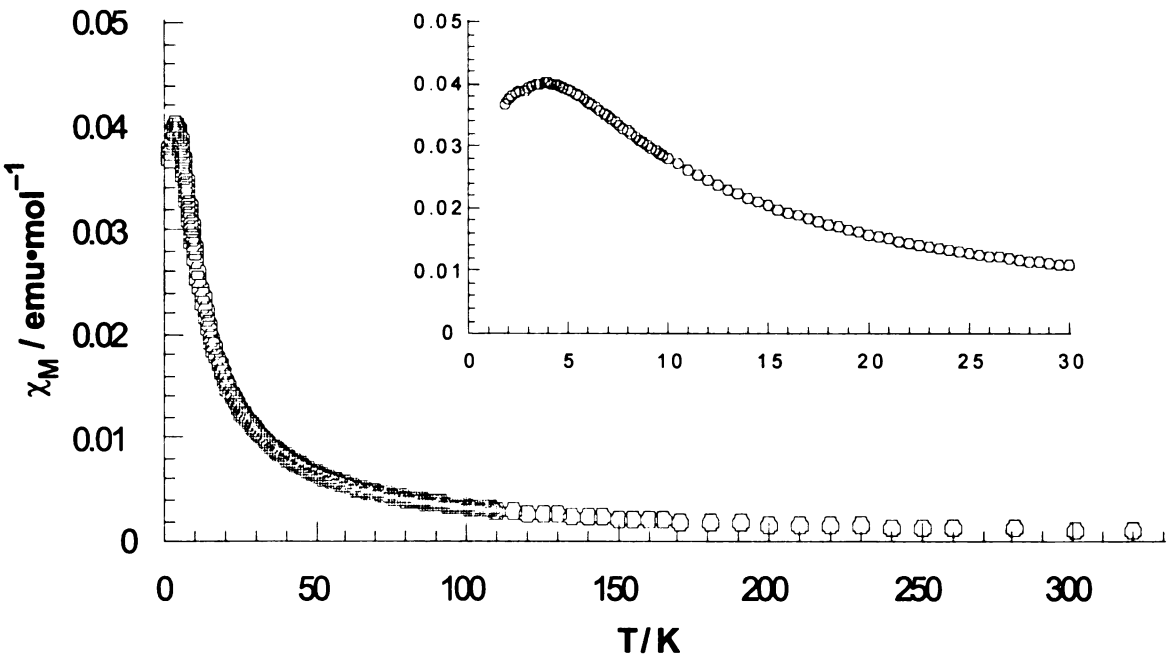

Figure 22. Thermal variation of the molar susceptibility of $VO(O_3PNp)(H_2O)$•0.7HexOH. The inset displays the maximum observed in the susceptibility, typical of low–dimensional antiferromagnetic behavior.

C. Discussion

Our studies on layered vanadyl phosphates and phosphonates have covered a wide range of structural environments. Interconnection of vanadium octahedra and phosphorus tetrahedra via various linking modes results in complex intralayer environments. The inner structure of the layers is influenced by the steric and electronic requirements of the phosphate/phosphonate units. The common building blocks of the intralayer lattice were identified by Villeneuve and coworkers[3,7], and all structural descriptions discussed in the previous sections were based upon their classification. Hence magnetostructural correlations presented below, will be derived by recognizing these structural units as potential exchange pathways and by estimating their relative contribution to the overall magnetic properties.

In Table 7 the layered vanadyl phosphates and phosphonates utilized in this study along with related materials are categorized to four structural types (types 1, 2, 3, and 4) according to the nature of the intralayer connectivity. The structural building blocks of each type are identified and the magnetic properties (in the form of the exchange constant *J/k*) are also reported. The common feature shared by all the vanadyl phosphates and phosphonates gathered in Table 7 is their layered character. The interlayer volume is filled by intercalated ions and water molecules (vanadyl phosphates), or by organic pendants (vanadyl phosphonates). The packing arrangement of these groups is accomplished according to their stereochemical demands, and intralayer lattices are then built up around the interlayer space. For example, although the fluoro– and nitro–substituted phenylphosphonates are isostructural to the parent vanadyl phenylphosphonate monohydrate[11], para–substitution by the bulky methyl– and chloro–constituents resulted in a change to a more open intralayer structure,

Table 7. Structural Types of Layered Vanadyl Phosphates and Phosphonates

Structural Type	Building Blocks	Examples	J/k / K
Type 1	M II	$Na_{0.5}VOPO_4 \cdot 2H_2O$	+ 0.6
		$K_{0.5}VOPO_4 \cdot 1.5H_2O$	+ 0.6
		$Rb_{0.5}VOPO_4 \cdot 1.5H_2O$	+ 0.6
	D VII	$Sr_{0.5}VOPO_4 \cdot 2H_2O$	– 2.5
		$VOHPO_4 \cdot 4H_2O$	– 4.7
		β–$VOHPO_4 \cdot 2H_2O$	– 5.0
		α–$VOSO_4$	+ 1.5
Type 2	O III	$VO(O_3PC_6H_5) \cdot H_2O$	– 5.5
		$VO(O_3PC_6H_4$–*p*-F)$\cdot H_2O$	– 4.5
	D V	$VO(O_3PC_6H_4$–*m*-F)$\cdot H_2O$	– 3.3
		$VO(O_3PC_6H_4$–*p*-$NO_2) \cdot H_2O$	0
		α–$VOHPO_4 \cdot 2H_2O$	– 23.0
Type 3	D II	$VO(O_3PC_6H_4$–*p*-$CH_3) \cdot 1.5\,H_2O$	– 48.0
		$VO(O_3PC_6H_4$–*p*-Cl)$\cdot 1.5\,H_2O$	– 42.0
	D III	$VOHPO_4 \cdot 0.5H_2O$	– 43.0
		$VO(O_3PCH_3) \cdot 1.5\,H_2O$	– 43.8
	D V	$VO(O_3PCH_2CH_3) \cdot 1.5\,H_2O$	– 51.6
		$VO(O_3P\,(CH_2)_2CH_3) \cdot 1.5\,H_2O$	– 52.0
Type 4	M II	$VO(O_3PNp)(H_2O) \cdot nROH$	– 1.6

similar to that of vanadyl alkyl phosphonates ($(CH_3(CH_2)_nPO_3)VO$ with n = 0, 1, and 2[43]). The more sterically demanding naphthylphosphonates are accommodated in even more open vanadyl phosphonate layers along with two water molecules per formula unit.

The magnetic properties of vanadyl phosphates and phosphonates differ from one structural type to the other. Both ferromagnetic and antiferromagnetic interactions are observed in type 1 materials (Table 7), while antiferromagnetism is the dominant effect in the other structural types. The strongest and the weakest antiferromagnetic couplings are observed in type 3 (table 7) and type 4 Table 7) compounds respectively, while in type 2 (table 7) materials a noticeable difference in the magnitude of the effect is perceived, with the exchange coupling in α–$VOHPO_4 \cdot 0.5H_2O$ being much stronger than that of the $VO(O_3PC_6H_4–X) \cdot H_2O$ series. Attempts to understand the magnetic properties in layered vanadyl phosphates and phosphonates must incorporate geometrical and electronic variables.

The first concern regarding the magnetic properties of these systems is whether exchange interactions are feasible among neighboring layers. Recent literature results[56] suggest that variation of the interlayer distance does not modify magnetic properties of layered metal phosphonates. To further address this question we have undertaken the investigation of the magnetic properties of a series of layered vanadyl naphthylphosphonate dihydrates. Substitution of one water molecule by alkanols provides the means to mechanically jack the layers apart, increasing the interlayer space without altering the intralayer environment. Our results confirm the literature observation, since all five compounds studied (covering a d–space range of 12.1 to 20.8 Å) displayed identical magnetic behaviour (Table 6). Hence for type 2, 3, and 4 materials where the interlayer space is within the studied range, the magnetic properties are solely due to

intralayer effects. Type 1 materials on the other hand display much smaller d–spacings. Nonetheless, since no evidence of three–dimensional magnetic order was traced down to 2 K, their magnetic behavior is also considered to originate from intralayer coupling.

The main factor responsible for the wide range of magnetic properties observed in layered vanadyl phopsphates and phosphonates should therefore be the nature of the intralayer connectivity. In order to evaluate the effect of geometrical distortion of individual building blocks and potential exchange pathways in the magnitude and sign of the exchange coupling, the role of the O — P — O links as spin conductors has first to be established. Recent literature work[5,17], with the exception of one study[57] supports the role of these diamagnetic linkages as valuable exchange pathways. Our own ^{31}P–NMR results provide additional evidence for the above hypothesis. The large isotropic shifts observed in the metal intercalated vanadyl phosphate series and their linear temperature dependence suggest the presence of finite spin density on phosphorus atomic *s* or molecular sp^3 orbitals. This spin density is identical among the mixed–valence alkali metal derivatives, where ferromagnetic interactions of the same magnitude are observed, while is almost double in the Co^{2+} derivative, where each vanadium site bears an unpaired electron. This difference in spin density is translated to a larger isotropic ^{31}P–NMR shift for the latter derivative.

The paramagnetic shifts of vanadyl phosphates and phosphonates containing only V^{4+} metal sites differ widely, covering a range of almost 2000 ppm. Such a large difference should be associated to the amount of spin density on the phosphorus orbitals. Irrespectively of the spin transfer mechanism (spin polarization versus dipolar coupling or both), the magnitude of the paramagnetic shift should correlate with features of the potential exchange pathways. In *Figure 23* the room temperature shifts of five layered vanadyl phosphates and

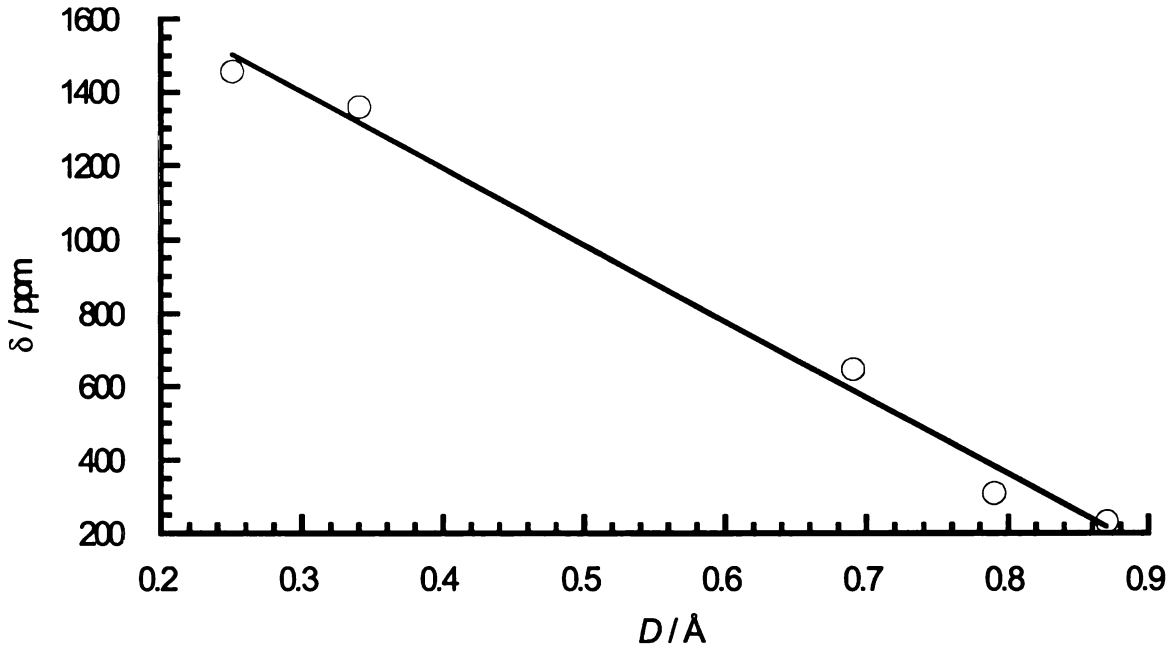

Figure 23. Plot of the isotropic ^{31}P–NMR chemical shift of selected vanadyl phosphates/phosphonates versus the phosphorous displacement *D* from the basal vanadyl plane.

phosphonates ($Sr_{0.5}VOPO_4 \cdot 2H_2O$, $VOHPO_4 \cdot 4H_2O$, β–$VOHPO_4 \cdot 2H_2O$, $VO(O_3PC_6H_5) \cdot H_2O$, and α–$VOHPO_4 \cdot 2H_2O$) are plotted against the displacement *D* in Å of the phosphorus atom from the vanadium basal plane (defined as the best plane passing through the four equatorial atoms). Small values of *D* (like those of $VO(O_3PC_6H_5) \cdot H_2O$, and α–$VOHPO_4 \cdot 2H_2O$), correlate with large ^{31}P–NMR isotropic shifts (and thus larger spin density on phosphorus orbitals). As *D* values approach the 1 Å displacement of phosphorus from the basal plane observed in chair–like building blocks of the D VII type, the isotropic chemical shift decreases significantly.

It should be pointed out that although a linear correlation is obtained, the usefulness of the plot is rather qualitative. Data were incorporated into it according to ^{31}P–NMR data availability, the presence of one major building block with the potential to act as an exchange pathway, and by considering the shortest value of *D* when two or more were available. Nevertheless *Figure 23* establishes that the magnitude of the paramagnetic chemical shift correlates to a geometric attribute of an exchange pathway and it further solidifies the hypothesis that O — P — O linkages are essential elements of spin communication.

Viable exchange pathways through the phosphate and phosphonate bridges therefore involve finite amounts of spin density on phosphorus orbitals. These orbitals should also have appropriate energies in order to sufficiently interact with the metal based *d*–orbitals. Theory predicts[58] that electron–withdrawing substituents, positioned in an influential manner to the structural core of the exchange pathway, will decrease the magnitude of the exchange interaction (Chapter 1) by tuning the energy levels of the phosphorus orbitals. This effect is demonstrated experimentally in the aryl phosphonate systems $VO(O_3PC_6H_4–X) \cdot H_2O$ (X = *p*-NO_2, *m*-F, *p*-F, -H), where the O — P — O pathway

dominates exchange between vanadyl centers. The magnetic coupling responds to variations in Hammett σ values which, in turn, reflect the electronic environment at the P atom (Table 5). Therefore, turning–off of the magnetic exchange in $VO(O_3PC_6H_4-NO_2)\cdot H_2O$ does not imply the absence of spin density on phosphorus orbitals; ^{31}P–NMR data on this compound consist of a low–field single line centered at 1421 ppm at room temperature.

The Hammett σ constant is defined via the acidity of the benzoic acids X–C_6H_4–COOH with X in the meta or para position on the phenyl ring. The value of σ for the *p*-NO_2 group, for instance, is then the difference in pK_a (acid strength) between parent and substituted benzoic acids [i.e. $\sigma = pK_a(X = H) - pK_a(X = p\text{-}NO_2)$]; the *p*-$NO_2$–benzoic acid is more readily ionized (i.e. stronger, pK_a lower) due to the electron accepting ability of the NO_2 group, so σ is positive for such electron withdrawing groups. The σ constants thus reflect composite resonance and sigmatropic electron withdrawal along with dipole changes in the molecules. As seen in *Figure 24*, a plot of J/k vs. σ is monotonic; for a simple linear fit, a slope of 6.8 is obtained. Other properties that depend on the electronic environment of phosphorus – specifically, the pK_a values in arylphosphonic acids[59] and ^{31}P–NMR chemical shifts in the related arylphosphonic dichlorides[60] – show linear correlations with σ. A trend to weaker coupling with increasing σ seems sensible on the terms of the active–electron approximation[61]; as substituents become more electron withdrawing, the energy mismatch between phosphonate orbital energies and vanadyl d levels widens, leading to decreased interaction and hence coupling (see equation 1.13, Chapter 1). In the *p*-NO_2 derivative for example, the energy mismatch becomes large enough to essentially turn off spin communication between adjacent vanadyl centers.

The effects described above make a relative small contribution to the magnitude of the exchange interaction. They establish however the presence of

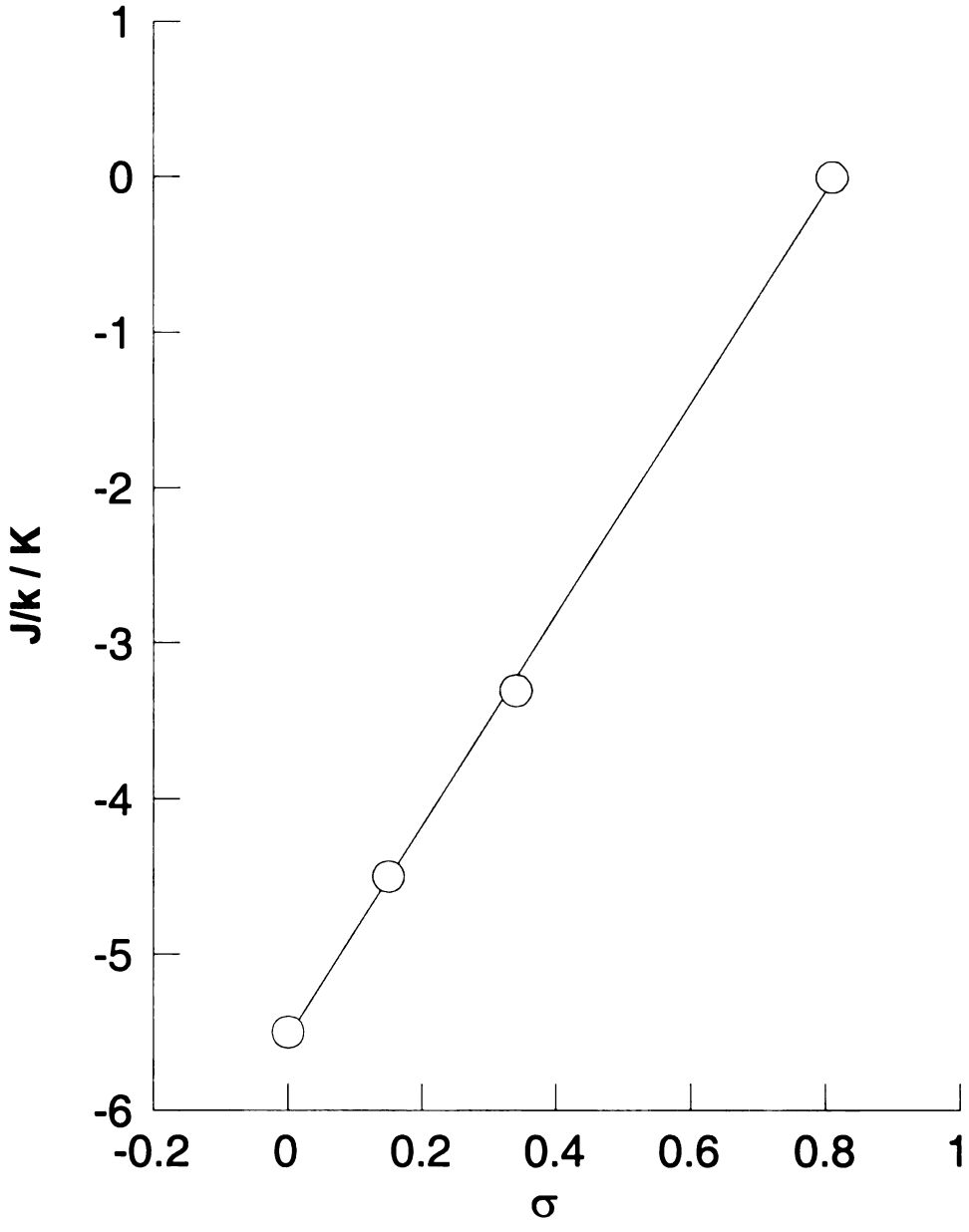

Figure 24. Plot of J/k vs. σ for the four LVPs $VO(O_3PC_6H_4–X)\cdot H_2O$ (X = *p*-NO_2, *m*-F, *p*-F, and H).

spin density on phosphorus orbitals and validate the hypothesis that O — P — O linkages are genuine magnetic coupling pathways. In types 1, 2, and 4 all the structural building blocks involve phosphate/phosponate links, indicating that spin communication propagates via one or more of these O — P — O linkages. Only type 3 materials contain the D II structural unit where a $V(\mu^2\text{-}O)_2V$ dimer assumes the role of the exchange pathway[3]. All six materials crystallizing in this structural type possess almost identical magnetic properties. The strong antiferromagnetic coupling is a consequence of the d_{xy} planes' coplanarity, in accordance with the calculation[58,62] studies performed for analogous copper systems within the framework of the active–electron approximation.

From the remaining structural types the simplest one is type 4, where the $VO(O_3PNp)(H_2O)\cdot nROH$ series of compounds crystallizes. The only structural element involved is of the M II type where adjacent vanadyl octahedra are connected through single–bridged phosphonate units. Weak antiferromagnetic interactions are observed as indicated by the broad maximum centered at 3.8 K in the χ vs T data (*Figure 22*). The susceptibility data were fitted adequately by a two dimensional Heisenberg model for a square lattice, resulting in a J/k value of –1.6 K. Such a small coupling is attributed to the M II exchange pathway, where adjacent metal centers are positioned almost 6 Å apart from each other.

The $VO(O_3PC_6H_4\text{–}X)\cdot H2O$ series of compounds with X = *p*-NO2, *m*-F, *p*-F, and -H, crystallizes along with α–VOHPO4•2H2O in the type 2 structural class. The magnetic properties along the isostructural vanadyl phosphonate series correlate well with the electronic properties of the substituted phosphonates, as was discussed above. The rigid nature of the intralayer framework, and its isolation from the substitution sites, preserve the structural block metric parameters. Structural comparisons are therefore validated among the parent vanadyl phenylphosphonate hydrate and the vanadyl hydrogen phosphate

dihydrate. Although both materials belong to the same structural type and ^{31}P–NMR data suggest that almost identical finite amounts of spin density are placed in phosphorus orbitals, the antiferromagnetic coupling is much stronger in the latter compound indicating significant geometrical differences within the basic structural building blocks. These are of the O III and D V type as indicated in Table 7 (*Figure 25*). The former assembles infinite linear chains while the latter comprises isolated dimers within the intralayer lattice. No significant coupling is expected through the O III pathway, since the orientation of the connecting links is orthogonal to the d_{xy} magnetic orbitals[3]. In addition, the susceptibility data were adequately fitted to a Bleaney–Bowers model for dimers[63], while no fit was possible by using 1–D models.

Variations in the strength of the magnetic exchange should be attributed to geometrical differences within the double–bridged D V pathways. The large inter–metal distance precludes the possibility of any significant contribution from through–space interactions. A superexchange mechanism, which necessarily involves the phosphate/phosphonate bridges and the metal orbitals, is more plausible. In order to qualitatively derive any valid magnetostructural correlations each exchange pathway has to be examined with respect to the geometrical aspects of the frontier orbitals involved. Although assigning the ligand orbitals does not present any difficulty the same is not true for the metal orbitals. The vanadium displacement from its basal plane complicates matters in terms of defining the orientation of the d_{xy} metal orbital. It is usually considered that the plane of this orbital coincides with the basal plane of the vanadium octahedron. However recent calculation studies[64] on copper complexes have shown a strong dependence of the magnitude of the antiferromagnetic coupling on the copper displacement from its basal plane; the larger the distortion, the less antiferromagnetic *J* becomes. These studies clearly point out that taking the d_{xy}

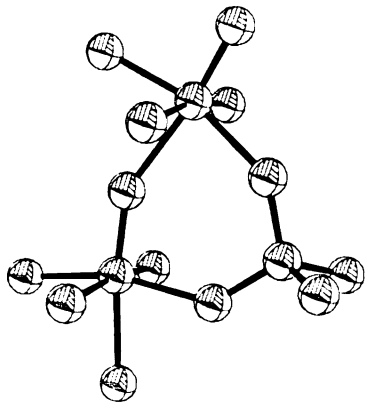

O III

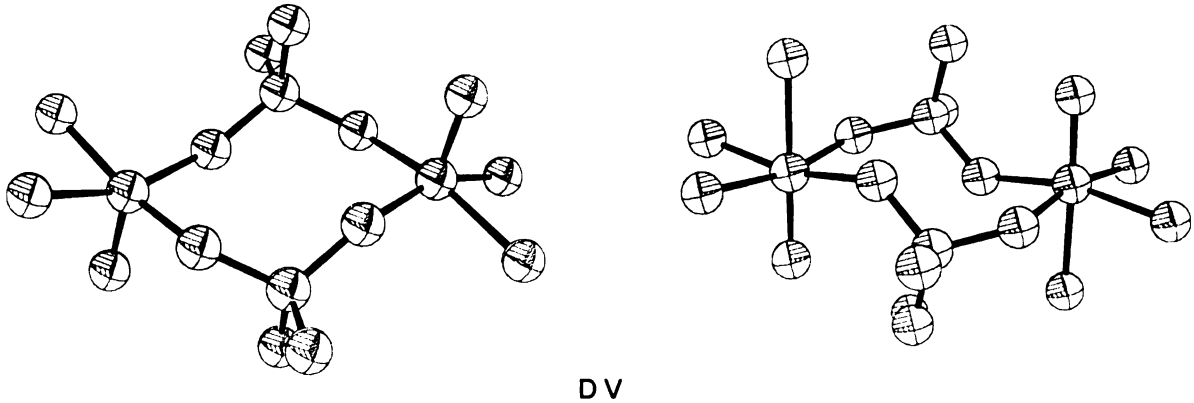

D V

Figure 25. O III structural building block (top) and the corresponding D V ones for the phospate (left) and the phosphonate (right).

orbital orientation for granted might lead to misinterpretation of the experimental results. In the materials examined here, the magnetic properties are due to isolated dimeric entities. Given the qualitative framework of this work, the d_{xy} orbital is then considered as either the vanadium basal plane (indicated as O_4^V) or as the plane defined by vanadium and the two basal oxygen atoms participating in the exchange pathway (indicated as VO_2). In the case of type 2 material the latter is considered as a more valid approximation.

Inspection of Table 8, where the metric parameters of the D V exchange pathways of the phosphonate and the phosphate are gathered, validates the above arguments. When the orientation of the d_{xy} plane is considered to coincide with that of the vanadium basal plane the two exchange pathways appear to be almost identical. The variance in the magnitude of the exchange coupling could then only arise from the energy mismatch between the metal orbitals and the phosphonate versus the phosphate frontier orbitals. Alternatively if the VO_2 plane coincides with the metal d_{xy} plane then the two exchange pathways present significant differences. The metal orbitals in the phosphate are almost coplanar while the same is not true for the phosponate. Under the theoretical framework of the active–electron approximation, an approach first developed by Hoffmann and coworkers[58], the dimer's magnetic orbitals are considered to be a symmetric (Φ_S) and an antisymmetric (Φ_A) combination of metal and ligand orbitals (*Figure 26*). The magnitude of the exchange interaction is then directly proportional to the square of the energy difference between these orbitals (see equation 1.8, Chapter 1). By using simple arguments, a qualitative energy diagram is constructed which relates the magnitude of this energy difference to the deviation from coplanarity ($d_v(VO_2|VO_2)$) of the metal orbitals. For $d_V = 0$, Φ_A is higher in energy than Φ_S, and as its value increases the energy difference becomes smaller reaching a point where the two should be practically degenerate.

Table 8. Metric Parameters for the D V Exchange Pathway

Metric Parameters	$VO(O_3PC_6H_5)\cdot H_2O$	α–$VOHPO_4\cdot 2H_2O$
d(V·····V) / Å[a]	5.010	5.138
$<VO_2IVO_2$ / ° [b]	0	0
$<VO_2IO_4^P$ / ° [c]	153.98	178.32
$d_V(VO_2I\ VO_2)$ / Å[d]	1.026	0.075
$<O_4^VIO_4^V$ / ° [e]	0	0
$<O_4^VIO_4^P$ / ° [f]	163.77	164.53
$d_O(O_4^VIO_4^V)$ / Å [g]	0.63	0.69
J/k / K [h]	– 5.5	– 23

[a]Distance between the vanadyl centers within the D V building block. [b]Dihedral angle between the VO_2 planes (defined by vanadium and the two basal oxygen atoms of the D V ring). [c]Dihedral angle between the VO_2 plane and the plane O_4^P (defined by the four D V ring oxygen atoms). [d]Distance between the VO_2 planes. [e]Dihedral angle between the O_4^V planes (defined by the four basal oxygens of the vanadium octhedron). [f]Dihedral angle between the O_4^V and the O_4^P planes. [g]Distance between the O_4^V planes. [h]From Bleaney–Bowers dimer model.

Table 9. Metric Parameters for the D VII Exchange Pathway

Metric	Na^{+} [a]	α–VOSO4	β–$VOHPO_4\cdot 2H_2O$	Sr^{2+} [b]	$VOHPO_4\cdot 4H_2O$
d(V·····V) / Å	4.608	4.530	4.805	4.680	4.595
$<O_4^VIO_4^V$ / °	0	0	0	2.38	6.66
$<O_4^VIO_4^P$ / °	119.1	131.8	145.3	133.8	131.0
$d_O(O_4^VIO_4^V)$ / Å	1.87	1.76	1.43	—	—
J/k / K	+ 0.6	+ 1.5	– 5.0	– 2.5	– 4.7

[a]$Na_{0.5}VOPO_4\cdot 2H_2O$. [b]$Sr_{0.5}VOPO_4\cdot 2H_2O$.

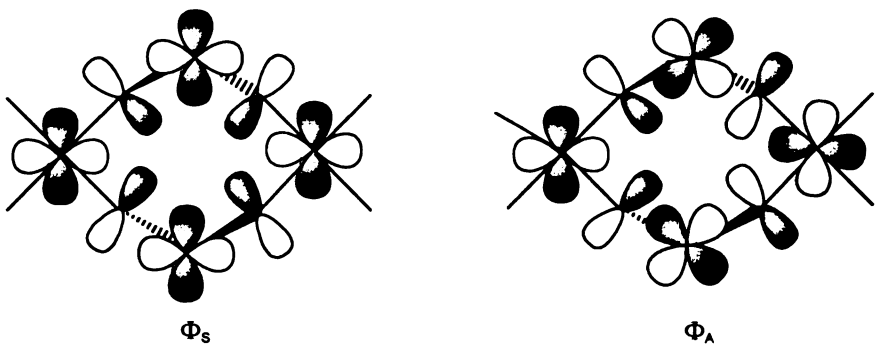

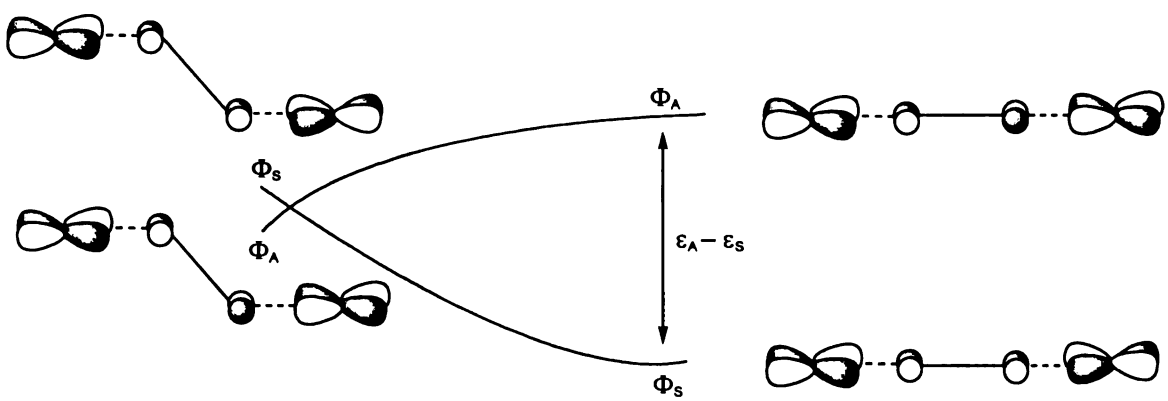

Figure 26. Symmetric (Φ_S) and antisymmetric (Φ_A) combination of vanadium d_{xy} and phosphate/phosphonate molecular orbitals and their energy dependence upon deviation from coplanarity of the local metal environments.

Therefore the smaller the value of d_V the higher the antiferromagnetic coupling should be, in accordance with equation 1.8. This behavior may be understood from the interactions of the *d* metal–based orbitals with the lower–lying filled orbitals of the diamagnetic phosphate/phosphonate links. The latter are a combination of oxygen *p* and phosporous *d* atomic orbitals, which form a pair of degenerate phosphate/phosphonate nonbonding MO's. Hence, the energy difference between the magnetic orbitals should be dependent on the manner that metal–based orbitals interact through the bridge. In *Figure 26* (bottom) a view of the section of the exchange pathway, for both the Φ_S and the Φ_A, at two extreme conformations is drawn. When the metal's local d_{xy} planes are coplanar, for both the symmetric and antisymmetric combinations, they can interact with the phosphate/phosphonate molecular orbitals. Such an interaction stabilizes Φ_S making it less antibonding in character while it has an opposite effect on the Φ_A combination. As deviations from coplanarity occur these overlaps decrease in magnitude, raising the energy of Φ_S and lowering that of Φ_A, since the latter combination becomes less antibonding.

In accordance with these arguments the exchange coupling in the phosphate is four times stronger than that of the phosphonate although both possess almost identical amounts of spin density on phosphorus orbitals. The relative orientation and displacement of the d_{xy} orbitals are thus the main factors that contribute to such a difference. In Chapter IV additional data on dimer complexes presenting similar exchange pathways will further validate these qualitative magnetostructural correlations.

The last structural class of extended materials discussed in this Chapter is type 1 materials where both ferromagnetic and antiferromagnetic interactions have been encountered. These two–dimensional compounds show an intralayered network assembled by interconnection of D VII and M II type

building blocks. Although they are structurally simple, their magnetic properties are quite complex with controversial reports in the literature[9,15] regarding the sign of the interaction. Such complications are prominent in the mixed–valence alkali metal intercalated series. The main concern in these materials is whether the electron is localized in distinct V^{4+} centers or electron delocalization occurs resulting in equivalent metal sites with an average oxidation state of +4.5. Single crystal X–ray studies performed at room temperature and at 173 K determined, in both instances, the presence of one crystallographically unique vanadium center. ^{31}P–NMR spectroscopy on the other hand, clearly shows that the single line observed at room temperature is split into three peaks at lower temperatures, indicating at least three different phosphorus environments within the intralayer network. In addition these lines display linear temperature dependence indicating the paramagnetic origin of their shift.

The ^{31}P–NMR results indicate the localization of the unpaired electron in half of the metal sites, at least on the experiment's time scale. Such a condition can be achieved in numerous ways, a few of which are drawn in *Figure 27*. All these electronic configurations should not be isoenergetic since one has to take into account electron–electron repulsions which are distance dependent. However the energy of interconversion from one to the other should be small in light of the relatively large distance among the potential spin carriers. Thus the system is best described by considering a dynamic equilibrium among the various configurations, which show temperature dependent populations. The establishment of equilibrium might account for the antiferromagnetic coupling observed in impure phases of the K^+ derivatives and the controversial magnetic results in the Na^+ derivatives. The weak ferromagnetic and antiferromagnetic couplings observed in these compounds are probably dependent on the purity of the studied material. The presence of impurities, which should be accommodated

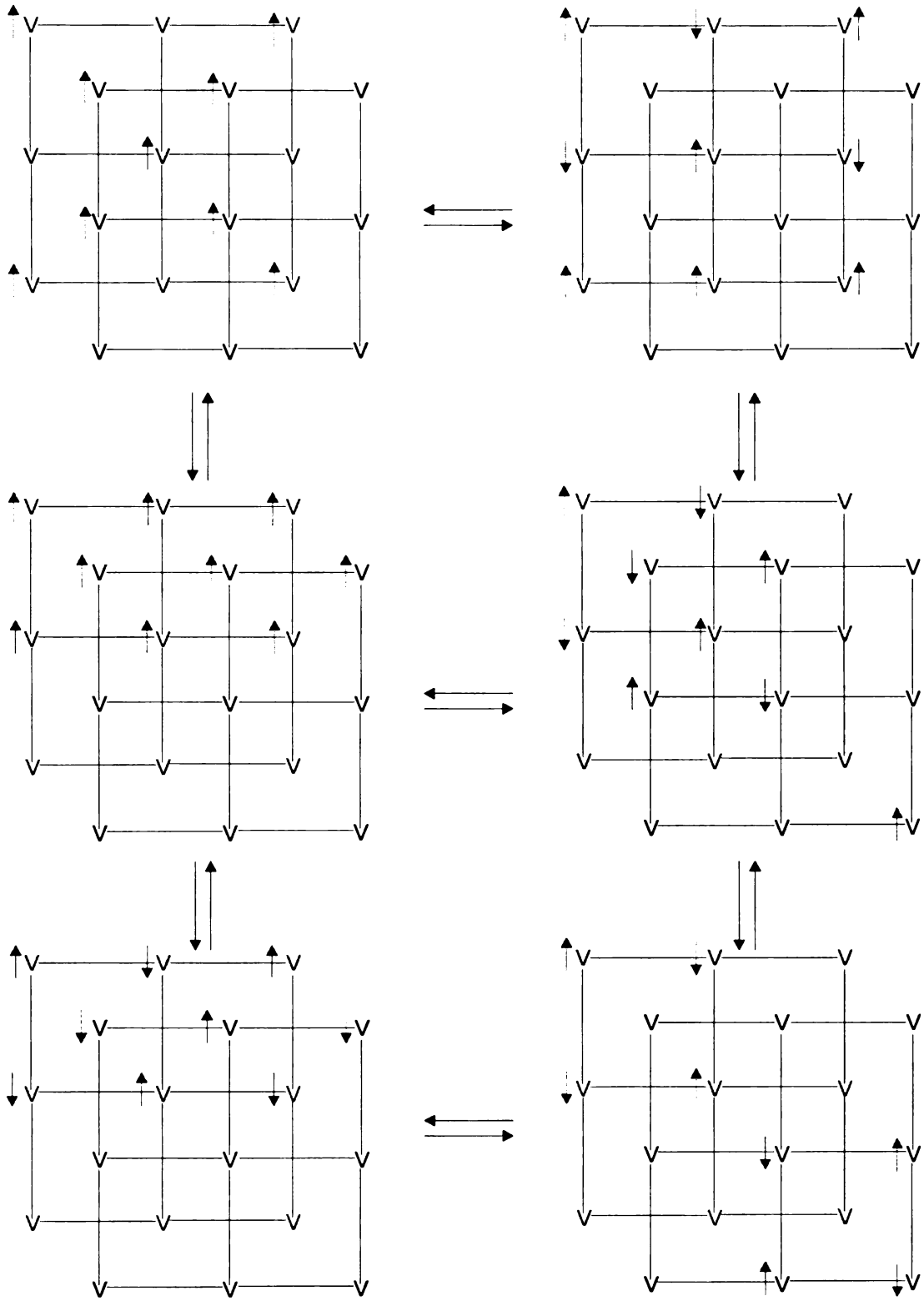

Figure 27. Various electronic configurations of the mixed valence alkali metal intercalated vanadyl phosphates hydrates.

within the interlayer space, might influence the relative weight of each electronic configuration. Since the observed magnetic couplings are weak in magnitude and basically are the sum of almost equal antiferromagnetic and ferromagnetic contributions, such small changes may very well enhance one factor over the other.

In this study all three isostructural alkali metal intercalated derivatives display weak ferromagnetic interactions of the same magnitude, correlating well with the ^{31}P–NMR results. In antithesis, the rest of the isostructural vanadyl phosphate layered materials, gathered in Table 7, are coupled antiferromagnetically, raising the question as to whether the sign of the interaction correlates with the layers' mixed–valency or not. The only compound that possesses ferromagnetically coupled layers with all vanadium sites bearing an unpaired electron is α–vanadyl sulfate, which is isostructural[65] to the parent vanadyl phosphate dihydrate and thus to its metal intercalated derivatives. Its magnetic properties have been studied by two different research groups; Longo and Arnott[65] who described the material as a ferrimagnet and Villeneuve and coworkers[66] who stated in their publications that repeated measurements in three independently prepared samples indicated weak intralayered ferromagnetic coupling. These authors also commented on the complexity of the problem, which results from the fact that the ferromagnetic and the antiferromagnetic components of the exchange interaction are both rather small and in fact of the same order of magnitude. Their study complements the results in alkali metal intercalated layered vanadyl phosphates presented in this thesis, indicating that there is at least an exchange pathway capable of ferromagnetically coupling neighboring vanadyl centers.

In light of the results in type 4 materials, where the single–bridged M II phosphonate units transmit antiferromagnetic interactions, the only potential

ferromagnetic exchange pathway is the double–bridged D VII structural block. In Table 9 the metric parameters of the latter exchange pathway are gathered for all materials belonging to structural type 1. From the alkali metal intercalated series only one of these, namely the Na^+ derivative, is displayed, since all three materials possess identical structural and magnetic properties. Inspection of Table 9 reveals one major difference; the d_{xy} planes within the D VII dimer core are parallel for $M_{0.5}VOPO_4 \cdot nH_2O$ (M = Na^+, K^+, and Rb^+), α–$VOSO_4$ and β–$VOHPO_4 \cdot 2H_2O$, while nonzero dihedral angles are exhibited in $Sr_{0.5}VOPO_4 \cdot 2H_2O$ and $VOHPO_4 \cdot 4H_2O$. In the latter compounds the layers are antiferromagnetically coupled, and, interestingly, the larger dihedral angle is also reflected in a larger antiferromagnetic exchange interaction.

By using the qualitative frontier orbital scheme depicted in *Figure 26*, the antiferromagnetic coupling in these compounds can be explained. The nonparallel alignment of the d_{xy} planes assures that overlap interactions are always present between them, through the diamagnetic phosphate group. Such a situation results in different energies for the Φ_S and Φ_A molecular orbitals even at large displacements of the metal's local environments. As a consequence a nonzero antiferromagnetic contribution is anticipated through the D VII exchange pathway.

On the other hand, when parallel d_{xy} planes are considered, qualitative arguments predict a large energy separation between the Φ_S and Φ_A orbitals for small d_{xy} displacements. When the latter separation becomes large enough, it was assumed in *Figure 26* that these orbitals become isoenergetic leading to a vanishing antiferromagnetic component. The magnetic results in the $M_{0.5}VOPO_4 \cdot nH_2O$ (M = Na^+, K^+, and Rb^+), α–$VOSO_4$ and β–$VOHPO_4 \cdot 2H_2O$ series of compounds can be understood under this qualitative treatment. The large displacement of the d_{xy} planes observed for the first four compounds,

results in a ferromagnetic contribution of the D VII pathway. The overall magnetic properties of these materials are then the sum of a weak antiferromagnetic component of the M II pathway and a weak ferromagnetic component of the D VII one. Thus in the mixed–valence series localization of the electrons in D VII versus M II pathways would have a marked influence on the magnetic properties of the materials. The smaller displacement of the d_{xy} planes on the other hand in β–$VOHPO_4 \cdot 2H_2O$ retains some energy difference between the Φ_S and Φ_A orbitals. Thus the D VII pathway in this compound contributes to the overall antiferromagnetic coupling.

A detailed calculation, which would be able to reproduce in reasonable accuracy the experimental results, will be crucial in determining the value of the qualitative energy diagram depicted in *Figure 26*. Only recently however Density Functional Theory (DFT) calculations, performed in complex systems, gave satisfactory agreement between theory and experiment[62,64]. The authors clearly pointed out that the magnetic properties of complex systems could be described in reasonable accuracy by the calculations only when simplifications regarding the bridging and the terminal ligands were avoided. In other words the actual complexes have to be utilized in the calculation studies as well. Small energy differences regarding the singlet–triplet splitting, such as these observed in these materials, are still hard to predict.

Our efforts therefore towards a better understanding of the magnetic properties of these layered materials, were focused on acquiring more experimental data, establishing the validity of the energy diagram depicted in *Figure 26*. We have accomplished it by synthesizing a series of dimer compounds modeling the geometrical features of the D VII structural building block. These data, along with data from other dimer model compounds, are presented in the next chapter.

LIST OF REFERENCES

(1) Laudise, R. A. *Chemical and Engineering News* **1987**, 30.

(2) Villeneuve, G.; Amoros, P.; Beltran, D.; Drillon, M. in *Organic and Inorganic Low Dimensional Crystalline Materials*, Delhaes, P.; Drillon, M.; Eds, Nato Asi Series, Plenum Press: New York 1987.

(3) Beltran, D.; Amoros, P.; Ibañez, R.; Martinez, E.; Beltran, A.; Le Bail A.; Ferey, G.; Villeneuve, G. *Solid State Ionics* **1989**, *32/33*, 57.

(4) (a) Leonowiez, M. E.; Johnson, J. W.; Brody, J. F.; Shanson, H. F.; Newsam, J. M. *J. Solid State Chem.* **1985**, *56*, 370. (b) Torardi, C. G.; Calabrese, J. C. *Inorg. Chem.* **1984**, *23*, 1308.

(5) Villeneuve, G.; Suh, K. S.; Amoros, P.; Casañ–Pastor, N.; Beltrán–Porter, D. *Chem. Mater.* **1992**, *4*, 108.

(6) Wrobleski, J. T. *Inorg. Chem.* **1988**, *27*, 946.

(7) Beltran–Porter, D.; Beltran–Porter, A.; Amoros, P.; Ibañez, R.; Martinez, E.; Le Bail, A.; Ferey, G.; Villeneuve, G. *Eur. J. Solid State Inorg. Chem.* **1991**, *28*, 131.

(8) Jacobson, A. J.; Johnson, J. W.; Brody, J. F.; Scanlon, J. C.; Lewandowski, J. T. *Inorg. Chem.* **1985**, *24*, 1782.

(9) Šišková, R.; Beneš, L.; Zima, V.; Vlcek, M.; Votinský, J.; Kalousová, J. *Polyhedron* **1993**, *12*, 181.

(10) Lii, K. H. *J. Chin. Chem. Soc.* **1992**, *39*, 569.

(11) Le Bideau, J.; Papoutsakis, D.; Jackson, J. E.; Nocera, D. G.; *J. Am. Chem. Soc.* **1997**, *119*, 1313.

(12) Torgerson, M. R. *Ph. D Dissertation* M.S.U. **1996**.

(13) Wang, S. L.; Kang, H. Y.; Cheng, C. Y.; Lii, K. H. *Inorg. Chem.* **1991**, *30*, 3496.

(14) Kang, H. Y.; Lee, W. C.; Wang, S. L.; Lii, K. H. *Inorg. Chem.* **1992**, *31*, 4743.

(15) Papoutsakis, D.; Jackson, J. E.; Nocera, D. G. *Inorg. Chem.* **1996**, *35*, 800.

(16) (a) Tietze, H. R. *Aust. J. Chem.* **1981**, *34*, 2035. (b) Tachez, M.; Theobald, F.; Bernard, J.; Hewat, A. W. *Rev. Chim. Min.* **1982**, *19*, 291.

(17) Sananes, M. T.; Tuel, A. *J. Chem. Soc. Chem. Commun.* **1995**, 1323.

(18) Fermi, E.; *Z. Phys.* **1930**, *60*, 320.

(19) (a) Horrocks, W. D., Jr. *Inorg. Chem.* **1970**, *9*, 690. (b) Horrocks, W. D., Jr.; Greenberg, E. S. *Inorg. Chem.* **1971**, *10*, 2190.

(20) Kurland, R. J.; McGarvey B. R. *J. Magn. Resonance* **1970**, *2*, 286.

(21) Carrington, A.; McLachlan, A. D. in *Introduction to Magnetic Resonance*; Harper: New York 1967; Ch. 6.

(22) (a) Turner, G. L.; Smith, K. A.; Kirkpatrick, R. J.; Oldfield, E. *J. Magn. Reson.* **1986**, *70*, 408. (b) Prabhakar, S.; Rao, K. J.; rao, C. N. R. *Chem. Phys. Lett.* **1987**, *139*, 96. (c) Hayashi, S.; Hayamizu, K. *Bull. Chem. Soc. Ipn.* **1989**, *62*, 3061.

(23) Kiely, C. J.; Burrows, A.; Hutchings, G. J.; Bere, K. E.; Volta, J.–C.; Tuel, A.; Abon, M. *Faraday Discuss.* **1996**, **105**, 103.

(24) Kurland, R. J.; McGarvey, B. *J. Magn. Reson.* **1970**, *2*, 286.

(25) Shulman, R. G.; Jaccarino, V. *Phys. Rev.* **1957**, *108*, 1219.

(26) (a) Gray, H. B.; Ballhausen, C. J. *Inorg. Chem.* **1962**, *1*, 111. (b) Selbin, J.; Holmes, L. H., Jr.; McGlynn, S. P. *J. Inorg. Nucl. Chem.* **1963**, *25*, 1359.

(27) Horrocks, W. DeW., Jr. in *NMR of Paramagnetic Molecules*; La Mar, G. N.; Horrocks, W. DeW., Jr.; Holm, R. H.; Eds.; Academic Press: New York 1973; Chapter 4.

(28) Drago, R. S. in *Phusical Methods in Chemistry*; W. B. Saunders Co.: Philadelphia 1977.

(29) Sananes, M. T.; Tuel, A.; Volta, J. C. *J. Catal.* **1994**, *145*, 251.

(30) Siskova, R.; Benes, L.; Zima, V.; Vlcek, M.; Votinsky, J.; Kalousova, J. *Polyhedron* **1993**, *12*, 181.

(31) Rusbrooke, G. S.; Wood, P. J. Mol. Phys. **1958**, *1*, 257.

(32) Hatfield, W. E. In *Magneto-Structural Correlations in Exchange Coupled Systems*; Willett, R. D., Gatteschi, D., Kahn, O., Eds.; NATO ASI Series; Reidel: Dordrecht, 1985.

(33) Plass, W. *Angew. Chem., Int. Ed. Engl.* **1996**, *35*, 627.

(34) Gorun, S. M.; Lippard, S. J. *Inorg. Chem.* **1991**, *30*, 1625.

(35) Niemann, A.; Bossek, U.; Wieghardt, K.; Butzlaff, C.; Trautwein, A. X.; Nuber, B. *Angew. Chem., Int. Ed. Engl.* **1992**, *31*, 311.

(36) Nanda, K. K.; Thompson, L. K.; Bridson, J. N.; Nag. K. *J. Chem. Soc., Chem. Commun.* **1994**, 1337.

(37) (a) Journaux, Y.; Kahn, O.; Morgenstern-Badarau, I.; Galy, J.; Jaud, J. *J. Am. Chem. Soc.* **1983**, *105*, 7585. (b) Kahn, O.; Galy, J.; Journaux, Y.; Morgenstern-Badarau, I. *J. Am. Chem. Soc.* **1982**, *104*, 2165. (c) Morgenstern-Badarau, I.; Rerat, M.; Kahn, O.; Jaud, J.; Galy, J. *Inorg. Chem.* **1982**, *21*, 3050.

(38) Lehn, J.-M. *Supramolecular Chemistry*; VCH: Weinheim, 1995.

(39) *Supramolecular Architecture*; Bein, T., Ed.; ACS Symposium Series No. 499; American Chemical Society: Washington, D.C., 1992.

(40) (a) Whitesides, G. M.; Simanek, E. E.; Mathias, J. P.; Seto, C. T.; Chin, D. N.; Mammen, M.; Gordon, D. M. *Acc. Chem. Res.* **1995**, *28*, 37. (b) Whitesides, G. M.; Mathias, J. P.; Seto, C. T. *Science* **1991**, *254*, 1312.

(41) Desiraju, G. R. *Angew. Chem., Int. Ed. Engl.* **1995**, *34*, 2311.

(42) Huan, G.; Jacobson, A. J.; Johnson, J. W.; Corcoran, E. W., Jr. *Chem. Mater.* **1990**, *2*, 91.

(43) Huan, G.; Johnson, J. W.; Brody, J. F.; Goshorn, D. P.; Jacobson, A. J. *Mater. Chem. Phys.* **1993**, *35*, 199.

(44) Lezama, L.; Villeneuve, G.; Marcos, M. D.; Pizarro, J. L.; Hagenmuller, P.; Rojo, T. *Solid State Commun.* **1989**, *70*, 899.

(45) Shin, Y.-g. K.; Nocera, D. G. *J. Am. Chem. Soc.* **1992** *114*, 1264.

(46) Carlin, R. L. *Magnetochemistry*; Springer-Verlag: Berlin, 1986.

(47) Clearfield, A. *Progress in Inorganic Chemistry* **1998**, *47*, 371.

(48) Johnson, J. W.; Jacobson, A. J.; Butler, W. M.; Rosenthal, S. E.; Brody, J. F.; Lewandowski, J. T. *J. Am. Chem. Soc.* **1989**, *111*, 381.

(49) Johnson, J. W.; Jacobson, A. J.; Brody, J. F.; Lewandowski, J. T. *Inorg. Chem.* **1984**, *23*, 3844.

(50) Costantino, U. in *Inorganic Ion–Exchange Materials*; Clearfield, A., Eds.; CRC Press: Boca Raton, FL, 1982; Chapter 3.

(51) Huan, G.; Jacobson, A. L.; Johnson, J. W.; Corcoran, E. W., Jr. *Chem.*

Mater. **1990**, *2*, 91.

(52) (a) Sutor, D. J. *Acta Crystallogr.* **1967**, *23*, 418. (b) Abbonna, F.; Boistelle, R.; Haser, R. *Acta Crystallogr.* **1979**, *B35*, 2514.

(53) Johnson, J. W.; Brody, J. F.; Alexander, R. M. *Chem. Mater.* **1990**, *2*, 198.

(54) Lines, M. E. *J. Phys. Chem. Solids* **1970**, *31*, 101.

(55) Torgerson, M. R.; Nocera, D. G. *J. Am. Chem. Soc.* **1996**, *118*, 8739.

(56) Le Bideau, J.; Payen, C.; Bujoli, B. *Comp. Rendu Acad. Sci. Paris* **1995**, *320*, 141.

(57) Canadell, E.; Provost, J.; Guesdon, A.; Borel, M. M.; Leclaire, A. *Chem. Mater.* **1997**, *9*, 68.

(58) Hay, P. J.; Thibeault, J. C.; Hoffmann, R. *J. Am. Chem. Soc.* **1975**, *97*, 4884.

(59) Nagarajan, K.; Shelly, K. P.; Perkins, R. R.; Stewart, R. *Can. J. Chem.* **1987**, *65*, 1729.

(60) Grabiak, R. C.; Miles, J. A.; Schwenzer, G. M. *Phosphorus and Sulfur* **1980**, *9*, 197

(61) Kahn, O. *Molecular Magnetism*; VCH Publishers: New York 1993.

(62) (a) Ruiz, E.; Alemany, P.; Santiago, A.; Cano, J. *J. Am. Chem. Soc.* **1997**, *119*, 1297. (b) Ruiz, E.; Alemany, P.; Santiago, A.; Cano, J. *Inorg. Chem.* **1997**, *36*, 3683.

(63) Carlin, R. L. *Magnetochemistry*; Springer-Verlag: Berlin, 1986.

(64) Cano, J. Alemany, P.; Alvarez, S.; Verdaguer, M.; Ruiz, E. *Chem. Eur. J.* **1998**, *4*, 476

(65) Longo, J. M.; Arnott, R. J. *J. Solid State Chem.* **1970**, *1*, 394.

(66) (a) Lezama, L.; Villeneuve, G.; Marcos, M. D.; Pizarro, J. L.; Hagenmuller, P. *Solid State Commun.* **1989**, *70*, 899. (b) Villeneuve, G.; Lezama, L. *Mol. Cryst. Liq. Cryst.* **1989**, *176*, 495.

CHAPTER 4

Magnetostructural Correlations in Dinuclear Vanadyl Phosphinate Complexes

A. Introduction

The structural and chemical properties of vanadyl phosphate/phosphonate extended materials continue to attract the attention of a growing audience of research scientists. Initial efforts to relate structure and magnetic properties afforded a series of qualitative rules, predicting the sign and the strength of the interaction[1,2]. Our work in layered vanadyl phosphates and phosphonates provided additional evidence as to the active role of the O — P — O linkages in the superexchange sequence. Their sensitivity to electronic[3] and structural tuning[4] has been established, although detailed magnetostructural correlations

were hard to derive. To further probe the sensitivity of magnetic properties to structural changes of the exchange pathway, geometrical distortions of the latter have to be induced by chemical means. This is hard to achieve in extended layered systems, since small structural changes often result in different intralayer frameworks.

The magnetic properties of most of these systems can be understood at a qualitative level by inspection of their structural building blocks, which usually consist of dimetallic fragments bridged by phosphate/phosphonate ligands in a single or double linking fashion. Hence, the synthesis of dimer compounds, whose connectivity resembles that of the vanadyl phosphate/phosphonate building blocks, could provide model systems for the study of magnetostructural correlations. In addition, such systems are readily modified via chemical means by proper selection of the bridging and terminal ligands.

We have synthesized and characterized two series of vanadyl dimers. They are based on bipyridyl–type and the hydrotris(1–pyrazolyl)borate terminal ligands, while bridging of the metals is accomplished by a series of bis–(*p*-phenyl) substituted phosphinates. The basic structure of the dimer core is mainly determined by the nature of the terminal ligands. *p*-Substitution of the phosphinate phenyl rings allows systematic introduction of small structural and electronic changes, which have a marked influence on the overall magnetic properties.

B. Results

1. Synthesis and Characterization of $\{LVO[\mu\text{–}(X\text{–}C_6H_4)_2PO_2]_{1.5}\}_2\{ClO_4\}$ Dimers, (L = substituted 2,2'–bipyridyl, and X = H–, CH_3O–, Cl–, F–)

a. Synthesis and Characterization

These complexes are formed by ligand substitution reactions, which occur exclusively at the vanadium(4+) level, so that there are no overall redox processes involved. The general synthetic scheme (*Figure 1*) involves initially the preparation of L_2VOCl_2 complexes[5], where L_2 is a substituted 2,2'–bipyridyl ligand. These compounds provide a stable L_2VO vanadyl fragment where three of the vanadium coordination sites are occupied and at the same time offer two labile V — Cl bonds which can be easily substituted upon treatment with the desired phosphinic acids.

The products are obtained in the form of small green crystals by allowing the methanolic reaction mixture to stand at room temperature for a few days. Although all compounds synthesized and structurally characterized in this manner possessed the same general formula — $\{L_2VO[\mu\text{–}(X\text{–}C_6H_4)_2PO_2]_{1.5}\}_2\{ClO_4\}$ with X = H–, CH_3O–, Cl–, F–, and L_2 = 2,2'–bipyridyl (bpy), 4,4'–dimethyl–2,2'–bipyridyl (dmbpy), and 3,3',4,4'–tetramethyl–2,2'–bipyridyl (tmbpy) — two different types of dimer cores were observed. The classification was based on the relative orientation of the vanadyl groups. In three complexes — $\{bpyVO[\mu\text{–}(C_6H_5)_2PO_2]_{1.5}\}_2\{ClO_4\}$ (**1**), $\{dmbpyVO[\mu\text{–}(C_6H_5)_2PO_2]_{1.5}\}_2\{ClO_4\}$ (**2**), and $\{tmbpyVO[\mu\text{–}(C_6H_5)_2PO_2]_{1.5}\}_2\{ClO_4\}$ (**3**) — the vanadyl groups are twisted and almost orthogonal with respect to each other. The remaining complexes — $\{bpyVO[\mu\text{–}(p\text{-}F\text{–}C_6H_4)_2PO_2]_{1.5}\}_2\{ClO_4\}$ (**4**), $\{bpyVO[\mu\text{–}(p\text{-}Cl\text{–}C_6H_4)_2PO_2]_{1.5}\}_2\{ClO_4\}$ (**5**), and $\{bpyVO[\mu\text{–}(p\text{-}CH_3O\text{–}C_6H_4)_2PO_2]_{1.5}\}_2\{ClO_4\}$ (**6**) — crystallized with the

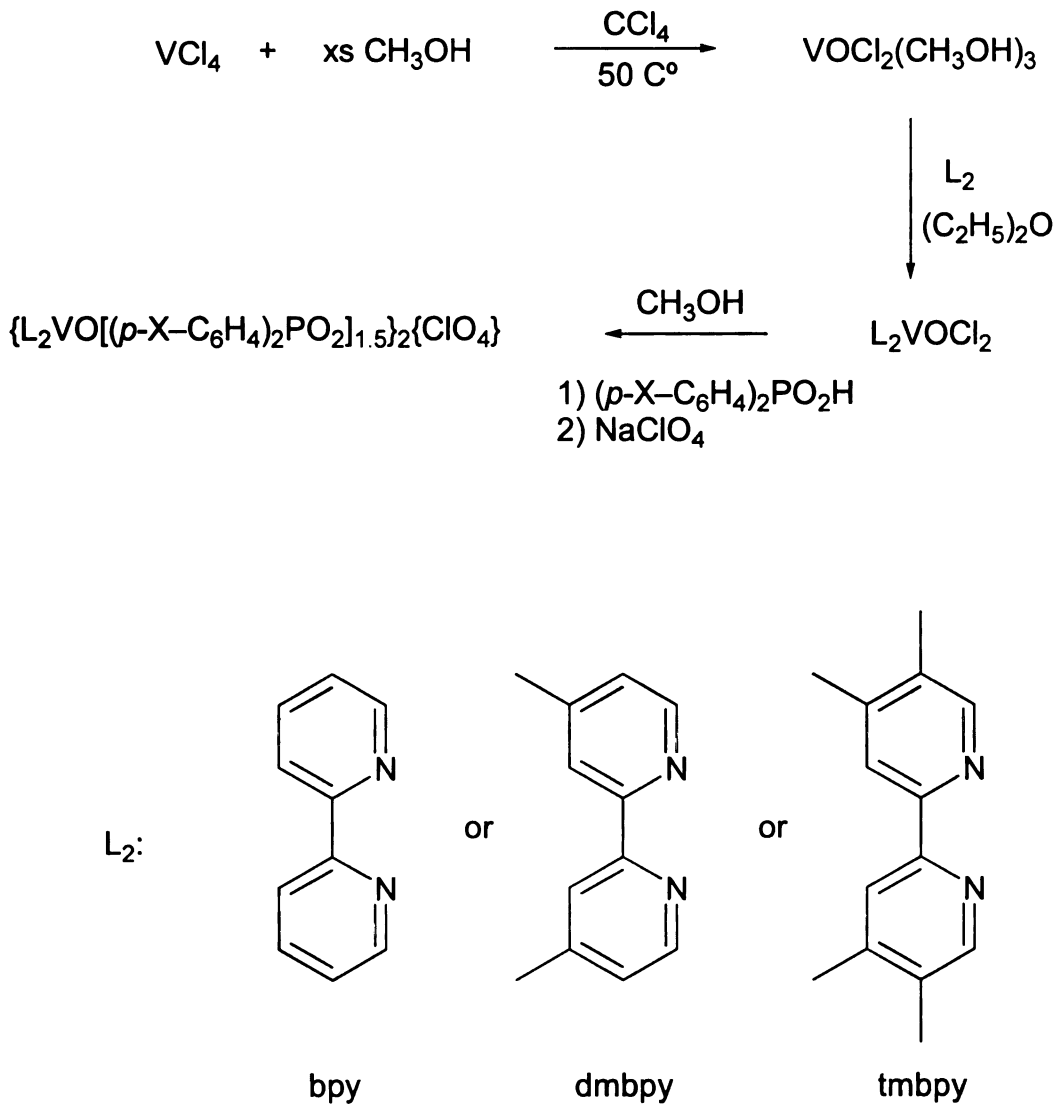

Figure 1. General synthetic scheme for vanadyl phosphinate dimers with bipyridyl–type terminal ligands.

vanadyl groups being *syn* to each other. Substitution of the bpy terminal ligands in complexes **5** and **6** by tmbpy afforded complexes {tmbpyVO[μ–(*p*-Cl–$C_6H_4)_2PO_2]_{1.5}\}_2\{ClO_4\}$ (**5A**), and {tmbpyVO[μ–(*p*-CH_3O–$C_6H_4)_2PO_2]_{1.5}\}_2\{ClO_4\}$ (**6A**). The structure of the former was not determined due to the lack of suitable single crystals, and the structure of the latter, which belongs to the *twist*–type, was only partially solved due to the poor quality of the data set.

Crystal data for compounds **1**, **2**, **3** and **6A** (*twist*–type dimers) are summarized in Tables 1 and 2, and selected bond distances and metric parameters of interest are gathered in Table 3. The first three complexes contain the diphenylphosphinate as the bridging link and only differ in the nature of the terminal 2,2'–bipyridyl ligand, which bears 0 (bpy), 2 (dmbpy), and 4 (tmbpy) methyl groups for **1**, **2**, and **3** respectively. In compound **6A**, where tmbpy was the terminal ligand, three bis (p-methoxyphenyl) phosphinate groups bridged the vanadyl octahedra. One crystallographically unique dimer molecule with a net charge of +1 crystallizes within the unit cell, along with one perchlorate anion and methanol molecules. 4 and 3.5 solvent molecules per dimer were located from Fourier differences maps in the unit cell of complexes **2** and 3, which although they possessed large anisotropic temperature factors, behaved reasonably well during structure refinement. The methanol molecules in the crystal structure of compounds **1** and **6A** could not be located and modeled to full or partial occupancy since they were highly disordered. The relatively large R1 factors for the latter two dimers are attributed to this difficulty. In compound **1** the data were corrected for the presence of solvent by the program PLATON[6], resulting in much better R1 values (see Chapter II for details) without actually modeling the solvent. All the atoms belonging to the dimer portion of the crystals were well behaved and refined with anisotropic temperature factors.

Table 1. Crystallographic Data for Compounds **1**, and **2**

	1	**2**
	(A) Crystal Parameters	
formula	$C_{56}H_{46}ClN_4O_{12}P_3V_2$	$C_{64}H_{70}ClN_4O_{16}P_3V_2$
crystal habit, color	block, green	block, green
FW	1197.21	1381.48
crystal size (mm^3)	0.50 × 0.40 × 0.16	0.77 × 0.73 × 0.62
crystal system	triclinic	triclinic
space group	$P\bar{1}$	$P\bar{1}$
a (Å)	11.8060(2)	14.7102(1)
b (Å)	16.8194(1)	14.8910(1)
c (Å)	17.0906(3)	17.0263(1)
α (deg)	67.459(1)	92.153(1)
β (deg)	77.146(1)	113.151(1)
γ (deg)	73.721(1)	95.862(1)
V ($Å^3$)	2983.33(7)	3398.90(5)
Z	2	2
d_{calc} (Mg/m^3)	1.333	1.350
F(000)	1228	1436
μ(Mo Kα), mm^{-1}	0.499	0.452
	(B) Data Collection	
$2\theta_{max}$ (deg)	50.0	50.0
index ranges	$-13 \le h \le 14$ $-18 \le k \le 19$ $0 \le l \le 20$	$-13 \le h \le 17$ $-17 \le k \le 15$ $-20 \le l \le 20$
temperature / K	173(2)	173(2)
reflections collected	17578	20469
independent reflections	10179	11568
R(int) (%)	2.01	1.10
	(C) Refinement	
Refinement method	Full–matrix least–squares on F^2	Full–matrix least–squares on F^2
R indices ($I > 2\sigma(I)$)	R1 = 0.0419 WR2 = 0.1018	R1 = 0.0363 WR2 = 0.1023
R indices all data	R1 = 0.0556 WR2 = 0.1094	R1 = 0.0413 WR2 = 0.1057
$\Delta(\rho)$ ($e^-/Å^3$)	0.881	0.887
GOF	1.035	1.034

Table 2. Crystallographic Data for Compounds **3**, and **6A**

	3	**6A**
	(A) Crystal Parameters	
formula	$C_{67.5}H_{76}ClN_4O_{15.5}P_3V_2$	$C_{76}H_{83}ClN_4O_{20}P_3V_2$
crystal habit, color	block, green	block, green
FW	1421.56	1602.70
crystal size (mm^3)	0.54 × 0.42 × 0.28	0.39 × 0.19 × 0.19
crystal system	triclinic	monoclinic
space group	$P\bar{1}$	$P2_1/n$
a (Å)	14.8345(2)	11.978(2)
b (Å)	18.3298(2)	19.284(2)
c (Å)	26.9275(1)	21.895(4)
α (deg)	74.511(1)	90
β (deg)	89.610(1)	95.51(3)
γ (deg)	88.934(1)	90
V ($Å^3$)	7055.1(1)	7644.0(9)
Z	4	4
d_{calc} (Mg/m^3)	1.388	1.393
F(000)	2964	3340
μ(Mo Kα), mm^{-1}	0.437	0.417
	(B) Data Collection	
$2\theta_{max}$ (deg)	50.0	50.0
index ranges	$-19 \le h \le 16$ $-24 \le k \le 24$ $-34 \le l \le 34$	$-14 \le h \le 14$ $-34 \le k \le 34$ $-26 \le l \le 26$
temperature / K	173.0(2)	131.0(2)
reflections collected	46838	71679
independent reflections	23782	13437
R(int) (%)	2.79	28.3
	(C) Refinement	
Refinement method	Full–matrix least–squares on F^2	Full–matrix least–squares on F^2
R indices ($I > 2\sigma(I)$)	R1 = 0.0782 WR2 = 0.213	R1 = 0.1049 WR2 = 0.1555
R indices all data	R1 = 0.0982 WR2 = 0.2404	R1 = 0.2463 WR2 = 0.2075
Δ(ρ) ($e^-/Å^3$)	1.642	0.743
GOF	0.989	1.040

Table 3. Bond Distances and Dimer Metric Parameters for $\{L_2VO[\mu\text{–}(X\text{–}C_6H_4)_2PO_2]_{1.5}\}_2\{ClO_4\}$, **1**, **2**, **3**, and **6A**[a]

Bond Distances	1	2	3	6A
V = O_{ax}	1.606(2)	1.606(1)	1.616(2)	1.596(5)
	1.600(2)	1.603(2)	1.612(3)	1.597(5)
V — N_{eq}	2.135(2)	2.129(2)	2.143(3)	2.126(7)
	2.130(2)	2.132(2)	2.136(3)	2.116(6)
V — N_{eq}	2.145(2)	2.150(2)	2.161(3)	2.136(6)
	2.131(2)	2.133(2)	2.145(3)	2.140(7)
V — O_{eq}	2.001(2)	1.999(1)	2.008(3)	1.984(5)
	1.991(2)	1.999(1)	1.999(3)	1.994(5)
V — O_{eq}	2.022(2)	2.014(1)	2.011(2)	1.998(5)
	1.992(2)	2.000(1)	2.014(3)	2.012(5)
V — O_{ax}	2.145(2)	2.128(1)	2.126(2)	2.113(5)
	2.144(2)	2.146(1)	2.109(2)	2.139(6)
T / K	173	173	173	131
$V_1 \cdots\cdots V_2$ / Å	4.906	4.906(1)	4.883(2)	4.835(2)
$\langle N_2O_2^{V1} / N_2O_2^{V2} \rangle$ / °[b]	39.2	45.3(1)	58.0(1)	55.0(1)
$\langle O_1 — V_1 — V_2 — O_2 \rangle$ / °[c]	126.8(3)	113.2(1)	100.5(2)	109.6(4)

[a] **1**: L = bpy; X = H. **2**: L = dmbpy; X = H. **3**: L = tmbpy; X = H. **6A**: L = tmbpy; X = CH_3O–. [b] Dihedral angle between the $N_2O_2^V$ planes (defined by the four basal atoms of the respective vanadium octhedron). [c] Dihedral angle between the axes defined by the vanadyl groups.

The four derivatives are found as tris(μ–phosphinato–*O,O'*)divanadyl complexes and have many structural features in common. *Figure 2(A)* displays an ORTEP view of the structure of compound **2**. Each crystallographically unique vanadium atom within the dimer core assumes a distorted octahedron coordination with the characteristic short vanadyl bond (Table 3). The equatorial plane is supplemented by the two nitrogen atoms of the dmbpy terminal ligand and by two phosphinate oxygens. The trans– to the vanadyl site is also occupied by a phosphinate oxygen, a feature which has never been observed in the dimeric structural building blocks of the phosphate/phosphonate extended materials, as remarked by Villeneuve and coworkers[2]. In fact bridging of the two metal sites by three phosphate–type ligands has been achieved only relatively recently in heterometallic vanadium(3+) clusters[7]. The axial V — O_P (where O_P is a phosphinate oxygen) bonds are slightly longer (2.145 Å) than the equatorial (~ 2.001 Å) ones, in accordance with the weak coordination ability of the trans–vanadyl site. Only one of the phosphinate groups binds to equatorial sites in both vanadyl centers, the other two binding one axial and one equatorial position of each octahedron (*Figure 2(B)*). The outcome of such ligand topology is an almost orthogonal twist between the vanadyl groups, as indicated by the O_1 — V_1 — V_2 — O_2 dihedral angles displayed in Table 3. They range from 126.8° for **1** to 100.5° in **3** resulting in an almost orthogonal arrangement between the vanadium basal planes.

When the phenyl rings of the phosphinate ligands are substituted in the para position with either electron withdrawing or donating substituents the bpy dimer core adopts a different structural framework. The structures of three such compounds were determined by single crystal X–ray studies (Table 4), and all were found to be tris(μ–bis–*p*-substituted–phenyl phosphinato–*O,O'*)divanadyl complexes. *Figure 3(A)* displays an ORTEP view of the *p*-CH_3O– derivative **6**.

(A)

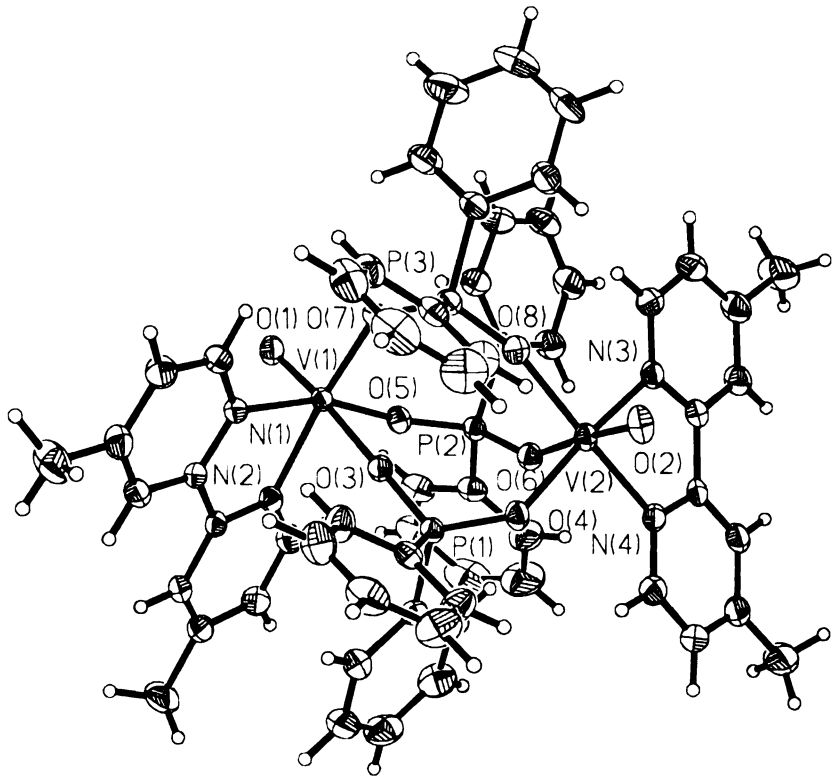

(B)

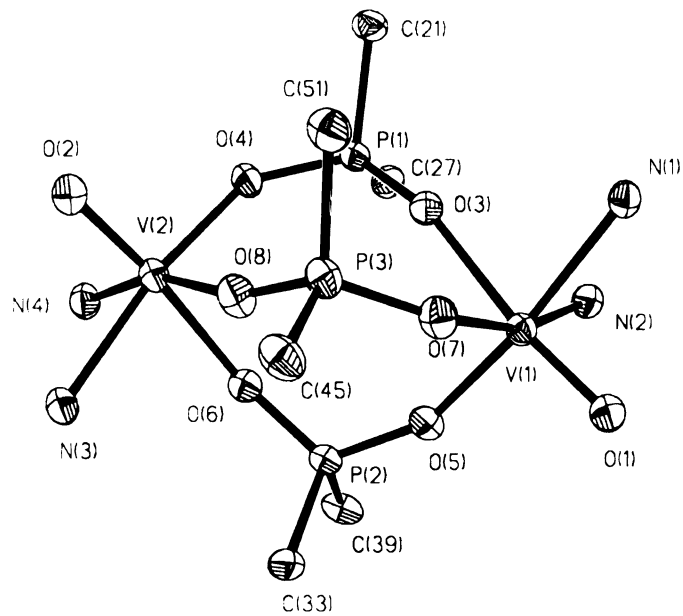

Figure 2. ORTEP representation of {dmbpyVO[μ–$(C_6H_5)_2PO_2]_{1.5}$}$_2${ClO_4}•$4CH_3OH$ (A), and view of its *twist* dimer core (B). The P(3) phosphinate group bridges the equatorial sites of the two vanadyl octahedra.

Table 4. Crystallographic Data for Compounds **4**, **5**, and **6**

	4	**5**
	(A) Crystal Parameters	
formula	$C_{57.5}H_{46}ClF_6N_4O_{13.5}P_3V$	$C_{56}H_{40}Cl_7N_4O_{12}P_3V_2$
cr. habit, color	facetted oval, green	plate, green
FW	1353.22	1403.86
cr. size (mm^3)	0.28 × 0.25 × 0.18	0.28 × 0.25 × 0.04
crystal system	orthorombic	monoclinic
space group	$P2_12_12_1$	$P2_1/c$
a (Å)	13.1898(2)	18.51111(1)
b (Å)	17.6206(3)	23.0689(3)
c (Å)	24.9142(1)	15.0155(2)
α (deg)	90	90
β (deg)	90	100.738(1)
γ (deg)	90	90
V ($Å^3$)	5790.36(13)	6299.8(1)
Z	4	4
d_{calc} (Mg/m^3)	1.552	1.480
F(000)	2756	2840
μ(Mo Kα), mm^{-1}	0.540	0.731
	(B) Data Collection	
$2\theta_{max}$ (deg)	50.1	50.2
index ranges	$-15 \le h \le 15$ $0 \le k \le 20$ $0 \le l \le 29$	$-22 \le h \le 21$ $0 \le k \le 27$ $0 \le l \le 17$
temperature / K	173(2)	173(2)
refl. collected	29058	29510
ind. reflections	10076	10923
R(int) (%)	3.98	9.83
	(C) Refinement	
Ref. method	Full–matrix least–squares on F^2	Full–matrix least–squares on F^2
R ind. ($I > 2\sigma(I)$)	R1 = 0.0535 WR2 = 0.1079	R1 = 0.0711 WR2 = 0.1389
R ind. all data	R1 = 0.0734 WR2 = 0.1185	R1 = 0.1545 WR2 = 0.1734
Δ(ρ) ($e^-/Å^3$)	0.679	0.682
GOF	1.025	0.901

Table 4 (cont'd)

	6
(A) Crystal Parameters	
formula	$C_{62}H_{58}ClN_4O_{18}P_3V_2$
cr. habit, color	block, green
FW	1377.36
cr. size (mm^3)	0.35 × 0.20 × 0.18
crystal system	triclinic
space group	$P\bar{1}$
a (Å)	12.5544(5)
b (Å)	14.6461(6)
c (Å)	18.8870(7)
α (deg)	76.375(1)
β (deg)	77.899(1)
γ (deg)	69.596(1)
V ($Å^3$)	3132.2(2)
Z	2
d_{calc} (Mg/m^3)	1.460
F(000)	1420
μ(Mo Kα), mm^{-1}	0.493
(B) Data Collection	
$2\theta_{max}$ (deg)	50.1
index ranges	$-14 \le h \le 14$ $-16 \le k \le 17$ $0 \le l \le 22$
temperature / K	173(2)
refl. collected	17417
ind. reflections	10509
R(int) (%)	3.34
(C) Refinement	
Ref. method	Full–matrix least–squares on F^2
R ind. ($I > 2\sigma(I)$)	R1 = 0.0721 WR2 = 0.1575
R ind. all data	R1 = 0.1275 WR2 = 0.1858
Δ(ρ) ($e^-/Å^3$)	1.009
GOF	1.016

The metric parameters of the vanadyl octahedra for all three compounds (Table 5) were similar to those observed in the twist structural type. Interconnection of the octahedra is accomplished by two phosphinates bridging equatorial sites and one bridging the axial sites (*Figure 3(B)*). Such an arrangement results in the formation of a convex boat[8], where vanadyl groups are *syn* with respect to each other. The axes defined by the vanadyl groups are almost coplanar as indicated by the small $O_1 — V_1 — V_2 — O_2$ dihedral angles, which range from 8.1° to 15.4° (Table 5).

Figure 4 depicts the electronic spectrum of {bpyVO[μ–(*p*-MeO–$C_6H_4)_2PO_2]_{1.5}\}_2\{ClO_4\}$ in acetone which represents a typical spectrum displayed by this series of compounds. The respective data for the remaining derivatives are gathered in Table 6. Three weak absorptions are observed which are attributed to d – d transitions, according to the molecular orbital scheme devised by Gray and Ballhausen[9] for vanadyl complexes with local C_{4V} symmetry. In this point group the energy ordering of the d levels is as, b_2 (d_{xy}), e (d_{xz}, d_{yz}), b_1 ($d_{x^2-y^2}$), and a_1 (d_{z^2}). Deviations in symmetry result in the lifting of the degeneracy of the e orbital set, as it is the case for the compounds in study, where the local metal symmetry is better approximated by the C_s point group. The crystal field transitions in the C_{4V} point group involve moving of the unpaired electron that resides in the b_2 orbital to the e, b_1, and a_1 MOs, which are essentially the 3d metal atomic orbitals, resulting in ^2E, $^2B_1$, and $^2A_1$ excited states, respectively. To a good approximation electron repulsion effects are considered to be the same for all these states, and hence transitions are expected to occur to ^2E, $^2B_1$, and $^2A_1$ in order of increasing energy. When the symmetry is lower than C_{4V}, the $^2B_2$ to ^2E transition is expected to appear as two separate absorption profiles resulting in a total of four bands, as has been observed in a few vanadyl complexes[10].

Table 5. Bond Distances and Dimer Metric Parameters for $\{L_2VO[\mu\text{–}(X\text{–}C_6H_4)_2PO_2]_{1.5}\}_2\{ClO_4\}$, **4**, **5**, and **6**[a]

Bond Distances	**4**	**5**	**6**
$V = O_{ax}$	1.612(3)	1.590(4)	1.597(4)
	1.601(3)	1.594(4)	1.600(4)
$V — N_{eq}$	2.122(4)	2.116(5)	2.126(4)
	2.129(4)	2.126(5)	2.118(4)
$V — N_{eq}$	2.124(4)	2.142(5)	2.139(4)
	2.130(4)	2.144(5)	2.122(4)
$V — O_{eq}$	1.982(3)	2.004(4)	1.984(3)
	1.989(3)	1.980(4)	1.979(3)
$V — O_{eq}$	1.989(3)	2.022(4)	2.008(3)
	1.995(3)	1.995(4)	1.993(4)
$V — O_{ax}$	2.133(3)	2.143(4)	2.113(4)
	2.148(3)	2.112(4)	2.125(3)
T / K	173	173	173
$V_1 \cdots\cdots V_2$ / Å	4.928	4.879	4.880
$<N_2O_2^{V1} / N_2O_2^{V2}>$ / ° [b]	103.4	102.2	99.8
$<O_1 — V_1 — V_2 — O_2>$ / ° [c]	8.1	13.0	15.4

[a] **4**: L = bpy; X = F–. **5**: L = bpy; X = Cl–. **6**: L = bpy; X = CH_3O–. [b] Dihedral angle between the $N_2O_2^V$ planes (defined by the four basal atoms of the respective vanadium octhedron). [c] Dihedral angle between the axes defined by the vanadyl groups.

(A)

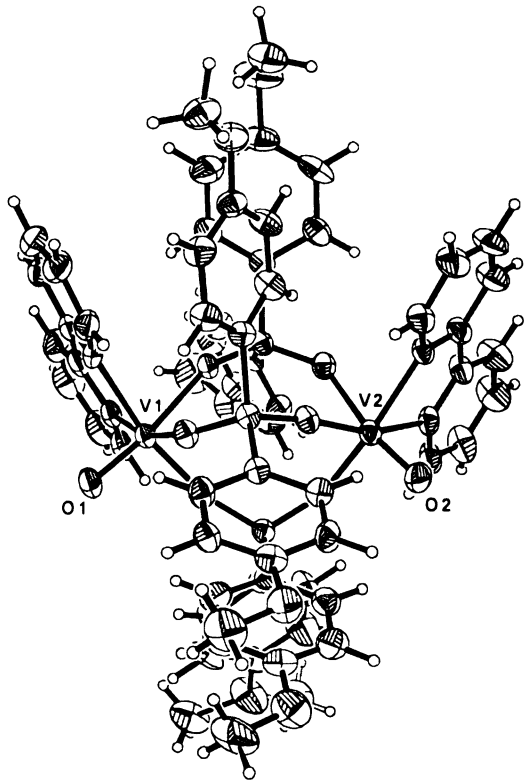

(B)

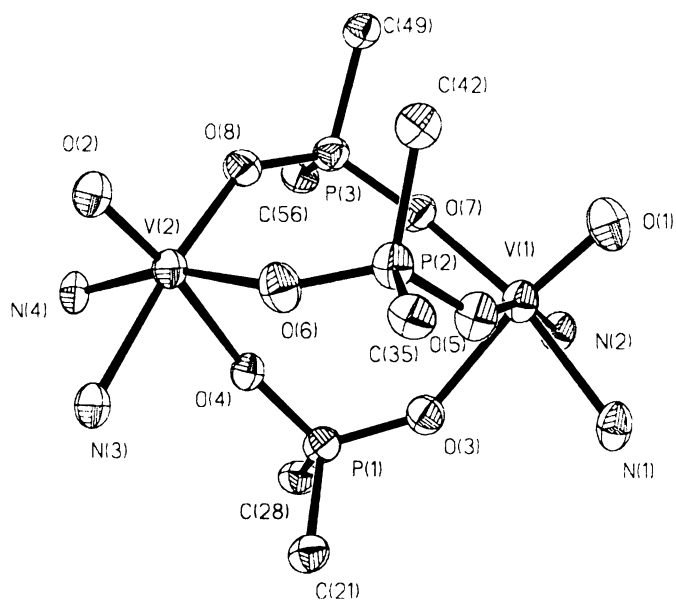

Figure 3. ORTEP representation of {bpyVO[μ–(p-CH_3O–C_6H_4)$_2PO_2$]$_{1.5}$}$_2${ClO_4} (A), and view of its *syn* dimer core (B). The P(1) phosphinate group bridges the axial sites of the two vanadyl octahedra.

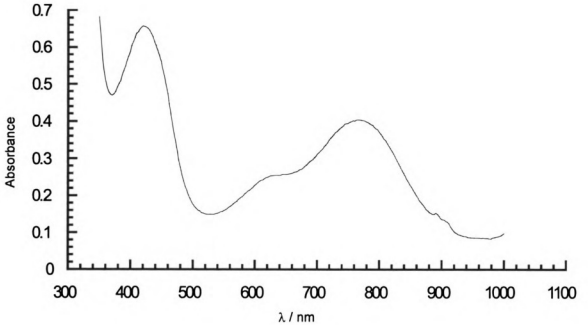

Figure 4. Absorption spectrum of {bpyVO[μ–(*p*-MeO–C_6H_4)$_2PO_2$]$_{1.5}$}$_2${ClO_4} in acetone solution. The three maxima are attributed to d – d transitions.

Table 6. Electronic Absorption Spectra of $\{bpyVO[(p\text{-}X\text{–}C_6H_4)_2PO_2]_{1.5}\}_2\{ClO_4\}$, 1, 4, 5, 6, and $\{tmbpyVO[(p\text{-}CH_3O\text{–}C_6H_4O)_2PO_2]\}_2\{ClO_4\}$, 6A, in acetone

– X	nm	cm^{-1}	ε	nm	cm^{-1}	ε	nm	cm^{-1}	ε
– H (**1**)	381	26212	206	617	16207	40	764	13089	66
– F (**4**)	404	24752	76	635	15748	17	758	13193	33
– Cl (**5**)	405	24716	91	652	15347	30	753	13280	49
– OCH_3 (**6**)	420	23798	94	633	15788	36	766	13055	57
– OCH_3 (**6A**) [a]	402	24876	68	631	15853	20	771	12967	50

Inspection of Table 6 reveals that three absorptions are observed for all dimer compounds belonging to this series. Hence, although lifting of the degeneracy is expected based on the structural environment of the vanadyl ion, the energy separation between the d_{xz} and d_{yz} orbitals should be small. The stronger transition, at low energies, is attributed to the $^2B_2$ to ^2E excitation. The second one, which appears as a weak shoulder, is assigned to a $^2B_2$ to $^2B_1$ transition and is only vibronically allowed. The final one is attributed to the also forbidden $^2B_2$ to $^2A_1$ transition.

b. Magnetic Susceptibilities Studies

The magnetic properties of the structurally characterized dimer complexes **1** – **6** and those of compounds **5A** and **6A** have been determined by powder susceptibility studies. The data for the diphenylphosphinate complexes **1**, **2**, and **3** are gathered in Table 7 along with metric parameters of the dimer core, while those of the remaining complexes **4**, **5**, **5A**, **6**, and **6A** are collected in Table 8. The molecular susceptibilities show a monotonic increase with decreasing temperature till they reach a maximum for complexes **2**, **3**, **4**, **5**, **6**, and **6A** (*Figures 5* and *6*). This maximum is characteristic of intradimer antiferromagnetic interaction, a behavior also indicated by the deviation towards zero of the $\chi_M T$ product as the temperature approaches zero. The latter is true even for complexes **1** and **5A** which do not display a maximum in the susceptibility versus temperature plot.

The data were fitted to a Bleaney–Bowers[11] model for an S = 1/2 system

$$\chi_M = \frac{2Ng^2\beta^2}{KT[3 + exp(-J/kT)} \qquad (4.1)$$

Table 7. Susceptibility Data and Dimer Metric Parameters for $\{(L_2VO[\mu\text{-}(Ph)_2PO_2]\}_2\{ClO_4\}$[a]

	1	2	3
J/k in K	– 2.9	– 8.9	– 11.3
g	1.97	2.02	1.98
T_{max} in K [b]	—	5.0	6.5
T_{max} in K [c]	1.8	5.5	7.0
% impurity	—	6.1	6.0
T / K	173	173	173
$V_1 \cdots\cdots V_2$ / Å	4.906	4.906(1)	4.881(3)
$<N_2O_2^{V1} / N_2O_2^{V2}>$ / ° [d]	39.2	45.3(1)	58.0(2)
<NVO / NVO> / ° [e]	51.4	43.4	27.5
$<O_1 — V_1 — V_2 — O_2>$ / ° [f]	126.8	113.2(1)	100.5(5)

[a] **1**: L = bpy. **2**: L = dmbpy. **3**: L = tmbpy. [b] Experimental. [c] From equation 4.2. [d] Dihedral angle between the $N_2O_2^V$ planes (defined by the four basal atoms of the vanadium octahedron). [e] Dihedral angles between the NVO planes (defined as the plane orthogonal to the V — O_{eq} bond). [f] Dihedral angle between the axes defined by the vanadyl groups.

Table 8. Susceptibility Data and Dimer Metric Parameters for $\{(L_2VO[\mu\text{–}(p\text{-X–Ph})_2PO_2]\}_2\{ClO_4\}$[a]

	4	**5**	**5A**	**6**	**6A**
J/k in K	– 26.0	– 25.0	– 4.5	– 23.9	– 11.3
g	1.97	2.06	1.98	1.90	1.94
T_{max} in K [b]	15.5	15.5	—	14.5	7.0
T_{max} in K [c]	16.3	15.6	2.8	15.0	7.1
% impurity	5.9	1.4	—	1.9	2.9
T / K	173	173	—	173	131
$V_1 \cdots\cdots V_2$ / Å	4.928	4.879	—	4.880	4.835
$<N_2O_2^{V1} / N_2O_2^{V2}>$ / ° [d]	103.4	102.2	—	99.8	55.0
$<O_1 — V_1 — V_2 — O_2>$ / ° [e]	8.1	13.0	—	15.4	109.6
σ_p [f]	0.06	0.23	0.23	– 0.27	– 0.27

[a] **4**: L = bpy; X = F–. **5**: L = bpy; X = Cl–. **5A**: L = tmbpy; X= Cl–. **6**: L = bpy; X = CH_3O–.**6A**: L = tmbpy; X = CH_3O–. [b] Experimental. [c] From equation 4.2. [d] Dihedral angle between the $N_2O_2^V$ planes (defined by the four basal atoms of the respective vanadium octhedron). [e] Dihedral angle between the axes defined by the vanadyl groups. [f] Hammett electronic parameters.

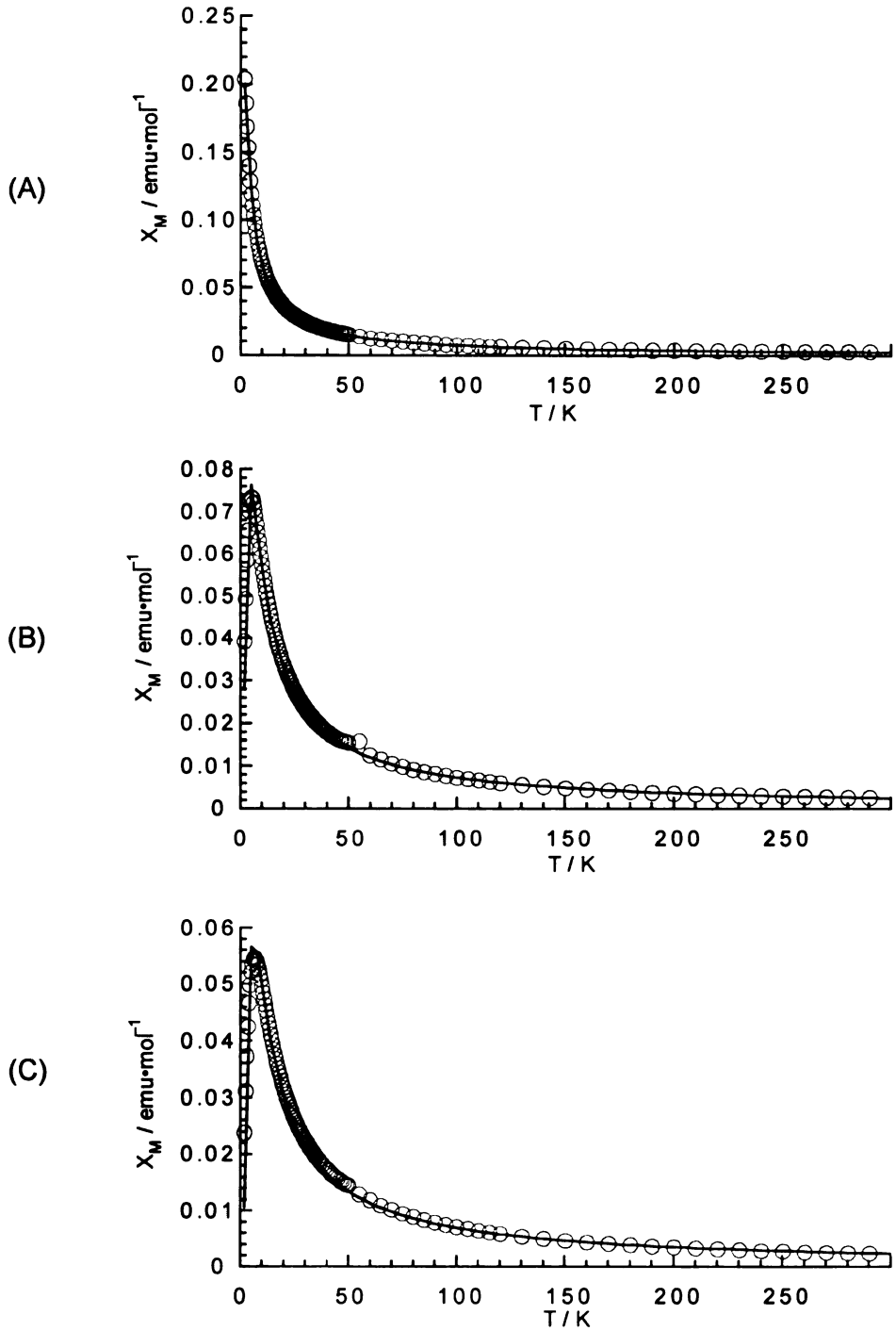

Figure 5. Molar susceptibility versus temperature plots of compmpounds **1** (A), **2** (B), and **3** (C). The solid line represents the best fit obtained by using a Bleaney–Bowers dimer model.

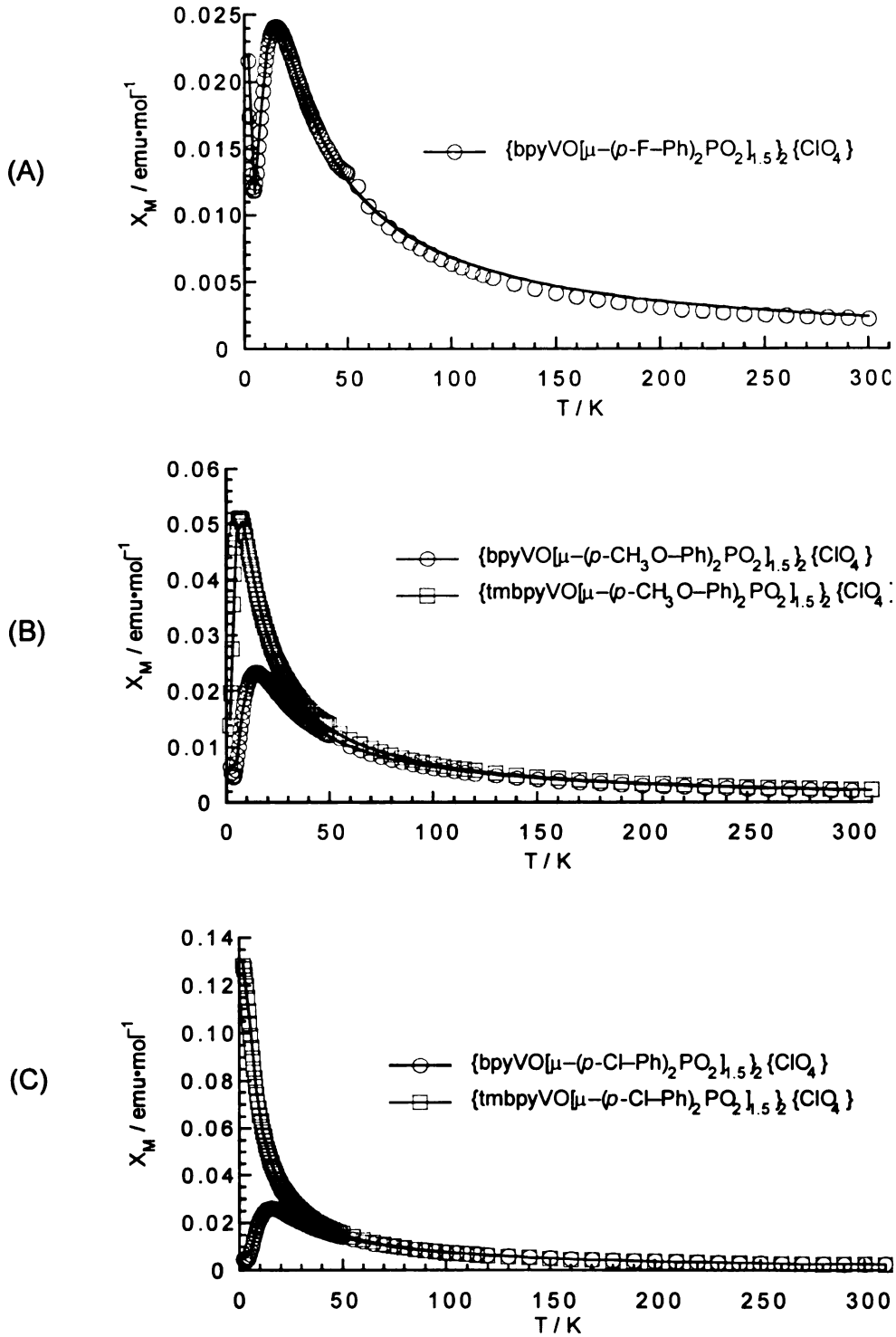

Figure 6. Molecular susceptibility versus temperature plots of compounds **4** (A), **6** and **6A** (B), and **5** and **5A** (C). The solid line represents the best fit obtained by using a Bleaney–Bowers dimer model.

where J is the singlet–triplet energy splitting. For J < 0, the model predicts a maximum for the magnetic susceptibility which tends toward zero when T approaches zero. The temperature at which the maximum occurs, which is a signature of antiferromagnetic interaction, is related to J through

$$\frac{|J|}{kT_{max}} = 1.599 \qquad (4.2)$$

Inspection of Tables 7 and 8 shows excellent agreement between the experimental and the calculated T_{max}, further strengthening the validity of the magnetic model utilized for data fitting.

The singlet–triplet energy splittings calculated by the data fit show an increase for the diphenylphosphinate derivatives upon methyl–substitution of the terminal ligands. In antithesis, the bpy complexes **5**, **6** display stronger and almost identical exchange couplings than their tmbpy analogs **5A**, and **6A**. The decrease upon methyl substitution of the terminal ligands was 5–fold for the *p*-CH_3O– derivatives and only 2–fold for the *p*-Cl– one.

2. Synthesis and Characterization of {LVO[μ–(*p*-X–C_6H_4)$_2PO_2$]}$_2$ Dimers, (L = hydrotris(1–pyrazolyl)borate, and X = H–, CH_3O–, CH_3–, F–), and of {LVO[μ–(*p*-NO_2–C_6H_4)$_2OPO_2$]}$_2$•S, (L = hydrotris(1–pyrazolyl)borate, and S = CH_2Cl_2, CH_3COCH_3, C_4H_5N, C_4H_4S, and $C_2H_6S_2$)

a. Synthesis and Characterization

Utilization of hydrotris(1–pyrazolyl)borate as a terminal ligand affords a new series of dimeric compounds, with dimer cores similar to the D VII exchange pathway of the extended layered vanadyl phosphates/phosphonates. The first dimer complex of this type was synthesized by Carrano and coworkers[8] who

devised the general synthetic scheme depicted in *Figure 7*. Reaction of the vanadyl mononuclear complex $HB(pz)_3VO(acac)$[12] in acetonitrile or dichloromethane with the desired phosphinic acid afforded the dimer compounds as blue polycrystalline powders. Recrystallization of the powder samples from either acetonitrile or dichloromethane produced blue crystals, the size and shape of which is a function of the crystallization medium.

In the original literature work two dimeric compounds were synthesized having as diamagnetic bridging groups the diphenylphosphinate and diphenylphosphonate ligands. By introducing substituents in the para– position of the phenyl rings we have synthesized a series of homologous complexes, where minor structural changes are introduced within the dimetallic core. Correlation of magnetic properties to these subtle geometrical variations was accomplished by X–ray structure determination of these compounds.

p–Substitution on the two phenyl rings of the diphenylphosphinate by CH_3–, CH_3O–, and F–, in addition to the unsubstituted parent compound, provides a series of four closely related dimer cores. The room temperature crystal structure of the parent compound crystallized in acetonitrile has been previously reported[13]. It was however repeated at 143 K, in crystals grown in dichloromethane. The crystallographic data of $\{HB(pz)_3VO[\mu\text{–}(Ph)_2PO_2]\}_2 \cdot 2CH_2Cl_2$ (**7**), $\{HB(pz)_3VO[\mu\text{–}(p\text{-}CH_3O\text{–}Ph)_2PO_2]\}_2 \cdot 2CH_3CN$ (**8**), and $\{HB(pz)_3VO[\mu\text{–}(p\text{-}F\text{–}Ph)_2PO_2]\}_2 \cdot 2CH_3CN$ (**9**), are gathered in Table 9. Table 10 displays the crystal data for $\{HB(pz)_3VO[\mu\text{–}(p\text{-}CH_3\text{–}Ph)_2PO_2]\}_2 \cdot 2CH_3CN$ (**10**), and $\{HB(pz)_3VO[\mu\text{–}(p\text{-}CH_3\text{–}Ph)_2PO_2]\}_2 \cdot 2CH_2Cl_2$ (**11**), from crystals grown in acetonitrile and dichloromethane and data collected at 173 and 133 K respectively. The crystal structure of the latter complex is described in detail while only notable differences of the remaining structures will be discussed.

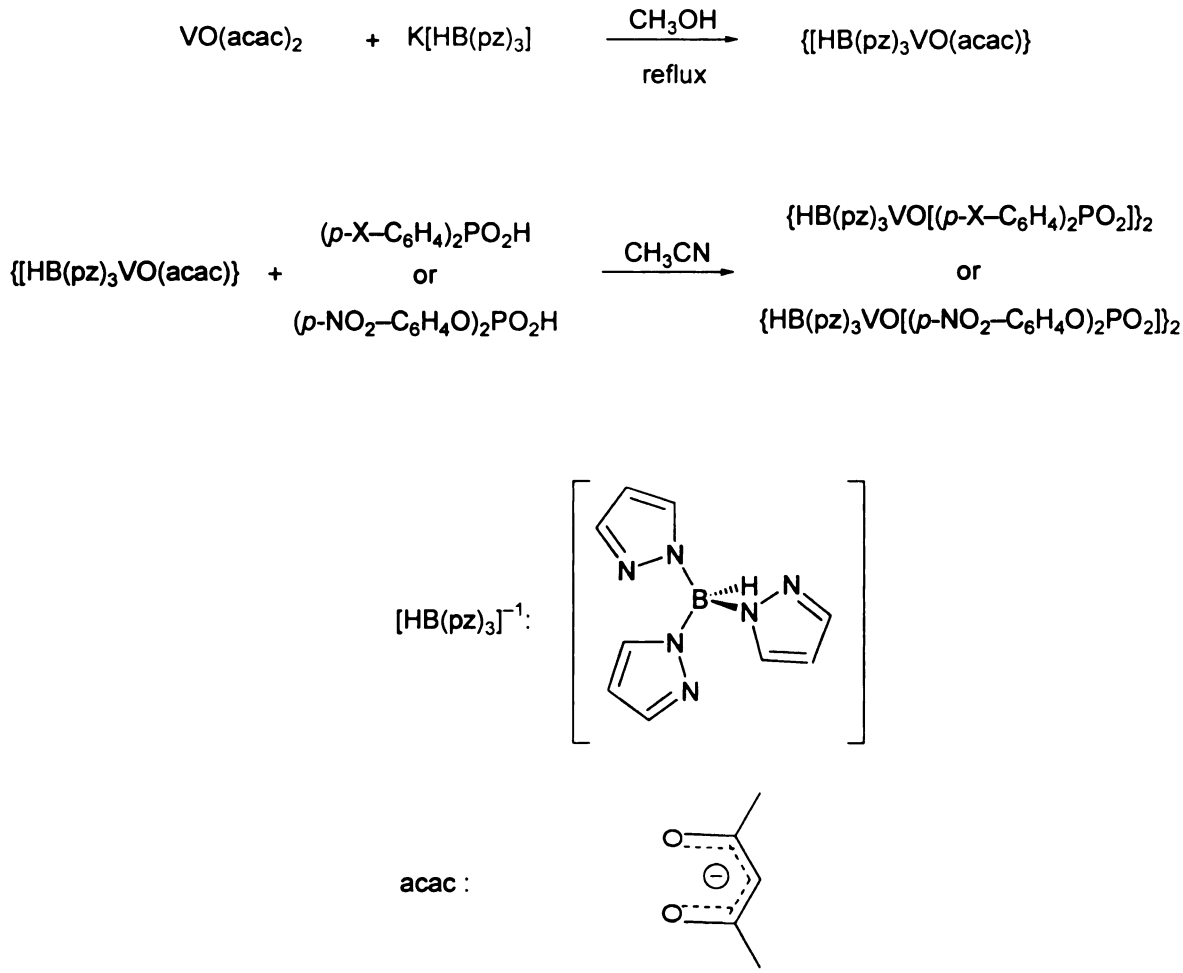

Figure 7. General synthetic scheme for phosphinate and phosphonate dimers with tris(1–pyrazolyl)borate as the terminal ligand.

Table 9. Crystallographic Data for Compounds **7**, **8**, and **9**

	7	**8**
	(A) Crystal Parameters	
formula	$C_{43}H_{42}B_2Cl_2N_{12}O_6P_2V_2$	$C_{48}H_{51}B_2N_{13}O_{10}P_2V_2$
crystal habit, color	block, blue	plate, blue
FW	1079.23	1155.46
crystal size (mm^3)	0.75 × 0.35 × 0.23	0.45 × 0.23 × 0.06
crystal system	triclinic	monoclinic
space group	$P\bar{1}$	*C2/c*
a (Å)	12.2553(1)	20.7757(4)
b (Å)	13.6377(2)	12.7340(3)
c (Å)	16.2773(1)	20.1158(4)
α (deg)	91.578(1)	90
β (deg)	99.998(1)	91.051(1)
γ (deg)	110.973(1)	90
V ($Å^3$)	2489.7(1)	5320.9(2)
Z	2	4
d_{calc} (Mg/m^3)	1.440	1.442
F(000)	1104	2384
μ(Mo Kα), mm^{-1}	0.606	0.481
	(B) Data Collection	
$2\theta_{max}$ (deg)	50.0	50.1
index ranges	$-14 \le h \le 14$ $-15 \le k \le 16$ $-19 \le l \le 19$	$-24 \le h \le 24$ $0 \le k \le 15$ $0 \le l \le 23$
temperature / K	143(2)	173(2)
reflections collected	17980	13029
independent reflections	8602	4657
R(int) (%)	1.74	2.51
	(C) Refinement	
Refinement method	Full–matrix least–squares on F^2	Full–matrix least–squares on F^2
R indices ($I > 2\sigma(I)$)	R1 = 0.0435 WR2 = 0.1106	R1 = 0.0456 WR2 = 0.1018
R indices all data	R1 = 0.0492 WR2 = 0.1135	R1 = 0.0570 WR2 = 0.1077
$\Delta(\rho)$ ($e^-/Å^3$)	1.115	0.753
GOF	1.089	1.048

Table 9 (cont'd)

	9
(A) Crystal Parameters	
formula	$C_{46}H_{42}B_2F_4N_{14}O_6P_2V_2$
crystal habit, color	block, blue
FW	1148.38
crystal size (mm^3)	0.54 × 0.50 × 0.38
crystal system	triclinic
space group	$P\bar{1}$
a (Å)	9.5497(7)
b (Å)	13.6622(9)
c (Å)	20.8945(14)
α (deg)	79.594(2)
β (deg)	85.006(1)
γ (deg)	76.554(1)
V ($Å^3$)	2604.9(3)
Z	2
d_{calc} (Mg/m^3)	1.464
F(000)	1172
μ(Mo Kα), mm^{-1}	0.496
(B) Data Collection	
$2\theta_{max}$ (deg)	46.6
index ranges	$-10 \le h \le 10$ $-15 \le k \le 15$ $-23 \le l \le 23$
temperature / K	131(2)
reflections collected	21560
independent reflections	7504
R(int) (%)	4.65
(C) Refinement	
Refinement method	Full–matrix least–squares on F^2
R indices ($I > 2\sigma(I)$)	R1 = 0.0333 WR2 = 0.0790
R indices all data	R1 = 0.0493 WR2 = 0.0849
Δ(ρ) ($e^-/Å^3$)	0.356
GOF	0.940

Table 10. Crystallographic Data for Compounds **11**, and **12**

	10	**11**
	(A) Crystal Parameters	
formula	$C_{50}H_{54}B_2N_{14}O_6P_2V_2$	$C_{48}H_{52}B_2Cl_4N_{12}O_6P_2V_2$
crystal habit, color	plate, blue	block, blue
FW	1132.51	1220.26
crystal size (mm^3)	0.22 × 0.19 × 0.04	0.75 × 0.65 × 0.31
crystal system	monclinic	monoclinic
space group	$P2_1/c$	$P2_1/c$
a (Å)	11.9355(5)	12.1590(2)
b (Å)	22.1526(9)	22.0256(2)
c (Å)	12.0009(5)	12.1094(1)
α (deg)	90	90
β (deg)	118.503(1)	118.585(1)
γ (deg)	90	90
V ($Å^3$)	2788.5(2)	2847.6(1)
Z	2	2
d_{calc} (Mg/m^3)	1.349	1.423
F(000)	1172	1252
μ(Mo Kα), mm^{-1}	0.453	0.629
	(B) Data Collection	
$2\theta_{max}$ (deg)	50.1	50.0
index ranges	$-14 \le h \le 12$ $0 \le k \le 26$ $0 \le l \le 14$	$-14 \le h \le 13$ $-26 \le k \le 26$ $-13 \le l \le 14$
temperature / K	173(2)	133(2)
reflections collected	13618	23433
independent reflections	4881	5006
R(int) (%)	3.72	5.53
	(C) Refinement	
Refinement method	Full–matrix least–squares on F^2	Full–matrix least–squares on F^2
R indices ($I > 2\sigma(I)$)	R1 = 0.0517 WR2 = 0.1058	R1 = 0.0388 WR2 = 0.1022
R indices all data	R1 = 0.0789 WR2 = 0.1157	R1 = 0.0458 WR2 = 0.1059
$\Delta(\rho)$ ($e^-/Å^3$)	0.666	0.559
GOF	1.029	1.028

The CH_3– derivative is found as bis(μ–di(tolyl) phosphinato–O,O') divanadyl complex (*Figure 8(A)*), with only half of the dimer being crystallographically unique since an inversion center relates one side of the dimer to the other. The vanadium atom is found in a distorted octahedral coordination environment with the typical short vanadyl bond occupying one of the axial positions. The hydrotris(1–pyrazolyl)borate capping ligand occupies three of the remaining coordination sites, one of which is trans– to the vanadyl oxygen. The equatorial V — N_{eq} bond distances are almost equivalent (2.116(2) and 2.119(2) Å), while the V — N_{ax} bond is much longer (2.310(2) Å). The remaining two free sites of the octahedron are supplemented by two oxygen atoms provided by different phosphinate ligands. The V — O_{eq} bonds are in the order of 1.986(2) and 1.992(2) Å, distances similar to those observed in the extended vanadyl phosphates/phosphonates. Bridging of the two metal sites is accomplished by the latter ligands affording an *anti* orientation of the vanadyl groups (*Figure 8(B)*), as expected from the presence of the inversion center within the dimer core. Such orientations, apart from the work of Carrano and coworkers[8,13], have also been observed in the other known dimer phosphonate complex reported by Zubieta and coworkers[14]. The local symmetry point group of each vanadium center is approximated as C_s, with the metal being slightly displaced from the basal plane of the octahedron (defined by the four equatorial atoms and symbolized as $N_2O_2^V$).

The remaining derivatives of this homologous series display dimer cores with similar metric parameters (Table 11). Even in the parent and the F–complexes, where two different dimers crystallized within the unit cell, the metric parameters of the individual dimers are almost identical. Small structural variations are observed only in the relative orientations of the aromatic rings in space and with respect to the five–membered pyrazolyl rings of the terminal

(a)

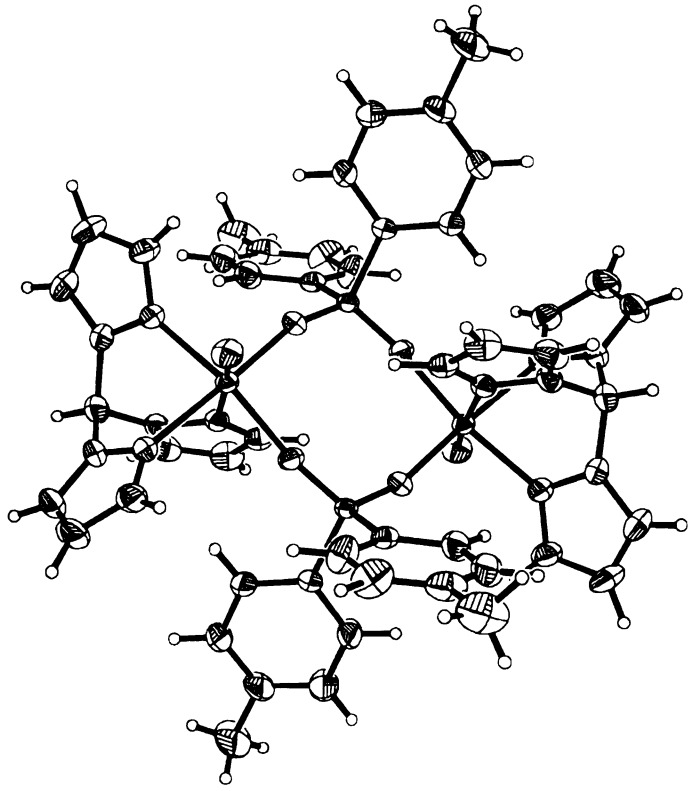

(B)

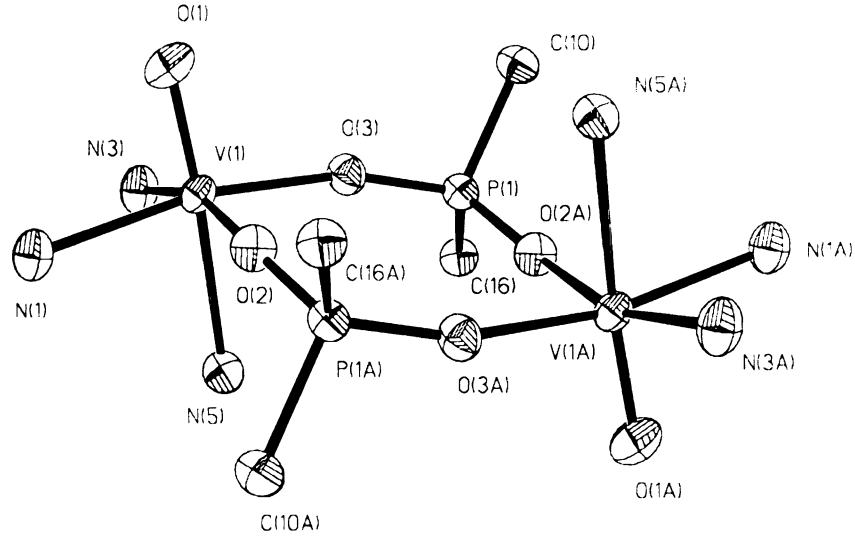

Figure 8. ORTEP view of $\{HB(pz)_3VO[\mu\text{–}(p\text{-}CH_3\text{–}Ph)_2PO_2]\}_2 \cdot 2CH_2Cl_2$ (**11**), where half of the atoms are crystallographically unique (A), and view of its *anti* dimer core (B).

Table 11. Bond Distances and Dimer Metric Parameters for $\{HB(pz)_3VO[\mu\text{–}(p\text{-}X\text{–}C_6H_4)_2PO_2]\}_2$ **7**, **8**, **9**, **10**, and **11**[a]

Bond Distances	H– (7)	CH_3– (10)	CH_3– (11)	CH_3O– (8)	F– (9)
V = O_{ax}	1.601(2) 1.600(2)	1.598(2)	1.594(2)	1.599(2)	1.592(2) 1.593(2)
V — N_{eq}	2.126(2) 2.117(2)	2.114(3)	2.116(2)	2.104(2)	2.100(2) 2.101(2)
V — N_{eq}	2.130(2) 2.148(3)	2.116(3)	2.119(2)	2.122(2)	2.115(2) 2.120(2)
V — O_{eq}	1.989(2) 1.983(2)	1.987(2)	1.986(2)	1.983(2)	1.981(2) 1.985(2)
V — O_{eq}	1.991(2) 1.989(2)	1.989(2)	1.992(2)	1.984(2)	1.986(2) 1.986(2)
V — N_{ax}	2.309(2) 2.310(2)	2.299(3)	2.310(2)	2.303(2)	2.321(2) 2.322(2)
T / K	143	173	133	173	131
V ····· V / Å (#1)[b]	5.291(1)	5.257(1)	5.233(1)	5.219(1)	5.265(1)
V ····· V / Å (#2)[c]	5.285(1)				5.270(1)
$<VO_2 / O_4^P>$ / °[d] (#1)	171.3(1)	164.2	164.6	162.1	172.7(1)
$<VO_2 / O_4^P>$ / °[d](#2)	175.3(1)				174.5(1)
$<N_2O_2^V / O_4^P>$ / °[e] (#1)	159.9(1)	153.2	153.3	152.2	161.6(1)
$<N_2O_2^V / O_4^P>$ / °[e] (#2)	163.9(1)				163.3(1)
$D(N_2O_2^V/N_2O_2^V)$ / Å[f] (#1)	0.852	1.160	1.154	1.181	0.772
$D(N_2O_2^V/N_2O_2^V)$ / Å[f] (#2)	0.689				0.696
$<C_3H_3N_2/C_6H_5>_{ax}$ / °[g] (#1)	22.1(2)	43.8(1)	41.2(1)	31.4(1)	17.3(1)
$<C_3H_3N_2/C_6H_5>_{ax}$ / °[g] (#2)	26.4(2)				11.3(1)

[a] **7**: X = H–. **8**: X = CH_3O–. **9**: X = F–. **10**: X = CH_3–; recrystallized fromacetonitrile. **11**: X = CH_3–; recrystallized in dichloromethane. [b] Refers to the first of the two crystallographically unique dimer molecules. [c] Refers to the second of the two crystallographically unique dimer molecules. [d] Dihedral angle between the VO_2 plane (defined by vanadium and the two basal oxygen atoms of the dimer ring) and the plane O_4^P (defined by the four phosphonate ring oxygen atoms). [e] Dihedral angle between the O_4^P and the $N_2O_2^V$ planes (defined by the four basal oxygens of the vanadium octahedron). [f] Distance between the $N_2O_2^V$ planes. [g] Dihedral angles between the axial pyrazolyl ($C_3H_3N_2$) and the respective aryl (C_6H_5) groups of the terminals and bridging ligands.

ligands. Thus, in the F– derivative, one of the *p*-fluorophenyl rings is almost parallel to the axial (to the vanadyl) pyrazolyl ring with angles of 11.3(1)° and 17.3(1)° for the two different dimers. The respective values for the remaining derivatives (Table 11) are 22.1(2)° and 26.4(2)° for the parent compound, 31.4(1)° for CH_3O–, and 43.8(1)° for CH_3–.

Such differences along with the packing requirements of each dimer imposed by substitution at the para position of the phenyl rings produce some notable discrepancies among the bridge cores of the various derivatives. They contribute to the flattening or not of the eight–membered ring that constitutes the bridge core. *Figure 9* displays two borderline conformations of the latter, one corresponding to an ideal chair–like and the other to a flat conformation. Since in the following sections the orientation of the vanadium d_{xy} orbital is approximated as the orientation of its basal plane, an ideal chair–like ring is considered as one having a 120° angle between the basal and the plane defined by the four oxygen ring atoms (symbolized as O_4^P). As the eight–membered ring flattens, the latter angle approaches 180°. In a flat ring the vanadium basal planes become coplanar — $d(N_2O_2^V \mid N_2O_2^V) = 0$ Å — while in a chair–like conformation these planes have a large displacement. *Figure 10* depicts the plot of that displacement versus the angle between the $N_2O_2^V$ and O_4^P planes, for the dimer cores utilized in this study (15 total number of points). A linear correlation was observed, from which the following equation was deduced:

$$d(N_2O_2^V \mid N_2O_2^V) = 7.23 - 0.03992 \bullet < N_2O_2^V \mid O_4^P > \qquad (4.3)$$

Equation 4.3 predicts that the displacement of the vanadium basal planes is 0.04 Å for the flat ring (where $<N_2O_2^V \mid O_4^P> = 180°$), a value which is very close to the actual 0 Å displacement expected for the coplanar arrangement. The value of 2.44 Å predicted for the chair conformation (where $<N_2O_2^V \mid O_4^P> = 120°$), on the

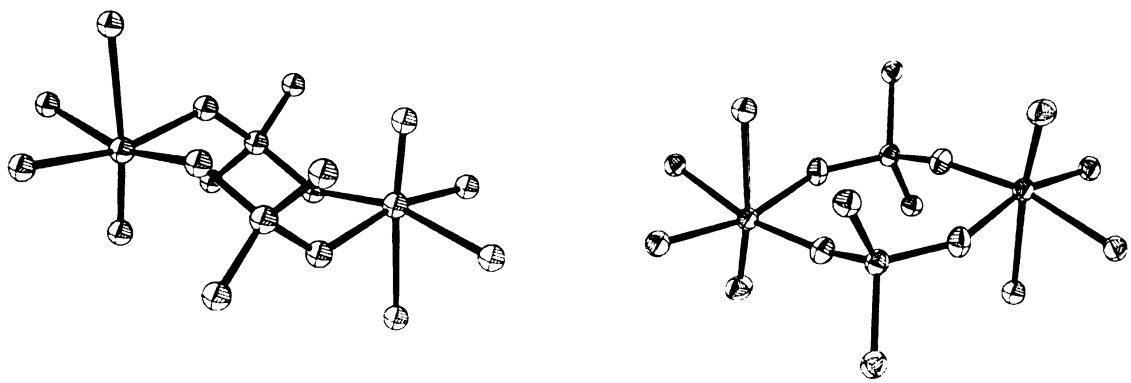

Chair Conformation		Flat Chair Conformation	
$<N_2O_2^{V} \mid O_4^{P}>$	120°	$<N_2O_2^{V} \mid O_4^{P}>$	180
$d(N_2O_2^{V} \mid N_2O_2^{V})$	~2.00 Å	$d(N_2O_2^{V} \mid N_2O_2^{V})$	0 Å

Figure 9. Chair (left) and flat (right) conformations of the eight–membered dimer core of the $\{HB(pz)_3VO[\mu\text{–}(p\text{-}X\text{–}Ph)_2PO_2]\}_2$ complexes.

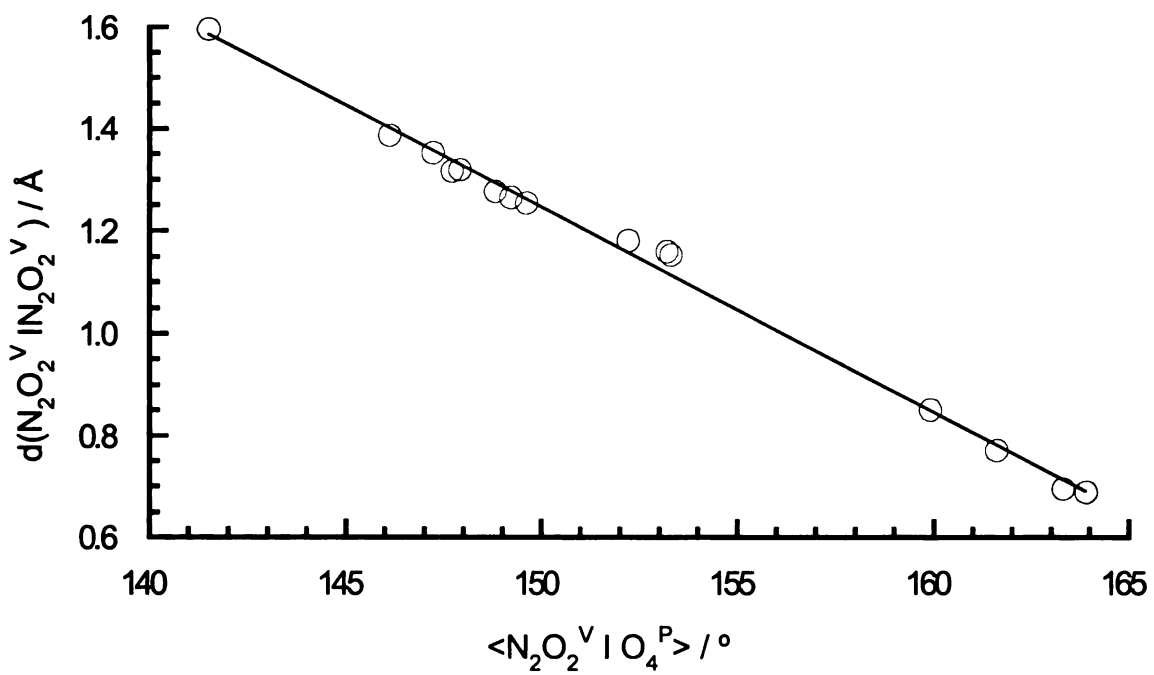

Figure 10. Basal plane displacement of the vanadyl octahedra plotted against the $<N_2O_2^V / O_4^P>$ dihedral angle.

other hand, is geometrically impossible if one considers the actual bond distances and angles. The corresponding values of the dimer units in the metal intercalated vanadyl phosphates were in the order of ~ 1.9 Å for almost ideal chair conformations, indicating that equation 4.3 will start deviating from linearity as $<N_2O_2^V \text{ I } O_4^P>$ approaches 120°. For the phosphinate derivatives presented in this study, the basal plane displacement ranges from 0.689 Å (for one of the parent dimer **8** crystallized in dichloromethane) to 1.181 Å (for the CH_3O– derivative **8**).

The dimer cores of the complexes described so far are closer to a flat conformation than to the idealized chair. This can probably be attributed to the relative orientations of the phosphinate aromatic rings and the pyrazolyl groups of the terminal ligand. A chair–like arrangement would bring them into close proximity enhancing unfavorable steric interaction, and therefore a flattened arrangement is preferred. In favor of this hypothesis, utilization of diphenylphosphonate as a bridging ligand results in a dimer core that better approximates a chair–like dimer ring ($< N_2O_2^V \text{ I } O_4^P> = 141.5°$, and $d(N_2O_2^V \text{ I } N_2O_2^V) = 1.597$ Å). The presence of the oxygen atom between the phosphorous and the phenyl group places the latter further apart from the pyrazolyl rings of the terminal ligands, diminishing steric interactions. When the terminal ligand is replaced by the bulkier hydridotris(3,5–dimethyl–1–pyrazolyl)borate steric interactions are again enhanced and a flat orientation is preffered[8].

In accordance with these observations, the *p*-NO_2– derivative of the $\{HB(pz)_3VO[\mu\text{–}(PhO)_2PO_2]\}_2$ complex was synthesized in an effort to prepare another dimer core that approximates the chair–like conformation of the eight–membered bridging core. The compound was synthesized following the general synthetic scheme depicted in *Figure 7*. Blue needles were obtained by slowly

cooling to room temperature a dichloromethane solution of the complex. A single crystal X–ray structure determination (Table 12) confirmed the preparation of the desired dimer, $\{HB(pz)_3VO[\mu\text{–}(p\text{-}NO_2\text{–}PhO)_2PO_2]\}_2 \cdot 2CH_2Cl_2$ (**12**). As in the phosphinate series, only half of the complex is crystallographically unique (*Figure 11(A)*). It displays similar metric parameters (Table 13) with the V — O_{eq} bonds being slightly longer (2.020(3) and 2.029(3) Å), in accordance with the less electronegative nature of the phosphonate oxygens. Shorter V — N_{eq} bonds compensate for the decreased electron density transferred from the bridging ligands to the metal center.

Surprisingly, the dimer core of the complex (*Figure 11(B)*) resembles more that of the phosphinate analogs, as judged by the $< N_2O_2^{V} \mid O_4^{P} >$ = 149.2° angle. This discrepancy can be understood by examining the relative orientations of the aryl and pyrazolyl rings in the unsubstituted and the *p*-NO_2–substituted compounds. In the former the angle between the phenyl and the axial pyrazolyl ring is on the order of 49.3°, with no close contacts among the atoms of these groups. In other words the phenyl rings point away from the terminal ligands. In the *p*-NO_2–substituted derivative on the other hand the corresponding rings are almost parallel (angle = 1.2°) with respect to each other, while the angle between the other aryl group and an equatorial pyrazolyl group is 20.7°. These π–π interaction effects[15] produce an energetically favorable situation, which is retained by the flat conformation of the dimer core.

We tested the strength of that interaction by crystallizing the compound in various solvents, of different steric requirements, hydrogen bonding abilities and electronic properties. The preservation or not of the dimer core was established by either single crystal X–ray structure determination or infrared and magnetic susceptibility measurements (described below). Tables 12, 14, and 15 display the crystal data for the $\{HB(pz)_3VO[\mu\text{–}(p\text{-}NO_2\text{–}PhO)_2PO_2]\}_2 \cdot S$ (where S = acetone

Table 12. Crystallographic Data for $\{HB(pz)_3VO[\mu\text{–}(p\text{-}NO_2\text{–}PhO)_2PO_2]\}_2 \cdot S$, with S = CH_2Cl_2 (**12**), CH_3COCH_3 (**13**) and C_4H_5N (**14**)

	12	**13**
	(A) Crystal Parameters	
formula	$C_{44}H_{40}B_2Cl_4N_{16}O_{18}P_2V_2$	$C_{48}H_{48}B_2N_{16}O_{20}P_2V_2$
crystal habit, color	plate, blue	plate, blue
FW	1408.16	1354.46
crystal size (mm^3)	0.54 × 0.31 × 0.08	0.46 × 0.19 × 0.08
crystal system	triclinic	triclinic
space group	$P\bar{1}$	$P\bar{1}$
a (Å)	8.5848(4)	8.5613(4)
b (Å)	11.9341(6)	12.3360(6)
c (Å)	14.8438(7)	15.4021(7)
α (deg)	99.781(1)	108.850(1)
β (deg)	96.6051)	94.937(1)
γ (deg)	102.852(1)	105.310(1)
V ($Å^3$)	1442.5(1)	1458.4(1)
Z	1	1
d_{calc} (Mg/m^3)	1.621	1.542
F(000)	714	694
μ(Mo Kα), mm^{-1}	0.650	0.465
	(B) Data Collection	
$2\theta_{max}$ (deg)	50.0	50.0
index ranges	$-10 \le h \le 10$ $-14 \le k \le 9$ $-17 \le l \le 17$	$-10 \le h \le 10$ $-14 \le k \le 13$ $-18 \le l \le 18$
temperature / K	143(2)	173(2)
reflections collected	5709	8921
independent reflections	4142	5018
R(int) (%)	3.32	2.64
	(C) Refinement	
Refinement method	Full–matrix least–squares on F^2	Full–matrix least–squares on F^2
R indices ($I > 2\sigma(I)$)	R1 = 0.0546 WR2 = 0.1240	R1 = 0.0395 WR2 = 0.0897
R indices all data	R1 = 0.0794 WR2 = 0.1367	R1 = 0.0592 WR2 = 0.0968
$\Delta(\rho)$ ($e^-/Å^3$)	0.638	0.253
GOF	0.963	1.019

Table 12 (cont'd)

	14
(A) Crystal Parameters	
formula	$C_{50}H_{46}B_2N_{18}O_{18}P_2V_2$
crystal habit, color	block, blue
FW	1372.49
crystal size (mm^3)	0.40 × 0.30 × 0.22
crystal system	triclinic
space group	$P\bar{1}$
a (Å)	8.5937(2)
b (Å)	12.4991(3)
c (Å)	14.7881(3)
α (deg)	101.922(1)
β (deg)	90.617(1)
γ (deg)	105.926(1)
V ($Å^3$)	1490.7(1)
Z	1
d_{calc} (Mg/m^3)	1.529
F(000)	702
μ(Mo Kα), mm^{-1}	0.454
(B) Data Collection	
$2\theta_{max}$ (deg)	50.0
index ranges	$-9 \le h \le 10$ $-14 \le k \le 14$ $-16 \le l \le 17$
temperature / K	173(2)
reflections collected	9152
independent reflections	5161
R(int) (%)	1.37
(C) Refinement	
Refinement method	Full–matrix least–squares on F^2
R indices ($I > 2\sigma(I)$)	R1 = 0.0317 WR2 = 0.0818
R indices all data	R1 = 0.0379 WR2 = 0.0845
Δ(ρ) ($e^-/Å^3$)	0.391
GOF	1.047

(A)

(B)

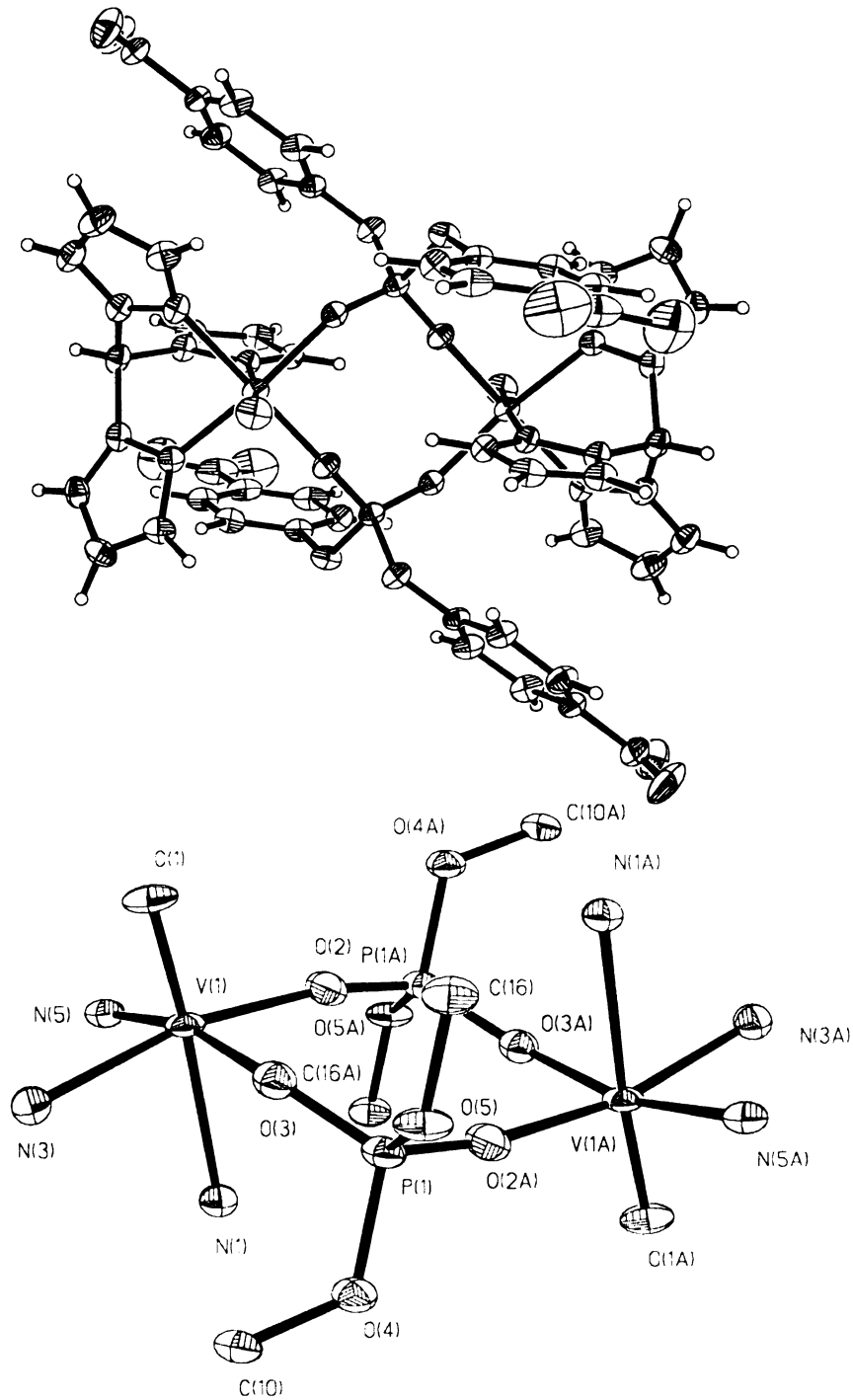

Figure 11. ORTEP view of $\{HB(pz)_3VO[\mu\text{–}(p\text{-}NO_2\text{–}PhO)_2PO_2]\}_2 \cdot 2CH_2Cl_2$ (**12**), where half of the atoms are crystallographically unique (A), and view of its *anti* dimer core (B).

(**13**), pyrrole (**14**), thiophene (**15**) and 1,2–ethanedithiol (**16**) derivatives and Tables 13 and 16 their metric parameters. Apart for the minor changes in bond distances and angles, the parameters of interest are the $d(N_2O_2^V \mid N_2O_2^V)$ distance and the $<N_2O_2^V \mid O_4^P>$ angle. The corresponding values are almost identical for the dichloromethane and acetone solvates, the small variance observed attributed to the 30 K difference in the data collection temperature. In the pyrrole, 1,2–ethanedithiol, and thiophene solvates on the other hand, these values differ widely, with the latter compound possessing a $d(N_2O_2^V \mid N_2O_2^V)$ = 1.387 Å. This value is 0.110 Å larger than the corresponding one in the acetone solvate (X–ray data collection for these derivatives was performed at the same temperature, 173K). Structure determination of the 1,2–ethanedithiol, and thiophene solvates was also performed at room temperature showing a variance in the parameters of interest (Table 16). In both derivatives as the temperature is lowered the vanadium basal plane displacement increases towards a more chair–like conformation.

Structural examination of the various solvates reveals that indeed the relative orientations of the aryl and pyrazolyl groups changes as solvent and temperature are varied. The angle between the axial pyrazolyl ring and the aryl group changed from 1.2° (dichloromethane) to 11.0° (thiophene), while that between the equatorial pyrazolyl and the aryl groups decreased from 20.7° (dichloromethane) down to 11.9° (thiophene). In addition the thiophene ring is almost parallel to the equatorial pyrazolyl group (3.3(2)°), forming thus a three molecule π–stack complex (*Figure 12(A)*), while pyrrole appears to be almost orthogonal (78.1(1)°) to the respective equatorial ring (*Figure 12(B)*).

The infrared spectra of the phosphinate dimers are almost identical (Table 17) with small differences in the B — H and V = O stretches. The aromatic ring breathing modes (1600 to 1400 cm^{-1}) also present little variation from one

Table 13. Bond Distances and Dimer Metric Parameters for $\{HB(pz)_3VO[\mu\text{–}(p\text{-}NO_2\text{–}C_6H_4O)_2PO_2]\}_2 \cdot S$ **12**, **13**, and **14**[a]

Bond Distances	**12**	**13**	**14**
$V = O_{ax}$	1.600(3)	1.595(2)	1.594(1)
$V — N_{eq}$	2.093(3)	2.088(2)	2.098(2)
$V — N_{eq}$	2.107(3)	2.092(2)	2.099(2)
$V — O_{eq}$	2.020(3)	2.006(2)	2.009(1)
$V — O_{eq}$	2.029(3)	2.026(2)	2.029(1)
$V — N_{ax}$	2.331(4)	2.329(2)	2.327(2)
T / K	143	173	173
V V	5.242(1)	5.231(1)	5.227(1)
$<VO_2 / O_4^P> / {}^{o}$ [b]	159.09	159.02	157.90
$<N_2O_2^V / O_4^P> / {}^{o}$ [c]	149.16	148.85	147.91
$D (N_2O_2^V / N_2O_2^V) / Å$ [d]	1.265	1.277	1.3205
$<C_3H_3N_2 / C_6H_5>_{ax} / {}^{o}$ [e]	1.2(1)	5.4(1)	7.5(1)
$<C_3H_3N_2 / C_6H_5>_{eq} / {}^{o}$ [f]	20.7(3)	19.0(2)	11.2(1)
$<C_3H_3N_2 / C_4H_5N> / {}^{o}$ [g]	—	—	78.1(1)

[a] **12**: S = CH_2Cl_2. **13**: S = CH_3COCH_3. **14**: S = C_4H_5N. [b] Dihedral angle between the VO_2 plane (defined by vanadium and the two basal oxygen atoms of the dimer ring) and the plane O_4^P (defined by the four phosphonate ring oxygen atoms). [c] Dihedral angle between the O_4^P and the $N_2O_2^V$ planes (defined by the four basal oxygens of the vanadium octhedron). [d] Distance between the $N_2O_2^V$ planes. [e] Dihdral angles between the axial pyrazolyl ($C_3H_3N_2$) and the respective aryl (C_6H_5) groups of the terminals and bridging ligands. [f] Dihedral angles between the equatorial pyrazolyl and the respective aryl groups of the terminals and bridging ligands. [g] Dihedral angles between the equatorial pyrazolyl group and the pyrrole solvent (C_4H_5N).

Table 14. Crystallographic Data of $\{HB(pz)_3VO[\mu\text{–}(p\text{-}NO_2\text{–}PhO)_2PO_2]\}_2 \cdot C_4H_4S$, at Room Temperature (**15A**) and at 173 K (**15B**)

	15A	**15B**
	(A) Crystal Parameters	
formula	$C_{50}H_{44}B_2N_{16}O_{18}P_2\ S_2V_2$	$C_{50}H_{44}B_2N_{16}O_{18}P_2\ S_2V_2$
crystal habit, color	block, blue	block, blue
FW	1406.57	1406.57
crystal size (mm^3)	0.85 × 0.77 × 0.15	0.62 × 0.54 × 0.23
crystal system	triclinic	triclinic
space group	$P\bar{1}$	$P\bar{1}$
a (Å)	8.5609(2)	8.5131(1)
b (Å)	12.5775(1)	12.4305(2)
c (Å)	15.4002(1)	15.2339(3)
α (deg)	101.172(2)	100.224(1)
β (deg)	100.246(2)	100.945(1)
γ (deg)	104.886(2)	104.419(1)
V ($Å^3$)	1526.2(1)	1489.5(1)
Z	1	1
d_{calc} (Mg/m^3)	1.530	1.568
F(000)	718	718
μ(Mo Kα), mm^{-1}	0.511	0.524
	(B) Data Collection	
$2\theta_{max}$ (deg)	50.0	50.0
index ranges	$-10 \le h \le 9$ $-14 \le k \le 14$ $-18 \le l \le 18$	$-9 \le h \le 10$ $-14 \le k \le 13$ $-18 \le l \le 17$
temperature / K	296(2)	173(2)
reflections collected	9219	9028
independent reflections	5229	5118
R(int) (%)	1.85	1.51
	(C) Refinement	
Refinement method	Full–matrix least–squares on F^2	Full–matrix least–squares on F^2
R indices ($I > 2\sigma(I)$)	R1 = 0.0484 WR2 = 0.1416	R1 = 0.0383 WR2 = 0.1066
R indices all data	R1 = 0.0568 WR2 = 0.1480	R1 = 0.0438 WR2 = 0.1103
Δ(ρ) ($e^-/Å^3$)	0.699	0.585
GOF	1.082	1.060

Table 15. Crystallographic Data of $\{HB(pz)_3VO[\mu\text{–}(p\text{-}NO_2\text{–}PhO)_2PO_2]\}_2 \cdot C_2H_6S_2$, at Room Temperature (**16A**) and at 173 K (**16B**)

	16A	**16B**
	(A) Crystal Parameters	
formula	$C_{46}H_{48}B_2N_{16}O_{18}P_2\ S_4V_2$	$C_{46}H_{48}B_2N_{16}O_{18}P_2\ S_4V_2$
crystal habit, color	plate, blue	plate, blue
FW	1426.68	1426.68
crystal size (mm^3)	0.66 × 0.31 × 0.08	0.66 × 0.31 × 0.08
crystal system	triclinic	triclinic
space group	$P\bar{1}$	$P\bar{1}$
a (Å)	8.718(1)	8.6036(2)
b (Å)	12.485(2)	12.1895(4)
c (Å)	16.033(3)	15.9203(5)
α (deg)	104.067(4)	103.507(1)
β (deg)	99.969(4)	100.688(1)
γ (deg)	105.493(4)	105.214(1)
V ($Å^3$)	1577.3(5)	1511.41)
Z	1	1
d_{calc} (Mg/m^3)	1.502	1.567
F(000)	730	730
μ(Mo Kα), mm^{-1}	0.559	0.583
	(B) Data Collection	
$2\theta_{max}$ (deg)	50.0	50.0
index ranges	$-9 \le h \le 10$ $-14 \le k \le 12$ $-19 \le l \le 17$	$-10 \le h \le 10$ $-14 \le k \le 12$ $-17 \le l \le 18$
temperature / K	296(2)	173(2)
reflections collected	6613	8942
independent reflections	5011	5122
R(int) (%)	3.03	2.70
	(C) Refinement	
Refinement method	Full–matrix least–squares on F^2	Full–matrix least–squares on F^2
R indices ($I > 2\sigma(I)$)	R1 = 0.0572 WR2 = 0.1171	R1 = 0.0459 WR2 = 0.1071
R indices all data	R1 = 0.1232 WR2 = 0.1398	R1 = 0.0711 WR2 = 0.1175
Δ(ρ) ($e^-/Å^3$)	0.388	0.720
GOF	0.934	1.023

Table 16. Bond Distances and Dimer Metric Parameters for $\{HB(pz)_3VO[\mu\text{–}(p\text{-}NO_2\text{–}C_6H_4O)_2PO_2]\}_2 \cdot S$ **15A**, **15B**, **16A**, and **16B**[a]

Bond Distances	**16A**	**16B**	**15A**	**15B**
$V = O_{ax}$	1.599(3)	1.594(2)	1.588(2)	1.592(1)
$V — N_{eq}$	2.097(4)	2.086(3)	2.089(2)	2.090(2)
$V — N_{eq}$	2.106(4)	2.095(3)	2.103(2)	2.099(2)
$V — O_{eq}$	2.013(3)	2.003(2)	2.008(2)	2.009(2)
$V — O_{eq}$	2.030(3)	2.005(2)	2.027(2)	2.027(2)
$V — N_{ax}$	2.339(4)	2.324(2)	2.335(2)	2.332(2)
T / K	296	173	296	173
V V	5.212(2)	5.216(1)	5.235(1)	5.240(1)
$<VO_2 / O_4^P> / {}^{o}$ [b]	159.87	158.02	157.25	156.14
$<N_2O_2^V / O_4^P> / {}^{o}$ [c]	149.59	147.73	147.16	146.1
$D (N_2O_2^V / N_2O_2^V) / Å$ [d]	1.254	1.317	1.353	1.387
$<C_3H_3N_2 / C_6H_5>_{ax} / {}^{o}$ [e]	10.6(1)	8.1(1)	11.0(1)	8.9(1)
$<C_3H_3N_2 / C_6H_5>_{eq} / {}^{o}$ [f]	14.5(3)	15.1(2)	11.9(3)	12.0(2)
$<C_3H_3N_2 / C_4H_4S> / {}^{o}$ [g]	—	—	1.1(4)	3.3(2)

[a] **15a**: S = C_4H_4S, structure determination at 296 K. **15b**: S = C_4H_4S, structure determination at 173 K. **16a**: S = $C_2H_6S_2$, structure determination at 296 K. **16b**: S = $C_2H_6S_2$, structure determination at 173 K. [b] Dihedral angle between the VO_2 plane (defined by vanadium and the two basal oxygen atoms of the dimer ring) and the plane O_4^P (defined by the four phosphonate ring oxygen atoms). [c] Dihedral angle between the O_4^P and the $N_2O_2^V$ planes (defined by the four basal oxygens of the vanadium octhedron). [d] Distance between the $N_2O_2^V$ planes. [e] Dihdral angles between the axial pyrazolyl ($C_3H_3N_2$) and the respective aryl (C_6H_5) groups of the terminals and bridging ligands. [f] Dihdral angles between the equatorial pyrazolyl and the respective aryl groups of the terminals and bridging ligands. [g] Dihedral angles between the equatorial pyrazolyl group and the thiophene solvent (C_4H_5N).

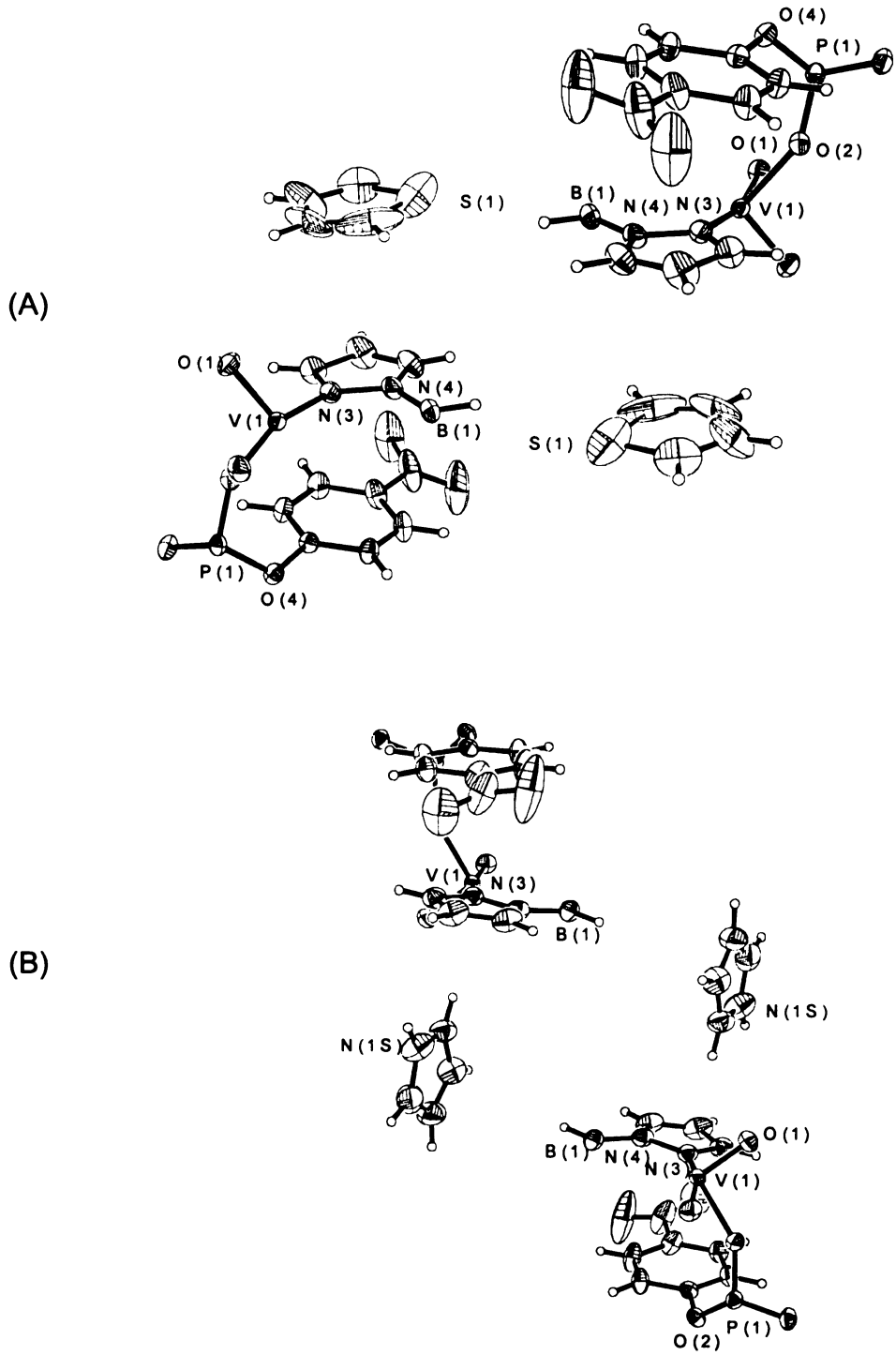

Figure 12. π–π Interactions between the solvent and the ligands in the thiophene (A) and pyrrole (B) solvates of $\{HB(pz)_3VO[\mu\text{–}(p\text{-}NO_2\text{–}PhO)_2PO_2]\}_2$.

Table 17. Infrared Data of $\{HB(pz)_3VO[(X)_2PO_2]\}_2 \cdot nCH_2Cl_2$ Complexes[a]

8	10	12	9	Assign.
3435	3432	3445	3432	
2474	2487	2477	2476	$\nu_{(B-H)}$
1625	1599	1605	1594	
1505	1503	1504	1502	
1404	1405	1403	1405	
1310	1308	1310	1310	
	1217		1220	$\nu_{as(P-O)}$
1199	1186	1192	1198	
1132	1129	1127	1129	
	1071		1071	
1053	1052	1053	1052	
969	968	972	971	$\nu_{(V=O)}$

[a] **8**: X = *p*-CH_3O–C_6H_4–. **9**: X = p-F– C_6H_4–. **10**: X = *p*-CH_3– C_6H_4–. **12**: *p*-NO_2– C_6H_4O–.

compound to the other. Recrystallization of $\{HB(pz)_3VO[(p\text{-}NO_2\text{–}PhO)_2PO_2\}_2$ from various solvents affords complexes that have identical infrared spectra (Table 18). Small differences are observed in the region of the V = O stretches, where three peaks are found. The two outer peaks remain identical for all the solvates studied, while the middle peak is shifted toward lower energies for thiophene, pyrrole and 1,2–ethanedithiol. Interestingly, these are the solvates that show geometrical distortions from the dichloromethane and acetone derivatives.

The electronic absorption data (*Figure 13*) for all five compounds are presented in Table 19 (due to their low solubility in CH_2Cl_2, absorption coefficients for the –H and $–NO_2$ derivatives were not determined). Although the local symmetry around the vanadyl centers is low (C_s point group) only two absorption bands were observed. The $^2B_2$ to $^2A_1$ transition is covered under charge transfer bands, while a small energy separation between the d_{xz}, d_{yz} orbital set is anticipated by the presence of a single band for the $^2B_2$ to ^2E excitation (energy states correspond to the C_{4V} point group). All four phosphinates have qualitatively similar spectra, while the absorption maxima of the phosphonates are slightly shifted toward higher energies.

b. Electron Paramagnetic Resonance and Magnetic Susceptibility Studies

EPR spectra of all five compounds utilized in this study were recorded in dichloromethane solutions at room temperature and at various temperatures in the range 4.1 to 77 K. *Figures 14* and *15* depict the room temperature spectra of the five compounds. Each of them displays a well resolved isotropic spectrum comprising fifteen lines, which is typical of divanadyl complexes[16]. The spectra of

Table 18. Infrared Data of $\{HB(pz)_3VO[(p\text{-}NO_2\text{–}C_6H_4O)_2PO_2]\}_2 \cdot S$

CH_2Cl_2	$CH_3O\text{–}C_6H_5$	CH_3COCH_3	$(HSCH_2)_2$	C_4H_5N	C_4H_4S	Assign.
3438	3438	3432	3438	3460	3439	
2510	2509	2505	2505	2511	2510	$\nu_{(B-H)}$
1614	1614	1614	1614	1614	1614	
1591	1591	1591	1591	1591	1591	
1519	1519	1519	1519	1519	1520	
1489	1489	1489	1489	1489	1489	
1407	1407	1407	1407	1407	1407	
1347	1347	1347	1346	1347	1346	
1310	1310	1310	1309	1310	1310	
1279	1279	1280	1281	1281	1281	
1213	1213	1213	1212	1212	1213	$\nu_{as(P-O)}$
1157	1157	1157	1159	1159	1158	
1128	1128	1128	1128	1128	1128	
1115	1115	1115	1115	1115	1116	
1055	1055	1055	1054	1053	1055	
976	976	976	976	976	976	$\nu_{(V=O)}$
957	957	957	948	951	951	
938	938	938	938	937	938	

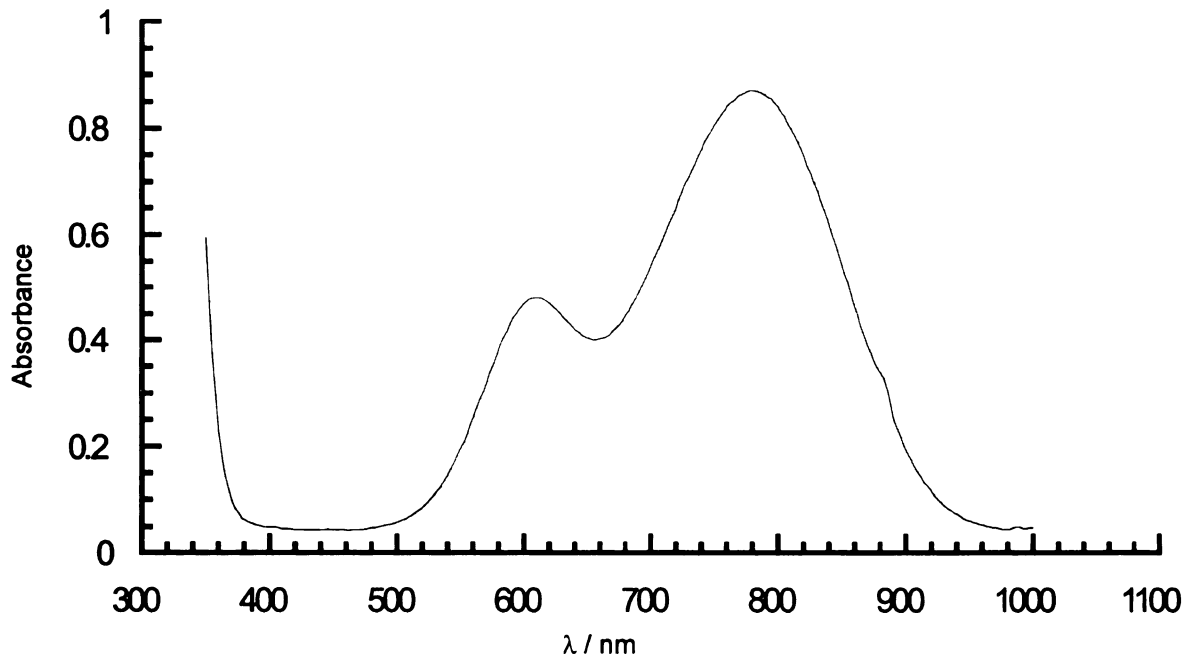

Figure 13. Absorption spectrum of $\{HB(pz)_3VO[\mu\text{–}(p\text{-}CH_3O\text{–}Ph)_2PO_2]\}_2$ **8**, in dichloromethane solution. The two maxima are attributed to d – d transitions.

Table 19. Electronic Absorption Spectra of $\{HB(pz)_3VO[(p\text{-}X\text{–}C_6H_4)_2PO_2]\}_2$ and $\{HB(pz)_3VO[(p\text{-}NO_2\text{–}C_6H_4O)_2PO_2]\}_2$ in Dichloromethane

– X	nm	cm^{-1}	ε	nm	cm–1	ε
– H (**7**)	615	16255	—	779	12837	—
– F (**9**)	610	16393	66	779	12837	103
– CH_3 (**11**)	610	16393	44	779	12837	84
– OCH_3 (**8**)	615	16255	51	776	12880	94
– NO_2 (**12**)	597	16750	—	750	13326	—

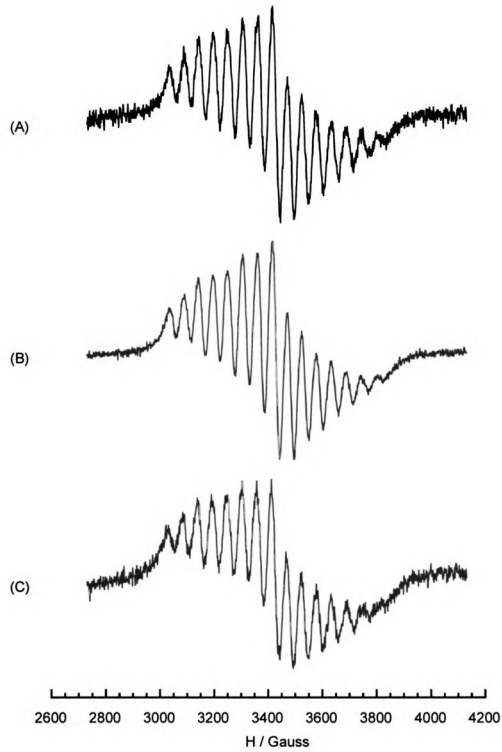

Figure 14. Room temperature EPR spectra of compounds **7** (A), **9** (B), and **12** (C).

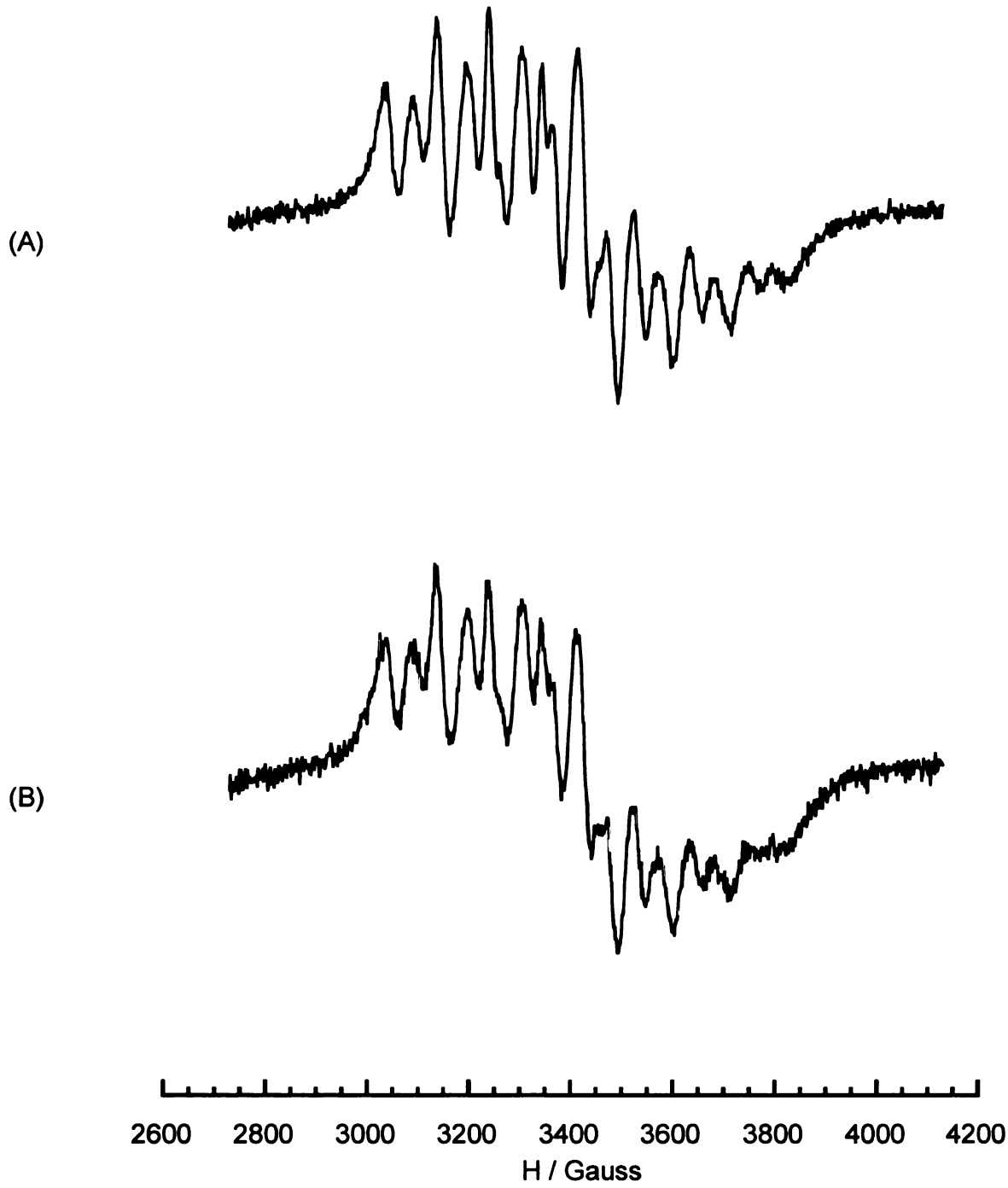

Figure 15. Room temperature EPR spectra of compounds **11** (A) and **8** (B).

the –H, –F, and $–NO_2$ derivatives were qualitatively similar (*Figure 14*) and could be simulated by considering the Hamiltonian

$$\mathbf{H} = g\beta_e B\mathbf{S} + A\mathbf{S} \bullet \mathbf{I} \qquad (4.4)$$

where A is the hyperfine constant. The simulation afforded g = 1.958 and A = 57 Gauss for the three compounds. These values are very close to the one observed by Carrano and coworkers[8] for $\{HB(pz)_3VO[\mu–(PhO)_2PO_2]\}_2$ in a dichloromethane/toluene solution. Mabbs[17] has pointed out however, that isotropic dimer complexes should be also treated for the effects of isotropic magnetic exchange (which adds a $J\mathbf{S}_1 \bullet \mathbf{S}_2$ term in the hamiltonian 4.4), in addition to the metal hyperfine interaction and the electron Zeeman term. As a result the shape of the fifteen–line spectra of divanadyl complexes is a function of the J/A ratio. Hence, the peculiar shape of the room temperature spectra of the electron donating CH_3– and CH_3O– derivatives (*Figure 15*) might be attributed to such effects.

The frozen–glass EPR spectra of these compounds are typical of triplets. More than fifteen lines were observed (*Figure 16*), which are attributed to the anisotropy of the g and A tensor and also to the presence of Zero Field Splitting. The latter was calculated by the point–dipole approximation[18] to be in the order of 0.0150 cm^{-1}. Attempts to simulate the spectra with the program SimFonia (which uses second order perturbation theory) were unsuccessful.

Variable temperature magnetic susceptibility data were determined on powder specimens. *Figure 17* displays the molar susceptibility versus temperature plot for the four phosphinate derivatives. The data show a monotonic increase with decreasing temperature till they reach a maximum at low temperature. This behavior is typical of antiferromagnetic exchange coupling

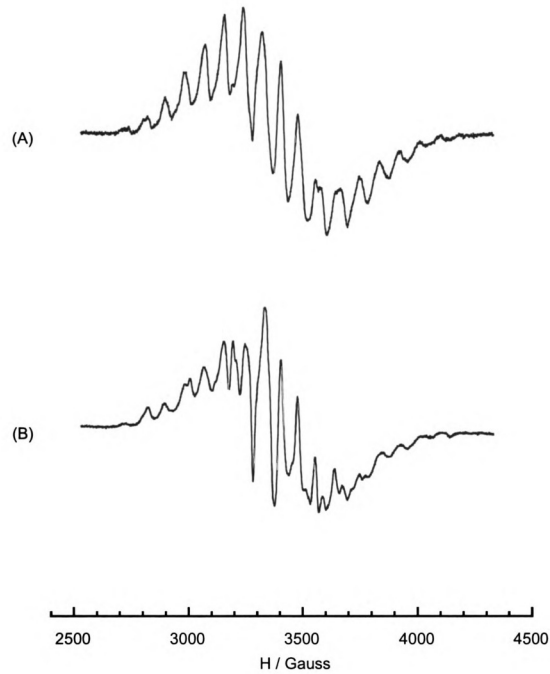

Figure 16. Frozen glass EPR spectra of compounds **7** (A), and **8** (B) at 4.1 K.

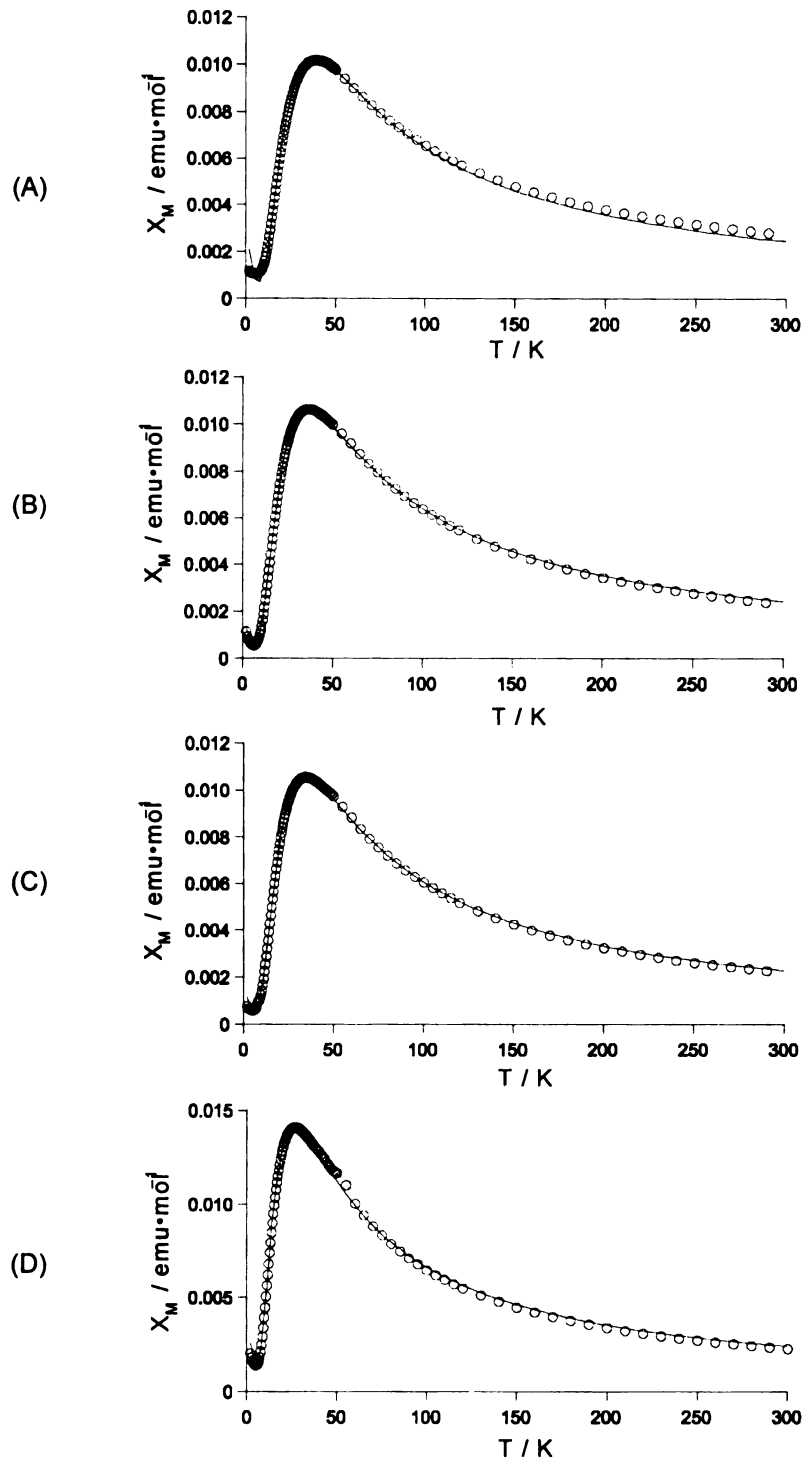

Figure 17. Susceptibility vesrus temperature plots of compounds **7** (A), **11** (B), **9** (C), and **8** (D). The solid lines represent the best fit obtained by using a Bleaney–Bowers dimer model.

and the data were fitted to a Bleany–Bowers[19] model for S = 1/2 system (equation 4.1).

The results of the fitting are gathered in Table 20, along with geometric parameters of the bridge core. The largest singlet–triplet splitting is observed for the parent compound **7**, where the solvent of recrystallization had a marked influence in the magnitude of the interaction, and the smallest for the *p*-CH_3O– derivative **8**. The best fit was obtained with the Landé factor being a free variable. The values obtained are close to the experimentally determined g_{iso} = 1.958 (from EPR) indicating the purity of the materials utilized in the study.

The corresponding data for the *p*-NO_2– solvate derivatives (*Figure 18*) are gathered in Table 21. The dichloromethane, acetone, and anisole solvates displayed identical magnetic properties; namely, weak antiferromagnetic coupling within the divanadyl core, with a singlet–triplet splitting of – 14 K. Deviations from that value were observed for the thiophene, 1,2–ethanedithiol, and pyrrole solvates, with the singlet–triplet splitting in the latter being 6.3 K larger.

C. Discussion

Extended vanadyl phosphates and phosphonates crystallize in a wide variety of structural frameworks. Their building blocks consist mainly of divanadyl octahedra bridged by phosphate–type ligands. The magnetic properties of these materials have been correlated to geometrical features of their structural building blocks, which include the phosphate/phosphonate bridges as active elements of the exchange pathways. Detailed magnetostructural correlation is not an easy task, due to the many variables involved. Part of the problem is the lack of a large body of compounds with closely related structures, which would enable the

Table 20. Susceptibility Data and Dimer Metric Parameters for $\{HB(pz)_3VO[\mu\text{–}(p\text{-X–Ph})_2PO_2]\}_2 \cdot S$

	H–[a]	H– (7)	CH_3–	F– (9)	CH_3O–
J/k in K	– 84.4	– 61.5	– 58.4	– 55.2	– 43.0
g	2.05	2.04	2.02	1.96	2.00
T_{max} in K [b]	52.5	39.0	37.0	35.0	26.5
T_{max} in K [c]	52.8	38.5	36.5	34.5	26.9
% impurity	1.8	0.5	0.3	0.3	0.7
T / K	296	143	133	131	173
V ····· V / Å (#1)[d]	5.258	5.291(1)	5.233(1)	5.265(1)	5.219(1)
V ····· V / Å (#2)[e]	5.294	5.285(1)		5.270(1)	
$<N_2O_2^V / O_4^P>$ / °[f] (#1)	163.12	159.9(1)	153.3	161.6(1)	152.2
$<N_2O_2^V / O_4^P>$ / °[f] (#2)	163.18	163.9(1)		163.3(1)	
$D(N_2O_2^V/N_2O_2^V)$ / Å [g] (#1)	0.722	0.852	1.154	0.772	1.181
$D(N_2O_2^V/N_2O_2^V)$ / Å [g] (#2)	0.716	0.689		0.696	

[a] Crystal data taken from reference 13, where crystals were grown in acetonitrile. [b] Experimental. [c] From equation 4.2. [d] Refers to the first of the two crystallographically unique dimer molecules. [e] Refers to the second of the two crystallographically unique dimer molecules. [f] Dihedral angle between the O_4^P (defined by the four phosphonate ring oxygen atoms) and the $N_2O_2^V$ planes (defined by the four basal oxygens of the vanadium octahedron). [g] Distance between the $N_2O_2^V$ planes.

(A)

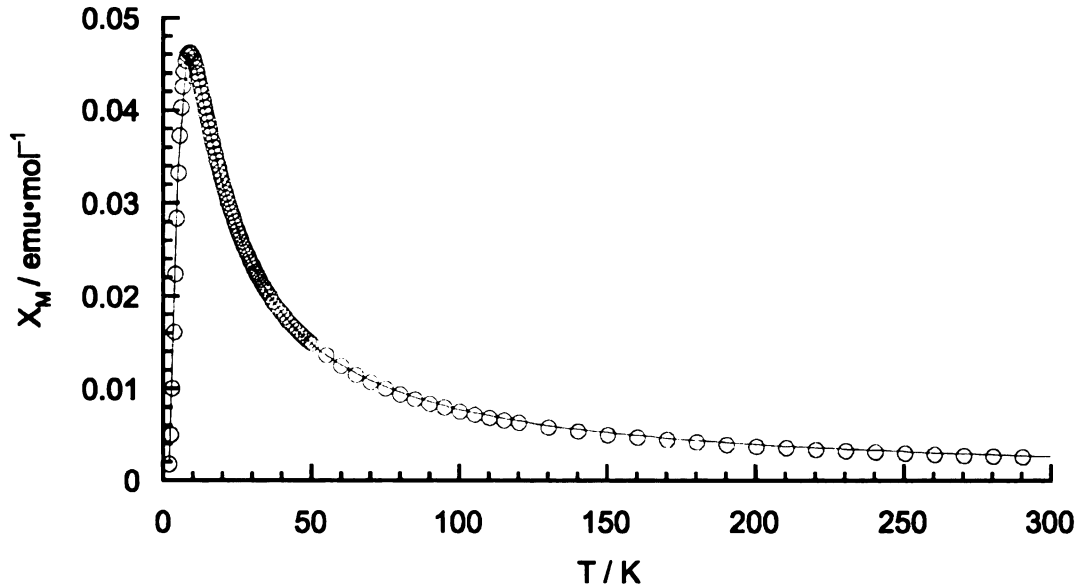

(B)

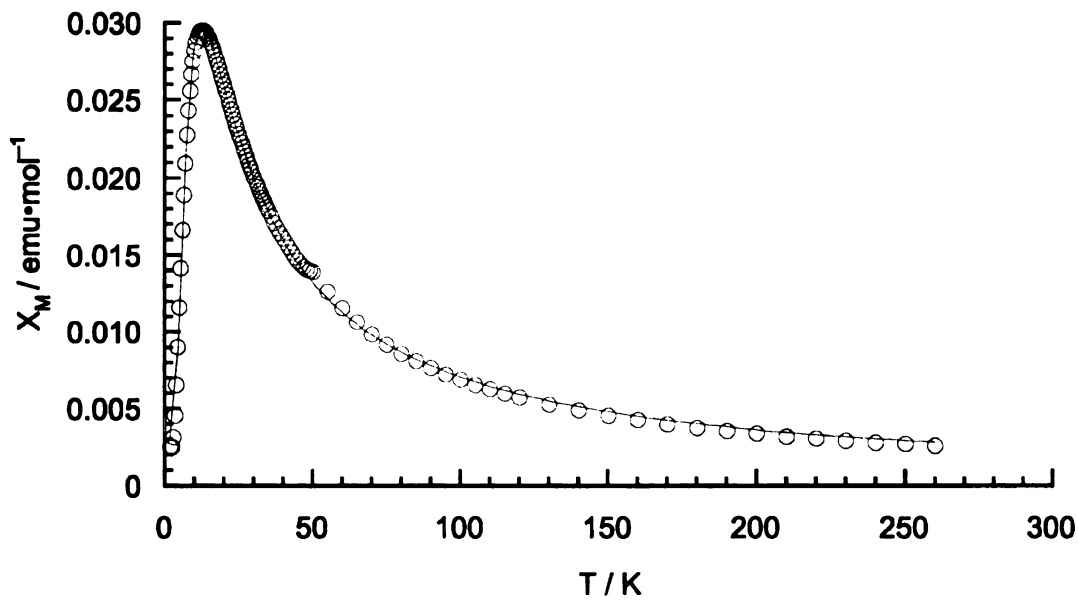

Figure 18. Susceptibility versus temperature plots of the dichloromethane (A) and pyrrole (B) solvates of $\{HB(pz)_3VO[\mu\text{–}(p\text{-}NO_2\text{–}PhO)_2PO_2]\}_2$. The solid lines represent the best fit obtained by using a Bleaney–Bowers dimer model.

Table 21. Susceptibility Data and Dimer Metric Parameters for $HB(pz)_3VO[\mu\text{–}(p\text{-}\ NO_2\text{–}PhO)_2PO_2]\}_2 \cdot S$

	CH_2Cl_2	$CH_3O\ CH_3$	$CH_3OC_6H_5$	C_4H_4S	$(HSCH_2$–	C_4H_5N
J/k in K	– 14.0	– 14.0	– 14.0	– 15.6	– 15.8	– 20.3
g	2,07	2.05	2.10	1.92	1.88	1.99
T_{max} in K [a]	8.5	8.5	8.5	9.5	10	12.5
T_{max} in K [b]	8.8	8.8	8.8	9.7	9.9	12.7
% impurity	0.08	—	0.003	—	—	0.8
T / K	143	173	—	173	173	173
V V	5.242(1)	5.231(1)	—	5.240(1)	5.216(1)	5.227(1)
$<N_2O_2^V / O_4^P> / {}^o$ [c]	149.16	148.85	—	146.1	147.7	147.9
D $(N_2O_2^V / N_2O_2^V)$ / Å [d]	1.265	1.277	—	1.387	1.317	1.3205
$<C_3H_3N_2 / C_6H_5>_{eq} / {}^o$ [e]	20.7(2)	19.0(2)	—	12.0(2)	15.1(2)	11.2(2)

[a] Experimental. [b] From equation 4.4. [c] Dihedral angle between the O_4^P (defined by the four phosphonate ring oxygen atoms) and the $N_2O_2^V$ planes (defined by the four basal oxygens of the vanadium octahedron). [d] Distance between the $N_2O_2^V$ planes. [e] Dihedral angles between the equatorial pyrazolyl ($C_3H_3N_2$) and the respective aryl groups of the terminals and bridging ligands.

systematic study of these variables. In addition, small changes in the ligand periphery sometimes lead to dramatic changes in the intralayer connectivity.

Our effort to synthesize molecular analogs of the extended material exchange pathways has targeted the detailed understanding of the factors affecting the strength and the sign of the magnetic interaction. The advantages that such molecular analogs offer are their ease of synthesis and the ability to introduce subtle changes within the dimer core. In addition, the proper choice of the terminal ligands is partially responsible for the generation of desirable model complexes. The inner geometry of the dimer however, cannot be totally designed. Weak noncovalent forces among the various ligands and the ligands with the solvent often dictate the way that vanadyl octahedra are interconnected. Unfortunately such forces are not well understood and only recently detailed studies[20] on their role in the design of molecular solids have been undertaken.

In the previous sections the synthesis and structural characterization of a series of phosphinate and phosphonate dimers has been described. Three types of dimer cores were identified — *twist*, *syn*, and *anti* — with the classification based on the relative orientation of the vanadyl groups. The *twist* dimer cores, where vanadyl groups are almost orthogonal with respect to each other, were observed in compounds **1**, **2**, **3**, and **6A**. The first three complexes contain the diphenylphosphonate as the bridging ligand and bpy, dmbpy and tmbpy respectively as terminal ligands. Compound **6A** on the other hand is a tmbpy derivative of bis(*p*-methoxyphenyl)phosphinate. All the bpy analogs of the remaining *p*-substituted phenylphosphinates crystallized with the *syn*–type dimer core. Examination of the structural cores of these complexes indicates that the driving force for the formation of one structural type over the other is the relative orientation of the compounds' aromatic units. In the *syn*–type dimer cores the volume between the bpy ligands is occupied by phenyl rings of the bridge. The

additional methyl groups in the dmbpy and tmbpy derivatives diminish this volume, inducing the relative twist of the vanadium octahedra. In the *twist* dimer core the terminal ligands point in opposite directions in space enabling the accommodation of the phosphinate's aromatic groups.

The 2,2'–bipyridyl terminal ligand analogs occupy two of the five open coordination sites of the vanadyl octahedron. The remaining three sites are occupied by oxygen atoms of the phosphinate bridging groups, each one binding in both vanadyl octahedra of the dimer complex. Linking of the metals by three phosphinate ligands precludes the generation of an *anti* dimer core. The latter arrangement is achieved by utilization of a tridentate ligand (hydrotris1–pyrazolyl borate), which blocks the site trans to the vanadyl group. The bridging of the vanadyl octahedra in this case is accomplished by two phosphinate/phosphonate ligands.

The structural framework of *anti* vanadyl dimers resembles that of the D VII exchange pathway of extended vanadyl phosphates/phosphonates. Substitution of the phenyl units with various groups introduces significant conformational changes. These are mainly attributed to the packing requirements of the individual dimer complexes. In some instances however, weak noncovalent interactions, primarily among the ligand aromatic units or between the latter groups and the crystallization solvent, also induce conformational variations. This is the case for complexes **9** and **12** where strong electron withdrawing substituents are attached to the phenyl rings of the bridging ligands. These groups are found to be in close proximity and possessing a parallel arrangement with the pyrazolyl rings of the terminal ligand (Tables 11, 13 and 16). Crystallization of compound **12** in various solvents, particularly thiophene and pyrrole, show further evidence for the existence of these ligand–solvent interactions, which are manifested in the parallel and almost orthogonal

arrangement of an equatorial pyrazolyl ring with thiophene and pyrrole respectively (*Figure 12*).

The current view on π–interactions considers them to be mainly electrostatic in nature[21]. According to this model the aromatic molecules consist of a positively charged σ framework sandwiched by the negatively charged π electron cloud. Hence the most favorable arrangement is either an offset π–stacked geometry (observed in the thiophene solvate) or an edge–on or T–shaped geometry (observed in the pyrrole solvate), where favorable π–σ electrostatic interactions are dominant. Ideal condition for strong π–interactions to occur is the presence of electron withdrawing substituents in the interacting molecules[22]. Contrary to popular beliefs, π–interactions between electron poor and electron rich molecules are only moderate in strength.

The dimer compounds reported in this study all display weak to moderate antiferromagnetic coupling, the only exception being $\{HB(pz)_3VO[\mu\text{–}(PhO)_2PO_2]\}_2$ synthesized and magnetically characterized by Carrano and coworkers[8]. The latter complex possesses a triplet ground state with an energy separation from the lowest singlet of 6.6 K. Substitution of the bridging and terminal ligands with electron withdrawing or donating substituents affects the strength and the sign of the interaction in two ways; first, by changing the energies of the metal and bridging ligands that participate in the exchange pathway (J_{el}), and second by inducing small but magnetically significant structural changes to the dimer core (J_{st}). The overall exchange constant is therefore the sum of these two contributions

$$J = J_F + J_{AF} = J_{el} + J_{st} \qquad (4.5)$$

which should affect both the ferromagnetic and the antiferromagnetic component of the exchange interaction. The dominant term is probably J_{st} in analogy to

copper[23] and vanadium[24] dimer systems where small structural variations had a marked influence to the strength of the interaction. Electronic effects, however, can be rather important for weakly coupled exchanged dimers[3]. For moderate antiferromagnetic interactions their contribution is additive to the J_{st} term resulting in significant complications, since other than theoretical calculations there are no means of determining the relative contribution of each term.

These observations are apparent in the three series of dimer complexes presented in this study. The magnetic properties and important metric parameters of the *syn*–type dimers cores are presented in Table 8. An unpaired electron in these complexes resides in a mainly d_{xy} type metal orbital with contributions from ligand orbitals. Its orientation is approximated as that of the vanadium basal plane, although this is not entirely correct due to the displacement of the vanadium atom from the plane. One of the phosphinate groups binds to the trans vanadyl sites in both metal octahedra, in a direction orthogonal to the magnetic orbital. As such, this group does not assume an active role in the superexchange pathway. The latter is considered to be the eight–membered ring depicted in *Figure 19(A)*, where the two vanadyl octahedra are linked by two phosphinate groups in a convex–boat arrangement. Under the framework of the active–electron approximation[25] the magnetic MOs are considered as a combination of metal and ligand–based orbitals.

The symmetric and antisymmetric metal–based orbitals, d_S and d_A in Scheme 1, can interact with the symmetry adapted combinations of phosphate type orbitals, l_S and l_A also shown in Scheme 1. The latter are isoenergetic, since each one consist of a phosphorous atomic *d* orbital interacting in a bonding fashion with two oxygen's *p* orbitals. Their energy however, can be tuned with electron withdrawing or donating substituents residing on the periphery of the phosphinate aromatic units. The substituent's ability to withdraw or donate

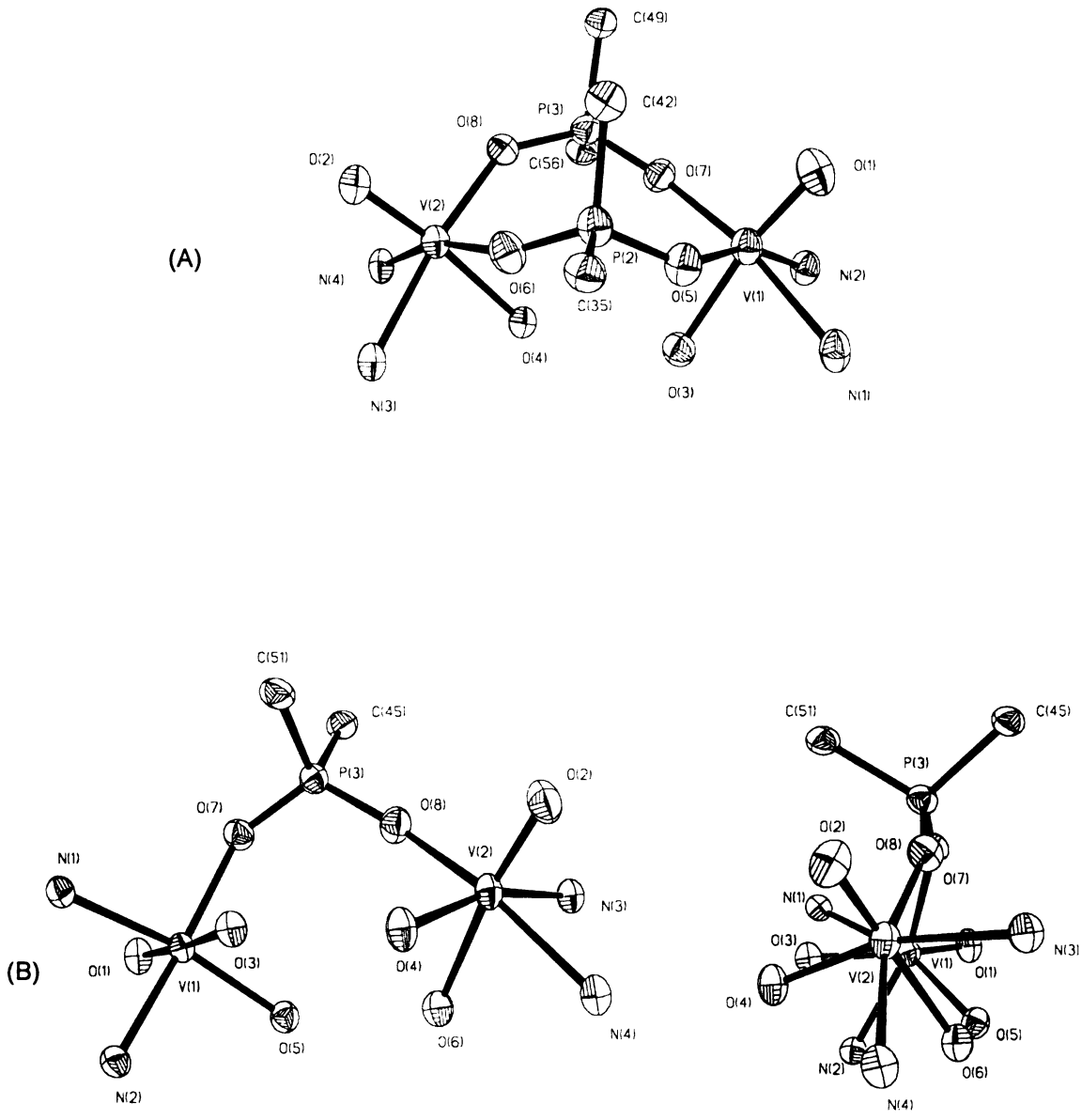

Figure 19. Superexchange pathways of *syn* (A) and *twist* (B) type dimer cores. The latter is displayed in two views, which show the relative orientation of the vanadium basal planes.

electrons is reflected in the value and the sign of the σ_p Hammett parameter[26], with negative values corresponding to electron donating groups (CH_3O–) and positive to electron withdrawing ones (Cl–, and F–). The combination of the metal

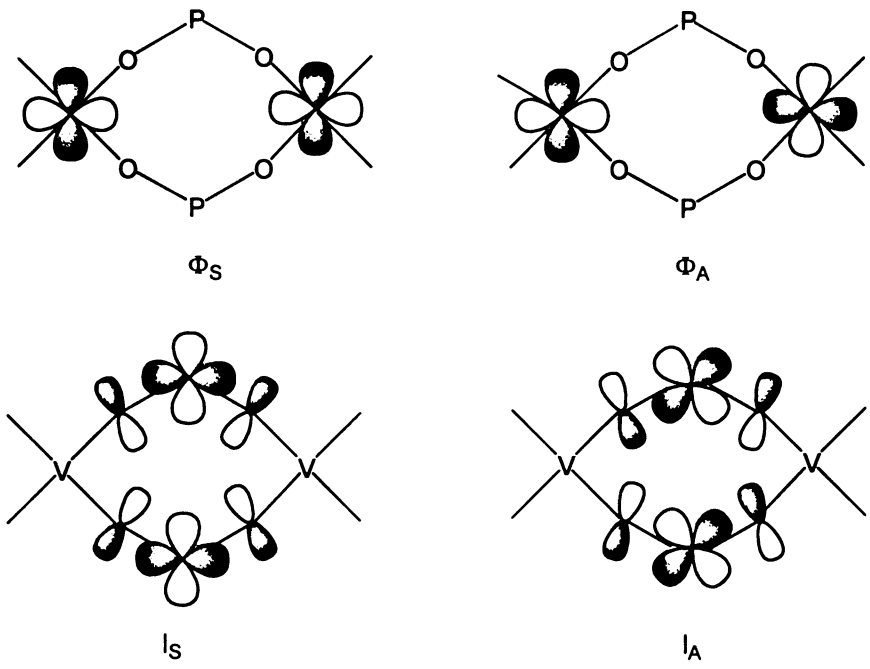

Scheme 1

and ligand orbitals generates the symmetric Φ_S and antisymmetric Φ_A magnetic MOs depicted in *Figure 20(A)*. In a coplanar arrangement — where $<N_2O_2^{V1}$ I $N_2O_2^{V2}> = 180°$ and $<O_1 — V_1 — V_2 — O_2> = 0°$ — the Φ_A orbital is higher in energy than Φ_S. When the angle between the basal planes deviates from coplanarity the antibonding character of Φ_A decreases while it becomes more pronounced for the Φ_S magnetic orbital. As they approach an orthogonal arrangement the energy mismatch between Φ_S and Φ_A decreases, reducing the magnitude of the antiferromagnetic term J_{AF}. The effect of that tilt is demonstrated in the qualitative energy diagram depicted in *Figure 20(B)*, which is in accordance with the experimental results in compounds **4**, **5**, and **6**. Inspection of Table 8 reveals that the exchange coupling constant J/k increases in the order,

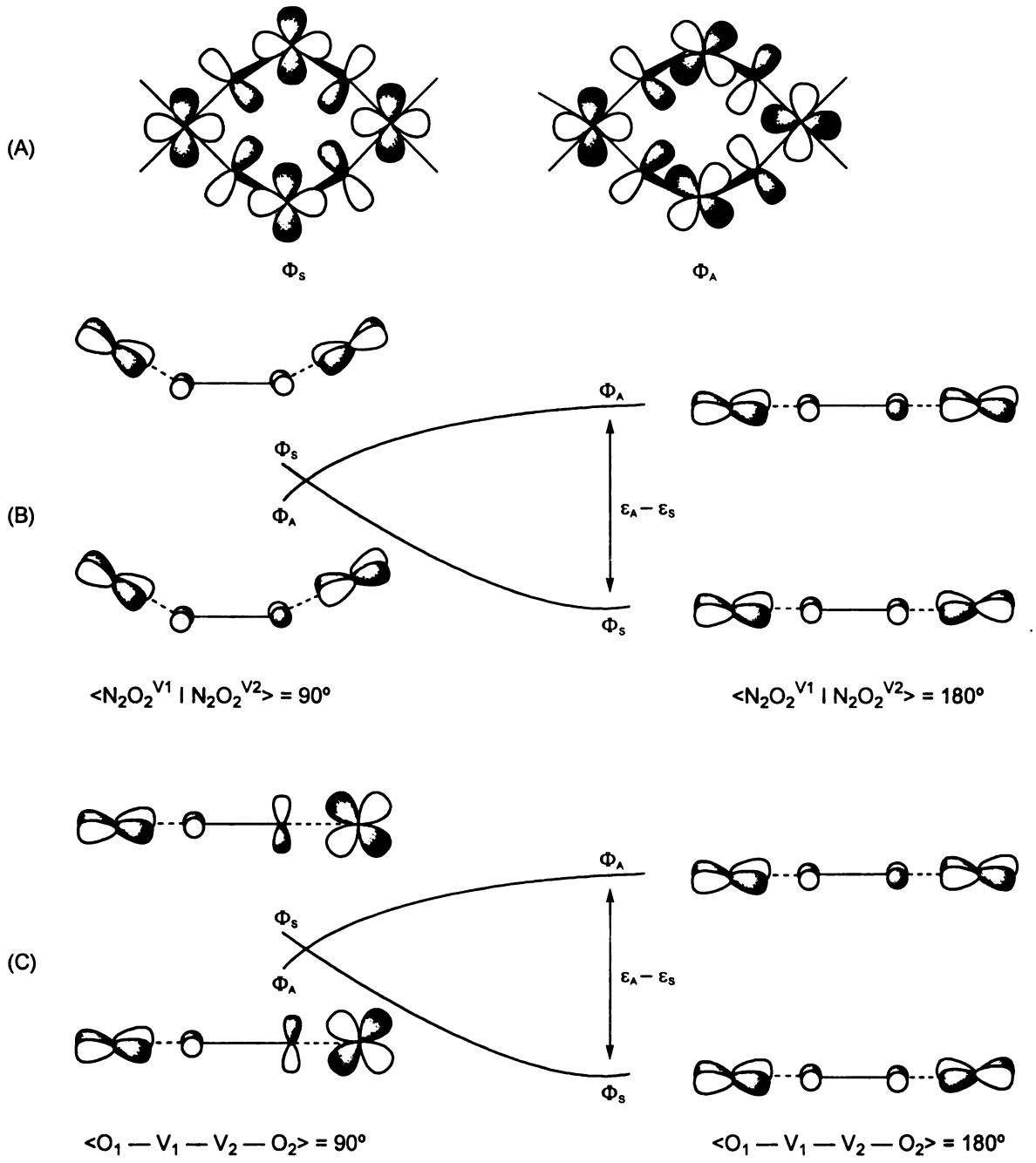

Figure 20. Symmetric (Φ_S) and antisymmetric (Φ_A) orthogonalized magnetic orbitals (A). Their energy separation is influenced by the relative orientation of the vanadium basal planes ($N_2O_2^{Vi}$) (B) and by the relative tilt of the vanadyl groups (C).

6 (CH_3O–) < **5** (Cl–) < **4** (F–) for the 2,2'–bipyridyl derivatives of the *syn*–type dimer cores, where the basal planes angles are 80.2°, 77.8°, and 76.6° respectively.

Figure 20(C) displays the variation of the $|\varepsilon_A - \varepsilon_S|$ energy difference upon the deviation from coplanarity of the vanadyl groups. A similar trend is predicted, namely decrease of the antiferromagnetic contribution as the $<O_1 — V_1 — V_2 — O_2>$ angle deviates from 0°, which also agrees with the J/k ordering **6** (CH_3O–) < **5** (Cl–) < **4** (F–) for deviations of 15.4°, 13.0°, and 8.1° respectively.

Substitution on the aromatic units of the bridging and terminal ligands also influences the magnitude of the antiferromagnetic component. The active–electron approximation accounts for substituent electronic effects[27] (see Chapter I), predicting that electron withdrawing (donating) groups on the bridging ligands should decrease (increase) the magnitude of the antiferromagnetic interaction by lowering (raising) the energy of the ligand's MOs. This effect is probably responsible for the small differences seen in the strength of the exchange coupling constant in compounds **4**, **5**, and **6**. The reduction of the J_{AF} term in **6** from structural effects is probably compensated by its enhancement from the electron donating ability of the *p*-CH_3O– group.

Replacement of the bpy ligand in complexes **5** and **6** by tmbpy generated complexes **5A** and **6A**, the magnetic properties of which differ widely form those of the parent derivatives. The reduction of the J/k constant was fivefold and twofold respectively. Such a great difference can be either attributed to the terminal ligands electronic effect or to a dramatic change of the dimer core geometry. The X–ray structure determination of compound **6A** revealed that indeed the dimer core of the complex is structurally quite different from the parent compound **6**. A *twist*–type arrangement is adopted by the vanadyl groups, as

judged by the large <O_1 — V_1 — V_2 — O_2> angle of 109.6°, a value which is similar to those of complexes **1**, **2**, and **3**. The structure of compound **5A** on the other hand, was not determined due to the lack of suitable single crystals. Its magnetic properties however, fall in the same range (Table 7) as those of the *twist*–type dimers, suggesting that this complex also belongs to the same structural type.

The significant twist of the vanadyl groups places these complexes in the intermediate regime between the *syn* and the *anti* structural types. Two of the phosphinate groups bridge the equatorial site of one vanadyl octahedron to the axial site of the other. Hence participation of these ligands in the exchange pathway may be excluded; there remains the single–bridged divanadyl fragment displayed in *Figure 19(B)*. Comparison of the magnetic data between the *syn* and the *twist*–type dimers indicates that the magnitude of the antiferromagnetic coupling in the latter complexes is consistently smaller. Two factors contribute to this reduction in the magnitude of the J_{AF} term. The first concerns the nature of the exchange pathway. As was also observed in the magnetic properties of extended vanadyl phosphates and phosphonates, the coupling among single–bridged vanadyl centers was much smaller than that of double–bridged ones. The second and probably most important factor is the significant tilt from coplanarity of the magnetic orbitals Φ_S and Φ_A introduced in the twist dimer cores (determined by the value of the dihedral angle <O_1 — V_1 — V_2 — O_2>). *Figure 20(C)* qualitatively describes this effect and predicts that as deviations from coplanarity increase, the energy difference between the magnetic orbitals is reduced. The outcome of this twist is the decrease of the kinetic exchange term, in accordance with the magnetic results presented in this study. Although the variance in the magnetic properties between the *syn* and the *twist*–type dimers is understood by utilization of the energy diagram of *Figure 20(C)*, the latter fails to

predict the magnitude of the antiferromagnetic coupling within the series of the twist–type dimers. The ordering predicted by the value of the $<O_1 — V_1 — V_2 — O_2>$ angle and assuming that the orientation of the d_{xy} orbitals coincide with the vanadium basal planes (**3** < **6A** < **2** < **1**), is exactly the opposite of the observed behavior.

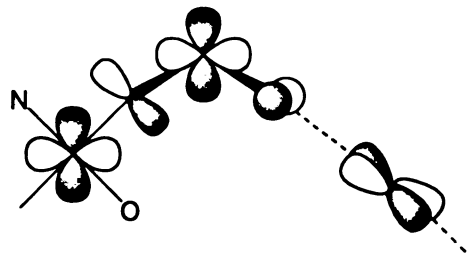

Scheme 2

The origin of this discrepancy, is either due to factors not accounted for by the active–electron approximation, or to errors introduced in the definition of the magnetic orbitals' orientations. In the *twist*–type exchange pathway depicted in Scheme 2, the metal d_{xy} orbitals interact with ligand MOs, which consist of oxygen *p* and phosphorous *d* orbitals. The twist of the d_{xy} levels is accompanied by a tilt of the ligand *p* orbitals, the relative orientation of which should play a prominent role in the magnitude of the kinetic exchange. If the orientation of each *p* orbital is approximated as the direction of the NVO plane normal to the respective oxygen atom, the angles between the *p* orbitals in the exchange pathway are 51.4° (**1**), 43.4° (**2**) and 27.5° (**3**). The magnitude of the kinetic exchange is expected to decrease as the *p* orbitals approach orthoganality, leading to a J/k ordering of **1** < **2** < **3**, which is exactly the experimentally observed order. The above assumption is purely qualitative and theoretical calculations are needed in order to define accurately the relative orientations of the magnetic orbitals.

The final class of molecular complexes synthesized is the *anti*–type, which is the only class that resembles the geometry of a structural building block of the extended vanadyl phosphates and phosphonates. Magnetic susceptibility studies by Carrano and coworkers[8] on $\{HB(pz)_3VO[\mu\text{–}(PhO)_2PO_2]\}_2$ indicated weak ferromagnetic coupling, while antiferromagnetic interactions were found to dominate in the $\{HB(3,4\text{–}Me_2pz)_3VO[\mu\text{–}(PhO)_2PO_2]\}_2$ and $\{HB(pz)_3VO[\mu\text{–}(Ph)_2PO_2]\}_2\bullet 2CH_3CN$ derivatives[13]. The authors explained the magnetic properties by using a direct overlap model. The ferromagnetic coupling is attributed to the chair conformation that facilitates direct overlap of the metal's d_{xy} orbital with the V = O π–system (the V = O π–orbital is orthogonal to the magnetic d_{xy} orbital). Antiferromagnetic interactions dominate on the other hand as the chair flattens and the d_{xy}– V = O π–overlap diminishes while the d_{xy}– d_{xy} overlap increases. This model assumes a distance dependent exchange coupling.

The magnetic studies on the *anti*–type dimer complexes presented in this thesis do not show a correlation of the magnetic properties to the intermetal separation (Tables 20 and 21). The latter is rather long (~5 Å) for direct overlap to make any significant contribution to the coupling interaction. Even in $Cu_2(CH_3COO)_4\bullet 2H_2O$[27] and $[L_2CuOH]_2X_2$[28] where metal distances are much shorter, superexchange interactions are considered to be the dominant magnetic coupling mechanism. In addition, ^{31}P solid state NMR data on extended vanadyl phosphates and phosphonates[29,30] support an active role for the diamagnetic link in the spin communication process. The magnetic properties of extended materials possessing a D VII chair–like dimer core as the main exchange pathway, were explained under the framework of the active–electron approximation. A qualitative energy diagram (*Figure 21*,) attributes the sign and the strength of the magnetic interaction to the vanadium basal plane displacement, $d(N_2O_2^V \text{ I } N_2O_2^V)$. Large displacements (1.87 Å for

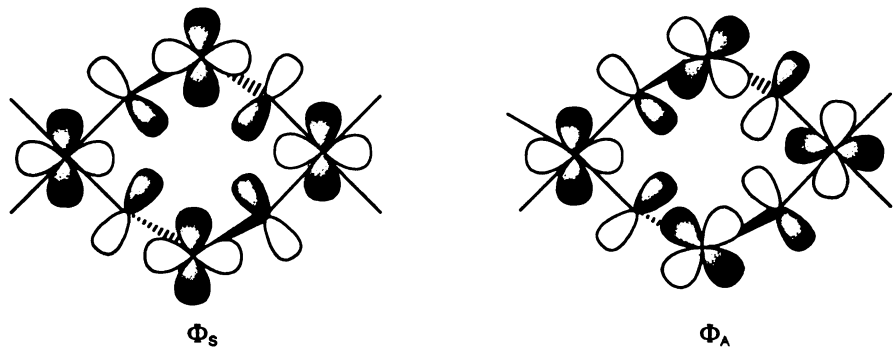

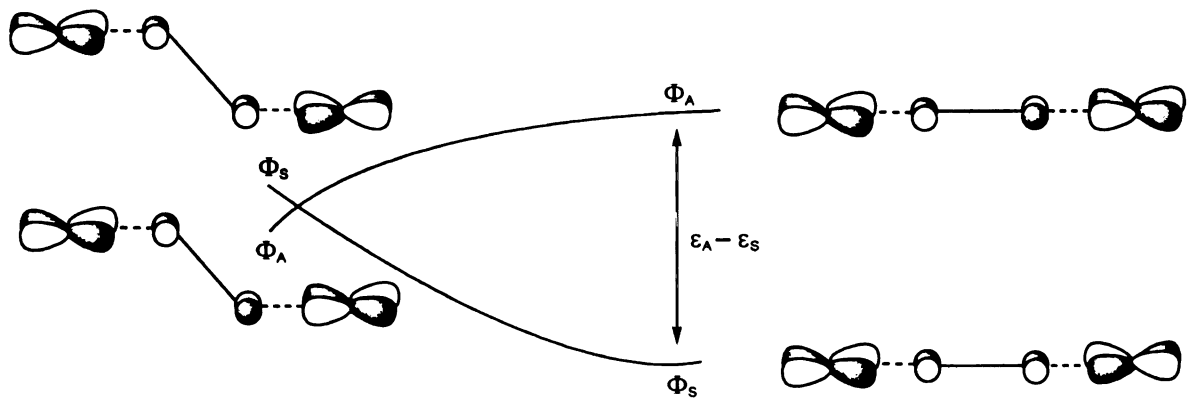

Figure 21. Symmetric (Φ_S) and antisymmetric (Φ_A) combination of vanadium d_{xy} and phosphate/phosphonate molecular orbitals and their energy dependence upon transformation of the flat ring conformation to the respective chair.

$A_{0.5}VOPO_4 \cdot nH_2O$ with A = Na, K, and Rb and 1.76 Å for α–VOSO4) diminish the kinetic exchange term (J_{AF}) leading to ferromagnetic interaction. Smaller displacements on the other hand (1.43 Å for β–$VOHPO_4 \cdot 2H_2O$) lift the degeneracy of the magnetic orbitals, resulting in a nonvanishing kinetic exchange contribution. In agreement with these qualitative arguments is the ferromagnetic coupling displayed by $\{HB(pz)_3VO[\mu\text{–}(PhO)_2PO_2]\}_2$, where the basal vanadium planes are 1.597 Å apart. The latter value is the lower experimental limit for the observation of ferromagnetic coupling in molecular complexes or extended materials that possess the D VII chair–like structural unit. On the other hand the value of 1.43 Å for β–$VOHPO_4 \cdot 2H_2O$ is the higher experimental limit for antiferromagnetic coupling. Inspection of Tables 20 and 21, where the magnetic and structural properties of the dimer cores utilized in this study are gathered, shows that these complexes possess smaller values of basal plane displacements.

These results also indicate that the magnitude of the exchange interaction is not solely dependent on the value of $d(N_2O_2^V \text{ I } N_2O_2^V)$. The magnetic properties of the $\{HB(pz)_3VO[\mu\text{–}(Ph)_2PO_2]\}_2$ derivative were determined for specimens recrystallized from acetonitrile and dichloromethane. Single crystal X–ray structure determination from crystals grown in these solvents revealed that the dimer metric parameters are different. The smaller $d(N_2O_2^V \text{ I } N_2O_2^V)$ displacement in the acetonitrile solvate (mean value 0.719 versus 0.770 Å for the dichloromethane solvate **7**) correlates to a larger singlet–triplet splitting (–81.4 and –61.5 K respectively).The corresponding values for the *p*–F– derivative (0.734 Å, –55.2 K) are similar to those of **7**. The small difference observed is attributed to the electron withdrawing nature of the fluoro–substituent.

Deviations from the energy scheme depicted in *Figure 21* are found for the derivatives **8** and **11** that possess the electron donating substituents CH_3O– and

CH_3– respectively. The electronic effect is expected to increase the antiferromagnetic contribution, while the larger d($N_2O_2^V$ I $N_2O_2^V$) values (1.181 and 1.154 Å respectively) to decrease it. Since both the electronic and metric parameters of the dimer cores are rather similar the observed difference in the singlet–triplet splittings (–43.0 K for **8** and –58.4 K for **11**) cannot be understood by the use of the qualitative arguments presented so far.

Additional complications were encountered in the series of the {$HB(pz)_3VO[\mu$–(*p*-NO_2–$PhO)_2PO_2$]}$_2$•S complexes. Inspection of Table 21 shows that the dichloromethane (**12**), acetone (**13**), and anisole solvates displayed identical magnetic properties. These three complexes possess identical infrared spectra, while X–ray structure determination for the first two revealed that the parameters of interest were similar. The basal plane displacement in these derivatives is 1.277 Å (determined at 173 K for the acetone solvate), a value much larger than those of the phosphinate analogs, and the singlet–triplet separation is smaller as expected. Attempts to increase the latter parameter (and thus decrease the magnitude of the antiferromagnetic exchange) by utilization of hydrogen–bonding donating and electron rich solvents were successful for 1,2–ethanedithiol (**16**), pyrrole (**14**), and thiophene (**15**). The corresponding d($N_2O_2^V$ I $N_2O_2^V$) values and magnetic parameters (given in parenthesis) were: 1.317 Å (–15.8 K), 1.320 Å (–20.3 K) and 1.387 Å (–15.6 K) respectively. Surprisingly the exchange constant is larger than the corresponding one in complexes **12** and **13** (–14 K) that have a smaller basal plane displacement (1.277 Å).

The magnetic properties of the *anti*–type dimers presented in this study, cannot be entirely understood with the qualitative model utilized in the magnetostructural correlations of the chair–like exchange pathways. These studies clearly show that large basal plane displacements correlate with ferromagnetic interactions and that as the chair core flattens antiferromagnetism

becomes the dominant effect. However additional factors adequately represented by the active–electron approximation probably influence the magnitude of the antiferromagnetic interactions. This model[27] considers that the antiferromagnetic component of the exchange interaction is dominated by only one term, namely the kinetic exchange. It is the latter that correlates with geometric features of the exchange pathways. Recent density functional calculations (DFT) displayed excellent agreement with experimental results[28,31], by using this model. However, the calculations were successful only when simplifications concerning the nature of the terminal ligands were avoided. These findings pointed out that the nature of the terminal ligands and their overall geometry might influence the magnitude of the interaction. Therefore one needs to go beyond the active–electron approximation to account for such effects. The pioneering work of de Loth and coworkers[32], who calculated directly the energy gap between the singlet and the triplet, show that there are other terms that contribute to the magnitude of the exchange interaction. The dominant contribution to the antiferromagnetic component was the kinetic exchange, but charge transfer terms were also found to have a significant magnitude. These involved stabilization of the singlet ground state by excited singlet states where electrons from the ligand (metal) are transfer to the metal (ligand), as shown in Scheme 3.

The magnitude of these contributions depends upon the relative energies of the singlet ground and excited states. The latter are sensitive to the structural and electronic environment of the terminal and bridging ligand. For example, although donor–acceptor interactions from π–π stacking are not important in ground state electronic configurations[21], they can significantly stabilize excited states[33] where some of the ligand orbitals are half–filled.

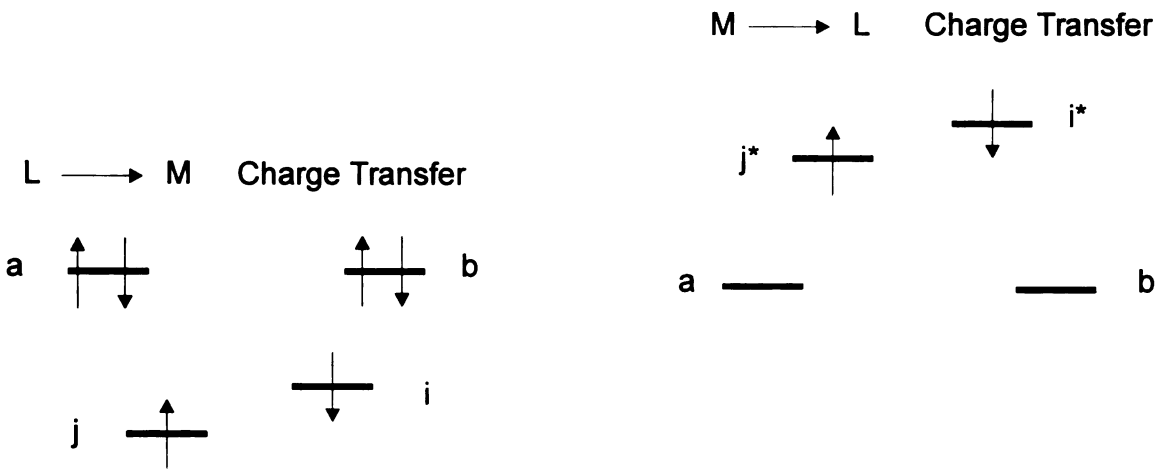

Scheme 3

It is interesting to note therefore the effect that the crystallization solvent has on some of the metric parameters of the $\{HB(pz)_3VO[\mu\text{–}(p\text{-}NO_2\text{–}PhO)_2PO_2]\}_2 \cdot S$ complexes. In the dichloromethane and acetone solvates one of the equatorial pyrazolyl groups and a *p*-nitrophenyl ring form an angle ($<C_3H_3N_2$ / $C_6H_5>_{eq}$) of approximately 20°. The magnetic properties of the two compounds are identical. In the 1,2–ethanedithiol (**16**), thiophene (**15**) and pyrrole (**14**) derivatives, $<C_3H_3N_2$ / $C_6H_5>_{eq}$ dropped to 15.1°, 12.0°, and 11.2° respectively. Although the basal plane displacement is identical in solvates **16** and **14**, the latter complex shows a larger J/k which correlates with a smaller $<C_3H_3N_2$ / $C_6H_5>_{eq}$ angle. In **15** and **14**, where similar $<C_3H_3N_2$ / $C_6H_5>_{eq}$ angles are observed, the larger J/k in **14** correlates with a smaller basal plane displacement d ($N_2O_2^V$ / $N_2O_2^V$).

D. **Conclusions**

The magnetic properties of extended layered vanadyl phosphates and phosphonates have been treated qualitatively under the framework of the active–electron approximation. The antiferromagnetic component was approximated as the kinetic exchange term, the magnitude of which correlates with geometric features of the exchange pathways. These were identified as dimer units with single– or double–bridged vanadyl centers. Synthesis of molecular analogs of the exchange pathways and the study of their magnetic properties provided additional information concerning the exchange coupling. Hence, for the chair–like D VII exchange pathway

- non–parallel vanadyl basal planes correlate with antiferromagnetic coupling
- parallel basal planes correlate with either antiferromagnetic or ferromagnetic coupling
- the sign of the interaction (ferro vs antiferro) for parallel basal planes depends upon their relative displacement d ($N_2O_2^V$ / $N_2O_2^V$)
- the conformation of the chair core (and thus the parameter d ($N_2O_2^V$ / $N_2O_2^V$)) varies with temperature
- ferromagnetism was observed for d ($N_2O_2^V$ / $N_2O_2^V$) values larger than 1.60 Å
- antiferromagnetism was observed for d ($N_2O_2^V$ / $N_2O_2^V$) values smaller than 1.43 Å
- the magnitude of the antiferromagnetic interaction displays a rough correlation to the d ($N_2O_2^V$ / $N_2O_2^V$) value, with smaller exchange couplings observed for larger d ($N_2O_2^V$ / $N_2O_2^V$) displacements

- substituent electronic effects influence directly the magnitude of the exchange interaction by changing the relative energies of the magnetic orbitals
- substituent electronic effects are probably influence indirectly the magnitude of the exchange interaction by changing the energy of the metal's d_{xy} orbital
- ligand–solvent non–covalent interaction have a pronounced influence in the conformation geometry of the chair core
- additional terms of ligand to metal and metal to ligand charge transfer have significant contribution to the magnitude of the antiferromagnetic term
- the charge transfer terms are sensitive to the interaction of the ligands π–systems with those of other ligands and those of surrounding solvent molecules

In addition, the synthesis and magnetostructural characterization of the *syn*– and *twist*–type dimer cores (based on 2,2'–bipyridyl ligands) provided information regarding the correlation of the antiferromagnetic coupling with the relative orientations of the vanadium basal planes. Hence,

- as the angle between the vanadium basal planes approaches 90° the magnitude of the antiferromagnetic interaction decreases
- a similar trend is observed as the $<O_1 — V_1 — V_2 — O_2>$ angle approaches 90°
- complications arise due to the complex geometry of the exchange pathway, which makes difficult to qualitatively define the orientation of the magnetic orbitals

The qualitative arguments presented in Chapters 3 and 4 correctly predicted the sign of the magnetic interaction in both the extended and the molecular compounds. The magnitude of the magnetic coupling, however, was harder to evaluate. Magnetostructural correlations beyond the qualitative approach utilized in this work should take under consideration both the conformational flexibility of the dimer core and the variety of factors that influence the energy of the ligand and metal molecular orbitals.

LIST OF REFERENCES

(1) Beltran, D.; Amoros, P.; Ibañez, R.; Martinez, E.; Beltran, A.; Le Bail A.; Ferey, G.; Villeneuve, G. *Solid State Ionics* **1989**, *32/33*, 57.

(2) Beltran–Porter, D.; Beltran–Porter, A.; Amoros, P.; Ibañez, R.; Martinez, E.; Le Bail, A.; Ferey, G.; Villeneuve, G. *Eur. J. Solid State Inorg. Chem.* **1991**, *28*, 131.

(3) Le Bideau, J.; Papoutsakis, D.; Jackson, J. E.; Nocera, D. G.; *J. Am. Chem. Soc.* **1997**, *119*, 1313.

(4) Papoutsakis, D.; Jackson, J. E.; Nocera, D. G. *Inorg. Chem.* **1996**, *35*, 800.

(5) Fowles, G. W. A.; Rice, D. A.; Wilkins, J. D. *Inorg. Chim. Acta* **1973**, *7*, 642.

(6) Spek, A. L. *Acta Cryst.* **1990**, *A46*, C34.

(7) (a) Dean, N. S.; Mokry, L. M.; Bond, M. R.; O'Connor, C. J.; Carrano, C. J. *Inorg. Chem.* **1996**, *35*, 3541. (b) Dean, N. S.; Mokry, L. M.; Bond, M. R.; Mohan, M.; Otieno, T.; O'Connor, C. J.; Spartalian, K.; Carrano, C. J. *Inorg. Chem.* **1997**, *36*, 1424.

(8) Bond, M. R.; Mokry, L. M.; Otieno, T.; Thompson, J.; Carrano, C. J. *Inorg. Chem.* **1995**, *34*, 1894.

(9) Ballhausen, C. J.; Gray, H. B. *Inorg. Chem.* **1962**, *1*, 111.

(10) (a) Beddoes, R. L.; Collison, D.; Mabbs, F. E.; Passand, M. A. *Polyhedron* **1990**, *9*, 2483. (b) Patel, K. S.; Kolawole, G. A.; Earnshaw, A. *J. Inorg. Nucl. Chem.* **1981**, *43*, 3107.

(11) Bleaney, B.; Bowers, K. D. *Proc. Roy. Soc. (London)* **1952**, *Ser. A 214*, 451.

(12) Mohan, M.; Holmes, S. M.; Butcher, R. J.; Jasinski, J. P.; Carrano, C. J. *Inorg. Chem.* **1992**, *31*, 2029.

(13) Dean, S.; Bond, M. R.; O'Connor, C. J.; Carrano, C. J. *Inorg. Chem.* **1996**, *35*, 7643.

(14) Chen, Q.; Salta, J.; Zubieta, J. Inorg. Chem. 1993, 32, 4485.

(15) (a) Hunter, C. A. Angew. Chem. Int. Ed. Engl. 1993, 32, 1584. (b) Hunter, C. A. Chem. Soc. Rev. 1994, 23, 101.

(16) Hahn, C. W.; Rasmussen, P. G.; Bayon, J. C. Inorg. Chem. 1992, 31, 1963.

(17) (a) Mabbs, F. E.; Collison, D. in Electron Paramagnetic Resonance of d Transition Metal Compounds; Elsevier: Amsterdam 1992. (b) Collison, D.; Mabbs, F. E.; Turner, S. S. J. Chem. Soc. Faraday Trans. 1993, 89, 3705. (c) Mabbs, F. E. Chem. Soc. Rev. , , 313.

(18) Belford, R. L.; Chasteen, N. D.; So, H.; Tapscott, R. E. J. Am. Chem. Soc. 1969, 91, 4675.

(19) Bleaney, B.; Bowers, K. D. Proc. Roy. Soc. (London) 1952, Ser. A 214, 451.

(20) (a) Whitesides, G. M.; Mathias, J. P.; Seto, C. T. Science 1991, 254, 1312. (b) MacDonald, J. C.; Whitesides, G. M. Chem. Rev. 1994, 94, 2383. (c) Etter, M. C. J. Phys. Chem. 1991, 95, 4601. (d) Etter, M. C. Acc. Chem. Res. 1990, 23, 120. (e) Russell, V. A.; Ward, M. D. Chem. Mater. 1996, 8, 1654. (f) Claessens, C. G.; Stoddart, J. F. J. Phys. Org. Chem. 1997, 10, 254.

(21) Hunter, C.; Sanders, J. K. M. *J. Am. Chem. Soc.* **1990**, *112*, 5525.

(22) (a) Cozzi, F.; Cinquini, M.; Annunziata, R.; Dwyer, T.; Siegel, J. S. *J. Am. Chem. Soc.* **1992**, *114*, 5729. (b) Cozzi, F.; Cinquini, M.; Annunziata, R.; Siegel, J. S. *J. Am. Chem. Soc.* **1993**, *115*, 5330. (c) Cozzi, F.; Ponzini, F.; Annunziata, R.; Cinquini, M.; Siegel, J. S. *Angew. Chem. Int. Ed. Engl.* **1995**, *34*, 1019.

(23) Hatfield, W. E. in *Magneto-Structural Correlations in Exchange Coupled Systems*; Willett, R. D., Gatteschi, D., Kahn, O., Eds.; NATO ASI Series; Reidel: Dordrecht, 1985.

(24) Plass, W. *Angew. Chem. Int. Ed. Engl.* **1996**, *35*, 627.

(25) Kahn, O. in *Molecular Magnetism*; VCH Publishers: New York 1993.

(26) Lowry, T. H.; Richardson, K. S. in *Mechanism and Theory in Organic Chemistry*; Harper Collins Publishers, New York 1987.

(27) Hay, P. J.; Thibeault, J. C.; Hoffmann, R. *J. Am. Chem. Soc.* **1975**, *97*, 4884.

(28) Ruiz, E.; Alemany, P.; Alvarez, S.; Cano, J. *J. Am. Chem. Soc.* **1997**, *119*, 1297.

(29) Sananes, M. T.; Tuel, A. *J. Chem. Soc. Chem. Commun.* **1995**, 1323.

(30) Villeneuve, G.; Suh, K. S.; Amoros, P.; Casañ–Pastor, N.; Beltrán–Porter, D. *Chem. Mater.* **1992**, *4*, 108.

(31) Cano, J.; Alemany, P.; Alvarez, S.; Verdaguer, M.; Ruiz, E. *Chem. Eur. J.* **1998**, *4*, 476.

(32) de Loth P.; Cassoux, P.; Daudey, J. P.; Malrieu, J. P. *J. Am. Chem. Soc.* **1981**, *103*, 4007.

(33) (a) Strong, R. L. in *Intermolecular Forces*; Pullman, B., Ed.; D. Reidel: Dordrecht 1981. (b) Claverie, P. in *Intermolecular Interactions: From Diatomics to Biopolymers*; Pullman, B., Ed.; Wiley: Chichester 1978.

CHAPTER 5

Amidinium–Carboxylate Salt Bridge: A Synthon for Structural Design and Transmission of Magnetic Properties

A. Introduction

The field of supramolecular chemistry, "the chemistry beyond the molecule" is defined by Lehn[1] as "the designed chemistry of the intermolecular bond, just as molecular chemistry is that of the covalent bond." The relatively new research field of supramolecular chemistry is rapidly expanding and attracting new researchers, due to the endless perspectives offered by its location at the intersection of chemistry, biology and physics. In supramolecular chemistry, the supramolecules are not anymore viewed as a collection of individual species or as random molecular aggregates. There are distinct

nanostructures with different properties from those of the individual building blocks that are the result of the supramolecule's tertiary structure[2]. The collective properties of nanostructures can be tuned or modified by chemical changes in the molecular building blocks. It is therefore clear that one has to take into account many different factors in the successful design of a supramolecule. It is this complexity that produces materials with unique functions and applications. Fortunately these challenges are guided by the study of natural systems, where composite structures are formed by the self–organization of molecular components which interact in certain, well–defined ways[3].

Although interpenetration between areas takes place, novel lines of investigation have been developed in the supramolecular chemistry[4] that involve molecular recognition effects, the synthesis and study of supramolecular devices that are able to mimic the functions of natural systems, and self–assembly phenomena (*Figure 1*).

Molecular recognition is defined as the selective binding of a substrate by a molecular receptor to form a supramolecule. Systems that meet the above definition include the two catalytic reactions reported by Kelly and coworkers[5], where a template molecule binds the reactants through a network of hydrogen bonds. The template molecule is acting as an artificial enzyme by bringing the reactants in close proximity and accelerating their reaction. When the reaction product can serve as template for its own formation and, in addition is capable of conserving and expressing its structure, then the reaction is termed a self–replication process. The first examples of self–replication were concerned with the nonenzymatic ligation of nucleotides[6,7]. Purely synthetic self–replicating systems were latter developed[8] with the simplest one (*Figure 2*) containing an amidinium–carboxylate salt bridge as a key component for the assembly of the supramolecule[9]. In this example, the condensation of 3–aminobenzidines and 2–

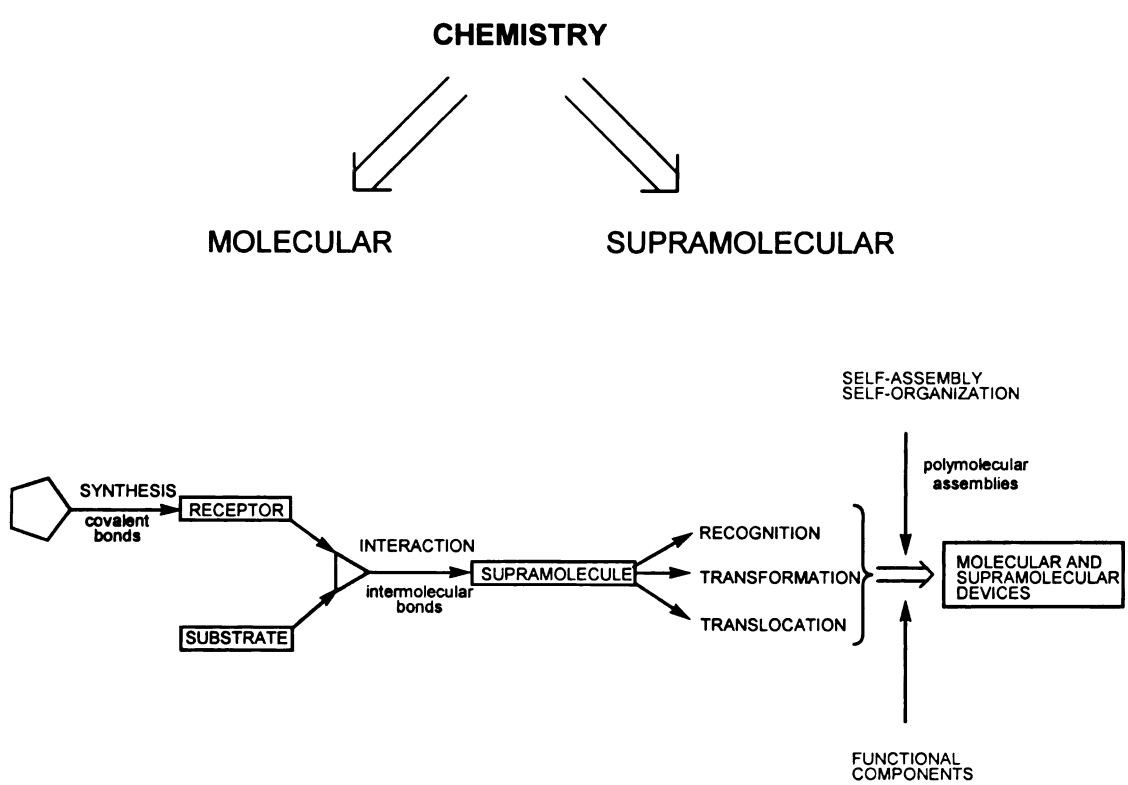

Figure 1. From molecular to supramolecular chemistry: molecules, supramolecules, molecular and supramolecular devices.

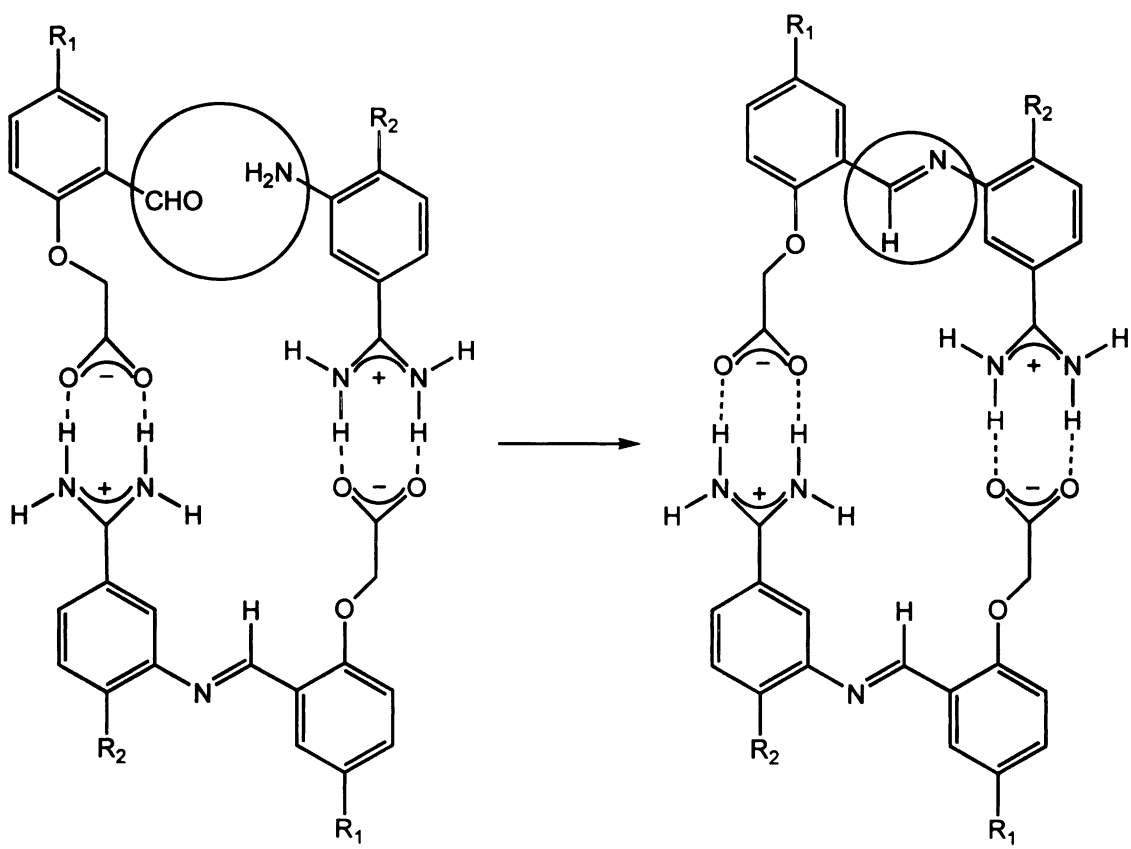

Figure 2. Condensation reaction of 3–aminobenzidines with 2–formyl phenoxyacetic acids via the assembly of a ternary complex, amiable by an amidinium–carboxylate salt bridge.

formylphenoxyacetic acids is facilitated by the close proximity of the reactants on the ternary complex formed by the strong interaction in the amidinium–carboxylate salt bridge.

Supramolecular devices on the other hand are structurally organized and functionally integrated chemical systems built into supramolecular arrays[1(c)]. The distinct molecular components, when placed in a proper order, performed specific functions characteristic of the supramolecule. This area of supramolecular chemistry is the focus of many research groups affording a vast variety of devices and has been the topic of many interested reviews[3,10] and monographs[11]. Such an example is selected from the work of Dr. J. A. Roberts[12], and is illustrated in *Figure 3* where donor–acceptor complexes for electron transfer reactions are drawn. The assembly of the two species is achieved in solution with the aid of an amidinium–carboxylate salt bridge. This structural element not only facilitates the formation of the ternary complex but also permits electronic communication and actively participates in the electron transfer event.

Self–assembly phenomena involve the spontaneous generation of supramolecular architectures, via molecular recognition sequences, by its individual components in the liquid or the solid state phase. These types of phenomena manifest the synthesis and functions of numerous complex biological systems, which are not entirely built up by covalently linked molecular units. Noncovalent bonding plays a prominent role to the self–organization of these macromolecules and it is by this intelligent design that Nature introduces synthetic economy, reduces structural errors upon reproduction and facilitates the formation of the desired supramolecules[10]. As progress in organic and inorganic synthesis is sustained by successful imitation of natural systems, there is a need for the development of novel synthetic routes that will allow the successful design and synthesis of supramolecular species. The lack of simple

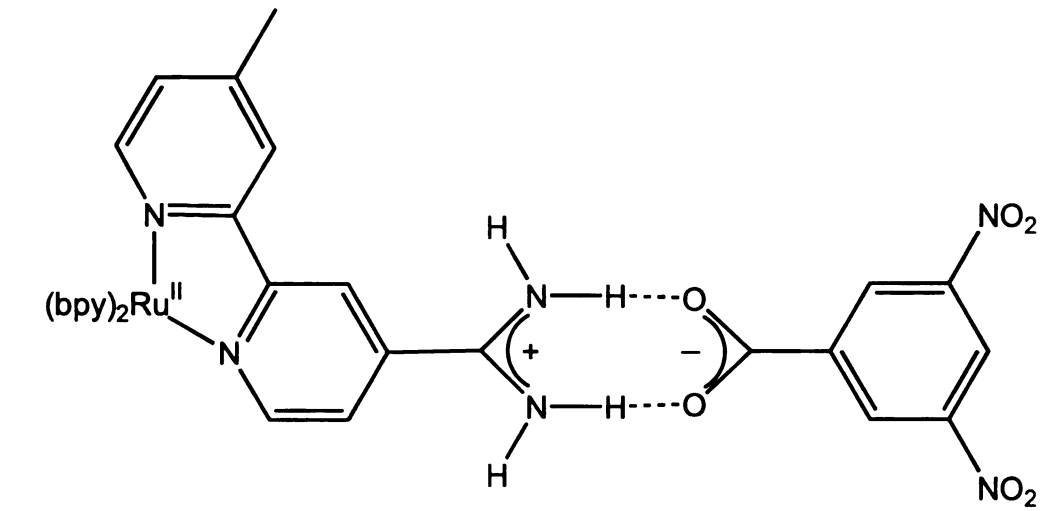

(A)

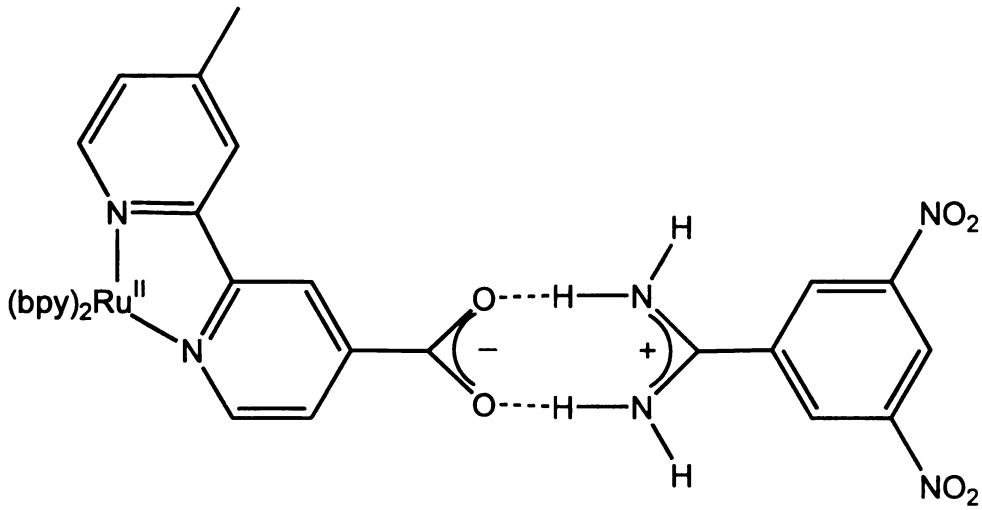

(B)

Figure 3. Supramolecular complexes (A) and (B) assembled in solution, for electron transfer studies, with an amidinium–carboxylate salt bridge as the connecting structural element.

rules, analogous to the ones applied for the formation of covalent and ionic bonds, is more prominent as the wealth of structural motifs increases, while at the same time the predictive powers of the researchers are very limited. It is through this necessity that the field of crystal engineering has emerged[13]. It was originated by the pioneering studies of Schmidt[14], who demonstrated that novel solid state packing arrangements of cinnamic acid derivatives displayed different photodimerization behavior. A recent definition given by Desiraju[15] lays the foundations of the field as: "the understanding of intermolecular interactions in the context of crystal packing and in the utilization of such understanding in the design of new solids with desirable physical and chemical properties." So, it is the goal of the field to systematize the principles that govern noncovalent bonding and apply them to supramolecular synthesis. Hydrogen–bonding, dipole, hydrophobic, aromatic π–stacking and van der Waals forces are some of the noncovalent intermolecular interactions that have been found to self–assemble molecules into solids[16]. This systematic analyses of structural data aided by the ongoing improvements and developments of the Cambridge Structural Database[17], not only unmasks the intermolecular forces responsible for the self–organization of molecular units to supramolecules but identifies common building blocks that interact in known ways. These are referred to as supramolecular synthons[2] or modules[16(e)] and their value is analogous to the value of respective structural features in a target molecule of organic synthesis. Most of the synthons are based on traditional hydrogen–bonding interactions involving the hydrogen atom of an —NHR or —OH moiety and a highly electronegative acceptor atom like O, N or F. Typical examples are synthons **1** and **2** shown in *Figure 4*, where the two carboxylic units comprising the building block can either form a two– or one–point hydrogen bond respectively. Various factors could govern the preference for one over the other, as it was demonstrated by Etter and

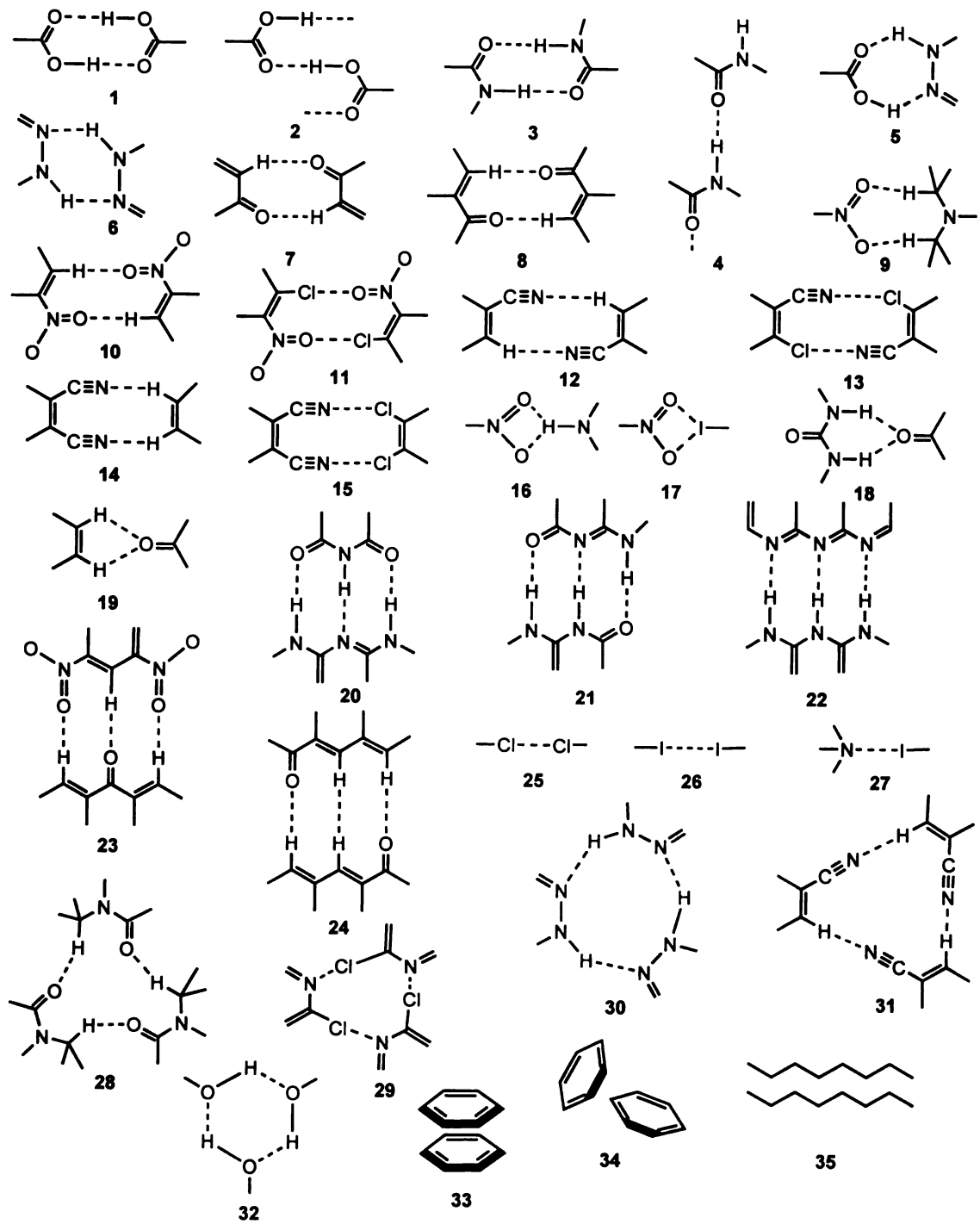

Figure 4. Representative supramolecular synthons.

coworkers[18], where the bonding mode was influenced by the steric demand imposed by the neighboring to the carboxylate alkyl groups. Attractive hydrogen–bonding interactions that involve weaker acceptor molecules or "unusual" donating hydrogen sources, have also been used quite successfully as molecular cement of superstructures. Synthons **7** – **12** and **31** – **32** (*Figure 4*) demonstrate such examples. It is noteworthy that the hydrogen atoms involved in hydrogen bonding, possess enhanced acidity by being always placed in the α–position of a double bond or other electron–rich groups. Apart from hydrogen–bonding, which most of the times sets the primary type of interactions in a supramolecular architecture, the overall tertiary structure of the material is determined by the synergistic contribution of weaker intermolecular forces. Their relative weight is hard to estimate since most of the times they remain masked due to the presence of stronger interactions. Relatively recently, some effort has been devoted to the subject by engineering structures based on synthons that do not involve hydrogen–bonding interactions (entries **17**, **25** – **27**, and **33** – **35** in *Figure 4*). For example Desiraju and coworkers[19], have assembled tapes and lamellar structures based on nitrogen — chlorine bonds, while three–dimensional diamond type networks[20] have been constructed with the aid of halogen — halogen interactions.

Charged species are seldom used as building blocks of extended structures. The nondirectionality of the electrostatic interaction along with the inability to desolvate charged species from polar environments and the need for counterions to maintain charge neutralization in the crystalline environment, are some of their drawbacks. These problems however can be overcome when the synthon is a salt bridge. These are charged species where in addition to hydrogen–bonding, the electrostatic attraction enhances the strength of the nonbonding interaction providing a powerful tool for crystal engineering.

Ammonium–carboxylate salt bridges[21] have led to successful examples of engineered structures, while the use of guanidinium–sulfonates as synthons by Ward and coworkers[22], has provided numerous tapes and layered motifs including a recent example of nanoporous materials with molecular–scale voids of controlled sizes[23].

Choosing the dimensionality between tapes or layers can be difficult. This is not the case in natural systems where the tertiary structure of proteins and enzymes is often determined by secondary electrostatic interactions of salt bridges buttressed and oriented with hydrogen bonding. Using Nature's example we have exploited the ability of salt bridges to set the dimensionality in engineered solids. Our approach is centered on the amidinium–carboxylate salt bridge as a synthon for self–assebly.

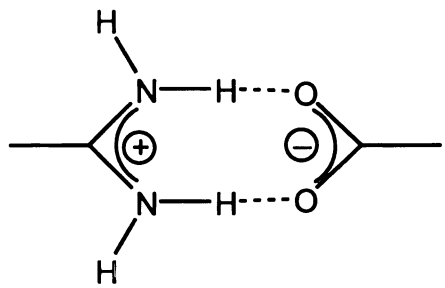

Scheme 1

As shown in Scheme 1, this synthon models the primary interaction of the guanidinium–carboxylate interface incorporated in arginine (Arg) and aspartate (Asp) residues of many natural systems[24], while the design strategy is simplified by offering only one carboxylate binding mode within the salt bridge. In addition, the successful use of this synthon for the assembly of the self–replicating system depicted in *Figure 2* and the supramolecular complex for electron transfer shown in *Figure 3* illustrates the strength of the primary interaction since these

supramolecules were assembled in solution. In the latter case, titration studies conducted by Dr. J. P. Kirby[25], have monitored the formation of the 1:1 amidinium–carboxylate complexes and indicated the presence of secondary interactions as this ratio is exceeded.

The main scope of this work is to explore possibilities of utilizing salt bridges not only as structural elements, but also as conductors of electronic communication. Work on electron transfer (*Figure 3*) places the amidinium–carboxylate salt bridge at the center of attention as a structural and communication element[12]. By the same reasoning, the salt bridge can be utilized as a coupling link for radical centers located on the oxygen atoms of organic nitroxides. The ability of the nitroxyl group to function as a crystal engineering element in conjunction with hydrogen donor groups has been explored relatively recently[26]. Veciana and coworkers[27], systematized the magnetostructural behavior of α–phenyl nitronyl nitroxide radicals by placing an O — H group at various positions on the aromatic ring. The structural motifs obtained, ranging from zero–dimensional to three–dimensional, were accompanied by a remarkable range of magnetic behaviors.

The first part of this chapter deals with the self–assembly of the bifunctional molecule 3–amidinium benzoate (**1**) and establishes the role of the amidinium–carboxylate salt bridge as a synthon for the successful organization of superstructures. It also demonstrates the ability of a nitroxyl radical group, in 2,2,5,5–tetramethyl–3–carboxypyrroline–1–oxyl (**2**), to form extensive structural networks even when other functional groups, traditionally used in crystal engineering, coexist in the same molecular framework. In the second part, the salt bridge in conjunction with the nitroxyl group is used for the assembly of the extended solids benzamidinium 2,2,5,5–tetramethyl–3–carboxypyrroline–1–oxyl hydrate (**3**), and 3–cyanobenzamidinium 2,2,5,5–tetramethyl–3–carboxypyrroline

–1–oxyl (**4**), where spin communication is turn–off and –on respectively, reflecting the synthons' interconnection.

B. Results

1. Synthesis and Structure of 3–Amidinium Benzoate (1)

The bifunctional molecule 3–amidinium benzoate (**1**) was synthesized in a one–pot step by modification of a known literature procedure[28], as described in detail in Chapter 2. In the first step, a sodium methoxide solution in methanol is added to 3–cyanobenzoic acid. Nucleophilic attack of the methoxide ion on the carbon–nitrogen triple bond, affords the intermediate imidate ester carboxylate depicted in Scheme 2. Addition of excess ammonium chloride, which also serves as a neutralizing agent for the extra sodium methoxide in the solution, promotes the nucleophilic attack of ammonia and generation of the amidinium functional group.

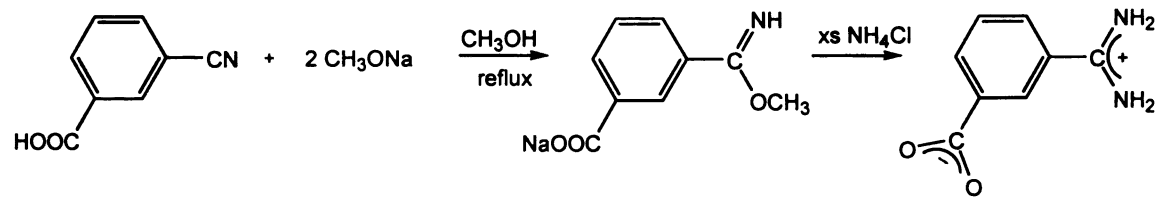

Scheme 2

Compound **1** forms white square–like crystals upon recrystallization from a hot aqueous solution. A single crystal X–ray study was undertaken, and the structural data are summarized in Table 1 (details of the experimental conditions, structure solution and refinement can be found in Chapter 2). Compound **1** self–assembles to a three dimensional structural network, built up by extensive

Table 1. Crystallographic Data for Compounds **1**, and **2**

	1	**2**
	(A) Crystal Parameters	
formula	$C_8H_8N_2O_2$	$C_9H_{14}NO_3$
FW	164.16	184.21
crystal size (mm^3)	0.65 × 0.40 × 0.20	0.58 × 0.58 × 0.38
crystal system	monoclinic	monoclinic
space group	$P2_1/n$	$P2_1/n$
a (Å)	7.253 (2)	5.9898 (1)
b (Å)	6.934 (3)	12.8092 (2)
c (Å)	14.602 (2)	26.3920 (5)
β (deg)	93.64 (2)	91.872 (1)
V ($Å^3$)	733.0 (4)	2023.83 (6)
Z	4	8
d_{calc} (g/cm^3)	1.488	1.209
F(000)	344	792
μ(Mo Kα), cm^{-1}	1.10	0.91
	(B) Data Collection	
$2\theta_{max}$ (deg)	50.0	50.0
index ranges	$0 \le h \le 8$ $0 \le k \le 8$ $-17 \le l \le 17$	$-7 \le h \le 7$ $-16 \le k \le 17$ $-30 \le l \le 35$
scan speed (deg/min in	2	
temperature	296 (2)	173
reflections collected	1397	10776
unique reflections	1288	3543
R(merg) (%)	3.27	2.45
	(C) Refinement	
Refinement method	Full–matrix least–squares on F^2	Full–matrix least–squares on F^2
R indices ($I > 2\sigma(I)$)	R1 = 0.0376 WR2 = 0.1195	R1 = 0.0326 WR2 = 0.0864
R indices all data	R1 = 0.0519 WR2 = 0.1291	R1 = 0.0400 WR2 = 0.0899
Δ(ρ) ($e^-/Å^3$)	0.180	0.246
Extinction coefficient	0.034 (9)	0.014 (2)
GOF	1.174	1.065

hydrogen–bonding. *Figure 5* illustrates the primary interaction involved to the organization of the structure, which consists of a two–point hydrogen bond between the amidinium–carboxylate salt bridge. The relatively short N to O distances of 2.776(1) and 2.790(2) Å, indicate the strength of such interactions which are enhanced by both hydrogen bonding and electrostatic forces[13]. In addition, two favorable secondary electrostatic interactions[29] confer further stability on the interface[12,30]. A zig–zag tape pattern results from the catenation of the salt bridges, as a consequence to their *meta* positioning on the aromatic ring. The tapes align in a head–to–head arrangement along the c–axis of the unit cell and pack together at a van der Waals contact distance to create the sheets of the bc plane. The repeat distance between positional atoms of neighboring tapes is 6.93 Å, thereby establishing the b–dimension of the unit cell. Whereas the phenyl rings lie in the bc plane, a rotation of the amidinium group by 30.0(1)° from the plane of the aromatic ring is complemented by a 23.3(1)° counter–rotation of the carboxylate group. This 7° difference in rotation results in a slight twist of the amidinium–carboxylate interface (dihedral angle of 8.41° for the planes defined by the CN2 and CO2 atoms of the salt bridge) with respect to the bc plane.

Although the self–assembly process is dictated by the two–point hydrogen bond described above, the canting of the salt bridges permits the formation of secondary hydrogen bonding interactions, which extend the dimensionality of the structure beyond the sheets of zig–zag tapes. The amidinium protons outside the salt bridge form hydrogen bonds to carboxylate oxygens of tapes from adjacent sheets above and below the bc plane. This secondary interaction involves one–point hydrogen bonds that generate ladders, as shown in *Figure 6* where the crystal structure has been rotated such that one of the ladders is projected in the plane of the paper. The hydrogen bonding arrangement of the ladder necessarily enforces the amidinium–carboxylate salt bridges in neighboring sheets to

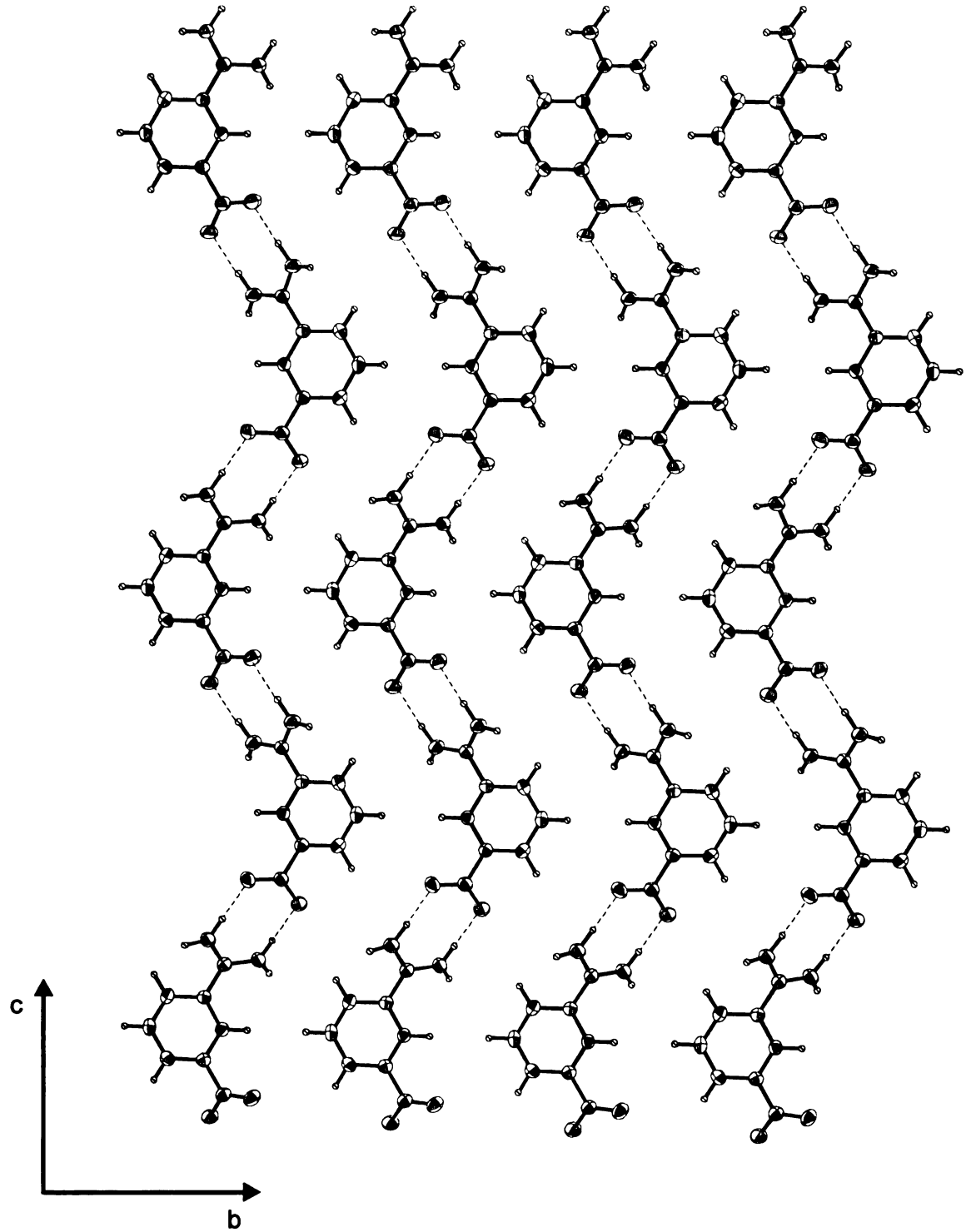

Figure 5. The packing of the zig–zag tapes in the bc plane of the crystal structure of 1. The amidinium–carboxylate salt bridge is rotated 26.1 (plane defined by the oxygen and nitrogen atoms of the salt bridge) out of the plane of the aromatic ring.

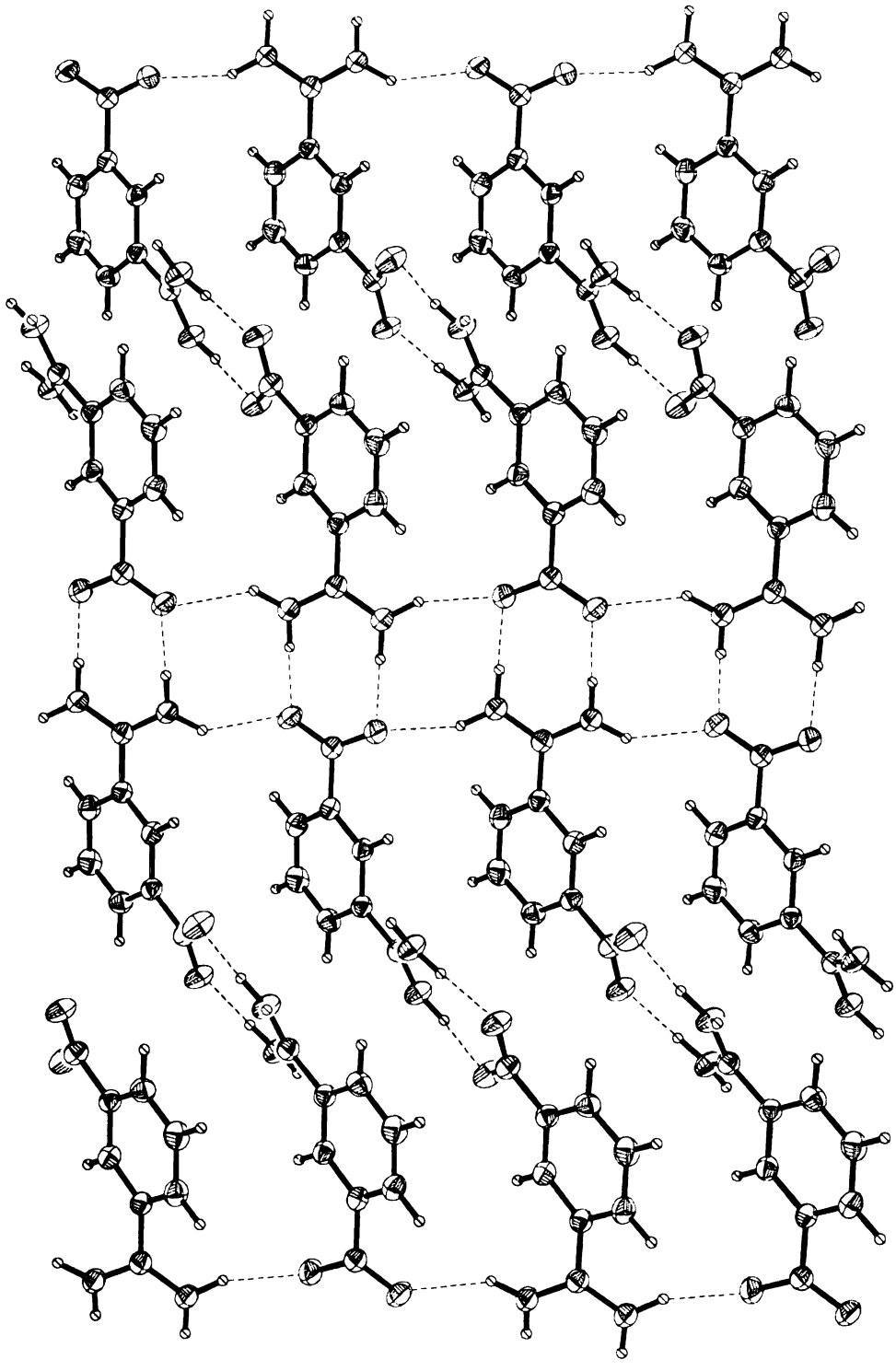

Figure 6. Rotation of the crystal structure of 1 such that the ladder is viewed in the plane of the paper. The ladder structure is formed from the hydrogen bonding between protons external to the salt bridge of a given tape and the carboxylate oxygens of salt bridges in neighboring interlayers.

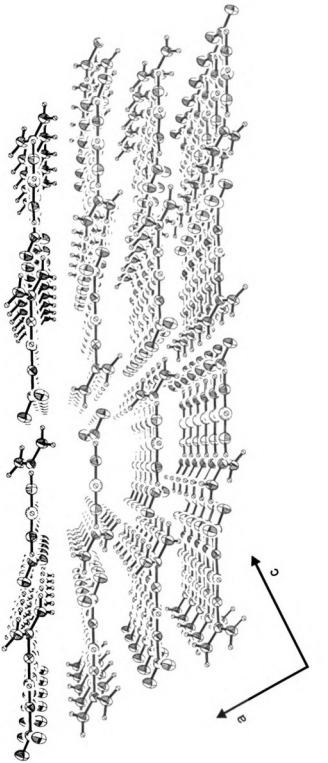

Figure 7. The ac plane of 1 showing the layered sheet structure supported by a ladder scaffold. The ladders tilt alternately in to and out of the plane of the paper by 30.0° and 23.3° respectively.

arrange such that their dipoles are opposed, thereby setting the head–to–tail orientation of tapes along the ladder. This orientation has the added benefit of satisfying the dominant dipole interaction within the three–dimensional structure. The dipoles of salt bridges above and below a plane in the ladder structure are at a distance of 3 Å whereas the dipoles within the bc plane are at a distance of 7 Å. Consequently, the maximum stabilization of the dipoles arising from the coulombic potential is derived from interlayer salt bridges in the head–to–tail arrangement.

A view of the ac plane (*Figure 7*) in the crystal structure of **1**, shows that the ladders intersect the bc plane at an oblique angle, further interconnecting the interlayer planes of zig–zag tapes within sheets to form a layered structure (d–spacing of 3.16 Å). The ladders are parallel to each other but alternately tilt in and out of the ac plane owing to the rotation of the amidinium and carboxylate groups with respect to the aromatic rings (*vide supra*). Although the one–point hydrogen bond is slightly weaker than the two–point interaction, as evidenced by the longer N to O distances of 2.878(5) Å and 2.904(6) Å, it composes the ladders that radiate from the aromatic subunits providing the scaffolding which supports the layer structure. The latter is further stabilized by the van der Waals interactions of the aromatic rings from neighboring sheets.

2. Synthesis and Structure of 2,2,5,5–tetramethyl–3–carboxypyrroline–1–oxyl (2)

Compound **2**, namely 2,2,5,5–tetramethyl–3–carboxypyrroline–1–oxyl, was synthesized by a known literature procedure[31] from the commercially available carboximide **I** as illustrated in Scheme 3. The carboxamide is catalytically oxidized by sodium tungstate, which is constantly regenerated by hydrogen peroxide. Subsequent hydrolysis under basic conditions and

recrystallization from benzene afforded **2** as a bright yellow solid.

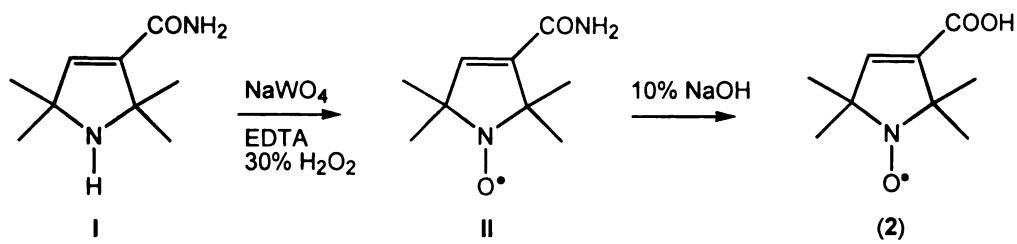

Scheme 3

Although compound **2** is utilized as a spin label and a spin trap for biological systems, an extensive search of the Cambridge Structural Database revealed no structural data. Since the carboxylate of **2** is used along with the benzamidinium and 3–cyanobenzamidinium cations for the engineering of magnetic solids, we decided to solve its crystal structure and study its magnetic properties. The structural and magnetic data of **2** in addition to those of analogous compounds[32,33,34], provide a solid basis for understanding the bonding preferences of the nitroxyl synthon.

Well formed yellow square–like crystals where prepared by slowly cooling to room temperature a benzene solution of compound **2**. Two crystallographically independent molecules A and B, crystallize in the monoclinic system, space group $P2_1/n$ (14) (Table 1). Inspection of covalent bond distances and angles for the two independent molecules reveals very small differences between them. The average N to O bond distance in the nitroxyl group is 1.275(1) Å, a value that compares well with the typical distances found in other similar molecules[26] bearing this functional group. The plane of the carboxylic group (defined by the CO2 atoms) is twisted from the plane of the pyrrolline five member ring by only 1.4(2)° and 3.0(2)° respectively for the A and B molecules.

Although carboxylic groups have the tendency to form two– or one–point hydrogen bonds among themselves (see synthons **1** and **2**, *Figure 4*), in compound **2** the presence of the nitroxyl moiety impedes this type of contact. Its enhanced electronegative character leads to the formation of a hydrogen bonding pattern involving itself and the O–H group of the carboxylic moiety. This primary interaction establishes one–dimensional chains running along the c–axis of the unit cell as shown in *Figure 8* where the bc plane is projected. Molecules A and B alternate along the chain with hydrogen bonding distances of 2.594(1) Å and 2.652(1) Å from the hydroxyl oxygen (O2 for A, O5 for B) to the nitroxyl oxygen (O6 for B, O3 for A) respectively (1.73(2) Å and 1.75(2) Å from the hydroxyl hydrogen atom). These chains are not simply a repetition of an ..ABAB.. pattern since another type of alternation is involved. The alternating A and B molecules are placed such that their carboxylate oxygen atoms (O1 for A, and O4 for B) are positioned antiparallel between adjacent molecules of the same type forming a pattern, where each unique molecule is repeated every fourth time along the chain.

This concrete pattern of the chain is not a coincidental choice of compound **2** for self–assembly. It establishes a hydrogen bonding interaction among adjacent chains that involves the olefinic hydrogen of the A type molecules and the carboxylate oxygen of the B type molecules. This is a relatively weak interaction judging from the long C3 to O4 distance of 3.259(1) Å (the H3 to O4 distance is 2.39(1) Å) but much stronger than similar contacts reported in the literature[27(a)]. No hydrogen bonding is established between the two–dimensional sheets, resulting in a simple stacking of the layers on the top of each other at van der Waals contact distances along the a–axis of the unit cell.

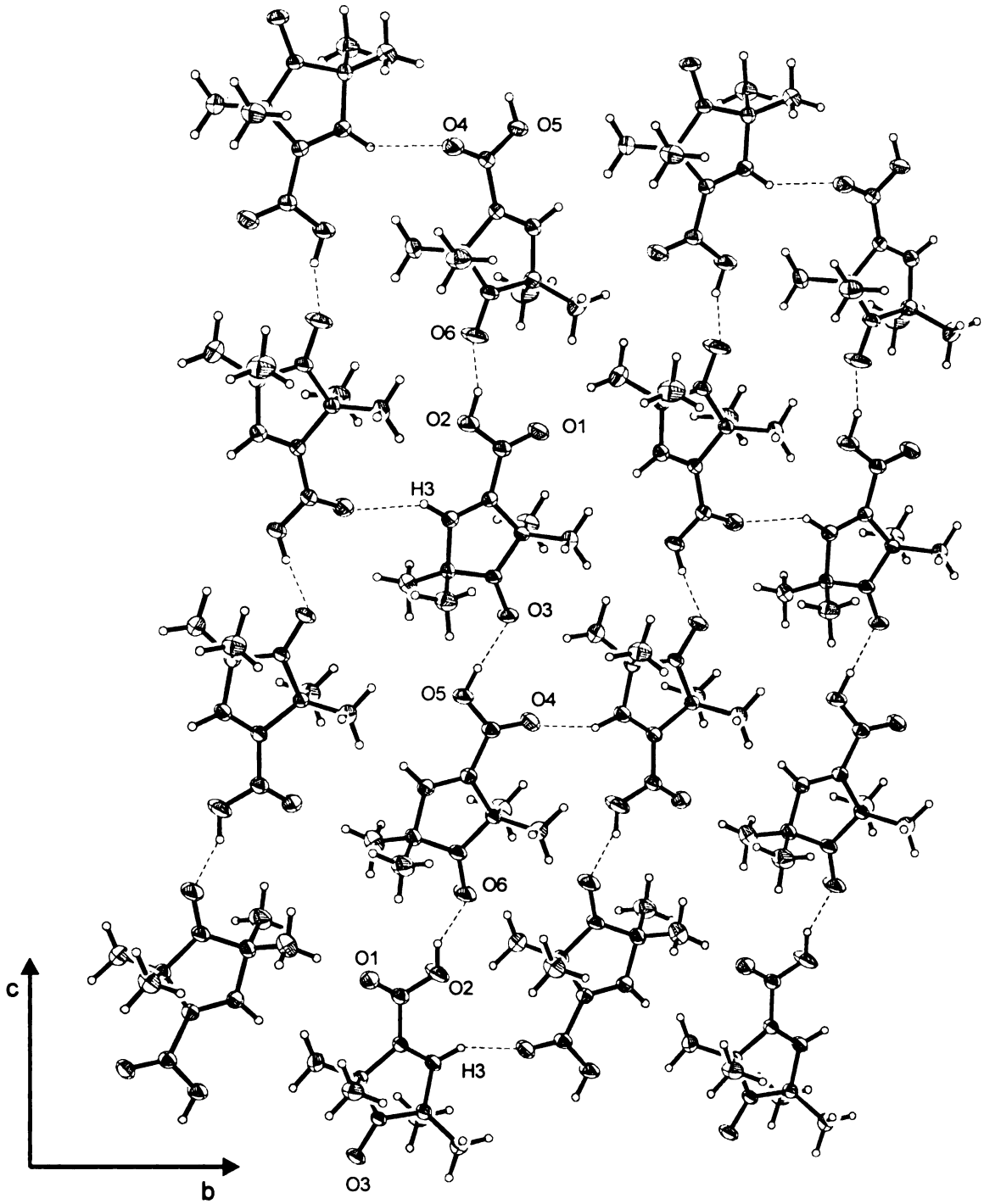

Figure 8 The layered structure of compound **2**. Only atoms involved in the hydrogen bonding pattern are numbered along one of the chains.

3. Synthesis and Structure of benzamidinium–2,2,5,5–tetramethyl–3–carboxypyrroline–1–oxyl hydrate (3)

The title compound **3** is prepared by mixing equimolar aqueous solutions of benzamidinium chloride and 2,2,5,5–tetramethyl–3–carboxypyrroline–1–oxyl neutralized by sodium hydroxide. Slow evaporation of the resulting solution afforded large, well–formed yellow crystals of a monohydrated amidinium–carboxylate salt (crystal data are gathered in Table 2). The average carbon to oxygen and carbon to nitrogen bond distances are 1.247(3) Å, and 1.307(3) Å for the carboxylate and the amidinium groups respectively, while the nitrogen to oxygen distance in the nitroxyl functional group is 1.274(3) Å, a value comparable to the one found in the parent compound **2**. The CO_2 plane of the carboxylate is rotated 12.8(3)° with respect to the plane defined by the pyrroline five–member ring, while the CN_2 plane of the amidinium deviates significantly from the benzene ring plane by 52.5(2)°.

The two–point hydrogen bond of the amidinium–carboxylate salt bridge is the primary interaction involved in the extended structure of **3**, as has been observed previously[35]. This type of bonding is directional and strong, as judged by the relatively short nitrogen to oxygen distances of 2.853(3) Å and 2.842(2) Å. Dimers of the benzamidinium (Am) and the 2,2,5,5–tetramethyl–3–carboxypyrroline–1–oxyl (Ca) ions form via this primary interaction, as shown in *Figure 9(A)*. Formation of a tape motif by this two–point hydrogen bond pattern is not possible in this case, as it was in the structure of compound **1**. If only this primary interaction were operative, the structure of compound **3** would be terminated by dimer formation of the (AmCa) type. However the external hydrogen atoms of the amidinium group are involved in a variety of one–point hydrogen bonds, also shown in *Figure 9(A)*. One of these interactions, involves

Table 2. Crystallographic Data for Compounds **3**, and **4**

	3	**4**
	(A) Crystal Parameters	
formula	$C_{16}H_{24}N_3O_4$	$C_{17}H_{21}N_4O_3$
FW	322.38	329.38
crystal size (mm^3)	0.57 × 0.32 × 0.30	0.46 × 0.23 × 0.15
crystal system	monoclinic	monoclinic
space group	$P2_1/n$	$P2_1/c$
a (Å)	9.232 (1)	8.107 (4)
b (Å)	9.479 (5)	18.463 (2)
c (Å)	20.695 (3)	12.231 (2)
β (deg)	97.94 (2)	103.15 (2)
V ($Å^3$)	1793.8 (9)	1782.9 (9)
Z	4	4
d_{calc} (g/cm^3)	1.194	1.227
F(000)	692	700
μ(Mo Kα), cm^{-1}	0.86	0.86
	(B) Data Collection	
$2\theta_{max}$ (deg)	50.0	50.0
index ranges	$0 \le h \le 9$ $0 \le k \le 11$ $-24 \le l \le 24$	$0 \le h \le 9$ $0 \le k \le 21$ $-14 \le l \le 14$
scan speed (deg/min in	2	2
temperature	296 (2)	296 (2)
reflections collected	2937	3369
unique reflections	2725	3140
R(merg) (%)	4.53	2.99
	(C) Refinement	
Refinement method	Full–matrix least–squares on F^2	Full–matrix least–squares on F^2
R indices ($I > 2\sigma(I)$)	R1 = 0.0459 WR2 = 0.1090	R1 = 0.0522 WR2 = 0.1054
R indices all data	R1 = 0.0918 WR2 = 0.1334	R1 = 0.1275 WR2 = 0.1370
Δ(ρ) ($e^-/Å^3$)	0.152	0.177
Extinction coefficient	0.016 (2)	0.005 (1)
GOF	1.135	1.030

A

iB

Figu
resul
the c

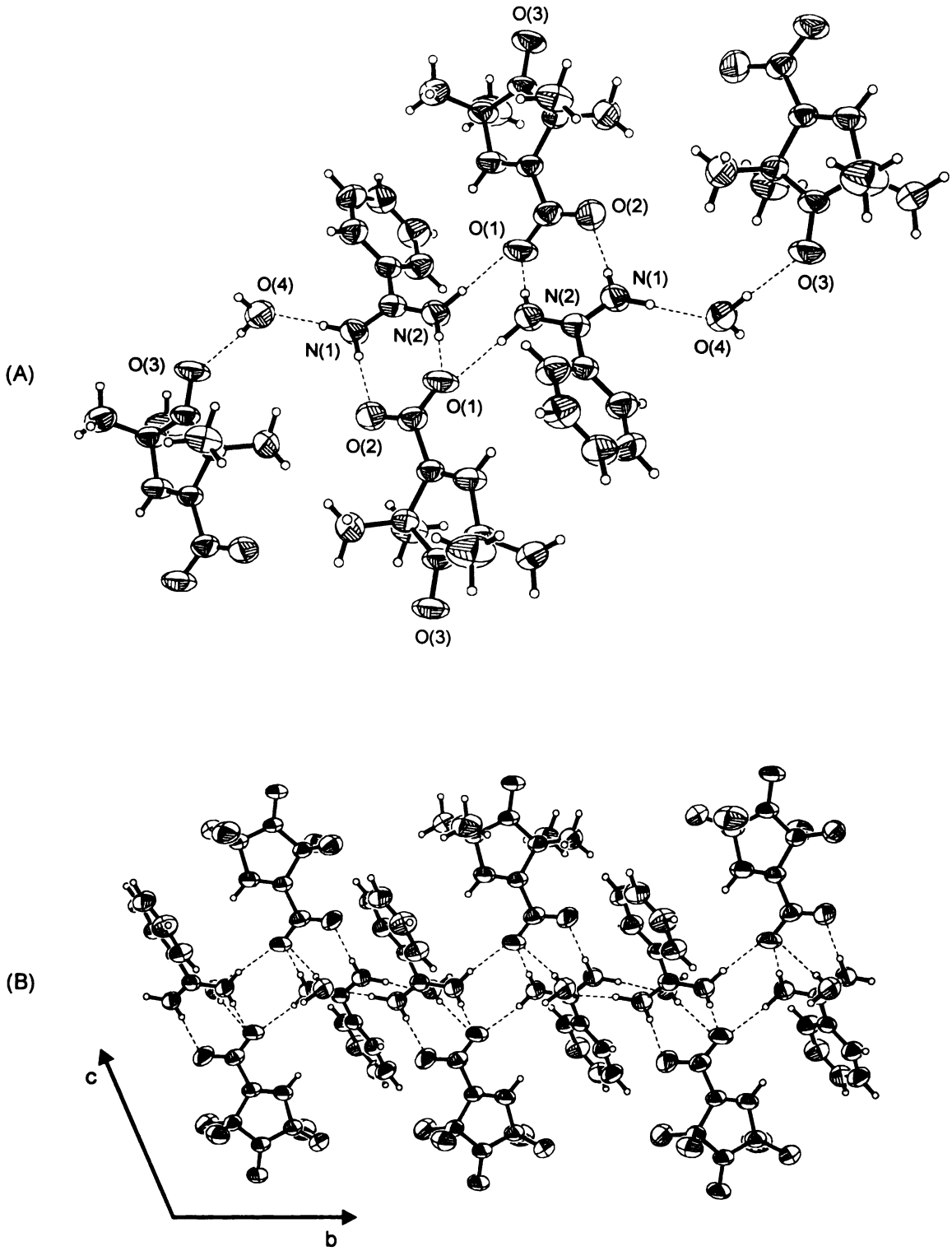

Figure 9. The molecular cluster of two cations and two anions (A) and the resulting infinite ladders along the b–axis of the unit cell that result upon bridging the clusters with the water molecules (B).

the carboxylate oxygen O(1) and the amidinium nitrogen N(2). These partners hydrogen bond at a distance of 2.886(4) Å (1.99(4) Å from the hydrogen atom) creating a cluster of four molecules, two of each ion, with the maximum number of hydrogen bonding and favorable dipole arrangement achieved. The other amidinium nitrogen, N(1), is connected to oxygen O(4) of the water molecule at a distance of 2.829(4) Å (1.87(4) Å from the hydrogen atom), a distance that is even shorter than the ones involved in the primary interaction of the salt bridge. The water molecules are coplanar to the amidinium group, but alternately placed above and below the plane of the carboxylate groups, to which are connected via the O(1) oxygen at a distance of 3.061(3) Å. The result of such an arrangement is the formation of infinite ladders running along the b–axis of the unit cell, by connecting the clusters via N(1) to O(4) and O(4) to O(1) hydrogen bonds, as shown in *Figure 9(B)*.

The dimensionality of the structure is further extended by the participation of the nitroxyl group in the bonding pattern. It forms strong one–point hydrogen bonds to the water molecule as judged by the sort distance of 2.793(3) Å (1.91(3) Å from the H(4A) water hydrogen). In *Figure 10(A)*, where the benzamidinium ions have been omitted for clarity, a view of the hydrogen bond pattern involving the 2,2,5,5–tetramethyl–3–carboxypyrroline–1–oxyl ions and the water molecules is drawn. Linear chains, running along the a–axis, are formed via the O(3), O(4) and O(1) oxygen atoms. In *Figure 10(B)* two neighboring chains are drawn along with the respective benzamidinium ions. The chains are connected in the hydrogen–bonded clusters of the salt bridge and the water molecules. The result is a double helix that runs along the a–axis of the unit cell.

The overall structure of compound **3** can be described as double helices, positioned parallel to each other along the a–axis, that intersect the infinite ladders running along the b–axis of the unit cell. This two–dimensional character

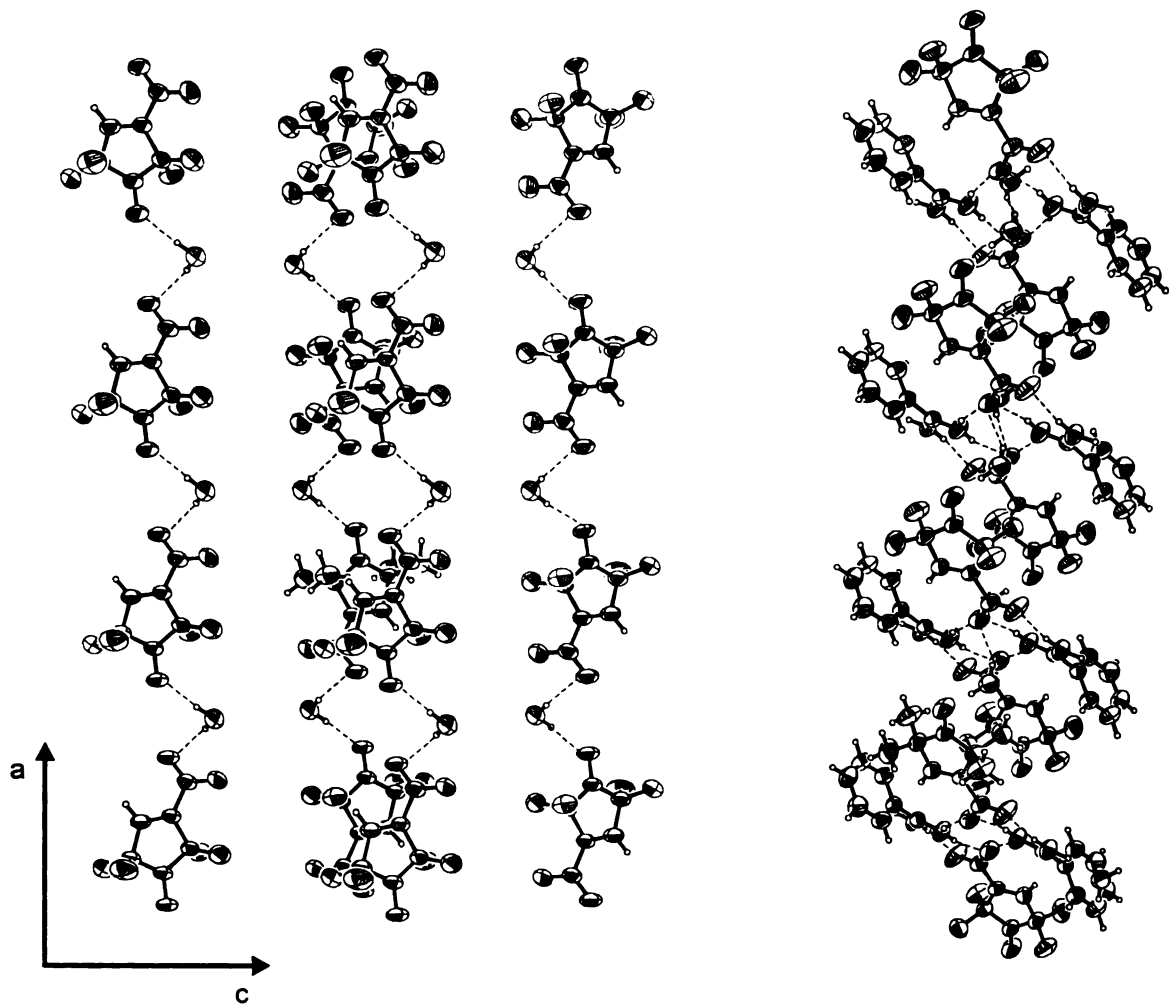

Figure 10. View (A) of the one–dimensional chains formed by the water hydrogen bonding to the carboxylate and the nitroxo group of the anion (the benzamidinium cations have been removed for clarity). Two neigboring chains are connected via the hydrogen bonding interaction of the salt bridge forming double helices that run along the a axis of the unit cell (B).

results from the interaction of this amidinium–carboxylate salt with the water of crystallization, which serves as a connecting piece for both the ladder and the helix parts of the structure.

4. Synthesis and Structure of *m*–cyanobenzamidinium–2,2,5,5–tetramethyl–3–carboxypyrroline–1–oxyl (4)

Cocrystallization of the 2,2,5,5–tetramethyl–3–carboxypyrroline–1–oxyl anion with the *m*–cyanobenzamidinium cation affords large yellow crystals of the title compound **4**. They were grown by the slow evaporation of an aqueous solution containning equimolar amounts of the two reactants. An X–ray structure determination revealed that no solvent crystallizes along with the two ions (Table 2). The structural features of the molecular components of the salt are very similar to the respective ones observed in compound **3**. Hence, the average carbon to oxygen and carbon to nitrogen bond distances are 1.255(3) Å and 1.312(4) Å respectively, and the length of the nitroxyl group bond is 1.273(3) Å. The biggest difference concerns the rotation of the CN_2 plane of the amidinium group with respect to the plane of the phenyl ring, which is 34.7(3)°, a value that is almost 17° smaller than the respective value of compound **3** and 5° larger from the one of compound **1**. The counter–rotation of the carboxylate group is 20.8(3)°.

Although the molecular units do not differ a lot, compound **4** adopts a totally different extended structure. The self–organization of the amidinium–carboxylate salt bridge via the two–point hydrogen bond is again the primary interaction. In this particular case a highly unsymmetrical salt bridge is assembled with one bond being 0.173 Å longer than the other, since the nitrogen to oxygen distances are 2.853(3) Å and 2.680(3) Å. As shown in *Figure 11* the

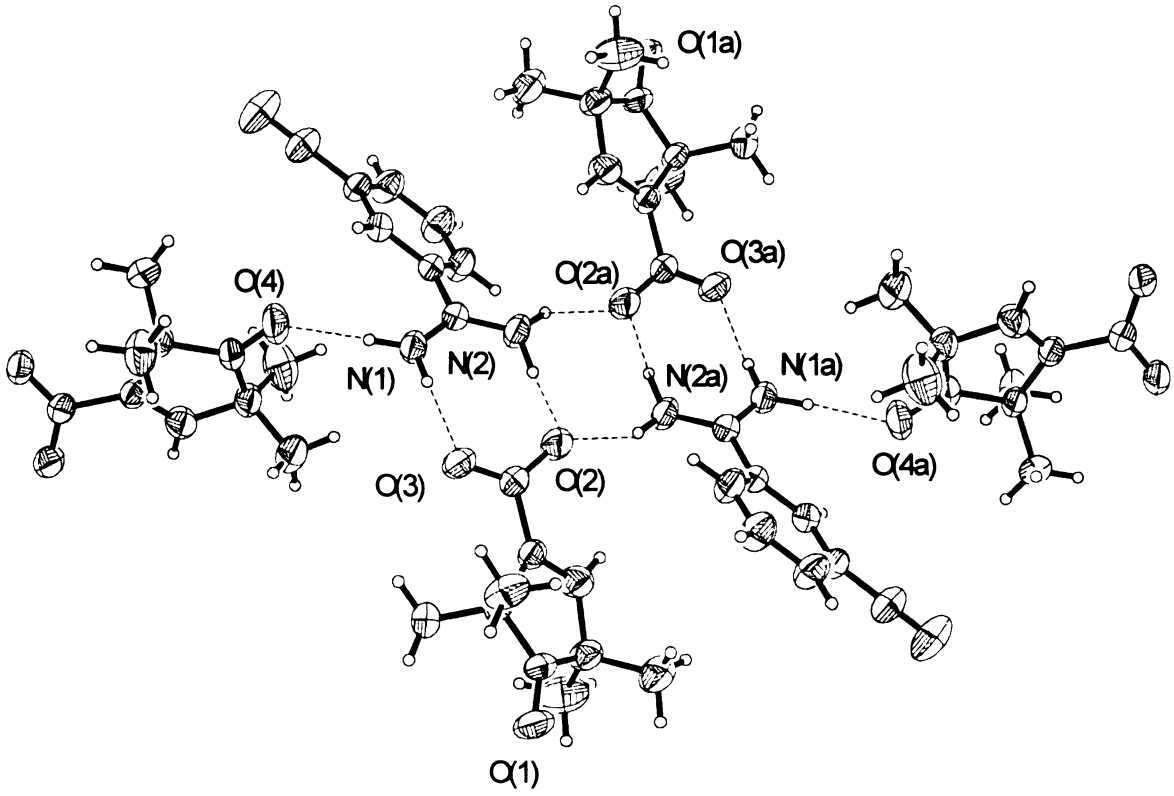

Figure 11. Structural building block of compound 4 built up by a molecular cluster of two anions and two cations held by the salt bridge interaction. The external amidinium protons of the cluster, hydrogen bond to the nitroxo oxygen atoms of anions belonging to different clusters.

external amidinium protons are able to participate in hydrogen bonding preventing the termination of the structure's dimensionality. A four molecule cluster, similar to the one observed in compound **3**, is formed via the bonding of N(2) to O(2) at a distance of 2.789(4) Å. The other external amidinium hydrogen of the N(1) atom binds to the nitroxyl oxygen O(1) of the anion with a nitrogen to oxygen distance of 2.851(3) Å. This position was occupied by the water molecule in the extended structure of compound **3** as it is revealed by a comparison of *Figure 9(A)* and *Figure 11* where the prime building blocks of the two structures are drawn. Apart from this noticeable similarity, the two salts self–assemble around these prime building blocks according to the different hydrogen bonding capabilities of their external to the cluster units. The extended structure of **4** is a repetition of the prime building block depicted in *Figure 11*. A two–dimensional network along the bc plane of the unit cell, shown in *Figure 12*, is formed where adjacent clusters are positioned vertically to each other and they are interconnected via the O(1) to N(1) hydrogen bond. The empty space of the layer is filled up by the aromatic units of the cation which are positioned in a face on arrangement. The cyano group is not involved in any type of hydrogen bonding and adjacent layers simply stack on the top of each other.

5. Magnetic Properties of Compounds 2, 3, and 4

The magnetic properties of the compounds containing the nitroxyl–moiety have been studied by electron spin resonance and magnetic susceptibility methods (experimental conditions are described in Chapter 2). The solution EPR spectrum of compound **4** shown in *Figure 13(A)* displays the typical three-line pattern, with the splitting arising from the ^{14}N hyperfine coupling to the free electron. The Landé g-factor is 2.010 and the value of the nitrogen isotropic

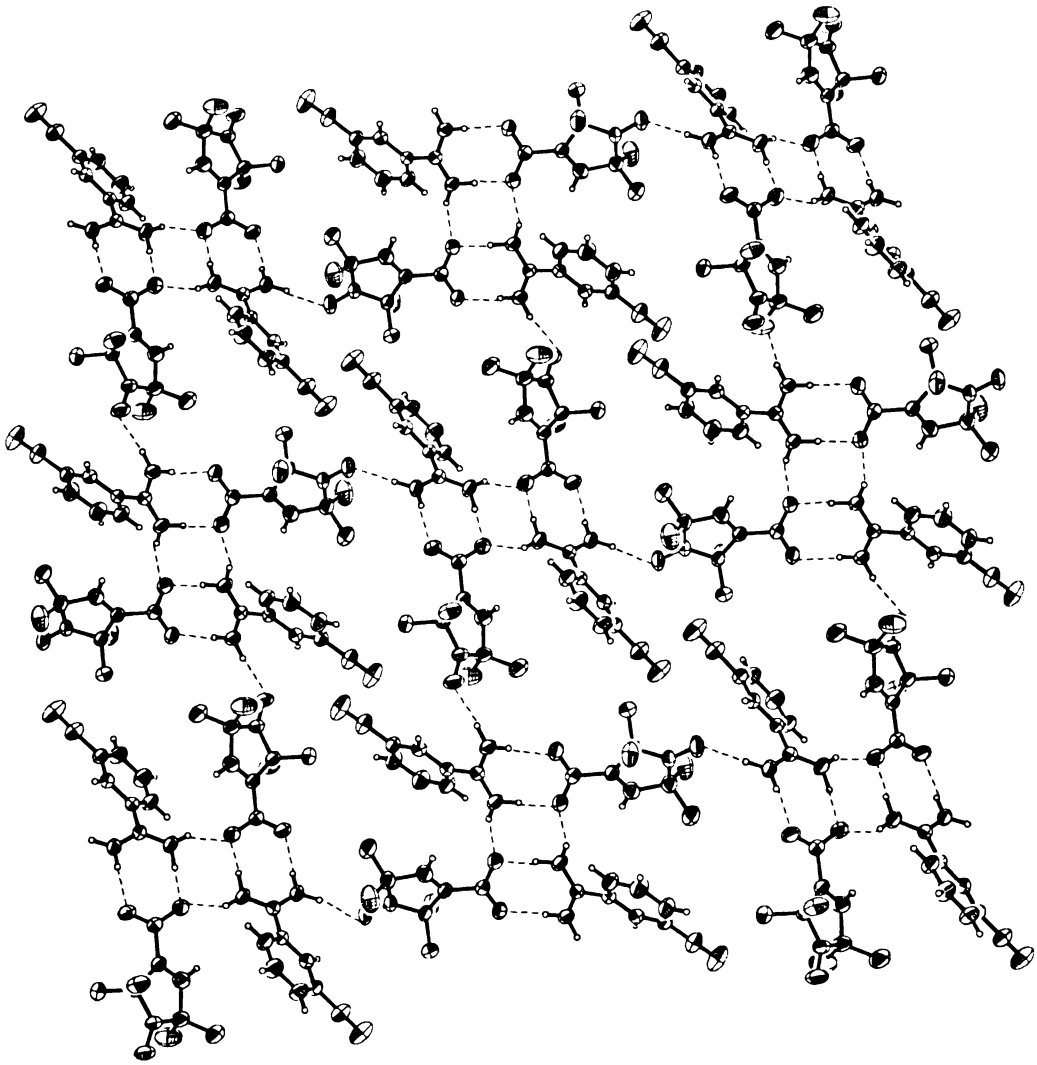

Figure 12. Two–dimensional sheets of compound 4 assembled by nitroxyl radicals interconnecting adjacent cluster subunits. The nitroxyl spin carriers compose a linera chain, diagonally situated within the layer.

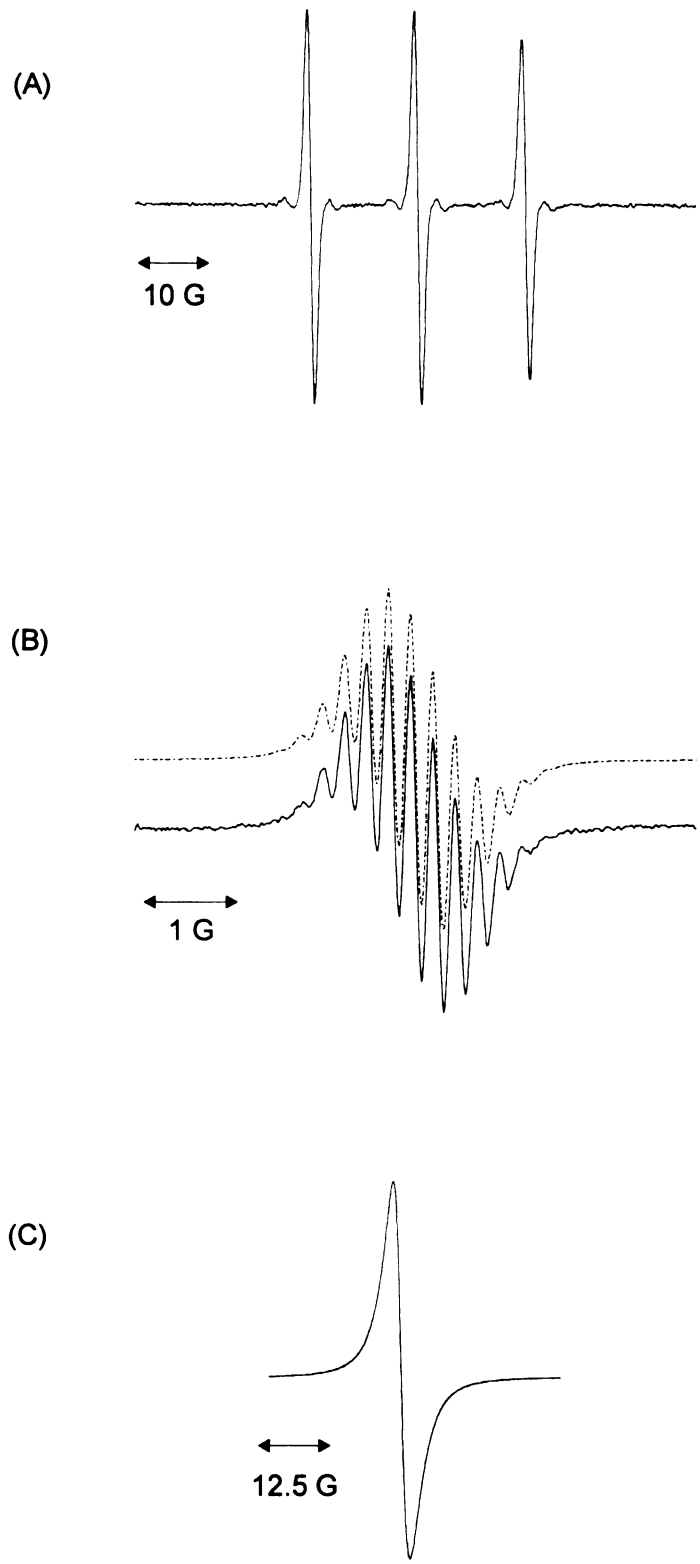

Figure 13. Room temperature EPR spectra of compound 4 (A) in deuterated methanol (B) its $m_N = 0$ line showing shf structure and (C) for a solid sample.

hyperfine coupling, obtained directly from the experimental spectrum, is 15.3 G, typical of the nitroxyl radical in solution[36,37]. As has been noted previously[38], oxygen–free solutions of nitroxyl compounds provide additional details regarding proton superhyperfine (shf) coupling. *Figure 13(B)* displays the central nitrogen hyperfine line of compound **4**, where good resolution of the proton hyperfine is observed. Computer simulation of the spectrum yields values of 0.235 G and 0.465 G for the coupling to the methyl and vinylic protons respectively, in agreement with literature results[36]. These values establish that delocalization of the unpaired electron is not limited to the nitroxyl moiety, but extends to the ring backbone of the radical.

Powder EPR experiments afforded featureless, relatively broad gaussian–shaped line profiles (*Figure 13(C)*). The lack of hyperfine splitting in the powder samples yields no information regarding exchange interactions, which were, however, studied via magnetic susceptibility measurements. The product of molar susceptibility and temperature is plotted versus temperature in *Figure 14*. Compound **3** affords a straight line with a X_MT value of 0.377 in the whole temperature range studied (2 to 300 K) indicating the purely paramagnetic behavior of the material. At high temperatures the X_MT product of compound **2** is also linear but it starts deviating from linearity below 40 K reaching a value of 0.166 at 2K. This behavior is indicative of weak antiferromagnetic exchange and the molar susceptibility was fitted by using the Heisenberg linear chain theory with a mean field approximation[39]. For an infinite linear chain, the general Heisenberg–Dirac–Van Vleck (HDVV) Hamiltonian[40] may be written as

$$H = -2J_{ij}\sum\{\alpha S_i^x S_j^x + \beta S_i^y S_j^y + \gamma S_i^z S_j^z\} \qquad (6.1)$$

where the subscripts i and j correspond to the two different interacting spins and

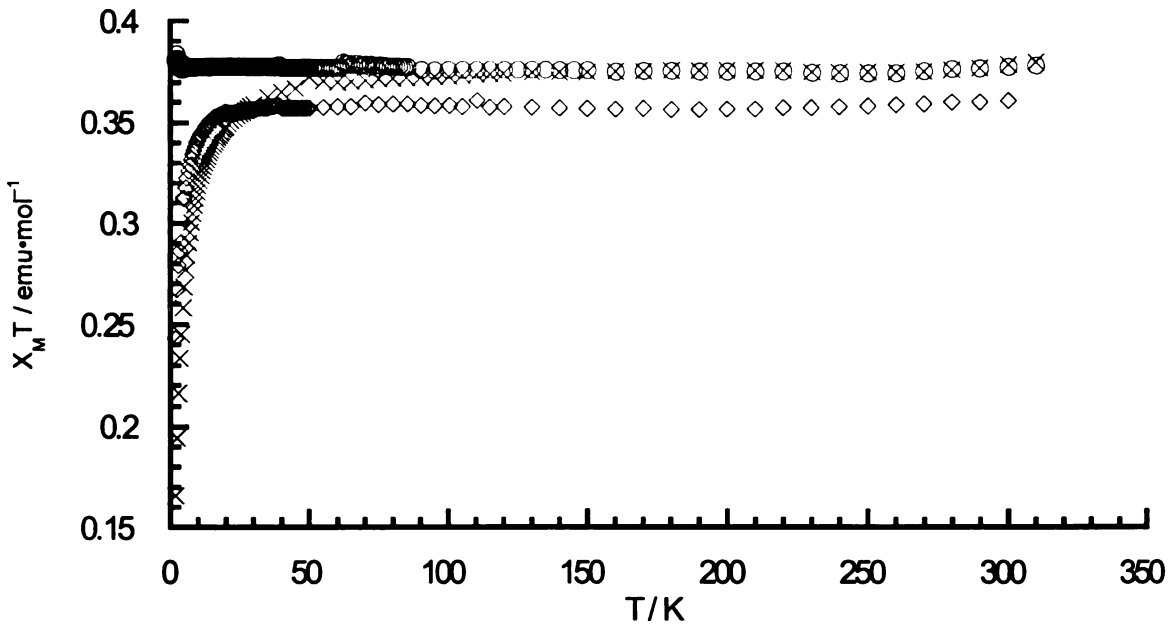

Figure 14. Magnetic susceptibility data for compounds **2** (×), **3** (o), and **4** (◊), expressed in the form of XT versus T plot.

J_{ij} is the exchange coupling constant. For $\alpha = \beta = \gamma$, the isotropic Heisenberg case arises, while anisotropy is taken into account when $\alpha = \beta = 0$, $\gamma = 1$ (Ising model), and when $\alpha = \beta = 1$, $\gamma = 0$ (XY model). For antiferromagnetically exchange–coupled spin 1/2 isotropic chain compounds an approximate solution was attained by Bonner and Fisher[41]. Hall[42] fit their numerical results to the above expression

$$\chi = \frac{Ng^2\mu_\beta^2}{k_B T} \times \frac{0.25 + 0.14995X + 0.30094X^2}{1 + 1.9862X + 0.68854X^2 + 6.0626X^3} \qquad (6.2)$$

where $X = |J_{ij}|/K_B T$. Interchain interaction is accounted as a correction to the linear chain model by a term arising from mean field theory and is expressed as[39]

$$\chi_m = \frac{\chi_H}{(1 - 2zJ'\chi_H / Ng^2 m_\beta^2)} \qquad (6.3)$$

where χ_H is the magnetic susceptibility of an isolated linear chain of S = 1/2 ions, z is the number of near neighbors in adjacent chains, and J' is the interchain exchange parameter. Analysis of the data of compound **2** using the Landé g–factor determined from EPR, gave $J_{ij}/k_B = -1.2\,\mathrm{K}$ and $zJ'/k_B = -0.9\,\mathrm{K}$.

The radical centers in compound **4** are also antiferromagnetically coupled, as judged by the deviation of the $X_M T$ product from the value of 0.360 at high temperatures to the value of 0.243 at 2K. The data were analyzed by using a one–dimensional Heisenberg model. The experimental data produce a satisfactory fit by using the experimentally determined Landé g–factor and a $J_{ij}/k_B = -0.8$ K.

C. Discussion

The amidinium–carboxylate salt bridge has been used successfully for the organization of molecular units into solids of higher dimensionality. The spontaneous self–assembly process even from solvents of enhanced polarity, is driven by the strength of the salt bridge interaction which is a combination of an electrostatic attraction and a two–point hydrogen bond between the internal amidinium protons and the carboxylate oxygens. Furthermore, favorable secondary electrostatic interactions (SEI) strengthen the primary forces[29], as illustrated in Scheme 4.

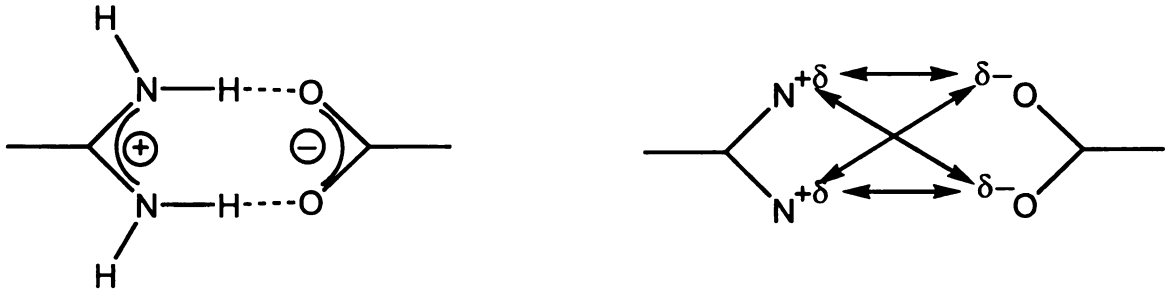

Scheme 4

The primary two–point hydrogen bond of the amidinium–carboxylate salt bridge is similar to the interaction established among carboxylic acid moieties (synthon **1** in *Figure 4*). For example the one–dimensional zig–zag tapes of compound **1** assembled by this primary interaction are also seen in the crystal of isophthalic acid[43]. However the overall structure of the latter remains one–dimensional due to the inability of the carboxylic group interfaces to further interconnect with each other. On the other hand the dimensionality of **1** is extended beyond the tapes by interconnecting them into infinite ladders. These one–dimensional ladders are a common feature of amidinium–carboxylate

bridges[35] and are assembled by hydrogen–bonding among the two external amidinium protons and carboxylate oxygens from above and below the plane of the salt bridge. This secondary interaction is further strengthened by electrostatic attractions, since the dipoles of adjacent salt bridges are arranged in a head to tail fashion along the ladders.

When other functional groups capable of hydrogen–bonding are present in the molecules, the formation of the salt bridge ladders is prevented. This is the case in compounds **3** and **4** where although the primary interaction of the amidinium–carboxylate bridge is still operative, the presence of the nitroxyl moiety sets a different mode for their interconnection. Additional insights of the role of the nitroxyl group as a synthon have been gained by the study of the structure of **2**, which along with recent literature examples[26], establishes its potential not only to act as a radical center but also as a structural building block. The configuration of the nitrogen atom in all three compounds is planar, as judged by the small deviation of the oxygen atom from the CNC plane which are in the order of 0.01(1) Å, 0.06(1) Å and 0.05(1) Å for **2**, **3** and **4** respectively. In addition the nitroxyl group is able to adjust its polarity according to the environment.

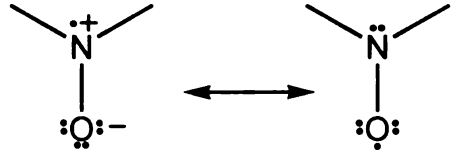

Scheme 5

As shown in Scheme 5, two resonance structures are possible: a zwitterionic one that places the radical center on the nitrogen atom and a neutral

one where the unpaired electron density resides on the oxygen atom. In polar environments the former is favored, as shown by EPR experiments. Spin densities of 0.60 and 0.55 are assigned on the nitrogen atom of the sodium salt[36(c)] and the amide[44] of compound **2** in ethanol and methanol respectively. The above effect increases the electronegative character of the nitroxyl oxygen atom enhancing its ability to perform as an acceptor of hydrogen–bonding. Therefore it is not surprising that the nitroxyl group is involved in the primary interaction in the structure of **2** by preventing the formation of the usual two–point hydrogen bond between acid moieties. In contrast the driving force for the assembly of the amidinium– carboxylate salt bridge is large enough that its formation is not hindered by the nitroxyl group in the structures of **3** and **4**. The assembly of ladders however, is hampered and new types of interactions are observed. Both structures share as a common building block a four molecule cluster shown in *Figures 9(A)* and *11*. The same type of cluster, which consists of two salt bridges assembled via the two–point hydrogen bond and joined together by a one–point hydrogen bond between an external amidinium proton and a carboxylate oxygen from each salt bridge, evolves to the ladders of compound **1** by direct cluster interconnection. In **3** and **4** interconnection of the salt bridges is not direct and is achieved via a water molecule and the nitroxyl radical anion respectively resulting in the formation of different two–dimensional patterns.

The structural organization of compounds **2**, **3**, and **4** is reflected in their magnetic properties, which, although they originate from the same radical center, differ remarkably. The antifferomagnetic behavior of **2** was analyzed by considering exchange interactions along head (nitroxide) to tail (carboxylate) linear chain arrangements of the radicals interconnected by N — O·····H — O hydrogen bonds (*Figure 8*). Although the radical centers are mainly localized on the nitroxyl moiety, small but appreciable amounts of spin density can be

transferred by the spin polarization mechanism[45] to remote atoms either intramolecularly via covalent bonding or intermolecularly via hydrogen–bonding. Direct evaluation of the intramolecularly induced spin density is accomplished by EPR and mainly ENDOR techniques by measuring the isotropic hyperfine coupling of a given magnetic nucleus in frozen or fluid solutions. Such a measurement of the A_{iso} of the carboxylic proton in compound **2** has not been reported, but a finite amount of spin density is probably transferred intramolecularly via covalent bonding, by analogy to the N — H protons of the corresponding amide[46] (A_{iso} values were on the order of – 0.010 and – 0.083 MHz). Additional contributions are rendered by the direct hydrogen bonding of the carboxylic proton to a neighboring radical center, in accordance with recent literature examples[26,27] where spin communication advances through hydrogen bonded networks of similar type as the one observed in **2**.

Magnetic communication also propagates among adjacent chains, which are joined by a weaker interaction involving the vinylic hydrogen atom and the carboxylate oxygen. The lack of the latter interaction in the saturated analogue of **2**, confines its dimensionality to linear chains[34]. Apart from their significance as a structural element (*Figure 4*), hydrogen bonds involving the vinylic proton apparently represent efficient exchange pathways for spin communication. ENDOR studies on radical **2**[36(a)] and its amide analogue[46] indicate the presence of substantial spin density on this proton as judged by the values of A_{iso} which are – 1.52 and – 1.81 MHz. The former value correspond to a fractional π–spin density of 0.026, localized on the $2p_z$ orbital of the vinylic carbon, but it is likely that the spin transfer in this unconjugated system is more complex, involving σ bond spin polarization.

The spin communication is turned off in the amidinium–carboxylate salt **3**. However examination of the possible exchange pathways in this composite two–

dimensional crystal facilitates magnetostructural analysis of the other two compounds. There are two pathways interconnecting adjacent radical centers. The first one, drawn in *Figure 10(A)*, resembles the head to tail linear chains of the parent nitroxide **2**. The absence of the carboxylic proton prevents direct hydrogen–bonding of adjacent radical molecules, which is now accomplished with the aid of water molecules alternatively placed among them. This indirect bonding increases the distance between neighboring radicals, in comparison to the parent compound **2**, and as a result turns off their magnetic communication. The radical centers are also connected by interactions involving the amidinium–carboxylate salt bridge itself, which assembles the molecular cluster depicted in *Figure 9(A)*. However spin communication here is not effective since this arrangement places the radical centers 14 bonds away from each other, with two of them being hydrogen bonds.

The antiferromagnetic coupling observed in the amidinium–carboxylate salt **4** is harder to understand due to the complexity of the intralayer network. Examination of *Figures 11* and *12* reveals four possible pathways for spin communication, all of which involve the salt bridge. Taking the nitroxyl oxygen as the seat of unpaired spin, and tracing paths in the six–subunit fragment shown in *Figure 11*, we designate O(1)·····O(4), O(1)·····O(4A), O(4)·····O(4A), and O(1)·····O(1A) as paths 1 – 4, respectively. The first, and shortest, is the one we believe to be magnetically significant (see below); it is a 9–bond path in which nitroxyl radicals internal and external to the four molecule ladder cluster are coupled via N — O(4)···H — N(1) — H···O(3) — C hydrogen bonding. Paths 2, 3 and 4 involve 11, 12 and 14 bonds, respectively; path 3, propagating along and across the ladder cluster, includes four hydrogen bonds rather than the two found in each of the other three paths. It is unlikely that the transfer of spin through paths 2 – 4 could effectively compete with the shorter path 1. The differing

magnetic behavior of **4** and **3** favors the latter statement. It suggests that coupling between external and internal nitroxyl radicals is the important exchange pathway since it is the presence or absence of this interaction that distinguishes the structures. If intracluster coupling were dominant, then similar behavior for both compounds would be expected on the basis of the retention of path 4 in both structures. Moreover, these data support our initial inference that path 1 should dominate the magnetic coupling; the extra H_2O in **3** adds one H–bond and one O–H covalent bond to path 1, making it an 11-bond pathway that includes three H–bonds. Noting that path 2 is an 11-bond linkage incorporating two hydrogen bonds, and that path 3 has 14 bonds with four hydrogen bonds, it seems unlikely that these connections contribute to the coupling in **4**.

D. Conclusions

The results presented in this chapter revealed the structural diversity accessible by combining amidinium–carboxylate salt bridges with moieties of interest, such as nitroxyl. Juxtaposition of such localized spin centers in a predictable crystal framework expands the possibilities for the controlable construction of organic–based magnetic materials. The primary two–point hydrogen bond bolstered by the coulombic attraction between the negatively charged carboxylate by the positively charged amidinum, is the robust framework from which each individual structure radiates. More specifically our work has shown that

- the strong two–point hydrogen bonding interaction of the amidinium–carboxylate salt bridge was the essential primary building block of all structures studied

- the presence of the nitroxyl functional group did not influence this two–point hydrogen bonding interaction
- expansion of the structures' dimensionality was achieved via secondary one–point hydrogen bonds between the amidinium protons external to the salt bridge interface and the proper Lewis basic sites
- in all cases studied the assembly of a four–molecule cluster was observed
- interconnection of the clusters by themselves or via the nitroxyl functional group afforded the extended solids
- weak magnetic exchange was the result of the direct interaction between the external to the salt bridge amidinium protons with the nitroxyl spin centers
- increasing the length of the exchange pathway by involvement of crystallization water in the bonding turned off the magnetic interaction

The studies presented in this chapter, although associated with negligible magnetic interactions, are of the first examples where crystal engineering is used to dictate the ways that spin centers interact with each other. Synthesis of related solids where both the carboxylate and the amidinium components of the salt bridge bear a nitroxyl radical or radical analogs of 3–amidiniumbenzoate could provide further information regarding the spin coupling via non–covalent bonding.

LIST OF REFERENCES

(1) (a) Lehn, J.–M. *Pure Appl. Chem.* **1978**, *50*, 871. (b) Lehn, J.–M. *Science* **1985**, *227*, 849. (c) Lehn, J.–M. *Angew. Chem. Int. Ed. Engl.* **1988**, *27*, 89.

(2) Desiraju, G. R. *Angew. Chem. Int. Ed. Engl.* **1995**, *34*, 2311.

(3) Philip, D.; Stoddart, J. F. *Angew. Chem. Int. Ed. Engl.* **1996**, *35*, 1154.

(4) Lehn, J.–M. *Angew. Chem. Int. Ed. Engl.* **1990**, *29*, 1304.

(5) (a) Kelly, T. R.; Zhao, C.; Bridger, G. J. *J. Am. Chem. Soc.* **1989**, *111*, 3744. (b) Kelly, T. R.; Bridger, G. J.; Zhao, C. *J. Am. Chem. Soc.* **1990**, *112*, 8024.

(6) (a) von Kiedrowski, G. *Angew. Chem. Int. Ed. Engl.* **1986**, *25*, 932. (b) von Kiedrowski, G.; Wlotzka, B.; Helbing, J. *Angew. Chem. Int. Ed. Engl.* **1989**, *28*, 1235. (c) von Kiedrowski, G.; Wlotzka, B.; Helbing, J.; Matzen, M.; Jordan, S. *Angew. Chem. Int. Ed. Engl.* **1991**, *30*, 423. (d) von Kiedrowski, G. *Bioorg. Chem. Front.* **1993**, *3*, 113. (e) Achilles, T.; von Kiedrowski, G. *Angew. Chem. Int. Ed. Engl.* **1993**, *32*, 1198. (f) Sievers, D.; von Kiedrowski, G. *Nature* **1994**, *369*, 221.

(7) (a) Zielinski, W. S.; Orgel, L. E. *Nature* **1987**, *327*, 346. (b) Wu, T.; Orgel, L. E. *J. Am. Chem. Soc.* **1992**, *114*, 317.

(8) (a) Rebek, J., Jr. *Angew. Chem. Int. Ed. Engl.* **1990**, *29*, 245. (b) Rebek, J., Jr. *Acc. Chem. Res.* **1990**, *23*, 399. (c) Tjivikua, T.; Ballester, P.; Rebek, J., Jr. *J. Am. Chem. Soc.* **1990**, *112*, 1249. (d) Nowick, J. S.; Feng, Q.; Tjivikua, T.; Ballester, P.; Rebek, J., Jr. *J. Am. Chem. Soc.* **1991**, *113*, 8831.

(9) Terfort, A.; von Kiedrowski, G. *Angew. Chem. Int. Ed. Engl.* **1992**, *31*, 654.

(10) Lawrence, D. S.; Jiang, T.; Levett, M. *Chem. Rev.* **1995**, *95*, 2229.

(11) (a) Vögtle, F.; *Supramolecular Chemistry*; Wiley: Chichesyer 1991. (b) Lehn, J.–M. *Macrocyclic Chemistry*; VCH: New York 1993. (c) Lehn, J.–M. *Supramolecular Chemistry*; VCH: Weinheim 1995. (d) Balzani, V.; Scandola, F. *Supramolecular Photochemistry*; Ellis Horwood: West Sussex 1991. (e) Cram, D. J. *Container Molecules and their Guests*; Royal Society of Chemistry: Cambridge 1994.

(12) (a) Roberts, J. A.; *Ph. D. Dissertation*, M. S. U. **1997**. (b) Roberts, J. A.;

Kirby, J. P.; Nocera, D. G. *J. Am. Chem. Soc.* **1995**, *117*, 8051. (c) Kirby, J. P.; Roberts, J. A.; Nocera, D. G. *J. Am. Chem. Soc.* In press.

(13) Aakeröy, C. B. *Acta Cryst.* **1997**, *B53*, 569.

(14) (a) Schmidt, G. M. J. *Pure Appl. Chem.* **1971**, *27*, 647. (b) Cohen, M. D.; Schmidt, G. M. J. *J. Chem. Soc.* **1996**, 1964.

(15) Desiraju, G. R. *Crystal Engineering: The Design of Organic Solids* **1989**, Amsterdam: Elsevier.

(16) (a) Whitesides, G. M.; Mathias, J. P.; Seto, C. T. *Science* **1991**, *254*, 1312. (b) MacDonald, J. C.; Whitesides, G. M. *Chem. Rev.* **1994**, *94*, 2383. (c) Etter, M. C. *J. Phys. Chem.* **1991**, *95*, 4601. (d) Etter, M. C. *Acc. Chem. Res.* **1990**, *23*, 120. (e) Russell, V. A.; Ward, M. D. *Chem. Mater.* **1996**, *8*, 1654. (f) Claessens, C. G.; Stoddart, J. F. *J. Phys. Org. Chem.* **1997**, *10*, 254.

(17) Allen, F. H.; Kennard, O.; Taylor, R. *Acc. Chem. Res.* **1983**, **16**, 146.

(18) (a) Reutzel, S. M.; Etter, M. C. *J. Phys. Org. Chem.* **1992**, *5*, 44. (b) Etter, M. C.; Britton, D.; Reutzel, S. M. *Acta Crystallogr.* **1991**, *C47*, 556. (c) Etter, M. C.; Reutzel, S. M. *J. Am. Chem. Soc.* **1991**, *113*, 2586.

(19) Reddy, D. S.; Ovchinnikov, Y. E.; Shishkin, O. V.; Struchkov, Y. T; Desiraju, G. R. *J. Am. Chem. Soc.* **1996**, *118*, 4085.

(20) Reddy, D. S.; Craig, D. C.; Desiraju, G. R. *J. Am. Chem. Soc.* **1996**, *118*, 4090.

(21) (a) Aakeröy, C. B.; Hitchcock, P. B.; Seddon, K. R. *J. Chem. Soc. Chem. Commun.* **1992**, 553. (b) Aakeröy, C. B.; Nieuwenhuyzen, M. *J. Am. Chem. Soc.* **1994**, *116*, 10983. (c) Aakeröy, C. B.; Nieuwenhuyzen, M. *J. Mol. Struct.* **1996**, *374*, 223.

(22) (a) Russell, V. A.; Etter, M. C.; Ward, M. D. *J. Am. Chem. Soc.* **1994**, *116*, 1941. (b) Russell, V. A.; Etter, M. C.; Ward, M. D. *Chem. Mater.* **1994**, *6*, 1206.

(23) Russell, V. A.; Evans, C. C.; Li, W.; Ward, M. D. *Science* **1997**, *276*, 575.

(24) (a) Puglisi, J. D.; Chen, L.; Frankel, A. D.; Williamson, J. R. *Proc. Natl. Acad. Sci. USA* **1993**, *90*, 3680. (b) Pavletich, N. P.; Pabo, C. O. *Science* **1991**, *252*, 809. (c) Berg, J. M. *Acc. Chem. Res.* **1995**, *28*, 14. (d) Howell, E. H.; Villafranca, J. E.; Warren, M. S.; Oatley, S. J.; Kraut, J. *Science* **1986**, *231*, 809. (e) Ramirez, E. B.; Malmström, G. B.; Winkler, R. J.; Gray, H. B. *Proc. Natl. Acad. Sci. USA* **1995**, *92*, 11949. (f) English, A. M.; Tsaprailis, G. *Adv. Inorg. Chem.* **1995**, *43*, 79. (g) Crane, B. R.; Lewis, M. S.; Getzoff, E. D. *Science* **1995**, *270*, 59. (h) Lippard, J. S.; Berg, M. J.

Principles of Bioinorganic Chemistry; University Science Books: Mill Valley, CA, 1994; p 141.

(25) Kirby, J. P. *Ph. D. Dissertation*, M. S. U. **1997**.

(26) (a) Lang, A.; Pei, Y.; Quahab, L.; Kahn, O. *Adv. Mater.* **1996**, *8*, 60. (b) Sugawara, T.; Matsushita, M. M.; Izuoka, A.; Wada, N.; Takeda, N.; Ishikawa, M. *J. Chem. Soc. Chem. Commun.* **1994**, 1723. (c) Tamura, M.; Nakazawa, Y.; Shiomi, D.; Nozawa, K.; Hosokoshi, Y.; Ishikawa, M.; Takahashi, M.; Kinoshita, M. *Chem. Phys. Lett.* **1991**, *186*, 401. (d) Nakazawa, Y.; Tamura, M.; Shirakawa, N.; Shiomi, D.; Takahashi, M.; Kinoshita, M.; Ishikawa, M.; *Phys. Rev.* **1992**, *B 46*, 8906.

(27) (a) Hernàndez, E.; Mas, M.; Molins, E.; Rovira, C.; Veciana, J. *Angew. Chem. Int. Ed. Engl.* **1993**, *32*, 882. (b) Cirujeda, J.; Ochando, L. E.; Amigó, J. M.; Rovira, C.; Rius, J.; Veciana, J. *Angew. Chem. Int. Ed. Engl.* **1995**, *34*, 55. (c) Cirujeda, J.; Mas, M.; Molins, E.; de Panthou, F. L.; Laugier, J.; Park, J. G.; Paulsen, C.; Rey, P.; Rovira, C.; Amigó, J. M.; Veciana, J *J. Chem. Soc. Chem. Commun.* **1995**, 709.

(28) Wagner, G.; Vieweg, H.; Kuehmstedt, H. *Pharmazie* **1973**, *28*, 288.

(29) (a) Pranata, J.; Wierschke, S. G.; Jorgensen, W. L. *J. Am. Chem. Soc.* **1991**, *113*, 2810. (b) Jorgensen, W. L.; Pranata, J. *J. Am. Chem. Soc.* **1990**, *112*, 2008.

(30) (a) Kirby, J. P.; Dantzig, N. A. van; Chang. C. K.; Nocera, D. G *Tetrahedron Lett.* **1995**, *36*, 3477.

(31) Rozantev, E. G.; Krinitzakaya, L. A. *Tetrahedron* **1965**, *21*, 491.

(32) Boeyens, J. C. A.; Kruger, G. J. *Acta. Cryst.* **1970**, *B 26*, 668.

(33) (a) Chion, P. B.; Lajzérowicz, J. *Acta. Cryst.* **1975**, *B 31*, 1430. (b) Turley, W.; Boer, F. P. *Acta. Cryst.* **1972**, *B 28*, 1641.

(34) Wetherington, J. B.; Ament, S. S.; Moncrief, J. W. *Acta. Cryst.* **1974**, *B 30*, 568.

(35) (a) Kratochvíl, B.; Ondrácek, J.; Malý, K.; Csordás, L. *Collect. Czech. Chem. Commun.* **1988**, *53*, 294. (b) Kratochvíl, B.; Ondrácek, J.; Krechl, J.; Hasek, J. *Acta. Cryst.* **1987**, *C43*, 2182. (c) Papoutsakis, D.; Kirby, J. P.; Jackson, J. E.; Nocera, D. G. *Submitted for Publication*.

(36) (a) Mustafi, D.; Joela, H. *J. Phys. Chem.* **1995**, *99*, 11370. (b) Bullock, A. T.; Howard, C. B. *J. Chem. Soc. Faraday I* **1980**, *76*, 1296. (c) Ottaviani, M. F.; Martini, G.; Nuti, L. *Magn. Reson. Chem.* **1987**, *25*, 897.

(37) Griffith, O. H.; Dehlinger, P. J.; Van, S. P. *J. Membr. Biol.* **1974**, *15*, 159.

(38) a) C. A. Popp, J. S. Hyde, J. Magn. Reson. 1981, 43, 249; b) J. S. Hyde, W. K. Subczynski, J. Magn. Reson. 1984, 56, 125.

(39) Hatfield, W. E. *J. Appl. Phys.* **1981**, *52*, 1985.

(40) (a) Heisenberg, W. Z. *Physik.* **1926**, *38*, 411. (b) Dirac, P. A. M. *Proc. Roy. Soc.* **1926**, *112A*, 661.

(41) Bonner, J. C.; Fisher, M. E. *Phys. Rev.* **1964**, *A133*, 768.

(42) (a) Hall, J. W. *Ph. D. Dissertation* **1977**, University of North Carolina, Chapel Hill, NC. (b) Hatfield, W. E.; Trojan, K. L. *Research Frontiers in Magnetochemistry* **1993**, Word Scientific Publishing Co. Pte. Ltd.: Singapore, 1.

(43) Derissen, J. L. *Acta. Cryst.* **1974**, *B30*, 2764.

(44) Mustafi, D.; Sachleben, J. R.; Wells, J. B.; Makinen, M. W. *J. Am. Chem. Soc.* **1990**, *112*, 2558.

(45) Kollamr, C.; Kahn, O. *Acc. Chem. Res.* **1993**, *26*, 259.

(46) Mustafi, D.; Joela, H.; Makinen, M. W. *J. Magn. Reson.* **1991**, *91*, 497.

APPENDIX

Table 1. Atomic Coordinates ($\times 10^4$) and Equivalent Isotropic Thermal Parameters ($Å^2 \times 10^2$) for $Rb_{0.5}VOPO_4 \cdot 1.5H_2O$ (T = 293 K), (**3.1A**).

Atom	x	y	z	U_{eq}	Occupancy
Rb(1)	0	0	0	6.0(1)	0.39
Rb(2)	627(32)	–5586(27)	–28(19)	3.3(5)	0.07
V(1)	2899(2)	–2518(2)	5957(2)	0.9(1)	1.0
P(1)	2494(2)	2496(2)	5047(2)	1.0(1)	1.0
O(1)	3118(8)	4397(7)	6502(8)	2.0(1)	1.0
O(2)	2907(8)	535(7)	6465(7)	1.7(1)	1.0
O(3)	3892(7)	2410(7)	3562(7)	1.6(1)	1.0
O(4)	56(7)	2597(7)	3665(8)	1.9(1)	1.0
O(5)	2144(8)	–2508(8)	3508(7)	2.1(1)	1.0
O(6)	3967(10)	–2500(10)	9555(8)	3.2(1)	1.0
O(7)	–267(47)	–4996(53)	–20(40)	1.7(5)	0.42
O(8)	251(17)	–390(16)	42(16)	8.2(2.8)	0.10

Table 2. Anisotropic Thermal Parameters ($Å^2 \times 10^3$) for $Rb_{0.5}VOPO_4 \cdot 1.5H_2O$ (T = 293 K), (**3.1A**).

Atom	U_{11}	U_{22}	U_{33}	U_{23}	U_{13}	U_{12}
Rb(1)	87(2)	62(1)	22(1)	–2(1)	5(1)	51(1)
Rb(2)	56(13)	22(7)	18(6)	4(5)	7(5)	–6(7)
V(1)	8(1)	8(1)	12(1)	0(1)	3(1)	0(1)
P(1)	7(1)	7(1)	17(1)	0(1)	4(1)	0(1)
O(1)	20(2)	8(2)	31(3)	–7(2)	6(2)	–2(2)
O(2)	19(2)	11(2)	22(2)	2(2)	7(2)	–2(2)
O(3)	8(2)	21(2)	17(2)	–1(2)	2(2)	–2(2)
O(4)	8(2)	19(2)	26(2)	1(2)	3(2)	2(2)
O(5)	24(2)	23(2)	15(2)	–1(2)	4(2)	3(2)
O(6)	39(3)	40(3)	16(2)	2(2)	7(2)	9(2)

Table 3. Atomic Coordinates ($\times 10^4$) and Equivalent Isotropic Thermal Parameters ($Å^2 \times 10^2$) for $Rb_{0.5}VOPO_4 \cdot 1.5H_2O$ (T = 173 K), (**3.1B**).

Atom	x	y	z	U_{eq}	Occupancy
Rb(1)	0	0	10000	29(1)	0.802
Rb(2)	36(70)	449(50)	128(60)	62(12)	0.080
V(1)	2912(2)	-2529(1)	5975(2)	8(1)	1
P(1)	7508(2)	-2497(2)	4948(3)	10(1)	1
O(1)	2149(8)	-2526(7)	3502(7)	16(1)	1
O(2)	3943(10)	-2466(10)	9574(8)	30(1)	1
O(3)	2866(7)	522(7)	6472(7)	14(1)	1
O(4)	6131(7)	-2385(7)	6473(7)	13(1)	1
O(5)	-65(7)	-2659(8)	6351(8)	18(1)	1
O(6)	3185(8)	-5627(7)	6528(9)	18(1)	1
O(7)	0	-5000	10000	17(4)	0.82
O(8)	-47(70)	-9(60)	895(100)	2(8)	0.01

Table 4. Anisotropic Thermal Parameters ($Å^2 \times 10^3$) for $Rb_{0.5}VOPO_4 \cdot 1.5H_2O$ (T = 173 K), (**3.1B**).

Atom	U_{11}	U_{22}	U_{33}	U_{23}	U_{13}	U_{12}
Rb(1)	41(1)	24(1)	20(1)	-1(1)	5(1)	20(1)
Rb(2)	100(20)	25(14)	28(11)	26(8)	-23(9)	-1(10)
V(1)	6(1)	2(1)	16(1)	0(1)	4(1)	0(1)
P(1)	6(1)	2(1)	23(1)	1(1)	5(1)	0(1)
O(1)	17(2)	15(2)	16(2)	0(2)	5(2)	4(2)
O(2)	31(3)	40(3)	16(2)	-1(2)	4(2)	19(2)
O(3)	14(2)	2(2)	24(2)	4(2)	4(2)	-1(1)
O(4)	4(2)	15(2)	19(2)	1(2)	1(2)	0(1)
O(5)	4(2)	15(2)	31(3)	4(2)	0(2)	1(2)
O(6)	15(2)	2(2)	36(3)	-5(2)	9(2)	-1(2)
O(7)	34(8)	6(12)	0(7)	25(7)	-11(7)	-9(8)

Table 5. Atomic Coordinates (× 10^4) and Equivalent Isotropic Thermal Parameters (Å^2 × 10^2) for {bpyVO[μ–$(C_6H_5)_2PO_2]_{1.5}$}$_2${ClO_4}, (**4.1**).

Atom	x	y	z	U_{eq}	Occupancy
V(1)	3587(1)	1651(1)	3681(1)	23(1)	1
V(2)	4618(1)	4472(1)	3101(1)	22(1)	1
O(1)	2738(2)	1043(1)	4379(1)	30(1)	1
O(2)	5864(2)	4746(1)	2947(1)	32(1)	1
O(3)	4848(2)	2307(1)	2711(1)	27(1)	1
O(4)	4915(2)	3958(1)	2182(1)	27(1)	1
O(5)	4418(2)	1804(1)	4513(1)	26(1)	1
O(6)	4919(2)	3325(1)	4055(1)	29(1)	1
O(7)	2431(2)	2817(1)	3425(1)	27(1)	1
O(8)	2834(2)	4300(1)	3287(1)	26(1)	1
N(1)	3080(2)	1482(2)	2641(1)	29(1)	1
N(2)	4934(2)	566(1)	3476(1)	26(1)	1
N(3)	3761(2)	5169(1)	3960(1)	24(1)	1
N(4)	3766(2)	5714(1)	2283(1)	25(1)	1
P(1)	5067(1)	3129(1)	1980(1)	24(1)	1
P(2)	5198(1)	2352(1)	4575(1)	24(1)	1
P(3)	1982(1)	3700(1)	3556(1)	22(1)	1
C(1)	2070(3)	1935(2)	2297(2)	37(1)	1
C(2)	1729(3)	1750(2)	1679(2)	47(1)	1
C(3)	2437(4)	1082(3)	1401(2)	58(1)	1
C(4)	3491(3)	620(2)	1742(2)	50(1)	1
C(5)	3792(3)	834(2)	2364(2)	33(1)	1
C(6)	4885(3)	372(2)	2783(2)	31(1)	1
C(7)	5811(3)	-210(2)	2495(2)	41(1)	1
C(8)	6799(3)	-612(2)	2927(2)	44(1)	1
C(9)	6829(3)	-439(2)	3652(2)	40(1)	1
C(10)	5879(2)	155(2)	3903(2)	31(1)	1
C(11)	3815(2)	4851(2)	4805(2)	31(1)	1
C(12)	3183(3)	5320(2)	5341(2)	37(1)	1
C(13)	2484(3)	6146(2)	4987(2)	42(1)	1
C(14)	2414(3)	6480(2)	4118(2)	36(1)	1
C(15)	3062(2)	5979(2)	3613(2)	28(1)	1
C(16)	3036(2)	6272(2)	2678(2)	27(1)	1
C(17)	2310(3)	7046(2)	2226(2)	36(1)	1

Table 5 (con't)

C(18)	2332(3)	7251(2)	1357(2)	44(1)	1
C(19)	3099(3)	6693(2)	954(2)	39(1)	1
C(20)	3805(3)	5933(2)	1438(2)	30(1)	1
C(21)	6575(2)	2890(2)	1472(2)	29(1)	1
C(22)	7229(3)	3543(2)	1105(2)	40(1)	1
C(23)	8391(3)	3356(3)	702(2)	57(1)	1
C(24)	8895(3)	2530(3)	663(2)	62(1)	1
C(25)	8260(3)	1877(3)	1033(2)	58(1)	1
C(26)	7107(3)	2043(2)	1450(2)	43(1)	1
C(28)	4076(2)	3404(2)	1198(2)	29(1)	1
C(29)	4273(3)	2942(2)	635(2)	42(1)	1
C(30)	3439(3)	3116(3)	97(2)	56(1)	1
C(31)	2397(3)	3745(3)	129(2)	57(1)	1
C(32)	2184(3)	4206(2)	680(2)	50(1)	1
C(33)	3025(3)	4043(2)	1207(2)	39(1)	1
C(35)	5022(2)	2278(2)	5683(2)	28(1)	1
C(36)	3874(3)	2601(2)	6041(2)	37(1)	1
C(37)	3673(3)	2641(2)	6858(2)	47(1)	1
C(38)	4606(3)	2335(2)	7342(2)	48(1)	1
C(39)	5736(3)	2003(2)	7003(2)	45(1)	1
C(40)	5950(3)	1981(2)	6174(2)	36(1)	1
C(42)	6747(2)	1901(2)	4275(2)	28(1)	1
C(43)	7384(2)	2399(2)	3549(2)	33(1)	1
C(44)	8555(3)	2052(2)	3296(2)	45(1)	1
C(45)	9118(3)	1216(2)	3765(2)	52(1)	1
C(46)	8494(3)	708(2)	4486(2)	46(1)	1
C(47)	7306(3)	1046(2)	4741(2)	35(1)	1
C(49)	727(2)	4303(2)	2960(2)	24(1)	1
C(50)	-219(2)	3913(2)	3057(2)	34(1)	1
C(51)	-1206(3)	4400(2)	2636(2)	44(1)	1
C(52)	-1259(3)	5271(2)	2124(2)	44(1)	1
C(53)	-322(3)	5662(2)	2008(2)	40(1)	1
C(54)	670(2)	5176(2)	2429(2)	31(1)	1
C(56)	1396(2)	3499(2)	4671(2)	26(1)	1
C(57)	1108(2)	2696(2)	5198(2)	33(1)	1
C(58)	708(3)	2548(2)	6066(2)	41(1)	1
C(59)	594(3)	3205(2)	6400(2)	42(1)	1

Table 5 (con't)

C(60)	863(2)	4007(2)	5880(2)	37(1)	1
C(61)	1263(2)	4155(2)	5017(2)	30(1)	1
Cl(1)	1711(1)	1573(1)	-907(1)	74(1)	1
O(100)	979(4)	1109(3)	-168(2)	113(1)	1
O(101)	1817(4)	2318(2)	-765(3)	127(2)	1
O(102)	1196(4)	1840(2)	-1667(2)	113(1)	1
O(103)	2829(4)	1008(3)	-966(2)	156(2)	1

Table 6. Anisotropic Thermal Parameters ($Å^2 \times 10^3$) for {bpyVO[μ–$(C_6H_5)_2PO_2]_{1.5}$}$_2${ClO_4}, (**4.1**).

Atom	U_{11}	U_{22}	U_{33}	U_{23}	U_{13}	U_{12}
V(1)	23(1)	22(1)	24(1)	-8(1)	-4(1)	-4(1)
V(2)	20(1)	23(1)	23(1)	-8(1)	-4(1)	-4(1)
O(1)	33(1)	27(1)	31(1)	-9(1)	-3(1)	-8(1)
O(2)	24(1)	38(1)	35(1)	-13(1)	-5(1)	-7(1)
O(3)	29(1)	26(1)	24(1)	-7(1)	-2(1)	-6(1)
O(4)	32(1)	24(1)	23(1)	-9(1)	-1(1)	-5(1)
O(5)	26(1)	30(1)	25(1)	-11(1)	-5(1)	-5(1)
O(6)	31(1)	26(1)	27(1)	-6(1)	-7(1)	-3(1)
O(7)	25(1)	25(1)	31(1)	-10(1)	-7(1)	-1(1)
O(8)	21(1)	28(1)	29(1)	-11(1)	-4(1)	-5(1)
N(1)	32(1)	31(1)	29(1)	-12(1)	-6(1)	-10(1)
N(2)	31(1)	23(1)	24(1)	-8(1)	-3(1)	-4(1)
N(3)	24(1)	28(1)	24(1)	-11(1)	-3(1)	-7(1)
N(4)	25(1)	24(1)	26(1)	-9(1)	-1(1)	-7(1)
P(1)	24(1)	25(1)	22(1)	-9(1)	-2(1)	-3(1)
P(2)	23(1)	25(1)	22(1)	-6(1)	-6(1)	-3(1)
P(3)	19(1)	23(1)	23(1)	-8(1)	-4(1)	-2(1)
C(1)	34(2)	40(2)	38(2)	-11(1)	-13(1)	-7(1)
C(2)	49(2)	53(2)	48(2)	-16(2)	-23(2)	-14(2)
C(3)	79(3)	60(2)	49(2)	-21(2)	-31(2)	-19(2)
C(4)	71(2)	42(2)	47(2)	-23(2)	-20(2)	-8(2)
C(5)	45(2)	29(2)	28(2)	-11(1)	-6(1)	-11(1)
C(6)	43(2)	23(1)	30(2)	-10(1)	-4(1)	-8(1)
C(7)	57(2)	31(2)	32(2)	-16(1)	0(2)	-1(2)
C(8)	47(2)	31(2)	39(2)	-12(1)	6(2)	4(1)
C(9)	39(2)	33(2)	40(2)	-10(1)	-6(1)	4(1)
C(10)	32(2)	29(2)	29(2)	-9(1)	-5(1)	-3(1)
C(11)	29(1)	40(2)	29(2)	-13(1)	-5(1)	-13(1)
C(12)	36(2)	58(2)	27(2)	-21(2)	-2(1)	-15(2)
C(13)	42(2)	50(2)	44(2)	-33(2)	2(1)	-10(2)
C(14)	32(2)	38(2)	41(2)	-22(2)	-2(1)	-4(1)
C(15)	27(1)	29(2)	33(2)	-16(1)	-3(1)	-7(1)
C(16)	27(1)	24(1)	30(2)	-10(1)	-3(1)	-6(1)
C(17)	40(2)	25(2)	38(2)	-12(1)	-4(1)	0(1)

Table 6 (con't)

C(18)	49(2)	30(2)	41(2)	-4(1)	-14(2)	3(1)
C(19)	48(2)	33(2)	28(2)	-3(1)	-8(1)	-5(1)
C(20)	36(2)	28(2)	26(2)	-10(1)	-2(1)	-7(1)
C(21)	28(1)	36(2)	21(1)	-10(1)	-4(1)	-1(1)
C(22)	32(2)	49(2)	37(2)	-11(2)	-3(1)	-12(1)
C(23)	32(2)	88(3)	43(2)	-12(2)	2(2)	-19(2)
C(24)	27(2)	107(4)	39(2)	-26(2)	-1(2)	6(2)
C(25)	45(2)	68(3)	48(2)	-29(2)	-8(2)	23(2)
C(26)	42(2)	40(2)	40(2)	-16(2)	-5(1)	5(2)
C(28)	31(2)	31(2)	23(1)	-7(1)	-3(1)	-9(1)
C(29)	43(2)	54(2)	36(2)	-24(2)	-1(1)	-10(2)
C(30)	61(2)	83(3)	41(2)	-33(2)	-7(2)	-25(2)
C(31)	54(2)	78(3)	40(2)	-9(2)	-22(2)	-18(2)
C(32)	45(2)	51(2)	49(2)	-10(2)	-20(2)	-4(2)
C(33)	41(2)	39(2)	34(2)	-8(1)	-12(1)	-7(1)
C(35)	32(2)	29(2)	24(1)	-5(1)	-7(1)	-11(1)
C(36)	34(2)	44(2)	31(2)	-12(1)	-11(1)	-3(1)
C(37)	46(2)	56(2)	35(2)	-19(2)	-4(2)	-5(2)
C(38)	61(2)	58(2)	29(2)	-17(2)	-8(2)	-15(2)
C(39)	50(2)	55(2)	37(2)	-12(2)	-18(2)	-18(2)
C(40)	33(2)	42(2)	33(2)	-11(1)	-11(1)	-8(1)
C(42)	25(1)	30(2)	29(2)	-12(1)	-8(1)	-5(1)
C(43)	29(2)	34(2)	37(2)	-11(1)	-5(1)	-6(1)
C(44)	31(2)	47(2)	51(2)	-16(2)	5(1)	-11(2)
C(45)	25(2)	52(2)	72(2)	-22(2)	0(2)	-1(2)
C(46)	32(2)	33(2)	66(2)	-12(2)	-13(2)	2(1)
C(47)	30(2)	29(2)	43(2)	-10(1)	-7(1)	-4(1)
C(49)	22(1)	30(2)	21(1)	-12(1)	-1(1)	-3(1)
C(50)	26(1)	37(2)	36(2)	-10(1)	-6(1)	-7(1)
C(51)	25(2)	60(2)	46(2)	-16(2)	-9(1)	-9(2)
C(52)	32(2)	57(2)	38(2)	-16(2)	-18(1)	7(2)
C(53)	43(2)	34(2)	33(2)	-6(1)	-14(1)	5(1)
C(54)	32(2)	29(2)	30(2)	-9(1)	-6(1)	-4(1)
C(56)	19(1)	31(2)	24(1)	-8(1)	-5(1)	0(1)
C(57)	27(2)	32(2)	34(2)	-9(1)	-2(1)	-2(1)
C(58)	31(2)	41(2)	34(2)	0(1)	1(1)	-3(1)
C(59)	30(2)	57(2)	28(2)	-13(2)	-1(1)	3(2)

Table 6 (con't)

C(60)	29(2)	49(2)	32(2)	-20(2)	-4(1)	1(1)
C(61)	24(1)	35(2)	30(2)	-11(1)	-7(1)	-2(1)
Cl(1)	99(1)	67(1)	37(1)	-20(1)	-11(1)	18(1)
O(100)	126(3)	139(3)	54(2)	-20(2)	4(2)	-28(3)
O(101)	178(4)	82(3)	143(4)	-54(3)	-87(3)	15(3)
O(102)	178(4)	107(3)	55(2)	-17(2)	-50(2)	-18(3)
O(103)	168(4)	124(3)	83(3)	-27(2)	17(3)	74(3)

Table 7. Atomic Coordinates (× 10^4) and Equivalent Isotropic Thermal Parameters (Å^2 × 10^2) for {dmbpyVO[μ–$(C_6H_5)_2PO_2]_{1.5}$}$_2${ClO_4}•4CH_3OH, (**4.2**).

Atom	x	y	z	U_{eq}	Occupancy
V(1)	656(1)	6948(1)	4146(1)	19(1)	1
O(1)	661(1)	7133(1)	5084(1)	27(1)	1
N(1)	1425(1)	5778(1)	4497(1)	21(1)	1
C(1)	2418(2)	5786(2)	4898(1)	27(1)	1
C(2)	2872(2)	5007(2)	5049(2)	32(1)	1
C(3)	2292(2)	4163(2)	4794(2)	31(1)	1
C(3A)	2755(2)	3291(2)	4931(2)	50(1)	1
C(4)	1265(2)	4156(2)	4407(1)	27(1)	1
C(5)	848(2)	4966(1)	4260(1)	22(1)	1
C(6)	-243(2)	5004(1)	3844(1)	21(1)	1
C(7)	-943(2)	4238(2)	3587(1)	26(1)	1
C(8)	-1961(2)	4319(2)	3222(1)	29(1)	1
C(8A)	-2721(2)	3491(2)	2950(2)	45(1)	1
C(9)	-2230(2)	5190(2)	3118(2)	30(1)	1
C(10)	-1497(2)	5926(2)	3376(1)	28(1)	1
N(2)	-516(1)	5848(1)	3741(1)	22(1)	1
V(2)	738(1)	8553(1)	1707(1)	22(1)	1
O(2)	1544(1)	8703(1)	1292(1)	33(1)	1
N(3)	604(1)	9958(1)	1833(1)	24(1)	1
C(11)	1215(2)	10551(2)	2487(1)	30(1)	1
C(12)	1084(2)	11454(2)	2543(2)	34(1)	1
C(13)	276(2)	11770(2)	1911(2)	36(1)	1
C(13A)	88(3)	12748(2)	1945(2)	57(1)	1
C(14)	-362(2)	11152(2)	1238(2)	32(1)	1
C(15)	-178(2)	10256(1)	1210(1)	25(1)	1
C(16)	-814(2)	9561(1)	501(1)	25(1)	1
C(17)	-1659(2)	9745(2)	-182(2)	31(1)	1
C(18)	-2210(2)	9070(2)	-838(2)	36(1)	1
C(18A)	-3119(2)	9267(2)	-1590(2)	53(1)	1
C(19)	-1879(2)	8220(2)	-772(2)	37(1)	1
C(20)	-1038(2)	8075(2)	-69(1)	33(1)	1
N(4)	-505(1)	8727(1)	561(1)	26(1)	1
O(3)	726(1)	6557(1)	2959(1)	23(1)	1
P(1)	399(1)	6385(1)	2006(1)	20(1)	1

Table 7 (con't)

C(21)	1158(2)	5591(1)	1814(1)	23(1)	1
C(22)	1787(2)	5156(2)	2490(2)	33(1)	1
C(23)	2378(2)	4547(2)	2347(2)	41(1)	1
C(24)	2340(2)	4374(2)	1532(2)	40(1)	1
C(25)	1723(2)	4805(2)	857(2)	44(1)	1
C(26)	1131(2)	5416(2)	996(2)	35(1)	1
C(27)	-877(2)	5834(1)	1537(1)	24(1)	1
C(28)	-1662(2)	6357(2)	1246(2)	32(1)	1
C(29)	-2642(2)	5941(2)	921(2)	44(1)	1
C(30)	-2845(2)	5008(2)	881(2)	46(1)	1
C(31)	-2076(2)	4480(2)	1167(2)	40(1)	1
C(32)	-1093(2)	4895(2)	1498(1)	31(1)	1
O(4)	443(1)	7203(1)	1506(1)	26(1)	1
O(5)	-321(1)	7790(1)	3544(1)	24(1)	1
P(2)	-702(1)	8497(1)	2915(1)	21(1)	1
C(33)	-279(2)	9605(1)	3503(1)	24(1)	1
C(34)	614(2)	9740(2)	4228(1)	29(1)	1
C(35)	956(2)	10594(2)	4678(2)	36(1)	1
C(36)	392(2)	11301(2)	4422(2)	38(1)	1
C(37)	-499(2)	11173(2)	3706(2)	40(1)	1
C(38)	-831(2)	10325(2)	3239(2)	34(1)	1
C(39)	-2053(2)	8345(1)	2528(2)	28(1)	1
C(40)	-2524(2)	8104(2)	3073(2)	35(1)	1
C(41)	-3558(2)	7965(2)	2767(2)	52(1)	1
C(42)	-4123(2)	8085(2)	1922(3)	66(1)	1
C(43)	-3667(2)	8340(2)	1374(2)	66(1)	1
C(44)	-2631(2)	8466(2)	1673(2)	44(1)	1
O(6)	-454(1)	8470(1)	2137(1)	25(1)	1
O(7)	1885(1)	7803(1)	4321(1)	25(1)	1
P(3)	2361(1)	8290(1)	3781(1)	23(1)	1
C(45)	3112(2)	9296(1)	4437(2)	28(1)	1
C(46)	3538(2)	9958(2)	4075(2)	36(1)	1
C(47)	4071(2)	10758(2)	4562(2)	45(1)	1
C(48)	4188(2)	10897(2)	5403(2)	50(1)	1
C(49)	3787(2)	10239(2)	5769(2)	53(1)	1
C(50)	3250(2)	9439(2)	5286(2)	39(1)	1
C(51)	3202(2)	7593(1)	3592(2)	28(1)	1

Table 7 (con't)

C(52)	3890(2)	7222(2)	4292(2)	33(1)	1
C(53)	4503(2)	6631(2)	4163(2)	44(1)	1
C(54)	4451(2)	6426(2)	3346(2)	50(1)	1
C(55)	3797(2)	6813(2)	2654(2)	49(1)	1
C(56)	3166(2)	7396(2)	2776(2)	37(1)	1
O(8)	1666(1)	8590(1)	2939(1)	28(1)	1
Cl(1)	5434(1)	7016(1)	6863(1)	48(1)	1
O(1C)	5635(2)	6892(2)	7745(2)	78(1)	1
O(2C)	6346(2)	7337(2)	6804(2)	78(1)	1
O(3C)	4749(2)	7674(2)	6583(2)	79(1)	1
O(4C)	5013(3)	6199(2)	6367(2)	113(1)	1
O(1S)	7500(3)	2148(2)	446(2)	110(1)	1
C(1S)	7255(4)	2471(4)	-381(3)	110(2)	1
O(2S)	5306(2)	5030(2)	2170(2)	91(1)	1
C(2S)	4770(3)	5245(3)	1344(3)	80(1)	1
O(3S)	5705(3)	1370(4)	2064(4)	167(2)	1
C(3S)	6556(6)	932(5)	2390(5)	153(3)	1
O(4SA)	5569(6)	2114(6)	655(4)	134(3)	0.616
C(4SA)	5135(6)	2929(5)	630(4)	85(2)	0.616
O(4SB)	5820(9)	1303(9)	303(7)	141(5)	0.384
C(4SB)	5743(16)	314(11)	-2(11)	176(9)	0.384

Table 8. Anisotropic Thermal Parameters ($Å^2 \times 10^3$) for {dmbpyVO[μ–$(C_6H_5)_2PO_2]_{1.5}\}_2\{ClO_4\}\cdot 4CH_3OH$, (**4.2**).

Atom	U_{11}	U_{22}	U_{33}	U_{23}	U_{13}	U_{12}
V(1)	23(1)	16(1)	19(1)	2(1)	9(1)	1(1)
O(1)	38(1)	22(1)	24(1)	3(1)	15(1)	6(1)
N(1)	23(1)	20(1)	20(1)	3(1)	9(1)	1(1)
C(1)	24(1)	27(1)	28(1)	3(1)	10(1)	-1(1)
C(2)	23(1)	34(1)	35(1)	7(1)	9(1)	4(1)
C(3)	30(1)	28(1)	35(1)	9(1)	13(1)	7(1)
C(3A)	34(1)	32(1)	77(2)	15(1)	14(1)	11(1)
C(4)	28(1)	22(1)	31(1)	5(1)	10(1)	2(1)
C(5)	24(1)	21(1)	19(1)	4(1)	9(1)	2(1)
C(6)	26(1)	22(1)	18(1)	5(1)	10(1)	3(1)
C(7)	29(1)	22(1)	26(1)	6(1)	9(1)	1(1)
C(8)	28(1)	30(1)	28(1)	5(1)	10(1)	-3(1)
C(8A)	34(1)	38(1)	54(2)	4(1)	10(1)	-9(1)
C(9)	21(1)	35(1)	34(1)	6(1)	10(1)	2(1)
C(10)	26(1)	28(1)	31(1)	6(1)	12(1)	7(1)
N(2)	23(1)	22(1)	23(1)	3(1)	11(1)	2(1)
V(2)	29(1)	18(1)	23(1)	5(1)	12(1)	5(1)
O(2)	41(1)	28(1)	40(1)	11(1)	25(1)	9(1)
N(3)	30(1)	20(1)	25(1)	6(1)	12(1)	4(1)
C(11)	33(1)	26(1)	27(1)	3(1)	9(1)	3(1)
C(12)	40(1)	24(1)	35(1)	-2(1)	12(1)	1(1)
C(13)	42(1)	21(1)	44(1)	3(1)	17(1)	6(1)
C(13A)	65(2)	23(1)	70(2)	-3(1)	11(2)	11(1)
C(14)	34(1)	22(1)	37(1)	8(1)	9(1)	6(1)
C(15)	29(1)	22(1)	27(1)	6(1)	13(1)	2(1)
C(16)	31(1)	20(1)	25(1)	8(1)	13(1)	1(1)
C(17)	32(1)	25(1)	34(1)	11(1)	11(1)	1(1)
C(18)	34(1)	36(1)	32(1)	11(1)	7(1)	-5(1)
C(18A)	43(2)	47(2)	46(2)	11(1)	-5(1)	-5(1)
C(19)	45(1)	31(1)	28(1)	1(1)	10(1)	-6(1)
C(20)	46(1)	24(1)	28(1)	2(1)	15(1)	3(1)
N(4)	34(1)	22(1)	23(1)	4(1)	13(1)	4(1)
O(3)	28(1)	20(1)	21(1)	2(1)	12(1)	3(1)
P(1)	26(1)	16(1)	20(1)	2(1)	11(1)	4(1)

Table 8 (con't)

C(21)	25(1)	17(1)	29(1)	0(1)	14(1)	2(1)
C(22)	42(1)	31(1)	33(1)	8(1)	19(1)	14(1)
C(23)	44(2)	34(1)	52(2)	12(1)	22(1)	18(1)
C(24)	38(1)	29(1)	56(2)	-5(1)	24(1)	9(1)
C(25)	50(2)	49(2)	39(1)	-10(1)	24(1)	15(1)
C(26)	40(1)	40(1)	28(1)	1(1)	13(1)	13(1)
C(27)	29(1)	24(1)	19(1)	-1(1)	9(1)	3(1)
C(28)	32(1)	32(1)	31(1)	-1(1)	10(1)	8(1)
C(29)	30(1)	53(2)	44(2)	2(1)	9(1)	11(1)
C(30)	29(1)	61(2)	40(1)	-3(1)	10(1)	-7(1)
C(31)	44(2)	35(1)	39(1)	-1(1)	15(1)	-8(1)
C(32)	34(1)	26(1)	32(1)	4(1)	12(1)	3(1)
O(4)	39(1)	18(1)	24(1)	4(1)	16(1)	6(1)
O(5)	27(1)	20(1)	27(1)	4(1)	12(1)	5(1)
P(2)	23(1)	17(1)	22(1)	2(1)	10(1)	4(1)
C(33)	30(1)	19(1)	28(1)	-1(1)	16(1)	3(1)
C(34)	32(1)	26(1)	32(1)	-2(1)	14(1)	4(1)
C(35)	33(1)	33(1)	39(1)	-8(1)	15(1)	0(1)
C(36)	44(1)	24(1)	48(2)	-10(1)	24(1)	-2(1)
C(37)	48(2)	24(1)	51(2)	1(1)	21(1)	11(1)
C(38)	38(1)	24(1)	40(1)	0(1)	13(1)	7(1)
C(39)	26(1)	21(1)	35(1)	-2(1)	9(1)	6(1)
C(40)	30(1)	30(1)	46(1)	-4(1)	18(1)	3(1)
C(41)	35(2)	45(2)	80(2)	-7(2)	30(2)	0(1)
C(42)	25(1)	61(2)	98(3)	-3(2)	10(2)	5(1)
C(43)	39(2)	70(2)	63(2)	5(2)	-9(2)	13(2)
C(44)	36(1)	44(2)	40(1)	6(1)	3(1)	11(1)
O(6)	32(1)	22(1)	25(1)	2(1)	13(1)	5(1)
O(7)	24(1)	22(1)	25(1)	1(1)	8(1)	-2(1)
P(3)	23(1)	19(1)	25(1)	3(1)	9(1)	1(1)
C(45)	23(1)	21(1)	37(1)	3(1)	9(1)	1(1)
C(46)	29(1)	31(1)	43(1)	11(1)	10(1)	1(1)
C(47)	32(1)	25(1)	73(2)	12(1)	18(1)	-4(1)
C(48)	40(2)	30(1)	72(2)	-14(1)	21(1)	-9(1)
C(49)	57(2)	46(2)	54(2)	-20(1)	26(2)	-17(1)
C(50)	42(1)	33(1)	41(1)	-4(1)	21(1)	-10(1)
C(51)	23(1)	22(1)	39(1)	3(1)	14(1)	-1(1)

Table 8 (con't)

C(52)	25(1)	32(1)	42(1)	9(1)	13(1)	0(1)
C(53)	26(1)	41(2)	67(2)	17(1)	19(1)	8(1)
C(54)	36(1)	43(2)	80(2)	2(1)	30(2)	12(1)
C(55)	44(2)	56(2)	56(2)	-3(1)	28(1)	13(1)
C(56)	34(1)	41(1)	41(1)	5(1)	18(1)	8(1)
O(8)	31(1)	24(1)	28(1)	5(1)	9(1)	4(1)
Cl(1)	38(1)	49(1)	48(1)	12(1)	8(1)	4(1)
O(1C)	81(2)	90(2)	56(1)	32(1)	15(1)	15(1)
O(2C)	60(2)	71(2)	118(2)	22(2)	49(2)	14(1)
O(3C)	64(2)	103(2)	81(2)	47(2)	31(1)	45(2)
O(4C)	110(3)	74(2)	111(2)	-26(2)	5(2)	-12(2)
O(1S)	104(3)	94(2)	101(2)	13(2)	3(2)	30(2)
C(1S)	125(4)	129(4)	70(3)	-4(3)	23(3)	68(4)
O(2S)	59(2)	94(2)	108(2)	28(2)	20(2)	1(1)
C(2S)	64(2)	107(3)	71(2)	18(2)	28(2)	19(2)
O(3S)	102(3)	193(5)	210(5)	-91(4)	88(3)	-26(3)
C(3S)	181(7)	116(5)	177(7)	21(5)	77(6)	68(5)
O(4SA)	149(6)	150(7)	94(5)	24(4)	28(4)	57(5)
C(4SA)	99(5)	72(4)	65(4)	1(3)	9(4)	27(4)
O(4SB)	115(8)	140(10)	125(8)	27(7)	1(7)	11(7)
C(4SB)	260(20)	96(12)	124(13)	39(10)	29(15)	24(13)

Table 9. Atomic Coordinates (× 10^4) and Equivalent Isotropic Thermal Parameters (Å^2 × 10^2) for {tmbpyVO[μ–$(C_6H_5)_2PO_2]_{1.5}$}$_2${ClO_4}•3.5CH_3OH, (**4.3**).

Atom	x	y	z	U_{eq}	Occupancy
V(1)	8072(1)	8719(1)	5154(1)	14(1)	1
O(1)	7820(2)	9541(1)	5233(1)	21(1)	1
N(1)	9019(2)	9164(2)	4539(1)	17(1)	1
C(1)	8817(3)	9373(2)	4033(1)	22(1)	1
C(2)	9465(3)	9625(2)	3644(2)	28(1)	1
C(2A)	9190(3)	9828(3)	3084(2)	41(1)	1
C(3)	10356(3)	9676(2)	3797(2)	31(1)	1
C(3A)	11106(4)	9950(3)	3405(2)	54(2)	1
C(4)	10557(3)	9466(2)	4321(2)	27(1)	1
C(5)	9885(2)	9199(2)	4685(1)	18(1)	1
C(6)	10061(2)	8931(2)	5250(1)	19(1)	1
C(7)	10912(3)	8950(2)	5470(2)	25(1)	1
C(8)	11036(3)	8666(2)	6004(2)	25(1)	1
C(8A)	11958(3)	8683(3)	6240(2)	37(1)	1
C(9)	10287(3)	8354(2)	6308(2)	28(1)	1
C(9A)	10348(3)	8004(3)	6884(2)	39(1)	1
C(10)	9461(3)	8376(2)	6058(2)	26(1)	1
N(2)	9336(2)	8652(2)	5545(1)	20(1)	1
V(2)	6434(1)	6401(1)	5246(1)	16(1)	1
O(2)	6383(2)	5618(1)	5694(1)	26(1)	1
N(3)	5010(2)	6497(2)	5102(1)	19(1)	1
C(11)	4402(3)	6863(2)	5326(2)	24(1)	1
C(12)	3477(3)	6881(2)	5239(2)	28(1)	1
C(12A)	2850(3)	7332(3)	5498(2)	41(1)	1
C(13)	3159(3)	6454(3)	4908(2)	33(1)	1
C(13A)	2158(3)	6398(4)	4816(2)	59(2)	1
C(14)	3791(3)	6089(2)	4672(2)	29(1)	1
C(15)	4705(2)	6134(2)	4757(1)	20(1)	1
C(16)	5416(2)	5802(2)	4489(1)	18(1)	1
C(17)	5234(3)	5462(2)	4096(1)	25(1)	1
C(18)	5933(3)	5168(2)	3850(1)	26(1)	1
C(18A)	5724(4)	4793(3)	3432(2)	45(1)	1
C(19)	6822(3)	5239(2)	4003(2)	27(1)	1
C(19A)	7625(3)	4956(3)	3754(2)	44(1)	1

Table 9 (con't)

C(20)	6957(3)	5599(2)	4398(2)	24(1)	1
N(4)	6278(2)	5864(2)	4640(1)	20(1)	1
O(3)	8576(2)	7701(1)	5009(1)	20(1)	1
P(1)	8641(1)	6850(1)	5124(1)	16(1)	1
C(21)	9243(2)	6453(2)	5718(1)	20(1)	1
C(22)	8858(3)	5875(2)	6108(1)	24(1)	1
C(23)	9312(3)	5576(2)	6572(2)	33(1)	1
C(24)	10155(3)	5849(3)	6651(2)	39(1)	1
C(25)	10543(3)	6418(3)	6271(2)	36(1)	1
C(26)	10099(3)	6719(2)	5800(2)	27(1)	1
C(27)	9307(3)	6633(2)	4611(2)	26(1)	1
C(28)	9454(3)	5882(3)	4599(2)	36(1)	1
C(29)	9910(3)	5715(3)	4188(2)	52(1)	1
C(30)	10226(4)	6290(4)	3793(2)	67(2)	1
C(31)	10131(4)	7049(4)	3804(2)	69(2)	1
C(32)	9667(3)	7218(3)	4214(2)	46(1)	1
O(4)	7774(2)	6409(1)	5165(1)	23(1)	1
O(5)	7048(2)	8667(1)	4680(1)	21(1)	1
P(2)	6444(1)	8219(1)	4416(1)	15(1)	1
C(33)	5302(2)	8561(2)	4457(1)	20(1)	1
C(34)	5073(3)	8982(2)	4804(2)	31(1)	1
C(35)	4173(3)	9205(3)	4851(2)	43(1)	1
C(36)	3513(3)	9019(3)	4552(2)	47(1)	1
C(37)	3720(3)	8598(3)	4209(2)	44(1)	1
C(38)	4614(3)	8361(2)	4159(2)	31(1)	1
C(39)	6769(3)	8437(2)	3739(1)	22(1)	1
C(40)	6382(3)	9015(3)	3349(2)	44(1)	1
C(41)	6691(4)	9148(3)	2840(2)	59(2)	1
C(42)	7380(4)	8729(3)	2713(2)	52(1)	1
C(43)	7802(4)	8166(3)	3102(2)	50(1)	1
C(44)	7484(3)	8019(3)	3605(2)	39(1)	1
O(6)	6469(2)	7366(1)	4611(1)	19(1)	1
O(7)	7526(2)	8067(1)	5803(1)	19(1)	1
P(3)	6752(1)	7550(1)	6036(1)	15(1)	1
C(45)	5887(2)	8110(2)	6246(1)	18(1)	1
C(46)	5112(3)	7760(2)	6500(2)	31(1)	1
C(47)	4454(3)	8185(3)	6675(2)	40(1)	1

Table 9 (con't)

C(48)	4552(3)	8956(3)	6591(2)	43(1)	1
C(49)	5316(3)	9317(2)	6343(2)	38(1)	1
C(50)	5983(3)	8890(2)	6168(2)	26(1)	1
C(51)	7154(2)	6878(2)	6618(1)	20(1)	1
C(52)	6856(3)	6130(2)	6753(2)	28(1)	1
C(53)	7162(3)	5615(2)	7207(2)	36(1)	1
C(54)	7752(3)	5838(3)	7524(2)	39(1)	1
C(55)	8065(3)	6578(3)	7402(2)	38(1)	1
C(56)	7747(3)	7093(2)	6951(2)	30(1)	1
O(8)	6309(2)	7122(1)	5692(1)	22(1)	1
V(3)	6924(1)	6274(1)	9872(1)	17(1)	1
O(9)	7185(2)	5424(2)	9847(1)	28(1)	1
N(5)	5931(2)	5931(2)	10470(1)	21(1)	1
C(57)	6076(3)	5832(2)	10977(2)	29(1)	1
C(58)	5396(3)	5606(3)	11350(2)	44(1)	1
C(58A)	5618(4)	5544(4)	11917(2)	70(2)	1
C(59)	4541(3)	5448(3)	11189(2)	50(1)	1
C(59A)	3782(4)	5151(5)	11564(2)	81(2)	1
C(60)	4391(3)	5580(3)	10661(2)	39(1)	1
C(61)	5084(2)	5838(2)	10311(1)	22(1)	1
C(62)	4948(3)	6033(2)	9744(2)	24(1)	1
C(63)	4127(3)	5979(2)	9514(2)	28(1)	1
C(64)	4033(3)	6200(3)	8979(2)	38(1)	1
C(64A)	3132(3)	6154(3)	8732(2)	49(1)	1
C(65)	4798(3)	6489(4)	8684(2)	53(2)	1
C(65A)	4777(4)	6772(5)	8099(2)	92(3)	1
C(66)	5601(3)	6492(3)	8946(2)	50(1)	1
N(6)	5691(2)	6279(2)	9462(1)	29(1)	1
V(4)	8593(1)	8610(1)	9664(1)	20(1)	1
O(10)	8721(2)	9377(2)	9207(1)	30(1)	1
N(7)	8710(2)	9170(2)	10261(1)	26(1)	1
C(67)	8023(3)	9468(2)	10468(2)	35(1)	1
C(68)	8115(4)	9792(2)	10878(2)	44(1)	1
C(68A)	7291(5)	10104(3)	11095(2)	63(2)	1
C(69)	8987(4)	9808(3)	11080(2)	48(1)	1
C(69A)	9162(5)	10169(3)	11515(2)	69(2)	1
C(70)	9698(4)	9487(3)	10865(2)	45(1)	1

Table 9 (con't)

C(71)	9552(3)	9173(2)	10458(2)	31(1)	1
C(72)	10276(3)	8803(2)	10216(2)	31(1)	1
C(73)	11191(3)	8765(3)	10351(2)	50(1)	1
C(74)	11823(3)	8406(4)	10108(2)	59(2)	1
C(74A)	12790(4)	8375(5)	10259(3)	97(3)	1
C(75)	11518(3)	8066(3)	9729(2)	45(1)	1
C(75A)	12141(3)	7650(3)	9446(2)	64(2)	1
C(76)	10598(3)	8126(2)	9614(2)	34(1)	1
N(8)	9994(2)	8487(2)	9843(1)	26(1)	1
O(11)	7891(2)	6357(1)	10373(1)	22(1)	1
P(4)	8556(1)	6841(1)	10563(1)	16(1)	1
C(77)	8423(3)	6678(2)	11255(1)	25(1)	1
C(78)	8316(3)	5946(2)	11580(2)	35(1)	1
C(79)	8224(4)	5831(3)	12111(2)	51(1)	1
C(80)	8266(5)	6429(4)	12321(2)	75(2)	1
C(81)	8394(5)	7166(3)	12008(2)	74(2)	1
C(82)	8466(4)	7287(3)	11477(2)	50(1)	1
C(83)	9685(2)	6494(2)	10477(1)	21(1)	1
C(84)	9845(3)	6070(2)	10119(2)	30(1)	1
C(85)	10721(3)	5817(2)	10052(2)	40(1)	1
C(86)	11419(3)	5972(3)	10337(2)	47(1)	1
C(87)	11278(3)	6387(3)	10690(2)	44(1)	1
C(88)	10411(3)	6657(2)	10757(2)	30(1)	1
O(12)	8498(2)	7689(1)	10334(1)	20(1)	1
O(13)	7520(2)	6852(2)	9213(1)	26(1)	1
P(5)	8252(1)	7390(1)	8943(1)	20(1)	1
C(89)	7786(3)	8051(2)	8372(1)	25(1)	1
C(90)	7168(3)	7826(3)	8056(2)	37(1)	1
C(91)	6815(3)	8335(3)	7612(2)	45(1)	1
C(92)	7107(3)	9076(3)	7478(2)	43(1)	1
C(93)	7729(3)	9304(3)	7776(2)	40(1)	1
C(94)	8078(3)	8803(2)	8223(2)	37(1)	1
C(95)	9096(3)	6834(2)	8717(1)	22(1)	1
C(96)	9010(3)	6044(2)	8810(2)	31(1)	1
C(97)	9663(4)	5617(3)	8625(2)	44(1)	1
C(98)	10390(3)	5982(3)	8344(2)	45(1)	1
C(99)	10484(3)	6758(3)	8244(2)	41(1)	1

Table 9 (con't)

C(100)	9843(3)	7187(2)	8429(2)	32(1)	1
O(14)	8730(2)	7834(2)	9262(1)	26(1)	1
O(15)	6437(2)	7340(2)	9919(1)	27(1)	1
P(6)	6375(1)	8190(1)	9794(1)	23(1)	1
C(101)	5865(3)	8419(2)	10346(2)	32(1)	1
C(102)	5195(4)	8978(3)	10310(2)	55(1)	1
C(103)	4879(4)	9146(4)	10760(3)	71(2)	1
C(104)	5196(4)	8772(3)	11231(2)	65(2)	1
C(105)	5858(5)	8219(4)	11270(2)	74(2)	1
C(106)	6195(4)	8038(3)	10831(2)	59(2)	1
C(107)	5661(3)	8541(2)	9235(2)	27(1)	1
C(108)	4876(3)	8158(3)	9175(2)	44(1)	1
C(109)	4373(3)	8376(3)	8721(2)	55(2)	1
C(110)	4628(3)	8988(3)	8334(2)	46(1)	1
C(111)	5396(4)	9379(3)	8385(2)	45(1)	1
C(112)	5909(3)	9152(2)	8833(2)	36(1)	1
O(16)	7245(2)	8631(2)	9670(1)	30(1)	1
Cl(1)	7355(1)	3494(1)	2754(1)	31(1)	1
O(1P)	7372(3)	2867(2)	2528(2)	64(1)	1
O(2P)	8216(4)	3839(3)	2644(2)	100(2)	1
O(3P)	6666(4)	4006(4)	2564(2)	129(2)	1
O(4P)	7299(3)	3233(2)	3310(1)	73(1)	1
Cl(2)	9312(1)	1604(1)	7698(1)	86(1)	1
O(5P)	9263(5)	1766(4)	8198(2)	128(2)	1
O(6P)	8837(5)	2213(4)	7355(3)	150(2)	1
O(7P)	10248(4)	1578(4)	7586(4)	151(3)	1
O(8P)	8970(5)	907(4)	7726(4)	172(3)	1
O(1S)	6789(7)	3418(5)	7934(3)	159(3)	1
C(1S)	6356(12)	2736(8)	8287(6)	240(8)	1
O(2S)	8553(6)	3224(6)	8134(4)	175(3)	1
C(2S)	9130(8)	3817(6)	7813(4)	138(4)	1
O(3S)	6389(5)	3725(5)	6928(4)	172(4)	1
C(3S)	7222(6)	3761(7)	6687(4)	122(3)	1
O(4S)	5728(6)	1219(5)	7435(5)	203(5)	1
C(4S)	6563(8)	1320(7)	7255(6)	169(5)	1
O(5S)	4272(6)	2915(5)	7059(4)	184(3)	1
C(5S)	5097(6)	2667(4)	6883(4)	106(3)	1

Table 9 (con't)

O(6S)	7266(16)	989(17)	8481(7)	411(10)	1
C(6S)	7374(7)	510(6)	8969(7)	203(7)	1
O(7S)	7791(6)	1393(5)	2174(3)	161(3)	1
C(7S)	7203(6)	1358(4)	2504(3)	102(3)	1

Table 10. Anisotropic Thermal Parameters ($Å^2 \times 10^3$) for {tmbpyVO[μ–$(C_6H_5)_2PO_2]_{1.5}$}$_2${ClO_4}•3.5CH_3OH, (**4.3**).

Atom	U_{11}	U_{22}	U_{33}	U_{23}	U_{13}	U_{12}
V(1)	10(1)	13(1)	19(1)	-6(1)	2(1)	-3(1)
O(1)	18(1)	17(1)	33(2)	-12(1)	4(1)	-4(1)
N(1)	15(2)	13(1)	23(2)	-4(1)	1(1)	-3(1)
C(1)	25(2)	17(2)	24(2)	-3(2)	1(2)	-5(2)
C(2)	33(2)	27(2)	25(2)	-8(2)	9(2)	-6(2)
C(2A)	46(3)	49(3)	25(2)	-2(2)	3(2)	-8(2)
C(3)	29(2)	33(2)	29(2)	-6(2)	13(2)	-7(2)
C(3A)	39(3)	78(4)	41(3)	-4(3)	21(2)	-18(3)
C(4)	18(2)	29(2)	33(2)	-9(2)	7(2)	-6(2)
C(5)	15(2)	14(2)	27(2)	-7(2)	1(2)	-4(1)
C(6)	15(2)	15(2)	29(2)	-9(2)	2(2)	-3(1)
C(7)	17(2)	23(2)	35(2)	-9(2)	1(2)	1(2)
C(8)	17(2)	25(2)	36(2)	-13(2)	-8(2)	1(2)
C(8A)	23(2)	44(3)	46(3)	-14(2)	-13(2)	4(2)
C(9)	27(2)	30(2)	28(2)	-9(2)	-6(2)	1(2)
C(9A)	34(3)	51(3)	31(2)	-1(2)	-8(2)	-6(2)
C(10)	22(2)	32(2)	24(2)	-9(2)	1(2)	-8(2)
N(2)	17(2)	22(2)	23(2)	-9(1)	0(1)	-5(1)
V(2)	16(1)	13(1)	20(1)	-6(1)	-2(1)	-4(1)
O(2)	32(2)	18(1)	26(1)	-2(1)	-5(1)	-7(1)
N(3)	20(2)	19(2)	20(2)	-7(1)	3(1)	-5(1)
C(11)	25(2)	21(2)	27(2)	-8(2)	6(2)	-5(2)
C(12)	23(2)	31(2)	25(2)	-3(2)	8(2)	0(2)
C(12A)	30(3)	46(3)	46(3)	-11(2)	13(2)	2(2)
C(13)	19(2)	45(3)	33(2)	-7(2)	1(2)	-6(2)
C(13A)	19(3)	103(5)	64(4)	-35(3)	0(2)	-1(3)
C(14)	22(2)	41(2)	26(2)	-11(2)	-2(2)	-8(2)
C(15)	17(2)	22(2)	19(2)	-3(2)	0(1)	-6(2)
C(16)	17(2)	18(2)	19(2)	-4(1)	-1(1)	-7(1)
C(17)	23(2)	28(2)	23(2)	-7(2)	-2(2)	-1(2)
C(18)	39(2)	24(2)	18(2)	-7(2)	4(2)	-5(2)
C(18A)	54(3)	56(3)	35(3)	-27(2)	1(2)	-8(3)
C(19)	31(2)	22(2)	29(2)	-9(2)	8(2)	-1(2)
C(19A)	45(3)	48(3)	48(3)	-29(2)	12(2)	1(2)

Table 10 (con't)

C(20)	19(2)	21(2)	33(2)	-13(2)	3(2)	-2(2)
N(4)	20(2)	14(1)	25(2)	-6(1)	0(1)	-3(1)
O(3)	19(1)	15(1)	27(1)	-7(1)	2(1)	1(1)
P(1)	13(1)	14(1)	22(1)	-6(1)	-1(1)	2(1)
C(21)	16(2)	21(2)	25(2)	-9(2)	-1(2)	5(2)
C(22)	22(2)	25(2)	27(2)	-8(2)	4(2)	0(2)
C(23)	35(3)	36(2)	23(2)	-3(2)	2(2)	9(2)
C(24)	40(3)	47(3)	30(2)	-1(2)	-11(2)	21(2)
C(25)	20(2)	47(3)	46(3)	-19(2)	-1(2)	6(2)
C(26)	15(2)	30(2)	35(2)	-7(2)	-1(2)	0(2)
C(27)	23(2)	28(2)	28(2)	-11(2)	-4(2)	8(2)
C(28)	35(3)	35(2)	42(3)	-17(2)	-1(2)	11(2)
C(29)	43(3)	64(3)	61(3)	-38(3)	2(3)	19(3)
C(30)	66(4)	101(5)	43(3)	-36(3)	5(3)	32(4)
C(31)	70(4)	90(5)	36(3)	0(3)	21(3)	12(4)
C(32)	51(3)	46(3)	35(3)	-4(2)	1(2)	9(2)
O(4)	16(1)	17(1)	37(2)	-9(1)	-6(1)	-1(1)
O(5)	17(1)	19(1)	28(1)	-6(1)	-4(1)	-4(1)
P(2)	12(1)	14(1)	19(1)	-5(1)	-1(1)	-1(1)
C(33)	16(2)	18(2)	26(2)	-4(2)	0(2)	0(1)
C(34)	33(2)	27(2)	36(2)	-12(2)	7(2)	-2(2)
C(35)	36(3)	35(2)	59(3)	-15(2)	20(2)	8(2)
C(36)	18(2)	43(3)	72(4)	0(3)	15(2)	6(2)
C(37)	16(2)	51(3)	62(3)	-7(3)	-7(2)	-1(2)
C(38)	16(2)	41(2)	37(2)	-9(2)	-5(2)	-1(2)
C(39)	23(2)	20(2)	21(2)	-4(2)	-2(2)	0(2)
C(40)	47(3)	38(3)	34(2)	12(2)	11(2)	15(2)
C(41)	71(4)	56(3)	33(3)	18(2)	6(3)	9(3)
C(42)	72(4)	52(3)	28(2)	-3(2)	15(2)	-9(3)
C(43)	57(3)	54(3)	39(3)	-14(2)	8(2)	8(3)
C(44)	48(3)	40(3)	29(2)	-8(2)	1(2)	12(2)
O(6)	19(1)	14(1)	23(1)	-5(1)	0(1)	-2(1)
O(7)	15(1)	23(1)	20(1)	-6(1)	4(1)	-8(1)
P(3)	15(1)	16(1)	16(1)	-6(1)	3(1)	-5(1)
C(45)	17(2)	22(2)	16(2)	-5(1)	2(1)	-3(2)
C(46)	26(2)	29(2)	38(2)	-11(2)	9(2)	-11(2)
C(47)	22(2)	44(3)	51(3)	-1(2)	18(2)	-7(2)

Table 10 (con't)

C(48)	34(3)	42(3)	53(3)	-11(2)	16(2)	1(2)
C(49)	43(3)	22(2)	47(3)	-9(2)	12(2)	5(2)
C(50)	26(2)	21(2)	30(2)	-4(2)	7(2)	-4(2)
C(51)	19(2)	23(2)	17(2)	-5(2)	5(1)	0(2)
C(52)	34(2)	26(2)	22(2)	-4(2)	6(2)	-9(2)
C(53)	50(3)	24(2)	28(2)	1(2)	12(2)	-3(2)
C(54)	46(3)	42(3)	23(2)	2(2)	8(2)	7(2)
C(55)	33(3)	52(3)	25(2)	-5(2)	-5(2)	-6(2)
C(56)	27(2)	36(2)	26(2)	-4(2)	-1(2)	-7(2)
O(8)	22(1)	24(1)	23(1)	-12(1)	1(1)	-6(1)
V(3)	13(1)	21(1)	19(1)	-9(1)	4(1)	-7(1)
O(9)	26(2)	26(1)	39(2)	-18(1)	9(1)	-11(1)
N(5)	20(2)	22(2)	20(2)	-6(1)	3(1)	-4(1)
C(57)	24(2)	38(2)	24(2)	-6(2)	1(2)	-2(2)
C(58)	43(3)	65(3)	17(2)	-1(2)	7(2)	1(2)
C(58A)	56(4)	126(6)	21(2)	-1(3)	5(2)	-2(4)
C(59)	29(3)	82(4)	30(2)	-2(2)	12(2)	-7(3)
C(59A)	46(4)	140(7)	47(3)	-6(4)	26(3)	-20(4)
C(60)	18(2)	62(3)	33(2)	-3(2)	7(2)	-8(2)
C(61)	15(2)	26(2)	23(2)	-3(2)	2(2)	-2(2)
C(62)	19(2)	28(2)	25(2)	-6(2)	3(2)	-8(2)
C(63)	18(2)	30(2)	34(2)	-4(2)	1(2)	-7(2)
C(64)	24(2)	54(3)	35(2)	-11(2)	-6(2)	-16(2)
C(64A)	26(3)	68(3)	51(3)	-9(3)	-15(2)	-13(2)
C(65)	36(3)	93(4)	26(2)	-7(3)	-7(2)	-24(3)
C(65A)	49(4)	188(8)	25(3)	-5(4)	-8(2)	-46(4)
C(66)	31(3)	96(4)	21(2)	-12(2)	3(2)	-29(3)
N(6)	18(2)	46(2)	23(2)	-8(2)	6(1)	-18(2)
V(4)	19(1)	18(1)	22(1)	-4(1)	0(1)	-6(1)
O(10)	34(2)	27(2)	26(1)	1(1)	-2(1)	-11(1)
N(7)	33(2)	16(2)	28(2)	-4(1)	-3(2)	-8(1)
C(67)	48(3)	21(2)	39(2)	-9(2)	2(2)	-6(2)
C(68)	71(4)	25(2)	41(3)	-15(2)	15(3)	-14(2)
C(68A)	90(5)	43(3)	63(4)	-28(3)	16(3)	2(3)
C(69)	87(4)	30(2)	28(2)	-9(2)	5(3)	-23(3)
C(69A)	112(6)	62(4)	43(3)	-27(3)	1(3)	-40(4)
C(70)	63(3)	38(3)	31(2)	-4(2)	-4(2)	-32(2)

Table 10 (con't)

C(71)	42(3)	24(2)	27(2)	-3(2)	2(2)	-18(2)
C(72)	30(2)	26(2)	31(2)	3(2)	-6(2)	-17(2)
C(73)	38(3)	64(3)	40(3)	-1(2)	-8(2)	-26(3)
C(74)	23(3)	80(4)	59(3)	1(3)	-4(2)	-13(3)
C(74A)	30(3)	163(8)	88(5)	-16(5)	-1(3)	-14(4)
C(75)	23(2)	48(3)	52(3)	7(2)	4(2)	-8(2)
C(75A)	26(3)	70(4)	81(4)	8(3)	18(3)	5(3)
C(76)	26(2)	31(2)	39(2)	-1(2)	7(2)	-7(2)
N(8)	23(2)	22(2)	31(2)	-3(1)	-1(1)	-9(1)
O(11)	19(1)	16(1)	32(1)	-6(1)	-6(1)	-6(1)
P(4)	16(1)	15(1)	18(1)	-5(1)	-2(1)	-3(1)
C(77)	27(2)	26(2)	22(2)	-4(2)	2(2)	-1(2)
C(78)	42(3)	30(2)	30(2)	-1(2)	-3(2)	-1(2)
C(79)	65(4)	46(3)	30(2)	1(2)	2(2)	-7(3)
C(80)	128(6)	68(4)	24(3)	-5(3)	14(3)	1(4)
C(81)	139(7)	55(3)	35(3)	-22(3)	14(3)	-6(4)
C(82)	84(4)	33(3)	33(3)	-1(2)	3(3)	0(3)
C(83)	21(2)	18(2)	21(2)	-2(2)	0(2)	-1(2)
C(84)	31(2)	27(2)	34(2)	-11(2)	1(2)	-2(2)
C(85)	40(3)	28(2)	52(3)	-11(2)	15(2)	5(2)
C(86)	24(2)	36(3)	73(4)	-1(2)	12(2)	2(2)
C(87)	19(2)	45(3)	63(3)	-5(2)	-8(2)	-3(2)
C(88)	24(2)	33(2)	35(2)	-1(2)	-6(2)	-5(2)
O(12)	22(1)	17(1)	22(1)	-5(1)	-1(1)	-3(1)
O(13)	23(2)	36(2)	22(1)	-1(1)	7(1)	-15(1)
P(5)	16(1)	26(1)	19(1)	-8(1)	6(1)	-8(1)
C(89)	21(2)	32(2)	23(2)	-9(2)	1(2)	-1(2)
C(90)	38(3)	34(2)	37(2)	-5(2)	-7(2)	-5(2)
C(91)	41(3)	52(3)	40(3)	-8(2)	-13(2)	-3(2)
C(92)	48(3)	46(3)	28(2)	0(2)	3(2)	9(2)
C(93)	56(3)	36(2)	23(2)	1(2)	8(2)	-1(2)
C(94)	47(3)	36(2)	27(2)	-4(2)	6(2)	-18(2)
C(95)	21(2)	28(2)	17(2)	-5(2)	4(2)	-4(2)
C(96)	36(2)	27(2)	28(2)	-5(2)	7(2)	-3(2)
C(97)	60(3)	28(2)	40(3)	-5(2)	7(2)	9(2)
C(98)	47(3)	45(3)	37(3)	-3(2)	11(2)	21(2)
C(99)	29(2)	54(3)	38(3)	-8(2)	17(2)	0(2)

Table 10 (con't)

C(100)	24(2)	30(2)	37(2)	-4(2)	11(2)	-6(2)
O(14)	22(1)	33(2)	28(1)	-16(1)	4(1)	-9(1)
O(15)	21(2)	26(1)	33(2)	-8(1)	2(1)	1(1)
P(6)	17(1)	22(1)	28(1)	-3(1)	2(1)	0(1)
C(101)	30(2)	26(2)	38(2)	-8(2)	6(2)	-2(2)
C(102)	57(4)	52(3)	57(3)	-17(3)	3(3)	16(3)
C(103)	63(4)	70(4)	91(5)	-42(4)	22(4)	15(3)
C(104)	78(4)	69(4)	54(3)	-29(3)	28(3)	-2(3)
C(105)	115(6)	63(4)	43(3)	-13(3)	19(3)	8(4)
C(106)	77(4)	57(3)	37(3)	-5(2)	7(3)	20(3)
C(107)	22(2)	28(2)	28(2)	-3(2)	3(2)	2(2)
C(108)	22(2)	50(3)	50(3)	8(2)	-4(2)	-8(2)
C(109)	26(3)	71(4)	59(3)	0(3)	-15(2)	2(2)
C(110)	40(3)	57(3)	37(3)	-6(2)	-8(2)	18(2)
C(111)	58(3)	40(3)	31(2)	3(2)	3(2)	8(2)
C(112)	41(3)	30(2)	38(2)	-7(2)	3(2)	0(2)
O(16)	21(2)	27(1)	38(2)	-1(1)	-1(1)	-2(1)
Cl(1)	31(1)	33(1)	29(1)	-1(1)	-4(1)	1(1)
O(1P)	91(3)	50(2)	61(2)	-33(2)	8(2)	0(2)
O(2P)	93(4)	122(4)	89(4)	-32(3)	25(3)	-58(3)
O(3P)	140(4)	177(5)	101(4)	-95(4)	-81(3)	122(4)
O(4P)	112(4)	69(3)	38(2)	-13(2)	1(2)	-6(2)
Cl(2)	87(1)	68(1)	102(1)	-20(1)	17(1)	-3(1)
O(5P)	170(6)	126(5)	78(4)	-15(3)	2(4)	42(4)
O(6P)	172(6)	150(5)	99(4)	14(4)	8(4)	58(5)
O(7P)	82(4)	114(4)	275(8)	-80(5)	39(4)	-15(3)
O(8P)	127(6)	108(5)	297(9)	-77(5)	9(5)	-49(4)
O(1S)	176(7)	142(6)	160(7)	-43(5)	0(6)	32(5)
C(1S)	327(20)	163(12)	192(15)	27(10)	37(13)	-116(12)
O(2S)	124(6)	254(10)	197(8)	-148(8)	-41(6)	26(6)
C(2S)	173(11)	97(7)	114(7)	20(6)	35(7)	37(7)
O(3S)	98(5)	171(7)	194(8)	45(7)	-40(5)	-22(5)
C(3S)	90(7)	180(10)	93(7)	-31(7)	-17(5)	8(7)
O(4S)	154(8)	121(6)	276(12)	46(7)	-9(8)	13(6)
C(4S)	125(10)	143(10)	245(15)	-66(10)	1(10)	58(9)
O(5S)	189(9)	135(7)	218(10)	-31(6)	52(7)	-15(6)
C(5S)	94(6)	70(5)	143(8)	-1(5)	-25(6)	5(4)

Table 10 (con't)

O(6S)	423(23)	539(28)	250(15)	-57(15)	68(14)	-186(18)
C(6S)	78(8)	151(10)	448(23)	-203(13)	-50(11)	25(7)
O(7S)	166(7)	214(8)	113(6)	-65(6)	-23(5)	58(6)
C(7S)	134(8)	75(5)	105(6)	-36(5)	51(6)	-28(5)

Table 11. Atomic Coordinates ($\times 10^4$) and Equivalent Isotropic Thermal Parameters ($Å^2 \times 10^2$) for {bpyVO[μ–(p-FC_6H_4)$_2PO_2$]$_{1.5}$}$_2${ClO4}•1.5CH_3OH, (**4.4**).

Atom	x	y	z	U_{eq}	Occupancy
V(1)	2133(1)	5119(1)	7441(1)	25(1)	1
O(1)	2140(3)	5703(2)	7939(1)	33(1)	1
O(2)	3365(2)	4514(2)	7611(1)	30(1)	1
O(3)	2105(3)	4493(2)	6709(1)	34(1)	1
O(4)	1151(2)	4366(2)	7724(1)	36(1)	1
V(2)	2756(1)	2362(1)	7410(1)	29(1)	1
O(5)	2900(3)	1749(2)	7877(1)	38(1)	1
O(6)	3830(2)	3098(2)	7626(1)	33(1)	1
O(7)	2544(2)	3063(2)	6713(1)	31(1)	1
O(8)	1636(3)	2950(2)	7747(1)	35(1)	1
P(1)	3929(1)	3876(1)	7879(1)	28(1)	1
N(1)	2955(3)	5884(2)	6947(2)	29(1)	1
C(1)	3954(4)	6000(3)	6977(2)	39(1)	1
C(2)	4449(4)	6528(3)	6664(2)	42(1)	1
C(3)	3889(5)	6944(3)	6292(2)	45(1)	1
C(4)	2858(4)	6831(3)	6262(2)	39(1)	1
C(5)	2401(4)	6289(2)	6592(2)	29(1)	1
C(6)	1305(4)	6127(3)	6594(2)	31(1)	1
C(7)	621(4)	6387(3)	6211(2)	41(1)	1
C(8)	-390(4)	6209(3)	6256(2)	43(1)	1
C(9)	-721(4)	5780(3)	6683(2)	43(1)	1
C(10)	-12(4)	5522(3)	7044(2)	35(1)	1
N(2)	980(3)	5681(2)	6999(2)	28(1)	1
N(3)	3790(3)	1801(2)	6887(2)	34(1)	1
C(11)	4801(4)	1860(3)	6920(2)	34(1)	1
C(12)	5442(4)	1459(3)	6583(2)	47(2)	1
C(13)	5022(4)	982(3)	6208(3)	50(2)	1
C(14)	3975(4)	915(3)	6166(2)	40(1)	1
C(15)	3372(4)	1329(3)	6513(2)	34(1)	1
C(16)	2253(4)	1290(2)	6518(2)	31(1)	1
C(17)	1690(4)	911(3)	6137(2)	42(1)	1
C(18)	641(4)	902(3)	6178(3)	47(2)	1
C(19)	186(4)	1269(3)	6600(3)	48(2)	1
C(20)	776(4)	1648(3)	6970(2)	37(1)	1

Table 11 (con't)

N(4)	1796(3)	1667(2)	6930(2)	33(1)	1
C(21)	3570(4)	3822(3)	8571(2)	30(1)	1
C(22)	3178(4)	4457(3)	8826(2)	37(1)	1
C(23)	2945(5)	4439(3)	9369(2)	48(2)	1
C(24)	3105(4)	3791(3)	9647(2)	45(1)	1
F(1)	2858(3)	3763(2)	10176(1)	71(1)	1
C(25)	3471(4)	3140(3)	9419(2)	45(1)	1
C(26)	3708(4)	3160(3)	8868(2)	39(1)	1
C(27)	5247(4)	4127(3)	7843(2)	31(1)	1
C(28)	5895(4)	4068(3)	8285(2)	36(1)	1
C(29)	6908(4)	4275(3)	8240(2)	40(1)	1
C(30)	7230(4)	4562(3)	7767(2)	42(1)	1
F(2)	8223(2)	4796(2)	7728(1)	57(1)	1
C(31)	6636(4)	4621(3)	7321(3)	50(2)	1
C(32)	5639(4)	4400(3)	7358(2)	40(1)	1
P(2)	2406(1)	3789(1)	6407(1)	31(1)	1
C(33)	3563(5)	3974(3)	6041(2)	44(1)	1
C(34)	3710(9)	4658(4)	5792(4)	133(5)	1
C(35)	4577(11)	4803(5)	5506(6)	209(9)	1
C(36)	5281(9)	4262(6)	5468(5)	138(5)	1
F(3)	6129(6)	4359(4)	5175(4)	224(5)	1
C(37)	5205(6)	3583(6)	5730(3)	89(3)	1
C(38)	4319(5)	3441(4)	6015(3)	61(2)	1
C(39)	1422(5)	3648(3)	5915(2)	41(1)	1
C(40)	856(5)	4238(3)	5702(2)	52(2)	1
C(41)	45(6)	4116(4)	5360(2)	63(2)	1
C(42)	-168(6)	3387(4)	5225(3)	64(2)	1
F(4)	-1002(4)	3261(3)	4902(2)	99(2)	1
C(43)	350(6)	2776(4)	5411(3)	69(2)	1
C(44)	1168(5)	2915(3)	5754(2)	51(2)	1
P(3)	860(1)	3556(1)	7861(1)	29(1)	1
C(45)	-287(3)	3340(2)	7495(2)	31(1)	1
C(46)	-394(4)	3598(3)	6967(2)	43(1)	1
C(47)	-1239(5)	3417(4)	6669(2)	54(2)	1
C(48)	-1977(4)	2976(3)	6909(2)	47(1)	1
F(5)	-2821(3)	2811(2)	6614(1)	71(1)	1
C(49)	-1910(4)	2717(3)	7412(2)	48(1)	1

Table 11 (con't)

C(50)	-1059(4)	2896(3)	7717(2)	40(1)	1
C(51)	544(3)	3505(3)	8563(2)	30(1)	1
C(52)	-213(4)	3963(3)	8772(2)	39(1)	1
C(53)	-475(4)	3923(3)	9317(2)	47(1)	1
C(54)	62(5)	3434(3)	9634(2)	41(1)	1
F(6)	-175(3)	3392(2)	10164(1)	56(1)	1
C(55)	815(4)	2970(3)	9443(2)	39(1)	1
C(56)	1053(4)	3009(3)	8897(2)	32(1)	1
Cl(1)	8282(1)	6089(1)	4817(1)	46(1)	1
O(9)	8103(5)	6650(3)	4427(2)	110(2)	1
O(10)	9329(4)	6009(4)	4905(3)	107(2)	1
O(11)	7858(4)	5399(2)	4648(2)	71(1)	1
O(12)	7792(4)	6325(3)	5306(2)	75(1)	1
O(13)	6687(13)	5458(12)	6092(7)	187(9)	0.5
C(57)	7274(11)	5016(10)	5997(6)	92(7)	0.5
O(14)	2237(10)	6418(10)	9268(6)	341(11)	1
C(58)	1727(11)	6361(8)	9613(4)	194(8)	1

Table 12. Anisotropic Thermal Parameters ($Å^2 \times 10^3$) for {bpyVO[μ–(p-$FC_6H_4)_2PO_2]_{1.5}$}$_2${ClO4}•1.5CH_3OH, (**4.4**).

Atom	U_{11}	U_{22}	U_{33}	U_{23}	U_{13}	U_{12}
V(1)	26(1)	22(1)	28(1)	1(1)	1(1)	-1(1)
O(1)	35(2)	33(2)	31(2)	1(1)	3(2)	0(2)
O(2)	25(2)	32(2)	33(2)	1(2)	0(2)	2(1)
O(3)	48(2)	22(2)	33(2)	-1(1)	-3(2)	-2(2)
O(4)	32(2)	29(2)	46(2)	9(2)	3(2)	-6(2)
V(2)	30(1)	22(1)	35(1)	2(1)	3(1)	0(1)
O(5)	43(2)	29(2)	43(2)	10(2)	-2(2)	2(2)
O(6)	27(2)	29(2)	44(2)	0(2)	0(2)	-1(2)
O(7)	39(2)	23(2)	31(2)	2(1)	5(2)	-1(2)
O(8)	36(2)	32(2)	36(2)	-2(2)	7(2)	2(2)
P(1)	24(1)	28(1)	32(1)	1(1)	1(1)	0(1)
N(1)	30(2)	24(2)	33(2)	1(2)	5(2)	4(2)
C(1)	34(3)	36(3)	46(3)	0(2)	5(2)	-6(3)
C(2)	31(3)	44(3)	50(3)	8(3)	6(2)	-9(3)
C(3)	53(4)	42(3)	41(3)	3(3)	8(3)	-11(3)
C(4)	51(3)	32(3)	33(3)	1(2)	-1(3)	0(3)
C(5)	42(3)	20(2)	26(2)	-3(2)	4(2)	-2(2)
C(6)	42(3)	21(2)	30(3)	-2(2)	-1(2)	5(2)
C(7)	50(4)	36(3)	35(3)	-1(2)	-2(3)	9(3)
C(8)	44(3)	32(3)	52(4)	-7(3)	-15(3)	5(3)
C(9)	33(3)	37(3)	58(4)	5(3)	-12(3)	1(3)
C(10)	32(3)	27(3)	47(3)	0(2)	1(2)	-2(2)
N(2)	31(2)	22(2)	30(2)	0(2)	-3(2)	0(2)
N(3)	34(2)	25(2)	43(3)	2(2)	2(2)	7(2)
C(11)	29(3)	27(3)	47(3)	1(2)	4(2)	4(2)
C(12)	38(3)	40(3)	64(4)	-4(3)	3(3)	6(3)
C(13)	41(3)	42(3)	66(4)	-10(3)	11(3)	12(3)
C(14)	51(4)	28(3)	42(3)	-6(2)	6(3)	2(3)
C(15)	37(3)	24(3)	42(3)	2(2)	0(2)	2(2)
C(16)	38(3)	16(2)	39(3)	0(2)	0(2)	3(2)
C(17)	40(3)	31(3)	55(4)	-4(3)	1(3)	-1(3)
C(18)	44(4)	27(3)	71(4)	-5(3)	-9(3)	-4(3)
C(19)	34(3)	36(3)	73(4)	7(3)	-3(3)	-4(3)
C(20)	32(3)	25(3)	53(3)	3(2)	5(3)	-2(2)

Table 12 (con't)

N(4)	32(2)	19(2)	47(3)	6(2)	2(2)	-2(2)
C(21)	29(3)	29(3)	31(3)	5(2)	-2(2)	-4(2)
C(22)	45(3)	34(3)	32(3)	3(2)	-1(2)	-5(3)
C(23)	64(4)	44(3)	36(3)	-4(3)	5(3)	-5(3)
C(24)	45(4)	60(4)	31(3)	8(3)	6(2)	-1(3)
F(1)	97(3)	87(3)	29(2)	14(2)	5(2)	0(2)
C(25)	43(3)	51(4)	41(3)	21(3)	-5(3)	3(3)
C(26)	30(3)	35(3)	51(3)	7(3)	2(2)	5(2)
C(27)	25(3)	25(3)	42(3)	-1(2)	2(2)	-2(2)
C(28)	31(3)	38(3)	39(3)	1(2)	2(2)	1(2)
C(29)	27(3)	45(3)	47(3)	-5(3)	-2(2)	-3(2)
C(30)	25(3)	39(3)	63(4)	-10(3)	5(3)	3(3)
F(2)	25(2)	64(2)	82(3)	-1(2)	11(2)	-11(2)
C(31)	35(3)	58(4)	58(4)	16(3)	13(3)	-2(3)
C(32)	33(3)	50(3)	37(3)	4(3)	1(2)	0(3)
P(2)	43(1)	23(1)	27(1)	0(1)	3(1)	-2(1)
C(33)	65(4)	27(3)	39(3)	-12(2)	15(3)	-16(3)
C(34)	205(11)	38(4)	156(9)	28(5)	136(9)	7(5)
C(35)	283(17)	52(5)	292(17)	-1(8)	244(16)	-19(8)
C(36)	156(10)	90(7)	168(10)	-26(7)	136(9)	-60(7)
F(3)	225(8)	149(5)	297(9)	-61(6)	221(8)	-84(6)
C(37)	71(5)	129(8)	67(5)	-13(5)	26(4)	-11(6)
C(38)	53(4)	73(5)	57(4)	20(4)	13(3)	-5(4)
C(39)	67(4)	31(3)	25(3)	6(2)	-1(3)	0(3)
C(40)	75(4)	36(3)	43(3)	4(3)	-6(3)	0(3)
C(41)	79(5)	65(4)	43(4)	10(3)	-22(3)	9(4)
C(42)	85(5)	65(5)	43(4)	1(3)	-25(4)	-10(4)
F(4)	113(4)	103(3)	82(3)	21(3)	-59(3)	-29(3)
C(43)	105(6)	48(4)	55(4)	4(3)	-25(4)	-16(4)
C(44)	75(5)	36(3)	43(3)	5(3)	-19(3)	-7(3)
P13)	27(1)	27(1)	33(1)	4(1)	4(1)	-2(1)
C(45)	34(3)	22(2)	37(3)	-2(2)	0(2)	3(2)
C(46)	33(3)	45(3)	51(4)	-5(3)	5(3)	-12(3)
C(47)	58(4)	68(4)	35(3)	3(3)	-5(3)	-12(4)
C(48)	40(3)	47(3)	53(4)	-4(3)	-9(3)	-8(3)
F(5)	58(2)	86(3)	68(2)	4(2)	-25(2)	-27(2)
C(49)	38(3)	45(3)	61(4)	10(3)	-6(3)	-12(3)

Table 12 (con't)

C(50)	40(3)	38(3)	43(3)	14(2)	-4(2)	-10(3)
C(51)	25(3)	24(2)	39(3)	1(2)	0(2)	-6(2)
C(52)	37(3)	36(3)	45(3)	4(3)	3(2)	5(3)
C(53)	50(4)	42(3)	48(4)	5(3)	15(3)	5(3)
C(54)	58(4)	38(3)	28(3)	-3(2)	4(3)	-15(3)
F(6)	73(2)	58(2)	36(2)	1(2)	12(2)	-8(2)
C(55)	43(3)	32(3)	42(3)	5(2)	-8(3)	-6(3)
C(56)	31(3)	21(2)	45(3)	0(2)	6(2)	1(2)
O(9)	173(7)	72(4)	85(4)	39(3)	-3(4)	14(4)
O(10)	46(3)	129(5)	144(5)	-1(4)	-6(3)	1(4)
O(11)	79(3)	37(2)	98(3)	-24(2)	-4(3)	-5(2)
O(12)	72(3)	96(4)	58(3)	-30(3)	-3(3)	0(3)
O(13)	131(16)	296(25)	134(14)	81(15)	10(12)	-21(14)
C(57)	65(10)	168(18)	44(8)	63(10)	-38(8)	-75(11)
O(14)	236(12)	505(24)	281(15)	309(17)	127(12)	130(15)
C(58)	253(17)	255(17)	73(7)	-67(8)	-36(7)	182(13)

Table 13. Atomic Coordinates (× 10^4) and Equivalent Isotropic Thermal Parameters (Å^2 × 10^2) for {bpyVO[μ–(p-ClC_6H_4)$_2PO_2$]$_{1.5}$}$_2${ClO4}, (**4.5**).

Atom	x	y	z	U_{eq}	Occupancy
V(1)	3568(1)	5097(1)	8471(1)	30(1)	1
O(1)	4327(2)	5000(2)	8139(3)	37(1)	1
O(2)	2579(2)	5123(2)	9017(2)	29(1)	1
O(3)	2988(2)	5466(2)	7355(2)	31(1)	1
O(4)	3841(2)	5855(2)	9122(3)	32(1)	1
V(2)	1868(1)	6714(1)	8465(1)	32(1)	1
O(5)	2034(2)	7374(2)	8264(3)	41(1)	1
O(6)	1514(2)	5862(2)	8671(3)	34(1)	1
O(7)	2204(2)	6393(2)	7377(2)	34(1)	1
O(8)	2760(2)	6509(2)	9357(3)	36(1)	1
N(1)	3824(2)	4549(2)	9639(3)	29(1)	1
C(1)	4166(3)	4705(3)	10471(4)	33(2)	1
C(2)	4140(3)	4384(3)	11240(4)	42(2)	1
C(3)	3736(3)	3871(3)	11149(5)	43(2)	1
C(4)	3409(3)	3695(3)	10288(5)	39(2)	1
C(5)	3465(3)	4028(2)	9542(4)	30(2)	1
C(6)	3142(3)	3865(3)	8601(4)	30(2)	1
C(7)	2880(3)	3308(3)	8356(5)	36(2)	1
C(8)	2625(4)	3188(3)	7467(5)	47(2)	1
C(9)	2616(4)	3618(3)	6820(5)	47(2)	1
C(10)	2880(3)	4162(3)	7110(5)	42(2)	1
N(2)	3147(3)	4280(2)	7986(3)	32(1)	1
N(3)	1319(3)	6896(2)	9557(4)	37(1)	1
C(11)	1646(4)	6929(2)	10426(5)	41(2)	1
C(12)	1256(5)	6957(3)	11126(5)	54(2)	1
C(13)	493(5)	6943(3)	10905(5)	57(2)	1
C(14)	163(4)	6927(3)	10016(5)	50(2)	1
C(15)	576(4)	6910(2)	9336(4)	34(2)	1
C(16)	263(4)	6902(2)	8370(5)	37(2)	1
C(17)	-471(4)	7027(3)	8007(5)	46(2)	1
C(18)	-718(4)	6990(3)	7094(5)	51(2)	1
C(19)	-232(4)	6834(3)	6539(5)	48(2)	1
C(20)	492(4)	6735(3)	6930(4)	37(2)	1
N(4)	740(3)	6779(2)	7803(3)	32(1)	1

Table 13 (con't)

P(1)	1767(1)	5248(1)	8871(1)	30(1)	1
C(21)	1449(3)	5029(2)	9886(4)	30(2)	1
C(22)	1719(4)	4542(3)	10379(5)	48(2)	1
C(23)	1476(4)	4375(3)	11161(5)	50(2)	1
C(24)	954(4)	4703(3)	11446(4)	41(2)	1
Cl(1)	633(1)	4499(1)	12412(1)	73(1)	1
C(25)	664(3)	5191(3)	10978(4)	41(2)	1
C(26)	909(3)	5343(3)	10191(4)	33(2)	1
C(27)	1286(3)	4801(3)	7956(4)	36(2)	1
C(28)	1165(4)	4214(3)	8088(5)	53(2)	1
C(29)	792(4)	3891(4)	7369(7)	69(3)	1
C(30)	541(4)	4126(5)	6548(7)	83(3)	1
C(31)	666(4)	4713(5)	6409(6)	83(3)	1
C(32)	1044(4)	5041(3)	7133(5)	57(2)	1
P(2)	2777(1)	6067(1)	6986(1)	32(1)	1
Cl(2)	38(1)	3731(2)	5666(2)	142(1)	1
C(33)	2406(3)	6000(3)	5807(4)	33(2)	1
C(34)	2254(5)	5484(3)	5369(5)	83(3)	1
C(35)	1938(6)	5449(4)	4445(6)	102(4)	1
C(36)	1787(4)	5948(3)	3977(5)	48(2)	1
Cl(3)	1383(1)	5918(1)	2833(1)	73(1)	1
C(37)	1916(4)	6461(3)	4392(5)	67(2)	1
C(38)	2225(4)	6483(3)	5297(5)	62(2)	1
C(39)	3587(3)	6510(3)	7068(4)	32(2)	1
C(40)	4231(4)	6271(3)	6894(4)	42(2)	1
C(41)	4863(4)	6601(3)	6940(4)	47(2)	1
C(42)	4828(4)	7181(3)	7149(4)	47(2)	1
Cl(4)	5628(1)	7597(1)	7226(1)	72(1)	1
C(43)	4196(4)	7435(3)	7320(4)	48(2)	1
C(44)	3577(4)	7097(3)	7274(4)	38(2)	1
P(3)	3550(1)	6330(1)	9656(1)	33(1)	1
C(45)	4110(4)	6966(3)	9640(4)	33(2)	1
C(46)	4849(4)	6926(3)	9587(4)	42(2)	1
C(47)	5278(4)	7420(3)	9592(4)	47(2)	1
C(48)	4953(4)	7953(3)	9639(4)	50(2)	1
Cl(5)	5496(1)	8572(1)	9646(1)	71(1)	1
C(49)	4221(4)	8006(3)	9670(4)	43(2)	1

Table 13 (con't)

C(50)	3804(4)	7515(3)	9673(4)	40(2)	1
C(51)	3650(4)	6100(3)	10815(4)	34(2)	1
C(52)	4313(4)	6115(3)	11418(5)	41(2)	1
C(53)	4411(4)	5892(3)	12278(5)	49(2)	1
C(54)	3810(5)	5641(3)	12547(5)	59(2)	1
Cl(6)	3913(2)	5331(1)	13626(1)	101(1)	1
C(55)	3128(5)	5621(3)	11975(5)	60(2)	1
C(56)	3057(4)	5846(3)	11121(5)	47(2)	1
Cl(7)	-1886(1)	7374(1)	9774(1)	44(1)	1
O(9)	-2069(3)	7040(2)	8955(3)	69(2)	1
O(10)	-2543(3)	7620(2)	9978(3)	63(2)	1
O(11)	-1548(3)	7012(2)	10519(3)	69(2)	1
O(12)	-1383(2)	7824(2)	9618(3)	62(1)	1

Table 14. Anisotropic Thermal Parameters ($Å^2 \times 10^3$) for {bpyVO[μ–(*p*-$ClC_6H_4)_2PO_2]_{1.5}$}$_2${ClO4}, (**4.5**).

Atom	U_{11}	U_{22}	U_{33}	U_{23}	U_{13}	U_{12}
V(1)	32(1)	25(1)	33(1)	-1(1)	7(1)	1(1)
O(1)	34(3)	34(3)	45(3)	-7(2)	11(2)	-2(2)
O(2)	29(2)	29(2)	30(2)	0(2)	7(2)	4(2)
O(3)	38(3)	26(2)	30(2)	1(2)	6(2)	0(2)
O(4)	35(3)	23(2)	38(3)	-4(2)	8(2)	-4(2)
V(2)	37(1)	26(1)	33(1)	0(1)	7(1)	2(1)
O(5)	52(3)	26(3)	46(3)	0(2)	14(2)	0(2)
O(6)	37(3)	23(2)	41(3)	0(2)	9(2)	1(2)
O(7)	36(3)	34(3)	35(3)	-1(2)	16(2)	1(2)
O(8)	36(3)	38(3)	34(3)	-2(2)	3(2)	-1(2)
N(1)	28(3)	25(3)	33(3)	3(2)	5(2)	0(2)
C(1)	28(4)	32(4)	35(4)	-7(3)	-5(3)	1(3)
C(2)	46(5)	47(5)	29(4)	-3(3)	-1(3)	1(4)
C(3)	39(4)	36(4)	53(5)	16(4)	4(4)	3(3)
C(4)	37(4)	35(4)	46(5)	8(4)	6(4)	6(3)
C(5)	26(4)	21(4)	44(4)	11(3)	7(3)	7(3)
C(6)	25(4)	32(4)	34(4)	1(3)	9(3)	-3(3)
C(7)	37(4)	28(4)	44(5)	3(3)	13(3)	7(3)
C(8)	54(5)	33(4)	56(5)	-10(4)	16(4)	-10(3)
C(9)	59(5)	30(4)	52(5)	-16(4)	8(4)	-8(4)
C(10)	53(5)	32(4)	40(5)	3(3)	4(4)	4(3)
N(2)	35(3)	29(3)	32(3)	1(3)	6(3)	1(2)
N(3)	50(4)	23(3)	38(4)	0(3)	13(3)	7(3)
C(11)	63(5)	22(4)	39(5)	0(3)	13(4)	9(3)
C(12)	98(7)	31(4)	33(5)	-2(3)	15(5)	16(4)
C(13)	88(7)	43(5)	50(6)	13(4)	39(5)	29(4)
C(14)	64(5)	43(5)	47(5)	1(4)	22(4)	14(4)
C(15)	46(5)	21(4)	38(4)	6(3)	17(4)	12(3)
C(16)	46(5)	21(4)	45(5)	3(3)	13(4)	-1(3)
C(17)	41(5)	48(5)	50(5)	5(4)	14(4)	7(3)
C(18)	42(5)	44(5)	64(6)	14(4)	4(4)	5(4)
C(19)	47(5)	54(5)	39(5)	7(4)	-5(4)	-5(4)
C(20)	44(5)	33(4)	33(4)	-3(3)	4(3)	-3(3)
N(4)	39(3)	22(3)	34(4)	5(2)	7(3)	6(2)

Table 14 (con't)

P(1)	32(1)	27(1)	32(1)	-3(1)	7(1)	0(1)
C(21)	29(4)	19(4)	43(4)	-1(3)	10(3)	6(3)
C(22)	55(5)	37(4)	60(5)	8(4)	30(4)	10(4)
C(23)	65(5)	37(4)	58(5)	13(4)	33(4)	9(4)
C(24)	49(5)	28(4)	50(5)	-8(3)	24(4)	-7(3)
Cl(1)	108(2)	57(1)	69(2)	6(1)	56(1)	-10(1)
C(25)	33(4)	38(4)	53(5)	-14(4)	14(4)	-2(3)
C(26)	37(4)	31(4)	29(4)	-3(3)	1(3)	0(3)
C(27)	27(4)	45(5)	33(4)	-15(3)	-1(3)	1(3)
C(28)	37(5)	51(5)	68(6)	-11(4)	5(4)	-7(4)
C(29)	56(6)	58(6)	95(8)	-42(6)	18(5)	-14(4)
C(30)	22(5)	127(10)	94(8)	-75(8)	-8(5)	3(5)
C(31)	55(6)	133(10)	52(6)	-27(6)	-12(4)	30(6)
C(32)	49(5)	66(6)	46(5)	-12(4)	-14(4)	20(4)
P(2)	37(1)	29(1)	31(1)	0(1)	9(1)	-2(1)
Cl(2)	60(2)	198(3)	156(3)	-140(3)	-12(2)	11(2)
C(33)	36(4)	23(4)	42(4)	1(3)	9(3)	2(3)
C(34)	161(9)	39(5)	34(5)	3(4)	-22(5)	28(5)
C(35)	197(11)	40(6)	54(6)	-18(5)	-15(6)	37(6)
C(36)	67(5)	41(5)	36(5)	2(4)	10(4)	0(4)
Cl(3)	103(2)	79(2)	30(1)	4(1)	-6(1)	-10(1)
C(37)	IO5(7)	40(5)	45(5)	19(4)	-18(4)	-22(4)
C(38)	108(7)	25(4)	41(5)	-1(4)	-18(4)	-17(4)
C(39)	29(4)	40(4)	27(4)	9(3)	3(3)	-6(3)
C(40)	39(4)	50(5)	37(4)	11(3)	8(3)	-5(4)
C(41)	35(4)	72(6)	34(4)	15(4)	6(3)	2(4)
C(42)	48(5)	53(5)	38(5)	9(4)	1(4)	-17(4)
C1(4)	55(1)	83(2)	74(2)	18(1)	4(1)	-31(1)
C(43)	60(5)	40(5)	45(5)	4(3)	11(4)	-13(4)
C(44)	41(4)	38(4)	34(4)	4(3)	5(3)	-5(3)
P(3)	36(1)	31(1)	31(1)	-4(1)	3(1)	-2(1)
C(45)	42(4)	35(4)	18(4)	4(3)	-1(3)	-4(3)
C(46)	48(5)	27(4)	51(5)	0(3)	10(4)	4(3)
C(47)	46(5)	38(5)	57(5)	6(4)	11(4)	-10(4)
C(48)	72(6)	29(5)	45(5)	1(3)	3(4)	-19(4)
Cl(5)	81(2)	41(1)	85(2)	7(1)	3(1)	-27(1)
C(49)	60(5)	19(4)	50(5)	3(3)	7(4)	-2(4)

Table 14 (con't)

C(50)	44(4)	36(4)	40(4)	3(3)	4(3)	3(3)
C(51)	38(4)	25(4)	38(4)	-6(3)	8(3)	6(3)
C(52)	52(5)	31(4)	41(5)	-5(3)	10(4)	-2(3)
C(53)	61(5)	43(5)	38(5)	-2(4)	-5(4)	-1(4)
C(54)	89(7)	48(5)	39(5)	3(4)	8(5)	2(5)
Cl(6)	150(2)	102(2)	46(1)	26(1)	5(1)	-29(2)
C(55)	67(6)	69(6)	46(5)	-1(4)	14(4)	-19(4)
C(56)	49(5)	5O(5)	40(5)	-1(4)	5(4)	-8(4)
Cl(7)	41(1)	37(1)	53(1)	9(1)	8(1)	-1(1)
O(9)	93(4)	59(4)	58(4)	-11(3)	20(3)	-5(3)
O(10)	57(3)	39(3)	100(4)	10(3)	35(3)	8(3)
O(11)	63(4)	74(4)	69(4)	34(3)	9(3)	11(3)
O(12)	50(3)	51(3)	81(4)	23(3)	3(3)	-19(3)

Table 15. Atomic Coordinates (× 10^4) and Equivalent Isotropic Thermal Parameters ($Å^2$ × 10^2) for {bpyVO[μ–(p-$CH_3OC_6H_4$)$_2PO_2$]$_{1.5}$}$_2${ClO4}, (**4.6**).

Atom	x	y	z	U_{eq}	Occupancy
V(1)	1634(1)	7380(1)	1367(1)	29(1)	1
O(1)	920(3)	7072(3)	908(2)	44(1)	1
N(1)	798(4)	8925(3)	1077(2)	34(1)	1
C(1)	-190(5)	9440(5)	1439(3)	45(2)	1
C(2)	-630(6)	10463(5)	1278(3)	54(2)	1
C(3)	-47(6)	10962(5)	721(4)	59(2)	1
C(4)	962(6)	10441(5)	325(4)	56(2)	1
C(5)	1372(5)	9419(4)	521(3)	38(1)	1
C(6)	2422(5)	8794(4)	132(3)	35(1)	1
C(7)	3086(5)	9174(5)	-469(3)	48(2)	1
C(8)	4032(5)	8538(5)	-816(3)	51(2)	1
C(9)	4306(5)	7536(5)	-551(3)	49(2)	1
C(10)	3604(5)	7199(4)	45(3)	38(1)	1
N(2)	2692(4)	7813(3)	391(2)	30(1)	1
V(2)	3157(1)	5598(1)	3656(1)	27(1)	1
O(2)	2978(3)	4709(3)	4296(2)	38(1)	1
N(3)	3130(4)	6500(3)	4391(2)	32(1)	1
C(11)	2179(5)	7109(4)	4710(3)	39(1)	1
C(12)	2220(6)	7698(5)	5175(3)	50(2)	1
C(13)	3245(7)	7662(5)	5308(3)	58(2)	1
C(14)	4246(6)	7045(5)	4983(3)	50(2)	1
C(15)	4167(5)	6462(4)	4524(3)	35(1)	1
C(16)	5177(5)	5791(4)	4131(3)	36(1)	1
C(17)	6316(5)	5695(5)	4152(3)	44(2)	1
C(18)	7180(6)	5070(5)	3757(4)	54(2)	1
C(19)	6914(5)	4535(5)	3356(4)	54(2)	1
C(20)	5773(5)	4632(4)	3358(3)	41(2)	1
N(4)	4921(4)	5260(3)	3731(2)	31(1)	1
P(1)	3277(1)	7803(1)	2425(1)	28(1)	1
O(3)	2595(3)	7991(3)	1807(2)	32(1)	1
O(4)	3565(3)	6790(2)	2892(2)	28(1)	1
C(21)	2512(5)	8732(4)	3001(3)	29(1)	1
C(22)	1320(5)	9097(4)	3072(3)	35(1)	1
C(23)	701(5)	9764(4)	3532(3)	42(2)	1

Table 15 (con't)

C(24)	1291(5)	10084(4)	3925(3)	42(2)	1
C(25)	2467(6)	9748(4)	3850(3)	44(2)	1
C(26)	3067(5)	9067(4)	3388(3)	41(2)	1
O(9)	596(4)	10744(3)	4374(2)	60(1)	1
C(27)	1160(7)	11024(6)	4828(4)	78(2)	1
C(28)	4633(5)	8003(4)	2013(3)	32(1)	1
C(29)	4775(5)	8500(4)	1289(3)	40(2)	1
C(30)	5859(6)	8551(5)	958(3)	51(2)	1
C(31)	6781(5)	8120(5)	1347(4)	50(2)	1
C(32)	6649(6)	7649(5)	2065(4)	65(2)	1
C(33)	5573(5)	7583(5)	2391(4)	53(2)	1
O(10)	7881(4)	8150(4)	1022(3)	71(2)	1
C(34)	8430(6)	7430(5)	575(4)	60(2)	1
P(2)	565(1)	6618(1)	3062(1)	29(1)	1
O(5)	645(3)	7356(3)	2351(2)	32(1)	1
O(6)	1523(3)	6316(3)	3519(2)	34(1)	1
C(35)	-734(4)	7167(4)	3637(3)	29(1)	1
C(36)	-1527(5)	8059(5)	3416(3)	55(2)	1
C(37)	-2532(6)	8454(6)	3872(4)	70(2)	1
C(38)	-2721(6)	7924(5)	4573(3)	49(2)	1
C(39)	-1963(6)	7034(5)	4807(3)	47(2)	1
C(40)	-983(5)	6672(4)	4336(3)	42(2)	1
O(11)	-3715(4)	8313(4)	5028(3)	70(2)	1
C(41)	-3726(12)	7846(11)	5841(7)	69(5)	0.516
C(41')	-4546(13)	9277(11)	4790(9)	74(6)	0.484
C(42)	381(4)	5566(4)	2856(3)	31(1)	1
C(43)	-238(5)	5690(5)	2283(3)	41(2)	1
C(44)	-480(5)	4924(5)	2139(3)	47(2)	1
C(45)	-103(5)	4007(4)	2539(3)	38(2)	1
C(46)	509(5)	3833(5)	3113(4)	50(2)	1
C(47)	740(5)	4641(4)	3263(4)	46(2)	1
O(12)	-404(4)	3281(3)	2354(3)	62(1)	1
C(48)	-98(7)	2320(5)	2790(5)	77(2)	1
P(3)	3541(1)	5094(1)	1981(1)	28(1)	1
O(7)	2782(3)	6067(2)	1626(2)	30(1)	1
O(8)	3490(3)	4911(2)	2811(2)	31(1)	1
C(49)	3183(4)	4104(4)	1780(3)	26(1)	1

Table 15 (con't)

C(50)	2600(5)	4255(4)	1192(3)	32(1)	1
C(51)	2321(5)	3497(4)	1040(3)	37(1)	1
C(52)	2645(5)	2565(4)	1470(3)	35(1)	1
C(53)	3230(5)	2391(4)	2056(3)	35(1)	1
C(54)	3499(5)	3164(4)	2206(3)	35(1)	1
O(13)	2339(4)	1857(3)	1268(2)	49(1)	1
C(55)	2680(7)	875(5)	1681(4)	62(2)	1
C(56)	4994(4)	5003(4)	1566(3)	29(1)	1
C(57)	5304(5)	5853(4)	1257(3)	38(1)	1
C(58)	6405(5)	5800(4)	943(3)	39(2)	1
C(59)	7250(5)	4895(4)	928(3)	35(1)	1
C(60)	6982(5)	4034(4)	1254(3)	39(1)	1
C(61)	5859(5)	4096(4)	1564(3)	37(1)	1
O(14)	8315(3)	4929(3)	593(2)	42(1)	1
C(62)	9190(5)	4007(5)	486(4)	47(2)	1
Cl(1)	6868(5)	1281(5)	2868(3)	99(2)	0.726
O(15)	7540(10)	861(6)	3411(5)	133(5)	0.726
O(16)	7361(10)	1856(7)	2312(6)	177(6)	0.726
O(17)	6739(16)	562(9)	2583(6)	315(10)	0.726
O(18)	5836(8)	1859(12)	3144(8)	371(12)	0.726
Cl(1')	7049(9)	1493(7)	2869(5)	58(3)	0.274
O(15')	8051(14)	741(12)	2955(11)	81(7)	0.274
O(16')	6776(14)	1587(12)	2189(6)	59(6)	0.274
O(17')	7161(21)	2360(10)	2940(9)	177(13)	0.274
O(18')	6212(17)	1286(19)	3404(8)	198(16)	0.274

Table 16. Anisotropic Thermal Parameters ($Å^2 \times 10^3$) for {bpyVO[μ–(*p*-$CH_3OC_6H_4)_2PO_2]_{1.5}\}_2\{ClO4\}$, (**4.6**).

Atom	U_{11}	U_{22}	U_{33}	U_{23}	U_{13}	U_{12}
V(1)	28(1)	33(1)	22(1)	-5(1)	-2(1)	-6(1)
O(1)	42(2)	60(3)	33(2)	-9(2)	-7(2)	-17(2)
N(1)	30(3)	42(3)	22(2)	-6(2)	-5(2)	0(2)
C(1)	39(4)	56(4)	24(3)	1(3)	-2(3)	-2(3)
C(2)	46(4)	41(4)	45(4)	-5(3)	2(3)	18(3)
C(3)	58(5)	37(4)	60(5)	-4(3)	4(4)	2(3)
C(4)	54(4)	42(4)	56(4)	-7(3)	9(3)	-7(3)
C(5)	41(3)	34(4)	28(3)	-1(3)	-3(3)	-3(3)
C(6)	35(3)	42(4)	24(3)	-5(3)	2(3)	-10(3)
C(7)	45(4)	46(4)	44(4)	-4(3)	8(3)	-13(3)
C(8)	44(4)	54(5)	44(4)	-3(3)	16(3)	-17(3)
C(9)	44(4)	60(5)	36(4)	-17(3)	11(3)	-11(3)
C(10)	40(4)	41(4)	29(3)	-12(3)	1(3)	-8(3)
N(2)	31(3)	31(3)	21(2)	-4(2)	-1(2)	-5(2)
V(2)	31(1)	28(1)	21(1)	-3(1)	-4(1)	-10(1)
O(2)	51(3)	36(2)	27(2)	1(2)	-10(2)	-16(2)
N(3)	41(3)	34(3)	20(2)	1(2)	-6(2)	-12(2)
C(11)	54(4)	38(4)	21(3)	0(3)	-7(3)	-13(3)
C(12)	72(5)	48(4)	30(4)	-16(3)	0(3)	-17(4)
C(13)	94(6)	49(4)	40(4)	-20(3)	-11(4)	-28(4)
C(14)	71(5)	49(4)	41(4)	-5(3)	-23(4)	-27(4)
C(15)	56(4)	36(3)	20(3)	5(3)	-10(3)	-26(3)
C(16)	44(4)	41(4)	23(3)	9(3)	-12(3)	-20(3)
C(17)	50(4)	56(4)	33(3)	5(3)	-19(3)	-26(3)
C(18)	37(4)	76(5)	46(4)	1(4)	-14(3)	-15(4)
C(19)	35(4)	67(5)	45(4)	-2(4)	-6(3)	-4(3)
C(20)	36(4)	43(4)	35(3)	-1(3)	-10(3)	-5(3)
N(4)	35(3)	32(3)	25(2)	1(2)	-13(2)	-7(2)
p(1)	31(1)	27(1)	25(1)	-5(1)	-1(1)	-7(1)
O(3)	34(2)	33(2)	26(2)	-7(2)	-4(2)	-7(2)
O(4)	34(2)	27(2)	22(2)	-1(2)	-6(2)	-10(2)
C(21)	36(3)	26(3)	23(3)	-2(2)	1(2)	-11(3)
C(22)	38(3)	37(3)	33(3)	-11(3)	-6(3)	-13(3)
C(23)	31(3)	44(4)	45(4)	-14(3)	4(3)	-8(3)

Table 16 (con't)

C(24)	47(4)	33(4)	39(4)	-16(3)	5(3)	-6(3)
C(25)	60(4)	43(4)	36(4)	-15(3)	-3(3)	-21(3)
C(26)	40(4)	42(4)	41(4)	-15(3)	-6(3)	-9(3)
O(9)	67(3)	51(3)	58(3)	-34(2)	3(2)	-5(2)
C(27)	93(6)	78(6)	75(5)	-57(5)	-1(5)	-20(5)
C(28)	37(3)	28(3)	30(3)	-8(3)	-1(3)	-11(3)
C(29)	52(4)	32(3)	36(3)	-4(3)	-1(3)	-16(3)
C(30)	67(5)	48(4)	39(4)	-7(3)	16(3)	-35(4)
C(31)	34(4)	42(4)	64(5)	-13(3)	15(3)	-11(3)
C(32)	35(4)	70(5)	76(5)	8(4)	-6(4)	-13(4)
C(33)	38(4)	59(5)	47(4)	13(3)	-4(3)	-11(3)
O(10)	55(3)	65(3)	90(4)	-33(3)	33(3)	-30(3)
C(34)	51(4)	64(5)	61(5)	-15(4)	10(4)	-21(4)
P(2)	26(1)	34(1)	23(1)	-7(1)	0(1)	-7(1)
O(5)	28(2)	38(2)	24(2)	-6(2)	3(2)	-6(2)
O(6)	30(2)	43(2)	28(2)	-10(2)	-3(2)	-9(2)
C(35)	30(3)	33(3)	25(3)	-8(2)	1(2)	-12(3)
C(36)	44(4)	52(4)	36(4)	5(3)	13(3)	9(3)
C(37)	56(5)	60(5)	58(5)	-4(4)	13(4)	9(4)
C(38)	50(4)	54(4)	42(4)	-22(3)	21(3)	-21(4)
C(39)	60(4)	42(4)	31(3)	-7(3)	20(3)	-23(3)
C(40)	47(4)	32(3)	37(3)	-4(3)	3(3)	-9(3)
O(11)	56(3)	67(3)	55(3)	-14(3)	28(2)	-1(3)
C(41)	61(10)	93(12)	42(9)	-27(8)	36(7)	-26(8)
C(41')	50(10)	75(12)	72(11)	-24(9)	11(8)	7(9)
C(42)	24(3)	33(3)	32(3)	-9(3)	2(2)	-5(3)
C(43)	45(4)	47(4)	34(3)	-7(3)	-3(3)	-20(3)
C(44)	54(4)	52(4)	42(4)	-15(3)	-5(3)	-23(4)
C(45)	37(3)	38(4)	45(4)	-19(3)	4(3)	-15(3)
C(46)	45(4)	35(4)	56(4)	1(3)	3(3)	-5(3)
C(47)	38(4)	40(4)	60(4)	-7(3)	-13(3)	-12(3)
C(48)	80(6)	30(4)	108(7)	5(4)	2(5)	-22(4)
P(3)	31(1)	25(1)	26(1)	-6(1)	-3(1)	-7(1)
O(7)	36(2)	26(2)	27(2)	-3(2)	-4(2)	-8(2)
O(8)	40(2)	28(2)	25(2)	-7(2)	-5(2)	-10(2)
C(49)	25(3)	22(3)	26(3)	-9(2)	0(2)	-2(2)
C(50)	34(3)	30(3)	33(3)	-7(3)	-6(3)	-9(3)

Table 16 (con't)

C(51)	47(4)	45(4)	27(3)	-7(3)	-12(3)	-17(3)
C(52)	37(3)	37(4)	34(3)	-14(3)	3(3)	-13(3)
C(53)	42(3)	27(3)	34(3)	0(3)	-7(3)	-10(3)
C(54)	47(4)	32(3)	28(3)	-6(3)	-10(3)	-13(3)
O(13)	69(3)	37(3)	51(3)	-9(2)	-17(2)	-25(2)
C(55)	86(6)	37(4)	71(5)	-14(4)	-14(4)	-24(4)
O(12)	77(4)	49(3)	64(3)	-13(2)	-6(3)	-24(3)
C(56)	31(3)	31(3)	29(3)	-10(2)	-1(2)	-11(3)
C(57)	44(4)	31(3)	38(3)	-9(3)	1(3)	-11(3)
C(58)	44(4)	30(3)	40(4)	-8(3)	7(3)	-16(3)
C(59)	29(3)	39(4)	37(3)	-13(3)	-1(3)	-10(3)
C(60)	31(3)	30(3)	48(4)	-11(3)	-3(3)	-1(3)
C(61)	40(4)	26(3)	43(4)	-8(3)	-2(3)	-11(3)
O(14)	36(2)	42(3)	45(2)	-15(2)	2(2)	-11(2)
C(62)	33(3)	51(4)	55(4)	-23(3)	1(3)	-7(3)
Cl(1)	94(3)	143(5)	47(3)	-16(2)	2(2)	-29(3)
O(15)	196(12)	71(7)	134(9)	-31(6)	-91(8)	3(7)
O(16)	223(15)	62(7)	162(10)	17(6)	52(8)	-12(7)
O(17)	709(31)	242(13)	138(11)	104(8)	-257(15)	-302(17)
O(18)	69(8)	667(35)	215(18)	-104(17)	24(7)	75(9)
Cl(1')	70(6)	54(5)	34(5)	-19(4)	2(4)	3(4)
O(15')	71(10)	78(11)	89(16)	-12(13)	-47(10)	1(7)
O(16')	54(12)	55(13)	59(8)	-19(9)	-24(7)	10(9)
O(17')	435(42)	55(9)	51(13)	-22(11)	-84(18)	-52(14)
O(18')	106(15)	516(49)	71(12)	-184(23)	69(15)	-178(25)

Table 17. Atomic Coordinates ($\times 10^4$) and Equivalent Isotropic Thermal Parameters ($Å^2 \times 10^2$) for {tmbpyVO[μ–(p-$CH_3OC_6H_4$)$_2PO_2$]$_{1.5}$}$_2${ClO4} •2CH_3COCH_3, (**4.6A**).

Atom	x	y	z	U_{eq}	Occupancy
V(1)	6097(1)	2305(1)	4149(1)	24(1)	1
V(2)	8546(1)	2480(1)	6022(1)	24(1)	1
Cl(1)	8572(2)	-37(1)	2755(1)	50(1)	1
P(1)	5828(2)	2753(1)	5584(1)	25(1)	1
P(2)	7450(2)	1585(1)	5124(1)	26(1)	1
P(3)	8759(2)	2790(1)	4580(1)	25(1)	1
O(1)	4910(4)	2065(2)	3982(2)	31(2)	1
O(2)	9730(4)	2237(2)	6188(2)	29(1)	1
O(3)	5732(4)	2582(2)	4932(2)	29(2)	1
O(4)	6926(4)	1763(2)	4515(2)	27(1)	1
O(5)	7628(4)	2667(2)	4275(2)	27(1)	1
O(6)	7751(4)	1937(2)	5621(2)	29(1)	1
O(7)	6975(4)	2832(2)	5904(2)	31(2)	1
O(8)	8912(4)	2819(2)	5277(2)	27(1)	1
O(9)	2925(6)	4401(2)	5630(3)	58(2)	1
O(10)	3091(5)	1584(2)	7087(3)	42(2)	1
O(11)	4482(5)	181(2)	6091(3)	50(2)	1
O(12)	11322(5)	383(2)	4745(3)	52(2)	1
O(13)	10213(5)	4523(2)	3468(3)	44(2)	1
O(14)	12071(5)	1488(2)	3708(3)	50(2)	1
O(15)	9517(6)	238(2)	2636(4)	78(2)	1
O(16)	8340(6)	-361(2)	2258(3)	58(2)	1
O(17)	7607(6)	252(2)	2797(4)	76(2)	1
O(18)	8823(6)	-281(2)	3328(3)	64(2)	1
N(1)	5638(5)	2897(2)	3622(3)	25(2)	1
N(2)	6683(5)	2160(2)	3279(3)	23(2)	1
N(3)	9016(5)	3063(2)	6578(3)	26(2)	1
N(4)	7967(5)	2312(2)	6878(3)	22(2)	1
C(1)	5217(7)	3284(3)	3825(4)	30(2)	1
C(2)	4829(7)	3653(3)	3451(4)	29(2)	1
C(3)	4865(7)	3596(3)	2818(4)	26(2)	1
C(4)	5341(6)	3201(3)	2609(4)	28(2)	1
C(5)	5740(7)	2861(3)	3009(4)	28(2)	1
C(6)	6338(6)	2453(3)	2823(3)	22(2)	1

Table17 (con't)

C(7)	6612(7)	2373(3)	2225(3)	26(2)	1
C(8)	7230(7)	1995(3)	2093(4)	29(2)	1
C(9)	7621(7)	1712(3)	2564(4)	29(2)	1
C(10)	7302(7)	1804(3)	3152(4)	28(2)	1
C(11)	4406(8)	4076(3)	3727(4)	44(3)	1
C(12)	4399(8)	3957(3)	2370(4)	44(3)	1
C(13)	7488(8)	1913(3)	1445(4)	43(3)	1
C(14)	8356(8)	1307(3)	2475(4)	46(3)	1
C(15)	9544(7)	3433(3)	6395(4)	27(2)	1
C(16)	9951(7)	3775(3)	6784(4)	27(2)	1
C(17)	9837(7)	3730(3)	7415(4)	28(2)	1
C(18)	9258(6)	3349(3)	7597(4)	26(2)	1
C(19)	8851(7)	3016(3)	7182(3)	23(2)	1
C(20)	8262(6)	2601(3)	7349(3)	23(2)	1
C(21)	7986(6)	2509(3)	7939(4)	26(2)	1
C(22)	7426(7)	2114(3)	8065(4)	28(2)	1
C(23)	7088(6)	1816(3)	7579(4)	21(2)	1
C(24)	7395(7)	1934(3)	7001(4)	25(2)	1
C(25)	10520(8)	4185(3)	6524(4)	43(3)	1
C(26)	10289(7)	4077(3)	7883(4)	39(2)	1
C(27)	7162(8)	2000(3)	8711(4)	41(3)	1
C(28)	6440(7)	1398(3)	7664(4)	38(2)	1
C(29)	5023(7)	3272(3)	5579(4)	26(2)	1
C(30)	5359(8)	3644(3)	5952(4)	42(3)	1
C(31)	4686(9)	4028(3)	5973(4)	46(3)	1
C(32)	3676(9)	4046(3)	5624(4)	41(3)	1
C(33)	3346(8)	3685(3)	5248(4)	35(2)	1
C(34)	3999(7)	3303(3)	5228(4)	32(2)	1
C(35)	5050(6)	2377(3)	6017(3)	23(2)	1
C(36)	5039(7)	2435(3)	6657(4)	29(2)	1
C(37)	4383(7)	2171(3)	6993(4)	31(2)	1
C(38)	3715(7)	1829(3)	6715(4)	33(2)	1
C(39)	3732(7)	1757(3)	6087(4)	34(2)	1
C(40)	4384(7)	2033(3)	5760(4)	35(2)	1
C(41)	8653(7)	1256(3)	4984(3)	22(2)	1
C(42)	8640(8)	973(3)	4468(4)	35(2)	1
C(43)	9502(8)	689(3)	4370(4)	38(2)	1

Table 17 (con't)

C(44)	10414(7)	668(3)	4797(5)	37(2)	1
C(45)	10461(8)	936(3)	5321(4)	39(3)	1
C(46)	9597(7)	1227(3)	5403(4)	35(2)	1
C(47)	6519(7)	1175(3)	5403(4)	23(2)	1
C(48)	5507(7)	1058(3)	5083(4)	33(2)	1
C(49)	4803(8)	727(3)	5283(4)	46(3)	1
C(50)	5110(8)	511(3)	5828(4)	34(2)	1
C(51)	6110(8)	612(3)	6158(4)	38(2)	1
C(52)	6798(7)	934(3)	5948(4)	32(2)	1
C(53)	9132(7)	3335(3)	4285(3)	24(2)	1
C(54)	8556(7)	3508(3)	3746(4)	35(2)	1
C(55)	8855(7)	3911(3)	3467(4)	35(2)	1
C(56)	9771(8)	4142(3)	3713(4)	34(2)	1
C(57)	10360(8)	3988(3)	4268(4)	37(2)	1
C(58)	10032(7)	3592(3)	4537(4)	29(2)	1
C(59)	9780(7)	2396(3)	4344(4)	24(2)	1
C(60)	10639(7)	2220(3)	4749(4)	35(2)	1
C(61)	11423(8)	1920(3)	4553(4)	40(3)	1
C(62)	11356(8)	1783(3)	3948(4)	36(2)	1
C(63)	10506(7)	1961(3)	3532(4)	34(2)	1
C(64)	9720(7)	2265(3)	3727(4)	31(2)	1
C(65)	3198(10)	4756(4)	6082(5)	80(4)	1
C(66)	2419(8)	1222(3)	6826(5)	57(3)	1
C(67)	3444(8)	41(3)	5776(5)	61(3)	1
C(68)	11313(9)	104(3)	4217(5)	64(3)	1
C(69)	9722(9)	4653(3)	2867(4)	55(3)	1
C(70)	12894(8)	1266(3)	4126(5)	57(3)	1
O(1S)	2940(8)	321(3)	2946(5)	116(3)	1
C(1S)	1778(10)	858(4)	2409(5)	78(4)	1
C(2S)	2268(10)	406(4)	2453(6)	98(5)	1
C(3S)	2039(13)	31(4)	2035(7)	116(6)	1
O(2S)	2817(11)	741(4)	966(7)	176(5)	1
C(4S)	2165(12)	861(5)	-65(6)	111(5)	1
C(5S)	2793(16)	587(6)	398(8)	167(8)	1
C(6S)	3496(15)	200(6)	277(8)	171(8)	1

Table 18. Anisotropic Thermal Parameters ($Å^2 \times 10^3$) for {tmbpyVO[μ–(*p*-$CH_3OC_6H_4)_2PO_2]_{1.5}\}_2\{ClO4\}\cdot 2CH_3COCH_3$, (**4.6A**).

Atom	U_{11}	U_{22}	U_{33}	U_{23}	U_{13}	U_{12}
V(1)	27(1)	31(1)	13(1)	0(1)	0(1)	-2(1)
V(2)	26(1)	34(1)	13(1)	0(1)	-1(1)	-2(1)
Cl(1)	43(2)	40(2)	66(2)	7(1)	6(1)	2(1)
P(1)	27(1)	36(1)	13(1)	-1(1)	1(1)	2(1)
P(2)	31(1)	31(1)	16(1)	0(1)	-2(1)	1(1)
P(3)	24(1)	33(1)	17(1)	1(1)	3(1)	-2(1)
O(1)	28(4)	46(4)	18(3)	5(3)	-2(3)	-6(3)
O(2)	29(3)	39(4)	17(3)	1(3)	-1(3)	-1(3)
O(3)	22(3)	53(4)	11(3)	-2(3)	0(2)	2(3)
O(4)	39(4)	25(3)	16(3)	2(3)	-2(3)	-1(3)
O(5)	25(3)	35(4)	20(3)	-2(3)	1(3)	-7(3)
O(6)	34(4)	34(4)	17(3)	-2(3)	-3(3)	-3(3)
O(7)	31(4)	44(4)	16(3)	4(3)	1(3)	-1(3)
O(8)	35(4)	40(4)	6(3)	1(3)	3(3)	-5(3)
O(9)	84(6)	42(5)	49(5)	0(4)	9(4)	17(4)
O(10)	48(4)	48(4)	30(4)	9(3)	5(3)	-11(3)
O(11)	40(4)	47(4)	65(5)	12(4)	8(4)	-9(4)
O(12)	47(4)	52(5)	58(5)	-14(4)	10(4)	13(4)
O(13)	52(4)	33(4)	45(4)	12(3)	0(3)	-12(3)
O(14)	39(4)	59(5)	52(4)	-7(4)	11(4)	16(4)
O(15)	49(5)	62(5)	124(7)	10(5)	19(5)	-15(4)
O(16)	71(5)	56(5)	43(4)	-2(4)	-7(4)	-8(4)
O(17)	47(5)	61(5)	123(7)	14(5)	23(5)	18(4)
O(18)	95(6)	58(5)	38(4)	7(4)	-2(4)	13(4)
N(1)	23(4)	28(4)	23(4)	-5(3)	5(3)	-5(3)
N(2)	18(4)	28(4)	20(4)	-1(3)	-3(3)	-1(3)
N(3)	25(4)	38(5)	14(4)	-1(3)	-2(3)	4(4)
N(4)	26(4)	24(4)	15(4)	4(3)	-3(3)	-7(3)
C(1)	26(5)	44(6)	18(5)	3(5)	-2(4)	-9(5)
C(2)	32(6)	27(5)	29(5)	7(4)	1(4)	-6(4)
C(3)	23(5)	33(6)	21(5)	-3(4)	-6(4)	-4(4)
C(4)	26(5)	47(6)	13(5)	0(4)	8(4)	-1(5)
C(5)	27(5)	42(6)	13(5)	0(4)	-5(4)	-12(4)
C(6)	22(5)	22(5)	21(5)	0(4)	4(4)	0(4)

Table 18 (con't)

C(7)	33(5)	40(6)	7(4)	0(4)	5(4)	-11(4)
C(8)	30(5)	36(6)	21(5)	-8(4)	4(4)	-2(5)
C(9)	29(5)	37(6)	20(5)	-2(4)	2(4)	-4(4)
C(10)	37(6)	20(5)	25(5)	4(4)	-9(4)	-6(4)
C(11)	50(7)	46(7)	37(6)	8(5)	3(5)	15(5)
C(12)	50(7)	37(6)	44(6)	6(5)	1(5)	3(5)
C(13)	47(6)	61(7)	24(5)	-13(5)	13(5)	-7(5)
C(14)	53(7)	47(7)	40(6)	4(5)	15(5)	4(6)
C(15)	34(6)	31(6)	17(5)	12(4)	3(4)	-4(5)
C(16)	21(5)	25(5)	33(6)	-4(4)	-4(4)	1(4)
C(17)	32(6)	24(5)	28(5)	1(4)	-3(4)	1(4)
C(18)	25(5)	34(6)	18(5)	-4(4)	-2(4)	7(4)
C(19)	23(5)	30(5)	16(5)	-4(4)	-3(4)	11(4)
C(20)	23(5)	30(6)	14(5)	8(4)	0(4)	3(4)
C(21)	26(5)	28(5)	23(5)	-6(4)	-4(4)	3(4)
C(22)	26(5)	37(6)	19(5)	2(4)	4(4)	8(4)
C(23)	23(5)	18(5)	21(5)	8(4)	1(4)	2(4)
C(24)	32(5)	25(5)	16(5)	-10(4)	-4(4)	4(4)
C(25)	63(7)	36(6)	28(6)	-8(5)	-5(5)	-13(5)
C(26)	47(6)	44(6)	27(5)	-12(5)	7(5)	-4(5)
C(27)	49(6)	51(7)	25(5)	3(5)	14(5)	11(5)
C(28)	44(6)	47(6)	22(5)	-3(5)	-1(4)	-5(5)
C(29)	36(6)	25(5)	17(5)	-1(4)	9(4)	-4(4)
C(30)	41(6)	43(7)	39(6)	6(5)	-5(5)	-6(5)
C(31)	61(8)	28(6)	50(7)	0(5)	4(6)	-6(6)
C(32)	56(7)	33(6)	37(6)	14(5)	13(6)	5(6)
C(33)	41(6)	42(6)	22(5)	-2(5)	-3(4)	3(5)
C(34)	32(6)	42(6)	22(5)	-8(4)	3(4)	0(5)
C(35)	20(5)	34(6)	13(4)	1(4)	-2(4)	5(4)
C(36)	22(5)	47(6)	17(5)	1(4)	4(4)	0(4)
C(37)	33(5)	47(6)	12(5)	-4(4)	2(4)	-2(5)
C(38)	27(6)	40(6)	34(6)	18(5)	13(5)	1(5)
C(39)	40(6)	35(6)	29(6)	-4(4)	8(5)	-16(5)
C(40)	35(6)	48(6)	21(5)	-5(5)	-2(4)	-16(5)
C(41)	26(5)	26(5)	13(5)	3(4)	2(4)	-3(4)
C(42)	43(6)	36(6)	24(5)	3(4)	-9(5)	10(5)
C(43)	42(6)	37(6)	34(6)	-14(5)	6(5)	5(5)

Table 18 (con't)

C(44)	22(6)	33(6)	55(7)	9(5)	3(5)	-3(5)
C(45)	34(6)	44(6)	35(6)	-7(5)	-24(5)	5(5)
C(46)	41(6)	36(6)	26(5)	-4(4)	-6(5)	3(5)
C(47)	24(5)	25(5)	20(5)	3(4)	-1(4)	-2(4)
C(48)	37(6)	37(6)	24(5)	9(4)	4(5)	-10(5)
C(49)	40(6)	51(7)	43(7)	7(5)	-9(5)	-3(5)
C(50)	34(6)	29(6)	42(6)	1(5)	11(5)	-2(5)
C(51)	48(7)	40(6)	26(5)	16(5)	-2(5)	1(5)
C(52)	32(6)	35(6)	30(5)	2(4)	-1(4)	-1(5)
C(53)	25(5)	36(6)	10(4)	-3(4)	2(4)	-7(4)
C(54)	36(6)	43(6)	26(5)	-1(5)	-7(4)	-18(5)
C(55)	33(6)	37(6)	33(6)	14(5)	-4(5)	-5(5)
C(56)	48(7)	19(5)	38(6)	8(4)	14(5)	9(5)
C(57)	47(6)	28(6)	38(6)	-6(5)	8(5)	-17(5)
C(58)	25(5)	37(6)	24(5)	-5(4)	-4(4)	5(4)
C(59)	35(5)	18(5)	19(5)	1(4)	7(4)	-6(4)
C(60)	32(6)	49(6)	25(5)	9(5)	3(4)	-1(5)
C(61)	36(6)	53(7)	32(6)	13(5)	4(5)	13(5)
C(62)	38(6)	30(6)	39(6)	-3(5)	12(5)	-5(5)
C(63)	23(5)	54(7)	24(5)	5(5)	-7(4)	-4(5)
C(64)	22(5)	37(6)	31(5)	0(5)	-7(4)	1(5)
C(65)	102(10)	49(8)	88(10)	-13(7)	6(8)	35(7)
C(66)	58(7)	56(7)	58(7)	5(6)	22(6)	-23(6)
C(67)	44(7)	59(8)	81(9)	-2(6)	5(6)	-20(6)
C(68)	68(8)	51(7)	75(9)	-13(6)	21(7)	23(6)
C(69)	78(8)	50(7)	39(6)	9(5)	11(6)	-2(6)
C(70)	43(7)	62(8)	67(8)	3(6)	13(6)	6(6)
O(1S)	96(8)	120(8)	134(9)	28(7)	24(7)	5(6)
C(1S)	83(10)	60(8)	83(10)	25(7)	-28(7)	4(7)
C(2S)	39(8)	163(18)	87(11)	21(12)	-14(8)	-7(9)
C(3S)	123(13)	71(10)	153(15)	-62(10)	7(11)	-15(9)
O(2S)	158(8)	173(8)	193(9)	-14(7)	-6(7)	18(7)
C(4S)	119(9)	114(8)	102(8)	17(7)	21(7)	21(7)
C(5S)	169(11)	175(11)	156(11)	-6(9)	14(9)	29(9)
C(6S)	189(11)	156(11)	164(11)	-13(8)	-2(9)	12(9)

Table 19. Atomic Coordinates (× 10^4) and Equivalent Isotropic Thermal Parameters (Å^2 × 10^2) for {HB(pz)$_3$VO[μ–(C$_6$H$_5$)$_2$PO$_2$]}$_2$•CH$_2$Cl$_2$ (**4.7**).

Atom	x	y	z	U_{eq}	Occupancy
V(1)	8389(1)	890(1)	4757(1)	16(1)	1
O(1)	7296(2)	189(2)	4027(1)	26(1)	1
N(1)	9822(2)	2048(2)	5808(1)	20(1)	1
C(1)	10787(2)	1993(2)	6302(2)	23(1)	1
C(2)	11341(3)	2890(2)	6885(2)	27(1)	1
C(3)	10644(3)	3488(2)	6716(2)	26(1)	1
N(2)	9739(2)	2979(2)	6068(1)	21(1)	1
B(1)	8669(3)	3240(3)	5631(2)	23(1)	1
N(3)	8587(2)	2335(2)	4224(1)	20(1)	1
C(4)	8562(3)	2554(2)	3427(2)	25(1)	1
C(5)	8634(3)	3590(2)	3352(2)	32(1)	1
C(6)	8705(3)	3996(2)	4156(2)	29(1)	1
N(4)	8674(2)	3237(2)	4679(2)	23(1)	1
N(5)	7303(2)	1320(2)	5474(1)	21(1)	1
C(7)	6265(2)	721(2)	5666(2)	25(1)	1
C(8)	5773(3)	1344(3)	6054(2)	30(1)	1
C(9)	6601(3)	2365(3)	6099(2)	28(1)	1
N(6)	7508(2)	2340(2)	5745(2)	22(1)	1
O(2)	8455(2)	-184(2)	5547(1)	22(1)	1
P(1)	9025(1)	-951(1)	5879(1)	17(1)	1
C(10)	7985(2)	-2263(2)	5456(2)	21(1)	1
C(11)	8279(3)	-3147(2)	5614(2)	37(1)	1
C(12)	7485(3)	-4148(3)	5267(3)	48(1)	1
C(13)	6402(3)	-4268(3)	4767(2)	45(1)	1
C(14)	6100(3)	-3402(3)	4611(2)	41(1)	1
C(15)	6888(3)	-2399(2)	4952(2)	29(1)	1
C(16)	9155(3)	-876(2)	7003(2)	22(1)	1
C(17)	8138(3)	-1056(3)	7347(2)	34(1)	1
C(18)	8224(4)	-992(3)	8218(2)	45(1)	1
C(19)	9324(4)	-753(3)	8736(2)	46(1)	1
C(20)	10340(4)	-569(3)	8407(2)	43(1)	1
C(21)	10261(3)	-631(3)	7539(2)	31(1)	1
O(3)	10249(2)	-780(2)	5699(1)	22(1)	1
V(2)	5990(1)	1511(1)	1250(1)	19(1)	1

Table 19 (con't)

O(4)	7185(2)	1367(2)	1698(1)	33(1)	1
N(7)	4355(2)	1888(2)	642(2)	24(1)	1
C(22)	3478(3)	1422(3)	-22(2)	29(1)	1
C(23)	2756(3)	2015(3)	-192(2)	41(1)	1
C(24)	3241(3)	2865(3)	409(2)	41(1)	1
N(8)	4196(2)	2779(2)	906(2)	30(1)	1
B(2)	5114(4)	3494(3)	1656(2)	34(1)	1
N(9)	6849(2)	3177(2)	1189(2)	29(1)	1
C(25)	7898(3)	3744(3)	1001(2)	38(1)	1
C(26)	8088(4)	4819(3)	1079(3)	53(1)	1
C(27)	7091(4)	4874(3)	1321(2)	48(1)	1
N(10)	6351(3)	3884(2)	1394(2)	34(1)	1
N(11)	5540(2)	1987(2)	2353(2)	24(1)	1
C(28)	5587(3)	1624(2)	3107(2)	28(1)	1
C(29)	5283(3)	2235(3)	3668(2)	36(1)	1
C(30)	5036(3)	2984(3)	3202(2)	37(1)	1
N(12)	5198(2)	2837(2)	2411(2)	29(1)	1
O(5)	3929(2)	-1186(2)	-69(1)	25(1)	1
P(2)	4044(1)	-1011(1)	866(1)	18(1)	1
C(31)	2555(3)	-1378(2)	1078(2)	23(1)	1
C(32)	2396(3)	-1340(3)	1908(2)	34(1)	1
C(33)	1253(3)	-1661(3)	2084(2)	44(1)	1
C(34)	268(3)	-2033(3)	1437(2)	45(1)	1
C(35)	417(3)	-2060(3)	609(2)	43(1)	1
C(36)	1553(3)	-1737(3)	429(2)	32(1)	1
C(37)	4660(2)	-1902(2)	1397(2)	22(1)	1
C(38)	5557(3)	-1538(2)	2111(2)	27(1)	1
C(39)	5964(3)	-2251(3)	2542(2)	35(1)	1
C(40)	5489(3)	-3314(3)	2263(2)	40(1)	1
C(41)	4610(3)	-3673(3)	1542(3)	46(1)	1
C(42)	4192(3)	-2974(3)	1108(2)	37(1)	1
O(6)	4784(2)	88(2)	1282(1)	25(1)	1
C(1SA)	1417(7)	5586(7)	1908(5)	52(2)	0.5
Cl(1A)	1113(4)	5068(5)	888(3)	130(2)	0.5
Cl(2A)	1958(10)	4802(5)	2576(4)	235(6)	0.5
C(1SB)	1288(16)	3515(8)	1918(8)	100(5)	0.5
Cl(1B)	1166(5)	4165(7)	1152(5)	202(3)	0.5
Cl(2B)	2381(17)	4278(11)	2557(8)	435(13)	0.5

Table 20. Anisotropic Thermal Parameters ($Å^2 \times 10^3$) for {$HB(pz)_3VO[\mu$-$(C_6H_5)_2PO_2]\}_2 \cdot CH_2Cl_2$, (**4.7**).

Atom	U_{11}	U_{22}	U_{33}	U_{23}	U_{13}	U_{12}
V(1)	15(1)	15(1)	18(1)	1(1)	2(1)	6(1)
O(1)	23(1)	23(1)	28(1)	-2(1)	0(1)	7(1)
N(1)	21(1)	19(1)	22(1)	0(1)	4(1)	9(1)
C(1)	19(1)	28(2)	24(1)	5(1)	5(1)	11(1)
C(2)	21(1)	32(2)	25(2)	-1(1)	-2(1)	7(1)
C(3)	26(2)	20(1)	24(2)	-2(1)	2(1)	3(1)
N(2)	23(1)	17(1)	21(1)	0(1)	3(1)	6(1)
B(1)	28(2)	18(2)	25(2)	-1(1)	4(1)	11(1)
N(3)	21(1)	17(1)	20(1)	2(1)	1(1)	8(1)
C(4)	24(2)	25(2)	20(1)	2(1)	0(1)	6(1)
C(5)	42(2)	26(2)	24(2)	8(1)	2(1)	9(1)
C(6)	38(2)	18(1)	31(2)	6(1)	3(1)	12(1)
N(4)	27(1)	18(1)	24(1)	2(1)	3(1)	10(1)
N(5)	21(1)	21(1)	24(1)	2(1)	4(1)	10(1)
C(7)	19(1)	30(2)	25(2)	5(1)	4(1)	6(1)
C(8)	22(2)	48(2)	25(2)	5(1)	9(1)	16(1)
C(9)	29(2)	41(2)	24(2)	-3(1)	4(1)	24(1)
N(6)	23(1)	23(1)	24(1)	1(1)	4(1)	14(1)
O(2)	23(1)	20(1)	26(1)	7(1)	9(1)	10(1)
P(1)	18(1)	16(1)	18(1)	3(1)	6(1)	6(1)
C(10)	22(1)	19(1)	22(1)	2(1)	8(1)	5(1)
C(11)	25(2)	24(2)	61(2)	6(2)	4(2)	9(1)
C(12)	42(2)	19(2)	86(3)	3(2)	19(2)	13(2)
C(13)	40(2)	26(2)	55(2)	-13(2)	12(2)	-4(2)
C(14)	30(2)	40(2)	39(2)	-2(2)	-3(2)	2(2)
C(15)	28(2)	27(2)	30(2)	3(1)	3(1)	8(1)
C(16)	26(2)	19(1)	21(1)	2(1)	6(1)	7(1)
C(17)	31(2)	40(2)	29(2)	5(1)	12(1)	9(1)
C(18)	56(2)	49(2)	34(2)	9(2)	26(2)	16(2)
C(19)	71(3)	45(2)	22(2)	5(2)	10(2)	20(2)
C(20)	52(2)	46(2)	26(2)	-1(2)	-6(2)	20(2)
C(21)	32(2)	35(2)	29(2)	1(1)	2(1)	16(1)
O(3)	20(1)	21(1)	26(1)	2(1)	8(1)	8(1)
V(2)	19(1)	20(1)	16(1)	-1(1)	1(1)	8(1)

Table 20 (con't)

O(4)	29(1)	44(1)	27(1)	-5(1)	-4(1)	19(1)
N(7)	26(1)	26(1)	24(1)	2(1)	5(1)	13(1)
C(22)	25(2)	40(2)	23(2)	3(1)	4(1)	14(1)
C(23)	34(2)	64(2)	32(2)	10(2)	-1(1)	29(2)
C(24)	46(2)	50(2)	44(2)	16(2)	10(2)	36(2)
N(8)	36(2)	29(1)	31(1)	6(1)	8(1)	20(1)
B(2)	48(2)	24(2)	35(2)	1(2)	9(2)	20(2)
N(9)	31(1)	23(1)	26(1)	-2(1)	3(1)	5(1)
C(25)	36(2)	35(2)	33(2)	-3(1)	5(1)	0(2)
C(26)	56(2)	33(2)	47(2)	2(2)	12(2)	-10(2)
C(27)	67(3)	21(2)	45(2)	-2(2)	10(2)	4(2)
N(10)	45(2)	20(1)	34(2)	-2(1)	6(1)	9(1)
N(11)	26(1)	23(1)	22(1)	-2(1)	2(1)	10(1)
C(28)	28(2)	31(2)	23(2)	4(1)	4(1)	9(1)
C(29)	39(2)	43(2)	21(2)	-3(1)	7(1)	10(2)
C(30)	41(2)	36(2)	31(2)	-12(1)	9(2)	13(2)
N(12)	38(2)	26(1)	26(1)	-4(1)	6(1)	15(1)
O(5)	30(1)	28(1)	18(1)	1(1)	6(1)	12(1)
P(2)	21(1)	19(1)	16(1)	2(1)	4(1)	9(1)
C(31)	26(2)	24(2)	24(2)	5(1)	5(1)	13(1)
C(32)	34(2)	51(2)	25(2)	13(1)	9(1)	22(2)
C(33)	44(2)	68(3)	35(2)	24(2)	22(2)	31(2)
C(34)	29(2)	62(2)	54(2)	27(2)	21(2)	22(2)
C(35)	24(2)	58(2)	47(2)	11(2)	2(2)	16(2)
C(36)	28(2)	43(2)	26(2)	5(1)	4(1)	15(1)
C(37)	22(1)	22(1)	25(1)	5(1)	7(1)	10(1)
C(38)	28(2)	30(2)	26(2)	0(1)	3(1)	14(1)
C(39)	34(2)	46(2)	30(2)	4(2)	-1(1)	24(2)
C(40)	43(2)	38(2)	50(2)	16(2)	6(2)	27(2)
C(41)	49(2)	25(2)	62(2)	4(2)	-4(2)	17(2)
C(42)	38(2)	25(2)	43(2)	0(1)	-9(2)	12(1)
O(6)	32(1)	20(1)	22(1)	1(1)	6(1)	9(1)
C(1SA)	44(4)	49(5)	64(5)	10(4)	23(4)	13(4)
Cl(1A)	79(2)	196(5)	92(2)	16(3)	24(2)	22(3)
Cl(2A)	440(14)	93(3)	114(4)	-9(3)	102(6)	10(6)
C(1SB)	212(16)	44(6)	76(8)	13(5)	56(9)	72(8)
Cl(1B)	90(3)	248(8)	253(9)	-44(7)	-5(4)	67(5)
Cl(2B)	810(30)	377(19)	351(17)	259(16)	440(20)	330(20)

Table 21. Atomic Coordinates ($\times 10^4$) and Equivalent Isotropic Thermal Parameters ($Å^2 \times 10^2$) for $\{HB(pz)_3VO[\mu\text{–}(p\text{-}CH_3OC_6H_4)_2PO_2]\}_2 \cdot CH_3CN$, (**4.8**).

Atom	x	y	z	U_{eq}	Occupancy
V(1)	2092(1)	1759(1)	1126(1)	19(1)	1
O(1)	2872(1)	2497(2)	816(1)	25(1)	1
O(2)	1813(1)	2653(2)	1598(1)	28(1)	1
B(1)	2219(2)	-728(3)	1599(2)	31(1)	1
N(1)	2614(1)	25(2)	2051(1)	28(1)	1
C(1)	2980(2)	-158(3)	2597(2)	34(1)	1
C(2)	3256(2)	766(3)	2803(2)	38(1)	1
C(3)	3031(2)	1513(3)	2352(1)	32(1)	1
N(2)	2646(1)	1068(2)	1896(1)	25(1)	1
N(3)	1512(1)	-337(2)	1581(1)	29(1)	1
C(4)	962(2)	-849(3)	1711(2)	40(1)	1
C(5)	454(2)	-182(3)	1608(2)	42(1)	1
C(6)	730(1)	758(3)	1406(2)	32(1)	1
N(4)	1371(1)	665(2)	1389(1)	25(1)	1
N(5)	2481(1)	-650(2)	893(1)	29(1)	1
C(7)	2744(2)	-1379(3)	495(2)	39(1)	1
C(8)	2907(2)	-903(3)	-90(2)	40(1)	1
C(9)	2727(1)	141(2)	-15(2)	29(1)	1
N(6)	2469(1)	299(2)	580(1)	24(1)	1
O(3)	1602(1)	2056(2)	292(1)	24(1)	1
P(1)	1549(1)	2088(1)	-459(1)	19(1)	1
C(10)	870(1)	2897(2)	-665(1)	23(1)	1
C(11)	238(1)	2522(3)	-597(2)	32(1)	1
C(12)	-284(2)	3186(3)	-676(2)	39(1)	1
C(13)	-191(2)	4241(3)	-824(1)	33(1)	1
C(14)	426(2)	4623(2)	-902(2)	32(1)	1
C(15)	949(1)	3946(2)	-830(2)	29(1)	1
O(4)	-737(1)	4828(2)	-891(1)	44(1)	1
C(16)	-664(2)	5935(3)	-979(2)	48(1)	1
C(17)	1370(1)	786(2)	-755(1)	21(1)	1
C(18)	1070(1)	55(2)	-346(1)	28(1)	1
C(19)	924(2)	-938(2)	-575(2)	31(1)	1
C(20)	1071(1)	-1228(2)	-1220(2)	29(1)	1
C(21)	1376(2)	-518(2)	-1634(2)	31(1)	1

Table 21 (con't)

C(22)	1518(1)	481(2)	-1398(1)	28(1)	1
O(5)	893(1)	-2224(2)	-1398(1)	42(1)	1
C(23)	1053(2)	-2565(3)	-2050(2)	56(1)	1
N(7)	0	4683(5)	2500	77(2)	1
C(24)	0	5587(5)	2500	54(1)	1
C(25)	0	6703(5)	2500	65(2)	1

Table 22. Anisotropic Thermal Parameters ($Å^2 \times 10^3$) for $\{HB(pz)_3VO[\mu\text{–}(p\text{-}CH_3OC_6H_4)_2PO_2]\}_2 \cdot CH_3CN$, (**4.8**).

Atom	U_{11}	U_{22}	U_{33}	U_{23}	U_{13}	U_{12}
V(1)	22(1)	17(1)	18(1)	0(1)	0(1)	1(1)
O(1)	22(1)	24(1)	28(1)	4(1)	0(1)	-3(1)
O(2)	34(1)	26(1)	24(1)	-1(1)	0(1)	4(1)
B(1)	37(2)	21(2)	37(2)	5(1)	0(2)	0(2)
N(1)	32(1)	24(1)	26(1)	7(1)	2(1)	4(1)
C(1)	35(2)	38(2)	28(2)	11(1)	0(1)	9(1)
C(2)	38(2)	48(2)	28(2)	2(2)	-11(1)	6(2)
C(3)	35(2)	34(2)	27(2)	-3(1)	-5(1)	0(1)
N(2)	29(1)	22(1)	25(1)	3(1)	-2(1)	4(1)
N(3)	31(1)	26(1)	30(1)	4(1)	2(1)	-5(1)
C(4)	44(2)	33(2)	43(2)	5(2)	3(2)	-15(2)
C(5)	27(2)	54(2)	46(2)	4(2)	2(1)	-14(2)
C(6)	26(2)	40(2)	30(2)	-1(1)	2(1)	-1(1)
N(4)	26(1)	26(1)	24(1)	1(1)	1(1)	0(1)
N(5)	34(1)	20(1)	33(1)	-1(1)	0(1)	3(1)
C(7)	45(2)	24(2)	48(2)	-7(2)	1(2)	9(1)
C(8)	44(2)	37(2)	40(2)	-13(2)	10(2)	6(2)
C(9)	26(2)	35(2)	27(2)	-1(1)	2(1)	0(1)
N(6)	26(1)	23(1)	25(1)	1(1)	-1(1)	0(1)
O(3)	27(1)	23(1)	21(1)	1(1)	-3(1)	2(1)
P(1)	20(1)	19(1)	19(1)	2(1)	-2(1)	-1(1)
C(10)	23(1)	26(2)	19(1)	-1(1)	-2(1)	2(1)
C(11)	28(2)	31(2)	36(2)	8(1)	-1(1)	-3(1)
C(12)	23(2)	49(2)	44(2)	7(2)	0(1)	3(1)
C(13)	31(2)	43(2)	24(2)	-2(1)	-8(1)	12(1)
C(14)	35(2)	27(2)	35(2)	0(1)	-8(1)	7(1)
C(15)	25(2)	29(2)	32(2)	1(1)	-5(1)	0(1)
O(4)	33(1)	52(2)	48(1)	1(1)	-8(1)	19(1)
C(17)	20(1)	21(1)	21(1)	1(1)	-1(1)	0(1)
C(18)	37(2)	28(2)	20(1)	-1(1)	6(1)	-3(1)
C(19)	41(2)	27(2)	26(2)	2(1)	7(1)	-8(1)
C(20)	32(2)	22(2)	32(2)	-2(1)	2(1)	-1(1)
C(21)	39(2)	32(2)	23(2)	-5(1)	9(1)	-2(1)
C(22)	32(2)	26(2)	25(2)	3(1)	6(1)	-3(1)

Table 22 (con't)

O(5)	62(2)	27(1)	37(1)	-9(1)	14(1)	-13(1)
N(7)	104(5)	72(4)	54(3)	0	-5(3)	0
C(24)	62(4)	62(4)	37(3)	0	2(3)	0
C(25)	92(5)	60(4)	43(3)	0	11(3)	0

Table 23. Atomic Coordinates (× 10^4) and Equivalent Isotropic Thermal Parameters (Å^2 × 10^2) for $\{HB(pz)_3VO[\mu\text{–}(p\text{-}F\text{–}C_6H_4)_2PO_2]\}_2 \cdot 2CH_3CN$, (**4.9**).

Atom	x	y	z	$U_{eq.}$	Occupancy
V(1)	2602(1)	3917(1)	277(1)	18(1)	1
O(1)	3492(2)	4641(1)	497(1)	28(1)	1
O(2)	687(2)	4451(1)	682(1)	23(1)	1
O(3)	1989(2)	4668(1)	-595(1)	24(1)	1
N(1)	3164(2)	2766(1)	1095(1)	22(1)	1
N(2)	3654(2)	1756(1)	1042(1)	23(1)	1
C(1)	3969(2)	1212(2)	1635(1)	28(1)	1
C(2)	3689(3)	1856(2)	2085(1)	32(1)	1
C(3)	3204(3)	2820(2)	1724(1)	27(1)	1
N(3)	4359(2)	3065(1)	-206(1)	21(1)	1
N(4)	4699(2)	2020(1)	-103(1)	22(1)	1
C(4)	5863(3)	1704(2)	-487(1)	28(1)	1
C(5)	6291(3)	2541(2)	-845(1)	33(1)	1
C(6)	5318(2)	3374(2)	-649(1)	26(1)	1
N(5)	1534(2)	2684(1)	22(1)	23(1)	1
N(6)	2233(2)	1682(1)	117(1)	24(1)	1
C(7)	1377(3)	1110(2)	-35(1)	33(1)	1
C(8)	103(3)	1740(2)	-239(1)	35(1)	1
C(9)	252(3)	2715(2)	-199(1)	25(1)	1
B(1)	3755(3)	1416(2)	374(1)	25(1)	1
P(1)	-814(1)	4604(1)	990(1)	19(1)	1
C(10)	-1343(2)	3399(2)	1188(1)	20(1)	1
C(11)	-2582(3)	3276(2)	937(1)	25(1)	1
C(12)	-2908(3)	2323(2)	1022(1)	29(1)	1
C(13)	-1990(3)	1517(2)	1362(1)	33(1)	1
C(14)	-764(3)	1601(2)	1628(1)	31(1)	1
C(15)	-448(3)	2553(2)	1540(1)	26(1)	1
F(1)	-2289(2)	572(1)	1433(1)	53(1)	1
C(16)	-748(2)	5089(2)	1730(1)	22(1)	1
C(17)	473(3)	5415(2)	1853(1)	26(1)	1
C(18)	509(3)	5833(2)	2408(1)	31(1)	1
C(19)	-667(3)	5899(2)	2835(1)	33(1)	1
C(20)	-1892(3)	5592(2)	2736(1)	37(1)	1
C(21)	-1918(3)	5180(2)	2178(1)	30(1)	1

Table 23 (con't)

F(2)	-628(2)	6290(1)	3388(1)	51(1)	1
V(2)	7436(1)	1092(1)	4661(1)	18(1)	1
O(4)	6510(2)	324(1)	4528(1)	26(1)	1
O(5)	8008(2)	528(1)	5569(1)	22(1)	1
O(6)	9351(2)	427(1)	4311(1)	21(1)	1
N(7)	6959(2)	2071(1)	3760(1)	21(1)	1
N(8)	6468(2)	3104(1)	3715(1)	21(1)	1
C(22)	6098(3)	3513(2)	3102(1)	28(1)	1
C(23)	6361(3)	2744(2)	2734(1)	29(1)	1
C(24)	6879(2)	1866(2)	3165(1)	25(1)	1
N(9)	5400(2)	3131(1)	4847(1)	23(1)	1
N(10)	5686(2)	2098(1)	5052(1)	22(1)	1
C(25)	4219(3)	3568(2)	5180(1)	31(1)	1
C(26)	3728(3)	2823(2)	5609(1)	36(1)	1
C(27)	4673(3)	1914(2)	5510(1)	29(1)	1
N(11)	8533(2)	2385(1)	4796(1)	23(1)	1
N(12)	7903(2)	3383(1)	4578(1)	24(1)	1
C(28)	8794(3)	3983(2)	4653(1)	32(1)	1
C(29)	10016(3)	3385(2)	4926(1)	35(1)	1
C(30)	9810(3)	2394(2)	5009(1)	27(1)	1
B(2)	6384(3)	3615(2)	4319(1)	24(1)	1
P(2)	10858(1)	200(1)	4012(1)	18(1)	1
C(31)	11468(2)	1363(2)	3752(1)	20(1)	1
C(32)	10609(3)	2188(2)	3368(1)	24(1)	1
C(33)	10999(3)	3121(2)	3220(1)	29(1)	1
C(34)	12253(3)	3201(2)	3468(1)	30(1)	1
C(35)	13142(3)	2405(2)	3834(1)	28(1)	1
C(36)	12742(2)	1477(2)	3979(1)	24(1)	1
F(3)	12622(2)	4120(1)	3338(1)	50(1)	1
C(37)	10768(2)	-362(2)	3304(1)	20(1)	1
C(38)	11940(3)	-521(2)	2862(1)	29(1)	1
C(39)	11891(3)	-993(2)	2334(1)	33(1)	1
C(40)	10650(3)	-1295(2)	2259(1)	32(1)	1
C(41)	9472(3)	-1159(2)	2682(1)	33(1)	1
C(42)	9534(3)	-684(2)	3209(1)	27(1)	1
F(4)	10588(2)	-1752(1)	1738(1)	50(1)	1
N(13)	4348(3)	6161(2)	2719(2)	66(1)	1

Table 23 (con't)

C(43)	3684(3)	6476(2)	3147(2)	44(1)	1
C(44)	2817(4)	6877(3)	3686(1)	62(1)	1
N(14)	5600(3)	8691(2)	2482(2)	82(1)	1
C(45)	6219(3)	8298(2)	2076(2)	50(1)	1
C(46)	7043(4)	7814(3)	1561(2)	63(1)	1

Table 24. Anisotropic Thermal Parameters ($Å^2 \times 10^3$) for $\{HB(pz)_3VO[\mu\text{–}(p\text{-}F\text{–}C_6H_4)_2PO_2]\}_2 \cdot 2CH_3CN$, (**4.9**).

Atom	U_{11}	U_{22}	U_{33}	U_{23}	U_{13}	U_{12}
V(1)	18(1)	17(1)	21(1)	-4(1)	-1(1)	-3(1)
O(1)	28(1)	23(1)	36(1)	-9(1)	-1(1)	-9(1)
O(2)	21(1)	21(1)	24(1)	-4(1)	2(1)	-3(1)
O(3)	22(1)	23(1)	22(1)	1(1)	0(1)	0(1)
N(1)	19(1)	20(1)	27(1)	-4(1)	-2(1)	-4(1)
N(2)	21(1)	18(1)	29(1)	0(1)	-6(1)	-4(1)
C(1)	23(1)	24(1)	32(2)	8(1)	-7(1)	-6(1)
C(2)	32(2)	43(2)	21(1)	2(1)	-4(1)	-10(1)
C(3)	27(2)	33(2)	23(1)	-7(1)	-3(1)	-8(1)
N(3)	20(1)	17(1)	26(1)	-4(1)	-4(1)	-4(1)
N(4)	22(1)	18(1)	27(1)	-7(1)	-4(1)	-1(1)
C(4)	21(1)	26(1)	38(2)	-14(1)	-1(1)	2(1)
C(5)	25(2)	39(2)	35(2)	-13(1)	6(1)	-6(1)
C(6)	24(1)	24(1)	30(1)	-6(1)	4(1)	-7(1)
N(5)	22(1)	23(1)	23(1)	-5(1)	-1(1)	-4(1)
N(6)	24(1)	17(1)	32(1)	-5(1)	-5(1)	-3(1)
C(7)	36(2)	23(1)	45(2)	-6(1)	-10(1)	-13(1)
C(8)	30(2)	40(2)	39(2)	-9(1)	-9(1)	-16(1)
C(9)	20(1)	31(2)	24(1)	-4(1)	-4(1)	-4(1)
B(1)	26(2)	17(1)	33(2)	-4(1)	-5(1)	-4(1)
P(1)	19(1)	18(1)	19(1)	-2(1)	1(1)	-3(1)
C(10)	20(1)	23(1)	18(1)	-4(1)	2(1)	-5(1)
C(11)	25(1)	27(1)	20(1)	-1(1)	-3(1)	-4(1)
C(12)	28(2)	37(2)	26(1)	-6(1)	-3(1)	-14(1)
C(13)	38(2)	25(1)	40(2)	-7(1)	5(1)	-16(1)
C(14)	27(2)	21(1)	40(2)	2(1)	-4(1)	-2(1)
C(15)	23(1)	28(1)	28(1)	-1(1)	-3(1)	-7(1)
F(1)	57(1)	29(1)	78(1)	-3(1)	-11(1)	-23(1)
C(16)	25(1)	17(1)	22(1)	-1(1)	-1(1)	-2(1)
C(17)	26(1)	22(1)	29(1)	-3(1)	0(1)	-5(1)
C(18)	36(2)	27(1)	34(2)	-5(1)	-9(1)	-9(1)
C(19)	44(2)	31(2)	25(2)	-12(1)	-1(1)	-5(1)
C(20)	34(2)	48(2)	32(2)	-16(1)	9(1)	-10(1)
C(21)	27(2)	36(2)	29(1)	-10(1)	4(1)	-12(1)

Table 24 (con't)

F(2)	63(1)	61(1)	39(1)	-31(1)	-1(1)	-16(1)
V(2)	16(1)	19(1)	19(1)	-5(1)	-1(1)	-3(1)
O(4)	24(1)	26(1)	30(1)	-6(1)	-2(1)	-7(1)
O(5)	21(1)	25(1)	18(1)	-3(1)	1(1)	-1(1)
O(6)	19(1)	23(1)	20(1)	-5(1)	1(1)	-2(1)
N(7)	18(1)	21(1)	24(1)	-7(1)	0(1)	-4(1)
N(8)	19(1)	20(1)	24(1)	-2(1)	-3(1)	-4(1)
C(22)	24(1)	29(1)	27(2)	5(1)	-2(1)	-6(1)
C(23)	27(2)	39(2)	18(1)	-1(1)	-3(1)	-8(1)
C(24)	22(1)	31(1)	23(1)	-9(1)	0(1)	-6(1)
N(9)	20(1)	23(1)	27(1)	-10(1)	-3(1)	-1(1)
N(10)	20(1)	24(1)	22(1)	-5(1)	-3(1)	-3(1)
C(25)	24(2)	32(2)	38(2)	-20(1)	-1(1)	2(1)
C(26)	24(2)	48(2)	36(2)	-18(1)	8(1)	-4(1)
C(27)	23(1)	38(2)	26(1)	-6(1)	5(1)	-7(1)
N(11)	20(1)	25(1)	24(1)	-7(1)	-2(1)	-3(1)
N(12)	21(1)	22(1)	31(1)	-8(1)	-2(1)	-4(1)
C(28)	30(2)	26(1)	44(2)	-16(1)	1(1)	-11(1)
C(29)	25(2)	43(2)	45(2)	-18(1)	-4(1)	-13(1)
C(30)	18(1)	36(2)	28(1)	-13(1)	-2(1)	-3(1)
B(2)	22(2)	19(2)	31(2)	-6(1)	-4(1)	-1(1)
P(2)	17(1)	21(1)	16(1)	-4(1)	0(1)	-2(1)
C(31)	18(1)	25(1)	15(1)	-6(1)	2(1)	-4(1)
C(32)	21(1)	30(1)	22(1)	-4(1)	-3(1)	-6(1)
C(33)	27(2)	27(1)	31(2)	1(1)	-3(1)	-6(1)
C(34)	32(2)	24(1)	37(2)	-4(1)	3(1)	-12(1)
C(35)	22(1)	38(2)	28(1)	-6(1)	-3(1)	-12(1)
C(36)	22(1)	27(1)	21(1)	-4(1)	-1(1)	-3(1)
F(3)	46(1)	31(1)	75(1)	4(1)	-14(1)	-20(1)
C(37)	21(1)	20(1)	19(1)	-3(1)	-2(1)	-1(1)
C(38)	25(2)	36(2)	27(1)	-10(1)	2(1)	-8(1)
C(39)	32(2)	42(2)	28(1)	-16(1)	6(1)	-6(1)
C(40)	40(2)	32(2)	24(1)	-15(1)	-5(1)	-3(1)
C(41)	31(2)	37(2)	35(2)	-11(1)	-7(1)	-10(1)
C(42)	22(1)	29(1)	29(1)	-8(1)	2(1)	-2(1)
F(4)	58(1)	64(1)	39(1)	-34(1)	-2(1)	-13(1)
N(13)	59(2)	57(2)	79(2)	-15(2)	12(2)	-7(2)

Table 24 (con't)

C(43)	36(2)	35(2)	58(2)	-2(2)	-13(2)	-3(1)
C(44)	65(2)	76(2)	43(2)	-15(2)	-14(2)	-4(2)
N(14)	51(2)	83(2)	111(3)	-31(2)	21(2)	-11(2)
C(45)	31(2)	47(2)	71(2)	-1(2)	-11(2)	-9(2)
C(46)	67(2)	71(2)	52(2)	-10(2)	-17(2)	-9(2)

Table 25. Atomic Coordinates ($\times 10^4$) and Equivalent Isotropic Thermal Parameters ($Å^2 \times 10^2$) for $\{HB(pz)_3VO[\mu\text{–}(p\text{-}CH_3C_6H_4)_2PO_2]\}_2 \cdot 2CH_3CN$, (**4.10**).

Atom	x	y	z	$U_{eq.}$	Occupancy
V(1)	8805(1)	3972(1)	4108(1)	24(1)	1
O(1)	8690(2)	4768(1)	3294(2)	28(1)	1
O(2)	9470(2)	3582(1)	3466(2)	35(1)	1
B(1)	6272(4)	3572(2)	4384(4)	36(1)	1
N(1)	5982(3)	3626(1)	2989(3)	35(1)	1
C(1)	4880(4)	3551(2)	1908(4)	46(1)	1
C(2)	5092(4)	3656(2)	893(4)	48(1)	1
C(3)	6376(3)	3801(2)	1432(3)	37(1)	1
N(2)	6917(3)	3786(1)	2699(2)	30(1)	1
N(3)	7391(3)	3134(1)	5060(3)	34(1)	1
C(4)	7508(4)	2648(2)	5783(3)	44(1)	1
C(5)	8713(4)	2417(2)	6232(4)	47(1)	1
C(6)	9304(4)	2787(2)	5741(3)	38(1)	1
N(4)	8313(3)	3226(1)	5041(2)	29(1)	1
N(5)	6698(3)	4193(1)	5010(2)	30(1)	1
C(7)	6252(3)	4553(2)	5605(3)	38(1)	1
C(8)	6996(3)	5060(2)	6017(3)	39(1)	1
C(9)	7918(3)	4976(2)	5638(3)	30(1)	1
N(6)	7741(2)	4451(1)	5025(2)	28(1)	1
O(3)	10354(2)	4206(1)	5694(2)	28(1)	1
P(1)	11315(1)	4555(1)	6822(1)	23(1)	1
C(10)	12874(3)	4272(2)	7208(3)	28(1)	1
C(11)	13041(4)	3663(2)	7095(4)	43(1)	1
C(12)	14241(4)	3431(2)	7414(4)	53(1)	1
C(13)	15297(4)	3800(2)	7855(3)	45(1)	1
C(14)	15129(3)	4409(2)	7980(4)	47(1)	1
C(15)	13935(3)	4644(2)	7660(3)	37(1)	1
C(16)	16597(4)	3545(2)	8195(4)	69(1)	1
C(17)	11083(3)	4388(1)	8162(3)	25(1)	1
C(18)	10169(3)	3983(2)	8088(3)	39(1)	1
C(19)	9985(4)	3877(2)	9130(3)	44(1)	1
C(20)	10675(4)	4179(2)	10253(3)	39(1)	1
C(21)	11593(4)	4577(2)	10329(4)	60(1)	1
C(22)	11793(4)	4679(2)	9301(3)	52(1)	1

Table 25 (con't)

C(23)	10422(4)	4085(2)	11338(4)	56(1)	1
N(7)	12599(5)	2839(2)	12582(6)	97(2)	1
C(24)	12355(5)	2722(2)	13355(6)	71(1)	1
C(25)	11978(6)	2550(3)	14316(5)	104(2)	1

Table 26. Anisotropic Thermal Parameters ($Å^2 \times 10^3$) for $\{HB(pz)_3VO[\mu\text{-}(p\text{-}CH_3C_6H_4)_2PO_2]\}_2 \cdot 2CH_3CN$, (**4.10**).

Atom	U_{11}	U_{22}	U_{33}	U_{23}	U_{13}	U_{12}
V(1)	28(1)	23(1)	20(1)	-1(1)	12(1)	-1(1)
O(1)	31(1)	27(1)	27(1)	4(1)	14(1)	0(1)
O(2)	43(2)	32(1)	35(1)	-8(1)	22(1)	-2(1)
B(1)	32(2)	41(2)	38(2)	3(2)	19(2)	-9(2)
N(1)	30(2)	37(2)	33(2)	-2(1)	12(1)	-10(1)
C(1)	34(2)	49(2)	43(2)	-6(2)	9(2)	-13(2)
C(2)	41(2)	59(3)	29(2)	-5(2)	4(2)	-8(2)
C(3)	44(2)	36(2)	24(2)	-3(2)	11(2)	-3(2)
N(2)	33(2)	28(2)	27(2)	0(1)	13(1)	-4(1)
N(3)	39(2)	28(2)	34(2)	3(1)	18(1)	-6(1)
C(4)	65(3)	32(2)	40(2)	4(2)	29(2)	-11(2)
C(5)	66(3)	31(2)	39(2)	11(2)	20(2)	1(2)
C(6)	46(2)	29(2)	32(2)	4(2)	13(2)	3(2)
N(4)	31(2)	25(2)	28(2)	2(1)	11(1)	-2(1)
N(5)	26(2)	37(2)	29(2)	4(1)	16(1)	1(1)
C(7)	33(2)	53(2)	36(2)	6(2)	22(2)	8(2)
C(8)	40(2)	46(2)	33(2)	-5(2)	19(2)	9(2)
C(9)	32(2)	29(2)	27(2)	-1(1)	13(2)	1(2)
N(6)	27(2)	32(2)	26(1)	2(1)	14(1)	-1(1)
O(3)	25(1)	32(1)	23(1)	-2(1)	8(1)	-2(1)
P(1)	24(1)	25(1)	21(1)	2(1)	11(1)	-1(1)
C(10)	28(2)	35(2)	22(2)	2(1)	12(1)	2(2)
C(11)	34(2)	37(2)	56(2)	-4(2)	19(2)	2(2)
C(12)	46(3)	50(3)	58(3)	-3(2)	22(2)	16(2)
C(13)	37(2)	70(3)	34(2)	13(2)	22(2)	15(2)
C(14)	26(2)	73(3)	41(2)	8(2)	16(2)	-4(2)
C(15)	34(2)	40(2)	36(2)	3(2)	17(2)	-4(2)
C(16)	46(3)	107(4)	63(3)	25(3)	33(2)	30(3)
C(17)	28(2)	23(2)	22(2)	1(1)	11(1)	-1(1)
C(18)	43(2)	45(2)	29(2)	-5(2)	17(2)	-14(2)
C(19)	44(2)	55(3)	41(2)	-2(2)	25(2)	-21(2)
C(20)	46(2)	47(2)	28(2)	2(2)	22(2)	-5(2)
C(21)	76(3)	76(3)	33(2)	-20(2)	30(2)	-44(3)
C(22)	63(3)	66(3)	33(2)	-9(2)	27(2)	-37(2)

Table 26 (con't)

C(23)	70(3)	69(3)	42(2)	-4(2)	37(2)	-15(2)
N(7)	87(4)	85(4)	138(5)	0(3)	69(4)	-8(3)
C(24)	52(3)	64(3)	84(4)	-17(3)	23(3)	0(2)
C(25)	99(5)	139(6)	64(4)	-11(4)	31(3)	25(4)

Table 27. Atomic Coordinates ($\times 10^4$) and Equivalent Isotropic Thermal Parameters ($Å^2 \times 10^2$) for $\{HB(pz)_3VO[\mu\text{–}(p\text{-}CH_3C_6H_4)_2PO_2]\}_2 \cdot 2CH_2Cl_2$, (**4.11**).

Atom	x	y	z	$U_{eq.}$	Occupancy
V(1)	1196(1)	3979(1)	900(1)	21(1)	1
O(1)	566(2)	3594(1)	1564(2)	35(1)	1
N(1)	3061(2)	3807(1)	2305(2)	30(1)	1
C(1)	3581(2)	3825(1)	3558(2)	39(1)	1
C(2)	4845(3)	3680(1)	4103(3)	54(1)	1
C(3)	5060(3)	3573(1)	3106(3)	52(1)	1
N(2)	3984(2)	3648(1)	2027(2)	36(1)	1
B(1)	3702(3)	3592(1)	642(3)	37(1)	1
N(3)	1502(2)	3231(1)	-18(2)	31(1)	1
C(4)	726(3)	2789(1)	-725(2)	40(1)	1
C(5)	1323(3)	2420(1)	-1202(3)	51(1)	1
C(6)	2498(3)	2654(1)	-747(3)	44(1)	1
N(4)	2608(2)	3142(1)	-26(2)	35(1)	1
N(5)	2231(2)	4470(1)	-20(2)	26(1)	1
C(7)	2054(2)	4993(1)	-631(2)	30(1)	1
C(8)	2969(2)	5081(1)	-998(2)	40(1)	1
C(9)	3711(2)	4575(1)	-579(2)	40(1)	1
N(6)	3270(2)	4212(1)	8(2)	30(1)	1
O(2)	1300(1)	4784(1)	1684(1)	27(1)	1
O(3)	-343(1)	4187(1)	-688(1)	26(1)	1
P(1)	-1295(1)	4535(1)	-1813(1)	21(1)	1
C(10)	-2826(2)	4241(1)	-2210(2)	26(1)	1
C(11)	-3860(2)	4616(1)	-2559(2)	37(1)	1
C(12)	-5023(2)	4370(1)	-2854(3)	47(1)	1
C(13)	-5186(2)	3751(1)	-2805(3)	45(1)	1
C(13A)	-6456(3)	3491(2)	-3107(4)	71(1)	1
C(14)	-4166(3)	3379(1)	-2482(3)	51(1)	1
C(15)	-2999(2)	3618(1)	-2192(3)	42(1)	1
C(16)	-1051(2)	4377(1)	-3137(2)	25(1)	1
C(17)	-62(2)	4022(1)	-3025(2)	33(1)	1
C(18)	144(3)	3934(1)	-4049(2)	41(1)	1
C(19)	-605(3)	4205(1)	-5193(3)	47(1)	1
C(19A)	-328(4)	4132(2)	-6280(3)	76(1)	1
C(20)	-1635(4)	4533(2)	-5318(3)	70(1)	1

Table 27 (con't)

C(21)	-1848(3)	4621(2)	-4308(3)	55(1)	1
C(1S)	2156(5)	6989(2)	-816(4)	96(1)	1
Cl(1)	1962(3)	7689(2)	-289(2)	88(1)	0.705
Cl(2)	2480(2)	7980(1)	2870(2)	72(1)	0.599
Cl(1A)	1949(7)	7712(4)	100(20)	178(5)	0.295
Cl(2A)	3203(4)	7023(2)	-1013(6)	130(2)	0.401

Table 28. Anisotropic Thermal Parameters ($Å^2 \times 10^3$) for $\{HB(pz)_3VO[\mu\text{-}(p\text{-}CH_3C_6H_4)_2PO_2]\}_2 \cdot 2CH_2Cl_2$, (**4.11**).

Atom	U_{11}	U_{22}	U_{33}	U_{23}	U_{13}	U_{12}
V(1)	25(1)	21(1)	18(1)	2(1)	9(1)	1(1)
O(1)	45(1)	32(1)	32(1)	7(1)	20(1)	-2(1)
N(1)	32(1)	29(1)	24(1)	1(1)	9(1)	5(1)
C(1)	43(2)	41(1)	23(1)	3(1)	8(1)	4(1)
C(2)	44(2)	66(2)	28(2)	5(1)	-2(1)	9(1)
C(3)	34(2)	60(2)	41(2)	0(1)	2(1)	16(1)
N(2)	29(1)	40(1)	31(1)	-2(1)	7(1)	11(1)
B(1)	29(1)	43(2)	37(2)	-6(1)	14(1)	8(1)
N(3)	34(1)	26(1)	26(1)	-2(1)	9(1)	5(1)
C(4)	47(2)	27(1)	35(1)	-5(1)	11(1)	-3(1)
C(5)	73(2)	29(1)	42(2)	-11(1)	20(2)	1(1)
C(6)	61(2)	31(1)	40(2)	-5(1)	25(1)	11(1)
N(4)	40(1)	29(1)	33(1)	-3(1)	15(1)	9(1)
N(5)	26(1)	31(1)	22(1)	-1(1)	12(1)	1(1)
C(7)	32(1)	34(1)	23(1)	1(1)	14(1)	-3(1)
C(8)	42(2)	46(2)	39(2)	2(1)	25(1)	-11(1)
C(9)	35(1)	54(2)	39(2)	-11(1)	24(1)	-10(1)
N(6)	24(1)	37(1)	31(1)	-7(1)	15(1)	-1(1)
O(2)	30(1)	26(1)	26(1)	-4(1)	14(1)	1(1)
O(3)	24(1)	32(1)	20(1)	1(1)	8(1)	1(1)
P(1)	20(1)	24(1)	17(1)	-2(1)	9(1)	0(1)
C(10)	24(1)	35(1)	19(1)	-2(1)	10(1)	-3(1)
C(11)	29(1)	42(1)	39(1)	-9(1)	16(1)	-1(1)
C(12)	25(1)	68(2)	49(2)	-18(1)	18(1)	0(1)
C(13)	31(1)	72(2)	36(2)	-15(1)	19(1)	-18(1)
C(13A)	43(2)	107(3)	72(2)	-30(2)	36(2)	-33(2)
C(14)	42(2)	50(2)	55(2)	3(1)	19(1)	-16(1)
C(15)	31(1)	39(1)	53(2)	7(1)	16(1)	-3(1)
C(16)	28(1)	27(1)	21(1)	-2(1)	13(1)	0(1)
C(17)	32(1)	43(1)	24(1)	2(1)	14(1)	8(1)
C(18)	39(2)	53(2)	35(2)	-1(1)	22(1)	14(1)
C(19)	64(2)	56(2)	33(2)	2(1)	32(1)	15(1)
C(19A)	106(3)	96(3)	51(2)	12(2)	58(2)	37(2)
C(20)	90(3)	96(3)	28(2)	20(2)	32(2)	56(2)

Table 28 (con't)

C(21)	62(2)	76(2)	29(1)	11(1)	24(1)	43(2)
C(1S)	111(4)	100(3)	67(3)	-6(2)	35(3)	-30(3)
Cl(1)	102(2)	81(2)	77(2)	-9(1)	41(1)	-8(1)
Cl(2)	72(1)	83(1)	80(2)	-21(1)	52(1)	-17(1)
Cl(1A)	63(4)	69(4)	387(15)	69(6)	97(7)	15(3)
Cl(2A)	88(3)	173(4)	160(5)	-51(3)	85(3)	-41(2)

Table 29. Atomic Coordinates ($\times 10^4$) and Equivalent Isotropic Thermal Parameters ($Å^2 \times 10^2$) for $\{HB(pz)_3VO[\mu\text{–}(p\text{-}NO_2C_6H_4O)_2PO_2]\}_2 \cdot 2CH_2Cl_2$, (**4.12**).

Atom	x	y	z	$U_{eq.}$	Occupancy
V(1)	8728(1)	4117(1)	3263(1)	19(1)	1
O(1)	6800(3)	3683(3)	3136(2)	30(1)	1
N(1)	11516(4)	4744(3)	3314(2)	22(1)	1
C(1)	12808(5)	5213(4)	3980(3)	22(1)	1
C(2)	14222(5)	5368(4)	3595(3)	27(1)	1
C(3)	13731(5)	4977(4)	2660(3)	25(1)	1
N(2)	12108(4)	4611(3)	2499(2)	21(1)	1
B(1)	10918(6)	4204(5)	1583(3)	26(1)	1
N(3)	8982(4)	2743(3)	2238(2)	24(1)	1
C(4)	8229(6)	1602(4)	2024(3)	31(1)	1
C(5)	8599(6)	1068(4)	1205(3)	39(1)	1
C(6)	9645(6)	1961(4)	917(3)	34(1)	1
N(4)	9863(4)	2968(3)	1549(2)	24(1)	1
N(5)	8767(4)	5106(3)	2225(2)	23(1)	1
C(7)	7985(5)	5939(4)	2077(3)	27(1)	1
C(8)	8503(6)	6438(4)	1349(3)	30(1)	1
C(9)	9633(5)	5863(4)	1062(3)	28(1)	1
N(6)	9787(4)	5068(3)	1584(2)	24(1)	1
O(2)	9055(4)	5597(2)	4228(2)	26(1)	1
O(3)	9261(3)	3209(2)	4246(2)	23(1)	1
P(1)	10380(1)	3266(1)	5105(1)	20(1)	1
O(4)	11985(3)	2885(2)	4883(2)	23(1)	1
C(10)	12060(5)	2082(4)	4095(3)	23(1)	1
C(11)	13402(5)	2382(4)	3662(3)	25(1)	1
C(12)	13576(6)	1603(4)	2900(3)	32(1)	1
C(13)	12385(6)	558(4)	2581(3)	28(1)	1
N(7)	12574(6)	-258(4)	1758(3)	41(1)	1
O(6)	11390(5)	-1032(4)	1348(2)	57(1)	1
O(7)	13935(5)	-140(3)	1533(3)	60(1)	1
C(14)	11053(6)	263(4)	3007(3)	29(1)	1
C(15)	10903(6)	1027(4)	3792(3)	28(1)	1
O(5)	9607(3)	2236(2)	5600(2)	25(1)	1
C(16)	8068(5)	2088(4)	5873(3)	22(1)	1
C(17)	8017(5)	2366(4)	6806(3)	26(1)	1

Table 29 (con't)

C(18)	6533(6)	2149(4)	7107(3)	30(1)	1
C(19)	5154(6)	1655(4)	6449(4)	31(1)	1
N(8)	3561(6)	1371(4)	6761(4)	50(1)	1
O(8)	2382(6)	833(4)	6172(4)	77(1)	1
O(9)	3522(5)	1700(4)	7597(3)	73(1)	1
C(20)	5213(6)	1394(4)	5519(3)	32(1)	1
C(21)	6709(6)	1631(4)	5219(3)	29(1)	1
C(1S)	4471(9)	-2344(7)	-104(6)	91(3)	1
Cl(1)	6304(2)	-2226(2)	-535(1)	74(1)	1
Cl(2)	3802(2)	-3618(2)	262(2)	89(1)	1

Table 30. Anisotropic Thermal Parameters ($Å^2 \times 10^3$) for $\{HB(pz)_3VO[\mu\text{-}(p\text{-}NO_2C_6H_4O)_2PO_2]\}_2 \cdot 2CH_2Cl_2$, (**4.12**).

Atom	U_{11}	U_{22}	U_{33}	U_{23}	U_{13}	U_{12}
V(1)	7(1)	23(1)	26(1)	3(1)	4(1)	2(1)
O(1)	9(2)	37(2)	44(2)	9(2)	6(1)	2(2)
N(1)	14(2)	26(2)	25(2)	3(2)	3(2)	4(2)
C(1)	15(3)	21(2)	26(2)	1(2)	2(2)	1(2)
C(2)	10(3)	24(3)	42(3)	5(2)	-2(2)	1(2)
C(3)	9(3)	27(3)	40(3)	9(2)	10(2)	3(2)
N(2)	8(2)	29(2)	25(2)	4(2)	4(2)	4(2)
B(1)	17(3)	36(3)	26(3)	2(2)	9(2)	9(3)
N(3)	16(2)	30(2)	25(2)	0(2)	4(2)	4(2)
C(4)	23(3)	22(3)	38(3)	0(2)	-2(2)	-3(2)
C(5)	34(3)	28(3)	47(3)	-8(2)	3(2)	7(3)
C(6)	28(3)	39(3)	31(3)	-6(2)	1(2)	13(3)
N(4)	16(2)	28(2)	27(2)	1(2)	4(2)	5(2)
N(5)	16(2)	28(2)	26(2)	6(2)	6(2)	7(2)
C(7)	12(3)	31(3)	38(3)	7(2)	-3(2)	7(2)
C(8)	21(3)	31(3)	36(3)	13(2)	-2(2)	6(2)
C(9)	23(3)	38(3)	23(2)	7(2)	3(2)	5(2)
N(6)	12(2)	33(2)	25(2)	5(2)	4(2)	5(2)
O(2)	22(2)	27(2)	30(2)	3(1)	8(1)	9(2)
O(3)	18(2)	24(2)	26(2)	4(1)	7(1)	5(1)
P(1)	13(1)	22(1)	27(1)	4(1)	7(1)	5(1)
O(4)	11(2)	26(2)	30(2)	0(1)	5(1)	3(1)
C(10)	16(3)	24(3)	31(2)	6(2)	7(2)	9(2)
C(11)	18(3)	23(2)	35(3)	5(2)	8(2)	3(2)
C(12)	33(3)	29(3)	38(3)	8(2)	14(2)	12(3)
C(13)	34(3)	22(3)	28(2)	0(2)	2(2)	11(2)
N(7)	65(4)	30(3)	31(2)	1(2)	13(2)	18(3)
O(6)	71(3)	51(3)	37(2)	-12(2)	-2(2)	13(2)
O(7)	73(3)	47(2)	64(3)	-1(2)	46(2)	17(2)
C(14)	19(3)	23(3)	38(3)	0(2)	-1(2)	1(2)
C(15)	16(3)	27(3)	42(3)	6(2)	8(2)	6(2)
O(5)	12(2)	27(2)	40(2)	14(1)	10(1)	6(2)
C(16)	12(3)	17(2)	37(3)	9(2)	8(2)	0(2)
C(17)	13(3)	22(2)	39(3)	8(2)	2(2)	-1(2)

Table 30 (con't)

C(18)	27(3)	26(3)	43(3)	14(2)	16(2)	9(2)
C(19)	17(3)	18(2)	63(3)	13(2)	17(2)	3(2)
N(8)	30(3)	36(3)	95(4)	27(3)	31(3)	12(3)
O(8)	23(3)	76(3)	126(4)	16(3)	22(3)	-4(3)
O(9)	45(3)	96(4)	91(3)	28(3)	45(3)	23(3)
C(20)	12(3)	22(3)	55(3)	4(2)	-3(2)	-1(2)
C(21)	22(3)	28(3)	32(3)	2(2)	2(2)	2(2)
C(1S)	63(5)	111(6)	129(7)	42(5)	49(5)	57(5)
Cl(1)	61(1)	105(1)	80(1)	45(1)	34(1)	40(1)
Cl(2)	51(1)	82(1)	120(2)	11(1)	25(1)	-12(1)

Table 31. Atomic Coordinates (× 10^4) and Equivalent Isotropic Thermal Parameters (Å^2 × 10^2) for $\{HB(pz)_3VO[\mu\text{-}(p\text{-}NO_2C_6H_4O)_2PO_2]\}_2 \cdot 2CH_3COCH_3$, (**4.13**).

Atom	x	y	z	$U_{eq.}$	Occupancy
V(1)	3760(1)	9065(1)	3212(1)	18(1)	1
O(1)	1793(2)	8613(2)	3020(1)	26(1)	1
N(1)	6610(3)	9762(2)	3347(1)	21(1)	1
C(1)	7914(3)	10261(2)	4044(2)	24(1)	1
C(2)	9385(3)	10460(2)	3707(2)	28(1)	1
C(3)	8897(3)	10054(2)	2758(2)	28(1)	1
N(2)	7230(3)	9643(2)	2540(1)	24(1)	1
B(1)	6040(4)	9159(3)	1604(2)	24(1)	1
N(3)	4023(3)	7669(2)	2088(1)	23(1)	1
C(4)	3357(3)	6477(2)	1812(2)	28(1)	1
C(5)	3859(4)	5900(2)	1001(2)	34(1)	1
C(6)	4885(3)	6815(2)	799(2)	31(1)	1
N(4)	4965(3)	7878(2)	1445(1)	24(1)	1
N(5)	3926(3)	10066(2)	2336(1)	22(1)	1
C(7)	3180(3)	10866(2)	2269(2)	26(1)	1
C(8)	3681(3)	11314(2)	1586(2)	30(1)	1
C(9)	4791(3)	10732(2)	1239(2)	29(1)	1
N(6)	4920(3)	9980(2)	1682(1)	24(1)	1
O(2)	4143(2)	8149(2)	4048(1)	22(1)	1
O(3)	4162(2)	10573(2)	4327(1)	26(1)	1
P(1)	5239(1)	8251(1)	4892(1)	19(1)	1
O(4)	4400(2)	7203(2)	5248(1)	25(1)	1
C(10)	2838(3)	7007(2)	5490(2)	22(1)	1
C(11)	1438(3)	6598(2)	4819(2)	24(1)	1
C(12)	-86(3)	6351(2)	5081(2)	26(1)	1
C(13)	-147(3)	6542(2)	6007(2)	27(1)	1
N(7)	-1784(3)	6274(2)	6275(2)	41(1)	1
O(6)	-3003(3)	5899(2)	5678(2)	61(1)	1
O(7)	-1820(3)	6450(3)	7092(2)	93(1)	1
C(14)	1250(4)	6957(2)	6686(2)	31(1)	1
C(15)	2776(3)	7197(2)	6423(2)	27(1)	1
O(5)	6847(2)	7910(1)	4638(1)	22(1)	1
C(16)	6922(3)	7006(2)	3828(2)	19(1)	1
C(17)	5809(3)	5864(2)	3509(2)	26(1)	1

Table 31 (con't)

C(18)	6040(3)	4986(2)	2752(2)	29(1)	1
C(19)	7394(3)	5278(2)	2354(2)	26(1)	1
N(8)	7709(3)	4323(2)	1586(2)	39(1)	1
O(8)	6691(3)	3324(2)	1283(2)	47(1)	1
O(9)	8990(3)	4573(2)	1297(2)	76(1)	1
C(20)	8515(3)	6423(2)	2672(2)	29(1)	1
C(21)	8257(3)	7302(2)	3411(2)	26(1)	1
C(1S)	-554(4)	1588(3)	511(3)	63(1)	1
C(2S)	595(4)	2427(3)	157(2)	38(1)	1
O(1S)	2041(3)	2846(2)	490(2)	47(1)	1
C(3S)	-153(6)	2703(4)	-616(3)	77(1)	1

Table 32. Anisotropic Thermal Parameters ($Å^2 \times 10^3$) for $\{HB(pz)_3VO[\mu\text{–}(p\text{-}NO_2C_6H_4O)_2PO_2]\}_2 \cdot 2CH_3COCH_3$, (**4.13**).

Atom	U_{11}	U_{22}	U_{33}	U_{23}	U_{13}	U_{12}
V(1)	14(1)	19(1)	21(1)	7(1)	6(1)	4(1)
O(1)	14(1)	30(1)	32(1)	11(1)	6(1)	5(1)
N(1)	20(1)	21(1)	23(1)	8(1)	9(1)	6(1)
C(1)	23(2)	19(1)	28(2)	8(1)	4(1)	5(1)
C(2)	16(1)	23(2)	42(2)	10(1)	2(1)	2(1)
C(3)	17(2)	25(2)	44(2)	13(1)	14(1)	5(1)
N(2)	18(1)	25(1)	26(1)	7(1)	10(1)	6(1)
B(1)	25(2)	26(2)	22(2)	7(1)	12(1)	6(1)
N(3)	20(1)	23(1)	24(1)	8(1)	7(1)	4(1)
C(4)	29(2)	18(1)	33(2)	7(1)	5(1)	4(1)
C(5)	38(2)	20(2)	37(2)	2(1)	5(1)	7(1)
C(6)	34(2)	30(2)	26(2)	2(1)	9(1)	13(1)
N(4)	25(1)	24(1)	21(1)	5(1)	8(1)	8(1)
N(5)	18(1)	26(1)	22(1)	8(1)	7(1)	6(1)
C(7)	18(1)	27(2)	34(2)	10(1)	2(1)	6(1)
C(8)	28(2)	27(2)	33(2)	16(1)	-3(1)	4(1)
C(9)	33(2)	28(2)	23(2)	12(1)	4(1)	2(1)
N(6)	27(1)	25(1)	19(1)	9(1)	8(1)	5(1)
O(2)	22(1)	21(1)	24(1)	10(1)	7(1)	6(1)
O(3)	28(1)	24(1)	24(1)	6(1)	10(1)	9(1)
P(1)	17(1)	18(1)	23(1)	8(1)	8(1)	7(1)
O(4)	18(1)	28(1)	38(1)	20(1)	13(1)	10(1)
C(10)	19(1)	16(1)	34(2)	14(1)	9(1)	4(1)
C(11)	24(2)	22(1)	26(1)	11(1)	5(1)	4(1)
C(12)	21(2)	21(1)	35(2)	12(1)	0(1)	3(1)
C(13)	22(2)	21(1)	40(2)	13(1)	14(1)	6(1)
N(7)	31(2)	39(2)	58(2)	24(1)	23(2)	9(1)
O(6)	21(1)	90(2)	93(2)	61(2)	16(1)	13(1)
O(7)	46(2)	152(3)	55(2)	23(2)	31(1)	1(2)
C(14)	34(2)	30(2)	28(2)	10(1)	12(1)	5(1)
C(15)	20(2)	29(2)	27(2)	11(1)	0(1)	1(1)
O(5)	17(1)	20(1)	26(1)	4(1)	7(1)	6(1)
C(16)	18(1)	20(1)	22(1)	7(1)	4(1)	9(1)
C(17)	20(1)	23(1)	36(2)	10(1)	12(1)	7(1)

Table 32 (con't)

C(18)	23(2)	20(1)	36(2)	6(1)	5(1)	3(1)
C(19)	28(2)	21(1)	27(2)	6(1)	8(1)	9(1)
N(8)	44(2)	29(2)	42(2)	7(1)	19(1)	13(1)
O(8)	55(2)	22(1)	49(1)	-1(1)	17(1)	5(1)
O(9)	70(2)	44(1)	94(2)	-4(1)	60(2)	6(1)
C(20)	31(2)	25(2)	33(2)	10(1)	16(1)	9(1)
C(21)	22(2)	19(1)	33(2)	9(1)	9(1)	3(1)
C(1S)	46(2)	50(2)	89(3)	20(2)	23(2)	10(2)
C(2S)	43(2)	37(2)	34(2)	4(1)	9(2)	21(2)
O(1S)	35(1)	58(2)	58(2)	30(1)	12(1)	14(1)
C(3S)	95(3)	95(3)	45(2)	22(2)	-2(2)	45(3)

Table 33. Atomic Coordinates ($\times 10^4$) and Equivalent Isotropic Thermal Parameters ($Å^2 \times 10^2$) for $\{HB(pz)_3VO[\mu\text{–}(p\text{-}NO_2C_6H_4O)_2PO_2]\}_2 \cdot 2C_4H_5N$, (**4.14**).

Atom	x	y	z	$U_{eq.}$	Occupancy
V(1)	4094(1)	4278(1)	3235(1)	21(1)	1
O(1)	2170(2)	3827(1)	3051(1)	31(1)	1
N(1)	6913(2)	4943(1)	3355(1)	24(1)	1
C(1)	8077(2)	5399(2)	4046(1)	26(1)	1
C(2)	9612(2)	5630(2)	3702(2)	33(1)	1
C(3)	9317(2)	5292(2)	2757(2)	34(1)	1
N(2)	7702(2)	4886(1)	2555(1)	28(1)	1
B(1)	6703(3)	4494(2)	1613(2)	31(1)	1
N(3)	4546(2)	3012(1)	2185(1)	27(1)	1
C(4)	3831(3)	1888(2)	1949(1)	35(1)	1
C(5)	4450(3)	1406(2)	1155(2)	46(1)	1
C(6)	5590(3)	2297(2)	919(1)	41(1)	1
N(4)	5633(2)	3259(1)	1537(1)	30(1)	1
N(5)	4459(2)	5318(1)	2264(1)	25(1)	1
C(7)	3784(2)	6128(2)	2143(1)	30(1)	1
C(8)	4469(3)	6625(2)	1429(2)	37(1)	1
C(9)	5599(3)	6067(2)	1117(1)	35(1)	1
N(6)	5584(2)	5278(1)	1616(1)	29(1)	1
O(2)	4347(2)	3332(1)	4159(1)	25(1)	1
O(3)	4230(2)	5648(1)	4254(1)	30(1)	1
P(1)	5303(1)	3310(1)	4999(1)	21(1)	1
O(4)	4389(2)	2231(1)	5399(1)	29(1)	1
C(10)	2775(2)	2000(2)	5632(1)	26(1)	1
C(11)	2496(2)	2074(2)	6559(1)	34(1)	1
C(12)	908(3)	1796(2)	6812(2)	40(1)	1
C(13)	-332(2)	1443(2)	6122(2)	33(1)	1
N(7)	-2024(2)	1150(2)	6386(2)	49(1)	1
O(6)	-3108(2)	845(2)	5783(2)	67(1)	1
O(7)	-2263(3)	1209(3)	7195(2)	129(1)	1
C(14)	-64(2)	1365(2)	5195(2)	31(1)	1
C(15)	1522(2)	1655(2)	4945(1)	29(1)	1
O(5)	6946(2)	3003(1)	4745(1)	25(1)	1
C(16)	7100(2)	2234(2)	3937(1)	23(1)	1
C(17)	6054(2)	1142(2)	3694(1)	28(1)	1

Table 33 (con't)

C(18)	6285(3)	413(2)	2901(1)	33(1)	1
C(19)	7571(3)	795(2)	2384(2)	37(1)	1
N(8)	7782(3)	34(2)	1525(2)	63(1)	1
O(8)	6692(3)	-828(2)	1216(2)	84(1)	1
O(9)	9069(4)	292(2)	1162(2)	118(1)	1
C(20)	8647(3)	1876(2)	2638(2)	41(1)	1
C(21)	8400(2)	2608(2)	3428(2)	33(1)	1
N(1S)	9150(3)	7960(2)	-37(2)	60(1)	1
C(1S)	8673(3)	6913(2)	-592(2)	47(1)	1
C(2S)	9417(3)	6238(2)	-268(2)	52(1)	1
C(3S)	10410(3)	6905(3)	512(2)	63(1)	1
C(4S)	10242(4)	7959(3)	635(2)	65(1)	1

Table 34. Anisotropic Thermal Parameters ($Å^2 \times 10^3$) for {$HB(pz)_3VO[\mu$–(*p*-$NO_2C_6H_4O)_2PO_2]\}_2 \cdot 2C_4H_5N$, (**4.14**).

Atom	U_{11}	U_{22}	U_{33}	U_{23}	U_{13}	U_{12}
V(1)	16(1)	26(1)	19(1)	4(1)	2(1)	6(1)
O(1)	20(1)	38(1)	32(1)	9(1)	1(1)	6(1)
N(1)	20(1)	29(1)	22(1)	5(1)	4(1)	7(1)
C(1)	24(1)	24(1)	28(1)	5(1)	-2(1)	5(1)
C(2)	21(1)	32(1)	43(1)	7(1)	-2(1)	3(1)
C(3)	19(1)	40(1)	43(1)	12(1)	9(1)	7(1)
N(2)	20(1)	38(1)	26(1)	8(1)	7(1)	9(1)
B(1)	29(1)	43(1)	22(1)	7(1)	9(1)	11(1)
N(3)	26(1)	33(1)	22(1)	4(1)	1(1)	9(1)
C(4)	42(1)	29(1)	32(1)	5(1)	-5(1)	9(1)
C(5)	71(2)	34(1)	32(1)	-4(1)	-3(1)	20(1)
C(6)	56(2)	47(1)	23(1)	0(1)	4(1)	26(1)
N(4)	33(1)	39(1)	19(1)	2(1)	4(1)	15(1)
N(5)	20(1)	32(1)	22(1)	7(1)	2(1)	6(1)
C(7)	23(1)	34(1)	32(1)	8(1)	-3(1)	9(1)
C(8)	35(1)	40(1)	38(1)	18(1)	-6(1)	7(1)
C(9)	34(1)	45(1)	26(1)	16(1)	1(1)	5(1)
N(6)	27(1)	38(1)	21(1)	8(1)	4(1)	7(1)
O(2)	23(1)	30(1)	24(1)	9(1)	3(1)	8(1)
O(3)	34(1)	34(1)	23(1)	3(1)	6(1)	12(1)
P(1)	20(1)	24(1)	22(1)	6(1)	5(1)	8(1)
O(4)	22(1)	33(1)	40(1)	18(1)	9(1)	10(1)
C(10)	21(1)	23(1)	34(1)	11(1)	5(1)	5(1)
C(11)	26(1)	42(1)	31(1)	10(1)	0(1)	1(1)
C(12)	32(1)	51(1)	31(1)	9(1)	7(1)	-1(1)
C(13)	22(1)	29(1)	45(1)	11(1)	8(1)	3(1)
N(7)	26(1)	54(1)	63(1)	19(1)	11(1)	-1(1)
O(6)	24(1)	92(2)	93(2)	57(1)	1(1)	3(1)
O(7)	40(1)	250(4)	60(2)	22(2)	20(1)	-15(2)
C(14)	27(1)	25(1)	41(1)	10(1)	-4(1)	2(1)
C(15)	32(1)	27(1)	28(1)	8(1)	2(1)	6(1)
O(5)	20(1)	26(1)	26(1)	1(1)	3(1)	7(1)
C(16)	20(1)	25(1)	26(1)	4(1)	2(1)	10(1)
C(17)	23(1)	28(1)	32(1)	5(1)	6(1)	5(1)

Table 34 (con't)

C(18)	33(1)	27(1)	36(1)	3(1)	4(1)	5(1)
C(19)	49(1)	29(1)	34(1)	5(1)	15(1)	16(1)
N(8)	98(2)	34(1)	53(1)	5(1)	39(1)	17(1)
O(8)	106(2)	57(1)	61(1)	-25(1)	20(1)	3(1)
O(9)	169(3)	43(1)	119(2)	-6(1)	115(2)	4(1)
C(20)	45(1)	30(1)	50(1)	10(1)	27(1)	12(1)
C(21)	29(1)	23(1)	44(1)	5(1)	14(1)	7(1)
N(1S)	86(2)	54(1)	49(1)	15(1)	9(1)	30(1)
C(1S)	51(2)	61(2)	32(1)	11(1)	2(1)	21(1)
C(2S)	55(2)	56(2)	52(2)	11(1)	11(1)	29(1)
C(3S)	45(2)	96(2)	62(2)	37(2)	2(1)	27(2)
C(4S)	67(2)	73(2)	37(1)	6(1)	5(1)	-6(2)

Table 35. Atomic Coordinates (× 10^4) and Equivalent Isotropic Thermal Parameters (Å^2 × 10^2) for {HB(pz)$_3$VO[μ–(*p*-$NO_2C_6H_4O)_2PO_2$]}$_2$•2C_4H_4S, (**4.15A**).

Atom	x	y	z	$U_{eq.}$	Occupancy
V(1)	3599(1)	4329(1)	3252(1)	32(1)	1
O(1)	1625(3)	3909(2)	3051(2)	50(1)	1
N(1)	6472(3)	4953(2)	3403(2)	36(1)	1
C(1)	7821(4)	5384(2)	4093(2)	40(1)	1
C(2)	9267(4)	5610(3)	3772(2)	51(1)	1
C(3)	8713(4)	5301(3)	2845(2)	53(1)	1
N(2)	7041(3)	4918(2)	2627(2)	43(1)	1
B(1)	5780(5)	4552(3)	1700(2)	49(1)	1
N(3)	3738(3)	5398(2)	2356(2)	41(1)	1
C(4)	2997(4)	6193(3)	2247(2)	52(1)	1
C(5)	3455(5)	6667(3)	1561(3)	64(1)	1
C(6)	4516(5)	6120(3)	1253(2)	61(1)	1
N(4)	4681(3)	5349(2)	1730(2)	45(1)	1
N(5)	3757(3)	3081(2)	2187(2)	42(1)	1
C(7)	2944(5)	1975(3)	1901(3)	61(1)	1
C(8)	3325(7)	1515(4)	1109(3)	82(1)	1
C(9)	4410(6)	2386(3)	922(2)	68(1)	1
N(6)	4672(3)	3330(2)	1570(2)	47(1)	1
O(2)	4049(3)	5684(2)	4300(1)	47(1)	1
O(3)	4054(2)	3361(2)	4118(1)	40(1)	1
P(1)	5242(1)	3300(1)	4927(1)	33(1)	1
O(4)	4430(3)	2218(2)	5263(2)	47(1)	1
C(10)	2898(4)	1974(2)	5502(2)	39(1)	1
C(11)	2936(4)	1967(3)	6397(2)	57(1)	1
C(12)	1443(5)	1654(4)	6645(3)	69(1)	1
C(13)	-19(4)	1375(3)	6001(2)	54(1)	1
N(7)	-1606(5)	1046(3)	6263(3)	82(1)	1
O(6)	-2894(4)	821(4)	5696(3)	125(2)	1
O(7)	-1576(6)	892(6)	7007(3)	194(3)	1
C(14)	-54(4)	1376(3)	5107(3)	52(1)	1
C(15)	1433(4)	1688(3)	4856(2)	48(1)	1
O(5)	6790(2)	2975(2)	4656(1)	39(1)	1
C(16)	6729(3)	2193(2)	3862(2)	36(1)	1
C(17)	7938(4)	2523(3)	3404(2)	47(1)	1

Table 35 (con't)

C(18)	8021(5)	1758(3)	2652(2)	58(1)	1
C(19)	6854(5)	696(3)	2368(2)	59(1)	1
N(8)	6920(7)	-121(3)	1562(3)	102(2)	1
O(8)	5828(7)	-1006(3)	1267(3)	156(2)	1
O(9)	8127(8)	126(4)	1244(4)	174(3)	1
C(20)	5645(5)	363(3)	2827(2)	58(1)	1
C(21)	5582(4)	1121(3)	3588(2)	49(1)	1
S(1)	9168(4)	7056(4)	795(3)	236(2)	1
C(1S)	10453(9)	8216(5)	657(5)	118(2)	1
C(2S)	10902(11)	7933(8)	-111(5)	142(3)	1
C(3S)	10290(13)	6737(10)	-577(4)	139(4)	1
C(4S)	9311(13)	6292(8)	-157(9)	195(6)	1

Table 36. Anisotropic Thermal Parameters ($Å^2 \times 10^3$) for $\{HB(pz)_3VO[\mu\text{–}(p\text{-}NO_2C_6H_4O)_2PO_2]\}_2 \cdot 2C_4H_4S$, (**4.15A**).

Atom	U_{11}	U_{22}	U_{33}	U_{23}	U_{13}	U_{12}
V(1)	29(1)	35(1)	31(1)	5(1)	9(1)	9(1)
O(1)	34(1)	57(1)	57(1)	12(1)	12(1)	12(1)
N(1)	33(1)	42(1)	34(1)	9(1)	12(1)	11(1)
C(1)	37(2)	34(2)	44(2)	6(1)	5(1)	8(1)
C(2)	32(2)	48(2)	65(2)	10(2)	6(1)	6(1)
C(3)	38(2)	56(2)	68(2)	16(2)	24(2)	11(2)
N(2)	37(1)	51(2)	42(1)	11(1)	18(1)	11(1)
B(1)	51(2)	61(2)	36(2)	12(2)	20(2)	14(2)
N(3)	39(1)	44(1)	38(1)	11(1)	7(1)	11(1)
C(4)	42(2)	46(2)	63(2)	15(2)	-1(2)	12(1)
C(5)	62(2)	55(2)	74(2)	32(2)	-1(2)	14(2)
C(6)	65(2)	66(2)	45(2)	27(2)	5(2)	6(2)
N(4)	49(2)	50(2)	34(1)	14(1)	9(1)	9(1)
N(5)	46(1)	41(1)	34(1)	4(1)	10(1)	11(1)
C(7)	73(2)	40(2)	60(2)	2(2)	14(2)	7(2)
C(8)	119(4)	48(2)	60(2)	-13(2)	20(2)	17(2)
C(9)	96(3)	63(2)	42(2)	-4(2)	22(2)	29(2)
N(6)	56(2)	51(2)	32(1)	2(1)	13(1)	18(1)
O(2)	55(1)	46(1)	39(1)	1(1)	16(1)	18(1)
O(3)	40(1)	44(1)	40(1)	14(1)	13(1)	13(1)
P(1)	36(1)	32(1)	35(1)	8(1)	15(1)	12(1)
O(4)	42(1)	48(1)	68(1)	30(1)	27(1)	20(1)
C(10)	39(2)	32(1)	50(2)	15(1)	18(1)	10(1)
C(11)	48(2)	68(2)	45(2)	17(2)	8(2)	-1(2)
C(12)	64(2)	83(3)	46(2)	14(2)	22(2)	-5(2)
C(13)	46(2)	44(2)	70(2)	13(2)	27(2)	5(2)
N(7)	65(2)	79(2)	102(3)	25(2)	45(2)	2(2)
O(6)	52(2)	168(4)	194(4)	117(4)	48(3)	31(2)
O(7)	92(3)	329(8)	93(3)	29(4)	50(2)	-52(4)
C(14)	40(2)	46(2)	70(2)	24(2)	8(2)	9(1)
C(15)	51(2)	48(2)	47(2)	19(1)	12(1)	12(2)
O(5)	35(1)	37(1)	42(1)	1(1)	13(1)	10(1)
C(16)	36(2)	34(1)	40(2)	6(1)	13(1)	15(1)
C(17)	52(2)	34(2)	56(2)	9(1)	28(2)	9(1)

Table 36 (con't)

C(18)	75(2)	44(2)	65(2)	14(2)	44(2)	18(2)
C(19)	85(3)	42(2)	53(2)	4(2)	32(2)	21(2)
N(8)	166(4)	53(2)	89(3)	-1(2)	82(3)	18(3)
O(8)	218(5)	73(2)	128(3)	-47(2)	104(3)	-27(3)
O(9)	257(6)	90(3)	171(4)	-21(3)	170(5)	7(3)
C(20)	65(2)	38(2)	61(2)	-3(2)	26(2)	3(2)
C(21)	46(2)	39(2)	58(2)	4(1)	25(2)	6(1)
S(1)	137(2)	284(4)	327(5)	138(4)	84(3)	69(3)
C(1S)	128(5)	78(4)	141(6)	19(4)	9(4)	40(4)
C(2S)	193(8)	151(7)	98(5)	77(5)	26(5)	49(6)
C(3S)	165(8)	213(11)	34(3)	-10(4)	-3(3)	95(8)
C(4S)	133(8)	115(6)	228(11)	-94(8)	-99(7)	51(6)

Table 37. Atomic Coordinates (× 10^4) and Equivalent Isotropic Thermal Parameters (Å^2 × 10^2) for {HB(pz)$_3$VO[μ–(*p*-NO$_2$C$_6$H$_4$O)$_2$PO$_2$]}$_2$•2C$_4$H$_4$S, (**4.15B**).

Atom	x	y	z	$U_{eq.}$	Occupancy
V(1)	3586(1)	4314(1)	3233(1)	17(1)	1
O(1)	1598(2)	3898(1)	3017(1)	27(1)	1
N(1)	6471(2)	4942(2)	3405(1)	20(1)	1
C(1)	7821(3)	5383(2)	4113(2)	23(1)	1
C(2)	9280(3)	5620(2)	3801(2)	28(1)	1
C(3)	8733(3)	5307(2)	2856(2)	29(1)	1
N(2)	7057(2)	4904(2)	2629(1)	24(1)	1
B(1)	5804(4)	4546(2)	1682(2)	27(1)	1
N(3)	3768(2)	3068(2)	2171(1)	23(1)	1
C(4)	2948(4)	1954(2)	1885(2)	35(1)	1
C(5)	3341(4)	1487(2)	1091(2)	47(1)	1
C(6)	4447(4)	2370(2)	904(2)	38(1)	1
N(4)	4692(3)	3321(2)	1556(1)	26(1)	1
N(5)	3722(2)	5393(2)	2317(1)	23(1)	1
C(7)	2963(3)	6199(2)	2192(2)	28(1)	1
C(8)	3443(3)	6690(2)	1495(2)	35(1)	1
C(9)	4530(3)	6139(2)	1204(2)	33(1)	1
N(6)	4688(2)	5354(2)	1697(1)	25(1)	1
O(2)	4026(2)	5663(1)	4288(1)	26(1)	1
O(3)	4044(2)	3335(1)	4126(1)	22(1)	1
P(1)	5265(1)	3297(1)	4954(1)	18(1)	1
O(4)	6831(2)	2973(1)	4687(1)	22(1)	1
C(10)	6766(3)	2190(2)	3889(2)	21(1)	1
C(11)	5604(3)	1118(2)	3615(2)	27(1)	1
C(12)	5666(3)	357(2)	2851(2)	34(1)	1
C(13)	6903(4)	682(2)	2398(2)	35(1)	1
N(7)	6986(4)	-141(2)	1603(2)	60(1)	1
O(6)	8258(5)	52(2)	1324(2)	93(1)	1
O(7)	5810(5)	-988(2)	1262(2)	99(1)	1
C(14)	8075(3)	1748(2)	2675(2)	33(1)	1
C(15)	7985(3)	2519(2)	3427(2)	26(1)	1
O(5)	4488(2)	2220(1)	5331(1)	26(1)	1
C(16)	2944(3)	1983(2)	5554(2)	22(1)	1
C(17)	1477(3)	1659(2)	4875(2)	27(1)	1

Table 37 (con't)

C(18)	-31(3)	1347(2)	5114(2)	28(1)	1
C(19)	-19(3)	1377(2)	6024(2)	31(1)	1
N(8)	-1628(3)	1035(2)	6270(2)	46(1)	1
O(8)	-2912(3)	766(2)	5671(2)	65(1)	1
O(9)	-1604(4)	978(4)	7057(2)	127(2)	1
C(20)	1441(4)	1707(3)	6707(2)	40(1)	1
C(21)	2956(3)	2014(2)	6469(2)	33(1)	1
S(1)	9175(2)	7077(1)	844(1)	96(1)	1
C(1S)	10449(5)	8233(3)	644(3)	69(1)	1
C(2S)	10932(7)	7988(4)	-131(3)	79(1)	1
C(3S)	10246(7)	6784(5)	-606(2)	85(2)	1
C(4S)	9251(6)	6249(4)	-127(4)	108(2)	1

Table 38. Anisotropic Thermal Parameters ($Å^2 \times 10^3$) for $\{HB(pz)_3VO[\mu\text{-}(p\text{-}NO_2C_6H_4O)_2PO_2]\}_2 \cdot 2C_4H_4S$, (**4.15B**).

Atom	U_{11}	U_{22}	U_{33}	U_{23}	U_{13}	U_{12}
V(1)	16(1)	19(1)	17(1)	2(1)	5(1)	4(1)
O(1)	19(1)	31(1)	31(1)	6(1)	7(1)	5(1)
N(1)	21(1)	23(1)	18(1)	4(1)	7(1)	6(1)
C(1)	23(1)	19(1)	24(1)	3(1)	3(1)	6(1)
C(2)	18(1)	26(1)	37(1)	5(1)	3(1)	3(1)
C(3)	22(1)	30(1)	38(1)	10(1)	14(1)	6(1)
N(2)	21(1)	28(1)	23(1)	6(1)	10(1)	6(1)
B(1)	29(1)	34(2)	19(1)	6(1)	10(1)	8(1)
N(3)	24(1)	23(1)	20(1)	2(1)	6(1)	6(1)
C(4)	43(2)	23(1)	33(1)	1(1)	10(1)	4(1)
C(5)	69(2)	27(1)	35(2)	-7(1)	12(1)	7(1)
C(6)	54(2)	36(2)	23(1)	-2(1)	12(1)	16(1)
N(4)	31(1)	29(1)	18(1)	1(1)	7(1)	10(1)
N(5)	21(1)	25(1)	22(1)	6(1)	4(1)	5(1)
C(7)	22(1)	25(1)	34(1)	6(1)	-1(1)	6(1)
C(8)	33(1)	30(1)	39(2)	16(1)	-2(1)	4(1)
C(9)	36(1)	35(1)	24(1)	14(1)	2(1)	1(1)
N(6)	27(1)	28(1)	19(1)	7(1)	6(1)	4(1)
O(2)	31(1)	25(1)	22(1)	1(1)	9(1)	8(1)
O(3)	23(1)	23(1)	23(1)	7(1)	8(1)	6(1)
P(1)	20(1)	18(1)	19(1)	4(1)	8(1)	6(1)
O(4)	20(1)	20(1)	23(1)	0(1)	7(1)	5(1)
C(10)	22(1)	19(1)	22(1)	3(1)	7(1)	9(1)
C(11)	27(1)	23(1)	31(1)	3(1)	13(1)	4(1)
C(12)	39(2)	23(1)	34(1)	0(1)	14(1)	2(1)
C(13)	53(2)	23(1)	31(1)	2(1)	21(1)	12(1)
N(7)	103(2)	30(1)	51(2)	0(1)	52(2)	10(2)
O(6)	133(3)	52(2)	102(2)	-7(2)	95(2)	11(2)
O(7)	140(3)	46(2)	78(2)	-33(1)	67(2)	-27(2)
C(14)	42(2)	27(1)	37(1)	11(1)	25(1)	11(1)
C(15)	28(1)	20(1)	31(1)	6(1)	13(1)	5(1)
O(5)	23(1)	26(1)	35(1)	15(1)	14(1)	11(1)
C(16)	24(1)	16(1)	28(1)	8(1)	10(1)	5(1)
C(17)	30(1)	26(1)	26(1)	10(1)	8(1)	6(1)

Table 38 (con't)

C(18)	26(1)	23(1)	36(1)	12(1)	5(1)	5(1)
C(19)	27(1)	23(1)	42(2)	7(1)	17(1)	2(1)
N(8)	38(2)	44(1)	57(2)	12(1)	26(1)	0(1)
O(8)	28(1)	87(2)	95(2)	58(2)	22(1)	15(1)
O(9)	53(2)	232(5)	51(2)	14(2)	29(1)	-37(2)
C(20)	40(2)	46(2)	26(1)	7(1)	14(1)	-2(1)
C(21)	28(1)	38(1)	26(1)	8(1)	5(1)	-1(1)
S(1)	63(1)	92(1)	134(1)	26(1)	34(1)	19(1)
C(1S)	77(3)	45(2)	79(3)	6(2)	7(2)	24(2)
C(2S)	123(4)	68(3)	49(2)	29(2)	10(2)	33(3)
C(3S)	112(4)	106(4)	22(2)	-8(2)	-15(2)	46(3)
C(4S)	73(3)	49(2)	140(5)	-19(3)	-65(3)	8(2)

Table 39. Atomic Coordinates ($\times 10^4$) and Equivalent Isotropic Thermal Parameters ($Å^2 \times 10^2$) for $\{HB(pz)_3VO[\mu\text{–}(p\text{-}NO_2C_6H_4O)_2PO_2]\}_2 \cdot 2C_2H_4S_2$, (**4.16A**).

Atom	x	y	z	$U_{eq.}$	Occupancy
V(1)	3536(1)	4196(1)	3305(1)	44(1)	1
O(1)	1578(3)	3731(3)	3133(2)	63(1)	1
N(1)	6357(4)	4863(3)	3405(3)	47(1)	1
C(1)	7750(5)	5326(3)	4061(3)	47(1)	1
C(2)	9132(6)	5551(4)	3729(4)	58(1)	1
C(3)	8528(6)	5193(4)	2826(4)	60(1)	1
N(2)	6861(5)	4788(3)	2631(2)	52(1)	1
B(1)	5541(7)	4345(5)	1746(4)	61(2)	1
N(3)	3579(4)	5221(3)	2436(2)	51(1)	1
C(4)	2838(6)	6024(4)	2365(4)	65(2)	1
C(5)	3231(7)	6487(5)	1703(4)	82(2)	1
C(6)	4263(7)	5923(5)	1370(4)	78(2)	1
N(4)	4459(5)	5153(3)	1809(3)	58(1)	1
N(5)	3616(5)	2863(3)	2244(2)	55(1)	1
C(7)	2852(7)	1695(4)	1978(4)	72(2)	1
C(8)	3204(8)	1182(5)	1195(4)	94(2)	1
C(9)	4212(8)	2090(5)	995(4)	83(2)	1
N(6)	4467(5)	3095(3)	1628(3)	59(1)	1
O(2)	4047(4)	5650(2)	4328(2)	56(1)	1
O(3)	4082(3)	3272(2)	4129(2)	50(1)	1
P(1)	5240(1)	3259(1)	4918(1)	44(1)	1
O(4)	4408(4)	2167(2)	5231(2)	60(1)	1
C(10)	2921(6)	1965(4)	5490(3)	48(1)	1
C(11)	3012(6)	2015(4)	6356(3)	66(1)	1
C(12)	1545(8)	1762(5)	6623(4)	77(2)	1
C(13)	86(7)	1454(4)	6005(4)	63(1)	1
N(7)	-1478(8)	1176(5)	6303(6)	104(2)	1
O(6)	-1393(11)	1040(8)	7050(6)	192(4)	1
O(7A)	-1710(140)	1710(100)	6820(90)	181(10)	0.079
O(7B)	-2774(7)	976(6)	5767(6)	145(3)	0.921
C(14)	-14(6)	1409(4)	5151(4)	64(2)	1
C(15)	1433(6)	1671(4)	4885(3)	57(1)	1
O(5)	6767(3)	2914(2)	4668(2)	49(1)	1
C(16)	6678(5)	2088(4)	3878(3)	45(1)	1

Table 39 (con't)

C(17)	7860(6)	2435(4)	3434(3)	60(1)	1
C(18)	7886(7)	1653(4)	2667(4)	77(2)	1
C(19)	6716(7)	546(4)	2360(3)	68(2)	1
N(8)	6704(9)	-289(5)	1530(4)	112(2)	1
O(8A)	7980(50)	-120(30)	1290(30)	159(11)	0.52
O(8B)	7510(60)	140(30)	1040(30)	164(11)	0.48
O(9A)	5900(50)	-1310(30)	1340(30)	122(9)	0.5
O(9B)	5380(40)	-1110(30)	1150(30)	121(8)	0.5
C(20)	5572(6)	204(4)	2807(4)	68(2)	1
C(21)	5565(6)	979(4)	3583(3)	59(1)	1
S(1S)	8622(4)	6710(3)	843(2)	215(1)	1
C(1SA)	9720(20)	7873(12)	665(13)	212(9)	0.7
C(2SA)	10071(17)	7623(13)	-339(11)	162(6)	0.7
S(2SA)	11429(13)	7211(11)	-558(10)	293(6)	0.7
C(1SB)	9430(60)	7680(20)	392(19)	220(20)	0.3
C(2SB)	9550(30)	6640(30)	-302(18)	167(14)	0.3
S(2SB)	11010(20)	6617(11)	-677(10)	141(5)	0.3

Table 40. Anisotropic Thermal Parameters ($Å^2 \times 10^3$) for $\{HB(pz)_3VO[\mu\text{–}(p\text{-}NO_2C_6H_4O)_2PO_2]\}_2 \cdot 2C_2H_4S_2$, (**4.16A**).

Atom	U_{11}	U_{22}	U_{33}	U_{23}	U_{13}	U_{12}
V(1)	40(1)	48(1)	43(1)	10(1)	14(1)	13(1)
O(1)	40(2)	72(2)	74(2)	21(2)	17(2)	14(2)
N(1)	45(2)	47(2)	44(3)	8(2)	10(2)	14(2)
C(1)	46(3)	45(3)	46(3)	13(2)	11(3)	11(2)
C(2)	38(3)	54(3)	73(4)	11(3)	16(3)	7(2)
C(3)	49(3)	67(3)	69(4)	20(3)	33(3)	15(3)
N(2)	49(3)	65(3)	44(3)	13(2)	24(2)	15(2)
B(1)	68(4)	75(4)	35(4)	11(3)	21(3)	15(4)
N(3)	44(2)	55(2)	50(3)	15(2)	8(2)	12(2)
C(4)	51(3)	65(3)	75(4)	26(3)	-1(3)	21(3)
C(5)	74(4)	79(4)	96(5)	49(4)	4(4)	20(3)
C(6)	78(4)	94(4)	61(4)	39(4)	9(3)	15(4)
N(4)	57(3)	69(3)	44(3)	18(2)	11(2)	14(2)
N(5)	60(3)	57(3)	42(3)	8(2)	15(2)	16(2)
C(7)	87(4)	50(3)	60(4)	4(3)	9(3)	10(3)
C(8)	126(6)	60(4)	67(5)	-13(3)	9(4)	26(4)
C(9)	107(5)	80(4)	48(4)	-10(3)	21(3)	32(4)
N(6)	65(3)	65(3)	35(3)	-4(2)	10(2)	21(2)
O(2)	61(2)	57(2)	46(2)	5(2)	18(2)	21(2)
O(3)	51(2)	55(2)	47(2)	17(2)	16(2)	19(2)
P(1)	48(1)	43(1)	46(1)	13(1)	22(1)	18(1)
O(4)	57(2)	57(2)	86(3)	38(2)	37(2)	26(2)
C(10)	48(3)	40(3)	59(4)	20(2)	20(3)	13(2)
C(11)	55(3)	79(4)	54(4)	23(3)	9(3)	6(3)
C(12)	80(4)	91(4)	54(4)	23(3)	29(4)	11(3)
C(13)	56(4)	50(3)	85(5)	19(3)	35(4)	11(3)
N(7)	76(4)	92(4)	155(6)	45(4)	65(4)	15(3)
O(6)	138(5)	263(10)	151(6)	64(6)	87(4)	-8(6)
O(7A)	130(40)	220(50)	230(30)	60(20)	194(19)	20(40)
O(7B)	67(4)	177(6)	259(9)	145(6)	79(4)	55(4)
C(14)	47(3)	59(3)	91(5)	37(3)	15(3)	16(3)
C(15)	60(4)	58(3)	58(4)	25(3)	18(3)	18(3)
O(5)	43(2)	48(2)	50(2)	3(2)	18(2)	14(1)
C(16)	45(3)	45(3)	49(3)	11(2)	18(2)	20(2)

Table 40 (con't)

C(17)	66(3)	44(3)	69(4)	7(3)	40(3)	13(2)
C(18)	93(4)	60(3)	83(4)	14(3)	58(4)	20(3)
C(19)	85(4)	55(3)	65(4)	4(3)	37(3)	25(3)
N(8)	158(6)	71(3)	98(5)	-2(3)	77(4)	19(4)
O(8A)	206(14)	96(15)	180(30)	-4(12)	150(17)	37(9)
O(8B)	300(30)	83(14)	109(14)	3(9)	136(17)	24(13)
O(9A)	170(20)	64(7)	110(20)	-4(8)	53(15)	13(10)
O(9B)	176(14)	79(13)	71(13)	-15(9)	39(11)	13(10)
C(20)	70(4)	43(3)	76(4)	0(3)	25(3)	5(3)
C(21)	55(3)	46(3)	68(4)	7(3)	28(3)	7(3)
S(1S)	213(3)	255(4)	184(3)	96(3)	87(3)	37(3)
C(1SA)	126(12)	143(11)	330(20)	15(12)	114(14)	11(9)
C(2SA)	108(11)	170(13)	259(18)	135(13)	60(10)	55(9)
S(2SA)	163(7)	540(17)	193(7)	74(11)	67(7)	162(10)
C(1SB)	470(70)	330(40)	130(20)	210(30)	240(40)	320(50)
C(2SB)	88(16)	200(30)	80(20)	-53(19)	-16(13)	-40(20)
S(2SB)	224(15)	129(6)	96(7)	10(5)	80(8)	98(8)

Table 41. Atomic Coordinates (× 10^4) and Equivalent Isotropic Thermal Parameters (Å^2 × 10^2) for $\{HB(pz)_3VO[\mu\text{–}(p\text{-}NO_2C_6H_4O)_2PO_2]\}_2 \cdot 2C_2H_4S_2$, **(4.16B)**.

Atom	x	y	z	$U_{eq.}$	Occupancy
V(1)	3459(1)	4130(1)	3300(1)	21(1)	1
O(1)	1483(3)	3629(2)	3125(2)	32(1)	1
N(1)	6290(3)	4843(2)	3393(2)	23(1)	1
C(1)	7705(4)	5321(3)	4054(2)	23(1)	1
C(2)	9090(4)	5548(3)	3711(2)	30(1)	1
C(3)	8442(4)	5186(3)	2803(2)	29(1)	1
N(2)	6766(3)	4774(2)	2615(2)	26(1)	1
B(1)	5416(4)	4332(3)	1721(2)	27(1)	1
N(3)	3579(3)	2795(2)	2237(2)	28(1)	1
C(4)	2856(4)	1619(3)	1985(2)	35(1)	1
C(5)	3169(5)	1100(3)	1184(2)	42(1)	1
C(6)	4130(4)	2031(3)	966(2)	37(1)	1
N(4)	4370(3)	3049(2)	1600(2)	28(1)	1
N(5)	3430(3)	5174(2)	2432(2)	23(1)	1
C(7)	2651(4)	5984(3)	2365(2)	31(1)	1
C(8)	2996(4)	6466(3)	1689(2)	37(1)	1
C(9)	4029(4)	5905(3)	1341(2)	35(1)	1
N(6)	4282(3)	5131(2)	1787(2)	27(1)	1
O(2)	3950(3)	5588(2)	4330(1)	29(1)	1
O(3)	4084(2)	3209(2)	4142(1)	25(1)	1
P(1)	5314(1)	3266(1)	4953(1)	21(1)	1
O(4)	4534(3)	2216(2)	5335(2)	29(1)	1
C(10)	3021(4)	2005(3)	5568(2)	23(1)	1
C(11)	3084(4)	2095(3)	6447(2)	33(1)	1
C(12)	1613(4)	1828(3)	6706(2)	37(1)	1
C(13)	125(4)	1468(3)	6060(2)	30(1)	1
N(7)	-1457(4)	1171(3)	6325(3)	48(1)	1
O(6)	-2750(4)	949(3)	5763(3)	77(1)	1
O(7)	-1386(4)	1129(4)	7085(2)	97(1)	1
C(14)	46(4)	1394(3)	5176(2)	31(1)	1
C(15)	1525(4)	1667(3)	4923(2)	27(1)	1
O(5)	6855(2)	2902(2)	4706(1)	24(1)	1
C(16)	6719(4)	2063(3)	3900(2)	23(1)	1
C(17)	5582(4)	931(3)	3634(2)	29(1)	1

Table 41 (con't)

C(18)	5510(4)	136(3)	2843(2)	33(1)	1
C(19)	6613(5)	502(3)	2351(2)	38(1)	1
N(8)	6505(5)	-329(3)	1496(2)	59(1)	1
O(8)	7498(5)	-22(3)	1076(3)	108(2)	1
O(9)	5414(5)	-1285(3)	1225(2)	90(1)	1
C(20)	7833(4)	2411(3)	3420(2)	31(1)	1
C(21)	7787(5)	1619(3)	2634(3)	41(1)	1
S(1)	8378(2)	6714(1)	772(1)	76(1)	1
C(1S)	9689(5)	7915(4)	508(3)	57(1)	1
C(2S)	9976(6)	7638(5)	-417(3)	74(2)	1
S(2A)	11201(4)	6687(4)	-614(1)	65(1)	0.763
S(2B)	11670(10)	7560(20)	-590(6)	115(5)	0.237

Table 42. Anisotropic Thermal Parameters ($Å^2 \times 10^3$) for $\{HB(pz)_3VO[\mu\text{-}(p\text{-}NO_2C_6H_4O)_2PO_2]\}_2 \cdot 2C_2H_4S_2$, (**4.16B**).

Atom	U_{11}	U_{22}	U_{33}	U_{23}	U_{13}	U_{12}
V(1)	17(1)	23(1)	21(1)	4(1)	7(1)	4(1)
O(1)	21(1)	36(1)	39(1)	12(1)	10(1)	6(1)
N(1)	23(1)	23(2)	22(1)	3(1)	9(1)	7(1)
C(1)	25(2)	21(2)	20(2)	2(1)	5(1)	6(1)
C(2)	20(2)	28(2)	35(2)	6(2)	7(1)	1(1)
C(3)	21(2)	29(2)	35(2)	7(2)	14(2)	4(1)
N(2)	22(1)	30(2)	26(2)	7(1)	12(1)	6(1)
B(1)	26(2)	32(2)	20(2)	4(2)	10(2)	4(2)
N(3)	27(2)	26(2)	26(2)	4(1)	7(1)	5(1)
C(4)	40(2)	25(2)	34(2)	5(2)	7(2)	5(2)
C(5)	54(2)	25(2)	34(2)	-5(2)	9(2)	7(2)
C(6)	40(2)	37(2)	27(2)	-5(2)	9(2)	11(2)
N(4)	27(1)	33(2)	20(2)	2(1)	7(1)	9(1)
N(5)	21(1)	24(2)	23(1)	6(1)	6(1)	5(1)
C(7)	23(2)	31(2)	39(2)	10(2)	6(2)	8(2)
C(8)	31(2)	36(2)	42(2)	18(2)	-1(2)	8(2)
C(9)	35(2)	38(2)	26(2)	14(2)	4(2)	5(2)
N(6)	27(1)	29(2)	23(2)	9(1)	8(1)	5(1)
O(2)	32(1)	28(1)	26(1)	4(1)	12(1)	9(1)
O(3)	26(1)	24(1)	27(1)	9(1)	11(1)	7(1)
P(1)	22(1)	20(1)	23(1)	6(1)	11(1)	7(1)
O(4)	26(1)	32(1)	40(1)	20(1)	18(1)	14(1)
C(10)	23(2)	16(2)	32(2)	9(1)	12(1)	6(1)
C(11)	28(2)	33(2)	31(2)	10(2)	6(2)	1(2)
C(12)	40(2)	37(2)	33(2)	10(2)	17(2)	3(2)
C(13)	29(2)	19(2)	45(2)	10(2)	20(2)	4(1)
N(7)	38(2)	36(2)	74(3)	18(2)	30(2)	5(2)
O(6)	31(2)	101(3)	134(3)	82(3)	36(2)	26(2)
O(7)	56(2)	146(4)	60(2)	12(2)	37(2)	-14(2)
C(14)	24(2)	26(2)	42(2)	13(2)	7(2)	6(2)
C(15)	30(2)	22(2)	31(2)	11(2)	10(2)	6(1)
O(5)	22(1)	24(1)	25(1)	2(1)	10(1)	7(1)
C(16)	21(2)	24(2)	26(2)	6(1)	7(1)	9(1)
C(17)	27(2)	25(2)	32(2)	6(2)	12(1)	4(2)

Table 42 (con't)

C(18)	37(2)	22(2)	35(2)	0(2)	12(2)	3(2)
C(19)	45(2)	27(2)	40(2)	1(2)	21(2)	11(2)
N(8)	81(3)	34(2)	52(2)	-6(2)	40(2)	4(2)
O(8)	138(3)	65(2)	90(3)	-27(2)	91(3)	-15(2)
O(9)	136(3)	35(2)	64(2)	-20(2)	56(2)	-18(2)
C(20)	31(2)	23(2)	38(2)	3(2)	18(2)	4(2)
C(21)	47(2)	32(2)	47(2)	5(2)	32(2)	8(2)
S(1)	76(1)	81(1)	58(1)	18(1)	21(1)	2(1)
C(1S)	51(3)	71(3)	53(3)	16(2)	17(2)	23(2)
C(2S)	59(3)	105(4)	62(3)	28(3)	22(2)	26(3)
S(2A)	63(2)	95(3)	46(1)	10(1)	18(1)	45(2)
S(2B)	68(5)	129(15)	117(7)	-10(6)	44(4)	9(6)

Table 43. Atomic Coordinates ($\times 10^4$) and Equivalent Isotropic Thermal Parameters ($Å^2 \times 10^2$) for 3–amidinium benzoate, (**5.1**).

Atom	x	y	z	$U_{eq.}$	Occupancy
O(1)	5823(2)	2374(2)	949(1)	43(1)	1
O(2)	7505(2)	4948(2)	592(1)	41(1)	1
N(1)	4215(2)	2360(2)	4330(1)	36(1)	1
N(2)	2179(2)	4790(2)	4550(1)	35(1)	1
C(1)	6377(2)	4083(3)	1069(1)	31(1)	1
C(2)	5641(2)	5182(3)	1864(1)	28(1)	1
C(3)	5631(2)	7184(3)	1874(1)	33(1)	1
C(4)	4900(2)	8168(3)	2593(1)	37(1)	1
C(5)	4214(2)	7177(3)	3323(1)	33(1)	1
C(6)	4273(2)	5168(3)	3333(1)	28(1)	1
C(7)	4968(2)	4181(3)	2596(1)	29(1)	1
C(8)	3537(2)	4069(3)	4101(1)	29(1)	1

Table 44. Anisotropic Thermal Parameters ($Å^2 \times 10^3$) for 3–amidinium benzoate, (**5.1**).

Atom	U_{11}	U_{22}	U_{33}	U_{23}	U_{13}	U_{12}
O(1)	46(1)	37(1)	47(1)	-12(1)	18(1)	-13(1)
O(2)	42(1)	41(1)	41(1)	-3(1)	19(1)	-8(1)
N(1)	35(1)	35(1)	39(1)	7(1)	12(1)	7(1)
N(2)	35(1)	37(1)	36(1)	5(1)	11(1)	7(1)
C(1)	29(1)	34(1)	32(1)	-3(1)	5(1)	-2(1)
C(2)	24(1)	31(1)	30(1)	0(1)	4(1)	-2(1)
C(3)	32(1)	33(1)	34(1)	5(1)	4(1)	-2(1)
C(4)	41(1)	23(1)	45(1)	1(1)	3(1)	1(1)
C(5)	35(1)	28(1)	36(1)	-5(1)	2(1)	4(1)
C(6)	25(1)	30(1)	29(1)	0(1)	2(1)	0(1)
C(7)	29(1)	26(1)	34(1)	-1(1)	6(1)	-1(1)
C(8)	26(1)	30(1)	30(1)	-2(1)	2(1)	0(1)

Table 45. Atomic Coordinates (× 10^4) and Equivalent Isotropic Thermal Parameters ($Å^2$ × 10^2) for 2,2,5,5–tetramethyl–3–carboxypyrroline–1–oxyl, (**5.2**).

Atom	x	y	z	$U_{eq.}$	Occupancy
O(1)	7549(2)	3779(1)	824(1)	38(1)	1
O(2)	7759(2)	2040(1)	809(1)	54(1)	1
C(1)	7101(2)	2937(1)	1000(1)	27(1)	1
C(2)	5744(2)	2785(1)	1456(1)	24(1)	1
C(3)	5199(2)	1867(1)	1651(1)	28(1)	1
C(4)	3788(2)	1959(1)	2109(1)	25(1)	1
C(4A)	4931(3)	1516(1)	2587(1)	38(1)	1
C(4B)	1473(2)	1478(1)	2024(1)	37(1)	1
N(1)	3632(2)	3113(1)	2141(1)	25(1)	1
O(3)	2552(2)	3593(1)	2479(1)	39(1)	1
C(5)	4841(2)	3700(1)	1749(1)	23(1)	1
C(5A)	3183(2)	4368(1)	1441(1)	36(1)	1
C(5B)	6666(3)	4367(1)	2003(1)	37(1)	1
O(4)	5765(2)	9337(1)	1664(1)	41(1)	1
O(5)	4700(2)	7690(1)	1791(1)	38(1)	1
C(6)	5796(2)	8427(1)	1545(1)	27(1)	1
C(7)	7037(2)	8019(1)	1111(1)	23(1)	1
C(8)	7203(2)	7023(1)	974(1)	28(1)	1
C(9)	8562(2)	6863(1)	511(1)	29(1)	1
C(9A)	10638(3)	6198(1)	613(1)	45(1)	1
C(9B)	7177(3)	6437(1)	63(1)	49(1)	1
N(2)	9209(2)	7962(1)	419(1)	30(1)	1
O(6)	10476(2)	8240(1)	66(1)	58(1)	1
C(10)	8256(2)	8749(1)	764(1)	24(1)	1
C(10A)	6678(3)	9462(1)	456(1)	38(1)	1
C(10B)	10142(3)	9366(1)	1025(1)	41(1)	1

Table 46. Anisotropic Thermal Parameters ($Å^2 \times 10^3$) for 2,2,5,5–tetramethyl–3–carboxypyrroline–1–oxyl, (**5.2**).

Atom	U_{11}	U_{22}	U_{33}	U_{23}	U_{13}	U_{12}
O(1)	51(1)	30(1)	35(1)	2(1)	18(1)	-6(1)
O(2)	89(1)	31(1)	44(1)	1(1)	43(1)	8(1)
C(1)	32(1)	27(1)	23(1)	-1(1)	6(1)	1(1)
C(2)	27(1)	22(1)	22(1)	-1(1)	4(1)	2(1)
C(3)	36(1)	22(1)	27(1)	-2(1)	9(1)	3(1)
C(4)	31(1)	18(1)	26(1)	2(1)	7(1)	1(1)
C(4A)	42(1)	39(1)	33(1)	10(1)	6(1)	7(1)
C(4B)	40(1)	34(1)	38(1)	-4(1)	7(1)	-10(1)
N(1)	33(1)	20(1)	24(1)	-2(1)	11(1)	1(1)
O(3)	55(1)	27(1)	36(1)	-4(1)	27(1)	2(1)
C(5)	28(1)	19(1)	22(1)	0(1)	8(1)	-1(1)
C(5A)	40(1)	31(1)	36(1)	7(1)	9(1)	10(1)
C(5B)	42(1)	35(1)	33(1)	-8(1)	8(1)	-11(1)
O(4)	61(1)	26(1)	38(1)	-4(1)	23(1)	0(1)
O(5)	53(1)	28(1)	36(1)	3(1)	26(1)	1(1)
C(6)	32(1)	25(1)	23(1)	3(1)	6(1)	3(1)
C(7)	25(1)	24(1)	20(1)	2(1)	2(1)	2(1)
C(8)	33(1)	23(1)	28(1)	3(1)	6(1)	0(1)
C(9)	37(1)	21(1)	29(1)	-2(1)	8(1)	1(1)
C(9A)	48(1)	34(1)	55(1)	2(1)	13(1)	13(1)
C(9B)	57(1)	50(1)	40(1)	-17(1)	6(1)	-6(1)
N(2)	42(1)	24(1)	25(1)	0(1)	16(1)	1(1)
O(6)	93(1)	38(1)	47(1)	-5(1)	50(1)	-10(1)
C(10)	33(1)	21(1)	21(1)	-1(1)	8(1)	1(1)
C(10A)	54(1)	29(1)	31(1)	9(1)	7(1)	10(1)
C(10B)	39(1)	40(1)	43(1)	-7(1)	10(1)	-11(1)

Table 47. Atomic Coordinates ($\times 10^4$) and Equivalent Isotropic Thermal Parameters ($Å^2 \times 10^2$) for benzamidinium–2,2,5,5–tetramethyl–3–carboxypyrroline–1–oxyl hydrate, (**5.3**).

Atom	x	y	z	$U_{eq.}$	Occupancy
O(1)	1913(2)	8874(2)	5620(1)	78(1)	1
O(2)	2941(2)	6904(2)	5352(1)	93(1)	1
O(3)	8261(2)	8608(2)	6449(1)	88(1)	1
O(4)	-20(2)	3519(2)	3961(1)	74(1)	1
N(1)	499(3)	6328(3)	4394(1)	62(1)	1
N(2)	-38(3)	8681(3)	4428(1)	67(1)	1
N(3)	6887(2)	8809(2)	6327(1)	60(1)	1
C(1)	-280(3)	7427(3)	4176(1)	52(1)	1
C(2)	-1467(3)	7247(3)	3620(1)	50(1)	1
C(3)	-1511(3)	8118(3)	3081(1)	67(1)	1
C(4)	-2586(4)	7944(4)	2553(2)	77(1)	1
C(5)	-3639(3)	6945(4)	2569(2)	74(1)	1
C(6)	-3621(3)	6108(3)	3103(2)	74(1)	1
C(7)	-2526(3)	6234(3)	3634(1)	62(1)	1
C(8)	6167(3)	9949(3)	6647(1)	64(1)	1
C(9)	4617(3)	9691(3)	6351(1)	62(1)	1
C(10)	4451(2)	8595(3)	5953(1)	49(1)	1
C(11)	5894(3)	7885(3)	5888(1)	51(1)	1
C(12)	6749(3)	11374(4)	6463(2)	95(1)	1
C(13)	6399(4)	9727(5)	7389(2)	106(1)	1
C(14)	6020(4)	6387(3)	6153(2)	86(1)	1
C(15)	6298(3)	7955(4)	5204(2)	76(1)	1
C(16)	2997(3)	8089(3)	5612(1)	59(1)	1

Table 48. Anisotropic Thermal Parameters ($Å^2 \times 10^3$) for benzamidinium–2,2,5,5–tetramethyl–3–carboxypyrroline–1–oxyl hydrate, (**5.3**).

Atom	U_{11}	U_{22}	U_{33}	U_{23}	U_{13}	U_{12}
O(1)	37(1)	96(2)	94(2)	-22(1)	-13(1)	7(1)
O(2)	66(1)	69(1)	129(2)	-15(1)	-42(1)	0(1)
O(3)	35(1)	98(2)	121(2)	-32(1)	-19(1)	11(1)
O(4)	63(1)	69(2)	93(2)	-16(1)	17(1)	-7(1)
N(1)	54(2)	63(2)	64(2)	-10(1)	-15(1)	6(1)
N(2)	56(2)	61(2)	76(2)	-16(1)	-17(1)	6(1)
N(3)	34(1)	71(2)	71(2)	-10(1)	-11(1)	2(1)
C(1)	41(1)	62(2)	52(2)	-5(1)	3(1)	2(1)
C(2)	39(1)	59(2)	48(1)	-5(1)	-1(1)	5(1)
C(3)	55(2)	78(2)	65(2)	8(2)	-2(1)	-8(2)
C(4)	73(2)	94(2)	59(2)	13(2)	-9(2)	-1(2)
C(5)	65(2)	83(2)	65(2)	-2(2)	-19(2)	3(2)
C(6)	55(2)	76(2)	84(2)	-2(2)	-12(2)	-13(2)
C(7)	53(2)	68(2)	63(2)	2(2)	-3(1)	-5(2)
C(8)	40(2)	77(2)	69(2)	-21(2)	-8(1)	1(1)
C(9)	36(1)	81(2)	67(2)	-13(2)	-1(1)	4(1)
C(10)	37(1)	59(2)	48(1)	6(1)	-4(1)	-2(1)
C(11)	41(1)	55(2)	53(2)	2(1)	-8(1)	0(1)
C(12)	56(2)	76(2)	148(4)	-29(2)	0(2)	-9(2)
C(13)	76(2)	163(4)	70(2)	-36(2)	-16(2)	5(2)
C(14)	68(2)	63(2)	118(3)	21(2)	-22(2)	0(2)
C(15)	59(2)	108(3)	60(2)	-7(2)	3(1)	11(2)
C(16)	43(2)	65(2)	63(2)	4(2)	-9(1)	-5(2)

Table 49. Atomic Coordinates ($\times 10^4$) and Equivalent Isotropic Thermal Parameters ($Å^2 \times 10^2$) for *m*–cyanobenzamidinium–2,2,5,5–tetramethyl–3–carboxypyrroline–1–oxyl, (**5.4**).

Atom	x	y	z	$U_{eq.}$	Occupancy
O(1)	-2413(3)	8572(1)	6679(2)	66(1)	1
O(2)	165(3)	5902(1)	9000(2)	59(1)	1
O(3)	2235(2)	6654(1)	8825(2)	55(1)	1
N(1)	4410(3)	5835(1)	10547(2)	45(1)	1
N(2)	2218(3)	5059(2)	10505(2)	53(1)	1
N(3)	10516(4)	4497(2)	13916(3)	80(1)	1
N(4)	-2029(3)	8029(1)	7329(2)	45(1)	1
C(1)	4685(3)	4948(2)	12046(2)	38(1)	1
C(2)	6437(3)	4893(2)	12307(2)	39(1)	1
C(3)	7261(3)	4613(2)	13335(2)	42(1)	1
C(4)	6351(4)	4384(2)	14100(3)	54(1)	1
C(5)	4611(4)	4432(2)	13835(3)	57(1)	1
C(6)	3779(4)	4710(2)	12808(3)	51(1)	1
C(7)	3734(3)	5288(2)	10982(2)	38(1)	1
C(8)	9085(4)	4552(2)	13633(3)	54(1)	1
C(9)	-292(3)	7719(2)	7603(2)	42(1)	1
C(10)	-605(3)	7069(2)	8280(2)	38(1)	1
C(11)	-2156(4)	7064(2)	8436(3)	50(1)	1
C(12)	-3239(3)	7681(2)	7905(3)	47(1)	1
C(13)	-3723(6)	8200(2)	8757(4)	83(1)	1
C(14)	-4823(4)	7435(2)	7057(4)	74(1)	1
C(15)	924(4)	8269(2)	8289(4)	65(1)	1
C(16)	217(4)	7525(2)	6513(3)	62(1)	1
C(17)	715(4)	6502(2)	8732(2)	41(1)	1

Table 50. Anisotropic Thermal Parameters ($Å^2 \times 10^3$) for *m*–cyanobenzamidinium–2,2,5,5–tetramethyl–3–carboxypyrroline–1–oxyl, (**5.4**).

Atom	U_{11}	U_{22}	U_{33}	U_{23}	U_{13}	U_{12}
O(1)	46(1)	58(2)	89(2)	30(1)	7(1)	16(1)
O(2)	44(1)	49(1)	75(2)	24(1)	-6(1)	-4(1)
O(3)	36(1)	52(2)	73(2)	18(1)	4(1)	4(1)
N(1)	38(2)	45(2)	47(2)	6(1)	-3(1)	-8(1)
N(2)	33(2)	53(2)	63(2)	19(2)	-8(1)	-9(1)
N(3)	41(2)	125(3)	68(2)	-1(2)	2(2)	13(2)
N(4)	36(1)	39(2)	58(2)	11(1)	4(1)	8(1)
C(1)	32(2)	33(2)	46(2)	3(1)	4(1)	-1(1)
C(2)	34(2)	37(2)	45(2)	-1(1)	7(1)	-2(1)
C(3)	33(2)	44(2)	46(2)	-3(2)	2(1)	3(1)
C(4)	45(2)	66(2)	45(2)	12(2)	0(2)	5(2)
C(5)	45(2)	73(2)	54(2)	15(2)	12(2)	-2(2)
C(6)	33(2)	61(2)	54(2)	6(2)	3(2)	-1(2)
C(7)	31(2)	35(2)	46(2)	0(1)	6(1)	-1(1)
C(8)	39(2)	73(3)	46(2)	0(2)	2(2)	8(2)
C(9)	30(2)	45(2)	48(2)	10(1)	2(1)	1(1)
C(10)	32(2)	42(2)	37(2)	0(1)	2(1)	1(1)
C(11)	48(2)	46(2)	56(2)	12(2)	14(2)	1(2)
C(12)	34(2)	50(2)	59(2)	9(2)	14(2)	7(2)
C(13)	83(3)	84(3)	88(3)	5(3)	35(3)	34(3)
C(14)	40(2)	72(3)	104(3)	16(3)	4(2)	1(2)
C(15)	43(2)	48(2)	94(3)	2(2)	-6(2)	-8(2)
C(16)	52(2)	77(3)	59(2)	23(2)	19(2)	18(2)
C(17)	36(2)	43(2)	40(2)	2(1)	1(1)	1(1)